

A TAILORED APPROACH TOWARDS THE RIGHT DOSE OF  
DASATINIB, (E)-CLOMIPHENE, IMATINIB AND INFLIXIMAB  
LEVERAGING PHYSIOLOGICALLY BASED PHARMACOKINETIC AND  
POPULATION PHARMACOKINETIC MODELING

DISSERTATION

zur Erlangung des Grades des Doktors der Naturwissenschaften  
der Naturwissenschaftlich-Technischen Fakultät  
der Universität des Saarlandes

von  
Christina Birgitte-Margaretha Kovar  
(geb. Schräpel)  
Apothekerin

Saarbrücken  
2025

Tag des Kolloquiums:	26. November 2025
Dekan:	Prof. Dr.-Ing. Dirk Bähre
Berichterstatter:	Prof. Dr. Thorsten Lehr Prof. Dr. Markus R. Meyer
Akad. Mitglied:	Dr. Michael Ring
Vorsitz:	Prof. Dr. Andriy Luzhetskyy

*Alle Dinge sind Gift, und nichts ist ohne Gift.  
Allein die Dosis macht, dass ein Ding kein Gift ist.*

– Paracelsus –





## PUBLICATIONS

---

The following publications have been included in this thesis:

- I Kovar, C., Loer, H. L. H., Rüdesheim, S., Fuhr, L. M., Marok, F. Z., Selzer, D., Schwab, M., & Lehr, T. (2024). A physiologically-based pharmacokinetic precision dosing approach to manage dasatinib drug-drug interactions. *CPT: pharmacometrics & systems pharmacology*, 13(7), 1144–1159. DOI: [10.1002/psp4.13146](https://doi.org/10.1002/psp4.13146).
- II Loer, H. L. H., Kovar, C., Rüdesheim, S., Marok, F. Z., Fuhr, L. M., Selzer, D., Schwab, M., & Lehr, T. (2024). Physiologically based pharmacokinetic modeling of imatinib and N-desmethyl imatinib for drug-drug interaction predictions. *CPT: pharmacometrics & systems pharmacology*, 13(6), 926–940. DOI: [10.1002/psp4.13127](https://doi.org/10.1002/psp4.13127).
- III Kovar, C., Kovar, L., Rüdesheim, S., Selzer, D., Ganchev, B., Kröner, P., Igel, S., Kerb, R., Schaeffeler, E., Mürdter, T. E., Schwab, M., & Lehr, T. (2022). Prediction of drug-drug-gene interaction scenarios of (*E*)-clomiphene and its metabolites using physiologically based pharmacokinetic modeling. *Pharmaceutics*, 14(12), 2604. DOI: [10.3390/pharmaceutics14122604](https://doi.org/10.3390/pharmaceutics14122604).
- IV Schräpel, C., Kovar, L., Selzer, D., Hofmann, U., Tran, F., Reinisch, W., Schwab, M., & Lehr, T. (2021). External model performance evaluation of twelve infliximab population pharmacokinetic models in patients with inflammatory bowel disease. *Pharmaceutics*, 13(9), 1368. DOI: [10.3390/pharmaceutics13091368](https://doi.org/10.3390/pharmaceutics13091368).



## CONTRIBUTION REPORT

---

The author Christina Kovar (née Schräpel) would like to declare her contributions to the publications related to projects I–IV included in this thesis according to the contributor roles taxonomy (CRediT) [1].

- I Conceptualization, Investigation, Visualization, Writing – Original Draft, Writing – Review & Editing
- II Conceptualization, Investigation, Writing – Review & Editing
- III Conceptualization, Data Curation, Formal Analysis, Investigation, Methodology, Software, Validation, Visualization, Writing – Original Draft, Writing – Review & Editing
- IV Conceptualization, Data Curation, Formal Analysis, Investigation, Methodology, Software, Visualization, Writing – Original Draft, Writing – Review & Editing



## ABSTRACT

---

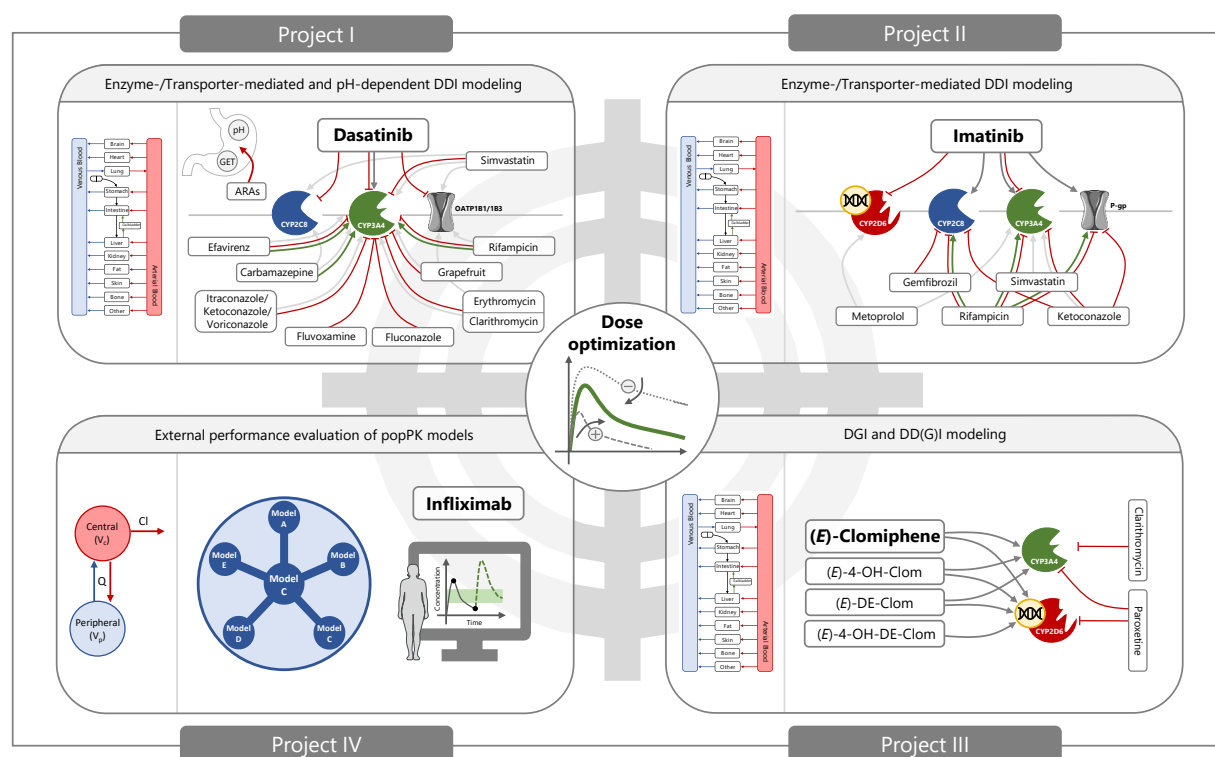
The overall aim of precision medicine is to provide the right treatment to the right patient at the right time and, consequently, improving clinical outcome and minimizing toxicities. However, substantial inter- and intra-individual variability in drug exposure and response often impedes successful treatment which calls for tailoring drug therapy to individual needs. Here, precision dosing represents an essential component of precision medicine to improve individual drug treatment. Despite the application of therapeutic drug monitoring or pharmacogenetic testing to optimize the dose for specific drugs, a significant need for advanced dosing strategies remains. Model-informed precision dosing, a crucial development in personalized medicine, uses pharmacometric models to guide clinicians in making dosing decisions by predicting tailored dosing regimens for individual patients or specific patient populations. This thesis aimed to develop and provide mechanistic pharmacometric models for the two tyrosine kinase inhibitors dasatinib and imatinib as well as for the selective estrogen receptor modulator (*E*)-clomiphene and an empirical pharmacometric model for the monoclonal antibody infliximab, helping to enhance treatment efficacy and reduce the risk of toxicities. These models and their presented applications may be leveraged to foster future precision dosing efforts in healthcare.

## ZUSAMMENFASSUNG

---

Zu den Hauptzielen der Präzisionsmedizin gehört die Anwendung der richtigen Therapie für den richtigen Patienten zum richtigen Zeitpunkt, um die klinische Wirksamkeit zu verbessern und Toxizitäten zu minimieren. Einer erfolgreichen Arzneimitteltherapie steht häufig eine hohe inter- und intra-individuelle Variabilität im Ansprechen an die Therapie entgegen. Das Konzept der Präzisionsdosierung ist daher eine wichtige Komponente der Präzisionsmedizin. Doch trotz der Anwendung von Therapeutischem Drug-Monitoring oder pharmakogenetischer Tests für vereinzelte Arzneistoffe zur individuellen Dosisoptimierung besteht weiterhin ein großer Bedarf an fortschrittlicheren Dosierungsstrategien: Mit der Modell-informierten Präzisionsdosierung, die eine Weiterentwicklung in der Präzisionsmedizin darstellt, können basierend auf pharmakometrischen Modellen und Patienten-bezogenen Informationen individuelle Dosen für Patienten oder Patientengruppen vorhergesagt werden. Das Ziel dieser Thesis war es, mechanistische pharmakometrische Modelle für die beiden Tyrosin Kinase Inhibitoren Dasatinib und Imatinib und den selektiven Estrogen-Rezeptor Inhibitor (*E*)-Clomifen zu entwickeln sowie ein empirisches pharmakometrisches Modell für den monoklonalen Antikörper Infliximab bereitzustellen. Diese Modelle können zukünftig für individuelle Dosisanpassungen in der Klinik angewendet werden, um höhere Therapieansprechraten zu erzielen und das Risiko für Toxizitäten zu minimieren.

## GRAPHICAL ABSTRACT



**Graphical abstract.** Drawings were obtained from Servier Medical Art [2], licensed under a Creative Commons Attribution 4.0 (CC BY 4.0) Unported License (<https://creativecommons.org/licenses/by/4.0/>). ARAs, acid-reducing agents; Cl, clearance; CYP, cytochrome P450; DDI, drug–drug interaction; DDGI, drug–drug–(gene) interaction; DGI, drug–gene interaction; (E)-4-OH-Clom, (E)-4-hydroxyclophenene; (E)-4-OH-DE-Clom, (E)-4-hydroxy-N-desethylclomiphene; (E)-DE-Clom, (E)-N-desethylclomiphene; GET, gastric emptying time; OATP, organic anion transporting polypeptides; P-gp, P-glycoprotein; popPK, population pharmacokinetic; Q, intercompartmental clearance; V<sub>c</sub>, central volume of distribution; V<sub>p</sub>, peripheral volume of distribution.





## DANKSAGUNG

---

Mit der Fertigstellung meiner Doktorarbeit geht ein prägender und herausfordernder Lebensabschnitt zu Ende. An dieser Stelle möchte ich mich von Herzen bei allen bedanken, die mich auf diesem Weg begleitet und unterstützt haben.

Allen voran gilt mein besonderer Dank meinem Doktorvater, Professor Thorsten Lehr, für die vertrauensvolle Unterstützung, die inspirierenden wissenschaftlichen Impulse und die wertvollen Anregungen während meiner Promotionszeit.

Ebenso möchte ich mich herzlichst bei meinen Kolleginnen und Kollegen vom Dr. Margarete Fischer-Bosch Institute of Clinical Pharmacology bedanken, insbesondere bei Professor Matthias Schwab, Dr. Thomas Mürdter und Dr. Ute Hofmann für die stetige wissenschaftliche Unterstützung während meiner Promotionszeit.

Mein weiterer Dank richtet sich an Professor Markus Meyer für die Übernahme des Zweitgutachtens dieser Arbeit und für seine wissenschaftliche Begleitung.

Ein großes Dankeschön geht an meine Kolleginnen und Kollegen aus der Arbeitsgruppe für den hilfreichen wissenschaftlichen Austausch, die Zusammenarbeit, die wertvolle gegenseitige Unterstützung und die vielen kleinen Momente, die den Alltag bereichern haben.

Auch bei meinen Co-Autorinnen und Co-Autoren möchte ich mich herzlich für ihre Unterstützung bei der Erstellung dieser Arbeit bedanken.

Ich möchte mich auch von Herzen bei meinen Freunden und meiner Familie bedanken, insbesondere bei meiner Mutter Michaela Schräpel und meinem Vater Günther Schräpel, für ihre Unterstützung und ihr Vertrauen in mich. Ohne eure Ermutigung und euren Rückhalt wäre diese Arbeit nicht möglich gewesen.

Schließlich gilt mein tiefster Dank meinem Ehemann, Dr. Lukas Kovar, der mich während dieser herausfordernden Zeit immer begleitet, an mich geglaubt und motiviert hat.

Ein großes Dankeschön – aus tiefstem Herzen!



# CONTENTS

---

1	Introduction	1
1.1	Motivation . . . . .	1
1.2	Personalized Medicine . . . . .	2
1.3	Precision Dosing . . . . .	2
1.3.1	Pharmacogenetics and pharmacogenomics (PGx) . . . . .	3
1.3.2	Therapeutic drug monitoring (TDM) . . . . .	5
1.3.3	Model-informed precision dosing (MIPD) . . . . .	7
1.4	Pharmacometric approaches: PBPK and popPK modeling . . . . .	9
1.4.1	Physiologically based pharmacokinetic (PBPK) modeling . . . . .	9
1.4.2	Population pharmacokinetic (popPK) modeling . . . . .	10
1.4.3	PopPK and PBPK modeling in MIDD . . . . .	11
1.4.4	PopPK and PBPK modeling in MIPD . . . . .	12
2	Objectives	15
3	Methods	17
3.1	Investigated compounds . . . . .	17
3.1.1	Imatinib and dasatinib . . . . .	17
3.1.2	( <i>E</i> )-clomiphene . . . . .	18
3.1.3	Infliximab . . . . .	18
3.2	PBPK modeling . . . . .	20
3.2.1	PBPK model building . . . . .	21
3.2.2	PBPK model evaluation . . . . .	22
3.2.3	Drug–gene interaction (DGI) modeling . . . . .	24
3.2.4	Drug–drug–(gene) interaction (DD(G)I) modeling . . . . .	24
3.2.5	Model performance evaluation of DGI and DD(G)I scenarios . . . . .	26
3.2.6	Software . . . . .	26
3.3	External performance evaluation of infliximab popPK models . . . . .	26
3.3.1	Literature search . . . . .	27
3.3.2	External dataset . . . . .	27
3.3.3	Handling below limit of quantification (BLQ) data . . . . .	27
3.3.4	Maximum a posteriori (MAP) Bayesian estimation process . . . . .	27
3.3.5	Graphical and quantitative evaluation . . . . .	28
4	Results	29
4.1	Project I – Physiologically based pharmacokinetic modeling of dasatinib . . . . .	29
4.1.1	Publication . . . . .	29
4.1.2	Author Contributions . . . . .	29
4.1.3	Copyright . . . . .	29
4.2	Project II – Physiologically based pharmacokinetic modeling of imatinib . . . . .	46
4.2.1	Publication . . . . .	46
4.2.2	Author Contributions . . . . .	46
4.2.3	Copyright . . . . .	46

4.3	Project III – Physiologically based pharmacokinetic modeling of (E)-clomiphene and its main metabolites . . . . .	62
4.3.1	Publication . . . . .	62
4.3.2	Author Contributions . . . . .	62
4.3.3	Copyright . . . . .	63
4.4	Project IV – External performance evaluation of infliximab population pharmacokinetic models . . . . .	84
4.4.1	Publication . . . . .	84
4.4.2	Author Contributions . . . . .	84
4.4.3	Copyright . . . . .	85
5	Discussion and future perspective . . . . .	107
5.1	Application of PBPK modeling to tailor drug therapy . . . . .	107
5.1.1	Rationale for MIPD of dasatinib . . . . .	107
5.1.2	Rationale for MIPD of imatinib . . . . .	109
5.1.3	Rationale for MIPD of clomiphene . . . . .	109
5.1.4	The virtual twin concept and individual PBPK predictions . . . . .	110
5.2	Application of popPK modeling to tailor drug therapy . . . . .	111
5.2.1	Rationale for MIPD of infliximab . . . . .	111
5.2.2	The “GUIDE-IBD” study . . . . .	112
5.2.3	Automated model selection and model averaging approach . . . . .	114
5.3	Outlook for clinical implementation of MIPD . . . . .	115
6	Conclusions . . . . .	117
	Bibliography . . . . .	119
A	Supplementary Documents . . . . .	141
A.1	Supplementary Document to Publication I . . . . .	141
A.2	Supplementary Document to Publication II . . . . .	197
A.3	Supplementary Document to Publication III . . . . .	244
A.4	Supplementary Document to Publication IV . . . . .	299
B	Publication History . . . . .	307
B.1	Research Articles . . . . .	307
B.2	Conference Abstracts . . . . .	308
B.3	Others . . . . .	309

## LIST OF FIGURES

---

Figure 1.1	Comparison of different dosing approaches . . . . .	3
Figure 1.2	Overview of the TDM strategy . . . . .	6
Figure 1.3	Summary of important criteria for drugs suited for TDM .	7
Figure 1.4	Exemplary representation of an MIPD dosing framework .	8
Figure 1.5	Structural overview of the multi-compartmental model implemented in PK-Sim® . . . . .	10
Figure 1.6	Structural illustration of a one-, two- and three-compartment model after intravenous application . . . . .	11
Figure 3.1	PBPK modeling workflow . . . . .	20
Figure 5.1	Clinical trial design overview for the “GUIDE-IBD” study	113
Figure 5.2	Workflow for generating an MIPD report . . . . .	114
Figure 5.3	Screenshot of a decision support system based on PBPK models . . . . .	116

## ACRONYMS

---

ABL	Abelson
ADA	anti-drug antibody
ADME	absorption, distribution, metabolism and excretion
ADR	adverse drug reaction
AGA	American Gastroenterological Association
ALL	acute lymphoblastic leukemia
ARA	acid-reducing agent
AS	activity score
AUC	area under the plasma concentration–time curve
AUC <sub>inf</sub>	AUC extrapolated to infinity
AUC <sub>last</sub>	AUC from the time of the first concentration measurement to the time of the last concentration measurement
BC	“best care”
BCR	breakpoint cluster region
BLQ	below the limit of quantification
CD	Crohn’s disease
CDSS	clinical decision support systems

Cl	clearance
C <sub>max</sub>	maximum plasma concentration
C <sub>min</sub>	trough concentration
CML	chronic myeloid leukemia
CPIC	Clinical Pharmacogenetics Implementation Consortium
CRedit	contributor roles taxonomy
CYP	cytochrome P450
DDGI	drug–drug–gene interaction
DDI	Drug–drug interaction
DGI	drug–gene interaction
(E)-4-OH-Clom	(E)-4-hydroxyclophene
(E)-4-OH-DE-Clom	(E)-4-hydroxy-N-desethylclomiphene
(E)-DE-Clom	(E)-N-desethylclomiphene
EBE	empirical Bayes PK parameter estimates
EHR	electronic health record
EMA	European Medicines Agency
FDA	U.S. Food and Drug Administration
FOCE-I	first-order conditional estimation with interaction
GET	gastric emptying time
GIST	gastrointestinal stromal tumors
GIT	gastrointestinal tract
GMFE	geometric mean fold error
IBD	inflammatory bowel disease
ICRP	International Commission on Radiological Protection
IM	intermediate metabolizer
k <sub>cat</sub>	catalytic rate constant
LLOQ	lower limit of quantification
MAP	maximum <i>a posteriori</i> probability
MIDD	model-informed drug development
MIPD	model-informed precision dosing
MMC	“molecular medicine care”
MRD	mean relative deviation
NHANES	National Health and Nutrition Examination Survey
NM	normal metabolizer
NTI	narrow therapeutic index
OATP	organic anion transporting polypeptide

OSP	Open Systems Pharmacology
P-gp	P-glycoprotein
PBPK	physiologically based pharmacokinetic
PCOS	polycystic ovary syndrome
PD	pharmacodynamic(s)
PGx	pharmacogenetic and pharmacogenomic
Ph	Philadelphia chromosome
Ph+	Philadelphia chromosome positive
PK	pharmacokinetic(s)
PM	poor metabolizer
popPK	population pharmacokinetic
Q	intercompartmental clearance
q.d.	once daily
SERM	selective estrogen receptor modulator
SSPB	symmetric signed percentage bias
TDM	therapeutic drug monitoring
TKI	tyrosine kinase inhibitor
TNF- $\alpha$	tumor necrosis factor alpha
UC	ulcerative colitis
UM	ultrarapid metabolizer
V <sub>c</sub>	central volume of distribution
V <sub>p</sub>	peripheral volume of distribution
$\zeta$	median symmetric accuracy





## INTRODUCTION

---

### 1.1 MOTIVATION

Approximately 50% of Phase II and III studies in drug development fail due to lack of efficacy of the tested drug product [3]. However, also approved drugs may show lack or loss of therapeutic response when evaluated in broader populations or real-world settings [4, 5].

In drug development, a “one-size-fits-all” paradigm is commonly applied including only a limited number of drug doses tested due to practicality and cost effectiveness [3]. In addition, drugs are typically investigated in a well-selected study population and eligibility criteria for clinical trial participation ensure the internal validity of studies and reduce the risk for vulnerable populations [3, 6]. As a result, however, populations in clinical studies usually do not represent the diversity of real-world patient populations including patients with organ dysfunctions, age-related physiological parameter changes (e.g., geriatrics) and others [6]. Consequently, the “one-size-fits-all” dosing, established by randomized controlled trials, often does not provide optimal dosing for all patients, especially if specific subpopulations were underrepresented in the trial cohorts [6]. Hence, tailoring drug therapy based on the drug, the disease state and the individual patient can be crucial to not only improve treatment efficacy but also to reduce the occurrence of adverse drug reactions (ADRs) [6].

ADRs – defined as a “response to a medicinal product which is noxious and unintended” [7] – have been estimated to be the fourth to sixth leading cause of mortality in the U.S., resulting in 100,000 deaths per year [8, 9]. Hospital admissions due to ADRs range from 2.4% to 16.5% in different studies [10, 11]. Moreover, the overall incidence of ADRs during hospitalization was found to be around 10%, leading to longer hospital stays [8, 12]. Consequently, ADR-related morbidity and mortality have been estimated to result in enormous costs ranging from 30 billion to more than 130 billion dollars annually in the U.S. [13, 14]. Especially the elderly population ( $\geq 65$  years) is affected by ADRs, showing a four times higher ADR-related hospitalization rate compared to younger people, likely due to co-morbidities, organ dysfunctions but also polypharmacy [15–17]: Drug–drug interactions (DDIs) following concomitant drug administrations, drug–gene interactions (DGIs) due to pharmacogenetic variations in metabolizing enzymes or transporters and the combination of both (drug–drug–gene interactions (DDGIs)) can significantly alter drug disposition and thereby represent important causes of preventable ADRs [18–20].

These aspects emphasize the need of shifting to a more personalized medicine approach for many drug therapies in the future.

## 1.2 PERSONALIZED MEDICINE

The area of medicine has experienced a revolution due to advances in the fields of genomics, proteomics, metabolomics, bioinformatics, molecular diagnostics and data science, leading to the emergence of personalized medicine, also termed as precision medicine [21, 22]. This new paradigm is defined as tailoring disease treatment and prevention by taking individual genetic and nongenetic characteristics, environmental as well as lifestyle factors into account [23, 24]. Personalized medicine aims for the right treatment to the right patient at the right time and consequently improving clinical outcomes and minimizing toxicities [23, 25]. This transformation was triggered by insights into the human genome, gained from novel technologies such as next-generation sequencing, identifying alterations and patterns in genes for potential predisposition and drivers for specific diseases [23, 26]. New treatments tailored to individual characteristics, such as a patient's genotype or the genetic profile of tumors, have since been approved by the U.S. Food and Drug Administration (FDA) [23]. Here, molecularly targeted cancer therapy in chronic myeloid leukemia (CML) illustrates a successful example of personalized medicine [27]. Since the advent of imatinib, the first tyrosine kinase inhibitor (TKI) applied in oncology, patients with CML now have a near-normal life expectancy [27]. In addition to selecting the right treatment for the right patient, the administration of the right dose and route at the right time (i.e., precision dosing) based on the genetic makeup and other individual attributes such as co-medications or concurrent diseases is an essential cornerstone of personalized medicine to ensure safer and more effective treatment strategies [28–30].

## 1.3 PRECISION DOSING

Precision dosing (also termed personalized or individualized dosing [24]) is an integral component of personalized medicine to optimize drug exposure [28] and has been defined "as dose selection by a prescriber for an individual patient at a given time" [3, 31]. The importance of finding the right dose has already been pointed out more than 500 years ago by Paracelsus: "All things are poison, and nothing is without poison, but the dose alone makes it so a thing is not a poison" (Paracelsus, 1493/1494–1541, translated into English) [31]. The administered dose of a given drug determines whether the patient will show the desired efficacy, non-response or sometimes even fatal toxicities, emphasizing the need of moving toward more individualized treatment strategies for many drug therapies [6]. This can be achieved by either stratified dosing or precision dosing. A stratified dosing approach categorizes patients into different subgroups based on common factors such as co-medication or patient characteristics like age, body weight, genetics or organ function and tailors the respective dose to each subgroup [24]. The precision dosing approach advances one step further, tailoring drug dosing individually based on patient characteristics that affect drug disposition and response [24]. To realize these personalized medicine approaches, various techniques such as pharmacogenetic and pharmacogenomic (PGx) testing, therapeutic drug monitoring (TDM) and/or the innovative model-informed precision dosing (MIPD) approach can be leveraged [32–35]. A graphical illustration of the

“one-size-fits-all”, stratified and precision dosing approaches is shown in **Figure 1.1**. **PGx** testing, **TDM** and **MIPD** approaches will be outlined in the following subsections.

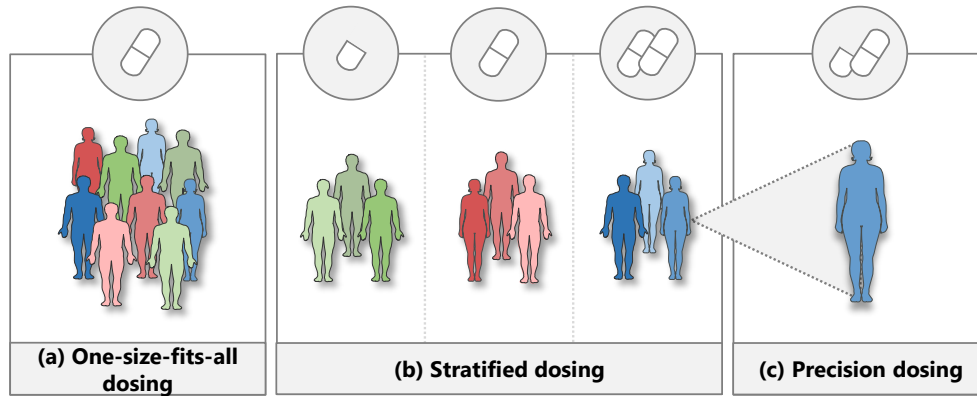


Figure 1.1: Comparison of different dosing approaches: (a) “One-size-fits-all” dosing: a uniform dose is applied to all patients; (b) Stratified dosing: the dose is adjusted for different subgroups based on co-medications or patient attributes; (c) Precision dosing: the dose is tailored to individual patient attributes. Drawings were adapted from Servier Medical Art [2], licensed under a Creative Commons Attribution 4.0 (CC BY 4.0) Unported License (<https://creativecommons.org/licenses/by/4.0/>).

### 1.3.1 Pharmacogenetics and pharmacogenomics (PGx)

Pharmacogenetics and Pharmacogenomics (**PGx**) are key components of personalized medicine to ensure safe and effective drug treatment based on individual genetic characteristics [30, 36]. While the discipline of pharmacogenetics focuses on genes determining a drug’s pharmacokinetic(s) (**PK**) (including absorption, distribution, metabolism and excretion (**ADME**)) or pharmacodynamic(s) (**PD**), the discipline of pharmacogenomics assesses the role of the human genome in drug response [36, 37]. Nevertheless, the distinction between the two terms is somewhat arbitrary and both terms are frequently used interchangeably [37]. In the last two decades, advances in genotyping and sequencing technologies, statistical genetic analysis and clinical trial designs have facilitated the understanding of the role of genetic variations in drug response [38]. As indicated by twin studies, 80–91% of variability in drug response might be explained by additive genetic effects and the remainder by unique environmental factors, highlighting the relevance of **PGx** testing for tailoring drug selection and dosing to the individual’s genetic characteristics [39, 40].

A prominent example is the cytochrome P450 (**CYP**) 2D6 enzyme encoded by the highly polymorphic **CYP2D6** gene [41]. While **CYP2D6** accounts for merely 2–4% of the hepatic **CYP** pool, it is involved in the metabolism of approximately 20–30% of commonly used drugs [30, 42]. **CYP2D6** metabolizes a broad spectrum of centrally acting drugs including opioids, antidepressants, antihypertensives or selective

estrogen receptor modulators (SERMs) [42]. The relatively short *CYP2D6* gene is located on chromosome 22 (22q13.2) and contains nine exons [42]. *CYP2D6* shows high expression in liver, brain, intestinal tissue and lymphoid cells [42]. Genetic variants in the *CYP2D6* gene, such as single nucleotide variations, copy number variants or structural rearrangements contribute to the pronounced variability in *CYP2D6* enzyme activity, and thus, may result in significant variability in drug response, both within a population and across ethnically differing populations [30, 43]. The predominant *CYP2D6* allelic variants are single nucleotide variations, consisting of single nucleotide polymorphisms as well as insertions or deletions of one or a small number of nucleotides [43].

Translation of these *CYP2D6* allelic variants and their enzymatic activities into clinically actionable guidelines was accomplished by grouping them into standard haplotypes and predicted metabolizer phenotypes [30, 44]. Here, the haplotype is assigned based on the star (\*)-allele nomenclature, cataloged by the Pharmacogene Variation Consortium, where each \*-allele comprises a predefined combination of variants [30, 43]. To date, > 160 distinct \*-alleles for *CYP2D6* have been described by the Pharmacogene Variation Consortium and assigned to one of the following enzymatic activities by the Clinical Pharmacogenetics Implementation Consortium (CPIC): no, decreased, normal, increased or unknown enzyme activity [45–47]. The individual diplotype (also known as the genotype) is determined by the combination of two *CYP2D6* alleles each of which can be allocated to a specific activity value of 0 for no activity, 0.25 or 0.5 for decreased, 1 for normal and 2 for increased activity [30, 41]. The sum of activity values from both alleles then constitutes the activity score (AS) [41, 48].

Furthermore, based on the *CYP2D6* diplotype, predicted phenotypes can be assigned which are categorized into four different *CYP2D6* metabolizer categories: poor metabolizer (PM) (AS = 0), intermediate metabolizer (IM) ( $0.25 \geq AS \leq 1$ ), normal metabolizer (NM) ( $1.25 \geq AS \leq 2.25$ ) and ultrarapid metabolizer (UM) (AS > 2.25) [30, 41]. For instance, *CYP2D6* \*1/\*1 refers to a NM with an AS of 2 [41]. An overview of selected *CYP2D6* alleles and their respective assigned activity value, required for calculating the AS of a specific genotype, is shown in Table 1.1.

Table 1.1: Assignment of *CYP2D6* activity values for selected *CYP2D6* alleles from the CPIC [45–47].

Allele Type	<i>CYP2D6</i> alleles	Activity Value
No function	*3, *4, *5, *6	0
Decreased function	*9, *10, *41	0.25
Decreased function	*17, *29	0.5
Normal function	*1, *2, *35	1
Increased function	*1x2, *2x2	2

*CYP2D6* allele frequencies have been observed to vary substantially, both within a population and across ethnically differing populations: About 2–3% of Asians and up to 7% of Europeans are *CYP2D6* PM, carrying two nonfunctional alleles that

encode for **CYP** enzymes not capable of metabolizing or bioactivating drugs via the **CYP2D6** pathway [45–47]. In contrast, **UM** carry a duplication or multiplication of a normal-function allele [49]. Consequently, **PM** typically have a higher risk for **ADRs** during treatment with **CYP2D6** substrates or, in the case of prodrugs bioactivated by **CYP2D6**, lack of therapeutic response [43]. For **UM**, these risks apply vice versa [43]. Yet, a patient's phenotype does not only depend on a patient's genotype [48]. In addition to genetic factors, (patho-)physiological factors (e.g., inflammation) and other factors (e.g., **DDIs**) can directly or indirectly affect **CYP2D6** activity [48]. Hence, inter-individual variability in populations with the same **CYP2D6** genotype can be observed [48]. Determining a patient's phenotype for a metabolizing enzyme such as **CYP2D6**, allows the application of precision dosing approaches for **DGIs** and **DDGIs**. To date, **PGx** testing is already recommended for many drugs [42]. However, its application in clinical practice translating **PGx** tests into clinical actions requires a comprehensive knowledge of clinical pharmacology [50]. Here, several professional societies including the **CPIC** and the Dutch Pharmacogenetics Working Group have developed clinical guidelines for several **DGIs** that are freely accessible ([www.pharmgkb.org](http://www.pharmgkb.org)) [42]. Nevertheless, there is still a significant need for further efforts from various stakeholders including pharmaceutical companies, academia and regulatory affairs to extend such **PGx** guidelines [51].

### 1.3.2 Therapeutic drug monitoring (TDM)

The discipline of **PK** studies what the body does to the drug and covers drug **ADME**, whereas the area of **PD** studies the effects of a drug on the body [52]. In clinical practice, therapeutic success can sometimes be monitored assessing surrogate **PD** parameters such as blood pressure or blood glucose [53]. However, such surrogate parameters are not available for many drugs [53]. Here, monitoring drug concentrations and adjusting drug doses using **TDM** can help to improve therapeutic responses if a significant relationship between the **PK** (i.e., drug concentrations) and **PD** effect (i.e., efficacy and/or safety) has been established [53].

In the early 1970s, **TDM** has emerged to individualize patient's drug therapy [54]. Subsequently, with the development of immunoassays during the 1980s, the implementation of **TDM** services was established in the clinic [54, 55]. In **TDM**, drug concentrations in biological fluids, typically in blood and plasma, are measured to adjust a patient's dosing regimen for optimal benefit [32, 56]. Thereby, the approach aims to improve therapeutic responses and prevent **ADRs** by maintaining drug concentrations within a predefined therapeutic target window where drug therapy is assumed to be both safe and effective [54, 56, 57]. An overview of the **TDM** strategy is depicted in **Figure 1.2**.

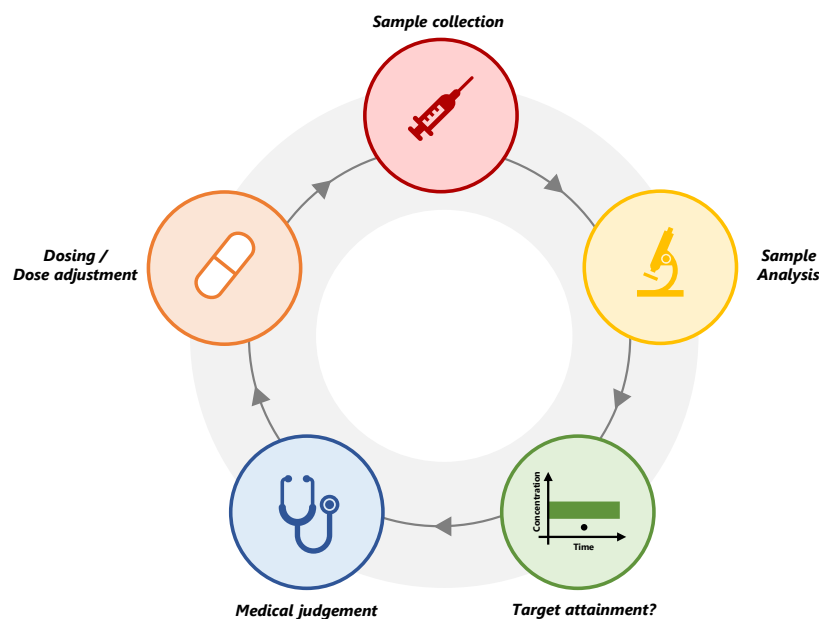


Figure 1.2: Overview of the **TDM** strategy. Blood samples are collected after drug administration and analyzed using validated bioanalytical assays [53]. The drug concentrations are clinically interpreted to determine if they fall within the therapeutic window [53]. After medical assessment, decisions about individual dose adjustments are made [53]. This process can be repeated in subsequent dosing intervals as required [53].

Especially narrow therapeutic index (**NTI**) drugs benefit from **TDM** [56]. **TDM** has shown to improve safety for **NTI** drugs such as digoxin, phenytoin, lithium, cyclosporine and aminoglycoside antibiotics [6, 56]. Moreover, **TDM** may also be advantageous in cases where a “one-size-fits-all” dosing approach results in significant differences in drug response among patients (inter-individual variability) or within the same patient over time (intra-individual variability) [54]. Here, **TDM** can be used to adjust individual dosing, accounting for variability in the **PK** and consequently variability in response [53]. A summary of the most important criteria for drugs suited for **TDM** is depicted in Figure 1.3.

While the area under the plasma concentration–time curve (**AUC**), the time above a threshold concentration, maximum plasma concentration ( $C_{\max}$ ) and trough concentration ( $C_{\min}$ ) all represent common measures of exposure [58], **TDM** is often based on  $C_{\min}$  samples [53]. For some drugs, prospective clinical studies investigating the suitability of **TDM** have been conducted and guidelines of potential dosing strategies provided [59–63]. Today, **TDM** is mainly applied in antiepileptic, immunosuppressive, antibiotic, antifungal, antipsychotic, cardiovascular system and anticancer drugs [64].

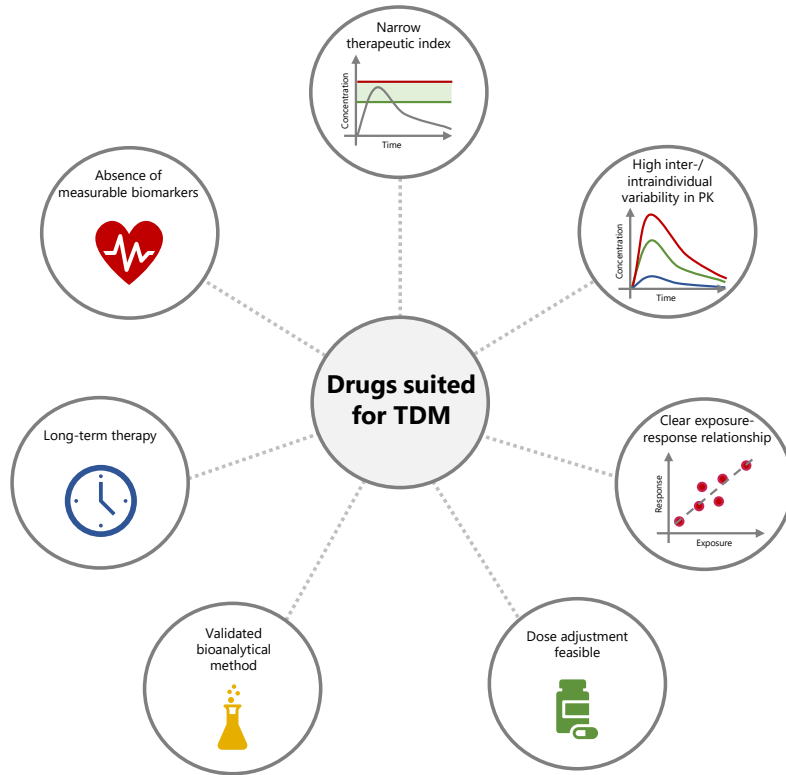


Figure 1.3: A summary of important criteria for drugs suited for **TDM**. These include absence of measurable biomarkers, a narrow therapeutic index, long-term therapy, high inter- and/or intra-individual variability, an exposure–response relationship as well as available validated bioanalytical methods and dose adjustment strategies [54, 65]. **PK**, pharmacokinetics; **TDM**, therapeutic drug monitoring.

### 1.3.3 Model-informed precision dosing (MIPD)

A rather novel and innovative approach individualizing patient's drug therapy is the application of pharmacometric models in **MIPD** [24]. The term pharmacometrics can be defined as "the science of developing and applying mathematical and statistical methods to characterize, understand, and predict a drug's pharmacokinetic, pharmacodynamic, and biomarker–outcomes behavior" [66]. This bridging discipline describes and quantifies interactions between xenobiotics and patients and can be leveraged in various ways [67]. For example, pharmacometric models can be used for personalized medicine, integrating various sources of information on the drug, disease and patient (population) to predict personalized dosing regimens for an individual patient or a specific patient group (**MIPD**) [58]. With that, **MIPD** can be seen as an advanced discipline of **TDM**, which provides individualized dosing strategies based on pharmacometric models, patient characteristics, intra- and inter-patient variability as well as, if available, **TDM** data for



better patient care [68]. An overview of an **MIPD** workflow is depicted in Figure 1.4.

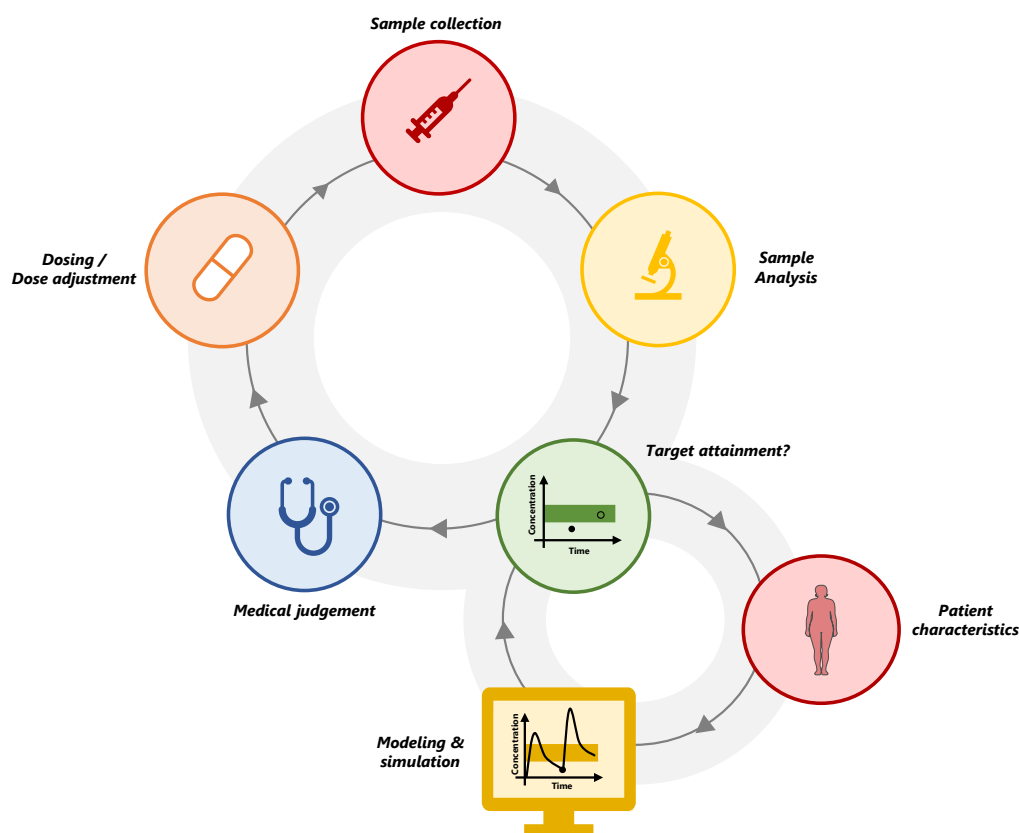


Figure 1.4: An exemplary representation of an **MIPD** framework. In contrast to **TDM**, the initial dose can be optimized based on drug- and patient-specific data using a pharmacometric model [55]. After drug administration, blood samples can be collected, followed by sample analysis to determine the respective drug concentration(s) [55]. A modeling and simulation approach can be utilized to find the optimal dosing regimen for the individual patient, integrating patient-specific and, if available, **TDM** data [55]. Based on model simulations, recommendations for dosing regimens can be provided to achieve the target threshold, supporting clinicians in the selection of the right dose for the right patient at the right time.

Different types of pharmacometric models, including primarily data-driven and descriptive models (i.e., non-mechanistic/empirical) as well as complex, mechanistic models, can be leveraged for **MIPD** [69]. Here, important pharmacometric modeling approaches include physiologically based pharmacokinetic (**PBPK**) and population pharmacokinetic (**popPK**) modeling [69].



#### 1.4 PHARMACOMETRIC APPROACHES: PHYSIOLOGICALLY BASED PHARMACOKINETIC (PBPK) AND POPULATION PHARMACOKINETIC (POPPK) MODELING

Both empirical (e.g., popPK) and mechanistic (e.g., PBPK) modeling approaches have attained considerable significance in driving model-informed drug development (MIDD) [70]. In MIDD, pharmacometric models are developed based on preclinical and/or clinical data and applied to inform pre-/clinical drug development and decision-making [70]. Consequently, MIDD and MIPD share the same idea to support and improve drug therapy through modeling and simulation techniques [71]. Differences lie in their respective application as MIDD primarily informs drug research and development, while MIPD aims to advance drug therapy through precision dosing [71]. In contrast to regulatory applications, the application of modeling and simulation for MIPD is still rare, yet has shown a notable growth in interest [55].

##### 1.4.1 PBPK modeling

In recent years, PBPK modeling has become a promising framework for assessing drug exposure in virtual individuals and populations and for gaining mechanistic insights into a drug's PK by integrating drug- and system-specific information into a dynamically interconnected model [72]. With that, PBPK models allow a mechanistic investigation of drug disposition in a biological system, enabling *a priori* simulations of drug and metabolite concentration–time profiles [73]. Thus, the PBPK modeling approach can be employed to predict unknown scenarios leveraging prior knowledge and information [73].

Whole-body PBPK models comprise of multiple compartments representing different organs and tissues, which are connected via the arterial and venous blood compartments and parameterized by the respective tissue and organ volumes, knowledge about their composition, blood flow rates, etc. [73]. Consequently, whole-body PBPK models can mimic the human body to simulate drug exposure in blood plasma and other organs and tissues of interest [74]. The above-mentioned compartments are subdivided into four sub-compartments including blood plasma, erythrocytes, intracellular and interstitial space [74]. The drug absorption and distribution between (sub-)compartments may occur passively or actively via transporters [74]. Drug metabolism and excretion from various organs can be implemented via enzymatic degradation or passive elimination through glomerular filtration, among other mechanisms [74]. To mechanistically model drug absorption in the gastrointestinal tract (GIT), the GIT is divided into multiple segments, consisting of a lumen, mucosa and non-mucosa and parametrized by sub-tissue volume, transit time and pH [75–77]. An overview of the whole-body PBPK model structure implemented in the modeling and simulation software PK-Sim® is shown in Figure 1.5.

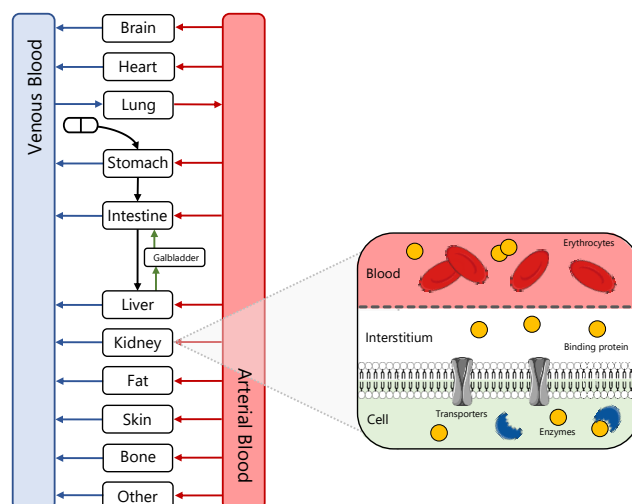


Figure 1.5: Structural overview of the multi-compartmental model implemented in PK-Sim®. Each organ or tissue is represented by a compartment, connected via the arterial and venous blood flow and subdivided into four sub-compartments including blood plasma, erythrocytes, intracellular and interstitial space [74]. Drawings were adapted from Servier Medical Art [2], licensed under a Creative Commons Attribution 4.0 (CC BY 4.0) Unported License (<https://creativecommons.org/licenses/by/4.0/>).

#### 1.4.2 PopPK modeling

The **popPK** modeling approach aims to quantify sources of **PK** variability and investigates sources of variability in drug concentrations over time across individuals [24]. In addition to drug concentration–time data from various individuals, relevant covariate information such as age, sex, race, organ dysfunction and co-medication is required to identify covariates that affect a drug’s **PK** [78].

Using the individual concentration–time and covariate data, a compartmental model can be developed that describes and partially explains the variability by categorical (e.g., sex) and continuous (e.g., body weight) covariates [78]. A **popPK** model consists of (i) a structural model, (ii) a statistical model and (iii) a covariate model [78]. The typical concentration–time profile of the studied population is described by the structural model [78]. One-, two- and three-compartment models are most commonly assessed [78]. Exemplary graphical illustrations of a one-, two- and three-compartment model after intravenous application are shown in Figure 1.6.

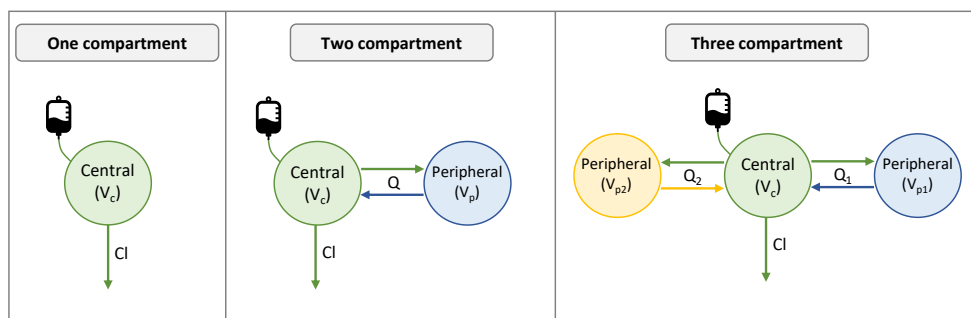


Figure 1.6: Structural illustration of a one-, two- and three-compartment model after intravenous application of a drug of interest. **Cl**, clearance; **Q**, intercompartmental clearance;  **$V_c$** , central volume of distribution;  **$V_p$** , peripheral volume of distribution.

Furthermore, the statistical model accounts for the random variability in the measured drug concentrations including inter-individual, inter-occasional and the random unexplained variability [78]: Variability between subjects is covered by the inter-individual, while variability between different occasions within a single individual is quantified by the inter-occasional variability [78]. Lastly, the random unexplained variability describes the remaining, unexplained variability in the drug concentrations [78]. Variability that can be explained by differences in subject characteristics (body weight, albumin levels, anti-drug antibody status, etc.) is captured by the covariate model [78]. With that, a **popPK** model describes the concentration–time profile for a typical individual with inter-individual variability partially explained by covariates and random unexplained variability [78].

#### 1.4.3 PopPK and PBPK modeling in MIDD

Early application of **MIDD** to inform regulatory decisions at the **FDA** date back to the 1990s, marking the advent of **popPK** and **PK/PD** modeling in regulatory submissions [70]. At this time, the main focus of these models was on drug and product characterization [70]. However, over the last 30 years, there has been a rapid growth in applying **MIDD** to inform drug development and in regulatory review [70]. The scope of **MIDD** applications primarily through empirical modeling approaches has been broadened to include supporting dose selection and trial design, assessing safety and contributing to the evaluation of efficacy [70]. Today, **MIDD** is widely applied in drug development and has not only become recognized but also encouraged by various regulatory agencies including **FDA** and European Medicines Agency (**EMA**) [79]. This entails the increasing application of **PBPK** modeling and simulation by pharmaceutical companies in the field of **MIDD** over the last years [79].

**PBPK** models can be used for a wide range of applications: These encompass but are not limited to the assessment of disposition characteristics of new drug candidates and the investigation and quantification of **PK** liabilities (i.e., poor bioavailability, **DDIs**, **DGIs** and **DDGIs**) as well as the application for dose adjustments in special populations (e.g., pediatrics, the elderly, patients with organ

impairment) [80, 81]. Over the period of 2019 to 2023, a total of 243 novel drugs were approved by the FDA, and approximately one third of novel drug applications involved the use of PBPK modeling and simulation [79]. While the annual number of FDA-approved drug applications which included a PBPK modeling package was seven on average during the period of 2013 to 2018, the number had doubled during the period of 2019 and 2023, with an average of ~15 approved novel drugs per year including PBPK model submissions [79]. Based on FDA data between 2019 and 2023, PBPK models involved in approved drug submissions were predominantly used in the area of DDI predictions (56.7% enzyme-mediated DDIs, 17.5% transporter-mediated DDIs and 4.2% gastric-mediated DDIs), DGI predictions (4.2%), organ impairment (4.2% hepatic impairment, 2.5% renal impairment), pediatrics (4.2%) as well as to investigate disease effects (2.5%) and food effects (1.7%) [79]. PBPK DDI study predictions with weak and moderate index inhibitors and inducers as alternatives to prospective clinical studies are supported by the FDA in case an adequate model performance has already been demonstrated using clinical data from prospective DDI studies with strong index perpetrator drugs [82].

#### 1.4.4 PopPK and PBPK modeling in MIPD

In addition to regulatory applications, pharmacometric models hold great potential for individualizing drug therapy, however, their implementation into clinical practice, especially of PBPK models, is still rare [55, 83]. While the application of empirical models in MIPD is usually restricted to the scope for which the model has been established, the power of PBPK models lies in the extrapolation to untested scenarios (e.g., different enzyme/transporter genotypes or diseases) [83]. A specific (sub-)population or individual, also referred to as “virtual twin” of the patient, can be created by integrating relevant information on demographics, results of liver and kidney function tests, co-medication or drug metabolizing enzyme genotypes and/or phenotypes into a PBPK model [84, 85]. Subsequently, model simulations of the drug’s PK can be used to provide dose adjustments, test different administration routes or predict drug exposure in a variety of clinical settings, e.g., untested (complex) DDI scenarios [72]. There are a noticeable number of FDA-approved drug labels containing PGx information that recommend PGx testing (e.g., irinotecan, carbamazepine, warfarin) to support clinical decision making [72, 81]. However, various drugs remain for which such guidelines are missing, for example due to the lack of clinical studies. Here, PBPK modeling demonstrates considerable promise as an approach to describe and quantify exposure differences in patients with different enzyme or transporter genotypes and could be leveraged to provide dosing guidance for precision medicine [72]. In addition, an increasing interest in the application of popPK modeling in the field of MIPD has been recently observed [33–35]. MIPD through the application of popPK(/PD) models can be implemented using two different approaches: *a priori* or *a posteriori* dose optimization [86, 87]. Here, a popPK(/PD) model serves as a Bayesian prior [86, 87]. In *a priori* dose optimization, dose recommendations are solely based on patient covariates that have been identified to affect the drug’s PK and/or PD [86, 87]. In contrast, *a posteriori* dose optimization, also

known as maximum *a posteriori* probability (MAP) Bayesian estimation approach, additionally leverages information on the individual patient from TDM drug concentration measurements [86, 87]. With that, based on patient characteristics and TDM drug concentration measurements, the individual PK parameters can be estimated (empirical Bayes PK parameter estimates (EBE)) and utilized to simulate and identify dosing regimens through which a predefined exposure target can be attained [86]. Hence, pharmacometric models not only present to be powerful tools in the field of MIDD but can also be leveraged to facilitate personalized medicine approaches by tailoring individual patient dosing and thereby improving individual treatment efficacy and preventing toxicities.



## OBJECTIVES

---

The overall aim of this thesis was to establish mechanistic and empirical pharmacometric models for selected drugs suited for the application of **MIPD**, helping to provide personalized dosing strategies for patients and encouraging precision dosing in drug therapy. Here, the **CYP3A4** substrates dasatinib and imatinib, the **CYP3A4** and **CYP2D6** substrate (*E*)-clomiphene as well as the monoclonal antibody infliximab, that often show supra- and/or subtherapeutic drug concentrations – for example as a result of **DDI**, **DGI**, **DDGI** or specific patient characteristics – were chosen as example candidates to demonstrate the benefits of shifting from a "one-size-fits-all dosing" to more personalized dosing approaches.

The work was supported by the German Federal Ministry of Education and Research (BMBF) funded project "GUIDE-IBD" in collaboration with Prof. Matthias Schwab and the Dr. Margarete Fischer-Bosch Institute of Clinical Pharmacology.

The aim of this thesis was realized within the scope of the following four projects:

### PROJECT I – PHYSIOLOGICALLY BASED PHARMACOKINETIC MODELING OF DASATINIB

The objectives of **project I** were (i) to develop a whole-body **PBPK** model for the **TKI** dasatinib, listed as sensitive **CYP3A4** substrate for the use in clinical **DDI** studies by the **FDA**, (ii) to describe and predict clinically tested enzyme-mediated **DDIs** involving dasatinib as victim drug and as **CYP2C8**, organic anion transporting polypeptide (**OATP**)<sub>1B1</sub> and **OATP**<sub>1B3</sub> perpetrator drug, (iii) to predict the effect of acid-reducing agents (**ARAs**) on the exposure of dasatinib, (iv) to apply the model for simulations of several untested **DDI** scenarios including single and multiple **DDIs** and (v) to provide model-based dose adaptations for those **DDI** scenarios, supporting precision dosing of dasatinib with **PBPK** modeling.

### PROJECT II – PHYSIOLOGICALLY BASED PHARMACOKINETIC MODELING OF IMATINIB

The objectives of **project II** were (i) to develop a whole-body parent-metabolite **PBPK** model for imatinib and its main metabolite *N*-desmethyl imatinib, listed as a moderate **CYP3A4** inhibitor for the use in clinical **DDI** studies by the **FDA**, (ii) to describe and predict clinically tested enzyme-mediated **DDIs** involving imatinib as victim drug and as **CYP2C8**, **CYP2D6** and **CYP3A4** perpetrator drug, and thereby (iii) to facilitate future investigations of various **DDI** scenarios and for **MIPD** of imatinib.

### PROJECT III – PHYSIOLOGICALLY BASED PHARMACOKINETIC MODELING OF (*E*)-CLOMIPHENE AND ITS MAIN METABOLITES

The objectives of **project III** were (i) to develop a whole-body parent-metabolite **PBPK** model for (*E*)-clomiphene and its three main metabolites

(*E*)-4-hydroxyclophene ((*E*)-4-OH-Clom), (*E*)-N-desethylclomiphene ((*E*)-DE-Clom) and (*E*)-4-hydroxy-N-desethylclomiphene ((*E*)-4-OH-DE-Clom), (ii) integrating an in vitro–in vivo extrapolation approach to predict DGIs, (iii) to investigate different DDI and DDGI scenarios with strong CYP3A4 and CYP2D6 inhibitors, (iv) to gain insights into the contribution of different metabolic pathways to (*E*)-clomiphene elimination and (v) to provide a basis for future investigations of DDI and DDGI scenarios involving additional moderate and weak CYP inhibitors and CYP3A4 inducers as well as for MIPD of (*E*)-clomiphene.

#### PROJECT IV – EXTERNAL PERFORMANCE EVALUATION OF INFlixIMAB POPULATION PHARMACOKINETIC MODELS

The objectives of project IV were (i) to obtain an overview of published infliximab popPK models in patients with inflammatory bowel disease (IBD), (ii) to perform a predictive external model performance evaluation of available models with a focus on differences between anti-drug antibody (ADA)-negative and ADA-positive subpopulations in a Bayesian forecasting setting and (iii) to provide guidance for a selection of a suitable popPK model for an MIPD framework to adapt individual infliximab dosing regimens, which could be applied in the observational clinical trial “GUIDE-IBD” to support clinicians in the selection of patient-specific, individual dosing regimens.



## METHODS

---

### 3.1 INVESTIGATED COMPOUNDS

Pharmacometric models were established for the following four drug candidates, covering different therapeutic areas.

#### 3.1.1 *Imatinib and dasatinib*

Imatinib (Gleevec®), the first generation TKI, has been approved by the FDA for the treatment of Philadelphia chromosome positive (Ph+) CML in pediatric and adult patients as well as Ph+ acute lymphoblastic leukemia (ALL), gastrointestinal stromal tumors (GIST) and multiple other oncologic diseases in adult patients [88, 89]. CML is commonly characterized by a reciprocal translocation between the Abelson (ABL) 1 gene on chromosome nine and the breakpoint cluster region (BCR) on chromosome 22 [90, 91]. The resulting so-called Philadelphia chromosome (Ph) encodes for the BCR-ABL1 oncoprotein with permanent tyrosine kinase activity, causing uncontrolled proliferation, differentiation arrest and resistance to cell death of myeloid cells [91]. Imatinib represents a selective inhibitor of the BCR-ABL1 oncoprotein, becoming the first-line standard therapy of newly diagnosed patients with CML [92]. As stated in the package insert, the recommended dosing regimen of imatinib is 400 mg once daily (q.d.) for adult patients in the chronic phase of CML, while a higher dose of 600 mg q.d. is proposed in the accelerated phase and blast crisis [89]. Since imatinib is a substrate of CYP2C8, CYP3A4 and different transporters, it is highly susceptible to DDIs [93–98]. Yet, specific dosing recommendations for DDI scenarios, are not provided in the current package insert [89].

Imatinib resistance caused mostly by point mutations in the BCR-ABL1 kinase domain as well as therapy relapses pose a rising issue in clinical practice and have led to the development of novel second and third generation TKIs [99–101]. Dasatinib (Sprycel®), a second generation and multi-targeted TKI, is approved for the treatment of Ph+ CML in the chronic, accelerated, or myeloid or lymphoid blast phase with resistance or intolerance to prior therapy (e.g., imatinib) [102]. Additionally, dasatinib is indicated for the treatment of Ph+ ALL [102]. In contrast to imatinib, dasatinib binds to both the active and the inactive conformation of BCR-ABL1, shows approximately 325-fold higher potency against wild-type BCR-ABL1 and retains activity against various imatinib-resistant BCR-ABL1 kinase domain mutations in vitro [103, 104]. For adult patients, 100 mg dasatinib is administered orally q.d. in the chronic phase of CML, while 140 mg q.d. is recommended for the accelerated, myeloid or lymphoid blast phase CML and for the Ph+ ALL [105]. However, as a sensitive CYP3A4 substrate and weak base with strong pH-sensitive solubility, dasatinib is also prone to enzyme-mediated DDIs involving CYP3A4 perpetrators and to pH-dependent DDIs with ARAs [106–109].

In contrast to imatinib, the package insert recommends to consider dasatinib dose adaptations in case of co-administration with strong CYP3A4 inhibitors, whereas dosing recommendations for concomitant administration of moderate CYP3A4 inhibitors are not provided [89, 102].

### 3.1.2 (E)-clomiphene

Clomiphene (Clomid®), a SERM, has been approved in 1967 by the FDA for the treatment of infertility in women with ovulation disorders that can be caused by polycystic ovary syndrome (PCOS) [110, 111]. Clomiphene is given orally as a racemic mixture of (E)- and (Z)-clomiphene following a recommended dosing regimen of 50 mg q.d. over five days [110]. If ovulation has not been induced after the first cycle, an increased dose of 100 mg q.d. for five days should be administered [110]. The therapeutic effect can be mainly attributed to the two active metabolites (E)-4-OH-Clom and (E)-4-OH-DE-Clom of (E)-clomiphene [112]. Both inhibit estrogen receptors at the hypothalamic arcuate nucleus, triggering the release of gonadotropin-releasing hormones and, subsequently, elevating follicle-stimulating and luteinizing hormone levels, which in turn induces ovulation [112, 113]. However, studies have shown that a large proportion of women do not respond to clomiphene therapy due to different factors such as hyperandrogenemia, obesity or CYP2D6 genotype [112–115]. (E)-clomiphene is primarily metabolized via CYP3A4 and the highly polymorphic CYP2D6 enzyme [112, 113, 115]. These two enzymes are also mainly responsible for the formation and elimination of the three main metabolites, making (E)-clomiphene prone to DDIs, DGIs and DDGIs [112, 113, 115]. In a clinical study, all CYP2D6 IM showed clinical response to clomiphene therapy, while 30% of NM failed to respond [116]. Recommendations to avoid concomitant intake of clomiphene with CYP2D6 and CYP3A4 inhibitors or CYP3A4 inducers are not provided in the current package insert [117]. Similarly, dose adaptations for different CYP2D6 phenotypes are not listed in the current package insert or the CPIC guidelines.

### 3.1.3 Infliximab

Infliximab (Remicade®), a tumor necrosis factor alpha (TNF- $\alpha$ ) antagonist, has been approved in 1999 by the EMA and is indicated and widely used for the treatment of immune-mediated diseases such as IBD (i.e., Crohn's disease (CD) and ulcerative colitis (UC)) in adult and pediatric patients as well as rheumatoid arthritis, ankylosing spondylitis, psoriatic arthritis and psoriasis in adult patients [118]. Infliximab is a recombinant chimeric human-murine monoclonal antibody and inhibits both soluble and membrane-bound TNF- $\alpha$  – a pro-inflammatory cytokine which plays a major role in the pathophysiology of the above-mentioned inflammatory indications [119, 120].

For the treatment of IBD, Remicade® can be administered intravenously with weight-based dosing of 5 mg/kg at weeks 0, 2 and 6 (induction phase) followed by maintenance therapy at 8-weekly intervals if patients have shown response [121, 122]. However, about one third of patients treated with infliximab do not show clinical response to induction therapy (called “primary non-response”) and

up to 50% of patients experience “secondary non-response” during maintenance therapy [4, 5, 122]. A correlation between negative clinical outcome and subtherapeutic infliximab  $C_{min}$  has been demonstrated in various studies [123–126]. As a result, and due its high inter- and intra-individual variability in drug exposure [122, 127–147], infliximab therapy is an ideal candidate for the application of MIPD to improve treatment efficiency. Several retrospective evaluations investigating the correlation between  $C_{min}$  and clinical outcome have established different target  $C_{min}$  [63, 122, 124, 148–153]. However, while the drug label suggests that a dose of 10 mg/kg every 8 weeks could be considered in case of secondary non-response, neither a particular target threshold nor specific dose adaptations have been included in the drug label yet [121].

## 3.2 PBPK MODELING

PBPK models in **project I** (for dasatinib), **project II** (for imatinib and its main metabolite) and in **project III** (for (*E*)-clomiphene and its three main metabolites) were developed and applied following the high-level workflow depicted in **Figure 3.1**.

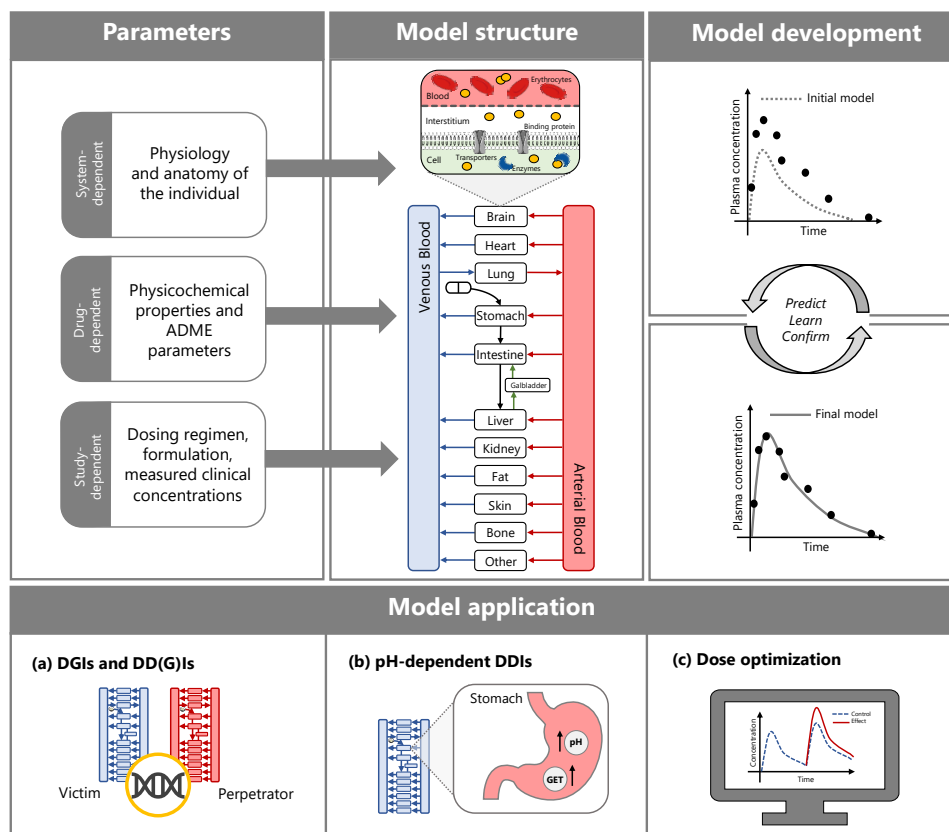


Figure 3.1: **PBPK** modeling workflow. **PBPK** models are commonly informed with system-, drug- and study-dependent parameters impacting model components. An exemplary **PBPK** model structure is depicted here. Each organ/tissue is represented by a compartment and subdivided into four sub-compartments [74]. **PBPK** models have been built and evaluated leveraging a stepwise predict-learn-confirm cycle. Subsequently, the models have been applied either for the prediction of different drug interactions and/or for dose optimization purposes. Drawings were adapted from Servier Medical Art [2], licensed under a Creative Commons Attribution 4.0 (CC BY 4.0) Unported License (<https://creativecommons.org/licenses/by/4.0/>). ADME, absorption, distribution, metabolism and excretion; DDGs, drug–drug–(gene) interactions; DDIs, drug–drug interactions; DGIs, drug–gene interactions; GET, gastric emptying time.

### 3.2.1 PBPK model building

#### 3.2.1.1 Data acquisition

PBPK modeling was initiated with a literature search for system-dependent (anatomical and physiological information) and drug-dependent parameters (physiochemical and ADME information) of the respective compound of interest. In addition, data from clinical PK studies including plasma concentration–time profiles and, if applicable, renal excretion profiles, information on dosing regimens and drug formulations as well as study population characteristics were collected.

#### 3.2.1.2 Creation of virtual typical individuals

“Virtual typical individuals” representing the mean individual of each clinical study were created in the applied software PK-Sim® based on reported mean or mode of age, sex, body weight, height, body mass index and ethnicity in the respective study. In case of missing study population characteristics for healthy volunteers, a 30-year-old male individual of respective ethnicity with values for body weight and height based on the corresponding database (e.g., the International Commission on Radiological Protection (ICRP) database for Europeans [154] or the third National Health and Nutrition Examination Survey (NHANES) database for Americans [155]) was used. For dasatinib and imatinib PBPK model development, plasma profiles of healthy subjects and cancer patients were included. In case of patients with missing demographics, the average age and mode of sex for the respective disease was selected and, subsequently, a standard individual with values for body weight and height according to the databases used.

#### 3.2.1.3 Enzymes and metabolic processes

Protein expressions across different organs were implemented according to the PK-Sim® expression database [156]. A detailed overview of expression and localization of relevant enzymes and transporters implemented in the PBPK models for dasatinib, (E)-clomiphene and imatinib is shown in the supplementary documents of the respective publication. Metabolism and transport via CYP enzymes and transporters, respectively, were implemented using Michaelis-Menten kinetics (Equation 3.1), while metabolism via other enzymes was described with an unspecific hepatic first-order clearance process (Equation 3.2) [74].

$$v = \frac{v_{\max} \cdot [S]}{K_m + [S]} = \frac{k_{\text{cat}} \cdot [E] \cdot [S]}{K_m + [S]} \quad (3.1)$$

with  $v$  = reaction velocity,  $v_{\max}$  = maximum reaction velocity,  $[S]$  = free substrate concentration,  $K_m$  = substrate concentration at half maximum velocity (Michaelis-Menten constant),  $k_{\text{cat}}$  = catalytic rate constant and  $[E]$  = amount of enzyme or transporter.

$$v = CL_{spec} \cdot [E] \cdot [S] \quad (3.2)$$

with  $v$  = reaction velocity,  $CL_{spec}$  = specific enzymatic clearance,  $[E]$  = enzyme concentration and  $[S]$  = free substrate concentration.

#### 3.2.1.4 Assignment of clinical data to test and training datasets

The available clinical PK profiles were divided into a training and a test dataset for model building and evaluation, respectively. PK profiles were allocated to the training and test datasets in a deliberate, non-randomized manner. This approach ensured that the training dataset included a broad range of doses, various dosing regimens (such as single and multiple dosing) and profiles with intensive PK sampling, as outlined in the respective publication. This strategy aimed for enriching the training dataset with diverse and informative data for robust model building, while also maximizing the number of PK profiles available in the test dataset for thorough model evaluation.

#### 3.2.1.5 Model parametrization

To estimate model parameters that could not be reliably informed via literature and/or were pivotal for critical quantitative structure-activity relationship estimations, a middle-out approach was leveraged, combining prior information on system- and drug-dependent information (bottom-up) with observed clinical data (top-down). Here, model predictions were fitted to the corresponding observed plasma concentrations of the training dataset using either the Levenberg-Marquardt or the Monte-Carlo optimization algorithm implemented in PK-Sim®. Here, the statistical optimization routines such as the Levenberg-Marquardt or the Monte-Carlo algorithm vary selected input parameters within a defined range, aiming to minimize the residuals between predicted and clinically observed concentrations [74].

#### 3.2.2 PBPK model evaluation

PBPK model performance was evaluated applying different graphical and statistical methods.

##### 3.2.2.1 Graphical evaluation

Graphical evaluation was conducted by comparing predicted plasma concentration–time and, if available, renal excretion profiles to the corresponding observed clinical data. This was complemented using goodness-of-fit plots assessing predicted versus observed AUC from the time of the first concentration measurement to the time of the last concentration measurement ( $AUC_{last}$ ),  $C_{max}$  values as well as plasma concentrations, respectively.

### 3.2.2.2 Quantitative measures for model evaluation

In addition, quantitative measures for model evaluation were calculated. These included the mean relative deviation (MRD) of predicted plasma concentrations (Equation 3.3) and the geometric mean fold error (GMFE) of predicted  $C_{\max}$  and  $AUC_{\text{last}}$  values, respectively (Equation 3.4).

$$MRD = 10 \sqrt{\frac{1}{m} \sum_{i=1}^m (\log_{10} \hat{c}_i - \log_{10} c_i)^2} \quad (3.3)$$

with  $\hat{c}_i = i$ -th predicted plasma concentration,  $c_i =$  corresponding observed plasma concentration and  $m =$  total number of observed values.

$$GMFE = 10^{\frac{1}{n} \sum_{i=1}^n \left| \log_{10} \left( \frac{\hat{c}_i}{c_i} \right) \right|} \quad (3.4)$$

with  $\hat{c}_i = i$ -th predicted  $AUC_{\text{last}}$  and  $C_{\max}$  value, respectively,  $c_i =$  corresponding observed value and  $n =$  total number of observed plasma profiles.

### 3.2.2.3 Creation of virtual populations

For the assessment of the models' capability to describe and predict the variability and central tendency in the observed clinical data, simulations with virtual populations matching the respective clinical study population demographics were performed (i.e., population simulations). The virtual populations were created using the implemented algorithm in PK-Sim<sup>®</sup> according to the respective demographic characteristics based on the NHANES database for white Americans [155], the ICRP database for Europeans [154] and according to [157] for Japanese populations. The algorithms for generating the virtual populations have been reported by Willmann et al. [158]. System-dependent parameters including enzyme and transporter reference concentrations that have been used in the projects are shown in the corresponding supplementary materials.

### 3.2.2.4 Sensitivity analysis

Sensitivity analyses allow the assessment of the impact of single parameter changes on model outputs [159]. In project I-III, the predicted  $AUC$  extrapolated to infinity ( $AUC_{\text{inf}}$ ) was used as model output of interest in the sensitivity analyses. Parameters were included in the sensitivity analyses if they (i) had been optimized during parameter optimization or (ii) if they were assumed to considerably affect drug exposure (e.g., as a result of their use in the calculation of drug permeabilities or partition coefficients). Sensitivity analyses were performed under steady-state conditions after oral administration of the recommended dose as stated in the respective package insert. The relative impact of each selected parameter on  $AUC_{\text{inf}}$  was calculated according to Equation 3.5 [74].

$$S = \frac{\Delta AUC_{\text{inf}}}{\Delta p} \cdot \frac{p}{AUC_{\text{inf}}} \quad (3.5)$$



with  $S$  = sensitivity of the  $AUC_{inf}$  to the investigated model parameter,  $\Delta AUC_{inf}$  = change of the  $AUC_{inf}$ ,  $\Delta p$  = variation of the model parameter value,  $p$  = original model parameter value and  $AUC_{inf}$  = simulated  $AUC_{inf}$  with the original model parameter value.

### 3.2.3 Drug–gene interaction (DGI) modeling

In **project III**, the impact of **CYP2D6** genetic polymorphisms on the **PK** of (E)-clomiphene and its metabolites was investigated. Here, **DGIs** were modeled by applying distinct catalytic rate constant ( $k_{cat}$ ) values for the different **CYP2D6 AS** groups. This was realized by extrapolating the metabolic process-specific  $k_{cat}$  values from the **AS=2 NM** population to other **AS** groups (**AS=0.5**, **AS=0.75**, **AS=1** and **AS=3**), leveraging data on in vitro **CYP2D6 AS**-dependent formation rates according to **Equation 3.6** [160]. **CYP2D6**  $k_{cat}$  values for the **PM** population were assumed to be zero.

$$k_{cat, AS=i} = k_{cat, AS=2} \cdot IVSF_i \quad (3.6)$$

with  $k_{cat, AS=i}$  = catalytic rate constant for the  $i$ th **CYP2D6 AS**,  $k_{cat, AS=2}$  = catalytic rate constant for the **AS=2 NM** population,  $IVSF_i$  = in vitro scaling factor for the  $i$ th **AS** group calculated based on the in vitro metabolite formation rate relative to the corresponding formation rate in **NM**.

### 3.2.4 Drug–drug–(gene) interaction (DD(G)I) modeling

The investigated **DDI** and **DDGI** scenarios can be categorized into the following two groups: (i) enzyme- and transporter-mediated **DDIs** and **DDGIs** as well as (ii) pH-dependent **DDIs**.

#### 3.2.4.1 Enzyme-and transporter-mediated DD(G)Is

Enzyme- and transporter-mediated **DDIs** and **DDGIs** were modeled coupling the developed **PBPK** models of dasatinib, imatinib and (E)-clomiphene with previously established **PBPK** models of enzyme and/or transporter substrates and/or perpetrator drugs. For dasatinib in **project I**, the model was linked with various **CYP3A4** inhibitors (clarithromycin, erythromycin, fluconazole, fluvoxamine, grapefruit juice, itraconazole, ketoconazole and voriconazole) and the **CYP3A4** inducer carbamazepine as well as efavirenz and rifampicin (inducer and inhibitor of **CYP3A4**) investigating dasatinib's **PK** as a **DDI** victim drug. In **project II**, **DDIs** between imatinib/N-desmethyl imatinib and the perpetrator drugs ketoconazole, rifampicin and gemfibrozil were investigated. In addition, the **DDI** perpetrator potential of dasatinib (**CYP3A4**, **CYP2C8** and **OATP1B1/OATP1B3** inhibition) and imatinib (**CYP3A4** and **CYP2D6** inhibition) was assessed, studying the following **DDI** scenarios in **project I** and **project II**, respectively: simvastatin-dasatinib-**DDI**, simvastatin-imatinib-**DDI** and metoprolol-imatinib-**DDI**. The parent–metabolite **PBPK** model of (E)-clomiphene was coupled with the strong **CYP3A4** inhibitor clarithromycin and the strong **CYP2D6** inhibitor paroxetine for **DDI** assessments.



Simultaneously, the effect of **CYP2D6** genetic variations on the clarithromycin and paroxetine **DDIs** (i.e., **DDGI** scenarios) was assessed. The investigated **DDI** and **DDGI** scenarios included both competitive and mechanism-based inhibition as well as induction processes. These were implemented according to **Equation 8a**, **Equation 8b**, **Equation 9a**, **Equation 9b**, **Equation 10a** and **Equation 10b**, respectively [74]. The interaction parameters were sourced from the literature and the published **PBPK** perpetrator models.

#### *Competitive inhibition*

$$K_{m, app} = K_m \cdot \left( 1 + \frac{[I]}{K_i} \right) \quad (8a)$$

$$v = \frac{v_{max} \cdot [S]}{K_{m, app} + [S]} = \frac{k_{cat} \cdot [E] \cdot [S]}{K_{m, app} + [S]} \quad (8b)$$

with  $K_{m, app}$  = Michaelis-Menten constant in the presence of inhibitor,  $K_m$  = Michaelis-Menten constant in the absence of inhibitor,  $[I]$  = free inhibitor concentration,  $K_i$  = dissociation constant of the inhibitor-protein complex,  $v$  = reaction velocity,  $v_{max}$  = maximum reaction velocity,  $[S]$  = free substrate concentration,  $k_{cat}$  = catalytic rate constant and  $[E]$  = amount of enzyme or transporter.

#### *Mechanism-based inhibition*

$$k_{deg, app} = k_{deg} + \frac{k_{inact} \cdot [I]}{K_I + [I]} \quad (9a)$$

$$\frac{d[E]}{dt} = R_{syn} - k_{deg, app} \cdot [E] \quad (9b)$$

with  $k_{deg, app}$  = enzyme degradation rate constant in the presence of mechanism-based inactivator,  $k_{deg}$  = enzyme degradation rate constant,  $k_{inact}$  = maximum inactivation rate constant,  $[I]$  = free mechanism-based inactivator concentration,  $K_I$  = inactivator concentration for half-maximal inactivation,  $\frac{d[E]}{dt}$  = enzyme turnover,  $R_{syn}$  = enzyme synthesis rate and  $[E]$  = enzyme concentration.

#### *Induction*

$$R_{syn, app} = R_{syn} \cdot \left( 1 + \frac{E_{max} \cdot [Ind]}{EC_{50} + [Ind]} \right) \quad (10a)$$

$$\frac{d[E]}{dt} = R_{syn, app} - k_{deg} \cdot [E] \quad (10b)$$

with  $R_{syn, app}$  = enzyme synthesis rate in the presence of inducer,  $R_{syn}$  = enzyme synthesis rate,  $E_{max}$  = maximum induction effect,  $[Ind]$  = free inducer concentration,  $EC_{50}$  = inducer concentration for half-maximal induction,  $\frac{d[E]}{dt}$  = enzyme turnover,  $k_{deg}$  = enzyme degradation rate constant and  $[E]$  = enzyme concentration.

### 3.2.4.2 pH-dependent DDIs

pH-dependent DDIs were investigated in **project I**: Gastric solubility of the weak base dasatinib may be reduced through pH elevation following intake of ARAs. The pH-dependent DDIs were modeled by increasing the gastric pH according to published values and adjusting the gastric emptying time if applicable.

### 3.2.5 Model performance evaluation of DGI and DD(G)I scenarios

DGI, DDI and DDGI model performance was evaluated comparing predicted plasma concentration–time profiles and, if available, renal excretion profiles to the corresponding observed clinical data. In addition,  $AUC_{last}$  and  $C_{max}$  effect ratios were calculated according to Equation 3.7 and goodness-of-fit plots created, showing predicted versus observed  $AUC_{last}$  and  $C_{max}$  effect ratios, respectively. For graphical assessment of DGIs, DDIs and DDGIs goodness-of-fit plots, the limits by Guest et al. with 1.25-fold variability were used [161].

$$PK \text{ effect ratio} = \frac{PK_{effect}}{PK_{control}} \quad (3.7)$$

with  $PK_{effect} = AUC_{last}$  or  $C_{max}$  value in the DGI, DDI or DDGI setting and  $PK_{control} = AUC_{last}$  or  $C_{max}$  value of the corresponding control setting.

### 3.2.6 Software

PBPK modeling and simulation was performed within PK-Sim® and MoBi® (part of the Open Systems Pharmacology (OSP) Suite, <http://www.open-systems-pharmacology.org>). GetData Graph Digitizer version 2.26.0.20 (S. Fedorov) was used to digitize published data according to guidelines introduced by Wojtyniak and coworkers [162]. Calculation of PK parameters, evaluation of model performance and generation of model output graphics was accomplished with the R programming language (R Foundation for Statistical Computing, Vienna, Austria) [163].

## 3.3 EXTERNAL PERFORMANCE EVALUATION OF INFLIXIMAB POPPK MODELS

For certain drugs, multiple non-linear mixed effects popPK models derived from different datasets are developed and published by various research groups, as is the case for the monoclonal antibody infliximab (**project IV**) [122, 127–147]. However, before applying one of these models in clinical practice for individualization of drug dosing (i.e., for MIPD), thorough model evaluation is crucial, assessing model accuracy, robustness and predictive performance [164, 165]. While an internal model evaluation assesses a model's ability to describe/predict the data that was used to develop the model, an external model evaluation assesses the model performance with an independent, new dataset, which was not used for model development [165, 166]. Hence, for an external model performance evaluation, the following three major components are required: a pharmacometric model, a modeling software and an external dataset.

### 3.3.1 Literature search

The external model performance evaluation in **project IV** was initiated with a literature search on published infliximab **popPK** models, gathering information about the respective structural models, the statistical models, the covariate models as well as study- and population-related information. Subsequently, **popPK** models matching the setting and patient population of interest (i.e., similar age groups, disease type, dose levels, co-morbidities, analytical assay(s), etc. [167]) were implemented in the non-linear mixed effects modeling software NONMEM®, setting fixed and random effect parameters to published values.

### 3.3.2 External dataset

Another important component in an external model performance evaluation is the external dataset that has neither been used for model building nor for internal model evaluation [165]. A dataset represents a time-ordered set-up of records showing the time course of a **PK** and/or **PD** event related to drug administration from one or several clinical trials [168]. For an external performance evaluation, relevant covariates from the investigated **popPK** models should be available in the dataset [165]. (Graphical) assessment of the data is an auxiliary step to identify, e.g., implausible/erroneous datapoints (such as a significant increase in serum concentrations without drug administration) or to investigate the number of concentrations below the limit of quantification (**BLQ**).

### 3.3.3 Handling below limit of quantification (**BLQ**) data

The lower limit of quantification (**LLOQ**) can be defined as the lowest concentration on the calibration curve associated with a coefficient of variation of <20% [169]. Stuart Beal has provided an overview of seven approaches how to handle **BLQ** data in **PK** modeling analyses (M1-M7 method) [170]. Since only three concentrations in the dataset available for external model evaluation were below **LLOQ** (<1% of samples), the M1 method was used, excluding the **BLQ** concentrations from the analysis.

### 3.3.4 Maximum a posteriori (**MAP**) Bayesian estimation process

A **MAP** Bayesian estimation approach using the first-order conditional estimation with interaction (**FOCE-I**) algorithm was leveraged to evaluate the predictive performance of the infliximab **popPK** models from the literature in the external model performance evaluation. To quantify and explain variability in drug concentrations across individuals, **popPK** models are generally developed [171]. The **MAP** Bayesian estimation approach grounds on this prior (i.e., *a priori*) distribution of inter-individual and residual variability and aims to identify point estimates of the most likely individual **PK** parameters (**EBE**) for an individual given a set of patient-specific data (i.e., covariates, drug concentration measurements, dosing history) [171]. With that, future drug concentration–time profiles can be predicted for this individual based on the *a posteriori* **EBEs** and various potential dosing

regimens investigated that could attain a desired target threshold (Bayesian forecasting) [171].

### 3.3.5 Graphical and quantitative evaluation

Graphical evaluation of predictive model performances was conducted comparing individual predicted serum concentrations to the corresponding observed clinical data from the external dataset in goodness-of-fit plots. In addition, prediction- and variability-corrected visual predictive checks were performed for each **popPK** model based on multiple replicates ( $n=1000$ ) of the original dataset. Here, observed concentrations were grouped into bins. For each bin and dataset, the median, 5th and 95th percentiles of simulated concentrations, their 95% confidence intervals as well as the median, 5th and 95th percentiles of the prediction- and variability-corrected observed concentrations were plotted against time after dose.

For quantitative predictive model performance evaluation, the median symmetric accuracy ( $\zeta$ ) (Equation 12a) and the symmetric signed percentage bias (**SSPB**) (Equation 12b) were calculated to assess model prediction accuracy and prediction bias, respectively [172].

$$\zeta = 100 \left[ e^{\left( \text{median} \left( \left| \ln \left( \frac{y_i}{x_i} \right) \right| \right) \right)} - 1 \right] \quad (12a)$$

$$\text{SSPB} = 100 \cdot \left[ \text{sign} \left( \text{median} \left( \ln \left( \frac{y_i}{x_i} \right) \right) \right) \right] \cdot \left[ e^{\left( \left| \text{median} \left( \ln \left( \frac{y_i}{x_i} \right) \right) \right| \right)} - 1 \right] \quad (12b)$$

with  $x_i = i$ th observed serum concentration and  $y_i =$  corresponding predicted serum concentration.

## RESULTS

---

### 4.1 PROJECT I – PHYSIOLOGICALLY BASED PHARMACOKINETIC MODELING OF DASATINIB

#### 4.1.1 *Publication*

Kovar, C., Loer, H. L. H., Rüdesheim, S., Fuhr, L. M., Marok, F. Z., Selzer, D., Schwab, M., & Lehr, T. (2024). A physiologically-based pharmacokinetic precision dosing approach to manage dasatinib drug-drug interactions. *CPT: pharmacometrics & systems pharmacology*, 13(7), 1144–1159. DOI: [10.1002/psp4.13146](https://doi.org/10.1002/psp4.13146). [173].

#### 4.1.2 *Author Contributions*

Author contributions according to the [CRediT](#) [1]:

Christina Kovar	Refer to <i>Contribution Report</i> (p. vii)
Helena Leonie Hanae Loer	Conceptualization, Investigation, Writing – Review & Editing
Simeon Rüdesheim	Conceptualization, Writing – Review & Editing
Laura Maria Fuhr	Conceptualization
Fatima Zahra Marok	Conceptualization
Dominik Selzer	Writing – Review & Editing
Matthias Schwab	Writing – Review & Editing, Funding Acquisition
Thorsten Lehr	Conceptualization, Writing – Review & Editing, Funding Acquisition

#### 4.1.3 *Copyright*

This is an open access article under the terms of CC BY-NC 4.0 (<https://creativecommons.org/licenses/by-nc-nd/4.0/>), which permits use and distribution in any medium, provided the original work is properly cited, the use is non-commercial and no modifications or adaptations are made. © 2024 The Authors. *CPT: Pharmacometrics & Systems Pharmacology* published by Wiley Periodicals LLC on behalf of American Society for Clinical Pharmacology and Therapeutics.



## ARTICLE

# A physiologically-based pharmacokinetic precision dosing approach to manage dasatinib drug–drug interactions

Christina Kovar<sup>1,2</sup> | Helena Leonie Hanae Loer<sup>1</sup> | Simeon Rüdesheim<sup>1,2</sup> |  
Laura Maria Fuhr<sup>1</sup> | Fatima Zahra Marok<sup>1</sup> | Dominik Selzer<sup>1</sup> |  
Matthias Schwab<sup>2,3,4</sup> | Thorsten Lehr<sup>1</sup>

<sup>1</sup>Clinical Pharmacy, Saarland University, Saarbrücken, Germany

<sup>2</sup>Dr. Margarete Fischer-Bosch Institute of Clinical Pharmacology, Stuttgart, Germany

<sup>3</sup>Departments of Clinical Pharmacology, and Pharmacy and Biochemistry, University of Tübingen, Tübingen, Germany

<sup>4</sup>Cluster of Excellence iFIT (EXC2180), Image-Guided and Functionally Instructed Tumor Therapies, University of Tübingen, Tübingen, Germany

## Correspondence

Thorsten Lehr, Clinical Pharmacy, Saarland University, Campus CS 3, Saarbrücken 66123, Germany.  
Email: [thorsten.lehr@mx.uni-saarland.de](mailto:thorsten.lehr@mx.uni-saarland.de)

## Abstract

Dasatinib, a second-generation tyrosine kinase inhibitor, is approved for treating chronic myeloid and acute lymphoblastic leukemia. As a sensitive cytochrome P450 (CYP) 3A4 substrate and weak base with strong pH-sensitive solubility, dasatinib is susceptible to enzyme-mediated drug–drug interactions (DDIs) with CYP3A4 perpetrators and pH-dependent DDIs with acid-reducing agents. This work aimed to develop a whole-body physiologically-based pharmacokinetic (PBPK) model of dasatinib to describe and predict enzyme-mediated and pH-dependent DDIs, to evaluate the impact of strong and moderate CYP3A4 inhibitors and inducers on dasatinib exposure and to support optimized dasatinib dosing. Overall, 63 plasma profiles from perorally administered dasatinib in healthy volunteers and cancer patients were used for model development. The model accurately described and predicted plasma profiles with geometric mean fold errors (GMFEs) for area under the concentration–time curve from the first to the last timepoint of measurement ( $AUC_{last}$ ) and maximum plasma concentration ( $C_{max}$ ) of 1.27 and 1.29, respectively. Regarding the DDI studies used for model development, all (8/8) predicted  $AUC_{last}$  and  $C_{max}$  ratios were within twofold of observed ratios. Application of the PBPK model for dose adaptations within various DDIs revealed dasatinib dose reductions of 50%–80% for strong and 0%–70% for moderate CYP3A4 inhibitors and a 2.3–3.1-fold increase of the daily dasatinib dose for CYP3A4 inducers to match the exposure of dasatinib administered alone. The developed model can be further employed to personalize dasatinib therapy, thereby help coping with clinical challenges resulting from DDIs and patient-related factors, such as elevated gastric pH.

This is an open access article under the terms of the [Creative Commons Attribution-NonCommercial-NoDerivs](https://creativecommons.org/licenses/by-nc-nd/4.0/) License, which permits use and distribution in any medium, provided the original work is properly cited, the use is non-commercial and no modifications or adaptations are made.

© 2024 The Authors. *CPT: Pharmacometrics & Systems Pharmacology* published by Wiley Periodicals LLC on behalf of American Society for Clinical Pharmacology and Therapeutics.

### Study Highlights

#### WHAT IS THE CURRENT KNOWLEDGE ON THE TOPIC?

As a sensitive cytochrome P450 (CYP) 3A4 substrate and weak base with strong pH-sensitive solubility, dasatinib is susceptible to enzyme-mediated and pH-dependent drug–drug interactions (DDIs) with CYP3A4 perpetrator drugs and acid-reducing agents, respectively.

#### WHAT QUESTION DID THIS STUDY ADDRESS?

This work aimed to develop a whole-body physiologically-based pharmacokinetic (PBPK) model of dasatinib to describe and predict enzyme-mediated and pH-dependent DDIs as well as to investigate a selection of clinically relevant DDIs, supporting optimized dasatinib precision dosing.

#### WHAT DOES THIS STUDY ADD TO OUR KNOWLEDGE?

A PBPK model for the CYP3A4 substrate dasatinib was developed and coupled with various strong and moderate CYP3A4 perpetrator models to provide model-based dasatinib dosing recommendations within single as well as complex multiple DDIs.

#### HOW MIGHT THIS CHANGE DRUG DISCOVERY, DEVELOPMENT, AND/OR THERAPEUTICS?

The presented dasatinib model may serve as a tool to further personalize dasatinib therapy, providing strategies to navigate clinical challenges that result from single and multiple DDIs and/or patient-related factors or to perform DDI simulations with drugs under development involving dasatinib as sensitive CYP3A4 substrate.

## INTRODUCTION

The introduction of tyrosine kinase inhibitors (TKIs) transformed the treatment and prognosis of chronic myeloid leukemia (CML), a myeloproliferative disorder accounting for approximately 15% of all newly diagnosed leukemias in adults.<sup>1</sup> Dasatinib (Sprycel®), an oral second-generation and multi-targeted TKI, is utilized in the treatment of Philadelphia chromosome positive (Ph+) CML in all phases and is also approved for Ph+ acute lymphoblastic leukemia (ALL).<sup>2</sup> Here, a comprehensive understanding of its pharmacokinetics (PK), encompassing absorption, distribution, metabolism and excretion (ADME) is vital for maximizing therapeutic efficacy and managing side effects.

Dasatinib, a weak base and a Biopharmaceutical Classification System (BCS) class II compound, demonstrates low solubility and high permeability, making it prone to drug–drug interactions (DDIs) with acid-reducing agents (ARAs) because of its pH-dependent solubility.<sup>3</sup> Given its strong pH-dependent solubility with improved solubility in acidic conditions, co-administration with proton pump inhibitors (PPIs), H<sub>2</sub>-antagonists, and antacids can modify its absorption and consequently, therapeutic efficacy.<sup>4,5</sup>

Dasatinib is primarily metabolized by cytochrome P450 (CYP) 3A4 via hydroxylation and N-dealkylation to three major metabolites.<sup>6,7</sup> Hence, systemic exposure of dasatinib can be significantly impacted by DDIs with both CYP3A4 inhibitors and inducers. The United States Food and Drug Administration has listed dasatinib as a sensitive CYP3A4 substrate for use in clinical DDI studies.<sup>8</sup> For instance, the strong CYP3A4 inhibitor ketoconazole increased dasatinib's area under the concentration–time curve (AUC) over one dosing interval nearly five-fold.<sup>9</sup> Conversely, pretreatment with rifampicin, a strong CYP3A4 inducer, can decrease the AUC by approximately 80%.<sup>3</sup> Moreover, dasatinib can affect the PK of other drugs, acting as a weak mechanism-based inhibitor of CYP3A4 and a competitive inhibitor of CYP2C8 and several transporters, such as organic anion transporting polypeptide (OATP) 1B1 and OATP1B3.<sup>10–12</sup>

Given dasatinib's susceptibility to both enzyme-mediated and pH-dependent DDIs, managing its therapeutic application presents clinical challenges. Here, physiologically-based pharmacokinetic (PBPK) modeling emerges as a valuable tool for exploring DDI scenarios and supporting precision dosing of dasatinib.<sup>13</sup> Specifically, the PBPK approach can provide insights into how various drugs might influence dasatinib PK





by modeling their complex biological ADME and interaction processes. Furthermore, these models can be utilized to simulate and predict the PK, guiding optimization of treatment regimens under complex conditions, such as multiple DDIs, thereby facilitating personalized and safer treatment strategies.<sup>14</sup>

Considering dasatinib's complex PK profile and its susceptibility to DDIs, this study aimed to develop a whole-body PBPK model with the objective to describe and predict the impact of various clinically studied DDIs including enzyme-mediated and pH-dependent DDIs on the exposure of dasatinib. As the package insert does not provide explicit dose adaptations for dasatinib when a specific perpetrator drug is co-administered,<sup>15</sup> our PBPK model was applied to simulate a selection of clinically relevant DDI scenarios involving various CYP3A4 perpetrator drugs, not previously explored in clinical DDI trials. Among others, simulations with the potent antifungal agents fluconazole, itraconazole, ketoconazole, and voriconazole as well as macrolide antibiotics such as clarithromycin were performed as patients with blood malignancies are more susceptible to opportunistic infections.<sup>16,17</sup> Notably, since around a third of CML patients suffer on anxiety and depression particularly during TKI therapy,<sup>18</sup> co-administration of selective serotonin reuptake inhibitors as effective antidepressants (e.g., fluvoxamine) frequently occurs. As a result, model-based dose adaptations for dasatinib, under co-treatment with these CYP3A4 inhibitors and additionally, with different CYP3A4 inducers, were performed to enhance support for precision dosing in patients. The model files will be made publicly available in the Clinical Pharmacy Saarland University GitHub repository (<http://models.clinicalpharmacy.me/>).

## METHODS

### Software

The dasatinib PBPK model was developed using PK-Sim® and MoBi® (Open Systems Pharmacology Suite version 11.0, <http://www.open-systems-pharmacology.org>).<sup>19</sup> Digitization of published concentration–time profiles was performed with GetData Graph Digitizer version 2.26.0.20 (© S. Fedorov) according to Wojtyniak and coworkers.<sup>20</sup> Model parameter estimation via the Levenberg–Marquardt algorithm and local sensitivity analysis were conducted within PK-Sim®. Calculation of PK parameters, model performance metrics as well as generation of graphics and dose adaptations were employed using R 4.2.1 (R Foundation for Statistical Computing, Vienna, Austria).<sup>21</sup>

### PBPK model building

PBPK model development was initiated with a comprehensive literature search to gather information about the physicochemical properties and ADME processes of dasatinib. Plasma concentration–time profiles following oral administration of dasatinib (as tablet, solution, or suspension) at fasted and fed state were extracted from 19 clinical trials including single- and multiple-dose studies with healthy volunteers and cancer patients. An overview of all clinical studies, including administration protocols and demographics of participants, is presented in [Tables S1, S7 and S9](#).

For the development of the dasatinib PBPK model, a middle-out approach was employed. The concentration–time profiles were digitized and divided into a training and test dataset for model building (5 profiles) and evaluation (58 profiles), respectively. The middle-out strategy merges prior information on drug- and system-specific parameters with a parameter estimation step based on clinical trial data.<sup>22</sup> Initial model input parameters were informed through a combination of *in vitro*, *in silico*, and clinical data. If model parameter values could not be reliably sourced via literature or were pivotal for critical quantitative structure–activity relationship estimations, parameter estimation was performed by fitting model simulations to the plasma profiles of the training dataset.

Dissolution kinetics of dasatinib tablets, suspensions and solutions were described using a mechanistic Noyes–Whitney type model, selected for its applicability to particle dissolution processes. Model parameterization utilized either particle size distributions derived from the literature (for suspensions and tablets)<sup>23</sup> or immediately dissolved particle radii of <0.01 µm (for solutions).<sup>24</sup> Dasatinib supersaturation in the intestine was considered, as indicated by prior research,<sup>25</sup> but redissolution processes of precipitated drug were discarded because of dasatinib's low intestinal solubility.<sup>23</sup>

Virtual “mean individuals” were created for each study as outlined in [Section S1.2](#). In addition, population simulations were employed to predict the drug's PK across a virtual population, accounting for variability in physiological factors (see [Section S1.3](#)). Here, we created virtual populations of 100 individuals for each study, mirroring the demographics of the actual study populations. The ethnicity and demographic characteristics for these simulations were selected based on the specific study participant profiles, utilizing distributions from relevant databases. These included the third National Health and Nutrition Examination Survey (NHANES) for White Americans,<sup>26</sup> the International Commission on Radiological Protection (ICRP) database for Europeans<sup>27</sup> and the integrated



database for the Japanese population.<sup>28</sup> Population variability in CYP3A4 expression was considered by varying the corresponding reference concentration within the virtual population according to Table S2.

### PBPK model evaluation

PBPK model performance was evaluated using graphical and quantitative approaches. The predicted plasma concentration–time profiles were compared with corresponding observed profiles. Goodness of fit plots were generated to compare predicted and observed AUC from the first to the last timepoint of measurement ( $AUC_{last}$ ), maximum plasma concentration ( $C_{max}$ ) values and plasma concentrations, respectively. As quantitative measures, the mean relative deviation (MRD) of predicted plasma concentrations and the geometric mean fold error (GMFE) of predicted  $AUC_{last}$  and  $C_{max}$  values were calculated as previously described.<sup>29</sup> Additionally, a local sensitivity analysis was performed as described in Section S2.4.1.

### PBPK drug–drug interaction modeling

Modeling of clinically studied DDI scenarios was performed with five perpetrator drugs (ketoconazole, rifampicin, rabeprazole, famotidine and Maalox®, an over-the-counter antacid containing aluminum hydroxide and magnesium hydroxide as active ingredients) and one victim drug (simvastatin).<sup>3–5,9</sup> The investigated DDI scenarios were categorized into two primary types: enzyme-mediated DDIs and pH-dependent DDIs. For the enzyme-mediated DDIs, the dasatinib PBPK model was coupled with previously published PBPK models of ketoconazole,<sup>29</sup> rifampicin<sup>30</sup> and simvastatin.<sup>31</sup> Here, inhibition and induction processes were implemented as described in the Open Systems Pharmacology Suite manual,<sup>32</sup> using interaction parameters sourced from published PBPK models for each perpetrator drug.<sup>29,30</sup> For the pH-dependent DDIs, the reduced gastric solubility due to intake of the ARAs rabeprazole,<sup>4</sup> famotidine<sup>5</sup> and Maalox®<sup>5</sup> was captured by increasing the gastric pH as previously performed<sup>33</sup> and adjusting the gastric emptying time for rabeprazole and Maalox®. Gastric pH values were only measured in the DDI study with rabeprazole.<sup>4</sup> Here, the mean gastric pH was measured to be 4.1 (2.8–5.2) following the administration of 20 mg rabeprazole and 0.7 (0.5–3.6) after intake of 20 mg rabeprazole plus 1500 mg betaine hydrochloride (BHCl), respectively, while the median gastric pH in the control group was 0.6 (0.5–1.8).<sup>4</sup> For administration of 40 mg famotidine (10 h prior to a 50 mg

dasatinib intake), the gastric pH was adjusted to 2.8, as reported in the literature.<sup>34</sup> In a separate instance involving the concomitant administration of 30 mL Maalox®, the gastric pH was adjusted to 3.0, as documented in a different study.<sup>35</sup> For the control setting, the PK-Sim® default gastric pH of 2.0 in the fasted state was utilized.

### PBPK drug–drug interaction model evaluation

Performance of the DDI model was evaluated by graphical comparison of predicted and observed plasma concentration–time profiles with and without concomitant use of the perpetrator drugs. DDI effects were evaluated by calculating predicted  $AUC_{last}$  and  $C_{max}$  effect ratios according to Equations 1 and 2 comparing predicted ratios to the respective observed values. Here, the prediction success limits proposed by Guest et al. were applied to assess predictive accuracy for DDI ratios, representing a stricter criterium for DDI predictions than the traditional twofold range, especially when the relative AUC and  $C_{max}$  change is small.

$$AUC_{last} \text{ ratio} = \frac{AUC_{last, \text{ effect}}}{AUC_{last, \text{ control}}} \quad (1)$$

$$C_{max} \text{ ratio} = \frac{C_{max, \text{ effect}}}{C_{max, \text{ control}}} \quad (2)$$

For DDI model performance evaluation,  $AUC_{last, \text{ effect}}$  and  $C_{max, \text{ effect}}$  represent the  $AUC_{last}$  and  $C_{max}$  values of the victim drug when administered with the perpetrator drug. Conversely,  $AUC_{last, \text{ control}}$  and  $C_{max, \text{ control}}$  represent the  $AUC_{last}$  and  $C_{max}$  values of the victim drug when administered alone.

### Exposure simulations for model-informed precision dosing

The developed PBPK model was applied to simulate dasatinib exposure in untested DDI scenarios with moderate and strong inhibitors as well as inducers of CYP3A4: The model was coupled with previously published PBPK perpetrator models of the inhibitors clarithromycin,<sup>30</sup> erythromycin,<sup>36</sup> fluconazole,<sup>37</sup> fluvoxamine,<sup>38</sup> grapefruit juice,<sup>39</sup> itraconazole,<sup>30</sup> and voriconazole<sup>40</sup> as well as the inducers carbamazepine<sup>41</sup> and efavirenz<sup>41,42</sup> to evaluate their impact on the exposure of dasatinib. Additionally, co-administration of dasatinib with two perpetrator drugs simultaneously was investigated. Inhibition and induction processes were implemented using interaction



parameters from the respective published PBPK models. The selected dosing regimens for each perpetrator drug and further information on the exposure simulations are given in Section S5.1. The magnitude of dose adjustments in the simulated DDI scenarios matching the exposure of dasatinib monotherapy was investigated for the two recommended daily dasatinib dosing regimens of 100 mg and 140 mg. Here, the simulated dasatinib doses were adapted in increments of 10 mg (in a range of 20–420 mg) until the steady-state AUC ( $AUC_{ss}$ ) matched the  $AUC_{ss}$  (80%–125%) of the monotherapy setting.

## RESULTS

### PBPK model building and evaluation

The training dataset for model building included five mean plasma concentration–time profiles from three single-dose and one multiple-dose study in healthy volunteers as well as a DDI study with ketoconazole in cancer patients, covering a dasatinib dose range from 20 to 140 mg. The test dataset consisted of 58 mean plasma profiles from healthy volunteers and cancer patients, who received single and multiple doses of dasatinib ranging from 15 to 200 mg.

Modeled elimination processes included metabolism via CYP3A4, implemented as Michaelis–Menten kinetics, an unspecific hepatic clearance to cover CYP3A4-independent metabolism and renal excretion through passive glomerular filtration. The Michaelis–Menten constant ( $K_m$ ) for metabolism via CYP3A4, inhibition constants for CYP2C8, OATP1B1, and OATP1B3 as well as the CYP3A4 mechanism-based inhibition parameters of dasatinib were derived from the literature.<sup>7,11,12</sup> Catalytic rate constant for CYP3A4-mediated metabolism ( $k_{cat,CYP3A4}$ ) and the unspecific hepatic clearance were fitted. Here,  $k_{cat,CYP3A4}$  was informed by including the ketoconazole DDI study for model training. Based on the estimated  $k_{cat,CYP3A4}$  and the corresponding  $K_m$  obtained from in vitro studies, an overall fraction metabolized via CYP3A4 resulting from metabolism in all tissues expressing this enzyme (see Table S3) was predicted to be ~92% of the absorbed drug. An overview of all integrated metabolic pathways and investigated DDIs is illustrated in Figure 1a–c, respectively. Drug-dependent model input parameters of dasatinib are listed in Table S4. The PBPK model file of dasatinib can be found in Appendix S2.

Plasma concentration–time profiles of the training dataset, a selection of plasma profiles of the test dataset and the corresponding goodness of fit plots showing predicted compared with observed  $AUC_{last}$ ,  $C_{max}$ , and plasma concentrations are depicted in Figure 2.

Overall, the developed whole-body PBPK model of dasatinib successfully described and predicted plasma concentration–time profiles of the training and test dataset including their shapes in both healthy volunteers and cancer patients. In addition, the model was able to capture minor effects of meal intake on dasatinib PK as demonstrated in Section S4. For the entire dasatinib dataset, 96% of predicted  $AUC_{last}$ , 98% of predicted  $C_{max}$  values, and 90% of predicted plasma concentrations were within the two-fold acceptance criterion of their observed values. GMFEs for predicted  $AUC_{last}$  and  $C_{max}$  values were 1.27 (training dataset: 1.12 and test dataset: 1.28) and 1.29 (training dataset: 1.18 and test dataset: 1.30), respectively, while the overall MRD value for predicted plasma concentrations was 1.54. Detailed values are presented in Tables S5 and S6. Considering the training and test dataset separately, MRD values were calculated to be 1.35 and 1.56, respectively. Moreover, 49 out of 53 plasma concentration–times profiles show MRD values  $\leq 2$ , supporting the adequate model predictions of longitudinal plasma concentration–time profile trajectories. As shown in Figure S6, residuals are randomly dispersed over time with no apparent trend, suggesting that the model does not exhibit systematic bias across the range of fits and predictions.

Of note, about half of the observed plasma profiles of cancer patients showed consistently lower plasma concentrations compared with the concentrations in healthy volunteers receiving similar dasatinib doses. As mentioned before, gastric pH plays a pivotal role in modulating dasatinib absorption. Moreover, co-morbidities and administration of ARAs could negatively affect the absorption of dasatinib. To mitigate these factors and refine model predictions, we adjusted the gastric pH for a subset of cancer patients showing consistently lower dasatinib exposure compared with healthy volunteers to the upper end of the physiological range in the fasted state (1.5–2.5).<sup>43</sup> As a result, the model performance could be improved, reducing the MRD for the corresponding plasma profiles from 1.92 to 1.60. Local sensitivity analysis, conducted for a 100 mg once daily dosing regimen, identified the two  $pK_a$  values, gastric pH and lipophilicity as the parameters most sensitive to dasatinib exposure at steady-state (details are presented in Section S2.4.2).

### PBPK drug–drug interaction modeling and evaluation

Eight dasatinib plasma profiles from five clinical DDI studies<sup>3–5,9</sup> were employed to prepare and evaluate the model predicting DDI scenarios. In enzyme-mediated DDI studies, dasatinib (acting as victim drug) was

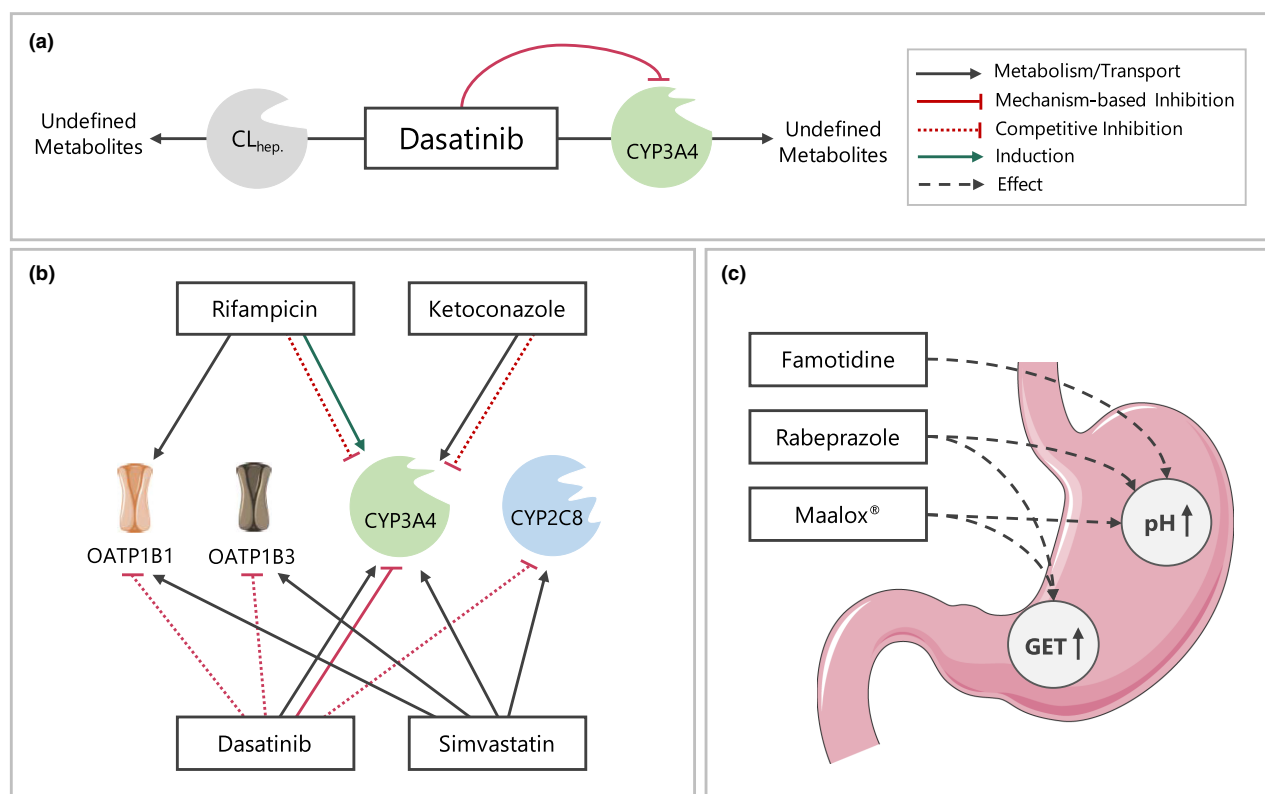


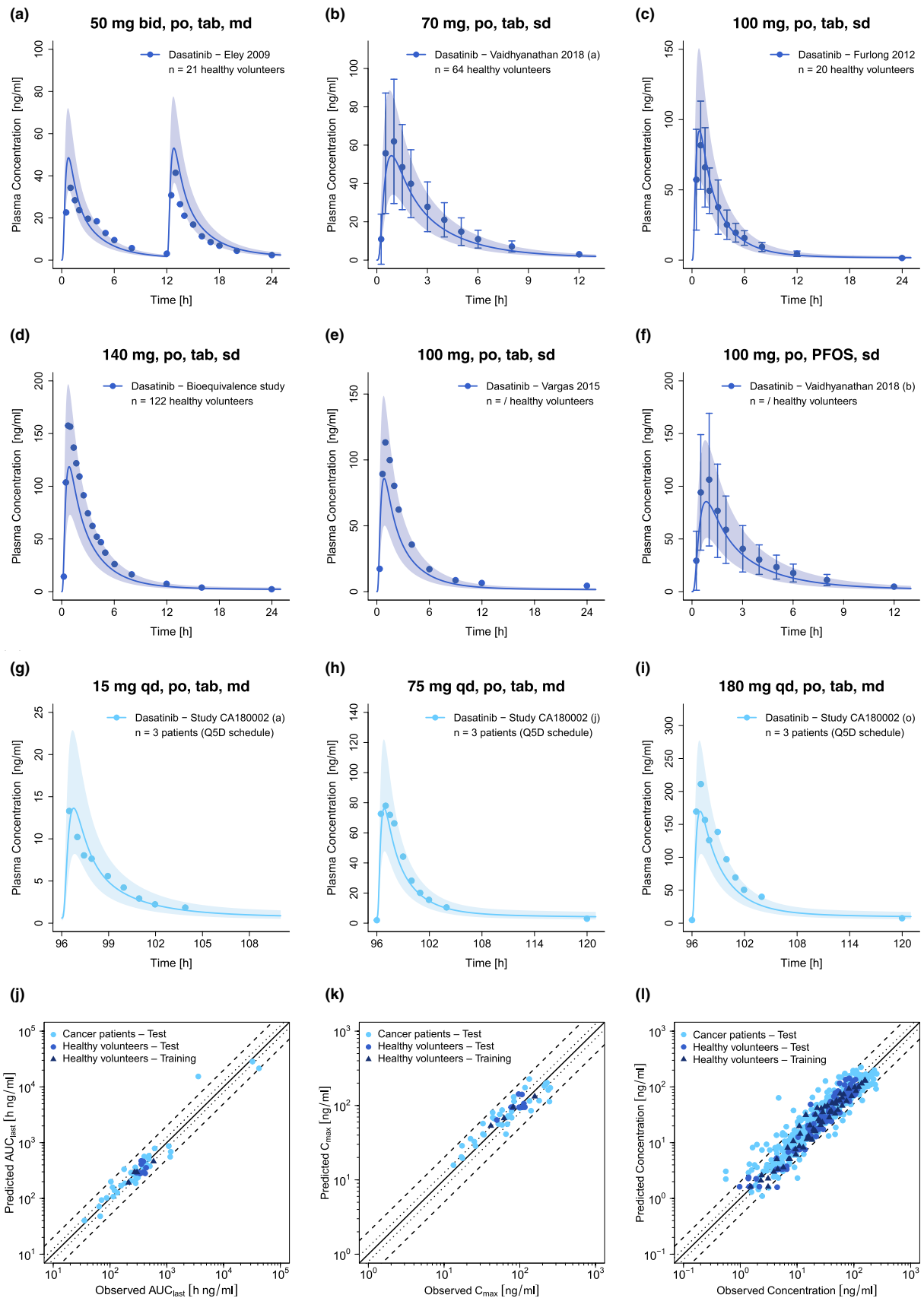
**FIGURE 1** Schematic overview of implemented metabolic processes in the dasatinib PBPK model (a) as well as investigated DDIs including enzyme-mediated (b) and pH-dependent DDIs (c). Drawings by Servier, licensed under CC BY 3.0.<sup>55</sup> CL<sub>hep.</sub>, unspecific hepatic clearance; CYP, cytochrome P450; DDIs, drug–drug interactions; GET, gastric emptying time; OATP, organic anion transporting polypeptide.

administered with and without the perpetrator drugs ketoconazole (CYP3A4 competitive inhibition<sup>29</sup>) and rifampicin (CYP3A4 induction and CYP3A4 competitive inhibition<sup>30</sup>), respectively. Furthermore, plasma profiles of the victim drug simvastatin lactone and its metabolite simvastatin acid administered with and without dasatinib were included for model evaluation. Here, dasatinib acts as a CYP3A4 mechanism-based inhibitor and CYP2C8, OATP1B1 and OATP1B3 competitive inhibitor. Simulated and observed plasma concentration–time profiles of all modeled enzyme-mediated DDIs are depicted in Figure 3. The DDI model files are included in Appendix S2.

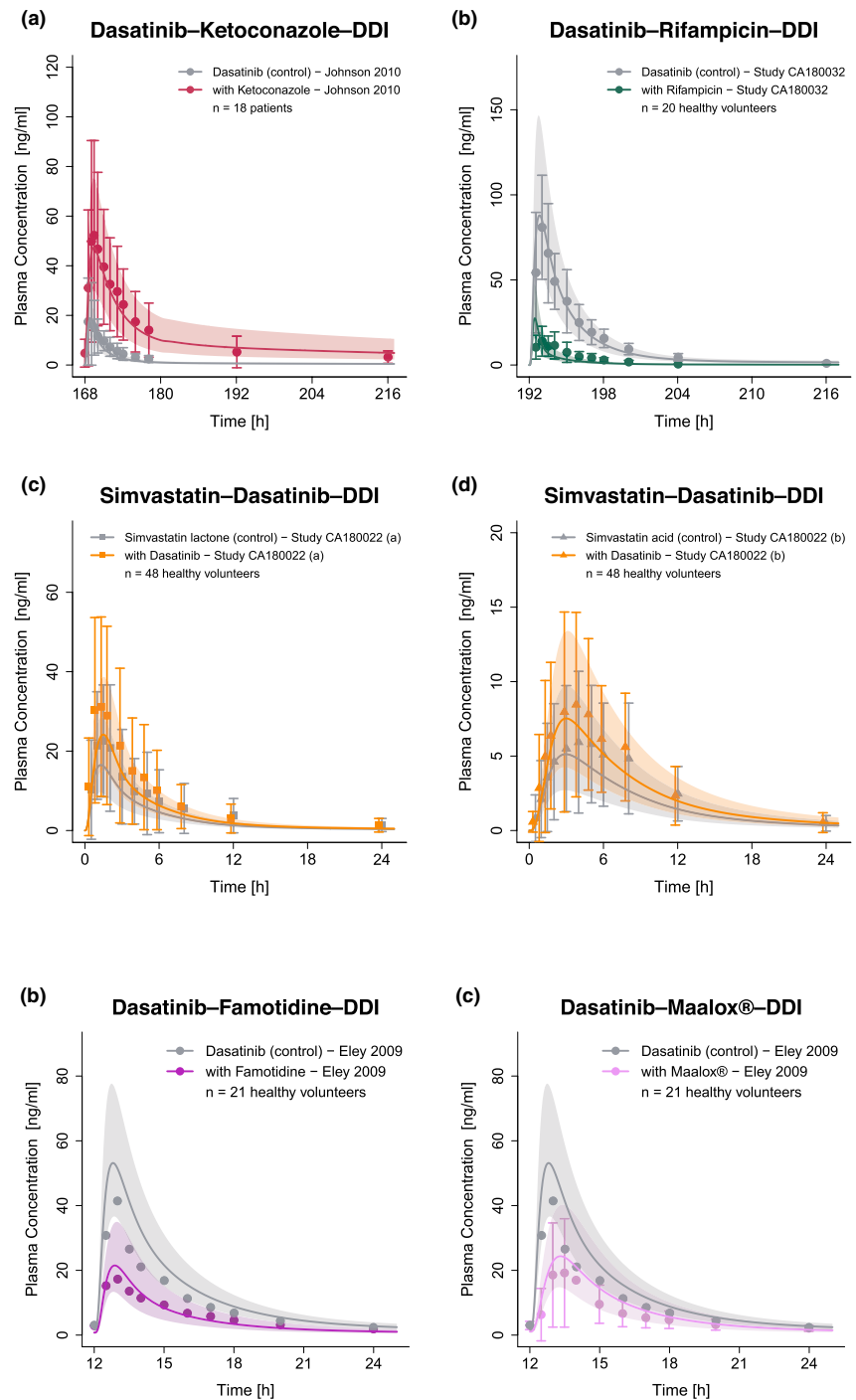
For the investigation of pH-dependent DDIs, plasma profiles of dasatinib with and without administration of the ARAs rabeprazole,<sup>4</sup> rabeprazole plus BHCl,<sup>4</sup> famotidine and Maalox<sup>®</sup><sup>5</sup> were available for model evaluation. The corresponding plasma profiles of the different pH-dependent DDI scenarios are depicted in Figure 4. Additional information on the DDI studies is provided in Table S7.

Figure 5 depicts the goodness of fit plots, comparing predicted to observed AUC<sub>last</sub> and C<sub>max</sub> ratios for dasatinib — modulated by intake of perpetrators ketoconazole, rifampicin, the antacid Maalox<sup>®</sup>, PPI rabeprazole, and

**FIGURE 2** Selection of predicted and observed dasatinib plasma concentration–time profiles of the training (a–d) and the test dataset (e–i) on a linear scale as well as goodness of fit plots of predicted versus observed AUC<sub>last</sub> (j), C<sub>max</sub> (k) and plasma concentrations (l). Blue and light blue solid lines show predicted geometric mean concentration–time profiles in healthy volunteers and cancer patients, respectively, with colored ribbons illustrating the corresponding geometric standard deviation of the population simulations ( $n=100$ ). Points demonstrate the mean observed data of dasatinib with the corresponding standard deviation (if depicted in the respective publication). Linear and semilogarithmic predicted and observed plasma concentration–time profiles of all studies are shown in Sections S2.1 and S2.2. In the goodness of fit plots, solid lines mark the lines of identity, dotted lines indicate 1.25-fold and dashed lines twofold deviation. /, no information available; AUC<sub>last</sub>, areas under the plasma concentration–time curves from the first to the last timepoint of measurement; bid, twice a day; C<sub>max</sub>, maximum plasma concentration; md, multiple dose;  $n$ , number of participants; PFOS, powder for oral suspension; po, peroral; Q5D, five consecutive days once daily dosing followed by two nontreatment days; qd, once a day; sd, single dose; tab, tablet.



**FIGURE 3** Predicted and observed plasma concentration–time profiles for enzyme-mediated DDIs with dasatinib acting as victim (a, b) and perpetrator drug (c, d). The solid lines show predicted geometric mean concentration–time profiles with (colored) and without (gray) intake of the perpetrator drug and ribbons show the corresponding geometric standard deviation of the population simulations ( $n=100$ ). Points depict mean observed data with corresponding standard deviation of dasatinib, while squares and triangles depict the observed data with corresponding standard deviation of simvastatin lactone and simvastatin acid, respectively. Predicted and observed plasma concentration–time profiles of all studies on a semilogarithmic scale are shown in Section S3.2.1. DDIs, drug–drug interactions; n, number of participants.



**FIGURE 4** Predicted and observed plasma concentration–time profiles of dasatinib for the pH-dependent DDIs. The solid lines show predicted geometric mean concentration–time profiles with (colored) and without (gray) the intake of the perpetrator drug and ribbons show the corresponding geometric standard deviation of the population simulations ( $n=100$ ). Points depict mean observed data with corresponding standard deviation of dasatinib (if depicted in the respective publication). Predicted and observed plasma concentration–time profiles of all studies on a semilogarithmic scale are shown in Section S3.2.2. BHCl, betaine hydrochloride; DDIs, drug–drug interactions; n, number of participants.

H<sub>2</sub>-blocker famotidine — as well as simvastatin lactone and its metabolite simvastatin acid, impacted by dasatinib administration. GMFEs for the predicted AUC<sub>last</sub> and

$C_{max}$  ratios were 1.19 and 1.08 for pH-dependent DDIs, 1.37 and 1.57 for enzyme-mediated DDIs with dasatinib acting as victim drug as well as 1.21 and 1.07 for DDIs with



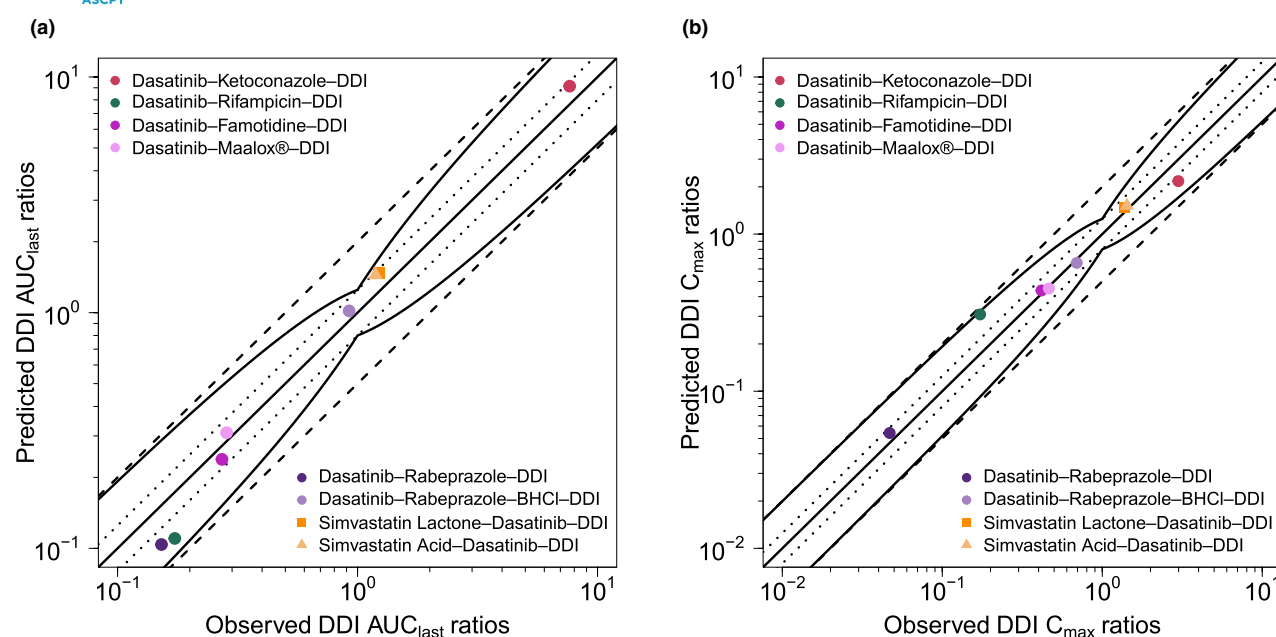


**FIGURE 5** Predicted versus observed DDI  $AUC_{last}$  ratios (a) and DDI  $C_{max}$  ratios (b) of dasatinib (circles), simvastatin lactone (squares) and simvastatin acid (triangles). The straight solid lines mark the lines of identity, the curved lines show the limits of the predictive measure proposed by Guest et al. with 1.25-fold variability.<sup>56</sup> Dotted lines indicate 1.25-fold and dashed lines twofold deviation.  $AUC_{last}$ , area under the plasma concentration–time curve from the first to the last timepoint of measurement; BHCl, betaine hydrochloride;  $C_{max}$ , maximum plasma concentration; DDI, drug–drug interaction.

dasatinib acting as perpetrator drug. Moreover, all  $AUC_{last}$  and  $C_{max}$  ratios lie within the limits proposed by Guest et al. (see Figure 5). Additionally, 7 out of 8  $AUC_{last}$  and  $C_{max}$  ratios were within 1.5-fold of observed ratios. Only the DDI with rifampicin, a strong CYP3A4 inducer and weak CYP3A4 inhibitor, was outside the stricter 1.5-fold range with  $AUC_{last}$  and  $C_{max}$  ratios of 0.64 and 1.79, respectively. All predicted and observed values for  $AUC_{last}$  and  $C_{max}$  ratios are listed in Table S8.

### Exposure simulations for model-informed precision dosing

The developed PBPK model was applied to simulate DDI scenarios of dasatinib with various strong and moderate CYP3A4 inhibitors and inducers. Subsequently, model-based dasatinib dose adaptations were simulated based on the exposure matching principle. A selection of the corresponding plasma concentration–time profiles with and without adapted dasatinib doses is provided in Figure 6 and profiles for all investigated DDI settings in Figures S13 and S14.

Model exposure simulations revealed that co-administration of the perpetrator drugs may result in mean dasatinib  $AUC_{ss}$  increases of up to 4.6-fold and reductions of up to 70% (see Table S12). Based on exposure matching

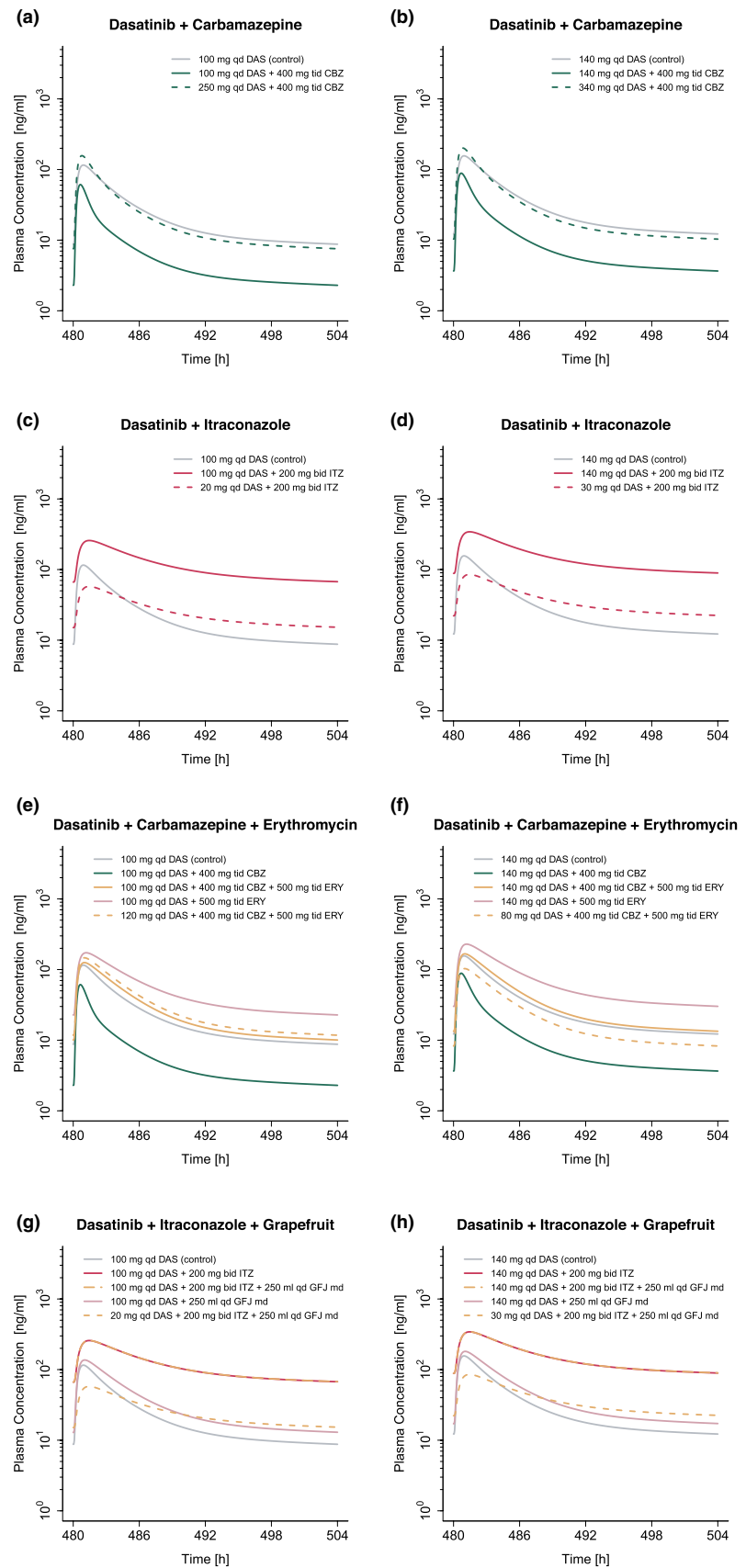
simulations, this translated into a dasatinib dose range of 20–310 (30–360) mg to match the PBPK simulated monotherapy  $AUC_{ss}$  from 100 (140) mg dasatinib (see Figure 7). Model simulations revealed dose reductions of 50%–80% for strong and 0%–70% for moderate inhibitors. In contrast, during co-administration of inducers, a 2.3–3.1-fold increase of dasatinib dose was required to match the exposure of dasatinib monotherapy.

Additionally, co-administration with drugs like carbamazepine and erythromycin or itraconazole and grapefruit juice resulted in dose reductions of up to 20% and 80%, respectively. Table S12 provides an overview of all DDI scenarios, including  $AUC_{ss}$  effect ratios and dose adjustments to match monotherapy exposure for 100 mg and 140 mg daily dasatinib.

## DISCUSSION

In this study, a whole-body PBPK model of dasatinib was successfully developed integrating data from a total of 19 clinical trials. The model was able to describe and predict dasatinib plasma concentration–time profiles in healthy volunteers and cancer patients, covering a dasatinib dose range of 15–200 mg. Several dasatinib PBPK models have been published in the literature, including three models that investigated either the DDI potential of

**FIGURE 6** Model-based dose adaptations for dasatinib within single (a–d) and multiple DDI scenarios (e–h) including moderate and strong CYP3A4 inhibitors and inducers. The first and second column represent the simulation results after administration of 100 mg and 140 mg dasatinib daily, respectively. Solid lines show the model predictions with (colored) and without (gray) intake of perpetrator drug. Colored dashed lines represent model predictions in the presence of perpetrator drug(s), using an adapted dasatinib dose. For the dosing simulations a virtual European male individual, 64 years of age and default values for body weight and height according to the International Commission on Radiological Protection (ICRP) database, was used. Bid, twice a day; CBZ, carbamazepine; DAS, dasatinib; DDI, drug–drug interaction; ERY, erythromycin; GFJ, grapefruit juice; ITZ, itraconazole; md, multiple dose; qd, once a day; tid, three times a day.



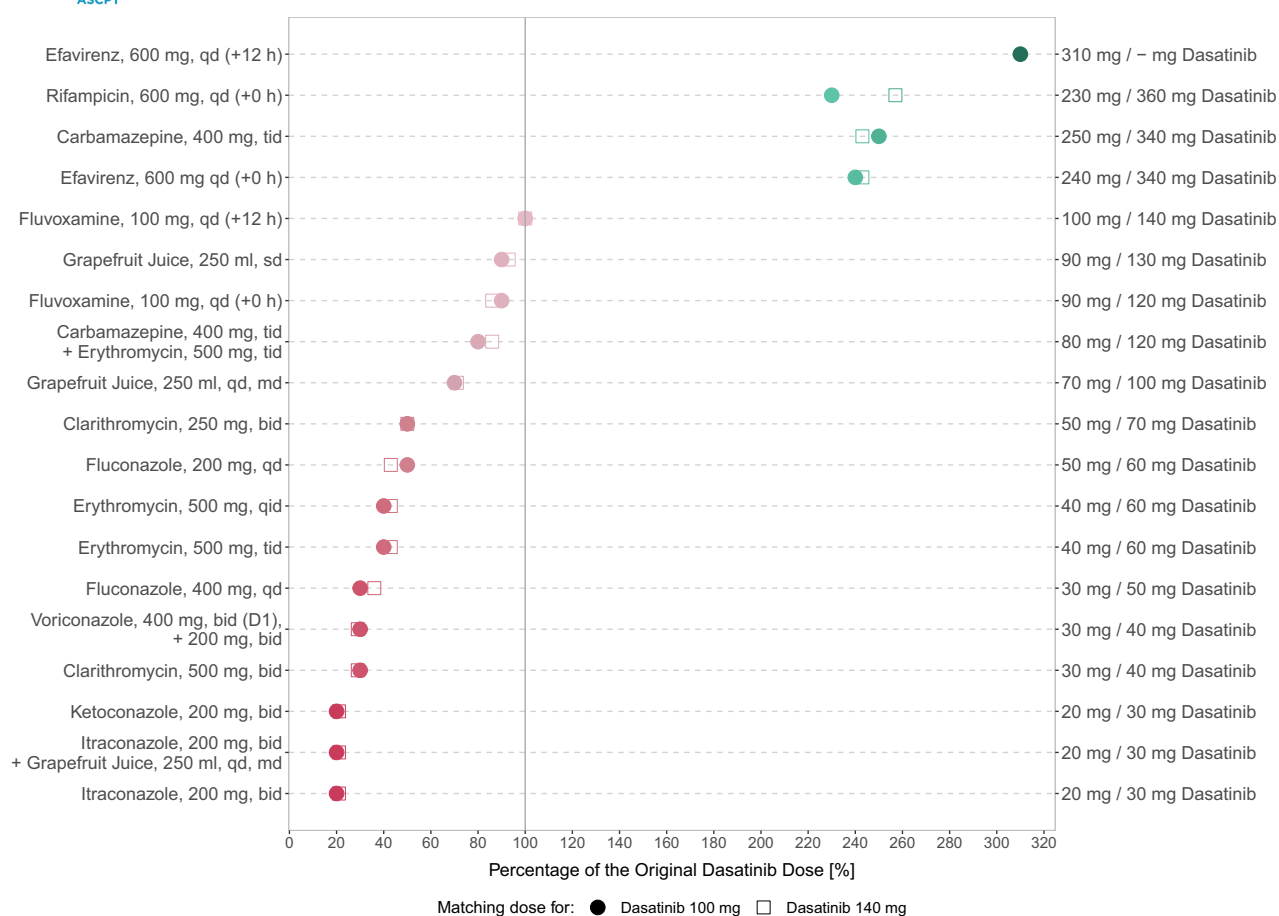


**FIGURE 7** Overview of model-based dose adaptations for dasatinib within single and multiple DDI scenarios based on the exposure matching principle, where points and squares show the percentage of the original dasatinib dose that match the PBPK simulated monotherapy  $AUC_{ss}$  at 100 mg and 140 mg, respectively. A virtual European male individual, 64 years of age and default values for body weight and height according to the International Commission on Radiological Protection (ICRP) database, was used for the dosing simulations. Red symbols depict dasatinib dose reductions and green symbols depict dasatinib dose elevations. The darker the color, the higher the magnitude of dasatinib dose adaptation. –, dose adaptations outside the simulated dose range;  $AUC_{ss}$ , steady-state area under the concentration–time curve; bid, twice a day; D, day; md, multiple dose; qd, once daily; qid, four times a day; sd, single dose; tab, tablet; tid, three times a day.

dasatinib mediated by enzymes and/or transporters<sup>11,12</sup> or the effects of varying formulations on dasatinib PK.<sup>23</sup> In contrast to previous work, the presented model was used to investigate a comprehensive range of clinically relevant enzyme-mediated and pH-dependent DDI scenarios in healthy volunteers and cancer patients within a single framework. For model development, a larger number of clinical studies involving a broader dose range (15–200 mg) of dasatinib was used compared with published PBPK models. Moreover, the model was utilized to simulate various DDI scenarios that have not yet been investigated in clinical trials and to provide model-based dose adaptations, supporting precision dosing approaches for dasatinib. Furthermore, our established PBPK model extends the openly accessible PBPK model library with an additional sensitive CYP3A4 substrate and can be applied

by the research community for various applications such as additional population-specific DDI simulations and dose adaptations, DDI simulations with drugs under development involving dasatinib as a sensitive CYP3A4 substrate, or to develop and evaluate new PBPK models.

In our PBPK model, fraction absorbed after administration of dasatinib tablets across the dose range of 20–420 mg varied between 80% and 41% (Table S14). Additionally, the respective modeled absolute bioavailability ranged from 20% to 28% for the dose range of 20–420 mg (Table S14). Due to lack of intravenous data the modeled bioavailability values could not be compared with clinically observed data.<sup>44</sup> Dasatinib is primarily metabolized via CYP3A4, accounting for ~92% of the absorbed drug, consistent with literature reports.<sup>7</sup> Moreover, only 0.1% of absorbed dasatinib was excreted unchanged in urine, which is in line



with results from a human ADME study.<sup>6</sup> In vitro studies suggested that dasatinib may be a substrate of the efflux transporters breast cancer resistance protein (BCRP) and P-glycoprotein (P-gp).<sup>45</sup> However, recent in vivo studies by Kamath et al. found no significant involvement of P-gp in modulating the rate and extent of intestinal absorption.<sup>46</sup> Consequently, and due to the absence of in vitro  $K_m$  values, P-gp and BCRP were not incorporated into the PBPK model.

A good descriptive and predictive performance for DDIs was demonstrated by GMFEs of 1.24 and 1.18 for predicted  $AUC_{last}$  and  $C_{max}$  effect ratios, respectively. The DDIs emphasize the significant role of CYP3A4 in dasatinib metabolism and the importance to adapt dasatinib therapy in DDI settings to increase both patient safety and treatment efficacy. Due to the potential risk of adverse events resulting from increased dasatinib exposure during CYP3A4 inhibition, the package insert advises against the concomitant use of dasatinib and strong CYP3A4 inhibitors.<sup>15,47</sup> However, if such combination is unavoidable, the package insert recommends considering dose adaptations to 20 (40) mg dasatinib daily instead of 100 (140) mg for all strong inhibitors, while dosing recommendations for moderate CYP3A4 inhibitors are not provided.<sup>15</sup> Consequently, our developed PBPK model was applied in tandem with models of various strong and moderate CYP3A4 perpetrators to conduct DDI simulations to support dasatinib precision dosing.

The performed model simulations suggest that a “one-dose-fits-all” approach during co-treatment with strong or moderate inhibitors may lead to suboptimal dasatinib exposures: If combination of dasatinib with strong CYP3A4 inhibitors is unavoidable, dasatinib dose reductions of 50%–80% should be considered, depending on the inhibitor and selected dosing regimen, to match dasatinib  $AUC_{ss}$  during monotherapy. This translates into a dasatinib dose range of 20–50 mg for the 100 mg dosing regimen and 30–70 mg for the 140 mg dosing regimen. Moreover, simulations suggest dose reductions of 0%–70% for co-treatment with moderate CYP3A4 inhibitors, depending on individual factors such as perpetrator drug and timing of drug administration (detailed numeric dasatinib dose adaptations are listed in Table S12). Furthermore, while simulations with a single dose of 250 mL grapefruit juice showed only a marginal increase in dasatinib exposure (~15%), a daily intake led to an  $AUC_{ss}$  increase of up to 40%, supporting the package insert guidance to avoid concomitant intake of dasatinib with grapefruit juice.

The PBPK model was additionally used to simulate the impact of CYP3A4 induction on dasatinib exposure, a situation for which only qualitative recommendations are available in the package insert: Concomitant strong inducers should be avoided, and if co-administration is

inevitable, a dose increase considered.<sup>15</sup> Our model simulations suggest that a 2.3–3.1-fold increase in dasatinib dose would match the exposure of dasatinib monotherapy. However, if adapting the dasatinib dose to higher values that were neither part of the model training/test dataset nor clinically studied, it is crucial to carefully monitor patients for potential toxicities (e.g., pleural effusion or hematological toxicities).<sup>15,47</sup>

Moreover, the effect of dose staggering was exemplarily investigated for fluvoxamine (moderate competitive CYP3A4 inhibitor) and efavirenz (moderate CYP3A4 inducer) as both drugs should be preferably taken in the evening according to the package insert. While no dose adaptations were needed for fluvoxamine with a 12 h staggered intake, the effect on dasatinib's  $AUC_{ss}$  increased when efavirenz was given 12 h staggered to dasatinib (see Figure 7 and Table S12).

Dasatinib's pH-dependent DDIs represent another type of clinical interaction. In the investigated pH-dependent DDIs, rabeprazole, famotidine and Maalox® co-treatment showed strong impact on dasatinib PK with simulated  $AUC_{last}$  effect ratios of 0.10, 0.24 and 0.31, respectively. Successful predictions of the DDI scenarios were attained by elevating the gastric pH constantly over time to the literature values of 4.1, 2.8, and 3.0, respectively, and estimating the elevated gastric emptying times to be 60.1 min for rabeprazole and 31.3 min for Maalox®. The impact of Maalox® on gastric emptying time has been reported in the literature,<sup>48</sup> while the effect of PPIs is volunteers of ongoing debate and necessitates further investigation.<sup>49,50</sup> Given the dynamic changes in gastric pH following the administration of ARAs, offering precise dosing recommendations for such DDI scenarios becomes challenging. However, the effect of antacids, which directly neutralize gastric acid, diminishes approximately 2 h post-dose.<sup>51</sup> Consequently, antacids taken 2 h before dasatinib do not significantly alter dasatinib exposure.<sup>5</sup> In contrast, the reduction in gastric acid production through  $H_2$ -antagonists can persist for up to 12 h and the suppression induced by PPIs can continue for several days after stopping the PPI treatment.<sup>51</sup> Therefore, ARAs that have a shorter duration of pH elevation, such as antacids, should be preferred.

Besides single DDIs, two exemplary multiple DDIs were investigated. While the single DDI with carbamazepine (strong CYP3A4 inducer) required a 2.4-fold increase in dasatinib dose to match the exposure of dasatinib monotherapy, the additional administration of erythromycin (moderate, irreversible CYP3A4 inhibitor) compensated this effect, overall resulting in a 20% dose reduction. In contrast, the additional intake of grapefruit juice to the strong CYP3A4 inhibitor itraconazole did not impact the simulated dose adaptation for the single dasatinib–itraconazole-DDI (80% dose reduction).



The dasatinib model was evaluated in a comprehensive PBPK DDI network, offering predictions for various clinical situations. It can explore single and multiple DDIs with dasatinib as the victim drug. The dasatinib perpetrator model, tested with the dasatinib–simvastatin DDI, holds potential for future research, especially concerning CYP3A4, CYP2C8, OATP1B1, and OATP1B3 substrates with a narrow therapeutic index. This underscores the importance of DDIs in long-term dasatinib treatment.

There are limitations to this study, which merit consideration and will be explored in the forthcoming paragraphs. Metabolites of dasatinib were not incorporated into the PBPK model, as they are not considered clinically relevant.<sup>6</sup> However, during strong CYP3A4 induction, plasma concentrations of active metabolites could potentially increase to clinically relevant exposures, which was not addressed in our dosing recommendations. Contrary to CYP3A4 genetic variants, CYP3A5 polymorphisms are known to significantly affect the PK of many CYP3A substrates.<sup>52</sup> Consequently, due to the minor contribution of CYP3A5 to the metabolism of dasatinib,<sup>7</sup> CYP3A genetic variants were not considered in this work. While our PBPK model accounts for differences in patient demographics, such as age, which affects various physiological parameters including glomerular filtration rate (GFR), blood flow rates and tissue volumes, pathophysiologic changes for cancer patients (e.g., enzyme expression or  $\alpha$ 1-acid glycoprotein levels [AGP]) were not integrated because of lack of specific information from clinical study reports. However, population variability in CYP3A4 enzyme expression or AGP levels was considered in the population simulations.

A less precise prediction performance compared with other explored DDIs could be observed for the DDI with rifampicin applying a stricter criterium of 1.5-fold range. Here, predicted  $AUC_{last}$  and  $C_{max}$  ratios deviated more than 1.5-fold from the observed ratios. Of note, rifampicin is not only an inhibitor and inducer of several enzymes, but also of several transporters like the efflux transporter P-gp. Incorporation of P-gp in the dasatinib PBPK model was investigated during model building; however, no significant improvement of DDI predictions involving rifampicin could be observed that has further encouraged to not include P-gp in the final model. Similar limitations regarding DDI predictions with rifampicin have also been reported in previous work because of the complex inhibition and induction mechanisms for several enzymes and transporters.<sup>53,54</sup>

The dosing simulations and subsequent dose adaptations were based on the exposure matching principle, utilizing dasatinib  $AUC_{ss}$  as exposure metric as described in the package insert.<sup>15</sup> However, it should be noted that despite achieving similar  $AUC_{ss}$  values for the control and

DDI scenarios through dose adaptations, differences in plasma profile trajectories and thus  $C_{max}$  and trough concentrations ( $C_{min}$ ) can lead to differences in drug efficacy and safety. Dose-adapted plasma profiles during CYP3A4 inducer co-treatment showed higher  $C_{max}$  values while plasma profiles during inhibitor co-treatment showed higher  $C_{min}$  values compared with the simulated plasma profiles during monotherapy. An exposure–response analysis identified elevation in  $C_{min}$  as the most significant predictor for pleural effusion, a key adverse event during dasatinib therapy.<sup>47</sup> Hence, close monitoring of patients for toxicities is inevitable particularly during CYP3A4 inhibitor co-treatment and concomitant use with strong inhibitors should be avoided in clinical practice.

Finally, the recommended dasatinib dose for each DDI scenario represents an estimated average dose that can be affected by different sources of variability and uncertainties (e.g., enzyme abundance). For dosing simulations, a virtual European male individual, 64 years of age and default values for body weight and height according to the ICRP database was used. While also complex scenarios like multiple DDIs were simulated, the applicability of the provided dosing recommendations to patients with diverse clinical characteristics (e.g., hepatic impairment) is not warranted and was beyond the scope of this study. However, our PBPK model offers a foundation for future applications to personalize dasatinib therapy by using individual demographics, physiology, and enzyme activity, creating a “virtual twin” of the patient. Clinical studies are yet required to confirm the advantage of such a precision dosing approach for dasatinib therapy including efficacy and safety over the broad dose range that was required in the various DDI simulations to match the dasatinib exposure during monotherapy.

To conclude, a comprehensive whole-body PBPK model was successfully developed for dasatinib, a sensitive CYP3A4 substrate. The established model was leveraged to simulate several previously unexplored DDI scenarios, resulting in model-based dosing recommendations for dasatinib. Moreover, the model could serve as a tool to further optimize and personalize dasatinib therapy, providing strategies to navigate clinical challenges that result from single and multiple DDIs and/or patient-related factors, such as elevated gastric pH. Finally, it extends the openly accessible PBPK model library with an additional sensitive CYP3A4 substrate and can be applied by the research community to investigate future single and multiple DDI scenarios involving dasatinib.

#### AUTHOR CONTRIBUTIONS

C.K., H.L.H.L., S.R., D.S., M.S. and T.L. wrote the manuscript; C.K., H.L.H.L., L.M.F., F.Z.M., S.R. and T.L. designed the research; C.K. performed the research; C.K. and H.L.H.L. analyzed the data.

## ACKNOWLEDGMENTS

We thank Elisabeth Emmerich for supporting this work during her internship at Saarland University. Open Access funding enabled and organized by Projekt DEAL.

## FUNDING INFORMATION

Matthias Schwab was supported by the Robert Bosch Stiftung (Stuttgart, Germany), a grant from the German Federal Ministry of Education and Research (BMBF, 031L0188D, “GUIDE-IBD”) and the DFG im Rahmen der Exzellenzstrategie des Bundes und der Länder-EXC 2180–390900677. Thorsten Lehr was supported by the German Federal Ministry of Education and Research (BMBF, Horizon 2020 INSPIRATION grant 643271), under the frame of ERACoSysMed and the European Union Horizon 2021 SafePolyMed (grant 101057639).

## CONFLICT OF INTEREST STATEMENT

The authors declared no competing interests for this work.

## ORCID

Christina Kovar  <https://orcid.org/0000-0003-0155-9861>

Simeon Rüdesheim  <https://orcid.org/0000-0002-5741-2511>

Dominik Selzer  <https://orcid.org/0000-0002-4126-0816>

Matthias Schwab  <https://orcid.org/0000-0002-9984-075X>

Thorsten Lehr  <https://orcid.org/0000-0002-8372-1465>

## REFERENCES

1. American Cancer Society. Cancer facts and figures. American Cancer Society website. <https://www.cancer.org/cancer/chronic-myeloid-leukemia/about/statistics.html>. Accessed February 1, 2023.
2. European Medicines Agency (EMA). Annex I: summary of product characteristics (Sprycel). European Medicines Agency website. [https://www.ema.europa.eu/en/documents/product-information/sprycel-epar-product-information\\_en.pdf](https://www.ema.europa.eu/en/documents/product-information/sprycel-epar-product-information_en.pdf). Accessed January 18, 2023.
3. Center for Drug Evaluation. Clinical pharmacology and biopharmaceutics review(s): NDA Review – Dasatinib. U.S. Food and Drug Administration website. [https://www.accessdata.fda.gov/drugsatfda\\_docs/nda/2006/021986s000\\_Sprycel\\_\\_ClinPharmR.pdf](https://www.accessdata.fda.gov/drugsatfda_docs/nda/2006/021986s000_Sprycel__ClinPharmR.pdf). Accessed August 04, 2022.
4. Yago MR, Frymoyer A, Benet LZ, et al. The use of betaine HCl to enhance dasatinib absorption in healthy volunteers with rabeprazole-induced hypochlorhydria. *AAPS J*. 2014;16:1358-1365.
5. Eley T, Luo FR, Agrawal S, et al. Phase I study of the effect of gastric acid pH modulators on the bioavailability of oral dasatinib in healthy subjects. *J Clin Pharmacol*. 2009;49:700-709.
6. Christopher LJ, Cui D, Wu C, et al. Metabolism and disposition of dasatinib after oral administration to humans. *Drug Metab Dispos*. 2008;36:1357-1364.
7. Wang L, Christopher LJ, Cui D, et al. Identification of the human enzymes involved in the oxidative metabolism of dasatinib: an effective approach for determining metabolite formation kinetics. *Drug Metab Dispos*. 2008;36:1828-1839.
8. U.S. Food and Drug Administration (FDA). Drug development and drug interactions | table of substrates, inhibitors and inducers. <https://www.fda.gov/drugs/drug-interactions-labeling/drug-development-and-drug-interactions-table-substrates-inhibitors-and-inducers>. Accessed February 01, 2023.
9. Johnson FM, Agrawal S, Burris H, et al. Phase 1 pharmacokinetic and drug-interaction study of dasatinib in patients with advanced solid tumors. *Cancer*. 2010;116:1582-1591.
10. Li X, He Y, Ruiz CH, Koenig M, Cameron MD, Vojtkovsky T. Characterization of dasatinib and its structural analogs as CYP3A4 mechanism-based inactivators and the proposed bioactivation pathways. *Drug Metab Dispos*. 2009;37:1242-1250.
11. Pahwa S, Alam K, Crowe A, et al. Pretreatment with rifampicin and tyrosine kinase inhibitor Dasatinib potentiates the inhibitory effects toward OATP1B1- and OATP1B3-mediated transport. *J Pharm Sci*. 2017;106:2123-2135.
12. Chang M, Bathena S, Christopher LJ, Shen H, Roy A. Prediction of drug-drug interaction potential mediated by transporters between dasatinib and metformin, pravastatin, and rosuvastatin using physiologically based pharmacokinetic modeling. *Cancer Chemother Pharmacol*. 2022;89:383-392.
13. Gonzalez D, Rao GG, Bailey SC, et al. Precision dosing: public health need, proposed framework, and anticipated impact. *Clin Transl Sci*. 2017;10:443-454.
14. Grimstein M, Yang Y, Zhang X, et al. Physiologically based pharmacokinetic modeling in regulatory science: an update from the U.S. Food and Drug Administration's Office of Clinical Pharmacology. *J Pharm Sci*. 2019;108:21-25.
15. Bristol-Myers Squibb Company. Sprycel U.S. prescribing information website. [https://packageinserts.bms.com/pi/pi\\_sprycel.pdf](https://packageinserts.bms.com/pi/pi_sprycel.pdf). Accessed 01 March 2023.
16. Rodriguez GH, Ahmed SI, Al-Akhrass F, Rallapalli V, Safdar A. Characteristics of, and risk factors for, infections in patients with cancer treated with dasatinib and a brief review of other complications. *Leuk Lymphoma*. 2012;53:1530-1535.
17. Shariati A, Moradabadi A, Chegini Z, Khoshbayan A, Didehdar M. An overview of the Management of the Most Important Invasive Fungal Infections in patients with blood malignancies. *Infect Drug Resist*. 2020;13:2329-2354.
18. Shi D, Li Z, Li Y, Jiang Q. Variables associated with self-reported anxiety and depression symptoms in patients with chronic myeloid leukemia receiving tyrosine kinase inhibitor therapy. *Leuk Lymphoma*. 2021;62:640-648.
19. Lippert J, Burghaus R, Edginton A, et al. Open systems pharmacology community-an open access, open source, Open Science approach to modeling and simulation in pharmaceutical sciences. *CPT Pharmacometrics Syst Pharmacol*. 2019;8:878-882.
20. Wojtyniak J-G, Britz H, Selzer D, Schwab M, Lehr T. Data digitizing: accurate and precise data extraction for quantitative systems pharmacology and physiologically-based pharmacokinetic modeling. *CPT Pharmacometrics Syst Pharmacol*. 2020;9:322-331.
21. R Core Team. *R: A Language and Environment for Statistical Computing*. R Foundation for Statistical Computing; 2021.





22. Tsamandouras N, Rostami-Hodjegan A, Aarons L. Combining the “bottom up” and “top down” approaches in pharmacokinetic modelling: fitting PBPK models to observed clinical data. *Br J Clin Pharmacol*. 2015;79:48-55.
23. Vaidhyanathan S, Wang X, Crison J, et al. Bioequivalence comparison of pediatric Dasatinib formulations and elucidation of absorption mechanisms through integrated PBPK modeling. *J Pharm Sci*. 2019;108:741-749.
24. Willmann S, Thelen K, Becker C, Dressman JB, Lippert J. Mechanism-based prediction of particle size-dependent dissolution and absorption: cilostazol pharmacokinetics in dogs. *Eur J Pharm Biopharm*. 2010;76:83-94.
25. Tsume Y, Takeuchi S, Matsui K, Amidon GE, Amidon GL. In vitro dissolution methodology, mini-gastrointestinal simulator (mGIS), predicts better in vivo dissolution of a weak base drug, dasatinib. *Eur J Pharm Sci*. 2015;76:203-212.
26. National Center for Health Statistics. Third National Health and Nutrition Examination Survey (NHANES III). Tech. rep., Hyattsville, MD, 20782. 1997.
27. Valentin J. Basic anatomical and physiological data for use in radiological protection: reference values. *Ann ICRP*. 2002;32:1-277.
28. Schlender J. A report including the description of the physiology base of the Japanese population implemented in PK-Sim. Github website. [https://github.com/Open-Systems-Pharmacology/OSPSuite.Documentation/blob/master/Japanese\\_Population/Report.md](https://github.com/Open-Systems-Pharmacology/OSPSuite.Documentation/blob/master/Japanese_Population/Report.md). Accessed August 4, 2022.
29. Marok FZ, Wojtyniak JG, Fuhr LM, et al. A physiologically based pharmacokinetic model of ketoconazole and its metabolites as drug–drug interaction perpetrators. *Pharmaceutics*. 2023;15:15.
30. Hanke N, Frechen S, Moj D, et al. PBPK models for CYP3A4 and P-gp DDI prediction: a modeling network of rifampicin, Itraconazole, clarithromycin, midazolam, Alfentanil, and digoxin. *CPT Pharmacometrics Syst Pharmacol*. 2018;7:647-659.
31. Wojtyniak J-G, Selzer D, Schwab M, Lehr T. Physiologically based precision dosing approach for drug-drug-gene interactions: a simvastatin network analysis. *Clin Pharmacol Ther*. 2021;109:201-211.
32. Open Systems Pharmacology Suite Community. Open systems pharmacology suite manual. Github website. <https://raw.githubusercontent.com/Open-Systems-Pharmacology/OSPSuite.Documentation/master/Open-Systems-Pharmacology-Suite.pdf>. Accessed November 23, 2021.
33. Dong Z, Li J, Wu F, et al. Application of physiologically-based pharmacokinetic modeling to predict gastric pH-dependent drug-drug interactions for Weak Base drugs. *CPT Pharmacometrics Syst Pharmacol*. 2020;9:456-465.
34. Okada M, Yao T, Sakurai T, et al. A comparative study of once-a-day morning and once-a-day bedtime administration of 40 mg famotidine in treating gastric ulcers. *Am J Gastroenterol*. 1992;87:1009-1013.
35. Decktor DL, Malcolm Robinson SG. Comparative effects of liquid antacids on esophageal and gastric pH in patients with heartburn. *Am J Ther*. 1995;2:481-486.
36. Dallmann A, Solodenko J, Wendl T, Frechen S. Building and evaluation of a PBPK model for erythromycin in healthy adults. Github website. [https://github.com/Open-Systems-Pharmacology/OSP-PBPK-Model-Library/blob/master/Erythromycin/Erythromycin\\_evaluation\\_report.pdf](https://github.com/Open-Systems-Pharmacology/OSP-PBPK-Model-Library/blob/master/Erythromycin/Erythromycin_evaluation_report.pdf). Accessed October 18, 2022.
37. Eriksson J, Solodenko J. Building and evaluation of a PBPK model for fluconazole in healthy adults. Github website. [https://github.com/Open-Systems-Pharmacology/OSP-PBPK-Model-Library/blob/master/Fluconazole/fluconazole\\_evaluation\\_report.pdf](https://github.com/Open-Systems-Pharmacology/OSP-PBPK-Model-Library/blob/master/Fluconazole/fluconazole_evaluation_report.pdf). Accessed August 17, 2023.
38. Britz H, Hanke N, Volz AK, et al. Physiologically-based pharmacokinetic models for CYP1A2 drug–drug interaction prediction: a modeling network of fluvoxamine, theophylline, caffeine, rifampicin, and midazolam. *CPT Pharmacometrics Syst Pharmacol*. 2019;8:296-307.
39. Fuhr LM, Marok FZ, Fuhr U, Selzer D, Lehr T. Physiologically based pharmacokinetic modeling of bergamottin and 6,7-dihydroxybergamottin to describe CYP3A4 mediated grapefruit-drug interactions. *Clin Pharmacol Ther*. 2023;114:470-482.
40. Li X, Frechen S, Moj D, et al. A physiologically based pharmacokinetic model of Voriconazole integrating time-dependent inhibition of CYP3A4, genetic polymorphisms of CYP2C19 and predictions of drug–drug interactions. *Clin Pharmacokinet*. 2020;59:781-808.
41. Fuhr LM, Marok FZ, Hanke N, Selzer D, Lehr T. Pharmacokinetics of the CYP3A4 and CYP2B6 inducer carbamazepine and its drug-drug interaction potential: a physiologically based pharmacokinetic modeling approach. *Pharmaceutics*. 2021;13:1-21.
42. Wendl T, Frechen S, Solodenko J, Dallmann A. Building and evaluation of a PBPK model for Efavirenz in healthy adults. Github website. [https://github.com/Open-Systems-Pharmacology/OSP-PBPK-Model-Library/blob/master/Efavirenz/efavirenz\\_evaluation\\_report.pdf](https://github.com/Open-Systems-Pharmacology/OSP-PBPK-Model-Library/blob/master/Efavirenz/efavirenz_evaluation_report.pdf). Accessed 18 October 2022.
43. Willmann S, Schmitt W, Keldenich J, Lippert J, Dressman JB. A physiological model for the estimation of the fraction dose absorbed in humans. *J Med Chem*. 2004;47:4022-4031.
44. Levêque D, Becker G, Bilger K, Natarajan-Amé S. Clinical pharmacokinetics and pharmacodynamics of Dasatinib. *Clin Pharmacokinet*. 2020;59:849-856.
45. Hiwase DK, Saunders V, Hewett D, et al. Dasatinib cellular uptake and efflux in chronic myeloid leukemia cells: therapeutic implications. *Clin Cancer Res*. 2008;14:3881-3888.
46. Kamath AV, Wang J, Lee FY, Marathe PH. Preclinical pharmacokinetics and in vitro metabolism of dasatinib (BMS-354825): a potent oral multi-targeted kinase inhibitor against SRC and BCR-ABL. *Cancer Chemother Pharmacol*. 2008;61:365-376.
47. Wang X, Roy A, Hochhaus A, Kantarjian HM, Chen T-T, Shah NP. Differential effects of dosing regimen on the safety and efficacy of dasatinib: retrospective exposure-response analysis of a phase III study. *Clin Pharm*. 2013;5:85-97.
48. Monés J, Carrio I, Sainz S, et al. Gastric emptying of two radio-labelled antacids with simultaneous monitoring of gastric pH. *Eur J Nucl Med*. 1995;22:1123-1128.
49. Jones MP, Shah D, Ebert CC. Effects of rabeprazole sodium on gastric emptying, electrogastrography, and fullness. *Dig Dis Sci*. 2003;48:69-73.
50. Anjiki H, Sanaka M, Kuyama Y. Dual effects of rabeprazole on solid-phase gastric emptying assessed by the <sup>13</sup>C-octanoate breath test. *Digestion*. 2005;72:189-194.
51. Patel D, Bertz R, Ren S, Boulton DW, Någård M. A systematic review of gastric acid-reducing agent-mediated drug–drug interactions with orally administered medications. *Clin Pharmacokinet*. 2020;59:447-462.

52. Wojnowski L, Kamdem LK. Clinical implications of CYP3A polymorphisms. *Expert Opin Drug Metab Toxicol*. 2006;2:171-182.
53. Jia G, Ren C, Wang H, Fan C. Prediction of drug–drug interactions between roflumilast and CYP3A4/1A2 perpetrators using a physiologically-based pharmacokinetic (PBPK) approach. *BMC Pharmacol Toxicol*. 2024;25:4.
54. Loer HLH, Feick D, Rüdesheim S, et al. Physiologically based pharmacokinetic modeling of tacrolimus for food-drug and CYP3A drug–drug-gene interaction predictions. *CPT Pharmacometrics Syst Pharmacol*. 2023;12:724-738.
55. Les Laboratoires Servier. Servier Medical Art. <https://smart.servier.com>. Accessed July 10, 2023.
56. Guest EJ, Aarons L, Houston JB, Rostami-Hodjegan A, Galetin A. Critique of the two-fold measure of prediction success for ratios: application for the assessment of drug-drug interactions. *Drug Metab Dispos*. 2011;39:170-173.

## SUPPORTING INFORMATION

Additional supporting information can be found online in the Supporting Information section at the end of this article.

**How to cite this article:** Kovar C, Loer HLH, Rüdesheim S, et al. A physiologically-based pharmacokinetic precision dosing approach to manage dasatinib drug–drug interactions. *CPT Pharmacometrics Syst Pharmacol*. 2024;13:1144-1159. doi:[10.1002/psp4.13146](https://doi.org/10.1002/psp4.13146)

## 4.2 PROJECT II – PHYSIOLOGICALLY BASED PHARMACOKINETIC MODELING OF IMATINIB

### 4.2.1 Publication

Loer, H. L. H., Kovar, C., Rüdesheim, S., Marok, F. Z., Fuhr, L. M., Selzer, D., Schwab, M., & Lehr, T. (2024). Physiologically based pharmacokinetic modeling of imatinib and N-desmethyl imatinib for drug-drug interaction predictions. *CPT: pharmacometrics & systems pharmacology*, 13(6), 926–940. DOI: [10.1002/psp4.13127](https://doi.org/10.1002/psp4.13127) [174].

### 4.2.2 Author Contributions

Author contributions according to the [CRediT](#) [1]:

Helena Leonie Hanae Loer	Conceptualization, Investigation, Visualization, Writing – Original Draft, Writing – Review & Editing
Christina Kovar	Refer to <i>Contribution Report</i> (p. <a href="#">vii</a> )
Simeon Rüdesheim	Conceptualization, Writing – Review & Editing
Fatima Zahra Marok	Conceptualization
Laura Maria Fuhr	Conceptualization
Dominik Selzer	Writing – Review & Editing
Matthias Schwab	Writing – Review & Editing, Funding Acquisition
Thorsten Lehr	Conceptualization, Writing – Review & Editing, Funding Acquisition

### 4.2.3 Copyright

This is an open access article under the terms of CC BY-NC 4.0 (<https://creativecommons.org/licenses/by-nc-nd/4.0/>), which permits use and distribution in any medium, provided the original work is properly cited, the use is non-commercial and no modifications or adaptations are made. © 2024 The Authors. *CPT: Pharmacometrics & Systems Pharmacology* published by Wiley Periodicals LLC on behalf of American Society for Clinical Pharmacology and Therapeutics.

Received: 30 December 2023 | Revised: 20 February 2024 | Accepted: 5 March 2024

DOI: [10.1002/psp4.13127](https://doi.org/10.1002/psp4.13127)

## ARTICLE

# Physiologically based pharmacokinetic modeling of imatinib and *N*-desmethyl imatinib for drug–drug interaction predictions

Helena Leonie Hanae Loer<sup>1</sup> | Christina Kovar<sup>1,2</sup> | Simeon Rüdesheim<sup>1,2</sup> |  
Fatima Zahra Marok<sup>1</sup> | Laura Maria Fuhr<sup>1</sup> | Dominik Selzer<sup>1</sup> |  
Matthias Schwab<sup>2,3,4</sup> | Thorsten Lehr<sup>1</sup>

<sup>1</sup>Clinical Pharmacy, Saarland University, Saarbrücken, Germany

<sup>2</sup>Dr. Margarete Fischer-Bosch-Institute of Clinical Pharmacology, Stuttgart, Germany

<sup>3</sup>Departments of Clinical Pharmacology, and Pharmacy and Biochemistry, University of Tübingen, Tübingen, Germany

<sup>4</sup>Cluster of Excellence iFIT (EXC2180), Image-Guided and Functionally Instructed Tumor Therapies, University of Tübingen, Tübingen, Germany

**Correspondence**

Thorsten Lehr, Clinical Pharmacy, Saarland University, Campus C4 3, 66123 Saarbrücken, Germany.  
Email: [thorsten.lehr@mx.uni-saarland.de](mailto:thorsten.lehr@mx.uni-saarland.de)

**Abstract**

The first-generation tyrosine kinase inhibitor imatinib has revolutionized the development of targeted cancer therapy and remains among the frontline treatments, for example, against chronic myeloid leukemia. As a substrate of cytochrome P450 (CYP) 2C8, CYP3A4, and various transporters, imatinib is highly susceptible to drug–drug interactions (DDIs) when co-administered with corresponding perpetrator drugs. Additionally, imatinib and its main metabolite *N*-desmethyl imatinib (NDMI) act as inhibitors of CYP2C8, CYP2D6, and CYP3A4 affecting their own metabolism as well as the exposure of co-medications. This work presents the development of a parent–metabolite whole-body physiologically based pharmacokinetic (PBPK) model for imatinib and NDMI used for the investigation and prediction of different DDI scenarios centered around imatinib as both a victim and perpetrator drug. Model development was performed in PK-Sim® using a total of 60 plasma concentration–time profiles of imatinib and NDMI in healthy subjects and cancer patients. Metabolism of both compounds was integrated via CYP2C8 and CYP3A4, with imatinib additionally transported via P-glycoprotein. The subsequently developed DDI network demonstrated good predictive performance. DDIs involving imatinib and NDMI were simulated with perpetrator drugs rifampicin, ketoconazole, and gemfibrozil as well as victim drugs simvastatin and metoprolol. Overall, 12/12 predicted DDI area under the curve determined between first and last plasma concentration measurements ( $AUC_{last}$ ) ratios and 12/12 predicted DDI maximum plasma concentration ( $C_{max}$ ) ratios were within twofold of the respective observed ratios. Potential applications of the final model include model-informed drug development or the support of model-informed precision dosing.

This is an open access article under the terms of the [Creative Commons Attribution-NonCommercial](https://creativecommons.org/licenses/by-nc/4.0/) License, which permits use, distribution and reproduction in any medium, provided the original work is properly cited and is not used for commercial purposes.

© 2024 The Authors. *CPT: Pharmacometrics & Systems Pharmacology* published by Wiley Periodicals LLC on behalf of American Society for Clinical Pharmacology and Therapeutics.

### Study Highlights

#### WHAT IS THE CURRENT KNOWLEDGE ON THE TOPIC?

As a victim drug of cytochrome P450 (CYP) 2C8, CYP3A4, and P-glycoprotein, imatinib is highly susceptible to drug–drug interactions (DDIs). Additionally, acting as a perpetrator, imatinib affects its own metabolism and the exposure of co-medications via inhibition of CYP2C8, CYP2D6, and CYP3A4.

#### WHAT QUESTION DID THIS STUDY ADDRESS?

This study presents the development of a new whole-body physiologically based pharmacokinetic model of imatinib and its main metabolite *N*-desmethyl imatinib (NDMI). The model was applied to describe and predict the role of imatinib and NDMI as victims and perpetrators within a newly established CYP2C8/CYP2D6/CYP3A4/P-glycoprotein-DDI network.

#### WHAT DOES THIS STUDY ADD TO OUR KNOWLEDGE?

The DDI network helps to evaluate the effects of co-medication on the pharmacokinetics of imatinib/NDMI and the inhibitory potential of imatinib/NDMI, highlighting the importance of considering imatinib as both victim and perpetrator in clinical practice.

#### HOW MIGHT THIS CHANGE DRUG DISCOVERY, DEVELOPMENT, AND/OR THERAPEUTICS?

The model can be used to support model-informed drug development and to improve clinical safety and efficacy of imatinib and co-medications through model-based precision dosing.

## INTRODUCTION

In 2001, approval of the tyrosine kinase inhibitor (TKI) imatinib for the treatment of Philadelphia chromosome-positive chronic myeloid leukemia (CML) revolutionized not only the therapy of CML, but also the development of targeted cancer therapy in general.<sup>1</sup> Imatinib selectively inhibits the *BCR-ABL* oncoprotein encoded by the Philadelphia chromosome, suppressing its constitutive tyrosine kinase activity and associated uncontrolled proliferation.<sup>2</sup> However, resistance to imatinib, primarily due to mutations in the *BCR-ABL* oncogene and other factors, necessitated the development of subsequent generations of TKIs.<sup>3</sup> Despite this, imatinib remains one of the front-line therapies for CML and has been approved for additional indications, such as acute lymphoblastic leukemia and gastrointestinal stromal tumors (GISTs).<sup>4</sup>

As a Biopharmaceutics Classification System class I drug, imatinib demonstrates high intestinal permeability and solubility.<sup>5</sup> When administered orally, it is completely absorbed, achieving an absolute bioavailability exceeding 97%.<sup>6</sup> Imatinib is primarily metabolized via cytochrome P450 (CYP) enzymes 2C8 and 3A4,<sup>7</sup> with its main metabolite, *N*-desmethyl imatinib (NDMI), accounting for 10%–15% of the overall drug level. NDMI's potency against *BCR-ABL* is approximately three times lower than that of imatinib itself.<sup>8,9</sup> Furthermore, imatinib has been

identified as a substrate of numerous influx and efflux transporters in vitro, such as organic cation transporter (OCT) 1, OCTN2, organic-anion-transporting polypeptide (OATP) 1A2, OATP1B3, breast cancer resistance protein (BCRP), and P-glycoprotein (P-gp).<sup>10–12</sup> Following oral administration, 67% and 13% of a single dose (SD) of imatinib are excreted as imatinib-related products in feces and urine, respectively, over a period of 7 days.<sup>13</sup>

Imatinib and its metabolite NDMI are highly susceptible to drug–drug interactions (DDIs), impacting their own metabolism and altering the exposure of co-administered drugs via inhibition of CYP2C8, CYP2D6, and CYP3A4.<sup>14,15</sup> For instance, pretreatment with imatinib resulted in a 2.6-fold increase in the area under the curve (AUC) of the active metabolite of simvastatin, which is formed by CYP3A4.<sup>16</sup> Consequently, the United States Food and Drug Administration (FDA) lists imatinib as a moderate inhibitor of CYP3A4.<sup>17</sup> However, imatinib does not only act as a perpetrator but also as a victim drug in DDI scenarios. Here, perpetrator drugs affecting imatinib's and NDMI's metabolism via CYP2C8 and CYP3A4 are of particular clinical importance. For example, concomitant administration with the antifungal agent ketoconazole, an inhibitor, increases imatinib exposure by 40%. In contrast, pretreatment with the antibiotic agent rifampicin, an inducer, leads to a 74% reduction in AUC of imatinib.<sup>18,19</sup> Given the typical



prescription of five to eight drugs per patient in oncology, these interactions present a substantial challenge in terms of therapeutic management during imatinib treatment. A co-medication review of over 4500 patients receiving imatinib identified potential DDIs associated with a decrease in imatinib effectiveness in 43% and an increase in toxicity in 68% of cases.<sup>20</sup>

Given these complexities, there is a critical need to understand the pharmacokinetics (PK) of imatinib and NDMI, especially regarding their interaction potential. This understanding is vital to enhance the safety and efficacy of imatinib therapy. Therefore, this study aimed to develop a whole-body physiologically based pharmacokinetic (PBPK) model for imatinib and its main metabolite NDMI. Such models are exceptionally useful in investigating the PK of drugs, both independently and within DDI frameworks, as emphasized by the substantial number of PBPK studies submitted to regulatory agencies concentrating on DDI research questions.<sup>21</sup> Furthermore, the versatility of PBPK modeling, especially in integrating patient-specific demographic, physiological, pathophysiological, and pharmacogenetic data, makes it instrumental in facilitating model-based precision dosing strategies.<sup>22</sup> Utilizing the developed imatinib model, this study further conducted predictions and analyses of various complex DDI scenarios, showcasing imatinib as both a victim and perpetrator of such interactions. Numerous PBPK models of imatinib have been developed to explore various research inquiries.<sup>23–25</sup> However, our approach uniquely extends this body of work by providing a comprehensive whole-body PBPK model that incorporates imatinib's main metabolite NDMI, and examines imatinib as both a victim and a perpetrator drug in DDI scenarios. To promote widespread access and encourage further research, the finalized model files will be made available to the public at <http://models.clinicalpharmacy.me/>.

## METHODS

### Software

Development of the imatinib PBPK model, including parameter identification and local sensitivity analyses, was performed using PK-Sim® and MoBi® version 11.0 (Open Systems Pharmacology Suite, [www.open-systems-pharmacology.org](http://www.open-systems-pharmacology.org), 2022). Engauge Digitizer version 12.1 (M. Mitchell, <https://markummittchell.github.io/engauge-digitizer/>, 2019) was utilized for the digitization of published clinical study data according to Wojtyniak et al.<sup>26</sup> The R programming language version 4.2.3 (R Foundation for Statistical Computing, Vienna,

Austria, 2023) was used to generate plots and calculate PK parameters as well as quantitative model performance measures.

### Clinical study data

Plasma concentration–time profiles of imatinib and its main metabolite NDMI were gathered from published literature covering a wide dosing range of imatinib administered either intravenously or orally in SD and multiple dose (MD) studies. Once digitized, the profiles were systematically divided into a training and a test dataset for model development and model evaluation, respectively. The allocation of profiles was conducted in a deliberate, non-randomized fashion. The goal was to construct a training dataset that encompassed a diverse range of dosages and administration forms, ensuring each profile included a wide array of sampling time points over an extended duration. Concurrently, the approach aimed to optimize the size of the test dataset, thereby enhancing its robustness for thorough model evaluation. Only profiles obtained from healthy individuals were selected for the training dataset, whereas CML and GIST patients were included in the test dataset.

### Physiologically based pharmacokinetic model building

Prior to building the imatinib parent–metabolite model, an extensive literature search was conducted regarding clinical study data and physicochemical parameters as well as information on the absorption, distribution, metabolism, and excretion (ADME) of imatinib and NDMI.

For model simulations, a representative virtual individual was created for each included study population based on the corresponding reported mean and mode data for age, sex, weight, height, body mass index, and ethnicity. If demographic information was missing or incomplete, a default individual was generated according to the population database provided in PK-Sim®. Relative expressions of relevant transporters and enzymes in the different organs were adopted from the expression database included in PK-Sim®. Tables S1 and S2 list the reference concentration in the respective organ of highest concentration as well as the relative expression profile for each implemented transporter/enzyme. To visually examine the influence of variation in demographic factors, plasma protein binding to  $\alpha$ 1-acid glycoprotein (AGP), as well as transporter and metabolizing enzyme abundances on the exposure of imatinib and NDMI, a virtual population of 1000 individuals was established for each study population. If no minimum

and maximum demographic values were provided, an age range of 20–50 years was assumed. Geometric standard deviations applied to the incorporated transporter/enzyme concentrations for the population sampling process are presented in Table S1.

During the parameter identification process, unknown parameter values not reported in the literature or parameters involved in PK-Sim®'s permeability and partition quantitative structure–activity relationship (QSAR) models were fitted using the training dataset. Following oral administration, the release of imatinib was incorporated via a Weibull function (Equation S1). Depending on the information available in the literature, transport and metabolic processes were implemented as either Michaelis–Menten (MM) (Equation S2) or first-order kinetics. The role of relevant enzymes in imatinib metabolism was informed by including published in vitro data, detailing the proportional contribution of each relevant enzyme to the total clearance of imatinib, thereby informing the PBPK model with more precise metabolic pathway information.

### Physiologically based pharmacokinetic model evaluation

The imatinib parent–metabolite model was evaluated both graphically and statistically. First, predicted plasma concentration–time profiles of imatinib and NDMI were plotted alongside corresponding observed data. Goodness-of-fit plots were generated to assess the deviation of predicted versus observed plasma concentrations, AUC determined between first and last plasma concentration measurements ( $AUC_{last}$ ), and maximum plasma concentration ( $C_{max}$ ) values for each profile. A twofold difference from observed values was set as the prediction success threshold. The statistical analysis covered the calculation of mean relative deviations (MRDs) for predicted concentration–time points (Equation 1) and geometric mean fold errors for predicted  $AUC_{last}$  and  $C_{max}$  values (Equation 2).

$$MRD = 10^x; x = \sqrt{\frac{\sum_{i=1}^k (\log_{10} \hat{c}_i - \log_{10} c_i)^2}{k}} \quad (1)$$

where  $c_i$  =  $i$ -th observed concentration,  $\hat{c}_i$  = predicted concentration corresponding to the  $i$ -th observed concentration, and  $k$  = number of observed values.

$$GMFE = 10^x; x = \frac{\sum_{i=1}^m \left| \log_{10} \left( \frac{\hat{p}_i}{p_i} \right) \right|}{m} \quad (2)$$

where  $p_i$  = observed  $AUC_{last}$  or  $C_{max}$  value of study  $i$ ,  $\hat{p}_i$  = corresponding predicted  $AUC_{last}$  or  $C_{max}$  value of study  $i$ , and  $m$  = number of studies.

Finally, local sensitivity analyses were conducted for imatinib and NDMI, which are described in Section S2.7.1.

### Drug–drug interaction network modeling

To investigate the role of imatinib and NDMI acting as either victims or perpetrators in DDI scenarios, the developed model was coupled with previously published PBPK models of rifampicin, ketoconazole, gemfibrozil, simvastatin, and metoprolol.<sup>27–31</sup> Relevant interaction types, including induction, competitive inhibition, non-competitive inhibition, and mechanism-based inactivation, were incorporated as described in the Open Systems Pharmacology Suite manual,<sup>32</sup> with the corresponding interaction parameters adopted from the literature.

The developed DDI network was graphically evaluated by comparing predicted with observed plasma concentration–time profiles of each victim drug with and without co-administration of the respective perpetrator drug. Predicted and observed  $AUC_{last}$  and  $C_{max}$  ratios were calculated for each DDI scenario according to Equation 3 and compared by applying the limits proposed by Guest et al.<sup>33</sup> to determine prediction accuracy (including 20% variability).

$$DDI \text{ PK parameter ratio} = \frac{PK \text{ parameter}_{DDI}}{PK \text{ parameter}_{Control}} \quad (3)$$

where  $PK \text{ parameter} = AUC_{last}$  or  $C_{max}$ ,  $PK \text{ parameter}_{DDI} = AUC_{last}$  or  $C_{max}$  of victim drug with perpetrator co-administration, and  $PK \text{ parameter}_{Control} = AUC_{last}$  or  $C_{max}$  of victim drug control.

Quantitative evaluation was performed by calculating GMFE values (Equation 2) for all predicted DDI  $AUC_{last}$  and  $C_{max}$  ratios.

## RESULTS

### Physiologically based pharmacokinetic model building and evaluation

The imatinib parent–metabolite model was developed using 24 clinical studies providing a total of 42 and 18 plasma concentration–time profiles of imatinib and NDMI, respectively. The profiles were allocated to either the training ( $n=8$ ) or the test ( $n=52$ ) dataset. Of these 60 profiles, 40 were collected in healthy subjects, while 20 were derived from CML and GIST patients. Given no apparent difference between plasma profiles of healthy subjects and patients, the developed PBPK model was applied to CML and GIST patients without modifications

to the drug-dependent parameters of imatinib and NDMI or the physiological parameters of the simulated virtual individuals. Routes of administration included intravenous dosing of imatinib via infusion (100 mg, SD) and oral intake as tablet or capsule (25–750 mg, SD and MD). Information on all profiles and study populations used is listed in Table S3.

Figure 1 provides a schematic representation of the transport and metabolic processes implemented in the model. Imatinib metabolism via CYP2C8 and CYP3A4 was incorporated in the model via MM kinetics, accounting for 67% and 33% of NDMI formation, respectively. The model further integrated the transformation of imatinib into unspecified metabolites through CYP3A4, following first-order kinetics. Additionally, P-gp was incorporated as a transport protein for imatinib, with its function modeled using MM kinetics. NDMI metabolism was implemented via CYP2C8, CYP3A4, and a nonspecific first-order hepatic clearance process. The effect of genetic polymorphisms on the incorporated transporters and enzymes was not accounted for in the model due to a lack of studies stratifying their cohorts by genotype or phenotype.

During model building, lipophilicities of imatinib and NDMI which are crucial parameters in several key QSAR equations were optimized. This fitting resulted in values within the reference range for imatinib and approximately one logarithmic unit lower than the reference for NDMI.

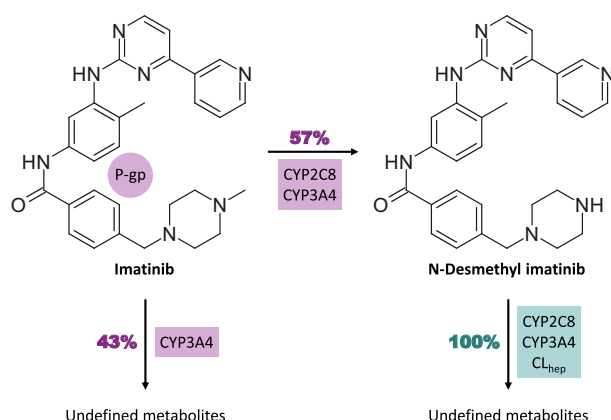


**FIGURE 1** Schematic overview of the processes incorporated in the developed imatinib parent-metabolite model. Following administration of a single dose of imatinib, 57% of modeled imatinib metabolism leads to the formation of *N*-desmethyl imatinib via CYP2C8 and CYP3A4, while the remaining pathway involves the conversion of imatinib to undefined metabolites via CYP3A4. In addition, transport via P-gp was included for imatinib. For the metabolism of *N*-desmethyl imatinib, the model incorporates CYP2C8, CYP3A4, and a nonspecific hepatic clearance process. CL<sub>hep</sub>: hepatic clearance, CYP: cytochrome P450, P-gp: P-glycoprotein.

Parameters for first-order clearance processes were also included in the parameter optimization procedure. For biotransformation steps modeled as MM kinetics, MM constants ( $K_M$ ) were adopted from the literature, while catalytic rate constants ( $k_{cat}$ ) were fitted within one magnitude of reported values. Conversely, both  $K_M$  and  $k_{cat}$  were optimized for the transport of imatinib via P-gp, as the  $K_M$  value could not be informed from the literature. In addition, (auto)inhibition was integrated using published data.<sup>14,34,35</sup> Here, for imatinib, mechanism-based inactivation of CYP3A4 was implemented. Moreover, competitive inhibition of CYP2C8, CYP2D6, P-gp, and BCRP was integrated. With respect to NDMI, competitive inhibition parameters of CYP2C8, CYP2D6, and CYP3A4 were informed via literature.<sup>14</sup> A Weibull function was applied to simulate the release of imatinib from both tablets and capsules, with parameters time to 50% dissolution and shape derived from a tablet dissolution profile of previous work according to Langenbucher et al.<sup>36,37</sup> The final model parameters for imatinib and NDMI are provided in Table S4.

The developed imatinib PBPK model demonstrated good performance in describing (training dataset) and predicting (test dataset) plasma concentration–time profiles of imatinib and NDMI following intravenous and oral administration of imatinib to healthy subjects and patients. Figure 2 presents a representative selection of imatinib/NDMI population predictions compared to corresponding observed data. Linear and semilogarithmic plots of all model predictions including observed data are provided in Sections S2.1–S2.3.

Goodness-of-fit plots of predicted versus observed plasma concentrations as well as AUC<sub>last</sub> and  $C_{max}$  values separated by dataset are shown in Figure 3. Overall, 92% of predicted imatinib and NDMI concentration measurements as well as 98% of predicted AUC<sub>last</sub> and 98% of predicted  $C_{max}$  values were within twofold of corresponding observed data. Moreover, statistical model evaluation resulted in a mean (range) MRD of predicted plasma concentrations of 1.46 (1.07–2.81) along with mean (range) GMFE<sub>AUClast</sub> and GMFE<sub>Cmax</sub> values of 1.28 (1.00–2.40) and 1.26 (1.00–2.08), respectively. Values for MRD, AUC<sub>last</sub>, and  $C_{max}$  of all profiles are listed in Tables S5 and S6.

Local sensitivity analyses were performed based on simulated steady-state conditions following oral administration of 400 mg imatinib once daily for 28 days. The steady-state AUC of imatinib and NDMI exhibited the greatest sensitivity to changes in the acid dissociation constant of the amino group within the piperazine ring and the unbound fraction ( $f_u$ ), respectively. Both parameters were adopted from the literature. Of note, given the proximity of the model parameter for the acid dissociation constant (7.84) to the physiological pH of 7.4, an increase of 10% causes only a small change in imatinib and NDMI

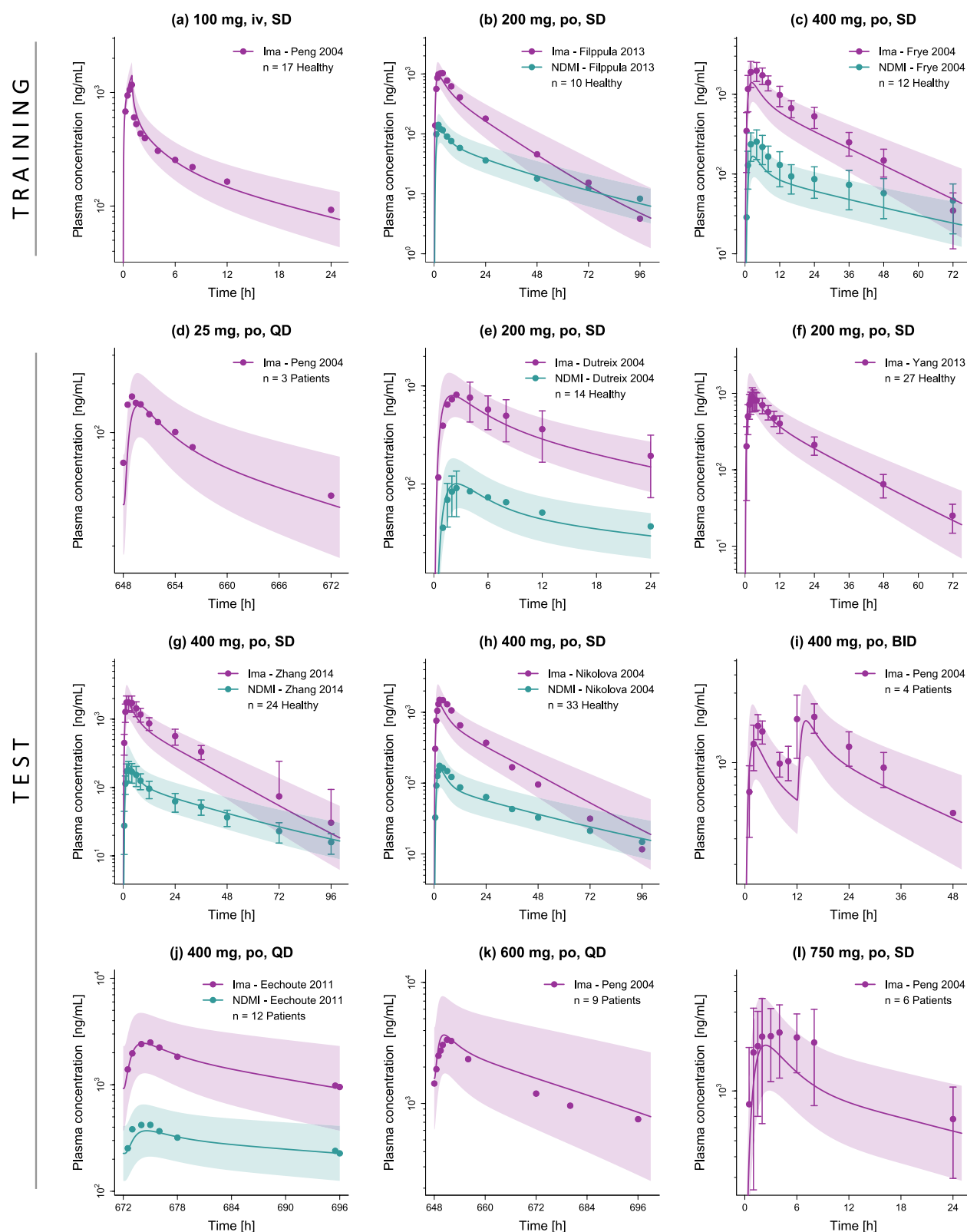


**FIGURE 2** Predicted compared to observed plasma concentration–time profiles of imatinib and NDMI of the training (a–c) and test (d–l) dataset. Solid lines and ribbons represent population predictions ( $n = 1000$ ; geometric mean and geometric standard deviation), while corresponding observed data are shown as dots ( $\pm$  standard deviation, if available).<sup>6,18,38,43,47–51</sup> Detailed information on all investigated profiles is provided in [Table S3](#). BID: twice daily, Healthy: healthy subjects, Ima: imatinib, iv: intravenous,  $n$ : number of study participants, NDMI: *N*-desmethyl imatinib, Patients: cancer patients, po: oral, QD: once daily, SD: single dose.



AUC values, while a reduction of 10% is associated with a large decrease in exposure. Section S2.7.2 provides a detailed evaluation of the sensitivity analyses.

## Drug–drug interaction modeling

The DDI network centered around imatinib as a victim and perpetrator drug was developed using five DDI studies. In total, three studies investigated the influence of perpetrator co-administration on the exposure of imatinib and NDMI. Here, one study examined pretreatment with the competitive CYP2C8/CYP3A4/P-gp inhibitor and inducer rifampicin, while a second study addressed co-treatment with the competitive CYP3A4/P-gp inhibitor and non-competitive CYP2C8 inhibitor ketoconazole.<sup>18,19</sup> Finally, one study analyzed the effect of pretreatment with the CYP2C8 mechanism-based inactivator gemfibrozil.<sup>38</sup>

Moreover, DDI studies assessing the influence of imatinib pretreatment on the PK of simvastatin and metoprolol as well as their active metabolites were available, with interactions predominantly caused by CYP3A4 mechanism-based inactivation and CYP2D6 competitive inhibition, respectively.<sup>15,16</sup> In the case of metoprolol, a drug–drug–gene interaction (DDGI) study was included in which the study population was additionally stratified into CYP2D6 normal metabolizers (NMs) and intermediate metabolizers (IMs). Here, the same  $K_M$  value was used for both study cohorts, while phenotype-specific  $k_{cat}$  values were applied.<sup>28</sup> Because most NMs and IMs were  $*1/*10$  and  $*10/*10$  genotypes, respectively,  $k_{cat}$  values equivalent to 64% and 19% of the wildtype  $k_{cat}$  were included in the DDI model. Figure 4 shows a schematic overview of the modeled DDI network, depicting the respective main interaction mechanisms. Detailed information on the DDI studies used and model parameters of each DDI partner are available in Sections S3.1–S3.2.

Predicted versus observed plasma concentration–time profiles of each victim drug with and without co-administration of the respective perpetrator drug are displayed in Figure 5. Table 1 presents the predicted versus observed impact of each perpetrator on the respective victim, stating the exposure (AUC) during perpetrator co-administration relative to the control exposure. Furthermore, predicted versus observed DDI  $AUC_{last}$  and  $C_{max}$  ratios are shown in Figure 6. In total, 11/12 of predicted DDI  $AUC_{last}$  and 10/12 of  $C_{max}$  ratios were within the limits proposed by Guest et al.<sup>33</sup> with mean (range) GMFE values of 1.21 (1.02–1.65) and 1.23 (1.01–1.87), respectively. Predicted and observed DDI profiles (linear and semilogarithmic) and corresponding DDI ratios are provided in Sections S3.3–S3.6.

## DISCUSSION

In the present work, a parent–metabolite whole-body PBPK model for imatinib was developed demonstrating its capability to accurately describe and predict plasma concentration–time profiles for both imatinib and its main metabolite NDMI. The model is robust across a wide dosing range of intravenously and orally administered imatinib (25–750 mg, SD and MD studies) in both healthy subjects and cancer patients. PK differences between these populations are documented in the literature and were investigated during model building. For instance, a 2–5-fold increase in AGP plasma levels is reported for CML patients compared to healthy subjects, potentially influencing imatinib  $f_u$ .<sup>39</sup> However, since elevated AGP levels were also observed to normalize during imatinib treatment, no CML-specific  $f_u$  value was incorporated in the model.<sup>40</sup> Overall, imatinib clearance in CML patients appears to depend on both the disease stage and the duration of imatinib use, while in GIST patients, for example, changes in liver function due to hepatic metastases or surgery have been reported.<sup>40</sup> Given the frequent unavailability of detailed physiological data for cancer patients, mechanistic modeling to account for these differences was constrained. Therefore, our approach remained focused on leveraging broadly applicable physiological parameters. Moreover, given the performance of the unmodified model in both populations (mean MRD: healthy subjects 1.39 vs. patients 1.59), no population-specific adjustments were made to minimize the model's complexity. The final PBPK model was further applied to predict different DDI scenarios involving imatinib and NDMI acting as both victims and perpetrators.

A key constraint of the model lies in the limitations of current knowledge as well as published clinical and in vitro data. For instance, consistent with literature data, when simulating an oral administration of 400 mg imatinib, the entire dose is absorbed.<sup>6</sup> However, at 83%, the predicted total bioavailability was moderately lower than the reported literature value of more than 97%.<sup>6</sup> One potential explanation for this discrepancy may lie in the in vivo deconjugation of imatinib glucuronides by gut microbes,<sup>41</sup> a process integral to the enterohepatic circulation (EHC). This phenomenon could lead to the reabsorption of imatinib, influencing its overall bioavailability. Although the model accounts for the EHC of imatinib with a modeled EHC fraction of 1, it does not incorporate the sequential formation and breakdown of imatinib glucuronides. This omission is primarily due to the complexity of these processes and the lack of comprehensive data regarding the conjugation and deconjugation of imatinib, as well as the PK of its various glucuronide forms.

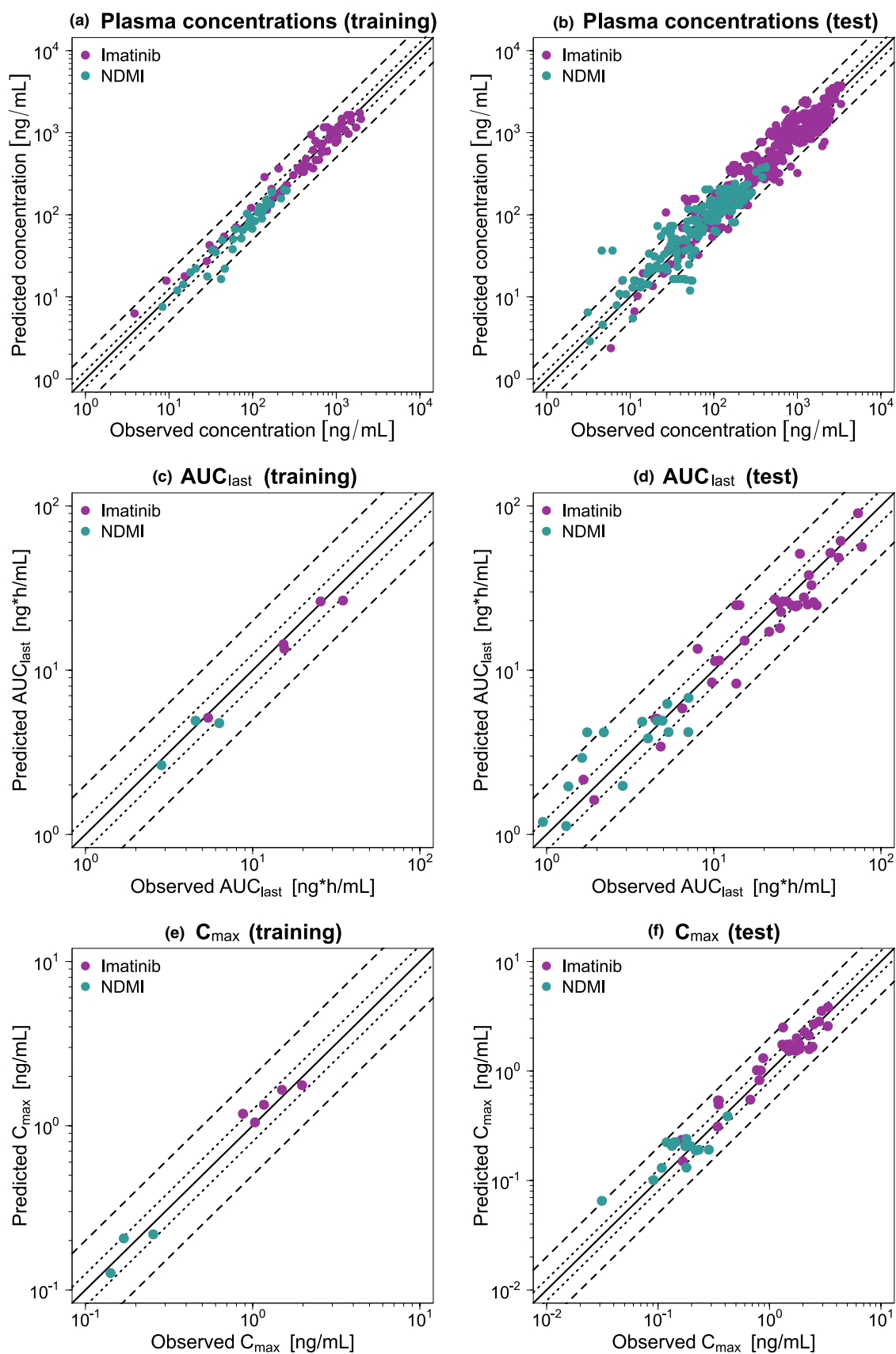


**FIGURE 3** Goodness-of-fit plots of the final imatinib parent–metabolite model. Stratified by training (left column) and test dataset (right column), predicted plasma concentration measurements (a, b) as well as  $AUC_{last}$  (c, d) and  $C_{max}$  (e, f) values are plotted against corresponding observed data. The solid line represents the line of identity, while dotted lines indicate 1.25-fold, and dashed lines twofold deviation from the respective observed value. Detailed information on all investigated profiles is provided in Table S3.  $AUC_{last}$ : area under the curve determined between first and last plasma concentration measurements,  $C_{max}$ : maximum plasma concentration, NDMI: *N*-desmethyl imatinib.

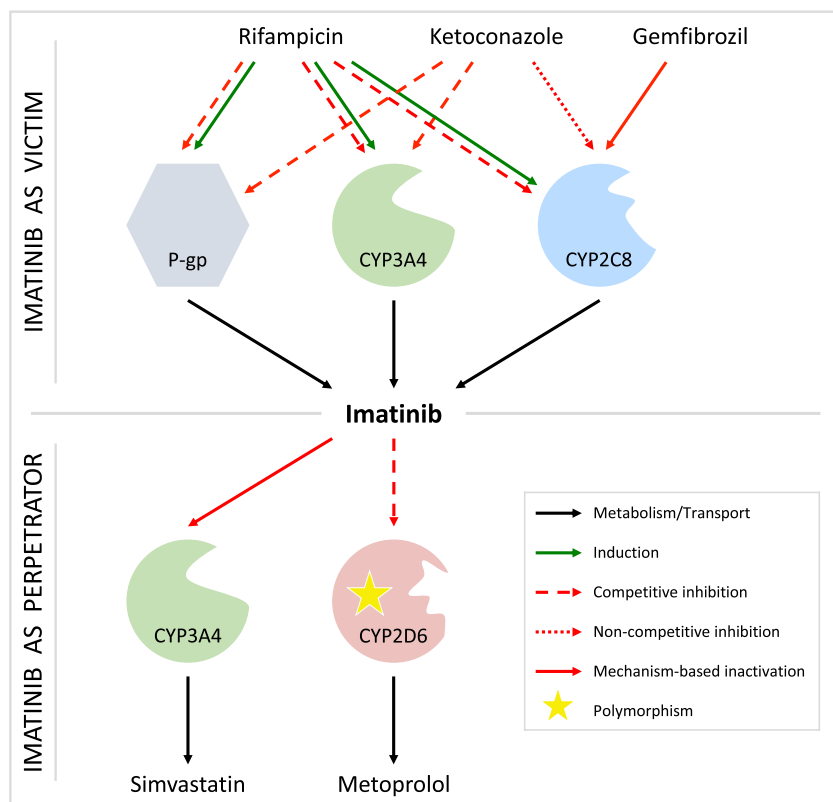
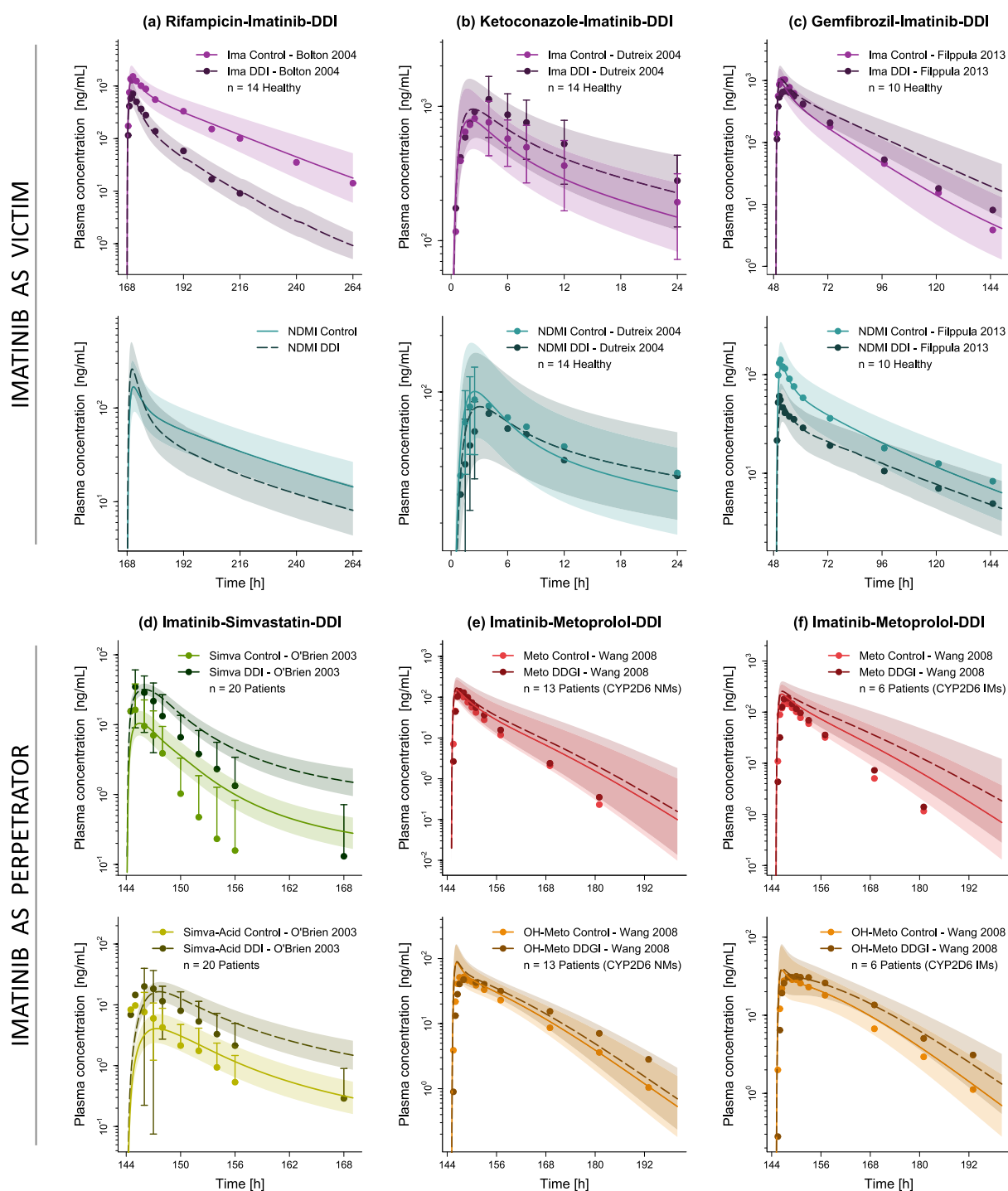


**FIGURE 4** Schematic overview of the modeled drug–drug interaction network. The network covers the effects of rifampicin, ketoconazole, and gemfibrozil on the pharmacokinetics of imatinib as a victim, as well as the impact of imatinib as a perpetrator on the plasma levels of simvastatin and metoprolol. The respective main mechanisms of interactions are presented. For simplicity, the interaction effects of and on the corresponding metabolites, such as *N*-desmethyl imatinib, are summarized under the name of the parent drug. CYP: cytochrome P450, P-gp: P-glycoprotein.

Furthermore, imatinib has been identified as a substrate of several influx and efflux transporters *in vitro*, such as OCT1, OCTN2, OATP1A2, OATP1B3, BCRP, and P-gp,<sup>10–12</sup> potentially influencing ADME processes. However, the relevance of these transporters *in vivo* remains uncertain due to conflicting study results. In our model, P-gp was selected as the efflux transporter over BCRP, primarily because the data for P-gp were more consistent and reliable compared to that for BCRP. Incorporating P-gp into the model led to an increase in the predicted urinary excretion of unchanged imatinib, rising from under 2% to about 5% following SD oral administration. This adjustment brings the model's predictions more in line with the urinary excretion rates observed *in vivo*.<sup>37,42</sup> During model building, the incorporation of various influx transporters such as OCT1, OCTN2, OATP1A2, and OATP1B3 was tested. Despite considering the integration of these transporters into the model, we ultimately did not include them in the final model. This decision was based on the observation

that their inclusion did not markedly alter the base model's predictive performance or the simulated DDIs, with the total bioavailability consistently estimated around 83%. Furthermore, the data on transport parameters necessary to inform the model were limited and often conflicting. For example, while some studies identified OATP1A2 as a key transporter in imatinib uptake, evidence from pre-treatment with the OATP1A2 inhibitor rosuvastatin indicated no significant impact on imatinib's PK, adding to the ambiguity in these transporters' roles.<sup>43,44</sup>

Overall, as only one mean intravenous imatinib profile was available from the literature, additional intravenous studies would be of particular interest to further investigate the discrepancy between modeled and reported total bioavailability. Moreover, dedicated studies on the parameterization and quantification of transport processes would be of great value to allow for an even more precise simulation of imatinib's PK. However, as both oral and intravenous administration of imatinib and metabolism to

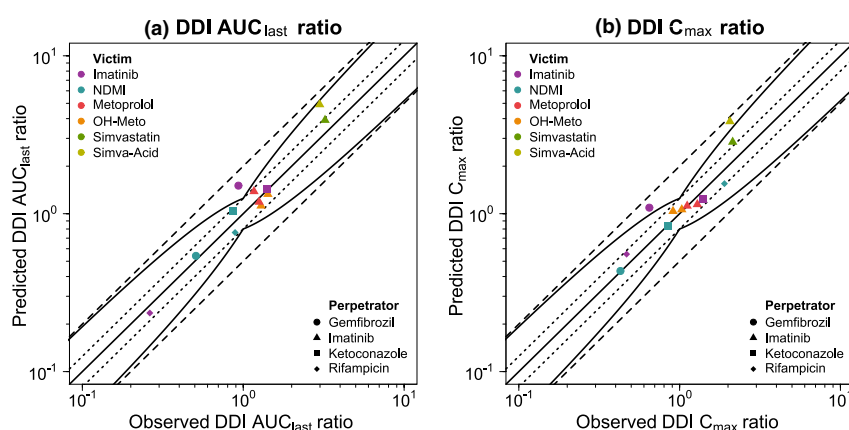


**FIGURE 5** Evaluation of the modeled drug–drug interaction network. Presented are predicted plasma concentration–time profiles of victim drugs imatinib (a–c), simvastatin (d), and metoprolol (e, f) without (Control) and with (DDI) co-administration of the respective perpetrator drug rifampicin (a), ketoconazole (b), gemfibrozil (c), or imatinib (d–f), alongside corresponding observed data.<sup>15,16,18,19,38</sup> Solid (Control) and dashed (DDI) lines and ribbons represent model population predictions ( $n=1000$ ; geometric mean and geometric standard deviation), while corresponding observed data are shown as dots ( $\pm$  standard deviation, if available). For the effect of rifampicin on NDMI, only DDI ratios were reported in the respective study (see Figure 6). Detailed information on all investigated DDI studies is provided in Table S8. CYP: cytochrome P450, DDI: drug–drug interaction, Healthy: healthy subjects, IM: intermediate metabolizer, Ima: imatinib, Meto: metoprolol,  $n$ : number of study participants, NDMI: *N*-desmethyl imatinib, NM: normal metabolizer, OH-Meto: hydroxymetoprolol, Patients: cancer patients, Simva: simvastatin, Simva-Acid: simvastatin hydroxy acid.



**TABLE 1** Predicted versus observed impact on the exposure of each victim drug upon perpetrator co-administration.

Victim	Perpetrator	Compound measured	DDI exposure <sup>a</sup> [%]		References
			Predicted	Observed	
Imatinib	Rifampicin	Imatinib	24	26	Bolton 2004 <sup>19</sup>
		NDMI	76	89	
Imatinib	Ketoconazole	Imatinib	144	140	Dutreix 2004 <sup>18</sup>
		NDMI	104	86	
Imatinib	Gemfibrozil	Imatinib	151	93	Filppula 2013 <sup>38</sup>
		NDMI	54	51	
Simvastatin	Imatinib	Simvastatin	391	322	O'Brien 2003 <sup>16</sup>
		Simva-Acid	491	299	
Metoprolol <sup>b</sup>	Imatinib	Metoprolol	119	126	Wang 2008 <sup>15</sup>
		OH-Meto	112	129	
Metoprolol <sup>c</sup>	Imatinib	Metoprolol	138	117	Wang 2008 <sup>15</sup>
		OH-Meto	133	142	

<sup>a</sup>Relative to the corresponding exposure without perpetrator co-administration.<sup>b</sup>CYP2D6 normal metabolizers.<sup>c</sup>CYP2D6 intermediate metabolizers, CYP: cytochrome P450, DDI: drug–drug interaction, NDMI: *N*-desmethyl imatinib, OH-Meto: hydroxymetoprolol, Simva-Acid: simvastatin hydroxy acid.**FIGURE 6** Evaluation of the modeled drug–drug interaction network. Predicted versus observed DDI  $AUC_{last}$  (a) and DDI  $C_{max}$  (b) ratios are shown with the solid line representing the line of identity, dotted lines indicating 1.25-fold, and dashed lines twofold deviation from the respective observed value. Curved lines mark the prediction success limits proposed by Guest et al.<sup>33</sup> including 20% variability. Detailed information on all investigated DDI studies is provided in Table S8.  $AUC_{last}$ : area under the curve determined between first and last plasma concentration measurements,  $C_{max}$ : maximum plasma concentration, DDI: drug–drug interaction, NDMI: *N*-desmethyl imatinib, OH-Meto: hydroxymetoprolol, Simva-Acid: simvastatin hydroxy acid.

NDMI were well described by the model, we consider hepatic clearance processes, and thus the fraction escaping first-pass liver metabolism, to be adequately represented in the model. Furthermore, the good prediction of mainly metabolic DDIs indicates a well-described relationship between fraction absorbed and fraction escaping gut wall metabolism.

In line with literature reports, CYP2C8 and CYP3A4 were implemented for the metabolism of imatinib and NDMI, while biotransformation via CYP3A5 was excluded

due to its relatively minor role in the biotransformation process.<sup>7</sup> Here, model predictions for the relative influence on NDMI formation of CYP2C8 (67%) and CYP3A4 (33%) are in close agreement with the approximate in vitro literature values of 69% and 31%, respectively.<sup>7</sup> Overall, 57% of the modeled total metabolism of imatinib is accounted for by the formation of NDMI, closely aligning with in vitro findings which reported a similar contribution of 51%.<sup>7</sup> Listed fractional contributions of CYP2C8 and CYP3A4 to the metabolism of imatinib refer to a simulated SD

administration of imatinib. However, a shift in the enzymatic contributions toward a greater influence of CYP2C8 was observed upon simulated MD administrations of imatinib, most likely due to the pronounced autoinhibition of CYP3A4. Under simulated steady-state conditions, 75% of imatinib metabolism leads to the formation of NDMI (SD: 57%), with an increasing role of CYP2C8 within the NDMI pathway (SD: 67% vs. MD: 84%). This modeled decrease in CYP3A4 contribution to the overall metabolism of imatinib at steady-state reflects the results from DDI studies involving CYP3A perpetrators. Here an effect of ketoconazole on SD administration of imatinib was observed, while ritonavir showed almost no influence on the steady-state AUC of imatinib.<sup>18,45</sup> This finding could be confirmed via modeling (see Section S3.7). The influence of different polymorphically expressed transporters and enzymes on imatinib exposure has been investigated in previous works. For example, one study showed that the *CYP3A4 rs2242480* polymorphism resulted in significantly lower steady-state imatinib trough concentrations, relative to the wild type.<sup>46</sup> However, the model does not account for genotype-specific activities of the incorporated transporters and enzymes, primarily due to the scarcity of comprehensive data. Future studies focusing on the impact of various genetic polymorphisms on the plasma levels of imatinib and NDMI, especially over extended periods and not just at trough concentrations, would be valuable. Such research could facilitate the integration of, for example, different CYP3A4 activities into the model, allowing more personalized predictions.

Following the model development process, a DDI network centered around imatinib acting as both a victim and perpetrator drug was successfully established by coupling the final imatinib model with previously published models of the perpetrator drugs rifampicin, ketoconazole, and gemfibrozil, as well as of the victim drugs simvastatin and metoprolol.<sup>27–31</sup> Good overall predictive performance was attained for the modeled DDI scenarios, reflected by 24/24 predicted  $AUC_{last}$  and  $C_{max}$  ratios being within twofold of observed ratios. However, the modeled DDI network has limitations due to incomplete or biased published data. For instance, the effect of co-treatment with ketoconazole on imatinib exposure was examined solely in the context of SD administration of ketoconazole. As the metabolites of ketoconazole also exhibit potent inhibition of CYP2C8, CYP3A4, and P-gp, DDI studies involving pretreatment with ketoconazole would be of great interest to analyze the maximum inhibitory effect of ketoconazole and its metabolites on the AUC of imatinib and NDMI.

Various other PBPK models for imatinib are documented in the literature. These models address aspects such as interethnic differences in imatinib PK as well as

dose optimizations for children and adults in DDI scenarios with imatinib as the victim drug.<sup>23–25</sup> Contrasting with these, our whole-body PBPK model of imatinib encompasses the formation and biotransformation of both imatinib and its main metabolite NDMI. This approach is crucial as NDMI not only contributes to imatinib's pharmacodynamic effects but also plays an important role in inhibiting enzymes such as CYP2C8, CYP2D6, and CYP3A4. Hence, the inclusion of NDMI in the model enhances the model's clinical relevance for imatinib application and provides a more robust framework for the prediction of DDIs. While the activity and the inhibitory effect of NDMI are not overly prominent when imatinib is administered alone given its rather low contribution to the overall exposure, the importance of NDMI can increase greatly depending on the concomitant medication. For example, pretreatment with the inducer rifampicin causes the contribution of NDMI to total exposure to increase from 15% to 38%.<sup>19</sup> In a clinical oncology environment with five to eight drugs prescribed per patient, the importance of NDMI might therefore increase considerably and should not be neglected.<sup>20</sup> Furthermore, to the best of our knowledge, the developed DDI network is the first to cover imatinib not only as a victim, but also as a perpetrator drug. In particular, the good model prediction regarding the effect of imatinib on simvastatin exposure, mainly via CYP3A4 inhibition, is of great value as it allows the verification of the appropriate implementation of imatinib autoinhibition.

In summary, the developed imatinib parent-metabolite whole-body PBPK model shows good descriptive and predictive performance for both imatinib and its active metabolite NDMI in healthy subjects and CML/GIST patients. In addition, the role of imatinib and NDMI as CYP2C8, CYP3A4, and P-gp (imatinib) substrates, as well as inhibitors of CYP3A4 and CYP2D6, was successfully investigated and predicted within a newly established DDI network. Potential application areas of the developed model and corresponding imatinib DDI network include model-informed drug development as well as model-based precision dosing for patients. After being evaluated across various DDI scenarios, the imatinib model is capable of integration with any existing and validated PK-Sim® victim or perpetrator model to predict clinically untested DDIs and even multiple DDIs involving more than two DDI partners (e.g., two perpetrators). Hence, the developed imatinib model enables the prediction of effects both by and on imatinib and NDMI across a wide array of clinically relevant polypharmacy scenarios. This capability facilitates the identification and quantification of potential drug interactions. Subsequently, the presented model may be used to generate dose recommendations for imatinib or



relevant victim drugs to improve both therapy safety and efficacy.

## AUTHOR CONTRIBUTIONS

H.L.H.L., C.K., D.S., M.S., and T.L. wrote the manuscript. H.L.H.L., C.K., S.R., F.Z.M., L.M.F., and T.L. designed the research. H.L.H.L. performed the research. H.L.H.L. and C.K. analyzed the data.

## ACKNOWLEDGMENTS

Open Access funding enabled and organized by Projekt DEAL.

## FUNDING INFORMATION

Matthias Schwab was supported by the Robert Bosch Stiftung (Stuttgart, Germany), a grant from the German Federal Ministry of Education and Research (BMBF, 031L0188D, “GUIDE-IBD”) and the DFG im Rahmen der Exzellenzstrategie des Bundes und der Länder-EXC 2180-390900677. Thorsten Lehr was supported by the German Federal Ministry of Education and Research (BMBF, Horizon 2020 INSPIRATION grant 643271), under the frame of ERA-CoSysMed and the European Union Horizon 2021 SafePolyMed (grant 101057639).

## CONFLICT OF INTEREST STATEMENT

The authors declared no competing interests for this work.

## ORCID

Simeon Rüdesheim <https://orcid.org/0000-0002-5741-2511>

Matthias Schwab <https://orcid.org/0000-0002-9984-075X>

Thorsten Lehr <https://orcid.org/0000-0002-8372-1465>

## REFERENCES

- Kantarjian HM, Jain N, Garcia-Manero G, et al. The cure of leukemia through the optimist's prism. *Cancer*. 2022;128:240-259. doi:10.1002/cncr.33933
- Kantarjian HM, Talpaz M, Giles F, Brien SO, Cortes J. New insights into the pathophysiology of chronic myeloid leukemia and imatinib resistance. *Ann Intern Med*. 2006;145:913-923. doi:10.7326/0003-4819-145-12-200612190-00008
- Bixby D, Talpaz M. Seeking the causes and solutions to imatinib-resistance in chronic myeloid leukemia. *Leukemia*. 2011;25:7-22. doi:10.1038/leu.2010.238
- Roskoski RJ. Properties of FDA-approved small molecule protein kinase inhibitors: a 2023 update. *Pharmacol Res*. 2023;187:106552. doi:10.1016/j.phrs.2022.106552
- O'Brien Z, Moghaddam MF. A systematic analysis of physicochemical and ADME properties of all small molecule kinase inhibitors approved by US FDA from January 2001 to October 2015. *Curr Med Chem*. 2017;24:3159-3184. doi:10.2174/0929867324666170523124441
- Peng B, Dutreix C, Mehrling G, et al. Absolute bioavailability of imatinib (Gleevec®) orally versus intravenous infusion. *J Clin Pharmacol*. 2004;44:158-162. doi:10.1177/0091270003262101
- Filppula AM, Neuvonen M, Laitila J, Neuvonen PJ, Backman JT. Autoinhibition of CYP3A4 leads to important role of CYP2C8 in imatinib metabolism: variability in CYP2C8 activity may alter plasma concentrations and response. *Drug Metab Dispos*. 2013;41:50-59. doi:10.1124/dmd.112.048017
- Duckett DR, Cameron MD. Metabolism considerations for kinase inhibitors in cancer treatment. *Expert Opin Drug Metab Toxicol*. 2010;6:1175-1193. doi:10.1517/17425255.2010.506873. [Metabolism](#)
- Manley PW. Investigations into the potential role of metabolites on the anti-leukemic activity of imatinib, nilotinib and midostaurin. *Chimia*. 2019;73:561-570. doi:10.2533/chimia.2019.561
- Hu S, Franke RM, Filipinski KK, et al. Interaction of imatinib with human organic ion carriers. *Clin Cancer Res*. 2008;14:3141-3148. doi:10.1158/1078-0432.CCR-07-4913
- Hamada A, Miyano H, Watanabe H, Saito H. Interaction of imatinib mesilate with human P-glycoprotein. *J Pharmacol Exp Ther*. 2003;307:824-828. doi:10.1124/jpet.103.055574
- Burger H, van Tol H, Boersma AWM, et al. Imatinib mesylate (STI571) is a substrate for the breast cancer resistance protein (BCRP)/ABCG2 drug pump. *Blood*. 2004;104:2940-2942. doi:10.1182/blood-2004-04-1398
- Gschwind HP, Pfaar U, Waldmeier F, et al. Metabolism and disposition of imatinib mesylate in healthy volunteers. *Drug Metab Dispos*. 2005;33:1503-1512. doi:10.1124/dmd.105.004283
- Filppula AM, Laitila J, Neuvonen PJ, Backman JT. Potent mechanism-based inhibition of CYP3A4 by imatinib explains its liability to interact with CYP3A4 substrates. *Br J Pharmacol*. 2012;165:2787-2798. doi:10.1111/j.1476-5381.2011.01732.x
- Wang Y, Zhou L, Dutreix C, et al. Effects of imatinib (Gleevec) on the pharmacokinetics of metoprolol, a CYP2D6 substrate, in Chinese patients with chronic myelogenous leukaemia. *Br J Clin Pharmacol*. 2008;65:885-892. doi:10.1111/j.1365-2125.2008.03150.x
- O'Brien SG, Meinhardt P, Bond E, et al. Effects of imatinib mesylate (STI571, Gleevec) on the pharmacokinetics of simvastatin, a cytochrome P450 3A4 substrate, in patients with chronic myeloid leukaemia. *Br J Cancer*. 2003;89:1855-1859. doi:10.1038/sj.bjc.6601152
- Drug development and drug interactions: FDA table of substrates, inhibitors and inducers. Accessed September 28, 2023. <https://www.fda.gov/drugs/drug-interactions-labeling/health-care-professionals-fdas-examples-drugs-interact-cyp-enzymes-and-transporter-systems>
- Dutreix C, Peng B, Mehrling G, et al. Pharmacokinetic interaction between ketoconazole and imatinib mesylate (Gleevec) in healthy subjects. *Cancer Chemother Pharmacol*. 2004;54:290-294. doi:10.1007/s00280-004-0832-z
- Bolton AE, Peng B, Hubert M, et al. Effect of rifampicin on the pharmacokinetics of imatinib mesylate (Gleevec, STI571) in healthy subjects. *Cancer Chemother Pharmacol*. 2004;53:102-106. doi:10.1007/s00280-003-0722-9
- Bowlin SJ, Xia F, Wang W, Robinson KD, Stanek EJ. Twelve-month frequency of drug-metabolizing enzyme and transporter-based drug-drug interaction potential in patients receiving oral

- enzyme-targeted kinase inhibitor antineoplastic agents. *Mayo Clin Proc.* 2013;88:139-148. doi:[10.1016/j.mayocp.2012.10.020](https://doi.org/10.1016/j.mayocp.2012.10.020)
21. Grimstein M, Yang Y, Zhang X, et al. Physiologically based pharmacokinetic modeling in regulatory science: an update from the U.S. Food and Drug Administration's Office of Clinical Pharmacology. *J Pharm Sci.* 2019;108:21-25. doi:[10.1016/j.xphs.2018.10.033](https://doi.org/10.1016/j.xphs.2018.10.033)
  22. Gonzalez D, Rao GG, Bailey SC, et al. Precision dosing: public health need, proposed framework, and anticipated impact. *Clin Transl Sci.* 2017;10:443-454. doi:[10.1111/cts.12490](https://doi.org/10.1111/cts.12490)
  23. Adiwidjaja J, Gross AS, Boddy AV, McLachlan AJ. Physiologically-based pharmacokinetic model predictions of inter-ethnic differences in imatinib pharmacokinetics and dosing regimens. *Br J Clin Pharmacol.* 2022;88:1735-1750. doi:[10.1111/bcp.15084](https://doi.org/10.1111/bcp.15084)
  24. Adiwidjaja J, Boddy AV, McLachlan AJ. Implementation of a physiologically based pharmacokinetic modeling approach to guide optimal dosing regimens for imatinib and potential drug interactions in paediatrics. *Front Pharmacol.* 2020;10:1672. doi:[10.3389/fphar.2019.01672](https://doi.org/10.3389/fphar.2019.01672)
  25. Gao D, Wang G, Wu H, Wu JH, Zhao X. Prediction for plasma trough concentration and optimal dosing of imatinib under multiple clinical situations using physiologically based pharmacokinetic modeling. *ACS Omega.* 2023;8:13741-13753. doi:[10.1021/acsomega.2c07967](https://doi.org/10.1021/acsomega.2c07967)
  26. Wojtyniak J-G, Britz H, Selzer D, Schwab M, Lehr T. Data digitizing: accurate and precise data extraction for quantitative systems pharmacology and physiologically-based pharmacokinetic modeling. *CPT Pharmacometrics Syst Pharmacol.* 2020;9:322-331. doi:[10.1002/psp4.12511](https://doi.org/10.1002/psp4.12511)
  27. Wojtyniak J-G, Selzer D, Schwab M, Lehr T. Physiologically based precision dosing approach for drug-drug-gene interactions: a simvastatin network analysis. *Clin Pharmacol Ther.* 2021;109:201-211. doi:[10.1002/cpt.2111](https://doi.org/10.1002/cpt.2111)
  28. Rüdesheim S, Wojtyniak JG, Selzer D, et al. Physiologically based pharmacokinetic modeling of metoprolol enantiomers and  $\alpha$ -hydroxymetoprolol to describe CYP2D6 drug-gene interactions. *Pharmaceutics.* 2020;12:1200. doi:[10.3390/pharmaceutics12121200](https://doi.org/10.3390/pharmaceutics12121200)
  29. Marok FZ, Wojtyniak JG, Fuhr LM, et al. A physiologically based pharmacokinetic model of ketoconazole and its metabolites as drug-drug interaction perpetrators. *Pharmaceutics.* 2023;12:679. doi:[10.3390/pharmaceutics15020679](https://doi.org/10.3390/pharmaceutics15020679)
  30. Hanke N, Frechen S, Moj D, et al. PBPK models for CYP3A4 and P-gp DDI prediction: a modeling network of rifampicin, itraconazole, clarithromycin, midazolam, alfentanil, and digoxin. *CPT Pharmacometrics Syst Pharmacol.* 2018;7:647-659. doi:[10.1002/psp4.12343](https://doi.org/10.1002/psp4.12343)
  31. Türk D, Hanke N, Wolf S, et al. Physiologically based pharmacokinetic models for prediction of complex CYP2C8 and OATP1B1 (SLCO1B1) drug-drug-gene interactions: a modeling network of gemfibrozil, repaglinide, pioglitazone, rifampicin, clarithromycin and itraconazole. *Clin Pharmacokinet.* 2019;58:1595-1607. doi:[10.1007/s40262-019-00777-x](https://doi.org/10.1007/s40262-019-00777-x)
  32. Open Systems Pharmacology Suite Community. Open Systems Pharmacology Suite Manual, Version 11 2023. Accessed September 30, 2023. <https://docs.open-systems-pharmacology.org/copyright>
  33. Guest EJ, Aarons L, Houston JB, Rostami-Hodjegan A, Galetin A. Critique of the two-fold measure of prediction success for ratios: application for the assessment of drug-drug interactions. *Drug Metab Dispos.* 2011;39:170-173. doi:[10.1124/dmd.110.036103](https://doi.org/10.1124/dmd.110.036103)
  34. Hegedus T, Orfi L, Seprodi A, Váradi A, Sarkadi B, Kéri G. Interaction of tyrosine kinase inhibitors with the human multidrug transporter proteins, MDR1 and MRP1. *Biochim Biophys Acta.* 2002;1587:318-325. doi:[10.1016/S0925-4439\(02\)00095-9](https://doi.org/10.1016/S0925-4439(02)00095-9)
  35. D'Cunha R, Bae S, Murry DJ, An G. TKI combination therapy: strategy to enhance dasatinib uptake by inhibiting Pgp- and BCRP-mediated efflux. *Biopharm Drug Dispos.* 2016;37:397-408. doi:[10.1002/bdd.2022](https://doi.org/10.1002/bdd.2022)
  36. Langenbucher F. Linearization of dissolution rate by the Weibull distribution. *J Pharm Pharmacol.* 1972;24:979-981. doi:[10.1111/j.2042-7158.1972.tb08930.x](https://doi.org/10.1111/j.2042-7158.1972.tb08930.x)
  37. Zidan DW, Hassan WS, Elmasry MS, Shalaby AA. A novel spectrofluorimetric method for determination of imatinib in pure, pharmaceutical preparation, human plasma, and human urine. *Luminescence.* 2018;33:232-242. doi:[10.1002/bio.3406](https://doi.org/10.1002/bio.3406)
  38. Filppula AM, Tornio A, Niemi M, Neuvonen PJ, Backman JT. Gemfibrozil impairs imatinib absorption and inhibits the CYP2C8-mediated formation of its main metabolite. *Clin Pharmacol Ther.* 2013;94:383-393. doi:[10.1038/clpt.2013.92](https://doi.org/10.1038/clpt.2013.92)
  39. Jørgensen HG, Elliott MA, Allan EK, Carr CE, Holyoake TL, Smith KD.  $\alpha$ 1-acid glycoprotein expressed in the plasma of chronic myeloid leukemia patients does not mediate significant in vitro resistance to STI571. *Blood.* 2002;99:713-715. doi:[10.1182/blood.V99.2.713](https://doi.org/10.1182/blood.V99.2.713)
  40. Peng B, Lloyd P, Schran H. Clinical pharmacokinetics of imatinib. *Clin Pharmacokinet.* 2005;44:879-894. doi:[10.2165/00003088-200544090-00001](https://doi.org/10.2165/00003088-200544090-00001)
  41. Friedecký D, Mičová K, Faber E, Hrdá M, Šíroká J, Adam T. Detailed study of imatinib metabolization using high-resolution mass spectrometry. *J Chromatogr A.* 2015;1409:173-181. doi:[10.1016/j.chroma.2015.07.033](https://doi.org/10.1016/j.chroma.2015.07.033)
  42. Rodríguez Flores J, Berzas JJ, Castañeda G, Rodríguez N. Direct and fast capillary zone electrophoretic method for the determination of Gleevec and its main metabolite in human urine. *J Chromatogr B Anal Technol Biomed Life Sci.* 2003;794:381-388. doi:[10.1016/S1570-0232\(03\)00518-X](https://doi.org/10.1016/S1570-0232(03)00518-X)
  43. Echoute K, Franke RM, Loos WJ, et al. Environmental and genetic factors affecting transport of imatinib by OATP1A2. *Clin Pharmacol Ther.* 2011;89:816-820. doi:[10.1038/clpt.2011.42](https://doi.org/10.1038/clpt.2011.42)
  44. Silva CG, Honeywell RJ, Dekker H, Peters GJ. Physicochemical properties of novel protein kinase inhibitors in relation to their substrate specificity for drug transporters. *Expert Opin Drug Metab Toxicol.* 2015;11:703-717. doi:[10.1517/17425255.2015.1006626](https://doi.org/10.1517/17425255.2015.1006626)
  45. van Erp NP, Gelderblom H, Karlsson MO, et al. Influence of CYP3A4 inhibition on the steady-state pharmacokinetics of imatinib. *Clin Cancer Res.* 2007;13:7394-7400. doi:[10.1158/1078-0432.CCR-07-0346](https://doi.org/10.1158/1078-0432.CCR-07-0346)
  46. Liu J, Chen Z, Chen H, et al. Genetic polymorphisms contribute to the individual variations of imatinib mesylate plasma levels and adverse reactions in Chinese GIST patients. *Int J Mol Sci.* 2017;18:603. doi:[10.3390/ijms18030603](https://doi.org/10.3390/ijms18030603)
  47. Frye RF, Fitzgerald SM, Lagattuta TF, Hruska MW, Egorin MJ. Effect of St John's wort on imatinib mesylate pharmacokinetics. *Clin Pharmacol Ther.* 2004;76:323-329. doi:[10.1016/j.clpt.2004.06.007](https://doi.org/10.1016/j.clpt.2004.06.007)



48. Peng B, Hayes M, Resta D, et al. Pharmacokinetics and pharmacodynamics of imatinib in a phase I trial with chronic myeloid leukemia patients. *J Clin Oncol*. 2004;22:935-942. doi:[10.1200/JCO.2004.03.050](https://doi.org/10.1200/JCO.2004.03.050)
49. Yang JS, Cho EG, Huh W, Ko JW, Jung JA, Lee SY. Rapid determination of imatinib in human plasma by liquid chromatography-tandem mass spectrometry: application to a pharmacokinetic study. *Bull Korean Chem Soc*. 2013;34:2425-2430. doi:[10.5012/bkcs.2013.34.8.2425](https://doi.org/10.5012/bkcs.2013.34.8.2425)
50. Zhang Y, Qiang S, Yu Z, et al. LC-MS-MS determination of imatinib and N-desmethyl imatinib in human plasma. *J Chromatogr Sci*. 2014;52:344-350. doi:[10.1093/chromsci/bmt037](https://doi.org/10.1093/chromsci/bmt037)
51. Nikolova Z, Peng B, Hubert M, et al. Bioequivalence, safety, and tolerability of imatinib tablets compared with capsules. *Cancer Chemother Pharmacol*. 2004;53:433-438. doi:[10.1007/s00280-003-0756-z](https://doi.org/10.1007/s00280-003-0756-z)

## SUPPORTING INFORMATION

Additional supporting information can be found online in the Supporting Information section at the end of this article.

**How to cite this article:** Loer HLH, Kovar C, Rüdesheim S, et al. Physiologically based pharmacokinetic modeling of imatinib and N-desmethyl imatinib for drug–drug interaction predictions. *CPT Pharmacometrics Syst Pharmacol*. 2024;13:926-940. doi:[10.1002/psp4.13127](https://doi.org/10.1002/psp4.13127)



### 4.3 PROJECT III – PHYSIOLOGICALLY BASED PHARMACOKINETIC MODELING OF (E)-CLOMIPHENE AND ITS MAIN METABOLITES

#### 4.3.1 Publication

Kovar, C., Kovar, L., Rüdesheim, S., Selzer, D., Ganchev, B., Kröner, P., Igel, S., Kerb, R., Schaeffeler, E., Mürdter, T. E., Schwab, M., & Lehr, T. (2022). Prediction of drug-drug-gene interaction scenarios of (E)-clomiphene and its metabolites using physiologically based pharmacokinetic modeling. *Pharmaceutics*, 14(12), 2604. DOI: [10.3390/pharmaceutics14122604](https://doi.org/10.3390/pharmaceutics14122604) [160].

#### 4.3.2 Author Contributions

Author contributions according to the [CRediT](#) [1]:


Christina Kovar	Refer to <i>Contribution Report</i> (p. <a href="#">vii</a> )
Lukas Kovar	Conceptualization, Investigation, Methodology, Validation, Visualization, Writing – Review & Editing
Simeon Rüdesheim	Formal Analysis, Methodology, Writing – Review & Editing
Dominik Selzer	Formal Analysis, Methodology, Software, Validation, Writing – Review & Editing
Boian Ganchev	Investigation, Methodology, Writing – Review & Editing
Patrick Kröner	Investigation, Methodology, Writing – Review & Editing
Svitlana Igel	Investigation, Writing – Review & Editing
Reinhold Kerb	Conceptualization, Investigation, Writing – Review & Editing
Elke Schaeffeler	Investigation, Methodology, Writing – Review & Editing
Thomas Mürdter	Conceptualization, Investigation, Methodology, Project Administration, Supervision, Validation, Writing – Review & Editing
Matthias Schwab	Conceptualization, Funding Acquisition, Project Administration, Resources, Supervision, Validation, Writing – Review & Editing
Thorsten Lehr	Conceptualization, Funding Acquisition, Project Administration, Resources, Supervision, Validation, Writing – Original Draft, Writing – Review & Editing

#### 4.3.3 *Copyright*

This article is an open access article distributed under the terms and conditions of the Creative Commons Attribution (CC BY) license (<https://creativecommons.org/licenses/by/4.0/>). © 2022 by the authors. Licensee MDPI, Basel, Switzerland.

## Article

# Prediction of Drug–Drug–Gene Interaction Scenarios of (E)-Clomiphene and Its Metabolites Using Physiologically Based Pharmacokinetic Modeling

Christina Kovar <sup>1,2</sup> , Lukas Kovar <sup>1</sup> , Simeon Rüdesheim <sup>1,2</sup> , Dominik Selzer <sup>1</sup>, Boian Ganchev <sup>2</sup>, Patrick Kröner <sup>2</sup>, Svitlana Igel <sup>2</sup>, Reinhold Kerb <sup>2</sup>, Elke Schaeffeler <sup>2</sup>, Thomas E. Mürdter <sup>2</sup>, Matthias Schwab <sup>2,3</sup> and Thorsten Lehr <sup>1,\*</sup> 

<sup>1</sup> Clinical Pharmacy, Saarland University, 66123 Saarbrücken, Germany

<sup>2</sup> Dr. Margarete Fischer-Bosch Institute of Clinical Pharmacology, University of Tübingen, 70376 Stuttgart, Germany

<sup>3</sup> Departments of Clinical Pharmacology, Pharmacy and Biochemistry, University of Tübingen, 72076 Tübingen, Germany

\* Correspondence: thorsten.lehr@mx.uni-saarland.de; Tel.: +49-681-302-70255



**Citation:** Kovar, C.; Kovar, L.; Rüdesheim, S.; Selzer, D.; Ganchev, B.; Kröner, P.; Igel, S.; Kerb, R.; Schaeffeler, E.; Mürdter, T.E.; et al. Prediction of Drug–Drug–Gene Interaction Scenarios of (E)-Clomiphene and Its Metabolites Using Physiologically Based Pharmacokinetic Modeling. *Pharmaceutics* **2022**, *14*, 2604. <https://doi.org/10.3390/pharmaceutics14122604>

Academic Editors: Yoon-Jee Chae and Kyeong-Ryoon Lee

Received: 24 October 2022

Accepted: 22 November 2022

Published: 25 November 2022

**Publisher's Note:** MDPI stays neutral with regard to jurisdictional claims in published maps and institutional affiliations.



**Copyright:** © 2022 by the authors. Licensee MDPI, Basel, Switzerland. This article is an open access article distributed under the terms and conditions of the Creative Commons Attribution (CC BY) license (<https://creativecommons.org/licenses/by/4.0/>).

**Abstract:** Clomiphene, a selective estrogen receptor modulator (SERM), has been used for the treatment of anovulation for more than 50 years. However, since (E)-clomiphene ((E)-Clom) and its metabolites are eliminated primarily via Cytochrome P450 (CYP) 2D6 and CYP3A4, exposure can be affected by CYP2D6 polymorphisms and concomitant use with CYP inhibitors. Thus, clomiphene therapy may be susceptible to drug–gene interactions (DGIs), drug–drug interactions (DDIs) and drug–drug–gene interactions (DDGIs). Physiologically based pharmacokinetic (PBPK) modeling is a tool to quantify such DGI and DD(G)I scenarios. This study aimed to develop a whole-body PBPK model of (E)-Clom including three important metabolites to describe and predict DGI and DD(G)I effects. Model performance was evaluated both graphically and by calculating quantitative measures. Here, 90% of predicted  $C_{max}$  and 80% of  $AUC_{last}$  values were within two-fold of the corresponding observed value for DGIs and DD(G)Is with clarithromycin and paroxetine. The model also revealed quantitative contributions of different CYP enzymes to the involved metabolic pathways of (E)-Clom and its metabolites. The developed PBPK model can be employed to assess the exposure of (E)-Clom and its active metabolites in as-yet unexplored DD(G)I scenarios in future studies.

**Keywords:** clomiphene; pharmacokinetics; cytochrome P450 2D6 (CYP2D6) polymorphisms; drug–drug interactions (DDIs); drug–drug–gene interactions (DDGIs); drug–gene interactions (DGIs); (E)-clomiphene; physiologically based pharmacokinetic (PBPK) modeling

## 1. Introduction

Ovulation disorders resulting in infertility can be caused by polycystic ovary syndrome (PCOS), which shows a prevalence of 4–20% in women of reproductive age worldwide [1,2]. Clomiphene has been used for the treatment of infertility in women with PCOS since the late 1960s and is administered orally as a racemic mixture of (E)- and (Z)-clomiphene ((E)-Clom and (Z)-Clom) [1,3]. As a selective estrogen receptor modulator (SERM), clomiphene—particularly (E)-Clom and its metabolites—inhibits the estrogen receptor at the hypothalamic arcuate nucleus [4–6]. Here, a rise in gonadotropin-releasing hormone levels leads to an increase in follicle-stimulating and luteinizing hormones, which in turn, induces ovulation [7]. In addition, antimicrobial activity of SERMs against different strains of bacteria has been shown in recent work [8,9].

During clomiphene therapy, 8–54% of women do not respond, while variability in response is affected by various factors such as hyperandrogenemia and obesity [10–12]. Additionally, research efforts have identified the importance of the highly polymorphic cytochrome



P450 (CYP) 2D6 enzyme in the bioactivation of (E)-Clom [6,13]. Here, the two metabolites (E)-4-hydroxyclophene ((E)-4-OH-Clom) and (E)-4-hydroxy-N-desethylclomiphene ((E)-4-OH-DE-Clom) were identified to exhibit the highest inhibitory affinity towards the estrogen receptor with half-maximal inhibitory concentrations of 2.2 and 0.9 nM, respectively [7]. In contrast, the parent drug (E)-Clom as well as (Z)-Clom and its metabolites showed lower inhibitory effects in in vitro assays [5,6]. Thus, (E)-4-OH-Clom and (E)-4-OH-DE-Clom are assumed to be key components in the bioactivation process of clomiphene with their pharmacokinetics (PK) strongly depending on CYP2D6 activity [5].

As a result, treatment with clomiphene can be subject to drug–gene interactions (DGIs) which has been confirmed in a study with healthy female volunteers [5]. Here, CYP2D6 poor metabolizers (PM) showed approximately ten-fold lower maximum plasma concentrations ( $C_{max}$ ) of (E)-4-OH-Clom and (E)-4-OH-DE-Clom compared with normal metabolizers (NM) [5]. Furthermore, the in vitro formation rates for both (E)-4-OH-Clom and (E)-4-OH-DE-Clom increased with CYP2D6 activity [5]. The impact of CYP2D6 polymorphisms has also been observed in a recent clinical trial, where all CYP2D6 intermediate metabolizers (IM) responded to clomiphene therapy, while 30% of NM were non-responders [14]. However, this non-classical gene–dose effect points to a more complex metabolic scheme.

As the biotransformation of its active metabolites does not only depend on CYP2D6, but also on CYP3A4 metabolism, among others, systemic exposure of (E)-Clom and its metabolites can be altered by drug–drug interactions (DDIs) with CYP2D6 inhibitors and additionally with CYP3A4 inhibitors/inducers [15,16]. This dependency of (E)-Clom PK and bioactivation on CYP2D6 and CYP3A4 leads to a complex network of possible DGI, DDI and drug–drug–gene interaction (DDGI) scenarios that can cause a high variability in the longitudinal trajectory of plasma concentrations for (E)-Clom and its metabolites. The fact, that not only the formation, but also the elimination, of the active metabolites depends on CYP2D6 and CYP3A4 activity, adds to the complexity of the PK. Here, physiologically based pharmacokinetic (PBPK) modeling can integrate available in vitro and in vivo information on these processes to quantify and investigate DGI, DDI and DDGI scenarios.

Thus, this study aimed to develop a whole-body parent–metabolite PBPK model of (E)-Clom and its metabolites (E)-4-OH-Clom, (E)-N-desethylclomiphene ((E)-DE-Clom) and (E)-4-OH-DE-Clom to support the investigation of CYP2D6 DGI effects on the PK and bioactivation of (E)-Clom. In addition, the model was applied to predict various DD(G)I scenarios with the CYP2D6 inhibitor paroxetine and the CYP3A4 inhibitor clarithromycin and to gain insights into the PK regarding the contribution of different metabolic pathways to the elimination of (E)-Clom and its metabolites. The supplementary document to this article serves as a model reference and includes a detailed evaluation of the model performance. In addition, the model files will be made publicly available (<http://models.clinicalpharmacy.me/>).

## 2. Materials and Methods

### 2.1. Clinical Study Data

Clinical data from a recently performed pharmacokinetic panel study (EudraCT-Nr.: 2009-014531-20, ClinicalTrials.gov: NCT01289756) were used for PBPK model development [6]. The study protocol, patient information sheet and consent form were approved by the Ethics Committee of the University of Tübingen and the German Federal Institute for Drugs and Medical Devices (BfArM). All study participants had signed an informed consent form.

The study was conducted in 20 healthy, Caucasian, premenopausal female volunteers that were genotyped for CYP2D6 polymorphisms and subsequently assigned to predicted phenotypes according to the respective CYP2D6 activity score (AS) as depicted in Table 1 [17,18]. All subjects received 100 mg clomiphene citrate (two 50 mg tablets Ratiopharm GmbH, Ulm, Germany, with 62:38 (E)-Clom:(Z)-Clom) as a single dose after an overnight fast and without any concomitant medication. After a wash-out phase of at least three weeks, clomiphene was administered concomitantly with the strong CYP3A4

inhibitor clarithromycin [19]. Here, the participants received 500 mg clarithromycin twice daily for four days. On day 5, a single dose of clomiphen citrate was administered together with 500 mg clarithromycin. Finally, in the third period, all subjects received clomiphen citrate together with the strong CYP2D6 inhibitor paroxetine [19]. Here, 40 mg paroxetine was administered once daily for two days. On day 3, participants received a single dose of clomiphen citrate concomitantly with 40 mg paroxetine (Figure 1).

**Table 1.** Overview of clinical data integrated from the pharmacokinetic panel study.

	AS = 0	AS = 0.5	AS = 0.75	AS = 1	AS = 2	AS = 3
<i>n</i>	6 <sup>#</sup>	4	1 <sup>+</sup>	2	3	3
CYP2D6 phenotypes	PM	IM	IM	IM	NM	UM
CYP2D6 genotypes	*4/*4 *4/*5 *4/*6	*4/*41 *4/*9	*9/*10	*1/*4	*1/*1	*1/*1 × 3
Demographics						
Age [years]	25.2 (22–29)	24.3 (21–30)	22.0 (–)	25.5 (23–28)	32.3 (26–43)	25.7 (22–28)
Weight [kg]	62.3 (50.0–70.0)	59.3 (55.5–64.0)	63.0 (–)	68.8 (63.5–74.0)	56.5 (48.0–63.5)	61.7 (54.0–73.0)
Height [cm]	1.70 (1.53–1.75)	1.68 (1.59–1.72)	1.66 (–)	1.71 (1.68–1.73)	1.63 (1.60–1.67)	1.65 (1.57–1.75)
BMI [kg/m <sup>2</sup> ]	21.6 (20.6–22.9)	21.1 (20.3–22.0)	22.9 (–)	23.6 (22.5–24.7)	21.3 (18.8–24.2)	22.6 (20.3–23.8)

<sup>#</sup> number of study participants decreased during the DDGI setting due to drop-outs (*n* = 5 for clarithromycin, *n* = 4 for paroxetine); <sup>+</sup> one study participant classified as AS = 0.75 was excluded from the analysis (see Section S1.1 of the supplementary document); demographic parameters are presented as mean (range); AS, CYP2D6 activity score; BMI, body mass index; IM, intermediate metabolizers; *n*, number of subjects; NM, normal metabolizers; PM, poor metabolizers; UM, ultrarapid metabolizers.

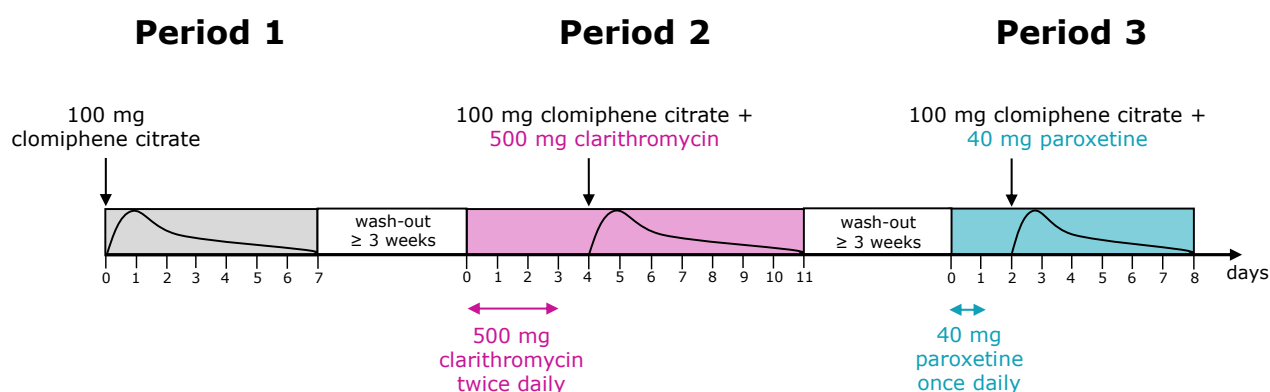


**Figure 1.** Drug administration schedule in the pharmacokinetic panel study. In period I, clomiphen citrate alone; in period II, combined with clarithromycin; and in period III, combined with paroxetine was administered.

Both plasma concentration–time profiles as well as renal excretion data of (*E*)-Clom and its metabolites (*E*)-4-OH-Clom, (*E*)-DE-Clom and (*E*)-4-OH-DE-Clom were obtained by validated liquid chromatography–tandem mass spectrometry (LC-MS/MS) methods [13,20]. The demographic and clinical characteristics of the study population are shown in Table 1.

Additionally, (*E*)-Clom plasma concentration–time profiles from two single-dose [21,22] and two multiple-dose [23,24] studies were identified in a literature search and plasma profiles were digitized for further model evaluation. In these clinical trials, CYP2D6 genotypes of study participants were not reported. Additional information including study populations and the corresponding administration protocols are listed in Table S2 of the supplementary document.

## 2.2. Software

PBPK modeling and simulation was performed in PK-Sim<sup>®</sup> and MoBi<sup>®</sup> (version 9.1 part of the Open Systems Pharmacology (OSP) Suite, <http://www.open-systems-pharmacology.org>) [25]. Published clinical data of (E)-Clom were digitized with GetData Graph Digitizer version 2.26.0.20 (S. Fedorov) according to Wojtyniak and coworkers [26]. PK parameter calculations, model performance evaluations and graphics were accomplished with the R programming language version 3.6.3 (R Foundation for Statistical Computing, Vienna, Austria) [27]. Model parameter estimation via Monte-Carlo optimization as well as local sensitivity analysis were performed within PK-Sim<sup>®</sup>.

## 2.3. PBPK Model Development

For PBPK model building, information on physicochemical properties, as well as absorption, distribution, metabolism and excretion (ADME) processes of all investigated compounds, were gathered from the literature. Clinical data were split into a training and a test dataset. The training dataset for model development comprised mean plasma and renal excretion profiles of (E)-Clom and its metabolites from NM and PM study populations ( $n = 8$  plasma concentration–time profiles and  $n = 8$  renal excretion profiles). This dataset was selected to inform catalytic rate constant ( $k_{cat}$ ) parameters associated with CYP2D6-dependent and -independent metabolic pathways, respectively. Plasma concentration–time profiles and renal excretion data of IM and ultrarapid metabolizers (UM) in the DGI setting, data from all phenotypes in the DD(G)I setting as well as digitized clinical study data from the published literature were utilized as the test dataset for PBPK model evaluation ( $n = 70$  plasma concentration–time profiles and  $n = 64$  renal excretion profiles).

Metabolic pathways of (E)-Clom and its metabolites comprising hydroxylation, N-de-ethylation and glucuronidation, among others, were implemented via CYP enzymes (CYP2D6, CYP3A4 and CYP2B6) and unspecific hepatic clearance mechanisms (Figure 2). In summary, (E)-Clom is primarily metabolized via CYP2D6 to the active metabolite (E)-4-OH-Clom as well as to (Z)-3-hydroxyclophene (implemented as an undefined metabolite) [6]. An additional biotransformation process via CYP2B6 to (E)-4-OH-Clom was implemented to cover the fraction of CYP2D6-independent metabolism observed in the PM population and in CYP2D6 DD(G)I scenarios [5,6]. Biotransformation of (E)-Clom to (E)-DE-Clom was implemented mainly through CYP3A4 with CYP2D6 playing only a minor role in this metabolic pathway [5,28].

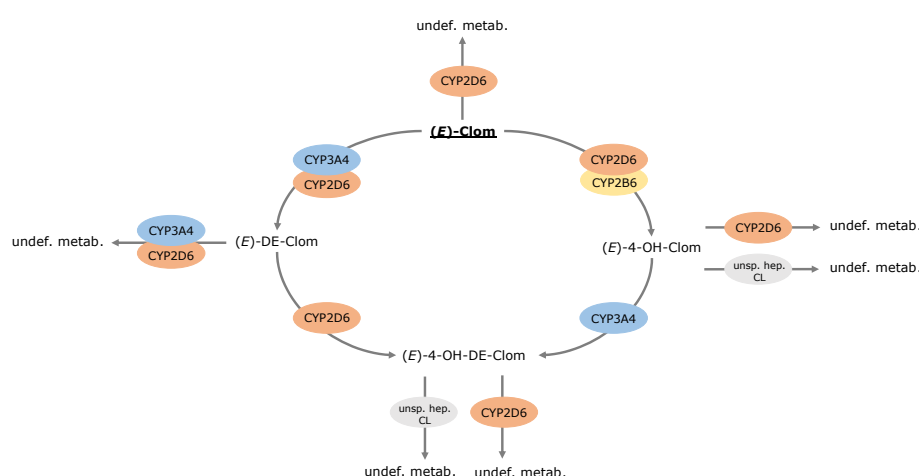


**Figure 2.** Overview of implemented metabolic processes in the (E)-Clom PBPK model. CYP, cytochrome P450; (E)-4-OH-Clom, (E)-4-hydroxyclophene; (E)-4-OH-DE-Clom, (E)-4-hydroxy-N-desethylclomiphene; (E)-Clom, (E)-clomiphene; (E)-DE-Clom, (E)-N-desethylclomiphene; undef. metab., undefined metabolite; unsp. hep. CL, unspecific hepatic clearance.

(*E*)-4-OH-Clom is metabolized via CYP2D6 to (*Z*)-3,4-dihydroxyclophene (implemented as an undefined metabolite), via an unspecific hepatic clearance mechanism and via CYP3A4 to the second active metabolite (*E*)-4-OH-DE-Clom [5,6,28]. (*E*)-4-OH-DE-Clom is also formed via CYP2D6 metabolism of (*E*)-DE-Clom, which in turn, represents the main route of elimination of (*E*)-DE-Clom [5,28]. Furthermore, (*E*)-DE-Clom is metabolized to minor extents through CYP2D6 and CYP3A4 to (*E*)-N,N-didesethylclomiphene (implemented as an undefined metabolite) [5,28]. The metabolism of (*E*)-4-OH-DE-Clom has not been extensively investigated, yet. According to work by Kröner [6], (*E*)-4-OH-DE-Clom is presumably metabolized through a CYP-mediated pathway to (*Z*)-3,4-dihydroxydesethylclomiphene. Additionally, glucuronidation, sulfation and potentially further unexplored pathways play a role in (*E*)-4-OH-DE-Clom biotransformation [6] and were grouped under an unspecific hepatic clearance process in the PBPK model (Figure 2).

Renal excretion through glomerular filtration was implemented and potential reabsorption or secretion processes were informed via renal excretion data. Model parameters that could not be informed from experimental reports during model development were optimized by fitting the model to the observed data of the training dataset. Moreover, a fraction of (*E*)-Clom metabolized via CYP3A4 was calculated (see Section S1.5 of the supplementary document) and used to inform  $k_{cat}$  model parameters associated with (*E*)-Clom metabolism. For detailed information on PBPK model building, see Section S1 of the supplementary document.

#### 2.4. DGI and DD(G)I Modeling

Using the training dataset,  $k_{cat}$  values for CYP2D6-mediated pathways were estimated for the NM population, while CYP2D6  $k_{cat}$  values for the PM population were set to zero. To predict DGIs and plasma concentration–time profiles in the IM and UM populations, IM and UM  $k_{cat}$  values for CYP2D6-dependent pathways were extrapolated from the estimated NM- $k_{cat}$  value (Equation (1)):

$$k_{cat, AS=i} = k_{cat, AS=2} \cdot IVSF_i \quad (1)$$

Here,  $k_{cat, AS=i}$  represents the catalytic rate constant for CYP2D6 AS = *i*,  $k_{cat, AS=2}$  is the catalytic rate constant for the NM population and IVSF<sub>*i*</sub> is the corresponding in vitro scaling factor (IVSF). IVSFs were obtained using in vitro information on CYP2D6 AS-specific formation rates regarding the metabolism of (*E*)-Clom and its three metabolites (see Table S8 of the supplementary document) [5]. For predictions of plasma concentrations from clinical trials that did not report CYP2D6 phenotypes, CYP2D6  $k_{cat}$  parameters were fitted to the respective plasma concentration–time profiles for each study.

In the DD(G)I setting, study participants in the pharmacokinetic panel study received clomiphene citrate together with the CYP3A4 inhibitor clarithromycin or the CYP2D6 inhibitor paroxetine that additionally acts as a weak inhibitor of CYP3A4 [19,29]. Predictions for DD(G)I scenarios of (*E*)-Clom and the investigated metabolites were performed for all CYP2D6 AS by coupling the developed parent–metabolite PBPK model with previously published PBPK models of the perpetrator drugs clarithromycin [16] and paroxetine [30]. Inhibition mechanisms of CYP3A4 and CYP2D6 were implemented as described in the OSP Suite manual [31]. Interaction parameters were used as published in the respective perpetrator PBPK models [16].

#### 2.5. PBPK DGI and DD(G)I Model Evaluation

The performance of the parent–metabolite PBPK model was evaluated, applying several graphical and quantitative methods. The predicted plasma concentration–time profiles of (*E*)-Clom, (*E*)-4-OH-Clom, (*E*)-DE-Clom and (*E*)-4-OH-DE-Clom were graphically compared with their respective observed plasma profiles for all investigated CYP2D6 AS populations. Additionally, goodness-of-fit plots were used to compare predicted and observed areas under the plasma concentration–time curves from the first to the last time point of measurements ( $AUC_{last}$ ),  $C_{max}$  values and plasma concentrations of all model

compounds for the DGI and DD(G)I scenarios. As quantitative measures, the mean relative deviation (MRD) of predicted plasma concentrations and the geometric mean fold error (GMFE) of predicted  $AUC_{last}$  and  $C_{max}$  were calculated according to Equations (2) and (3), respectively:

$$MRD = 10^x \text{ with } x = \sqrt{\frac{1}{n} \sum_{i=1}^n (\log_{10} \hat{c}_i - \log_{10} c_i)^2} \quad (2)$$

Here,  $\hat{c}_i$  represents the  $i$ -th predicted plasma concentration,  $c_i$  is the corresponding observed plasma concentration and  $n$  equals the number of observed values.

$$GMFE = 10^x \text{ with } x = \frac{1}{n} \sum_{i=1}^n \left| \log_{10} \left( \frac{\hat{a}_i}{a_i} \right) \right| \quad (3)$$

Here,  $\hat{a}_i$  represents the  $i$ -th predicted  $AUC_{last}$  and  $C_{max}$  value, respectively,  $a_i$  is the corresponding observed value and  $n$  equals the number of predicted plasma profiles.

For the evaluation of DGI and DD(G)I effects, the predicted  $AUC_{last}$  and  $C_{max}$  effect ratios were calculated according to Equations (4) and (5) and compared with the corresponding observed values. Here, model performance was assessed using the prediction acceptance limits proposed by Guest et al. with 1.25-fold variability [32].

$$AUC_{last, AS=i} \text{ ratio} = \frac{AUC_{last, effect, AS=i}}{AUC_{last, control}} \quad (4)$$

$$C_{max, AS=i} \text{ ratio} = \frac{C_{max, effect, AS=i}}{C_{max, control}} \quad (5)$$

For the calculation of DGI ratios,  $AUC_{last, effect, AS=i}$  and  $C_{max, effect, AS=i}$  represent the  $AUC_{last}$  and  $C_{max}$  for CYP2D6 AS =  $i$ , while  $AUC_{last, control}$  and  $C_{max, control}$  are the  $AUC_{last}$  and  $C_{max}$  values for the NM (AS = 2) population. For the calculation of DD(G)I ratios,  $AUC_{last, effect, AS=i}$  and  $C_{max, effect, AS=i}$  represent the  $AUC_{last}$  and  $C_{max}$  for the CYP2D6 AS =  $i$  in the DD(G)I scenario with clarithromycin or paroxetine, while  $AUC_{last, control}$  and  $C_{max, control}$  are the  $AUC_{last}$  and  $C_{max}$  values for the CYP2D6 AS =  $i$  without the concomitant use of perpetrator drugs.

Moreover, a local sensitivity analysis was performed using PK-Sim<sup>®</sup>. A detailed description of the analysis and results is provided in Section S4.4 of the supplementary document.

### 3. Results

#### 3.1. PBPK Model Building and Evaluation

The developed whole-body parent–metabolite PBPK model successfully described plasma concentration–time profiles and renal excretion profiles in NM and PM populations. In addition, DGI effects in IM and UM populations as well as DD(G)I scenarios with clarithromycin and paroxetine in various phenotypes could be successfully predicted. With that, the PBPK model of (E)-Clom and the three metabolites (E)-4-OH-Clom, (E)-DE-Clom and (E)-4-OH-DE-Clom was able to capture the complexity of the parent–metabolite network and was used to characterize the contribution of various elimination pathways.

For model building and evaluation, plasma concentration–time and renal excretion–time profiles of various CYP2D6 AS from a pharmacokinetic panel study as well as from four published clinical studies with a dose range from 6.25 mg to 62 mg of orally administered (E)-Clom citrate were included. In total, 22 plasma concentration–time profiles for (E)-Clom, 16 plasma profiles each for (E)-4-OH-Clom, (E)-DE-Clom and (E)-4-OH-DE-Clom as well as 64 renal excretion profiles were available. With the observed increase in exposure for NM during concomitant clarithromycin administration, a fraction metabolized ( $f_m$ ) of (E)-Clom via CYP3A4 of approximately 13% could be estimated (cf., Section S1.5 of the supplementary document) and subsequently integrated into the model building process to inform the contribution of the CYP3A4-dependent pathway. The drug-dependent model input parameters of (E)-Clom, (E)-4-OH-Clom, (E)-DE-Clom and (E)-4-OH-DE-Clom are provided in Tables S4–S7 of the supplementary document.

### 3.2. DGI Modeling and Evaluation

The final PBPK model precisely captured mean plasma concentration–time profiles of the NM ( $AS = 2$ ) population for (*E*)-Clom and all three integrated metabolites (see Figure 3, third column). All predicted  $AUC_{last}$  and  $C_{max}$  values were in good agreement with the observed values: GMFEs for  $AUC_{last}$  and  $C_{max}$  in the NM population were 1.11 and 1.13, respectively. The overall MRD value for predicted plasma concentrations was 1.37.

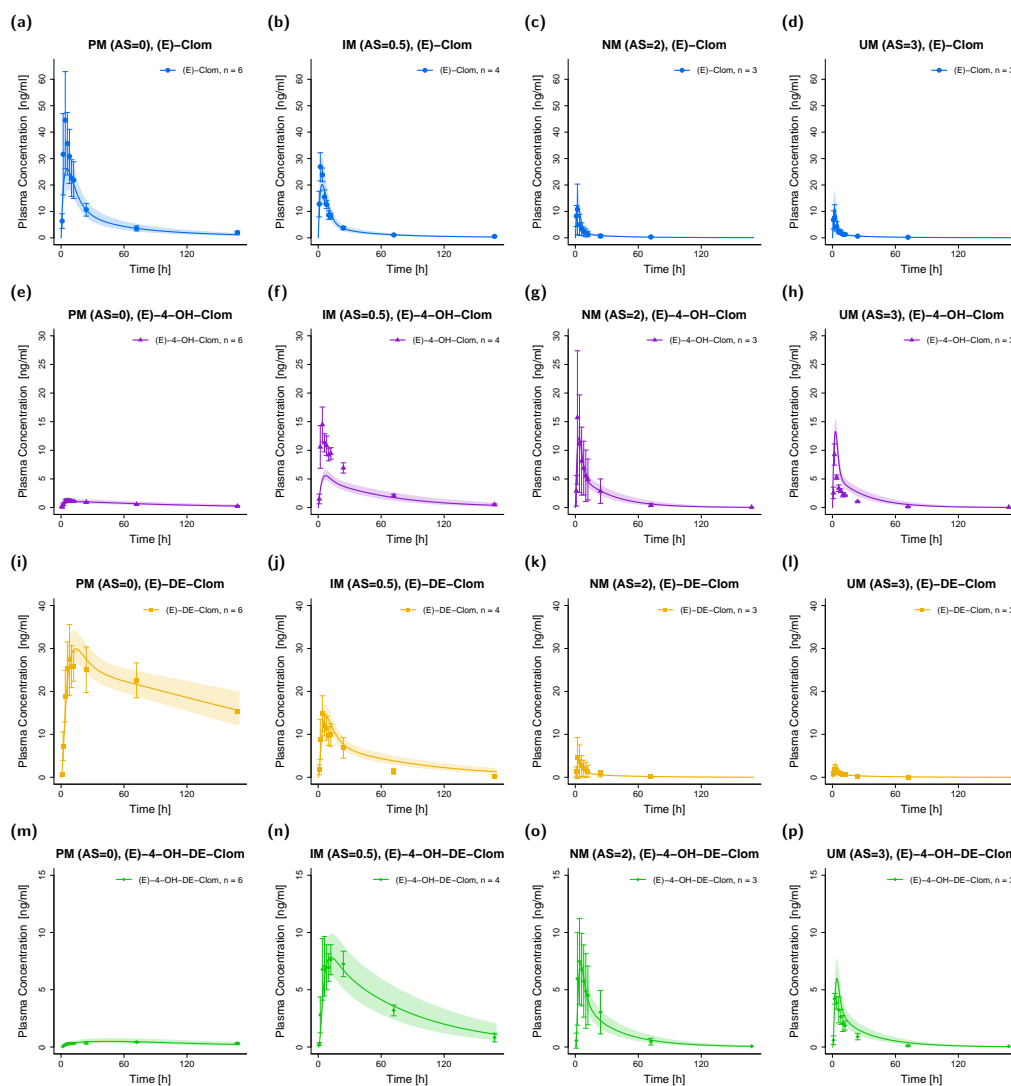


**Figure 3.** Predicted and observed plasma concentration–time profiles of (*E*)-Clom (a–d), (*E*)-4-OH-Clom (e–h), (*E*)-DE-Clom (i–l) and (*E*)-4-OH-DE-Clom (m–p) in PM (first column), IM (only  $AS = 0.5$  shown; second column), NM (third column) and UM (last column) for DGI scenarios. Solid lines depict predicted geometric mean concentration–time profiles in the PM, IM ( $AS = 0.5$ ), NM and UM populations. Colored ribbons show the corresponding geometric standard deviation of the population simulations ( $n = 1000$ ). Mean observed data are shown as symbols with the corresponding standard deviation. Linear and semilogarithmic predicted and observed plasma concentration–time profiles of all studies and AS are shown in Section S4.1 of the supplementary document. AS, CYP2D6 activity score; DGI, drug–gene interaction; (*E*)-4-OH-Clom, (*E*)-4-hydroxyclophene; (*E*)-4-OH-DE-Clom, (*E*)-4-hydroxy-N-desethylclomiphene; (*E*)-Clom, (*E*)-clomiphene; (*E*)-DE-Clom, (*E*)-N-desethylclomiphene; IM, intermediate metabolizers;  $n$ , number of subjects; NM, normal metabolizers; PM, poor metabolizers; UM, ultrarapid metabolizers.



For DGI model predictions, CYP2D6  $k_{cat}$  values were extrapolated from NM to IM (AS = 0.5, AS = 0.75 and AS = 1) and UM populations. The extrapolation of  $k_{cat}$  parameters based on in vitro scaling factors led to successful predictions of plasma profiles in IM and UM phenotypes. Plasma profiles in PM volunteers that were part of the training dataset were also well captured in model simulations (Figure 3).

Since (E)-Clom is primarily metabolized via CYP2D6 (predicted  $f_m = 86\%$ ), the PM population showed the highest  $AUC_{last}$  for the parent compound (E)-Clom ( $AUC_{PM} > AUC_{IM} > AUC_{NM} > AUC_{UM}$ ), but the lowest  $AUC_{last}$  for the two most active metabolites (E)-4-OH-Clom and (E)-4-OH-DE-Clom. However, since (E)-4-OH-Clom and (E)-4-OH-DE-Clom were not only formed but also degraded via CYP2D6, their highest  $AUC_{last}$  could not be found in UM, but in IM with AS = 0.5 ( $AUC_{IM (AS = 0.5)} > AUC_{NM} > AUC_{UM} > AUC_{PM}$ ). A detailed listing of all predicted and observed  $AUC_{last}$  and  $C_{max}$  values for all phenotypes in the DGI study setting is depicted in Table S11 of the supplementary document.

Goodness-of-fit plots for all modeled compounds showing predicted compared with observed plasma concentrations,  $AUC_{last}$  and  $C_{max}$  values in the DGI study setting are depicted in Figure 4. Here, 90% of  $C_{max}$ , 80% of  $AUC_{last}$  and 78% of the predicted concentrations were within the two-fold acceptance criterion. GMFEs for the predicted  $C_{max}$  and  $AUC_{last}$  values were 1.41 and 1.43, respectively, and the overall MRD value for predicted plasma concentrations was 1.95.

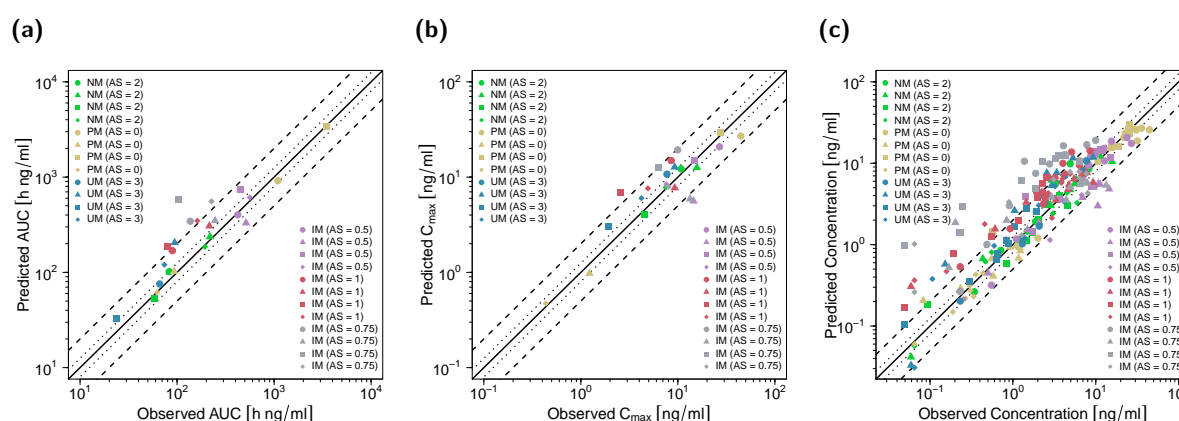


**Figure 4.** Predicted versus observed  $AUC_{last}$  (a),  $C_{max}$  (b) and plasma concentrations (c) of (E)-Clom (circles), (E)-4-OH-Clom (triangles), (E)-DE-Clom (squares) and (E)-4-OH-DE-Clom (diamonds) in PM, IM, NM and UM (DGI scenarios). The black solid lines mark the lines of identity. Black dotted lines indicate 1.25-fold; black dashed lines indicate two-fold deviation. Goodness-of-fit plots of digitized studies are depicted in Figure S8 of the supplementary document. AS, CYP2D6 activity score; DGI, drug–gene interaction; (E)-4-OH-Clom, (E)-4-hydroxyclophene; (E)-4-OH-DE-Clom, (E)-4-hydroxy-N-desethylclomiphene; (E)-Clom, (E)-clomiphene; (E)-DE-Clom, (E)-N-desethylclomiphene; IM, intermediate metabolizers; NM, normal metabolizers; PM, poor metabolizers; UM, ultrarapid metabolizers.

The predicted impact of CYP2D6 polymorphisms on the PK of (E)-Clom and its three metabolites (DGI effect ratios) is shown in Figure 5 and is highly consistent with observed effects. GMFEs for the predicted  $C_{max}$  and  $AUC_{last}$  ratios in the DGI setting were 1.46 and 1.65, respectively. Predicted and observed renal excretion profiles are visualized in Section S4.1 of the supplementary document. Moreover, complementary prediction results of concentration–time profiles for the remaining AS and included published clinical studies are shown in Sections S4.1.3 and S4.1.7, respectively, of the supplementary document.

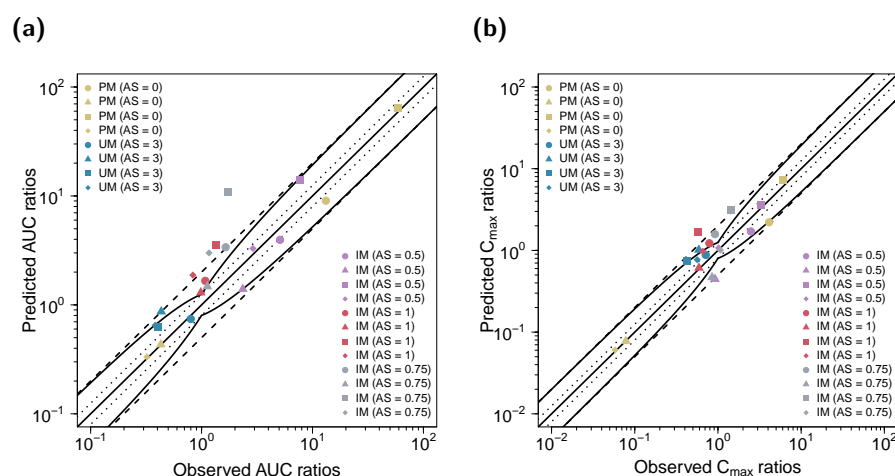


**Figure 5.** Predicted versus observed DGI (a)  $AUC_{last}$  and (b)  $C_{max}$  ratios of (E)-Clom (circles), (E)-4-OH-Clom (triangles), (E)-DE-Clom (squares) and (E)-4-OH-DE-Clom (diamonds). The straight black lines mark the lines of identity; the curved solid black lines show the limits of the predictive measure proposed by Guest et al. with 1.25-fold variability [32]. Black dotted lines indicate 1.25-fold; black dashed lines indicate two-fold deviation. AS, CYP2D6 activity score; (E)-4-OH-Clom, (E)-4-hydroxyclophene; (E)-4-OH-DE-Clom, (E)-4-hydroxy-N-desethylclomiphene; (E)-Clom, (E)-clomiphene; (E)-DE-Clom, (E)-N-desethylclomiphene; IM, intermediate metabolizers; NM, normal metabolizers; PM, poor metabolizers; UM, ultrarapid metabolizers.

### 3.3. DD(G)I Modeling and Evaluation

In total, 40 plasma concentration–time profiles and 40 renal excretion profiles of (E)-Clom and its metabolites were used for the investigation of DD(G)I scenarios with clarithromycin (mechanism-based inhibitor of CYP3A4) and paroxetine (mechanism-based inhibitor of CYP3A4 and CYP2D6) for various CYP2D6 AS (AS = 0, AS = 0.5, AS = 1, AS = 2 and AS = 3). Here, the impact of clarithromycin- and paroxetine-induced DD(G)I effects on plasma concentration–time profiles,  $AUC_{last}$  and  $C_{max}$  values of (E)-Clom and its metabolites was assessed. For this, published PBPK model parameters for clarithromycin [16] and paroxetine [30] were used including the respective competitive inhibition ( $K_i$ ) and the maximum inactivation rate ( $k_{inact}$ ) constants. Plasma and renal excretion profiles were predicted, compared with observed profiles and served for evaluations of DD(G)I model performance. DD(G)I model prediction performance is visually demonstrated in the concentration–time profiles (Figure 6) and the corresponding goodness-of-fit plots (Figure 7). GMFEs for the predicted  $AUC_{last}$  and  $C_{max}$  values were 1.30 and 1.40, respectively, and the overall MRD value for predicted plasma concentrations was 1.83.

Since the metabolism of (E)-Clom is predominantly mediated via CYP2D6, the  $AUC_{last}$  of (E)-Clom substantially increased with concomitant administration of the CYP2D6 inhibitor paroxetine (2.5–12-fold) for all phenotypes, except PM, which possess no CYP2D6 activity. Furthermore, due to inhibition of CYP2D6,  $C_{max}$  of the metabolite (E)-4-OH-Clom decreased in all phenotypes except for PM. However, as (E)-4-OH-Clom is not only formed but also degraded via CYP2D6, a substantial decrease in  $AUC_{last}$  during paroxetine DD(G)I was only predicted for the IM population in concordance with observed values. The minor involvement of CYP3A4 in the metabolism of (E)-Clom and (E)-4-OH-Clom is supported by the slight increase in the respective  $AUC_{last}$  during CYP3A4 inhibition in all phenotypes.



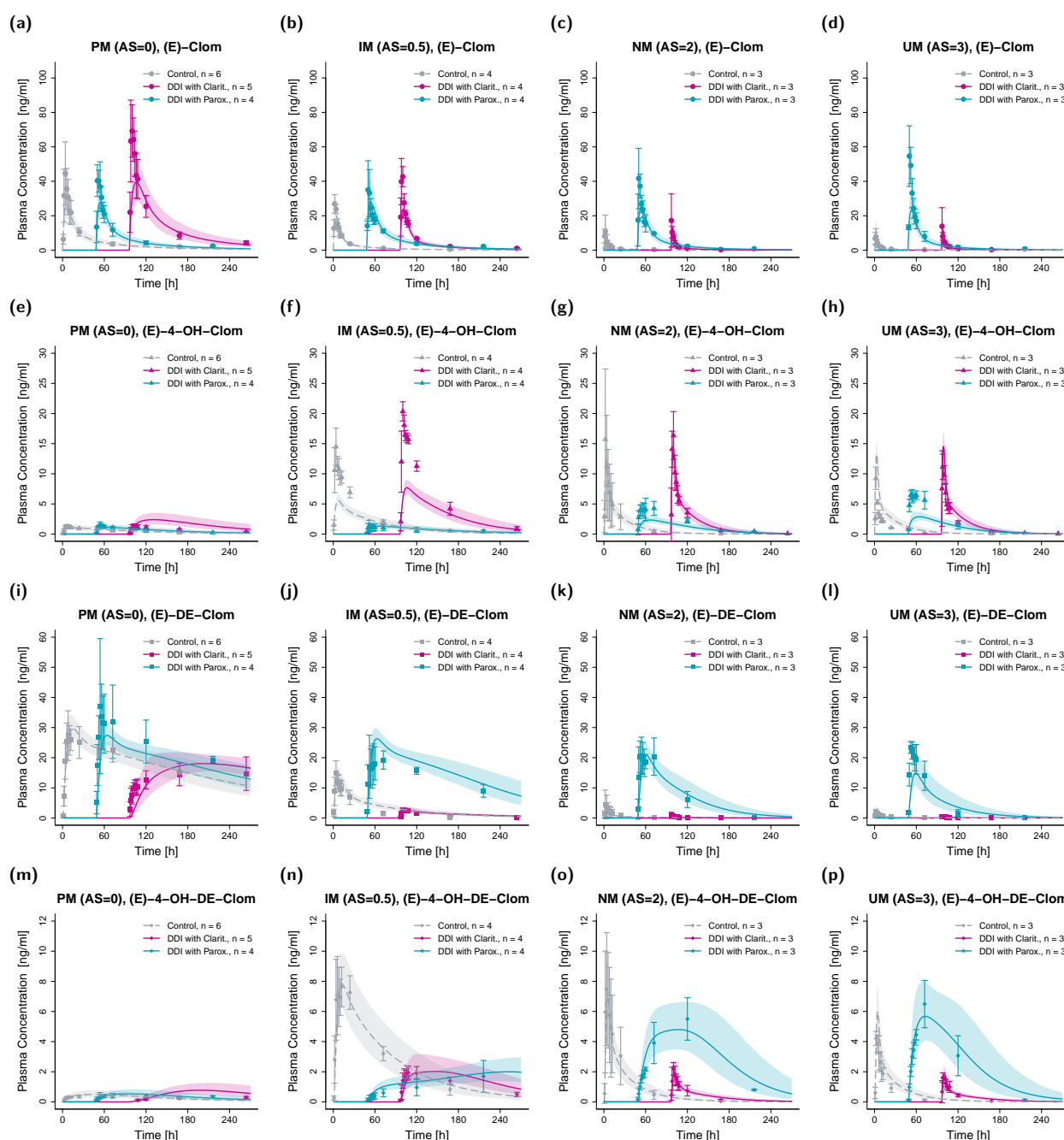


**Figure 6.** Predicted and observed plasma concentration–time profiles of (E)-Clom (a–d), (E)-4-OH-Clom (e–h), (E)-DE-Clom (i–l) and (E)-4-OH-DE-Clom (m–p) for DD(G)I scenarios in PM (first column), IM (only AS = 0.5 shown; second column), NM (third column) and UM (last column). Grey dashed lines depict the predicted geometric mean concentration–time profiles in absence of clarithromycin and paroxetine (control); turquoise solid lines represent the predicted geometric mean profiles in the presence of paroxetine; and pink solid lines represent the predicted geometric mean profiles in the presence of clarithromycin (DD(G)I). Colored ribbons show the corresponding geometric standard deviation of the population simulations ( $n = 1000$ ). Mean observed data are shown as symbols with the corresponding standard deviation. Linear and semilogarithmic predicted and observed plasma concentration–time profiles of all AS are shown in Section S4.2 of the supplementary document. For better visibility, DD(G)I scenarios were plotted with a time offset with  $t = 0$  at the first dose of the perpetrator drug. AS, CYP2D6 activity score; Clarit., Clarithromycin; DD(G)I, drug–drug

and drug–drug–gene interactions; (*E*)-4-OH-Clom, (*E*)-4-hydroxyclophiphen; (*E*)-4-OH-DE-Clom, (*E*)-4-hydroxy-N-desethylclomiphene; (*E*)-Clom, (*E*)-clomiphene; (*E*)-DE-Clom, (*E*)-N-desethylclomiphene; IM, intermediate metabolizers; *n*, number of subjects; NM, normal metabolizers; Parox., Paroxetine; PM, poor metabolizers; UM, ultrarapid metabolizers.

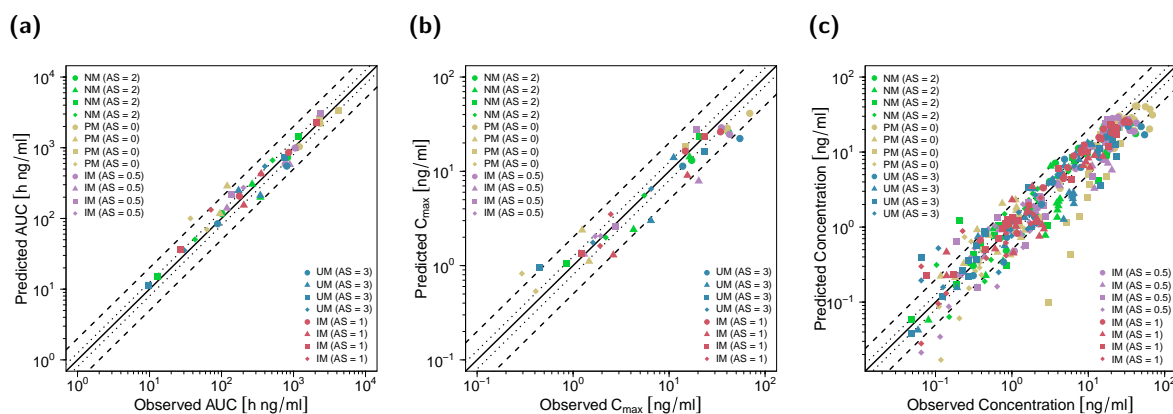


**Figure 7.** Predicted versus observed  $AUC_{last}$  (a),  $C_{max}$  (b) and plasma concentrations (c) of (*E*)-Clom (circles), (*E*)-4-OH-Clom (triangles), (*E*)-DE-Clom (squares) and (*E*)-4-OH-DE-Clom (diamonds) for DD(GI) scenarios with clarithromycin and paroxetine, respectively. The black solid lines mark the lines of identity. Black dotted lines indicate 1.25-fold; black dashed lines indicate two-fold deviation. AS, CYP2D6 activity score; DD(GI), drug–drug and drug–drug–gene interactions; (*E*)-4-OH-Clom, (*E*)-4-hydroxyclophiphen; (*E*)-4-OH-DE-Clom, (*E*)-4-hydroxy-N-desethylclomiphene; (*E*)-Clom, (*E*)-clomiphene; (*E*)-DE-Clom, (*E*)-N-desethylclomiphene; IM, intermediate metabolizers; NM, normal metabolizers, PM, poor metabolizers; UM, ultrarapid metabolizers.

The  $AUC_{last}$  of (*E*)-DE-Clom is substantially reduced in all phenotypes by values between ~70% and 80% (NM and IM) and ~34% (PM) during concomitant clarithromycin administration, demonstrating that CYP3A4 is likely the major enzyme in the formation of (*E*)-DE-Clom. During CYP3A4 inhibition,  $AUC_{last}$  and  $C_{max}$  values, as well as the corresponding DDGI effects for (*E*)-4-OH-Clom and (*E*)-4-OH-DE-Clom in PM, were overpredicted by ~2.5-fold.

Predicted and observed  $AUC_{last}$  and  $C_{max}$  ratios of (*E*)-Clom, (*E*)-4-OH-Clom, (*E*)-DE-Clom and (*E*)-4-OH-DE-Clom for the DD(GI) setting are shown in Figure 8. GMFEs for the predicted  $C_{max}$  and  $AUC_{last}$  ratios in the DD(GI) setting were 1.50 and 1.40, respectively. All predicted and observed values for  $AUC_{last}$  and  $C_{max}$ , DD(GI) effect ratios as well as calculated MRDs and GMFEs are listed in Section S4.3 of the supplementary document.

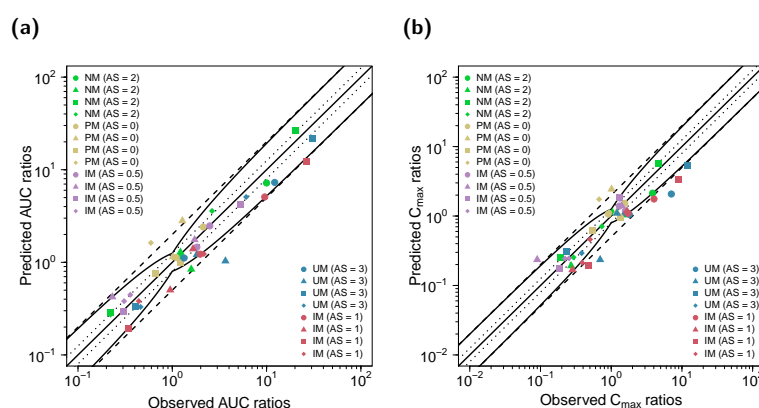


**Figure 8.** Predicted versus observed DD(GI)  $AUC_{last}$  (a) and  $C_{max}$  (b) ratios of (*E*)-Clom (circles), (*E*)-4-OH-Clom (triangles), (*E*)-DE-Clom (squares) and (*E*)-4-OH-DE-Clom (diamonds). The straight

### 3.4. Contribution of Metabolic Pathways to (E)-Clom and Metabolite Disposition

**Metabolic Pathway of Clomipramine**

**Oral Dose** (Fa=100%) → **First Pass Effect** (BA=11%) → **Systemic Drug**

**Systemic Drug** → **Metabolism** → **Excretion**

**Metabolism Pathways:**

- (E)-Clom** (42% CYP2D6) → undef. metab.
- (E)-Clom** (13% CYP3A4, 4% CYP2D6) → (E)-DE-Clom
- (E)-DE-Clom** (1% CYP3A4, 1% CYP2D6) → undef. metab.
- (E)-Clom** (40% CYP2D6, 1% CYP2B6) → (E)-4-OH-Clom
- (E)-4-OH-Clom** (28% CYP2D6) → undef. metab.
- (E)-4-OH-Clom** (6% unsp. hep. CL) → undef. metab.
- (E)-4-OH-Clom** (7% CYP3A4) → (E)-4-OH-DE-Clom
- (E)-4-OH-DE-Clom** (14% CYP2D6) → undef. metab.
- (E)-4-OH-DE-Clom** (8% unsp. hep. CL) → undef. metab.

**Excretion Pathways:**

- (E)-Clom (0.01%)
- (E)-DE-Clom (0.05%)
- (E)-4-OH-Clom (0.09%)
- (E)-4-OH-DE-Clom (0.23%)

The metabolism of the active metabolite (*E*)-4-OH-Clom in NM is mediated primarily via CYP2D6 (69%) and, to a minor extent, via an unspecific hepatic clearance (15%). Only 17% of (*E*)-4-OH-Clom is degraded to the second active metabolite (*E*)-4-OH-DE-Clom via CYP3A4. In addition, (*E*)-4-OH-DE-Clom is formed of (*E*)-DE-Clom via CYP2D6 (90% of (*E*)-DE-Clom elimination), while 10% of (*E*)-DE-Clom is metabolized via CYP2D6 and CYP3A4 to (*E*)-N,N-didesethylclomiphene. The renal excretion of (*E*)-Clom and its three metabolites can be considered negligible (0.01–0.23%). Calculated contributions for all

implemented metabolic pathways and fractions of dose excreted in urine of (*E*)-Clom and its metabolites in PBPK model simulations for NM as well as fractions of dose excreted in urine are illustrated in Figure 9.

#### 4. Discussion

Since the approval of clomiphene for the treatment of anovulation in women by the U.S. Food and Drug Administration (FDA) in the late 1960s, several efforts have been made to explain the inter-individual variability in clomiphene PK and drug response [13,14,34–36]. While early studies identified obesity, hyperandrogenemia and high levels of serum anti-Müllerian hormone as predictors for non-response [34,35,37–39], polymorphisms of CYP2D6 were additionally identified to alter drug disposition and response [5,14,36]. This study presents the first (*E*)-Clom PBPK model that investigates and characterizes the impact of CYP2D6 polymorphisms and the concomitant use of CYP3A4 and CYP2D6 inhibitors on the PK of (*E*)-Clom and its three important metabolites (*E*)-4-OH-Clom, (*E*)-DE-Clom and (*E*)-4-OH-DE-Clom.

For this, a whole-body parent–metabolite PBPK model of (*E*)-Clom has been successfully built and evaluated, predicting plasma concentration–time profiles for various CYP2D6 AS in DGI and DD(G)I scenarios. The predicted DGI and DD(G)I effects on the PK of (*E*)-Clom and its active metabolites were in good agreement with the effects observed in a pharmacokinetic panel study. Despite the complex nature of the disposition of (*E*)-Clom and its metabolites, the PBPK model could capture and quantify the contribution of the different metabolic pathways. The developed model described and predicted plasma profiles of the training and test dataset for the DGI setting with GMFEs of 1.43 and 1.41 for predictions of  $AUC_{last}$  and  $C_{max}$ , respectively. GMFEs in the DD(G)I settings with clarithromycin and paroxetine were 1.30 and 1.40 for predictions of  $AUC_{last}$  and  $C_{max}$ , respectively, highlighting the good descriptive and predictive model performance.

DGI predictions for IM and UM populations were based on in vitro–in vivo extrapolation of CYP2D6 activity. Here, the application of AS-specific  $k_{cat}$  values based on estimated in vivo NM- $k_{cat}$  and published in vitro information on differences in metabolic activity between CYP2D6 AS led to successful predictions of observed plasma concentrations and DGI effect ratios. The predicted DGI effects of CYP2D6 polymorphisms on the AUC of the four modeled compounds ranged from a ~60-fold increase ((*E*)-DE-Clom in PM vs. NM) to a ~70% decrease ((*E*)-4-OH-DE-Clom in PM vs. NM).

The observed DGI  $AUC_{last}$  effect ratio for (*E*)-Clom in IM (AS = 1) was ~1 representing “no effect”, while the model predicted effect ratio was about 1.7, suggesting a ~70% increase in AUC from NM to IM (AS = 1), which seems reasonable due to the strong CYP2D6 involvement in (*E*)-Clom degradation. The corresponding predicted effect on (*E*)-4-OH-DE-Clom exposure (~1.9) was also higher than the effect observed (~0.8). Similarly, DGI  $AUC_{last}$  effect ratios for IM (AS = 0.75) were higher than the corresponding effect ratios observed for (*E*)-Clom and its metabolites. Several genetic and non-genetic factors in addition to the CYP2D6 genotype have previously been described to affect CYP2D6 activity in vivo, resulting in substantial interindividual variability in the PK of CYP2D6 substrates [5,40,41]. Here, the pharmacokinetic panel study might lack the required power to reliably predict the low observed mean effect ratios for IM (AS = 1 and AS = 0.75) individuals ( $n = 2$  and  $n = 1$ , respectively). Thus, additional studies with an increased number of CYP2D6 genotyped individuals would be helpful to further evaluate these prediction scenarios.

The underprediction of (*E*)-4-OH-Clom  $AUC_{last}$  DGI effects in IM (AS = 0.5) and UM populations based on the in vitro–in vivo extrapolation of CYP2D6 activity could hint towards a stronger involvement of CYP2D6 in the metabolism of (*E*)-4-OH-Clom or indicate lower CYP2D6  $k_{cat}$  values in IM and higher values in UM than was extrapolated from in vitro. Moreover, the relative importance of other enzymes for pathways mediated by CYP2D6 increases for lower CYP2D6 AS. Consequently, the impact of variability in activity for alternative pathways (e.g., due to polymorphisms in CYP2B6) increases [41,42]. Notably, only a small number of participants ( $n = 3$ ) in the pharmacokinetic panel study

were assigned to the IM (AS = 0.5) group and were genotyped for *CYP2D6* only. Hence, as a result of the underprediction (IM (AS = 0.5)) and overprediction (UM) of (E)-4-OH-Clom exposure, respectively, DD(G)I model predictions for this metabolite should be interpreted carefully in these populations.

Since (E)-Clom is primarily metabolized via *CYP2D6* ( $f_m$  of ~86% according to model simulations) PM showed the highest exposure for the parent compound ( $AUC_{last, (E)-Clom}$  order: PM > IM > NM > UM). Additionally, as (E)-4-OH-DE-Clom is primarily formed via *CYP2D6*-dependent pathways, PM showed the lowest  $AUC_{last}$  for the active metabolite. However, the complex metabolic network with additional involvement of other CYP enzymes and contribution of multiple *CYP2D6*-dependent pathways resulted in a different order for (E)-4-OH-DE-Clom AUC values compared with (E)-Clom. Here, the  $AUC_{last}$  of (E)-4-OH-DE-Clom was highest in IM (AS = 0.5), while it was lowest for PM and second-lowest for UM, proposing a contribution of *CYP2D6* not only in the formation but also in the degradation of (E)-4-OH-DE-Clom. This is supported by model simulations, where the integration of a *CYP2D6* metabolic route for (E)-4-OH-Clom and (E)-4-OH-DE-Clom degradation [6,28] was crucial for successful predictions of the respective plasma profiles. The involvement of *CYP2D6* in the degradation of the active metabolites might also explain findings from a study by Ji et al., where all nine study participants with IM phenotype responded to clomiphene therapy, whereas 30% of NM were non-responders [14].

For the investigated clarithromycin DD(G)I scenario, (E)-Clom exposure increased by only ~15% for NM compared with the control scenario without *CYP3A4* inhibition. In contrast, for PM, (E)-Clom exposure increased ~2.4-fold, which was successfully predicted by the PBPK model. The increase in (E)-Clom  $AUC_{last}$ , however, also led to a model-predicted increase in (E)-4-OH-Clom  $AUC_{last}$  (~2.8-fold) and consequently to an increase in (E)-4-OH-DE-Clom  $AUC_{last}$  (~1.6-fold) for PM. This elevation was not observed in the available clinical data (effect ratio ~1.3-fold and ~0.6-fold, respectively). These differences between observation and prediction might be attributed to a saturated *CYP2B6* metabolism from (E)-Clom to (E)-4-OH-Clom in vivo that was not reflected in the PBPK model or to non-implemented alternative metabolic pathways that are active in scenarios of low *CYP3A4* and *CYP2D6* activity.

The underprediction of paroxetine DDGI effects on (E)-4-OH-Clom  $AUC_{last}$  in the IM (AS = 0.5) and UM population supports the aforementioned hint towards lower *CYP2D6*  $k_{cat}$  values in IM and higher values in UM or a stronger involvement of *CYP2D6* in the metabolism of (E)-4-OH-Clom than was extrapolated from in vitro.

Many different CYP enzymes are involved in the metabolic pathways of (E)-Clom and its metabolites [5,28]; therefore, the implementation of biotransformation generally focused on main CYP enzymes. However, of note, the implementation of *CYP2D6* as an additional enzyme, complementing *CYP3A4* in the formation of (E)-DE-Clom [43], led to a substantial improvement in the prediction of clarithromycin DD(G)I scenarios, preventing an underprediction of  $AUC_{last}$  values for (E)-DE-Clom. Here, *CYP2D6* was incorporated with a ~20% contribution to the formation of the desethyl metabolite [43].

In contrast, the initial assumption of a *CYP3A4*-mediated desethylation of (E)-4-OH-DE-Clom (as for (E)-4-OH-Clom, cf. Figure 9) was rejected, since this implemented process led to a consistent overprediction of (E)-4-OH-DE-Clom  $AUC_{last}$  in the clarithromycin DD(G)I scenarios for all phenotypes. Instead, the metabolic pathway was replaced by an unspecific hepatic clearance process representing glucuronidation, sulfation and potential other metabolic processes of (E)-4-OH-DE-Clom as suggested by Kröner [6].

PBPK modeling was also leveraged to gain insights into the PK of (E)-Clom and to investigate contributions of the different metabolic pathways for (E)-Clom and its metabolites. According to model simulations in NM, about 22% of the administered (E)-Clom dose is eventually metabolized to the metabolite with the highest target affinity ((E)-4-OH-DE-Clom [28]), mainly via the (E)-DE-Clom-pathway (~69%) and ~31% via the (E)-4-OH-Clom pathway. This is of note, as only ~17% of (E)-Clom is initially metabolized to (E)-DE-Clom, while ~41% is metabolized to (E)-4-OH-Clom. However, ~90% of (E)-DE-Clom metabolism



results in (*E*)-4-OH-DE-Clom formation (vs. only ~17% of (*E*)-4-OH-Clom metabolism), eventually representing the main pathway of (*E*)-4-OH-DE-Clom formation according to model simulations.

Clomiphene is typically administered as a racemic mixture of (*E*)- and (*Z*)-Clom (62:38) [22]. Both isomers show highly distinct pharmacokinetic characteristics and also differ in affinity to the target receptor [22,28]. In contrast to (*Z*)-Clom, (*E*)-Clom undergoes an extensive first-pass metabolism resulting in a lower bioavailability [44]. The model predicted bioavailability for (*E*)-Clom in NM was ~11%, which is in congruence with the low bioavailability of ~6.3% for the (*E*)-isomer calculated from the reported AUC<sub>0-24h</sub> after oral [21] and intravenous application of 50 mg clomiphene citrate [45]. While the calculated value from the literature is based on an intravenous study with a small number of study participants ( $n = 2$ ) [45], a low bioavailability can be supported with the developed PBPK model. The model calculated bioavailabilities in PM, IM (AS = 0.5, AS = 0.75, AS = 1) and UM were 49%, 30%, 27%, 18% and 9%, respectively.

In the pharmacokinetic panel study, renal excretion of the parent compound (*E*)-Clom and the three modeled metabolites was quantified and showed negligible overall contribution to the respective compound elimination. The PBPK model was able to quantify this small contribution of renal excretion for the four investigated compounds. The respective simulated fractions of dose excreted in urine for NM were calculated to be 0.01‰, 0.09‰, 0.05‰ and 0.23‰, for (*E*)-Clom, (*E*)-4-OH-Clom, (*E*)-DE-Clom and (*E*)-4-OH-DE-Clom, respectively. This is in concordance with recent studies, where unchanged (*E*)-Clom and unconjugated metabolites could only be detected in small amounts, or not at all in urine samples [46,47].

The pharmacokinetic panel study was conducted in a cross-over design [28]. One limitation of this work is the small number of participants in the panel study ( $n = 20$ ), with only one to six individuals per AS group available for model development. Additionally, from the PM group, one participant dropped out of the clinical trial during the clarithromycin DDGI scenario and two participants during the paroxetine DDGI scenario. In the case of the IM (AS = 0.75) group, no data for the DDGI scenarios were available due to drop-out.

When additional pharmacokinetic data become available, the PBPK model can be further evaluated according to the “learn–confirm–refine” principle [48,49] to be used for further model applications. Moreover, the presented parent–metabolite PBPK model of (*E*)-Clom provides a basis for future investigations of different covariates (e.g., body mass index), individual CYP2D6 genotypes and the concomitant use of additional perpetrator drugs influencing the PK of (*E*)-Clom and its metabolites. The evaluated model can be leveraged to simulate plasma concentration–time profiles and investigate the exposure of (*E*)-Clom and its active metabolites in as-yet unexplored DD(G)I scenarios with the concomitant administration of moderate and weak CYP enzyme inhibitors as well as CYP enzyme inducers (e.g., carbamazepine [15]). Here, future clinical investigations of DD(G)I scenarios with concomitant use of (*E*)-Clom and CYP enzyme inducers are required for evaluation of such model predictions with clinically observed data. For the translation of exposure differences into dose recommendations, studies quantifying the efficacy- and safety-related contributions of (*E*)-Clom and its metabolites would be of high interest.

## 5. Conclusions

A whole-body parent–metabolite PBPK model of (*E*)-Clom including the metabolites (*E*)-4-OH-Clom, (*E*)-DE-Clom and (*E*)-4-OH-DE-Clom was successfully developed. The model predicted plasma concentration–time profiles of (*E*)-Clom and its metabolites for CYP2D6 DGI, as well as CYP2D6 and CYP3A4 DDI and DDGI scenarios in six different CYP2D6 AS groups. For this, an in vitro–in vivo extrapolation approach to obtain CYP2D6  $k_{cat}$  values for different AS was successfully integrated to predict plasma profiles for IM (AS = 0.5, AS = 0.75, AS = 1) and UM populations. Furthermore, the model was applied to investigate the contribution of metabolic pathways to the elimination of (*E*)-Clom and its metabolites. The developed PBPK model will be made publicly available ([http:](http://)

[//models.clinicalpharmacy.me/](https://models.clinicalpharmacy.me/)) and can be further leveraged to investigate the PK of (E)-Clom and its metabolites for various DD(G)I scenarios.

**Supplementary Materials:** The following supporting information can be downloaded at: <https://www.mdpi.com/article/10.3390/pharmaceutics14122604/s1>, Figure S1: Predicted and observed plasma concentration-time profiles (linear scale) of (E)-Clom (a–f), (E)-4-OH-Clom (g–l), (E)-DE-Clom (m–r) and (E)-4-OH-DE-Clom (s–x) for DGI scenarios; Figure S2: Predicted and observed plasma concentration-time profiles (semilogarithmic scale) of (E)-Clom (a–f), (E)-4-OH-Clom (g–l), (E)-DE-Clom (m–r) and (E)-4-OH-DE-Clom (s–x) for DGI scenarios; Figure S3: Predicted versus observed AUC<sub>last</sub> (a), C<sub>max</sub> (b) and plasma concentrations (c) of (E)-Clom (circles), (E)-4-OH-Clom (triangles), (E)-DE-Clom (squares) and (E)-4-OH-DE-Clom (diamonds) in PM, IM, NM and UM (DGI scenarios); Figure S4: Predicted versus observed DGI AUC<sub>last</sub> (a) and C<sub>max</sub> (b) ratios of (E)-Clom (circles), (E)-4-OH-Clom (triangles), (E)-DE-Clom (squares) and (E)-4-OH-DE-Clom (diamonds) in PM, IM and UM; Figure S5: Predicted and observed renal excretion profiles (linear scale) of (E)-Clom (a–f), (E)-4-OH-Clom (g–l), (E)-DE-Clom (m–r) and (E)-4-OH-DE-Clom (s–x) for DGI scenarios; Figure S6: Predicted and observed plasma concentration-time profiles (linear scale) of digitized studies from literature after single (a,b) and multiple (c–f) dosing; Figure S7: Predicted and observed plasma concentration-time profiles (semilogarithmic scale) of digitized studies from literature after single (a,b) and multiple (c–f) dosing; Figure S8: Predicted versus observed (a) AUC<sub>last</sub>, (b) C<sub>max</sub> and (c) plasma concentrations of (E)-Clom; Figure S9: Predicted and observed plasma concentration-time profiles (linear scale) of (E)-Clom (a–e), (E)-4-OH-Clom (f–j), (E)-DE-Clom (k–o) and (E)-4-OH-DE-Clom (p–t) for DD(G)I scenarios in PM, IM, NM and UM; Figure S10: Predicted and observed plasma concentration-time profiles (semilogarithmic scale) of (E)-Clom (a–e), (E)-4-OH-Clom (f–j), (E)-DE-Clom (k–o) and (E)-4-OH-DE-Clom (p–t) for DD(G)I scenarios in PM, IM, NM and UM; Figure S11: Predicted versus observed AUC<sub>last</sub> (a), C<sub>max</sub> (b) and plasma concentrations (c) of (E)-Clom (circles), (E)-4-OH-Clom (triangles), (E)-DE-Clom (squares) and (E)-4-OH-DE-Clom (diamonds) for DD(G)I scenarios with clarithromycin and paroxetine, respectively in PM, IM, NM and UM; Figure S12: Predicted versus observed DD(G)I AUC<sub>last</sub> (a) and C<sub>max</sub> (b) ratios of (E)-Clom (circles), (E)-4-OH-Clom (triangles), (E)-DE-Clom (squares) and (E)-4-OH-DE-Clom (diamonds) in PM, IM, NM and UM; Figure S13: Predicted and observed renal excretion profiles (linear scale) of (E)-Clom (a–e), (E)-4-OH-Clom (f–j), (E)-DE-Clom (k–o) and (E)-4-OH-DE-Clom (p–t) for DD(G)I scenarios in PM, IM, NM and UM; Figure S14: Sensitivity analysis of the PBPK model for (E)-Clom, (E)-4-OH-Clom, (E)-DE-Clom and (E)-4-OH-DE-Clom; Figure S15: Molecular structures of (E)-Clom (a) and its metabolites (E)-DE-Clom (b), (E)-4-OH-Clom (c) and (E)-4-OH-DE-Clom (d); Table S1: Optimized CYP2D6 k<sub>cat</sub> values for each study; Table S2: Overview of clinical study data from literature used for model evaluation; Table S3: System-dependent parameters and expression of relevant enzymes; Table S4: Drug-dependent parameters for (E)-clomiphene; Table S5: Drug-dependent parameters for (E)-N-desethylclomiphene; Table S6: Drug-dependent parameters for (E)-4-hydroxyclophene; Table S7: Drug-dependent parameters for (E)-4-hydroxy-N-desethyl-clomiphene; Table S8: Employed in vitro scaling factors (IVSFs) for individual CYP2D6 activity scores; Table S9: Mean relative deviation (MRD) values of DGI plasma concentration predictions; Table S10: Mean relative deviation (MRD) values of DD(G)I plasma concentration predictions; Table S11: Geometric Mean Fold Error (GMFE) of AUC<sub>last</sub> and C<sub>max</sub> DGI Predictions; Table S12: Geometric Mean Fold Error (GMFE) of DGI AUC<sub>last</sub> and C<sub>max</sub> ratio; Table S13: Geometric Mean Fold Error (GMFE) of AUC<sub>last</sub> and C<sub>max</sub> DD(G)I Predictions; Table S14: Geometric Mean Fold Error (GMFE) of DD(G)I AUC<sub>last</sub> and C<sub>max</sub> ratios. References [50–80] are cited in the Supplementary Materials.

**Author Contributions:** Conceptualization, C.K., L.K., R.K., T.E.M., M.S. and T.L.; Data curation, C.K.; Formal analysis, C.K., S.R. and D.S.; Funding acquisition, M.S. and T.L.; Investigation, C.K., L.K., B.G., P.K., S.I., R.K., E.S. and T.E.M.; Methodology, C.K., L.K., S.R., D.S., B.G., P.K., E.S. and T.E.M.; Project administration, T.E.M., M.S. and T.L.; Resources, M.S. and T.L.; Software, C.K. and D.S.; Supervision, T.E.M., M.S. and T.L.; Validation, C.K., L.K., D.S., T.E.M., M.S. and T.L.; Visualization, C.K. and L.K.; Writing—original draft, C.K. and T.L.; Writing—review and editing, C.K., L.K., S.R., D.S., B.G., P.K., S.I., R.K., E.S., T.E.M., M.S. and T.L. All authors have read and agreed to the published version of the manuscript.

**Funding:** This research was funded by the Robert Bosch Stiftung, Stuttgart, Germany, the European Commission Horizon 2020 UPGx grant 668353 and the German Federal Ministry of Education and Research (BMBF) grant 031L0188D “GUIDE-IBD”.

**Institutional Review Board Statement:** The pharmacokinetic panel study (EudraCT-Nr.: 2009-014531-20, ClinicalTrials.gov: NCT01289756) was conducted in accordance with the Declaration of Helsinki, and approved by the Ethics Committee of the University of Tübingen (408/2009AMG1) and the German Federal Institute for Drugs and Medical Devices (BfArM: 4035694).

**Informed Consent Statement:** Informed consent was obtained from all subjects involved in the study.

**Data Availability Statement:** The developed PBPK model will be made publicly available (<http://models.clinicalpharmacy.me/>).

**Conflicts of Interest:** The authors declare no conflict of interest.

## References

- Legro, R.S.; Barnhart, H.X.; Schlaff, W.D.; Carr, B.R.; Diamond, M.P.; Carson, S.A.; Steinkampf, M.P.; Coutifaris, C.; McGovern, P.G.; Cataldo, N.A.; et al. Clomiphene, metformin, or both for infertility in the polycystic ovary syndrome. *N. Engl. J. Med.* **2007**, *356*, 551–566. [\[CrossRef\]](#) [\[PubMed\]](#)
- Deswal, R.; Narwal, V.; Dang, A.; Pundir, C.S. The prevalence of polycystic ovary syndrome: A brief systematic review. *J. Hum. Reprod. Sci.* **2022**, *13*, 261–271. [\[CrossRef\]](#)
- Jungheim, E.S.; Odibo, A.O. Fertility treatment in women with polycystic ovary syndrome: A decision analysis of different oral ovulation induction agents. *Fertil. Steril.* **2010**, *94*, 2659–2664. [\[CrossRef\]](#) [\[PubMed\]](#)
- European Medicines Agency (2018) Assessment Report EnCyzix. Available online: [https://www.ema.europa.eu/en/documents/assessment-report/encyzix-epar-public-assessment-report\\_en.pdf](https://www.ema.europa.eu/en/documents/assessment-report/encyzix-epar-public-assessment-report_en.pdf) (accessed on 12 August 2021).
- Mürdter, T.E.; Kerb, R.; Turpeinen, M.; Schroth, W.; Ganchev, B.; Böhmer, G.M.; Igel, S.; Schaeffeler, E.; Zanger, U.; Brauch, H.; et al. Genetic polymorphism of cytochrome p450 2D6 determines oestrogen receptor activity of the major infertility drug clomiphene via its active metabolites. *Hum. Mol. Genet.* **2012**, *21*, 1145–1154. [\[CrossRef\]](#) [\[PubMed\]](#)
- Kröner, P. Hydroxylierte Metaboliten des Clomifens: In vitro und in vivo Untersuchungen zur Bildung, Aktivität und Konjugation. Ph.D. Thesis, Eberhard-Karls-University Tübingen, Tübingen, Germany, 2018.
- Dickey, R.P.; Holtkamp, D.E. Development, pharmacology and clinical experience with clomiphene citrate. *Hum. Reprod. Update* **1996**, *2*, 483–506. [\[CrossRef\]](#)
- Garg, A.; Singh, B.; Sharma, R.; Singh, A.; Kumar, A. Selective Estrogen Receptor Modulators (SERMs): Mechanistic insights against microbial infections. *Curr. Mol. Med.* **2019**, *20*, 102–115. [\[CrossRef\]](#)
- Garg, A.; Singh, A.; Kumar, A. Selective estrogen receptor modulators against Gram-positive and Gram-negative bacteria: An experimental study. *Future Microbiol.* **2021**, *16*, 987–1001. [\[CrossRef\]](#)
- Homburg, R. Clomiphene citrate—end of an era? A mini-review. *Hum. Reprod.* **2005**, *20*, 2043–2051. [\[CrossRef\]](#)
- Rostami-Hodjegan, A.; Lennard, M.S.; Tucker, G.T.; Ledger, W.L. Monitoring plasma concentrations to individualize treatment with clomiphene citrate. *Fertil. Steril.* **2004**, *81*, 1187–1193. [\[CrossRef\]](#)
- Saha, L.; Kaur, S.; Saha, P.K. Pharmacotherapy of polycystic ovary syndrome—An update. *Fundam. Clin. Pharmacol.* **2012**, *26*, 54–62. [\[CrossRef\]](#)
- Kröner, P.; Heinkel, G.; Kerb, R.; Igel, S.; Schwab, M.; Mürdter, T.E. Stereoselective quantification of phase 1 and 2 metabolites of clomiphene in human plasma and urine. *Talanta* **2021**, *221*, 121658. [\[CrossRef\]](#)
- Ji, M.; Kim, K.-R.; Lee, W.; Choe, W.; Chun, S.; Min, W.-K. Genetic polymorphism of CYP2D6 and clomiphene concentrations in infertile patients with ovulatory dysfunction treated with clomiphene citrate. *J. Korean Med. Sci.* **2016**, *31*, 310–314. [\[CrossRef\]](#) [\[PubMed\]](#)
- Fuhr, L.M.; Marok, F.Z.; Hanke, N.; Selzer, D.; Lehr, T. Pharmacokinetics of the CYP3A4 and CYP2B6 inducer carbamazepine and its drug-drug interaction potential: A physiologically based pharmacokinetic modeling approach. *Pharmaceutics* **2021**, *13*, 270. [\[CrossRef\]](#) [\[PubMed\]](#)
- Hanke, N.; Frechen, S.; Moj, D.; Britz, H.; Eissing, T.; Wendl, T.; Lehr, T. PBPK models for CYP3A4 and P-gp DDI prediction: A modeling network of rifampicin, itraconazole, clarithromycin, midazolam, alfentanil, and digoxin. *CPT Pharmacomet. Syst. Pharmacol.* **2018**, *7*, 647–659. [\[CrossRef\]](#) [\[PubMed\]](#)
- Schroth, W.; Winter, S.; Mürdter, T.; Schaeffeler, E.; Eccles, D.; Eccles, B.; Chowbay, B.; Khor, C.C.; Tfayli, A.; Zgheib, N.K.; et al. Improved prediction of endoxifen metabolism by CYP2D6 genotype in breast cancer patients treated with tamoxifen. *Front. Pharmacol.* **2017**, *8*, 582. [\[CrossRef\]](#)
- Caudle, K.E.; Sangkuhl, K.; Whirl-Carrillo, M.; Swen, J.J.; Haidar, C.E.; Klein, T.E.; Gammal, R.S.; Relling, M.V.; Scott, S.A.; Hertz, D.L.; et al. Standardizing CYP2D6 genotype to phenotype translation: Consensus recommendations from the clinical pharmacogenetics implementation consortium and dutch pharmacogenetics working group. *Clin. Transl. Sci.* **2020**, *13*, 116–124. [\[CrossRef\]](#)



19. FDA Drug Development and Drug Interactions. Table of Substrates, Inhibitors and Inducers. Available online: <https://www.fda.gov/drugs/drug-interactions-labeling/drug-development-and-drug-interactions-table-substrates-inhibitors-and-inducers> (accessed on 13 January 2022).
20. Ganchev, B.; Heinkele, G.; Kerb, R.; Schwab, M.; Mürdter, T.E. Quantification of clomiphene metabolite isomers in human plasma by rapid-resolution liquid chromatography-electrospray ionization-tandem mass spectrometry. *Anal. Bioanal. Chem.* **2011**, *400*, 3429–3441. [CrossRef] [PubMed]
21. Mikkelsen, T.J.; Kroboth, P.D.; Cameron, W.J.; Dittert, L.W.; Chungi, V.; Manberg, P.J. Single-dose pharmacokinetics of clomiphene citrate in normal volunteers \*\*Supported by a grant from Serono Laboratories, Inc., Randolph, Massachusetts. *Fertil. Steril.* **1986**, *46*, 392–396. [CrossRef]
22. Ratiopharm GmbH Clomifen-ratiopharm®50 mg Tabletten (Study 1991). Available online: <https://www.ratiopharm.de/produkte/details/paeparate/paeparedaten/detail/pzn-3884844.html> (accessed on 23 November 2021).
23. Wiehle, R.; Cunningham, G.R.; Pitteloud, N.; Wike, J.; Hsu, K.; Fontenot, G.K.; Rosner, M.; Dwyer, A.; Podolski, J. Testosterone restoration by enclomiphene citrate in men with secondary hypogonadism: Pharmacodynamics and pharmacokinetics. *BJU Int.* **2013**, *112*, 1188–1200. [CrossRef]
24. Miller, G.D.; Moore, C.; Nair, V.; Hill, B.; Willick, S.E.; Rogol, A.D.; Eichner, D. Hypothalamic-pituitary-testicular axis effects and urinary detection following clomiphene administration in males. *J. Clin. Endocrinol. Metab.* **2019**, *104*, 906–914. [CrossRef]
25. Lippert, J.; Burghaus, R.; Edginton, A.; Frechen, S.; Karlsson, M.; Kovar, A.; Lehr, T.; Milligan, P.; Nock, V.; Ramusovic, S.; et al. Open systems pharmacology community-an open access, open source, open science approach to modeling and simulation in pharmaceutical sciences. *CPT Pharmacomet. Syst. Pharmacol.* **2019**, *8*, 878–882. [CrossRef]
26. Wojtyniak, J.-G.; Britz, H.; Selzer, D.; Schwab, M.; Lehr, T. Data digitizing: Accurate and precise data extraction for quantitative systems pharmacology and physiologically-based pharmacokinetic modeling. *CPT Pharmacomet. Syst. Pharmacol.* **2020**, *9*, 322–331. [CrossRef] [PubMed]
27. R Core Team. *R: A Language and Environment for Statistical Computing*; R Foundation for Statistical Computing: Vienna, Austria, 2021.
28. Ganchev, B. Charakterisierung der Metabolischen Bioaktivierung des Clomifens unter Besonderer Berücksichtigung Genetischer Polymorphismen. Ph.D. Thesis, Eberhard Karls University Tübingen, Tübingen, Germany, 2014.
29. Obach, R.S.; Walsky, R.L.; Venkatakrishnan, K. Mechanism-based inactivation of human cytochrome p450 enzymes and the prediction of drug-drug interactions. *Drug Metab. Dispos.* **2007**, *35*, 246–255. [CrossRef] [PubMed]
30. Rüdesheim, S.; Selzer, D.; Mürdter, T.; Igel, S.; Kerb, R.; Schwab, M.; Lehr, T. Physiologically based pharmacokinetic modeling to describe the CYP2D6 activity score-dependent metabolism of paroxetine, atomoxetine and risperidone. *Pharmaceutics* **2022**, *14*, 1734. [CrossRef] [PubMed]
31. Open Systems Pharmacology Suite Community. Open Systems Pharmacology Suite Manual. Available online: <https://raw.githubusercontent.com/Open-Systems-Pharmacology/OSPSuite.Documentation/master/OpenSystemsPharmacologySuite.pdf> (accessed on 23 November 2021).
32. Guest, E.J.; Aarons, L.; Houston, J.B.; Rostami-Hodjegan, A.; Galetin, A. Critique of the two-fold measure of prediction success for ratios: Application for the assessment of drug-drug interactions. *Drug Metab. Dispos.* **2011**, *39*, 170–173. [CrossRef]
33. Les Laboratoires Servier Servier Medical Art. Available online: <https://smart.servier.com/> (accessed on 12 August 2021).
34. Kousta, E.; White, D.M.; Franks, S. Modern use of clomiphene citrate in induction of ovulation. *Hum. Reprod. Update* **1997**, *3*, 359–365. [CrossRef]
35. Imani, B.; Eijkemans, M.J.C.; Te Velde, E.R.; Habbema, J.D.F.; Fauser, B.C.J.M. Predictors of patients remaining anovulatory during clomiphene citrate induction of ovulation in normogonadotropic oligoamenorrhoeic infertility. *J. Clin. Endocrinol. Metab.* **1998**, *83*, 2361–2365. [CrossRef]
36. Kim, M.-J.; Byeon, J.-Y.; Kim, Y.-H.; Kim, S.-H.; Lee, C.-M.; Jung, E.H.; Chae, W.K.; Lee, Y.J.; Jang, C.-G.; Lee, S.-Y.; et al. Effect of the CYP2D6\*10 allele on the pharmacokinetics of clomiphene and its active metabolites. *Arch. Pharm. Res.* **2018**, *41*, 347–353. [CrossRef]
37. Ellakwa, H.E.; Sanad, Z.F.; Hamza, H.A.; Emara, M.A.; Elsayed, M.A. Predictors of patient responses to ovulation induction with clomiphene citrate in patients with polycystic ovary syndrome experiencing infertility. *Int. J. Gynaecol. Obstet.* **2016**, *133*, 59–63. [CrossRef]
38. Mahran, A.; Abdelmeged, A.; El-Adawy, A.R.; Eissa, M.K.; Shaw, R.W.; Amer, S.A. The predictive value of circulating anti-Müllerian hormone in women with polycystic ovarian syndrome receiving clomiphene citrate: A prospective observational study. *J. Clin. Endocrinol. Metab.* **2013**, *98*, 4170–4175. [CrossRef]
39. Amer, S.A.; Mahran, A.; Abdelmaged, A.; El-Adawy, A.R.; Eissa, M.K.; Shaw, R.W. The influence of circulating anti-Müllerian hormone on ovarian responsiveness to ovulation induction with gonadotrophins in women with polycystic ovarian syndrome: A pilot study. *Reprod. Biol. Endocrinol.* **2013**, *11*, 115. [CrossRef]
40. Ghobadi, C.; Gregory, A.; Crewe, H.K.; Rostami-Hodjegan, A.; Lennard, M.S. CYP2D6 is primarily responsible for the metabolism of clomiphene. *Drug Metab. Pharmacokinet.* **2008**, *23*, 101–105. [CrossRef] [PubMed]
41. Rüdesheim, S.; Selzer, D.; Fuhr, U.; Schwab, M.; Lehr, T. Physiologically-based pharmacokinetic modeling of dextromethorphan to investigate interindividual variability within CYP2D6 activity score groups. *CPT Pharmacomet. Syst. Pharmacol.* **2022**, *11*, 494–511. [CrossRef]

42. Gaedigk, A.; Dinh, J.C.; Jeong, H.; Prasad, B.; Leeder, J.S. Ten years' experience with the CYP2D6 activity score: A perspective on future investigations to improve clinical predictions for precision therapeutics. *J. Pers. Med.* **2018**, *8*, 15. [CrossRef] [PubMed]
43. Mazzarino, M.; Biava, M.; de la Torre, X.; Fiacco, I.; Botrè, F. Characterization of the biotransformation pathways of clomiphene, tamoxifen and toremifene as assessed by LC-MS/(MS) following in vitro and excretion studies. *Anal. Bioanal. Chem.* **2013**, *405*, 5467–5487. [CrossRef] [PubMed]
44. Hill, S.; Arutchelvam, V.; Quinton, R. Enclomiphene, an estrogen receptor antagonist for the treatment of testosterone deficiency in men. *IDrugs* **2009**, *12*, 109–119.
45. Szutu, M.; Morgan, D.J.; McLeish, M.; Phillipou, G.; Blackman, G.L.; Cox, L.W.; Dollman, W. Pharmacokinetics of intravenous clomiphene isomers. *Br. J. Clin. Pharmacol.* **1989**, *27*, 639–640. [CrossRef]
46. Mazzarino, M.; Fiacco, I.; de la Torre, X.; Botrè, F. A mass spectrometric approach for the study of the metabolism of clomiphene, tamoxifen and toremifene by liquid chromatography time-of-flight spectroscopy. *Eur. J. Mass Spectrom.* **2008**, *14*, 171–180. [CrossRef]
47. Lu, J.; He, G.; Wang, X.; Xu, Y.; Wu, Y.; Dong, Y.; He, Z.; Liu, X.; Bo, T.; Ouyang, G. Mass spectrometric identification and characterization of new clomiphene metabolites in human urine by liquid chromatography-quadrupole time-of-flight tandem mass spectrometry. *J. Chromatogr. A* **2012**, *1243*, 23–32. [CrossRef]
48. Sheiner, L.B. Learning versus confirming in clinical drug development. *Clin. Pharmacol. Ther.* **1997**, *61*, 275–291. [CrossRef]
49. Jones, H.; Rowland-Yeo, K. Basic concepts in physiologically based pharmacokinetic modeling in drug discovery and development. *CPT Pharmacomet. Syst. Pharmacol.* **2013**, *2*, 63. [CrossRef] [PubMed]
50. Van der Lee, M.; Allard, W.G.; Vossen, R.H.A.M.; Baak-Pablo, R.F.; Menafrà, R.; Deiman, B.A.L.M.; Deenen, M.J.; Neven, P.; Johansson, I.; Gastaldello, S.; et al. Toward predicting CYP2D6-mediated variable drug response from CYP2D6 gene sequencing data. *Sci. Transl. Med.* **2021**, *13*, eabf3637. [CrossRef] [PubMed]
51. Valentin, J. Basic anatomical and physiological data for use in radiological protection: Reference values. A report of age- and gender-related differences in the anatomical and physiological characteristics of reference individuals. ICRP Publication 89. *Ann. ICRP* **2002**, *32*, 5–265.
52. Open Systems Pharmacology Suite Community. PK-Sim@Ontogeny Database Documentation, Version 7.3. Available online: <https://github.com/Open-Systems-Pharmacology/OSPSuite.Documentation/blob/master/PK-Sim%20Ontogeny%20Database%20Version%207.3.pdf> (accessed on 25 March 2020).
53. National Center for Health Statistics Hyattsville. 20782 Third National Health and Nutrition Examination Survey, NHANES III (1988–1994). Available online: <https://www.cdc.gov/nchs/nhanes/nhanes3/default.aspx> (accessed on 25 March 2020).
54. Willmann, S.; Höhn, K.; Edginton, A.; Sevestre, M.; Solodenko, J.; Weiss, W.; Lippert, J.; Schmitt, W. Development of a physiology-based whole-body population model for assessing the influence of individual variability on the pharmacokinetics of drugs. *J. Pharmacokinet. Pharmacodyn.* **2007**, *34*, 401–431. [CrossRef]
55. Rodrigues, A.D. Integrated cytochrome P450 reaction phenotyping. Attempting to bridge the gap between cDNA-expressed cytochromes P450 and native human liver microsomes. *Biochem. Pharmacol.* **1999**, *57*, 465–480. [CrossRef]
56. Nishimura, M.; Naito, S. Tissue-specific mRNA Expression Profiles of Human ATP-binding Cassette and Solute Carrier Transporter Superfamilies. *Drug Metab. Pharmacokinet.* **2005**, *20*, 452–477. [CrossRef]
57. Rowland Yeo, K.; Walsky, R.L.; Jamei, M.; Rostami-Hodjegan, A.; Tucker, G.T. Prediction of time-dependent CYP3A4 drug-drug interactions by physiologically based pharmacokinetic modelling: Impact of inactivation parameters and enzyme turnover. *Eur. J. Pharm. Sci.* **2011**, *43*, 160–173. [CrossRef]
58. Greenblatt, D.J.; von Moltke, L.L.; Harmatz, J.S.; Chen, G.; Weemhoff, J.L.; Jen, C.; Kelley, C.J.; LeDuc, B.W.; Zinny, M.A. Time course of recovery of cytochrome p450 3A function after single doses of grapefruit juice. *Clin. Pharmacol. Ther.* **2003**, *74*, 121–129. [CrossRef]
59. Tsamandouras, N.; Rostami-Hodjegan, A.; Aarons, L. Combining the 'bottom up' and 'top down' approaches in pharmacokinetic modelling: Fitting PBPK models to observed clinical data. *Br. J. Clin. Pharmacol.* **2015**, *79*, 48–55. [CrossRef]
60. Austin, R.P.; Barton, P.; Cockroft, S.L.; Wenlock, M.C.; Riley, R.J. The influence of nonspecific microsomal binding on apparent intrinsic clearance, and its prediction from physicochemical properties. *Drug Metab. Dispos.* **2002**, *30*, 1497–1503. [CrossRef]
61. Obach, R.S. Nonspecific binding to microsomes: Impact on scale-up of in vitro intrinsic clearance to hepatic clearance as assessed through examination of warfarin, imipramine, and propranolol. *Drug Metab. Dispos. Biol. Fate Chem.* **1997**, *25*, 1359–1369. [PubMed]
62. Watanabe, R.; Esaki, T.; Kawashima, H.; Natsume-Kitatani, Y.; Nagao, C.; Ohashi, R.; Mizuguchi, K. Predicting Fraction Unbound in Human Plasma from Chemical Structure: Improved Accuracy in the Low Value Ranges. *Mol. Pharm.* **2018**, *15*, 5302–5311. [CrossRef] [PubMed]
63. Siramshetty, V.B.; Grishagin, I.; Nguyễn, Đ.T.; Peryea, T.; Skovpen, Y.; Stroganov, O.; Katzel, D.; Sheils, T.; Jadhav, A.; Mathé, E.A.; et al. NCATS Inxight Drugs: A comprehensive and curated portal for translational research. *Nucleic Acids Res.* **2022**, *50*, D1307–D1316. [CrossRef] [PubMed]
64. Developed by ChemAxon (2009), Chemicalize Was Used for Prediction of (E)-Clomiphene Properties. Available online: <https://chemicalize.com/> (accessed on 9 August 2021).
65. Das, P.; Prajapati, M.; Maity, A. Study of equilibrium solubility of Clomiphene Citrate as model compound by Saturation orbital shake flask method. *J. Pharm. Adv. Res.* **2020**, *3*, 843–847.

- 
66. Smith, D.A.; Dalvie, D. Why do metabolites circulate? *Xenobiotica* **2012**, *42*, 107–126. [[CrossRef](#)] [[PubMed](#)]
  67. Wishart, D.S.; Knox, C.; Guo, A.C.; Shrivastava, S.; Hassanali, M.; Stothard, P.; Chang, Z.; Woolsey, J. DrugBank: A comprehensive resource for in silico drug discovery and exploration. *Nucleic Acids Res.* **2006**, *34*, D668–D672. [[CrossRef](#)]
  68. Güngör, S.; Delgado-Charro, M.B.; Masini-Etévé, V.; Potts, R.O.; Guy, R.H. Transdermal flux predictions for selected selective oestrogen receptor modulators (SERMs): Comparison with experimental results. *J. Control. Release Off. J. Control. Release Soc.* **2013**, *172*, 601–606. [[CrossRef](#)]
  69. Schmitt, W. General approach for the calculation of tissue to plasma partition coefficients. *Toxicol. Vitro. Int. J. Publ. Assoc. BIBRA* **2008**, *22*, 457–467. [[CrossRef](#)]
  70. Kawai, R.; Lemaire, M.; Steimer, J.L.; Bruelisauer, A.; Niederberger, W.; Rowland, M. Physiologically based pharmacokinetic study on a cyclosporin derivative, SDZ IMM 125. *J. Pharmacokinet. Biopharm.* **1994**, *22*, 327–365. [[CrossRef](#)] [[PubMed](#)]
  71. Developed by ChemAxon (2009), Chemicalize Was Used for Prediction of (E)-N-Desethylclomiphene Properties. Available online: <https://chemicalize.com/> (accessed on 9 August 2021).
  72. Kim, S.; Chen, J.; Cheng, T.; Gindulyte, A.; He, J.; He, S.; Li, Q.; Shoemaker, B.A.; Thiessen, P.A.; Yu, B.; et al. PubChem in 2021: New data content and improved web interfaces. *Nucleic Acids Res.* **2021**, *49*, D1388–D1395. [[CrossRef](#)]
  73. Rodgers, T.; Leahy, D.; Rowland, M. Physiologically based pharmacokinetic modeling 1: Predicting the tissue distribution of moderate-to-strong bases. *J. Pharm. Sci.* **2005**, *94*, 1259–1276. [[CrossRef](#)] [[PubMed](#)]
  74. Rodgers, T.; Rowland, M. Physiologically based pharmacokinetic modelling 2: Predicting the tissue distribution of acids, very weak bases, neutrals and zwitterions. *J. Pharm. Sci.* **2006**, *95*, 1238–1257. [[CrossRef](#)] [[PubMed](#)]
  75. Developed by ChemAxon (2009), Chemicalize Was Used for Prediction of (E)-4-Hydroxyclophene Properties. Available online: <https://chemicalize.com/> (accessed on 9 August 2021).
  76. Berezhkovskiy, L.M. Volume of distribution at steady state for a linear pharmacokinetic system with peripheral elimination. *J. Pharm. Sci.* **2004**, *93*, 1628–1640. [[CrossRef](#)]
  77. Developed by ChemAxon (2009), Chemicalize Was Used for Prediction of (E)-4-Hydroxy-N-desethylclomiphene Properties. Available online: <https://chemicalize.com/> (accessed on 9 August 2021).
  78. T'jollyn, H.; Snoeys, J.; Vermeulen, A.; Michelet, R.; Cuyckens, F.; Mannens, G.; Van Peer, A.; Annaert, P.; Allegaert, K.; Van Bocxlaer, J.; et al. Physiologically Based Pharmacokinetic Predictions of Tramadol Exposure Throughout Pediatric Life: An Analysis of the Different Clearance Contributors with Emphasis on CYP2D6 Maturation. *AAPS J.* **2015**, *17*, 1376–1387. [[CrossRef](#)]
  79. United States Pharmacopeial Convention. United States Pharmacopeia and National Formulary (USP 29-NF 24). 2006, p. 553. Available online: [http://www.pharmacopeia.cn/v29240/usp29nf24s0\\_m18490.html](http://www.pharmacopeia.cn/v29240/usp29nf24s0_m18490.html) (accessed on 24 August 2021).
  80. Beal, S.L. Ways to fit a PK model with some data below the quantification limit. *J. Pharmacokinet. Pharmacodyn.* **2001**, *28*, 481–504. [[CrossRef](#)]

#### 4.4 PROJECT IV – EXTERNAL PERFORMANCE EVALUATION OF INFLIXIMAB POPULATION PHARMACOKINETIC MODELS

##### 4.4.1 *Publication*

Schräpel, C., Kovar, L., Selzer, D., Hofmann, U., Tran, F., Reinisch, W., Schwab, M., & Lehr, T. (2021). External model performance evaluation of twelve infliximab population pharmacokinetic models in patients with inflammatory bowel disease. *Pharmaceutics*, 13(9), 1368. DOI: [10.3390/pharmaceutics13091368](https://doi.org/10.3390/pharmaceutics13091368) [175].

##### 4.4.2 *Author Contributions*

Author contributions according to the [CRediT](#) [1]:





Christina Kovar	Refer to <i>Contribution Report</i> (p. vii)
Lukas Kovar	Conceptualization, Formal Analysis, Investigation, Methodology, Software, Visualization, Writing – Original Draft, Writing – Review & Editing
Dominik Selzer	Data Curation, Formal Analysis, Methodology, Software, Visualization, Writing – Original Draft, Writing – Review & Editing
Ute Hofmann	Conceptualization, Funding Acquisition, Project Administration, Supervision, Writing – Review & Editing
Florian Tran	Conceptualization, Funding Acquisition, Project Administration, Supervision, Writing – Review & Editing
Walter Reinisch	Conceptualization, Funding Acquisition, Investigation, Project Administration, Resources, Supervision, Writing – Review & Editing
Matthias Schwab	Conceptualization, Funding Acquisition, Project Administration, Resources, Supervision, Writing – Review & Editing
Thorsten Lehr	Conceptualization, Funding Acquisition, Investigation, Project Administration, Resources, Supervision, Writing – Original Draft, Writing – Review & Editing

#### 4.4.3 *Copyright*

This article is an open access article distributed under the terms and conditions of the Creative Commons Attribution (CC BY) license (<https://creativecommons.org/licenses/by/4.0/>). © 2021 by the authors. Licensee MDPI, Basel, Switzerland.

## Article

# External Model Performance Evaluation of Twelve Infliximab Population Pharmacokinetic Models in Patients with Inflammatory Bowel Disease

Christina Schräpel <sup>1,2</sup> , Lukas Kovar <sup>1</sup> , Dominik Selzer <sup>1</sup>, Ute Hofmann <sup>2</sup> , Florian Tran <sup>3,4</sup>, Walter Reinisch <sup>5</sup>, Matthias Schwab <sup>2,6</sup> and Thorsten Lehr <sup>1,\*</sup> 

- <sup>1</sup> Clinical Pharmacy, Saarland University, 66123 Saarbrücken, Germany; christina.schraepel@uni-saarland.de (C.S.); lukas.kovar@uni-saarland.de (L.K.); dominik.selzer@uni-saarland.de (D.S.)
- <sup>2</sup> Dr. Margarete Fischer-Bosch-Institute of Clinical Pharmacology, University of Tübingen, 70376 Stuttgart, Germany; ute.hofmann@ikp-stuttgart.de (U.H.); matthias.schwab@ikp-stuttgart.de (M.S.)
- <sup>3</sup> Institute of Clinical Molecular Biology, Kiel University and University Medical Center Schleswig-Holstein, 24105 Kiel, Germany; f.tran@ikmb.uni-kiel.de
- <sup>4</sup> Department of Internal Medicine I, University Medical Center Schleswig-Holstein, 24105 Kiel, Germany
- <sup>5</sup> Department of Internal Medicine III, Medical University of Vienna, 1090 Vienna, Austria; walter.reinisch@meduniwien.ac.at
- <sup>6</sup> Departments of Clinical Pharmacology, Pharmacy and Biochemistry, University of Tübingen, 72076 Tübingen, Germany
- \* Correspondence: thorsten.lehr@mx.uni-saarland.de; Tel.: +49-681-302-70255



check for  
updates

**Citation:** Schräpel, C.; Kovar, L.; Selzer, D.; Hofmann, U.; Tran, F.; Reinisch, W.; Schwab, M.; Lehr, T. External Model Performance Evaluation of Twelve Infliximab Population Pharmacokinetic Models in Patients with Inflammatory Bowel Disease. *Pharmaceutics* **2021**, *13*, 1368. <https://doi.org/10.3390/pharmaceutics13091368>

Academic Editor: Neal M. Davies

Received: 31 July 2021

Accepted: 27 August 2021

Published: 31 August 2021

**Publisher's Note:** MDPI stays neutral with regard to jurisdictional claims in published maps and institutional affiliations.

**Abstract:** Infliximab is approved for treatment of various chronic inflammatory diseases including inflammatory bowel disease (IBD). However, high variability in infliximab trough levels has been associated with diverse response rates. Model-informed precision dosing (MIPD) with population pharmacokinetic models could help to individualize infliximab dosing regimens and improve therapy. The aim of this study was to evaluate the predictive performance of published infliximab population pharmacokinetic models for IBD patients with an external data set. The data set consisted of 105 IBD patients with 336 infliximab concentrations. Literature review identified 12 published models eligible for external evaluation. Model performance was evaluated with goodness-of-fit plots, prediction- and variability-corrected visual predictive checks (pvcVPCs) and quantitative measures. For anti-drug antibody (ADA)-negative patients, model accuracy decreased for predictions > 6 months, while bias did not increase. In general, predictions for patients developing ADA were less accurate for all models investigated. Two models with the highest classification accuracy identified necessary dose escalations (for trough concentrations < 5 µg/mL) in 88% of cases. In summary, population pharmacokinetic modeling can be used to individualize infliximab dosing and thereby help to prevent infliximab trough concentrations dropping below the target trough concentration. However, predictions of infliximab concentrations for patients developing ADA remain challenging.

**Keywords:** infliximab; population pharmacokinetics; inflammatory bowel disease; model-informed precision dosing; dose individualization



**Copyright:** © 2021 by the authors. Licensee MDPI, Basel, Switzerland. This article is an open access article distributed under the terms and conditions of the Creative Commons Attribution (CC BY) license (<https://creativecommons.org/licenses/by/4.0/>).

## 1. Introduction

Infliximab is an intravenously administered recombinant chimeric monoclonal antibody that inhibits both soluble and membrane-bound tumor necrosis factor alpha (TNF-α) [1]. Infliximab is approved for treatment of various chronic inflammatory diseases including the inflammatory bowel diseases (IBD) Crohn's disease (CD) and ulcerative colitis (UC) [2,3]. After its approval in 1999 by the European Medicines Agency (EMA), infliximab revolutionized the treatment of CD and UC because of its ability to induce long-term remission, reduce hospitalizations, and restore quality of life [4,5]. Today, infliximab is still widely used and available as different biosimilars [3].



Infliximab exhibits linear pharmacokinetic behavior, while low trough concentrations are associated with impaired or even loss of response to infliximab therapy [6–9]. UC patients with detectable serum infliximab trough concentrations showed a 4 times higher probability and CD patients even a 13 times higher probability of being in clinical remission, making serum infliximab levels a predictor of clinical response [6,9–12]. According to a recent guideline from the American Gastroenterological Association Institute, infliximab should be dosed to achieve target trough concentrations of  $\geq 5 \mu\text{g/mL}$  in order to improve therapy outcome [13]. However, a high inter-individual variability in infliximab trough levels has been observed contributing to a high rate of treatment failure [9,12–14]. About 10–40% of patients fail to respond to induction therapy (primary non-response) [15], and subsequently, 13% of patients lose response annually after initially responding (secondary non-response) [16]. One of the reasons for primary and secondary non-response is the formation of anti-drug antibodies (ADAs) against infliximab, leading to an increased infliximab clearance (CL) [9,17,18].

A good understanding of the high variability in infliximab trough levels is essential for dose individualization strategies [4,19–22]. In the past, several efforts have been made to characterize infliximab pharmacokinetics (PK), including the quantification and explanation of inter-individual variability, and to develop population pharmacokinetic models for dose individualization [21,23–27]. While these analyses identified various covariates (e.g., albumin levels, sex, weight, ADA development, and use of concomitant immunomodulators) that influence infliximab CL and volume of distribution ( $V_d$ ), the covariates could only partly explain the observed inter-individual and inter-occasion variability (IOV) [23,24,26,27].

Thus, population pharmacokinetic models combined with data from therapeutic drug monitoring could help to optimize drug dosing regimens in individual patients via model-informed precision dosing (MIPD) [28–32]. Infliximab models have recently been used to simulate dosing regimens for different patient populations or for evaluation of individualized dose adjustments and incidences of loss of response [31,33,34]. However, a comprehensive external evaluation of the different infliximab population pharmacokinetic modeling approaches including assessment of accuracy and bias of model predictions over time as well as the ability to predict the need for dose escalation is still pending. Hence, the aim of this work was to provide an overview of published infliximab population pharmacokinetic models for patients with IBD as well as to evaluate and compare model performance with a focus on differences between ADA-negative and ADA-positive subpopulations in a Bayesian forecasting setting using an external data set.

## 2. Materials and Methods

### 2.1. External Evaluation Data Set

For predictive external model evaluation, data originated from a previously published observational study that was reviewed and approved by the institutional review board of the Medical University of Vienna [35]. All participating patients had signed an informed consent form.

Patients with an established diagnosis of CD and UC were enrolled in the study. All participants had previously responded to induction therapy, receiving three infusions at weeks zero, two, and six, and were assigned to a maintenance dosing regimen. Serum samples of patients (median 2, range 1–12 samples) were collected during infliximab therapy at both midpoint and trough times of a dosing interval while exact time points were not specified in the protocol. Laboratory and demographic data were collected, including serum infliximab concentrations, ADA levels, serum albumin concentrations, C-reactive protein levels, weight, use of concomitant immunomodulators, Harvey–Bradshaw index (HBI), and smoking status.

Serum infliximab concentrations used in this analysis were measured with a commercially available enzyme-linked immunosorbent assay (ELISA) method (Immundiagnostik Germany, Bensheim, Germany) with a lower limit of quantification (LLOQ) of

2.68 ng/mL [36]. ADA concentrations were determined using the homogeneous mobility shift assay (HMSA) from Prometheus Labs Inc., San Diego, CA, USA with an LLOQ of 3.13 U/mL [37]. Patients were assigned to the ADA-positive patient cohort if any measured ADA concentration was above the threshold of 6.6 U/mL [37,38].

## 2.2. Population Pharmacokinetic Models and Software

A comprehensive and systematic literature search in PubMed was performed for infliximab population pharmacokinetic analyses in patients with IBD. The search terms were “infliximab” AND “population” AND “pharmacokinetics” and reference lists of identified articles were manually screened for further eligible studies. Subsequently, modeling and study information was collected, including model structure, population pharmacokinetic parameter values, covariates, inter-individual variability, residual variability, information on patient cohorts, disease type, number of patients, number of collected blood samples, and ADA immunogenicity rate. The population pharmacokinetic models described in the gathered studies were implemented and evaluated using the nonlinear mixed effects modeling software NONMEM<sup>®</sup> version 7.4 (Icon Development Solutions, Ellicott City, MD, USA). Computations for prediction- and variability-corrected visual predictive checks (pvcVPCs) were generated with the PsN (version 4.9.0) tool “vpc” [39,40]. Data management, graphics, and quantitative model diagnostics were carried out using the R programming language version 3.6.3 (R Foundation for Statistical Computing, Vienna, Austria) and R Studio<sup>®</sup> version 1.2.5019 (R Studio, Inc., Boston, MA, USA).

## 2.3. Model Performance Evaluation

For the implemented population pharmacokinetic models, all parameters (fixed and random effects) were set to published values of the respective study. To assess the potential applications in a clinical setting, model performances to predict serum infliximab concentrations with a Bayesian approach were evaluated with the external data set. Here, the first measured serum infliximab concentration of each patient ( $C_{MAP}$ ) was used for maximum a posteriori (MAP) estimation of individual pharmacokinetic parameters (empirical Bayes pharmacokinetic parameter estimates [EBEs]) considering interaction between inter-individual variability and residual variability for prediction of subsequent serum infliximab concentrations (Bayesian forecasting). As recommended by Abrantes and coworkers, IOV was included in the estimation of EBEs but excluded in the calculation of individual pharmacokinetic parameters used for predictions [41]. For prospective predictions, individual patient covariates for times after  $C_{MAP}$  were imputed using last observation carried forward.

Visual and quantitative methods were applied for the evaluation of predictive model performances. Goodness-of-fit plots of individual predicted infliximab concentrations vs. observed infliximab concentrations were generated for visual evaluation. Moreover, two quantitative measures were calculated, including the median symmetric accuracy ( $\zeta$ , Equation (1)) and the symmetric signed percentage bias (SSPB, Equation (2)) to evaluate the model regarding prediction accuracy and prediction bias.

$$\zeta = 100 \times \left[ e^{\left( \text{median} \left( \left| \ln \left( \frac{y_i}{x_i} \right) \right| \right) \right)} - 1 \right], \quad (1)$$

$$\text{SSPB} = 100 \times \left[ \text{sign} \left( \text{median} \left( \ln \left( \frac{y_i}{x_i} \right) \right) \right) \right] \times \left[ e^{\left( \left| \text{median} \left( \ln \left( \frac{y_i}{x_i} \right) \right| \right) \right)} - 1 \right]. \quad (2)$$

In Equations (1) and (2)  $x_i$  represents the  $i$ th observed infliximab serum concentration and  $y_i$  the corresponding predicted serum concentration.

$\zeta$  represents the typical absolute percentage error with 50% of absolute percentage errors below  $\zeta$  [42]. The SSPB, a measure of bias, estimates the central tendency of the error penalizing underprediction and overprediction equally as illustrated by Morley and coworkers [42].



As mentioned before, dose escalation can be beneficial in patients with trough concentrations below the target threshold of 5 µg/mL. Hence, a model's ability to correctly predict the need for dose escalation was further investigated. For that, observed and predicted trough concentrations were split into two categories:  $C_{\text{trough}} < 5 \mu\text{g/mL}$  (dose escalation needed) and  $C_{\text{trough}} \geq 5 \mu\text{g/mL}$  (no dose escalation needed). Correct predictions of need for dose escalation are referred to as “true positive” while correct predictions of no need for dose escalation are referred to as “true negative”. Model accuracy, i.e., the fraction of observed and corresponding predicted trough concentrations, both  $< 5 \mu\text{g/mL}$  or both  $\geq 5 \mu\text{g/mL}$ , were calculated for all models. Here, model classification performance was evaluated for trough samples in which ADA status was negative and for trough samples in which ADA status was positive individually.

In addition, pvcVPCs were performed with multiple replicates ( $n = 1000$ ) of the study population. The simulated concentrations (median, 5th, and 95th percentiles), the corresponding 95% confidence intervals as well as prediction- and variability-corrected observed concentrations (with median, 5th, and 95th percentiles) were plotted against time after dose.

### 3. Results

#### 3.1. Characteristics of Published Population Pharmacokinetic Models of Infliximab in Patients with IBD

The comprehensive literature search in PubMed for population pharmacokinetic analyses of infliximab in patients with IBD revealed 25 population pharmacokinetic models, which are listed in Table 1 together with the respective model characteristics. The models partially differ both in base model structure as well as tested and integrated covariates. The majority of the studies used a 2-compartment model ( $n = 18$ ) with first-order elimination, while seven models implemented a 1-compartment model. Yet, five out of seven studies that used a 1-compartment base model were developed with sparse data including only infliximab trough samples in the model building process.

Integrated covariates on infliximab CL and central volume of distribution ( $V_c$ ) include patient characteristics (sex, weight, and age), clinical characteristics (albumin levels, HBI, ADA status, etc.) as well as concomitant medication of immunomodulators (IMM).

Of the 25 models, 14 included albumin concentrations, 14 weight, and four sex as a covariate on CL. Moreover, four models included an IOV for the CL parameter. Eighteen models integrated ADA as a covariate (sixteen as binary, one as ordinal, and one as continuous covariate), two models implemented a risk function of developing ADA, and three did not include ADA status in the model since only a small fraction of patients in the respective model building data set were ADA positive ( $\leq 3\%$ ). Two studies did not include ADA-positive patients for the model building process (see Table 1).

Furthermore, model building data sets vastly differed in patient and sample numbers, patient cohort (patients with CD/UC; adult/pediatric patients) as well as sampling times (see Table 1). Eleven models used data from both patients with CD and UC, eleven from patients with CD, and three from patients with UC. The majority of models were developed with data from adult patients (19/25), three with data from both adult and pediatric patients, and three with data from pediatric patients only.

#### 3.2. Eligible Population Pharmacokinetic Models for Evaluation

Twelve out of 25 population pharmacokinetic models (entries marked with an asterisk in Table 1) were eligible for model performance evaluation with the external data set. From Fasanmade et al., 2011, two of three models that were developed using a data set of adult patients and a data set of both pediatric and adult patients, respectively, were included in the analysis [24]. Edlund et al. published three different approaches for handling the ADA covariate [43]. All three models based on ADA measurements by HMSA were included in the analysis and are, hereafter, referred to as I (ADA covariate on the patient level), II (ADA covariate on sample level), and III (ADA concentrations as a continuous covariate). Eleven out of 25 models (Ternant et al., 2008 [44], Dotan et al., 2014 [45], Ter-

nant et al., 2015 [46], Brandse et al., 2017 [47], Kevans et al., 2018 [48], Dreesen et al., 2019 [49], Matsuoka et al., 2019 [50], Petitcollin et al., 2019 [51], Dreesen et al., 2020 [27], Bauman et al., 2020 [21], and Kantasiripitak et al., 2021 [26]) could not be evaluated because of data set incompatibility (e.g., missing covariates in our data set) or lack of reported model implementation details. The model by Grišić et al. was not included in the analysis as it was specifically focused on modeling the effects of pregnancy affecting infliximab PK [52]. In summary, models developed by Aubourg et al., 2015 [53], Buurman et al., 2015 [54], Brandse et al., 2016 [55], Edlund et al., 2017 (I–III) [43], Fasanmade et al., 2009 [23], Fasanmade et al., 2011 (adults and adults/children) [24], Passot et al., 2016 [56], Petitcollin et al., 2018 [25], and Xu et al., 2012 [57] were implemented and included in the external evaluation. Additional information on the investigated models regarding assumptions for model implementation (e.g., handling of missing units or ambiguities) are outlined in Section 1 of the Supplementary Materials.

### 3.3. External Evaluation Data Set

Four hundred serum infliximab concentrations from 124 patients were available in the data set. Data from 11 patients (33 infliximab concentrations total) were excluded because of insufficient information on the respective dosing regimen (e.g., unknown time of dosing). Three concentrations below the LLOQ (<1% of samples) were excluded from the external evaluation (M1 method) [58]. Moreover, 28 concentrations classified as pharmacokinetically implausible (concentrations that did not decrease over a sampling period of at least seven days within a dosing interval) were removed from the analysis. Consequently, eight patients lacked informative infliximab PK data, i.e., at least one sample with detectable infliximab concentrations, and were therefore excluded from the analysis.

As a result, a total of 336 infliximab concentrations from 105 patients with IBD, including 76 cases of CD and 29 cases of UC, were available for external evaluation (median number of infliximab samples per patient: 2; range: 1–12). Twenty-two patients had at least one positive ADA sample. In total, ADA levels above the threshold of 6.6 U/mL were measured in 49 samples. An overview of clinical and demographic patient characteristics of the external data set is presented in Table 2. Infliximab was administered to patients using various dosing regimens with a median (interquartile range (IQR)) infliximab dose of 5.5 (5.1–5.9) mg/kg and a median (IQR) dosing interval of 8.0 (7.7–8.6) weeks.

**Table 1.** Overview of published pharmacokinetic models for infliximab in patients with IBD.

Publication	CD/UC	Patient Cohort	No. of Patients (Samples)	Sampling Times	Base Model	Covariates on CL	Covariates on $V_c$	IOV	Induction/Maintenance <sup>1</sup>	Inclusion of ADA+ Patients	Ref.
Ternant et al., 2008	both	adults	33 (478)	peak, trough	2-CMT	ADA	sex, weight	-	both	yes (15%)	[44]
Fasanmade et al., 2009 *	UC	adults	482 (4145)	peak, midpoint, trough	2-CMT	ADA, alb, sex	sex, weight	-	both	yes (7%)	[23]
Fasanmade et al., 2011 (a) *	CD	adults	580 (/)	peak, midpoint, trough	2-CMT	ADA, alb, IMM, weight	weight <sup>2</sup>	CL	both	yes (11%)	[24]
Fasanmade et al., 2011 (c)	CD	children	112 (/)	peak, midpoint, trough	2-CMT	alb, weight	weight <sup>2</sup>	CL	both	yes (3%)	[24]
Fasanmade et al., 2011(a/c) *	CD	both	692 (5757)	peak, midpoint, trough	2-CMT	ADA, alb, IMM, weight	weight <sup>2</sup>	CL	both	yes (10%)	[24]
Xu et al., 2012 *	both	both	655 <sup>3</sup> (/)	/	2-CMT	ADA, alb, weight <sup>4</sup>	weight <sup>2</sup>	-	/	yes (/)	[57]
Dotan et al., 2014	both	adults	54 (169)	trough	2-CMT	ADA, alb, weight <sup>4</sup>	weight <sup>2</sup>	-	both	yes (31%)	[45]
Aubourg et al., 2015 *	CD	adults	133 (/)	trough, peak	2-CMT	sex	sex, weight	-	treatment initiation	no	[53]
Buurman et al., 2015 *	both	adults	42 (188)	trough	2-CMT	ADA, period <sup>5</sup> , sex	HBI	-	both	yes (5%)	[54]
Ternant et al., 2015	CD	adults	111 (546)	throughout dosing interval	1-CMT	FCGR3A-158V/V, hsCRP	-	-	maintenance	yes (2%)	[46]
Brandse et al., 2016 *	UC	adults	19 (/)	throughout dosing interval	2-CMT	ADA, alb	-	-	induction	yes (32%)	[55]
Passot et al., 2016 *	both	both	79 <sup>6</sup> (/)	trough	1-CMT	CD/UC, sex, weight	CD/UC, sex, weight	-	both	no	[56]
Brandse et al., 2017	both	adults	332 (997)	throughout dosing interval	2-CMT	ADA, alb, previous exposure, weight <sup>4</sup>	weight <sup>2</sup>	-	both	yes (23%)	[47]
Edlund et al., 2017(I–III) <sup>*,7</sup>	CD	adults	68 (152)	midpoint, trough	2-CMT	ADA <sup>8</sup> , weight <sup>4,9</sup>	weight <sup>2,9</sup>	-	maintenance	yes (37%)	[43]
Kevans et al., 2018	both	adults	51 (/)	throughout dosing interval	2-CMT	ADA, alb, weight <sup>4</sup> , time-varying CL <sup>10</sup>	weight <sup>2</sup>	-	induction	yes (11%)	[48]
Petitcollin et al., 2018 *	CD	children	20 (145)	trough	1-CMT	alb, time-varying CL/risk of immunization <sup>11</sup>	-	-	both	yes (15%)	[25]
Dreesen et al., 2019	UC	adults	204 (583)	trough	1-CMT	alb, CRP, Mayo	FFM, CS, panc.	CL	induction	yes (1%) <sup>12</sup>	[49]
Matsuoka et al., 2019	CD	adults	121 (832)	trough	1-CMT	ADA, alb, weight	-	-	maintenance	yes (26%)	[50]

Table 1. Cont.

Publication	CD/UC	Patient Cohort	No. of Patients (Samples)	Sampling Times	Base Model	Covariates on CL	Covariates on $V_c$	IOV	Induction/Maintenance <sup>1</sup>	Inclusion of ADA+ Patients	Ref.
Petitcollin et al., 2019	both	adults	91 (607)	trough	1-CMT	CD/UC, CRP, dose, Mayo, AZA, time-varying CL/risk of immunization <sup>11</sup> , weight <sup>13</sup>	-	-	maintenance	yes (1%)	[51]
Bauman et al., 2020	both	children	135 (289)	trough	2-CMT	ADA <sup>14</sup> , alb, ESR, weight	weight <sup>2</sup>	-	maintenance	yes (62%)	[21]
Dreesen et al., 2020	CD	adults	116 (1329)	midpoint, trough	2-CMT	ADA, alb, CDAI, fCal	-	-	both	yes (18%)	[27]
Grišić et al., 2020	both	pregnant	19 (172)	throughout dosing interval	1-CMT	ADA, 2nd/3rd trimester	-	-	both	yes (30%) <sup>12,15</sup>	[52]
Kantasiripitak et al., 2021	both	adults	104 (272)	trough	2-CMT	ADA, age, alb, CRP, FFM	-	-	induction	yes (13%)	[26]

Note: -: none; /: unknown; (a): (adults); (a/c): (adults/children); ADA: anti-drug antibodies; ADA+: anti-drug antibody positive; alb: albumin concentrations; AZA: azathioprine; (c): children; CD: Crohn's disease; CDAI: Crohn's disease activity index; CL: clearance; CMT: compartment; CRP: C-reactive protein; CS: corticosteroids; ESR: erythrocyte sedimentation rate; fCal: fecal calprotectin; FCGR3A-158V/V: Fc fragment of IgG, low affinity IIIa, receptor (CD16a) polymorphism; FFM: fat-free mass; HBI: Harvey–Bradshaw index; hsCRP: high-sensitivity C-reactive protein; IBD: inflammatory bowel disease; IMM: immunomodulators; IOV: inter-occasion variability; Mayo: Mayo score; No.: number; panc.: pancolitis; Ref.: reference; UC: ulcerative colitis;  $V_c$ : volume of central compartment; \* included in the external model performance evaluation; <sup>1</sup> blood sample data collected during induction and/or maintenance therapy; <sup>2</sup> covariate also on volume of peripheral compartment ( $V_p$ ); <sup>3</sup> 133 more pediatric patients with other inflammatory diseases were included; <sup>4</sup> covariate also on intercompartmental clearance (Q); <sup>5</sup> induction or maintenance phase; <sup>6</sup> 139 more patients with other inflammatory diseases were included; <sup>7</sup> three similar models with different handling of the ADA covariate; <sup>8</sup> ADA as binary or continuous covariate; <sup>9</sup> allometric scaling; <sup>10</sup> a component of CL that varies over time independent of patient factors; <sup>11</sup> describing varying infliximab CL over time (independent from ADA testing); <sup>12</sup> percentage of ADA-positive blood samples; <sup>13</sup> as a covariate on the CL increase over time; <sup>14</sup> ADA was included as an ordinal covariate with four categories; <sup>15</sup> samples with infliximab concentrations  $\leq 5 \mu\text{g/mL}$  were assessed for ADAs.

Table 2. Clinical and demographic patient characteristics.

Characteristic	Median or No.	Range	IQR
Patients, n	105		
Sex, female, n (%)	50 (48)		
Patients with CD, n (%)	76 (72)		
Patients with UC, n (%)	29 (28)		
ADA-positive patient status, n (%)	22 (21)		
IMM <sup>1</sup> , n (%)	17 (16)		
Nonsmoker, n (%)	35 (33)		
Smoker, n (%)	41 (39)		
Past smoker, n (%)	28 (27)		
Unknown smoking status, n (%)	1 (1)		
Body weight <sup>1</sup> [kg]	70	47–115	59–80
Height <sup>1</sup> [cm]	171	155–190	165–178
Albumin <sup>1</sup> [g/dL]	4.35	2.53–5.08	4.12–4.54
CRP <sup>1</sup> [mg/dL]	0.29	0.02–7.49	0.11–0.49
HBI <sup>1</sup>	1	0–18	1–3
Total serum samples, n	336		
ADA-positive serum samples, n (%)	49 (15)		

Note: ADA: anti-drug antibodies; CD: Crohn's disease; CRP: C-reactive protein; HBI: Harvey–Bradshaw index; IMM: immunomodulators (including azathioprine and methotrexate); IQR: interquartile range; No.: number; UC: ulcerative colitis; <sup>1</sup> at the time of first drug sampling.

#### 3.4. Predictive Model Evaluation Goodness-of-Fit Plots

The first concentration ( $C_{MAP}$ ) was used for MAP estimation of EBEs, and all subsequent concentrations were predicted. Data was split into two sets of ADA-positive and ADA-negative patients. Additionally, for ADA-negative patients, predictions were stratified for different time intervals after  $C_{MAP}$  (i.e., “within 1 month”, “between 1 and 6 months” and “>6 months”). For ADA-positive patients, predicted concentrations were stratified as follows: infliximab concentrations for patients that have not been tested ADA positive yet (“before ADA+”), concentrations measured within one month or at first ADA detection (“1st time ADA+ and  $\leq 1$  month”), and concentrations measured after one month of first ADA detection (“>1 month of being ADA+”).

Goodness-of-fit plots (Figure 1) show that model predictions of infliximab concentrations for most ADA-negative patients (turquoise symbols) matched precisely with the observed concentrations. However, predictions of concentrations of ADA-positive patients (pink symbols), especially those measured within and after one month of first ADA detection, were less accurate (turquoise symbols). Additionally, in ADA-negative patients, predictions of concentrations measured more than six months after  $C_{MAP}$  showed larger deviation from the corresponding observed concentrations compared to predictions of concentrations measured within the first six months after  $C_{MAP}$  in this study setting.

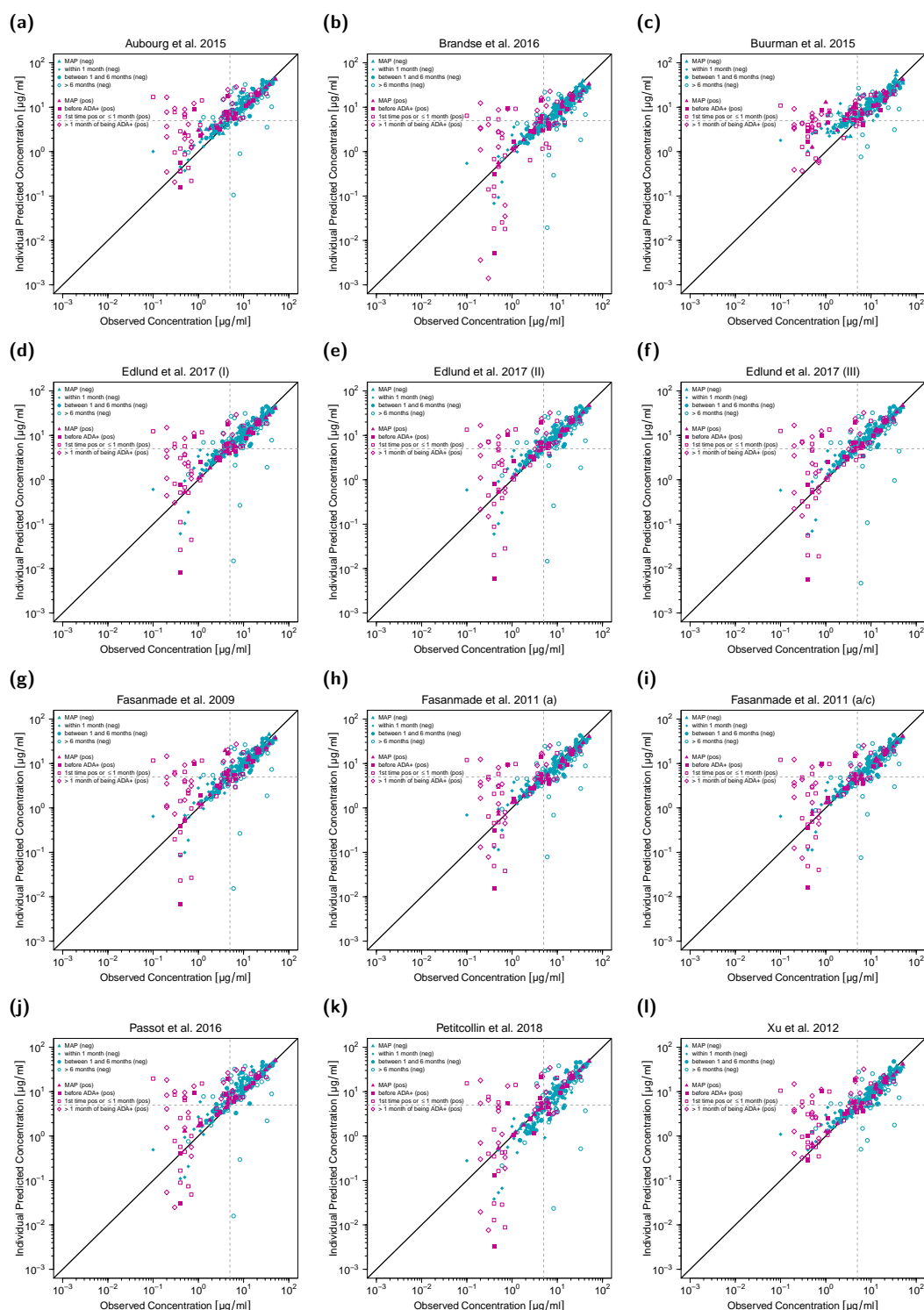


**Figure 1.** Individual predicted versus observed serum infliximab concentrations for twelve different population pharmacokinetic models (a–l). Concentrations of anti-drug antibody (ADA) negative patients are shown in turquoise, concentrations of ADA-positive patients in pink. Concentrations used for maximum a posteriori (MAP) estimation ( $C_{MAP}$ ) are depicted as triangles, the remaining symbols depict predictions in different time intervals after  $C_{MAP}$ . Black solid lines represent the lines of identity, gray dashed lines mark the target trough concentration of 5  $\mu\text{g/mL}$ . In (k), one serum concentration falls outside the plotting range but is included in the full plot depicted in the Supplementary Materials. a: adults; a/c: adults/children; (neg): ADA-negative patients; (pos): ADA-positive patients.

### 3.5. Accuracy and Bias of Model Predictions

$\zeta$  values represent a measure of accuracy with smaller values indicating higher accuracy, while SSPB values represent a measure of bias with values closer to zero indicating less bias. Figure 2 shows the development of  $\zeta$  and SSPB values over time for all included population pharmacokinetic models in the ADA negative (Figure 2a,b) and ADA-positive (Figure 2c,d) patient subpopulations. The last category (“all pred”) subsumes unstratified results for all predicted concentrations excluding  $C_{MAP}$ . The corresponding  $\zeta$  values were calculated for all 12 models to be within 26–44% (median: 30%) for ADA-negative patients and 77–215% (median: 92%) for ADA-positive patients. SSPB values for all models were within –22–27% (median: 6%) for ADA-negative patients and 8–145% (median: 43%) for ADA-positive patients.

The models exhibiting the highest overall accuracy (lowest  $\zeta$ ) for predicted concentrations in ADA-negative patients were the two models by Fasanmade et al., 2011, both with  $\zeta$  values of ~26%. Regarding bias in model predictions, four models had absolute SSPB values of  $\leq 5\%$  (with SSPB values for Fasanmade et al., 2009: –3%; Xu et al., 2012: –1%; and the two models from Fasanmade et al., 2011: –5%).

$\zeta$  values for predictions in ADA-negative patients increased from a median of 25% (predictions within one month of  $C_{MAP}$ ) and 28% (predictions one to six months after  $C_{MAP}$ ) to 54% (predictions more than six months after  $C_{MAP}$ ) over time (see Figure 2a). In contrast, the median SSPB value for model predictions in ADA-negative patients did not increase over time (median (SSPB  $< 1$  month): 7%, median (SSPB 1–6 months): 8%, median (SSPB  $> 6$  months): 2%; Figure 2b). All calculated  $\zeta$  and SSPB values for each model are listed in Table S1 and Table S2 of the Supplementary Materials.

In ADA-positive patients, predictions of infliximab concentrations were less accurate, especially for concentrations measured within and after one month of first ADA detection (Figure 3c, median ( $\zeta$  1st time ADA+ and  $\leq 1$  month): 97%, median ( $\zeta > 1$  month ADA+): 301%). For some models, bias (SSPB) was still low for predictions of concentrations when patients were tested ADA positive for the first time and within one month of detection (Petitcollin et al., 2018: –1%, Fasanmade et al., 2009: –2%, Fasanmade et al., 2011 (adults/children): 5%, Edlund et al., 2017 (II): 9%, and Edlund et al., 2017 (III): –9%) but was high for all models regarding concentrations measured more than one month after patients tested ADA positive for the first time (range of SSPB values: 78–344%).

$\zeta$  values for model simulations of  $C_{MAP}$  were 0–24% (median: 9%) for ADA-negative patients and 0–43% for ADA-positive patients (median: 12%). The corresponding SSPB values were –24–0% (median: –5%) for ADA-negative patients and –13–22% for ADA-positive patients (median: –4%).

The model by Edlund et al., 2017 (III) included ADA concentrations measured by HMSA (Prometheus Laboratories, San Diego, CA) as a continuous covariate on infliximab CL [43] in contrast to a binary covariate (i.e., ADA negative or ADA positive) as implemented in other evaluated models. However, since model predictions were executed with individual patient covariates imputed from time of  $C_{MAP}$ , model predictions for later time points could not benefit from continuous measurements of ADA concentrations and other time-varying covariates. In order to examine these potential benefits for the model by Edlund et al., 2017 (III), predictions were also performed with fully informed covariates for the ADA-positive subpopulation and results are depicted in Figure 2c,d (green dashed line). This led to an improvement in both model accuracy and bias, especially for concentrations measured more than one month after patients tested ADA positive for the first time ( $\zeta$ : 130% vs. 206% and SSPB: 11% vs. 206%).

Predictions with fully informed time-varying covariates were also performed for all other evaluated models for both ADA-negative and ADA-positive patients, and results are shown in Tables S3 and S4, as well as in Figures S1 and S2 in the Supplementary Materials.



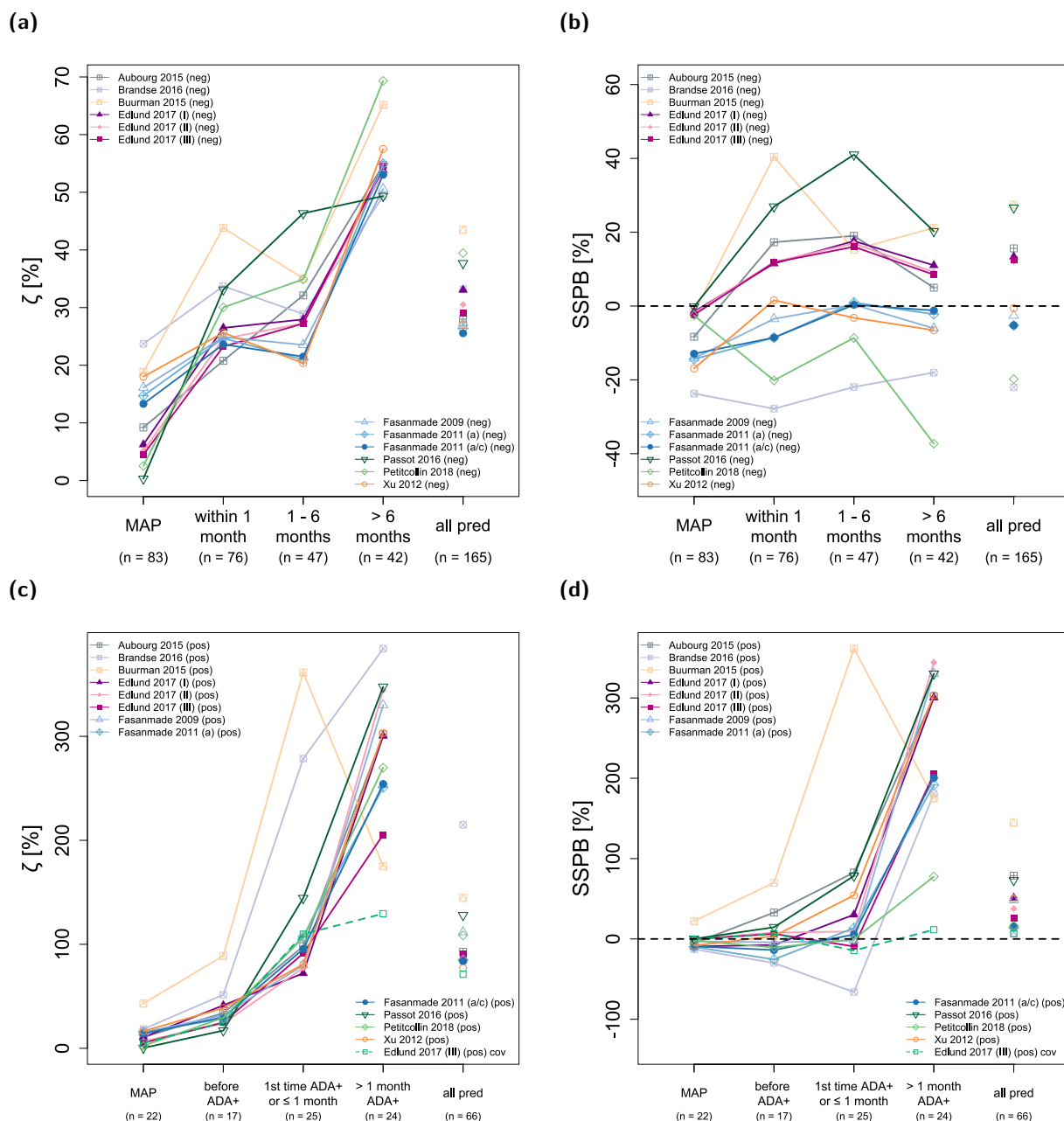


**Figure 2.** Model prediction accuracy ( $\zeta$ , (a,c)) and bias (SSPB, (b,d)) over time. The upper panel shows results for anti-drug antibody (ADA) negative patients, the lower panel for ADA-positive patients. Numbers in parentheses refer to the number of observed concentrations in the respective time interval. “all pred” covers all predicted concentrations excluding concentrations used for maximum a posteriori (MAP) estimation ( $C_{MAP}$ ) of individual pharmacokinetic parameters. Solid lines depict the results for model predictions using patient covariates determined at the time of  $C_{MAP}$ . The green dashed line shows the results for predictions with the model by Edlund et al., 2017 (III), using measured time-varying covariates. a: adults; a/c: adults/children; ADA+: anti-drug antibody positive; cov: covariates; (neg): ADA-negative patients, (pos): ADA-positive patients; pred: predictions; SSPB: symmetric signed percentage bias;  $\zeta$ : median symmetric accuracy.

### 3.6. Predictions of “Need for Dose Escalation”

According to the American Gastroenterological Association Institute Guideline, the target trough concentration for infliximab is  $\geq 5 \mu\text{g/mL}$  [13]. In total, 69 serum trough samples from the external data set exhibited infliximab concentrations  $\geq 5 \mu\text{g/mL}$  (no dose



escalation needed), 90 trough samples exhibited infliximab concentrations  $< 5 \mu\text{g/mL}$  (dose escalation needed). For serum trough samples in which ADA status was negative, 67 samples showed infliximab trough levels  $\geq 5 \mu\text{g/mL}$  (50%) and 67 showed infliximab trough levels  $< 5 \mu\text{g/mL}$  (50%). In contrast, for serum trough samples in which ADA status was positive, only 2 samples showed infliximab levels  $\geq 5 \mu\text{g/mL}$  (8%) and 23 showed infliximab levels  $< 5 \mu\text{g/mL}$  (92%).

Table 3 presents the results regarding model abilities to correctly predict the need for dose escalation in the external data set. Results were split into two groups—predictions for serum trough samples in which ADA status was negative and predictions for serum trough samples in which ADA status was positive. Models with the highest accuracy for the ADA-negative sample cohort were the models by Edlund et al., 2017 (II + III), and the models by Fasanmade et al., 2011, with 113/134 (84%) correct predictions. For the ADA-positive sample cohort, the model by Buurman et al., 2015, correctly classified 20 of 25 (80%) concentrations to be above or below the threshold of  $5 \mu\text{g/mL}$ . In summary, the investigated models correctly identified the need for dose escalation (i.e., trough concentration  $< 5 \mu\text{g/mL}$ ) in 63–89% of cases. In 4–43% of cases a dose escalation would have been recommended (predicted trough concentration  $< 5 \mu\text{g/mL}$ ) although the measured concentration was above the target concentration.

**Table 3.** Predictions of “need for dose escalation” (i.e., trough concentration  $< 5 \mu\text{g/mL}$  [13]).

Dose Escalation Needed? (Cobs $< 5 \mu\text{g/mL}$ )	ADA Negative					ADA Positive				
	Yes (n = 67)		No (n = 67)			Yes (n = 23)		No (n = 2)		
Correctly Predicted?	Yes	No	Yes	No	Accuracy	Yes	No	Yes	No	Accuracy
Aubourg et al., 2015	48	19	63	4	82.8%	13	10	2	0	60.0%
Brandse et al., 2016	62	5	39	28	75.4%	18	5	0	2	72.0%
Buurman et al., 2015	38	29	62	5	74.6%	19	4	1	1	80.0%
Edlund et al., 2017 (I)	51	16	61	6	83.6%	16	7	2	0	72.0%
Edlund et al., 2017 (II)	50	17	63	4	84.3%	15	8	1	1	64.0%
Edlund et al., 2017 (III)	50	17	63	4	84.3%	16	7	1	1	68.0%
Fasanmade et al., 2009	54	13	58	9	83.6%	17	6	1	1	72.0%
Fasanmade et al., 2011 (a/c)	60	7	53	14	84.3%	19	4	0	2	76.0%
Fasanmade et al., 2011 (a)	60	7	53	14	84.3%	19	4	0	2	76.0%
Passot et al., 2016	44	23	64	3	80.6%	13	10	2	0	60.0%
Petitcollin et al., 2018	62	5	48	19	82.1%	15	8	0	2	60.0%
Xu et al., 2012	56	11	52	15	80.6%	18	5	1	1	76.0%

Note: a: adults; a/c: adults/children; ADA: anti-drug antibody; C<sub>obs</sub>: observed trough concentration.

### 3.7. Prediction- and Variability-Corrected Visual Predictive Checks (pvcVPCs)

The results of pvcVPCs for each investigated population pharmacokinetic model are presented in Figure 3. The pvcVPCs showed a clear overprediction of the 95th percentile of observations for the models by Aubourg et al., 2015, Edlund et al., 2017 (II), Fasanmade et al., 2009, and Xu et al., 2012, but predictions of median infliximab concentrations were reasonable for all four models. The model by Petitcollin et al., 2018, overpredicted and the model by Brandse et al., 2016, underpredicted both the median and 95th percentile of observations. In contrast, the model by Buurman et al., 2015, overpredicted the 5th percentile while slightly underpredicting the 95th percentile. Model simulated median and 95th percentile showed high agreement with the corresponding median/percentile observed for the model by Passot et al., 2016. However, the 5th percentile was overpredicted

most of the time. The remaining four models showed high congruence with a slight initial underprediction of the median observations for the two models by Fasanmade et al., 2011, and the model by Edlund et al., 2017 (III).

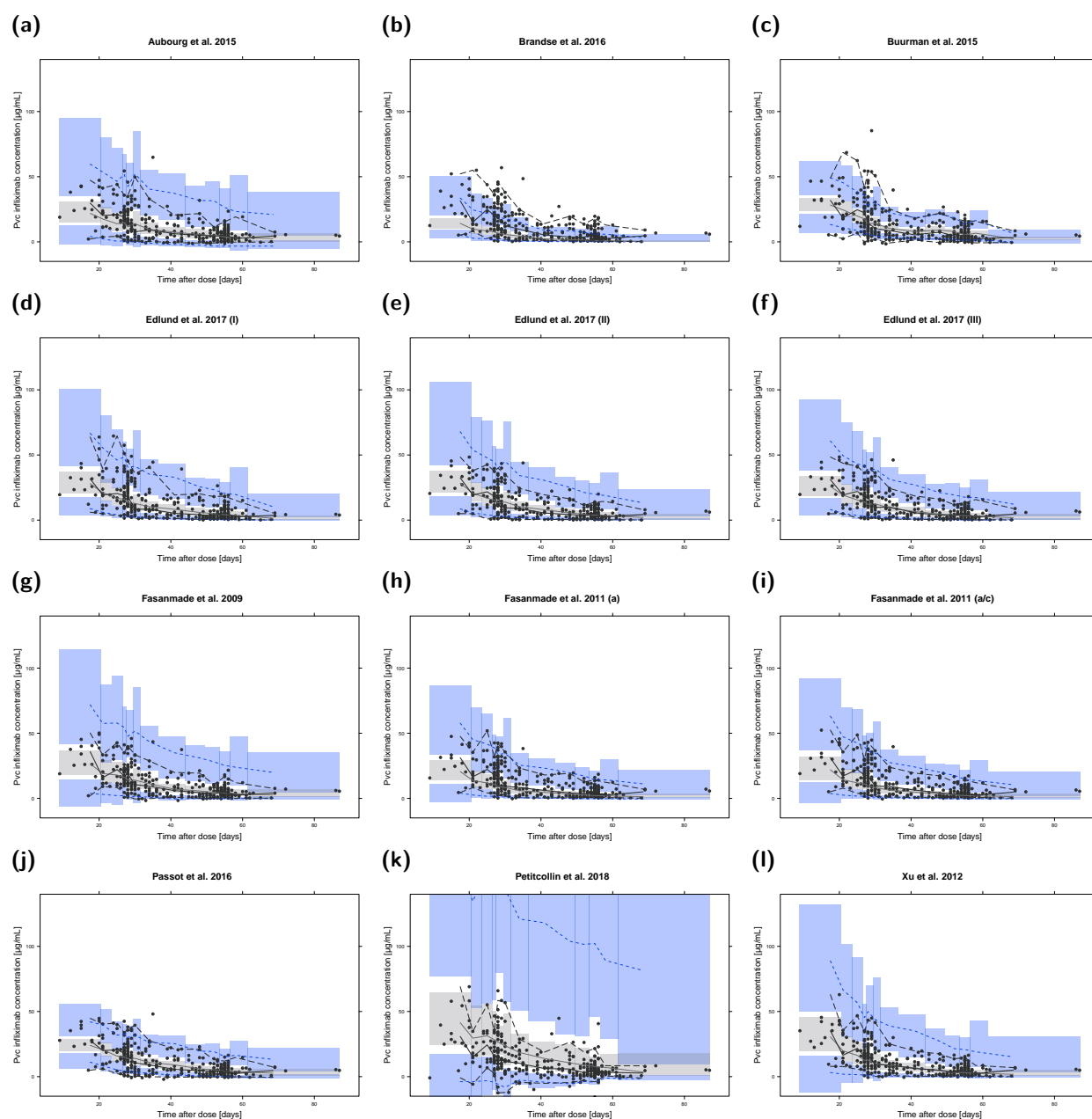


**Figure 3.** Prediction- and variability-corrected visual predictive checks (pvcVPCs) of serum infliximab concentrations for each investigated population pharmacokinetic model (a–l). Prediction- and variability-corrected observed concentrations are shown as black circles, observed medians are depicted as black solid lines, 5th and 95th data percentiles as black dashed lines. The model simulations ( $n = 1000$  replicates) are depicted as gray solid lines (median) and blue dashed lines (5th and 95th percentiles). Colored areas represent the simulation-based 95% confidence intervals for the corresponding model-predicted median (gray areas) and 5th and 95th percentiles (blue areas). For ease of comparison, y-axis upper limits were set to  $140 \mu\text{g/mL}$ . Plots with automatic y-axis limits are shown in the Supplementary Materials. a: adults; a/c: adults/children; Pvc: prediction- and variability-corrected.

#### 4. Discussion

Several MIPD approaches have recently shown major success in supporting and optimizing dosing regimen selection for various drugs [28,59–62]. As infliximab trough concentrations exhibit high inter-individual variability and, hence, contribute to a high rate of primary and secondary non-response [9,12–14,18] and as infliximab drug exposure is a predictor of clinical response [6,10–12], dose selection for infliximab could benefit considerably from population pharmacokinetic modeling and MIPD [31,63]. Consequently, many efforts have been made to analyze infliximab PK, quantifying and explaining inter-individual variability in various population pharmacokinetic models [21,23–27,43–49,51–57].

However, for the application of population pharmacokinetic models, an extensive assessment including internal and external evaluation regarding accuracy, robustness, and predictive performance is crucial [64]. While different methods have been applied in the respective internal model evaluations, only a fraction of the models has been evaluated with an independent data set [34,65–68], and a comprehensive external evaluation for predictive model performances has not been conducted yet. External evaluation with an independent data set allows the evaluation of model performance regarding prediction and variability in patients with a clinical background similar to the internal data set and thus evaluates not only the modeling approach itself, but also other study-related factors [64].

As shown in this analysis, differences in the predictive performances of the 12 investigated models could be observed by external evaluation, and trends in the predictability of infliximab concentrations could be identified for the ADA-negative as well as the ADA-positive subpopulation when using first measured infliximab concentration for estimation of EBEs.

While in ADA-negative patients the absolute SSPB values, as a measure of model bias, did not increase for virtually all models from the predictions of concentrations within one month (SSPB median of 7%) to the predictions of concentrations after more than six months of  $C_{MAP}$  (SSPB median of 2%), model accuracy decreased noticeably for predictions of concentrations more than six months after  $C_{MAP}$  in this study setting (median ( $\zeta < 1$  month): 25%, median ( $\zeta_{1-6}$  months): 28%, median ( $\zeta > 6$  months): 54%). As this observation also held true for model predictions performed with time-varying covariates, yet to a lesser extent, long-term predictions should be treated carefully because of the deterioration in model accuracy.

Different analytical methods have been used to measure infliximab and ADA concentrations in the population pharmacokinetic analyses, leading to differences in immunogenicity rate [17]. While in some studies, “drug sensitive” methods (ADAs not detectable in the presence of infliximab because of analytic interferences) were used to measure ADA concentrations, “drug-tolerant” assays were applied in other investigations, yielding a much higher rate of ADA-positive patients (up to 62% compared to as low as 1%) [21,51]. Nevertheless, 18 out of 23 models that included ADA patients implemented ADA status as a covariate. The five remaining studies identified only  $\leq 3\%$  of patients as ADA positive or used a risk function of developing ADA. The implementation of ADA status in the majority of models highlights the importance of ADA for the PK of infliximab.

Predictions in ADA-positive patients showed much larger deviations from the corresponding observed values compared to predictions in ADA-negative patients: While prediction accuracy for concentrations before the first ADA-positive blood sample (median( $\zeta$ ): 31%, range: 17–89%) were similar compared to predictions for ADA-negative patients, predictions became much less accurate as soon as ADA status turned positive (median( $\zeta$ ): 97%, range 72–361%). As noted, for predictions in this analysis, individual patient covariates for times after  $C_{MAP}$  were imputed (last observation carried forward). This especially affected predictions of concentrations in patients showing changes in important covariates such as ADA status. Hence, model predictions were also performed with time-varying covariates (depicted in the Supplementary Materials). While improvements in model predictions were especially noted for concentrations in ADA-positive blood samples, predictions still exhibited  $\zeta$  values of  $>100\%$  for concentrations more than one month after patients tested ADA positive for the first time, albeit the inclusion of ADA status in most models.

The study by Edlund et al., 2017, aimed to tackle the challenges of predicting infliximab CL in ADA-positive patients [43]. The corresponding population pharmacokinetic model was based on the models by Fasanmade et al., 2011, and Ternant et al., 2015, with the advancement of including ADA concentrations as a continuous covariate [43]. As a result, when using time-varying covariates, the model by Edlund et al., 2017 (III), showed the highest accuracy and least bias for model predictions in ADA-positive patients for “all pred”. However, the respective model predictions were still less accurate and showed a higher bias compared to predictions for the ADA-negative patient cohort. Additionally, the implemented covariates albumin and IMM in the model by Fasanmade et al., 2011, were not found to be statistically significant with the data set used for model development by Edlund et al., 2017 [43]. This may have contributed to the slightly lower accuracy and higher bias for predictions in ADA-negative patients compared to the models by Fasanmade et al., 2011.

One reason for the observed overprediction in ADA-positive patients could be due to the fact that the exact time of ADA onset is often unknown. ADA-positive patients develop ADA during a time period of unknown length before they test positive for the first time, which is supported by findings from Petitcollin and coworkers [51]. A close and regular monitoring for ADA using drug-tolerant assays as well as the development and application of models identifying predictors of ADA development [69] might help to improve predictive performances for ADA-positive patients.

For predictive performance evaluation in Bayesian forecasting, only the first measured serum infliximab concentration of each patient was used for MAP estimation of EBEs ( $C_{MAP}$ ). Due to the design of the study,  $C_{MAP}$  was usually a midpoint concentration and results should be interpreted with this in mind. However, using a midpoint infliximab concentration for estimation of EBEs to predict the subsequent trough level allows potential adjustment of the current dosing interval before infliximab concentrations drop below the target concentration of 5 µg/mL.

As infliximab therapy can be adapted based on trough levels [13], model performances to correctly predict the need for dose escalation (i.e., trough concentration <5 µg/mL) were further investigated. The two examined models by Fasanmade et al., 2011, correctly identified 79 of 90 (88%) trough concentrations to be below the target trough concentration (true positive) while correctly identifying 53 of 69 (77%) trough concentrations to be above the target trough concentration (true negative). This represented the highest classification accuracy of correctly identified infliximab trough samples (132/159, 83%) in this study setting. The model by Brandse et al., 2016 [55], exhibited the highest true positive rate (89%); however, it was accompanied by a low true negative rate of 57%. The model by Passot et al., 2016 [56], showed the highest true negative rate (96%) with a low true positive rate of only 63%. While a high false negative rate yields an increased number of patients with insufficient infliximab levels and, hence, decreased drug effect, a high false positive rate corresponds to an increased number of patients with higher exposure and potentially higher rates of adverse effects (e.g., rate of infection [70]). It should be noted that these measures only reflect whether model predictions were correctly below or above the target trough concentration and do not assess how much predictions deviated from the actual measured concentration.

The investigation of factors leading to differences in model performances was outside the scope of this study, but it is worth mentioning that the vast majority of blood samples from the external data set were collected during infliximab maintenance therapy. In contrast, three examined models were developed with data only from the first 6 weeks (Brandse et al., 2016 [55]), “treatment initiation” (Aubourg et al., 2015 [53]), and the first 22 weeks of infliximab treatment (Passot et al., 2016 [56]), which might have affected prediction performance. The model by Petitcollin et al., 2018, was included in the analysis to study the performance of a model with implemented ADA risk function instead of an ADA covariate, although the model was developed with data from pediatric patients [25]. While the corresponding CL and  $V_d$  model parameters appear comparable to

parameters in infliximab models developed with adult patients [25,43,46,56], the difference in patient cohorts might still explain larger deviations between predicted and measured infliximab concentrations observed in the corresponding pvcVPC and goodness-of-fit plot.

There are some limitations of this analysis, which are discussed in the following paragraphs. Since the study was based on routine therapeutic drug monitoring data, a full dosing schedule was not available for all patients. In such cases, regular dosing from the start of treatment with infliximab and from every change in dosing regimen was assumed. Moreover, sampling times as well as the included patient cohort, treatment period (induction vs. maintenance therapy), analytical methods, or dosing regimens in the external data set could have affected the results of the analysis. Hence, further evaluations with independent data sets should be conducted in future studies.

Another factor influencing the results of an analysis is the choice of quantitative measure. Here, median symmetric accuracy ( $\zeta$ ) and symmetric signed percentage bias (SSPB) values were computed. As illustrated by Morley et al.,  $\zeta$  attenuates the issues with asymmetric penalty and effects of outliers while maintaining interpretability [42].  $\zeta$  is a robust measure of accuracy minimizing the effect of the skewness of the distribution of absolute errors [42]. The SSPB estimates the central tendency of the error and can be interpreted similar to a mean percentage error (MPE) [42]. However, in contrast to the MPE, SSPB is not affected by the likely asymmetries in the distribution [42]. As illustrated throughout the analysis, different performance metrics stratified by different patient cohorts (here, ADA-negative and ADA-positive patients) can be of interest when evaluating population pharmacokinetic models in the framework of MIPD. Since different models showed strengths in different measures, we could not appraise which published model was the “best” model, as this also depends on the question of interest and was beyond the scope of this analysis.

Additionally, because of data set incompatibility (e.g., missing covariates) or the lack of reported model implementation details, only 12 of the 25 identified population pharmacokinetic models of infliximab in IBD could be evaluated. While this work already adds a comprehensive analysis to recently published evaluations of single models, an external evaluation including additional covariates (such as the erythrocyte sedimentation rate or fecal calprotectin [21,27]) would be of interest for future studies. Moreover, new modeling approaches (e.g., pharmacokinetic/pharmacodynamic models [27,49]) regarding treatment efficacy could investigate recent findings such as the relation of intestinal microbiota to anti-TNF- $\alpha$  treatment outcome in IBD patients [71,72]. Improvement in gut microbial dysbiosis in IBD patients has been observed during infliximab therapy [71,73], and fecal microbiota has been suggested as a response indicator of infliximab treatment [72]. Future pharmacokinetic/pharmacodynamic studies that examine therapeutic outcome could further investigate this interplay of intestinal microbiota and infliximab therapy. For this, the presented comprehensive external evaluation can also serve as guidance to adopt a suitable population pharmacokinetic model in order to explore these complex response mechanisms.

## 5. Conclusions

This work presents an external evaluation of the predictive performance of 12 published infliximab population pharmacokinetic models in IBD patients using an independent data set. Differences in predictive performance regarding model accuracy, model bias, and need for dose escalation have been observed for both ADA-negative and ADA-positive patients. Using the first measured infliximab concentration for MAP estimation ( $C_{MAP}$ ) in a Bayesian forecasting setting, overall model accuracy decreased for predictions more than six months after  $C_{MAP}$  for ADA-negative patients, while bias did not increase. The two investigated models by Fasanmade et al., 2011, showed the highest dose escalation classification accuracy of correctly identified infliximab trough samples (83%) in this study setting. Overall, the investigated population pharmacokinetic models showed a classification accuracy of 75–84% for ADA-negative samples and of 60–80% for ADA-positive



samples. The results of this predictive performance evaluation could help to guide and plan future MIPD approaches with infliximab population pharmacokinetic models to improve individual dosing strategies and prevent infliximab trough concentrations dropping below the target concentration. Yet clinical application needs to be tested and confirmed in larger, prospective clinical trials. In comparison to predictions for ADA-negative patients, model predictions of serum concentrations for ADA-positive patients showed lower accuracy and higher bias. Thus, predictions with population pharmacokinetic models remain particularly challenging for ADA-positive patients and for patients with unknown ADA status.

**Supplementary Materials:** The following are available online at <https://www.mdpi.com/article/10.3390/pharmaceutics13091368/s1>, Electronic Supplementary Materials: Additional evaluation results. Figure S1: Individual predicted versus observed serum infliximab concentrations for the population pharmacokinetic model by Petitcollin et al. 2018. Concentrations of anti-drug antibody (ADA) negative patients are shown in turquoise, concentrations of ADA positive patients in pink. Concentrations used for maximum a posteriori (MAP) estimation (CMAP) are depicted as triangles, the remaining symbols depict predictions in different time intervals after CMAP. The black solid line represents the line of identity, grey dashed lines mark the target trough concentration of 5 µg/mL. (neg): ADA negative patients; (pos): ADA positive patients, Figure S2: Model prediction accuracy ( $\zeta$ , a and b) and bias (SSPB, c and d) for anti-drug antibody (ADA) negative patients over time. The left panel shows  $\zeta$  and SSPB values for model predictions with fixed covariates determined at the time of the first measured serum infliximab concentration of each patient (CMAP), the right panel shows  $\zeta$  and SSPB values for model predictions with time-varying covariates. “all pred” covers all predicted concentrations excluding CMAP. Numbers in parentheses refer to the number of observed concentrations in the respective time interval. (neg): ADA negative patients, pred: predictions; SSPB: symmetric signed percentage bias;  $\zeta$ : median symmetric accuracy, Figure S3: Model prediction accuracy ( $\zeta$ , a and b) and bias (SSPB, c and d) for anti-drug antibody (ADA) positive patients over time. The left panel shows  $\zeta$  and SSPB values for model predictions with fixed covariates determined at the time of the first measured serum infliximab concentration of each patient (CMAP), the right panel shows  $\zeta$  and SSPB values for model predictions with time-varying covariates. “all pred” covers all predicted concentrations excluding CMAP. Numbers in parentheses refer to the number of observed concentrations in the respective time interval. (pos): ADA positive patients, pred: predictions; SSPB: symmetric signed percentage bias;  $\zeta$ : median symmetric accuracy, Figure S4: Prediction- and variability-corrected visual predictive check (pvcVPC) of serum infliximab concentrations for the population pharmacokinetic model by Petitcollin et al. 2018. Prediction- and variability-corrected observed concentrations are shown as black circles, observed median is depicted as black solid line, 5th and 95th data percentiles as black dashed lines. The model simulations ( $n = 1000$  replicates) are depicted as grey solid line (median) and blue dashed lines (5th and 95th percentiles). Colored areas represent the simulation-based 95% confidence intervals for the corresponding model-predicted median (grey areas) and 5th and 95th percentiles (blue areas). Pvc: prediction- and variability-corrected, Table S1:  $\zeta$  and SSPB values for model predictions with fixed covariates at time of CMAP for ADA negative patients, Table S2:  $\zeta$  and SSPB values for model predictions with fixed covariates at time of CMAP for ADA positive patients, Table S3:  $\zeta$  and SSPB values for model predictions with time-varying covariates for ADA negative patients, Table S4:  $\zeta$  and SSPB values for model predictions with time-varying covariates for ADA positive patients.

**Author Contributions:** Conceptualization, C.S., L.K., U.H., F.T., W.R., M.S. and T.L.; data curation, C.S. and D.S.; formal analysis, C.S., L.K. and D.S.; funding acquisition, U.H., F.T., W.R., M.S. and T.L.; investigation, C.S., L.K., W.R. and T.L.; methodology, C.S., L.K. and D.S.; project administration, U.H., F.T., W.R., M.S. and T.L.; resources, W.R., M.S. and T.L.; software, C.S., L.K. and D.S.; supervision, U.H., F.T., W.R., M.S. and T.L.; visualization, C.S., L.K. and D.S.; writing—original draft, C.S., L.K., D.S. and T.L.; writing—review and editing, C.S., L.K., D.S., U.H., F.T., W.R., M.S. and T.L. All authors have read and agreed to the published version of the manuscript.

**Funding:** This research was funded by the Robert Bosch Stiftung (Stuttgart, Germany), the German Federal Ministry of Education and Research (BMBF), 031L0188D “GUIDE-IBD”, and the Horizon 2020 ERACoSysMed project INSPIRATION (grant 643271).

**Institutional Review Board Statement:** For predictive external model evaluation, data originated from a previously published observational study that was reviewed and approved by the institutional review board of the Medical University of Vienna [35].

**Informed Consent Statement:** All participating patients signed an informed consent form.

**Data Availability Statement:** Not applicable.

**Conflicts of Interest:** C.S., L.K., D.S., U.H., M.S. and T.L. declare no conflicts of interest. F.T. has served as a speaker for Falk Pharma GmbH and Janssen. W.R. has served as a speaker for Abbott Laboratories, Abbvie, Aesca, Aptalis, Astellas, Centocor, Celltrion, Danone Austria, Elan, Falk Pharma GmbH, Ferring, Immundiagnostik, Mitsubishi Tanabe Pharma Corporation, MSD, Otsuka, PDL, Pharmacosmos, PLS Education, Schering-Plough, Shire, Takeda, Therakos, Vifor, Yakult. Moreover, W.R. has served as a consultant for Abbott Laboratories, Abbvie, Aesca, Algenon, Amgen, AM Pharma, AMT, AOP Orphan, Arena Pharmaceuticals, Astellas, Astra Zeneca, Avaxia, Roland Berger GmbH, Bioclinica, Biogen IDEC, Boehringer-Ingelheim, Bristol-Myers Squibb, Cellerix, Chemocentryx, Celgene, Centocor, Celltrion, Covance, Danone Austria, DSM, Elan, Eli Lilly, Ernest & Young, Falk Pharma GmbH, Ferring, Galapagos, Gatehouse Bio Inc., Genentech, Gilead, Grünenthal, ICON, Index Pharma, Inova, Intrinsic Imaging, Janssen, Johnson & Johnson, Kyowa Hakko Kirin Pharma, Lipid Therapeutics, LivaNova, Mallinckrodt, Medahead, MedImmune, Millenium, Mitsubishi Tanabe Pharma Corporation, MSD, Nash Pharmaceuticals, Nestle, Nippon Kayaku, Novartis, Ocera, OMass, Otsuka, Parexel, PDL, Periconsulting, Pharmacosmos, Philip Morris Institute, Pfizer, Procter & Gamble, Prometheus, Protagonist, Provention, Quell Therapeutics, Robarts Clinical Trial, Sandoz, Schering-Plough, Second Genome, Seres Therapeutics, Setpointmedical, Sigmoid, Sublimity, Takeda, Therakos, Theravance, Tigenix, UCB, Vifor, Zealand, Zyngenia, and 4SC. Additionally, W.R. has served as an advisory board member for Abbott Laboratories, Abbvie, Aesca, Amgen, AM Pharma, Astellas, Astra Zeneca, Avaxia, Biogen IDEC, Boehringer-Ingelheim, Bristol-Myers Squibb, Cellerix, Chemocentryx, Celgene, Centocor, Celltrion, Danone Austria, DSM, Elan, Ferring, Galapagos, Genentech, Grünenthal, Inova, Janssen, Johnson & Johnson, Kyowa Hakko Kirin Pharma, Lipid Therapeutics, MedImmune, Millenium, Mitsubishi Tanabe Pharma Corporation, MSD, Nestle, Novartis, Ocera, Otsuka, PDL, Pharmacosmos, Pfizer, Procter & Gamble, Prometheus, Sandoz, Schering-Plough, Second Genome, Setpointmedical, Takeda, Therakos, Tigenix, UCB, Zealand, Zyngenia, and 4SC, and W.R. has received research funding from Abbott Laboratories, Abbvie, Aesca, Centocor, Falk Pharma GmbH, Immundiagnostik, Janssen, MSD, Sandoz, Takeda.

## References

1. European Medicines Agency Remicade—EPAR. Product Information, Annex I—Summary of Product Characteristics—EMA/H/C/000240. 2020, pp. 1–59. Available online: [https://www.ema.europa.eu/en/documents/product-information/remicade-epar-product-information\\_en.pdf](https://www.ema.europa.eu/en/documents/product-information/remicade-epar-product-information_en.pdf) (accessed on 25 November 2020).
2. Prescribing Information REMICADE®(Infliximab), Janssen Biotech, Inc. Available online: [https://www.accessdata.fda.gov/drugsatfda\\_docs/label/2013/103772s5359lbl.pdf](https://www.accessdata.fda.gov/drugsatfda_docs/label/2013/103772s5359lbl.pdf) (accessed on 8 January 2021).
3. Feagan, B.G.; Choquette, D.; Ghosh, S.; Gladman, D.D.; Ho, V.; Meibohm, B.; Zou, G.; Xu, Z.; Shankar, G.; Sealey, D.C.; et al. The challenge of indication extrapolation for infliximab biosimilars. *Biologicals* **2014**, *42*, 177–183. [CrossRef]
4. Dreesen, E.; Gils, A.; Vermeire, S. Pharmacokinetic Modeling and Simulation of Biologicals in Inflammatory Bowel Disease: The Dawning of a New Era for Personalized Treatment. *Curr. Drug Targets* **2018**, *19*, 757–776. [CrossRef]
5. European Medicines Agency Remicade—EPAR. Summary for the Public, EMA/76495/2012. 2018, pp. 1–3. Available online: [https://www.ema.europa.eu/en/documents/overview/remicade-epar-summary-public\\_en.pdf](https://www.ema.europa.eu/en/documents/overview/remicade-epar-summary-public_en.pdf) (accessed on 9 March 2020).
6. Hemperly, A.; Vande Castele, N. Clinical Pharmacokinetics and Pharmacodynamics of Infliximab in the Treatment of Inflammatory Bowel Disease. *Clin. Pharmacokinet.* **2018**, *57*, 929–942. [CrossRef]
7. Klotz, U.; Teml, A.; Schwab, M. Clinical pharmacokinetics and use of infliximab. *Clin. Pharmacokinet.* **2007**, *46*, 645–660. [CrossRef] [PubMed]
8. Ryman, J.T.; Meibohm, B. Pharmacokinetics of Monoclonal Antibodies. *CPT Pharmacomet. Syst. Pharmacol.* **2017**, *6*, 576–588. [CrossRef]
9. Buhl, S.; Dorn-Rasmussen, M.; Brynskov, J.; Ainsworth, M.A.; Bendtzen, K.; Klausen, P.H.; Bolstad, N.; Warren, D.J.; Steenholdt, C. Therapeutic thresholds and mechanisms for primary non-response to infliximab in inflammatory bowel disease. *Scand. J. Gastroenterol.* **2020**, *55*, 884–890. [CrossRef] [PubMed]
10. Lee, L.Y.W.; Sanderson, J.D.; Irving, P.M. Anti-infliximab antibodies in inflammatory bowel disease. *Eur. J. Gastroenterol. Hepatol.* **2012**, *24*, 1078–1085. [CrossRef]
11. Seow, C.H.; Newman, A.; Irwin, S.P.; Steinhart, A.H.; Silverberg, M.S.; Greenberg, G.R. Trough serum infliximab: A predictive factor of clinical outcome for infliximab treatment in acute ulcerative colitis. *Gut* **2010**, *59*, 49–54. [CrossRef] [PubMed]
12. Maser, E.A.; Villela, R.; Silverberg, M.S.; Greenberg, G.R. Association of trough serum infliximab to clinical outcome after scheduled maintenance treatment for Crohn's disease. *Clin. Gastroenterol. Hepatol.* **2006**, *4*, 1248–1254. [CrossRef]



13. Feuerstein, J.D.; Nguyen, G.C.; Kupfer, S.S.; Falck-Ytter, Y.; Singh, S.; Gerson, L.; Hirano, I.; Rubenstein, J.H.; Smalley, W.E.; Stollman, N.; et al. American Gastroenterological Association Institute Guideline on Therapeutic Drug Monitoring in Inflammatory Bowel Disease. *Gastroenterology* **2017**, *153*, 827–834. [\[CrossRef\]](#)
14. Santacana, E.; Rodríguez-Alonso, L.; Padullés, A.; Guardiola, J.; Bas, J.; Rodríguez-Moranta, F.; Serra, K.; Morandeira, F.; Colom, H.; Padullés, N. Predictors of Infliximab Trough Concentrations in Inflammatory Bowel Disease Patients Using a Repeated-Measures Design. *Ther. Drug Monit.* **2020**, *42*, 102–110. [\[CrossRef\]](#)
15. Papamichael, K.; Gils, A.; Rutgeerts, P.; Levesque, B.G.; Vermeire, S.; Sandborn, W.J.; Vande Casteele, N. Role for therapeutic drug monitoring during induction therapy with TNF antagonists in IBD: Evolution in the definition and management of primary nonresponse. *Inflamm. Bowel Dis.* **2015**, *21*, 182–197. [\[CrossRef\]](#)
16. Gisbert, J.P.; Panés, J. Loss of response and requirement of infliximab dose intensification in Crohn's disease: A review. *Am. J. Gastroenterol.* **2009**, *104*, 760–767. [\[CrossRef\]](#)
17. Chirmule, N.; Jawa, V.; Meibohm, B. Immunogenicity to therapeutic proteins: Impact on PK/PD and efficacy. *AAPS J.* **2012**, *14*, 296–302. [\[CrossRef\]](#) [\[PubMed\]](#)
18. Roda, G.; Jharap, B.; Neeraj, N.; Colombel, J.F. Loss of Response to Anti-TNFs: Definition, Epidemiology, and Management. *Clin. Transl. Gastroenterol.* **2016**, *7*, e135. [\[CrossRef\]](#)
19. Mould, D.R.; Dubinsky, M.C. Dashboard systems: Pharmacokinetic/pharmacodynamic mediated dose optimization for monoclonal antibodies. *J. Clin. Pharmacol.* **2015**, *55*, S51–S59. [\[CrossRef\]](#)
20. Wojciechowski, J.; Upton, R.N.; Mould, D.R.; Wiese, M.D.; Foster, D.J.R. Infliximab Maintenance Dosing in Inflammatory Bowel Disease: An Example for In Silico Assessment of Adaptive Dosing Strategies. *AAPS J.* **2017**, *19*, 1136–1147. [\[CrossRef\]](#)
21. Bauman, L.E.; Xiong, Y.; Mizuno, T.; Minar, P.; Fukuda, T.; Dong, M.; Rosen, M.J.; Vinks, A.A. Improved Population Pharmacokinetic Model for Predicting Optimized Infliximab Exposure in Pediatric Inflammatory Bowel Disease. *Inflamm. Bowel Dis.* **2020**, *26*, 429–439. [\[CrossRef\]](#) [\[PubMed\]](#)
22. Vande Casteele, N.; Ferrante, M.; Van Assche, G.; Ballet, V.; Compernelle, G.; Van Steen, K.; Simoons, S.; Rutgeerts, P.; Gils, A.; Vermeire, S. Trough concentrations of infliximab guide dosing for patients with inflammatory bowel disease. *Gastroenterology* **2015**, *148*, 1320–1329.e3. [\[CrossRef\]](#)
23. Fasanmade, A.A.; Adedokun, O.J.; Ford, J.; Hernandez, D.; Johanns, J.; Hu, C.; Davis, H.M.; Zhou, H. Population pharmacokinetic analysis of infliximab in patients with ulcerative colitis. *Eur. J. Clin. Pharmacol.* **2009**, *65*, 1211–1228. [\[CrossRef\]](#)
24. Fasanmade, A.A.; Adedokun, O.J.; Blank, M.; Zhou, H.; Davis, H.M. Pharmacokinetic Properties of Infliximab in Children and Adults with Crohn's Disease: A Retrospective Analysis of Data from 2 Phase III Clinical Trials. *Clin. Ther.* **2011**, *33*, 946–964. [\[CrossRef\]](#)
25. Petitcollin, A.; Leuret, O.; Tron, C.; Lemaître, F.; Verdier, M.C.; Paintaud, G.; Bouguen, G.; Willot, S.; Bellissant, E.; Ternant, D. Modeling Immunization to Infliximab in Children with Crohn's Disease Using Population Pharmacokinetics: A Pilot Study. *Inflamm. Bowel Dis.* **2018**, *24*, 1745–1754. [\[CrossRef\]](#)
26. Kantasiripitak, W.; Verstockt, B.; Alsoud, D.; Lobatón, T.; Thomas, D.; Gils, A.; Vermeire, S.; Ferrante, M.; Dreesen, E. The effect of aging on infliximab exposure and response in patients with inflammatory bowel diseases. *Br. J. Clin. Pharmacol.* **2021**, 1–14. [\[CrossRef\]](#)
27. Dreesen, E.; Berends, S.; Laharie, D.; D'Haens, G.; Vermeire, S.; Gils, A.; Mathôt, R. Modelling of the relationship between infliximab exposure, faecal calprotectin and endoscopic remission in patients with Crohn's disease. *Br. J. Clin. Pharmacol.* **2020**, 1–13. [\[CrossRef\]](#)
28. Darwich, A.S.; Ogungbenro, K.; Vinks, A.A.; Powell, J.R.; Reny, J.-L.; Marsousi, N.; Daali, Y.; Fairman, D.; Cook, J.; Lesko, L.J.; et al. Why Has Model-Informed Precision Dosing Not Yet Become Common Clinical Reality? Lessons From the Past and a Roadmap for the Future. *Clin. Pharmacol. Ther.* **2017**, *101*, 646–656. [\[CrossRef\]](#)
29. Gonzalez, D.; Rao, G.G.; Bailey, S.C.; Brouwer, K.L.R.; Cao, Y.; Crona, D.J.; Kashuba, A.D.M.; Lee, C.R.; Morbitzer, K.; Patterson, J.H.; et al. Precision Dosing: Public Health Need, Proposed Framework, and Anticipated Impact. *Clin. Transl. Sci.* **2017**, *10*, 443–454. [\[CrossRef\]](#)
30. Santacana Juncosa, E.; Rodríguez-Alonso, L.; Padullés Zamora, A.; Guardiola, J.; Rodríguez-Moranta, F.; Serra Nilsson, K.; Bas Minguet, J.; Morandeira Rego, F.; Colom Codina, H.; Padullés Zamora, N. Bayes-based dosing of infliximab in inflammatory bowel diseases: Short-term efficacy. *Br. J. Clin. Pharmacol.* **2021**, *87*, 494–505. [\[CrossRef\]](#)
31. Strik, A.S.; Löwenberg, M.; Mould, D.R.; Berends, S.E.; Ponsioen, C.I.; van den Brande, J.M.H.; Jansen, J.M.; Hoekman, D.R.; Brandse, J.F.; Duijvestein, M.; et al. Efficacy of dashboard driven dosing of infliximab in inflammatory bowel disease patients; a randomized controlled trial. *Scand. J. Gastroenterol.* **2021**, *56*, 145–154. [\[CrossRef\]](#)
32. Buclin, T.; Gotta, V.; Fuchs, A.; Widmer, N.; Aronson, J. Monitoring drug therapy. *Br. J. Clin. Pharmacol.* **2012**, *73*, 917–923. [\[CrossRef\]](#) [\[PubMed\]](#)
33. Frymoyer, A.; Piester, T.L.; Park, K.T. Infliximab Dosing Strategies and Predicted Trough Exposure in Children With Crohn Disease. *J. Pediatr. Gastroenterol. Nutr.* **2016**, *62*, 723–727. [\[CrossRef\]](#)
34. Frymoyer, A.; Hoekman, D.R.; Piester, T.L.; de Meij, T.G.; Hummel, T.Z.; Benninga, M.A.; Kindermann, A.; Park, K.T. Application of Population Pharmacokinetic Modeling for Individualized Infliximab Dosing Strategies in Crohn Disease. *J. Pediatr. Gastroenterol. Nutr.* **2017**, *65*, 639–645. [\[CrossRef\]](#)
35. Eser, A.; Primas, C.; Reinisch, S.; Vogelsang, H.; Novacek, G.; Mould, D.R.; Reinisch, W. Prediction of Individual Serum Infliximab Concentrations in Inflammatory Bowel Disease by a Bayesian Dashboard System. *J. Clin. Pharmacol.* **2018**, *58*, 790–802. [\[CrossRef\]](#) [\[PubMed\]](#)

36. IDKmonitor® Infliximab Drug Level ELISA, Immundiagnostik AG. Available online: [http://www.immundiagnostik.com/fileadmin/pdf/IDKmonitor\\_Infliximab\\_K9655.pdf](http://www.immundiagnostik.com/fileadmin/pdf/IDKmonitor_Infliximab_K9655.pdf) (accessed on 20 January 2021).
37. Prometheus Therapeutics & Diagnostics Prometheus Anser IFX Monograph. Available online: [www.anserifx.com/PDF/AnserIFX-Monograph.pdf](http://www.anserifx.com/PDF/AnserIFX-Monograph.pdf) (accessed on 8 January 2021).
38. Wang, S.L.; Ohrmund, L.; Hauenstein, S.; Salbato, J.; Reddy, R.; Monk, P.; Lockton, S.; Ling, N.; Singh, S. Development and validation of a homogeneous mobility shift assay for the measurement of infliximab and antibodies-to-infliximab levels in patient serum. *J. Immunol. Methods* **2012**, *382*, 177–188. [\[CrossRef\]](#)
39. Lindbom, L.; Ribbing, J.; Jonsson, E.N. Perl-speaks-NONMEM (PsN)—A Perl module for NONMEM related programming. *Comput. Methods Programs Biomed.* **2004**, *75*, 85–94. [\[CrossRef\]](#)
40. Lindbom, L.; Pihlgren, P.; Jonsson, N. PsN-Toolkit—A collection of computer intensive statistical methods for non-linear mixed effect modeling using NONMEM. *Comput. Methods Programs Biomed.* **2005**, *79*, 241–257. [\[CrossRef\]](#)
41. Abrantes, J.A.; Jönsson, S.; Karlsson, M.O.; Nielsen, E.I. Handling interoccasion variability in model-based dose individualization using therapeutic drug monitoring data. *Br. J. Clin. Pharmacol.* **2019**, *85*, 1326–1336. [\[CrossRef\]](#)
42. Morley, S.K.; Brito, T.V.; Welling, D.T. Measures of Model Performance Based On the Log Accuracy Ratio. *Sp. Weather* **2018**, *16*, 69–88. [\[CrossRef\]](#)
43. Edlund, H.; Steenholdt, C.; Ainsworth, M.A.; Goebgen, E.; Brynskov, J.; Thomsen, O.; Huisinga, W.; Kloft, C. Magnitude of Increased Infliximab Clearance Imposed by Anti-infliximab Antibodies in Crohn's Disease Is Determined by Their Concentration. *AAPS J.* **2017**, *19*, 223–233. [\[CrossRef\]](#)
44. Ternant, D.; Aubourg, A.; Magdelaine-Beuzelin, C.; Degenne, D.; Watier, H.; Picon, L.; Paintaud, G. Infliximab Pharmacokinetics in Inflammatory Bowel Disease Patients. *Ther. Drug Monit.* **2008**, *30*, 523–529. [\[CrossRef\]](#)
45. Dotan, I.; Ron, Y.; Yanai, H.; Becker, S.; Fishman, S.; Yahav, L.; Ben Yehoyada, M.; Mould, D.R. Patient Factors That Increase Infliximab Clearance and Shorten Half-life in Inflammatory Bowel Disease. *Inflamm. Bowel Dis.* **2014**, *20*, 2247–2259. [\[CrossRef\]](#)
46. Ternant, D.; Berkane, Z.; Picon, L.; Gouilleux-Gruart, V.; Colombel, J.F.; Allez, M.; Louis, E.; Paintaud, G. Assessment of the Influence of Inflammation and FCGR3A Genotype on Infliximab Pharmacokinetics and Time to Relapse in Patients with Crohn's Disease. *Clin. Pharmacokinet.* **2015**, *54*, 551–562. [\[CrossRef\]](#)
47. Brandse, J.F.; Mould, D.; Smeeke, O.; Ashruf, Y.; Kuin, S.; Strik, A.; van den Brink, G.R.; D'Haens, G.R. A Real-life Population Pharmacokinetic Study Reveals Factors Associated with Clearance and Immunogenicity of Infliximab in Inflammatory Bowel Disease. *Inflamm. Bowel Dis.* **2017**, *23*, 650–660. [\[CrossRef\]](#)
48. Kevans, D.; Murthy, S.; Mould, D.R.; Silverberg, M.S. Accelerated clearance of infliximab is associated with treatment failure in patients with corticosteroid-refractory acute ulcerative colitis. *J. Crohn's Colitis* **2018**, *12*, 662–669. [\[CrossRef\]](#)
49. Dreesen, E.; Faelens, R.; Van Assche, G.; Ferrante, M.; Vermeire, S.; Gils, A.; Bouillon, T. Optimising infliximab induction dosing for patients with ulcerative colitis. *Br. J. Clin. Pharmacol.* **2019**, *85*, 782–795. [\[CrossRef\]](#)
50. Matsuoka, K.; Hamada, S.; Shimizu, M.; Nanki, K.; Mizuno, S.; Kiyohara, H.; Arai, M.; Sugimoto, S.; Iwao, Y.; Ogata, H.; et al. Factors contributing to the systemic clearance of infliximab with long-term administration in Japanese patients with Crohn's disease: Analysis using population pharmacokinetics. *Int. J. Clin. Pharmacol. Ther.* **2020**, *58*, 89–102. [\[CrossRef\]](#)
51. Petitcollin, A.; Brochard, C.; Siproudhis, L.; Tron, C.; Verdier, M.C.; Lemaitre, F.; Lucidarme, C.; Bouguen, G.; Bellissant, É. Pharmacokinetic Parameters of Infliximab Influence the Rate of Relapse After De-Escalation in Adults With Inflammatory Bowel Diseases. *Clin. Pharmacol. Ther.* **2019**, *106*, 605–615. [\[CrossRef\]](#)
52. Grišić, A.M.; Dorn-Rasmussen, M.; Ungar, B.; Brynskov, J.; Ilvemark, J.F.K.F.; Bolstad, N.; Warren, D.J.; Ainsworth, M.A.; Huisinga, W.; Ben-Horin, S.; et al. Infliximab clearance decreases in the second and third trimesters of pregnancy in inflammatory bowel disease. *United Eur. Gastroenterol. J.* **2020**, *9*, 91–101. [\[CrossRef\]](#)
53. Aubourg, A.; Picon, L.; Lecomte, T.; Bejan-Angoulvant, T.; Paintaud, G.; Ternant, D. A robust estimation of infliximab pharmacokinetic parameters in Crohn's disease. *Eur. J. Clin. Pharmacol.* **2015**, *71*, 1541–1542. [\[CrossRef\]](#)
54. Buurman, D.J.; Maurer, J.M.; Keizer, R.J.; Kosterink, J.G.W.; Dijkstra, G. Population pharmacokinetics of infliximab in patients with inflammatory bowel disease: Potential implications for dosing in clinical practice. *Aliment. Pharmacol. Ther.* **2015**, *42*, 529–539. [\[CrossRef\]](#)
55. Brandse, J.F.; Mathôt, R.A.; van der Kleij, D.; Rispens, T.; Ashruf, Y.; Jansen, J.M.; Rietdijk, S.; Löwenberg, M.; Ponsioen, C.Y.; Singh, S.; et al. Pharmacokinetic Features and Presence of Antidrug Antibodies Associate With Response to Infliximab Induction Therapy in Patients With Moderate to Severe Ulcerative Colitis. *Clin. Gastroenterol. Hepatol.* **2016**, *14*, 251–258.e2. [\[CrossRef\]](#)
56. Passot, C.; Mulleman, D.; Bejan-Angoulvant, T.; Aubourg, A.; Willot, S.; Lecomte, T.; Picon, L.; Goupille, P.; Paintaud, G.; Ternant, D. The underlying inflammatory chronic disease influences infliximab pharmacokinetics. *MAbs* **2016**, *8*, 1407–1416. [\[CrossRef\]](#)
57. Xu, Z.; Mould, D.R.; Hu, C.; Ford, J.; Keen, M.; Davis, H.M.; Zhou, H. Population pharmacokinetic analysis of infliximab in pediatrics using integrated data from six clinical trials. *Clin. Pharmacol. Drug Dev.* **2012**, *1*, 203.
58. Xu, X.S.; Dunne, A.; Kimko, H.; Nandy, P.; Vermeulen, A. Impact of low percentage of data below the quantification limit on parameter estimates of pharmacokinetic models. *J. Pharmacokinet. Pharmacodyn.* **2011**, *38*, 423–432. [\[CrossRef\]](#)
59. Janssen, E.J.H.; Väitalo, P.A.J.; Allegaert, K.; de Cock, R.F.W.; Simons, S.H.P.; Sherwin, C.M.T.; Mouton, J.W.; van den Anker, J.N.; Knibbe, C.A.J. Towards Rational Dosing Algorithms for Vancomycin in Neonates and Infants Based on Population Pharmacokinetic Modeling. *Antimicrob. Agents Chemother.* **2016**, *60*, 1013–1021. [\[CrossRef\]](#)

- 
60. Smits, A.; De Cock, R.F.W.; Allegaert, K.; Vanhaesebrouck, S.; Danhof, M.; Knibbe, C.A.J. Prospective Evaluation of a Model-Based Dosing Regimen for Amikacin in Preterm and Term Neonates in Clinical Practice. *Antimicrob. Agents Chemother.* **2015**, *59*, 6344–6351. [\[CrossRef\]](#)
  61. Neely, M.; Philippe, M.; Rushing, T.; Fu, X.; van Guilder, M.; Bayard, D.; Schumitzky, A.; Bleyzac, N.; Goutelle, S. Accurately Achieving Target Busulfan Exposure in Children and Adolescents With Very Limited Sampling and the BestDose Software. *Ther. Drug Monit.* **2016**, *38*, 332–342. [\[CrossRef\]](#) [\[PubMed\]](#)
  62. Krekels, E.H.J.; Tibboel, D.; de Wildt, S.N.; Ceelie, I.; Dahan, A.; van Dijk, M.; Danhof, M.; Knibbe, C.A.J. Evidence-Based Morphine Dosing for Postoperative Neonates and Infants. *Clin. Pharmacokinet.* **2014**, *53*, 553–563. [\[CrossRef\]](#) [\[PubMed\]](#)
  63. Darwich, A.S.; Polasek, T.M.; Aronson, J.K.; Ogungbenro, K.; Wright, D.F.B.; Achour, B.; Reny, J.-L.; Daali, Y.; Eiermann, B.; Cook, J.; et al. Model-Informed Precision Dosing: Background, Requirements, Validation, Implementation, and Forward Trajectory of Individualizing Drug Therapy. *Annu. Rev. Pharmacol. Toxicol.* **2021**, *61*, 225–245. [\[CrossRef\]](#)
  64. Zhao, W.; Kaguelidou, F.; Biran, V.; Zhang, D.; Allegaert, K.; Capparelli, E.V.; Holford, N.; Kimura, T.; Lo, Y.; Peris, J.; et al. External evaluation of population pharmacokinetic models of vancomycin in neonates: The transferability of published models to different clinical settings. *Br. J. Clin. Pharmacol.* **2013**, *75*, 1068–1080. [\[CrossRef\]](#) [\[PubMed\]](#)
  65. Santacana, E.; Rodríguez-Alonso, L.; Padullés, A.; Guardiola, J.; Rodríguez-Moranta, F.; Serra, K.; Bas, J.; Morandeira, F.; Colom, H.; Padullés, N. External Evaluation Of Population Pharmacokinetic Models Of Infliximab In Inflammatory Bowel Disease Patients. *Ther. Drug Monit.* **2017**, *40*, 120–129. [\[CrossRef\]](#)
  66. Santacana Juncosa, E.; Padullés Zamora, A.; Colom Codina, H.; Rodríguez Alonso, L.; Guardiola Capo, J.; Bas Minguet, J.; Padullés Zamora, N. Contribution of infliximab population pharmacokinetic model for dose optimization in ulcerative colitis patients. *Rev. Esp. Enferm. Dig.* **2016**, *108*, 104–105. [\[CrossRef\]](#)
  67. Candel, M.G.; Gascón Cánovas, J.J.; Espín, R.G.; Nicolás de Prado, I.; Redondo, L.R.; Sanz, E.U.; Navalón, C.I. Usefulness of population pharmacokinetics to optimize the dosage regimen of infliximab in inflammatory bowel disease patients. *Rev. Esp. Enfermedades Dig.* **2020**, *112*, 590–597. [\[CrossRef\]](#)
  68. Dave, M.B.; Dherai, A.J.; Desai, D.C.; Mould, D.R.; Ashavaid, T.F. Optimization of infliximab therapy in inflammatory bowel disease using a dashboard approach—An Indian experience. *Eur. J. Clin. Pharmacol.* **2021**, *77*, 55–62. [\[CrossRef\]](#)
  69. Eser, A.; Reinisch, W.; Schreiber, S.; Ahmad, T.; Boulos, S.; Mould, D.R. Increased Induction Infliximab Clearance Predicts Early Antidrug Antibody Detection. *J. Clin. Pharmacol.* **2020**, *61*, 224–233. [\[CrossRef\]](#)
  70. Landemaine, A.; Petitcollin, A.; Brochard, C.; Miard, C.; Dewitte, M.; Le Balc'h, E.; Grainville, T.; Bellissant, E.; Siproudhis, L.; Bouguen, G. Cumulative Exposure to Infliximab, But Not Trough Concentrations, Correlates With Rate of Infection. *Clin. Gastroenterol. Hepatol.* **2021**, *19*, 288–295.e4. [\[CrossRef\]](#)
  71. Magnusson, M.K.; Strid, H.; Sapnara, M.; Lason, A.; Bajor, A.; Ung, K.; Öhman, L. Anti-TNF Therapy Response in Patients with Ulcerative Colitis Is Associated with Colonic Antimicrobial Peptide Expression and Microbiota Composition. *J. Crohn's Colitis* **2016**, *10*, 943–952. [\[CrossRef\]](#)
  72. Seong, G.; Kim, N.; Joung, J.; Kim, E.R.; Chang, D.K.; Chun, J.; Hong, S.N.; Kim, Y.-H. Changes in the Intestinal Microbiota of Patients with Inflammatory Bowel Disease with Clinical Remission during an 8-Week Infliximab Infusion Cycle. *Microorganisms* **2020**, *8*, 874. [\[CrossRef\]](#)
  73. Wang, Y.; Gao, X.; Ghazlane, A.; Hu, H.; Li, X.; Xiao, Y.; Li, D.; Yu, G.; Zhang, T. Characteristics of Faecal Microbiota in Paediatric Crohn's Disease and Their Dynamic Changes During Infliximab Therapy. *J. Crohn's Colitis* **2018**, *12*, 337–346. [\[CrossRef\]](#)

## DISCUSSION AND FUTURE PERSPECTIVE

---

Pharmaceutical products continue to be a significant source of patient harm [31]: Despite the development of new drugs and many initiatives established to improve safety of drug therapies, the occurrence of ADRs is still a prevailing issue [31]. ADRs even represent the fourth to sixth leading cause of mortality in the U.S. [8]. Up to 50% of ADRs have been found to be preventable and are often a result of altered drug exposure caused by DGIs, DDIs and DDGIs [18–20]. Moreover, lack or loss of therapeutic response due to subtherapeutic drug concentrations present an additional risk for therapy failure and are typically more difficult to quantify compared to the incidence of ADRs [4, 6]. This supports the application of innovative approaches including popPK and PBPK modeling to provide tailored dosing recommendations.

This thesis delves into the innovative field of MIPD using pharmacometric modeling approaches. In projects 1–3, mechanistic modeling and simulation is leveraged to (i) predict enzyme-/transporter-mediated and pH-dependent DDI scenarios, (ii) investigate DGIs, DDIs and DDGIs across CYP2D6 AS groups and subsequently (iii) provide dosing strategies for various CYP3A4 DDI scenarios and powerful frameworks to be applied in future activities to individually tailor dosing regimens to the patient’s need. Here, new whole-body PBPK models were thoroughly developed for the TKIs dasatinib and imatinib as well as for the SERM (E)-clomiphene. Additionally, an external performance evaluation of infliximab popPK models was conducted to select an empirical pharmacometric model for its application in the observational clinical trial “GUIDE-IBD”, supporting clinicians in the selection of individualized dosing regimens. With that, this work aims to contribute shifting from the “one-size-fits-all” paradigm to a more individualized dosing approach for dasatinib, (E)-clomiphene, imatinib and infliximab by leveraging pharmacometric modeling and simulation.

### 5.1 APPLICATION OF PBPK MODELING TO TAILOR DRUG THERAPY

#### 5.1.1 *Rationale for MIPD of dasatinib*

While the standard dosing approach for chemotherapy has traditionally been based on body surface area, early studies of oral TKIs indicated large therapeutic indices, resulting in the approval of fixed dosing regimens [62, 176]. However, subtherapeutic or toxic drug exposures associated with fixed, “one-size-fits-all” dosing approaches, as approved at the time of commercialization of anticancer agents including dasatinib and imatinib, are increasingly acknowledged and underscore the need for efforts to optimize dosing after drug approval to better tailor treatments to individual patient needs [61, 176, 177]. Of note, adequate exposure during treatment with oral targeted therapies was found for only 45% of the treated patients, while 17% were overexposed and 38% underexposed,

resulting in an increased risk of toxicity and lack of response, respectively [178]. At the approved flat dose, dasatinib shows high variability in  $C_{\max}$  and AUC [179]. A popPK analysis conducted by Dai and colleagues highlighted that variability in dasatinib exposure can be primarily attributed to a high variability in relative bioavailability which was even larger within than between subjects [180]. Here, dasatinib exposure may be affected by multiple individual-specific factors, including the use of ARAs such as antacids, proton pump inhibitors or H<sub>2</sub>-receptor antagonists, which alter stomach pH and reduce dasatinib's limited solubility, and other DDIs with concomitant medications, particularly through CYP3A4 inhibition or induction [106–109]. While an exposure–response relationship between  $C_{\min}$  levels and efficacy could not be established based on results from five Phase II trials [181], an exposure–response analysis of a Phase III trial found a positive relationship between average steady-state plasma concentrations and the probability of achieving major cytogenic response [65, 182]. In addition, a target threshold of  $C_{\max} \geq 50$  ng/mL measured two hours after drug intake has been recommended [65, 179]. Moreover, an exposure–safety analysis identified higher  $C_{\min}$  and advanced age as the most significant predictors for pleural effusion, a key ADR during dasatinib therapy, suggesting to not exceed a  $C_{\min}$  of 2.5 ng/mL during dasatinib treatment [173, 179, 182]. Thus, implementation of a precision medicine approach, adapting dasatinib dosing to individual patient factors in clinical practice may benefit cancer patients. This is supported by a recent study investigating dasatinib TDM for patients with CML which showed that keeping  $C_{\min}$  levels below a certain threshold led to a significant reduction of pleural effusion events without impairing molecular responses [176].

In addition, as a sensitive CYP3A4 substrate, the concomitant intake of dasatinib with CYP3A4 inhibitors and inducers significantly affects dasatinib exposure, increasing the likelihood of therapy failure either due to ADRs or lack of response [106, 107]. However, the package insert does not include explicit instructions for dose adaptations under specific perpetrator drug co-treatment [102, 173]. Here, the presented work (project I) aimed to fill this gap, providing recommendations for individualized dasatinib therapy. The developed dasatinib PBPK model – able to describe pH-dependent as well as transporter- and enzyme-mediated DDIs – was leveraged to simulate various (complex) DDI scenarios. The simulations were then successfully translated into clinical actionable guidelines by providing model-based dose adaptations for various single and multiple DDI scenarios (e.g., concomitant intake of dasatinib, carbamazepine and erythromycin), supporting dasatinib precision dosing [173]. An overview of the model-based dose recommendations is depicted in Figure 7 of project I.



### 5.1.2 Rationale for MIPD of imatinib

Similar to dasatinib, imatinib also exhibits significant inter- and intra-individual PK variability following standard dosing [62]. For example, after fixed dosing of 400 mg imatinib q.d.,  $C_{min}$  levels ranged from 340 ng/mL to 2100 ng/mL [62]. Since this variability correlates with both treatment efficacy and drug resistance and since a positive exposure–response relationship has been observed in several studies, imatinib is a suitable candidate for TDM [62, 183–186].

The International Association of Therapeutic Drug Monitoring and Clinical Toxicology advises a target  $C_{min}$  of  $\geq 1000$  ng/mL and  $\geq 1100$  ng/mL in CML and GIST, respectively [62, 187]. In some studies the occurrence of ADRs were reported for  $C_{min}$  levels  $> 3000$  ng/mL, while other studies could not identify a clear toxicity threshold [62, 188]. The OPTIM-imatinib trial assessed the benefit of TDM for patients with CML who received imatinib as first-line therapy [61]. Here, patients in the TDM arm were considered underdosed if  $C_{min}$  levels were below 1000 ng/mL [61]. This TDM dose adaptation strategy yielded higher major molecular response rates at 12 months (67% vs. 39%) [61]. However, the treatment benefit for patients extends beyond the use of TDM; the application of MIPD has been retrospectively studied for imatinib therapy using popPK modeling and simulation [177]. Here, the application of a model-based simulation approach resulted in around 75% of  $C_{min}$  levels attaining the target threshold of 1000–2000 ng/mL, while a fixed dosing approach had been associated with only 16.5% of target attainment in a real world setting, highlighting the limitations of the “one-size-fits-all” dosing approach [177]. However, dose recommendations based on this simulation study only included age, weight, sex and disease covariates [177], while CYP3A4 and CYP2C8 DDIs as well as genetic variations in the involved CYP enzymes and transporters are also known to significantly affect imatinib exposure [96–98, 178, 189]. Here, the newly developed imatinib PBPK model presented in this thesis (project II) may be leveraged in the future to guide imatinib dosing strategies for specific subpopulations (e.g., patients under specific drug co-treatment) and for individual patients.

### 5.1.3 Rationale for MIPD of clomiphene

The SERM clomiphene citrate was approved nearly 60 years ago, providing a treatment for infertile women with PCOS [110, 111]. Yet, studies have revealed high variability in response to clomiphene therapy [114, 190, 191]. For example, according to results from Huyghe and colleagues, about one third of women did not respond to the 50 mg dose during the first cycle of treatment, supporting the need of a more personalized clomiphene therapy [191]. Multiple factors, including hyperandrogenemia, obesity, levels of specific hormones (e.g., anti-Müllerian hormone) and polymorphisms in CYP2D6, have been identified to affect the response to clomiphene therapy [112, 116, 192–197]. While clomiphene citrate has served as first-line infertility treatment for decades, its metabolism and activity profile had remained unclear for some time [112, 114]. Mürdter et al. thoroughly investigated the metabolism of clomiphene and its metabolites and identified (E)-4-OH-Clom and (E)-4-OH-DE-Clom as the compounds with the highest

inhibitory affinity for the estrogen receptor [112, 113, 115, 198, 199]. At the same time, CYP3A4 and the polymorphic enzyme CYP2D6 were identified to be highly involved in both the formation and the metabolism of (*E*)-clomiphene and its main metabolites [112, 113, 115]. As a result, co-treatment with clomiphene and CYP3A4/CYP2D6 perpetrator drugs as well as polymorphisms in the CYP2D6 gene lead to high variability in drug exposure, which in turn can affect therapy outcome [112, 113, 115]. In a study of 14 women under clomiphene citrate therapy, plasma concentrations for both (*E*)- and (*Z*)-clomiphene varied up to 40-fold between study participants, highlighting the large variability in clomiphene metabolism and exposure [190]. Variability in exposure across different CYP2D6 AS populations as well as the impact of clarithromycin and paroxetine co-medication on the exposure of (*E*)-clomiphene and its three main metabolites has been investigated in project III utilizing the established PBPK model of (*E*)-clomiphene and its three main metabolites. The developed model presents a powerful tool to support future activities to tailor clomiphene dosing to different CYP2D6 genotypes and phenotypes as well as complex DDI and DDGI scenarios. Clinical studies confirming the benefit of genotype- or phenotype-guided clomiphene dosing strategies are yet to be conducted.

#### 5.1.4 *The virtual twin concept and individual PBPK predictions*

PBPK models have advanced stratified dosing strategies by providing tailored dosing for subpopulations with the same attributes (e.g., CYP2D6 genotypes/phenotypes, co-medication, organ impairment) affecting a drug's PK [85]. However, by implementing individual demographics, physiology and enzyme activity into an established PBPK model, a "virtual twin" of the patient can be created to predict drug exposure in the respective individual [84, 85, 173]. Here, results from PGx tests on the individual genotype/phenotype of specific enzymes and/or transporters, among others, can be integrated to improve the predictive performance quality of the individual plasma concentration–time profiles or of drug concentrations in the target organ [84, 85]. With that, the "virtual twin" concept is a promising new approach in MIPD, integrating individual patient characteristics in PBPK models [85]. While proof-of-concept studies have been conducted for drugs such as olanzapine, demonstrating the benefit of using a "virtual twin" approach [84], the approach has not yet been assessed for many drugs including dasatinib, imatinib and (*E*)-clomiphene, respectively. The developed PBPK models could be leveraged as a profound basis for such an assessment. Since the models were developed with aggregated data only, evaluating their predictive performance with individual data is necessary before applying them in a "virtual twin" clinical setting.

Identification of individual-specific PK parameters has gained increasing interest also for PBPK-based MIPD. As described before, this concept has been successfully applied in MIPD with popPK(/PD) models based on *a priori* distribution of inter-/intra-individual variability, residual unexplained variability and MAP Bayesian estimation, leveraging individual drug concentrations [33–35, 171]. A combination of PBPK models, estimation of population parameters and inter-individual



variability as well as MAP Bayesian estimation represents a promising approach to identify individual PK parameters for PBPK-based MIPD [200].

## 5.2 APPLICATION OF POPPK MODELING TO TAILOR DRUG THERAPY

### 5.2.1 Rationale for MIPD of infliximab

Accumulating evidence suggests that the approved weight-based dosing of infliximab fails to achieve the expected positive outcome in a substantial number of patients due to significant inter- and intra-individual variability in infliximab PK [122, 127–147]. Up to 30% of infliximab-treated patients experience primary non-response [4, 5, 201]. Secondary loss of response occurs in up to 50% of patients during maintenance therapy with standard weight-based dosing [4, 5, 122]. As a result and since treatment efficacy has been shown to correlate with infliximab serum concentrations not only in IBD but also in rheumatoid arthritis and other indications, infliximab therapy is a suitable candidate for MIPD [123–126].

Several retrospective evaluations have recommended specific  $C_{min}$  values to target, which differ due to various factors such as disease type and severity [122]. For example, studies have shown that attaining infliximab  $C_{min}$  values at steady state above 3  $\mu\text{g/mL}$  for CD patients and 3.7  $\mu\text{g/mL}$  for UC patients can minimize treatment failure and help sustain clinical remission [122, 124, 148]. Furthermore, recent data recommend  $C_{min}$  values of at least 5  $\mu\text{g/mL}$  for CD and 7.5  $\mu\text{g/mL}$  for UC to achieve endoscopic healing and at least 8  $\mu\text{g/mL}$  for sustained histologic remission [122, 149–151]. For severe course of disease, such as perianal fistulizing CD, higher  $C_{min}$  levels ( $\geq 10 \mu\text{g/mL}$ ) are needed for fistula healing [5, 122, 153]. A retrospective study by Vande Castelle et al. has shown that the proportion of patients who are not in remission during maintenance therapy successively decreased with increasing infliximab  $C_{min}$ : from 25% of patients with an infliximab threshold of  $\geq 1 \mu\text{g/mL}$  to 15% with an infliximab  $C_{min}$  of  $\geq 3 \mu\text{g/mL}$  to 8% with an infliximab  $C_{min}$  of  $\geq 5 \mu\text{g/mL}$  and finally to 4% with infliximab  $C_{min}$  of  $\geq 7 \mu\text{g/mL}$  and  $\geq 10 \mu\text{g/mL}$ , respectively [202]. Therefore, the study proposed an infliximab  $C_{min}$  of at least 5  $\mu\text{g/mL}$  during maintenance therapy, yielding only a small portion of patients being not in remission [202]. Similarly, the American Gastroenterological Association (AGA), that endorses TDM for infliximab, proposed a maintenance infliximab target  $C_{min}$  of  $\geq 5 \mu\text{g/mL}$  [63]. Nevertheless, this target threshold is consistently not achieved in a large number of patients when applying the standard body-weight dosing regimen; often considerably higher infliximab doses are required [122]. To date, it remains unclear whether and to which extent higher infliximab exposure leads to an increased risk of toxicity [34]. Starting precision dosing during the induction phase would be of high benefit since patients are suffering from an active disease associated with higher clearance, resulting in higher risk of subtherapeutic drug exposure, early formation of ADAs and lack of therapeutic response [203]. A respective target threshold for the induction phase has been under investigation [204–206]. Several studies have demonstrated a correlation between higher induction infliximab  $C_{min}$  and favorable therapeutic outcomes, however, a high variability in the recommended infliximab target  $C_{min}$ s for week 2 and week 6 across studies could be observed:

For week 2, levels range from  $> 9.2 \mu\text{g/mL}$  to  $\geq 29 \mu\text{g/mL}$  and for week 6 from  $> 6.6 \mu\text{g/mL}$  to  $> 22 \mu\text{g/mL}$  [203–206].

MIPD approaches using Bayesian forecasting and patient-specific factors that impact infliximab clearance (e.g., serum albumin, body weight, gender and ADA titers), can be used early on and can help to achieve predefined target thresholds. First studies, such as the PRECISION study, evaluating a Bayesian approach for infliximab dosing, indicate a benefit of TDM combined with Bayesian forecasting [34, 207]. Moreover, according to an *in silico* assessment, a model-based approach using a popPK model and Bayesian forecasting may be superior over TDM with stepwise dosing or standard labeled dosing [165, 208]. Here, further prospective studies are warranted to assess, quantify and validate the benefits of personalized dosing and MIPD approaches in infliximab therapy.

### 5.2.2 The “GUIDE-IBD” study

One of these studies is the multi-center, randomized, open-label, prospective clinical trial “GUIDE-IBD”. Here, anti-TNF- $\alpha$  treatment-naïve patients suffering from CD or UC with moderate to severe disease activity were recruited at three German university hospitals and randomly assigned to a “best care” (BC) and a “molecular medicine care” (MMC) arm, which included MIPD and biomarker-informed molecular guidance (DRKS00032030) [209–212]. Best-care diagnostics and treatment were applied for patients in the BC arm, while medical decisions for infliximab dose adjustments in the MMC arm were taken based on molecular disease assessments and model-based dosing recommendations (i.e., MIPD) using Bayesian forecasting (cf., Figure 5.1) [209–211].

When selecting a model for MIPD, several factors must be considered including the age of the studied population (e.g., pediatrics, elderly), indications, health status, patient body composition (e.g., normal, obese, cachectic), genetic factors, evaluated dose levels, administration route, sampling scheme, investigated covariates and assay methods [55]. A predictive external model performance evaluation can help to assess the suitability of different models before applying them in clinical practice [55]. Hence, such an external model evaluation investigating the predictivity of various infliximab popPK models was conducted (see project IV). Based on the results of the assessment, the model developed and published by Fasanmade et al. [128] was selected as the most suitable one for the clinical trial “GUIDE-IBD”.

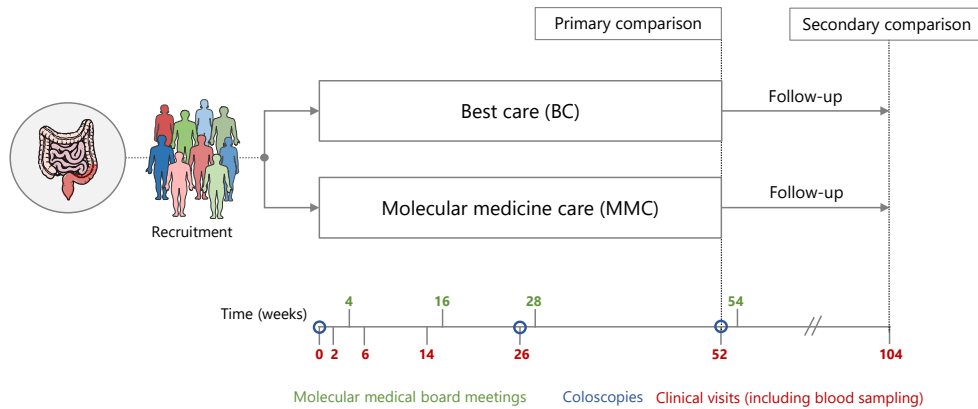


Figure 5.1: Clinical trial design overview for the “GUIDE-IBD” study. Anti-TNF- $\alpha$  treatment-naïve patients suffering from CD or UC were enrolled and randomized into one of the two treatment arms – the BC or the MMC arm. Molecular medical board meetings were held by a multidisciplinary team of healthcare professionals to discuss patients’ individual molecular disease behavior and individual model-based dosing recommendations (MMC arm only). Drawings were adapted from Servier Medical Art [2], licensed under a Creative Commons Attribution 4.0 (CC BY 4.0) Unported License (<https://creativecommons.org/licenses/by/4.0/>).

In “GUIDE-IBD”, blood samples were taken at weeks 0 (post-infusion concentration measurement), 2, 6, 14, 26, 52 and 104 ( $C_{\min}$  measurements), respectively [209, 210]. Using the first two measured infliximab concentrations from the induction phase (i.e., one peak and one  $C_{\min}$ ) in a Bayesian forecasting setting allowed dose simulations for each individual patient in the MMC arm after two weeks of infliximab therapy, predicting infliximab  $C_{\min}$  values in the maintenance phase [209, 210]. For predicted  $C_{\min}$  of  $< 5 \mu\text{g/mL}$ , (i.e., below the recommended minimum target trough threshold from the AGA guideline [63]), dose adjustments were proposed early on [209, 210]. Model-based dosing regimen recommendations were re-assessed, verified and/or adapted after weeks 14, 26 and 52, respectively [209, 210]. In addition, molecular assessments were conducted using published mRNA-based biomarkers from blood and biopsies [212]. Molecular and MIPD reports were provided for patients in the MMC arm after weeks 2, 14, 26 and 52, respectively, and results were presented to a multidisciplinary team of healthcare professionals. To facilitate MIPD report generation, an R-Shiny application was established. The workflow how to generate the reports is depicted in Figure 5.2.

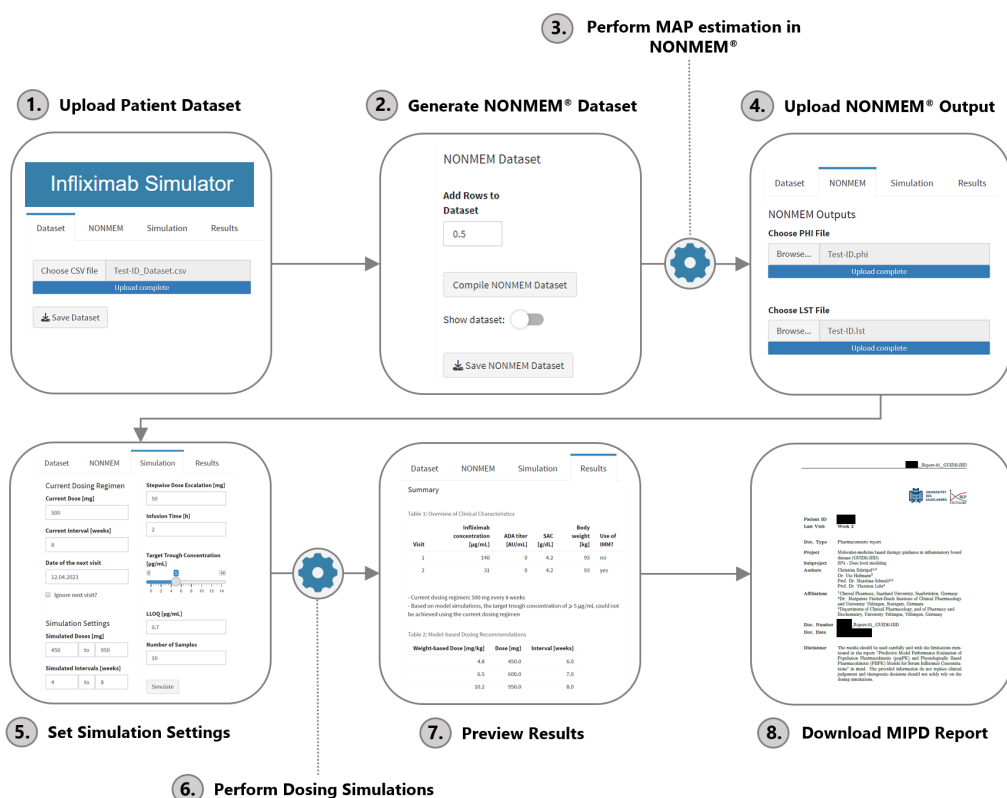


Figure 5.2: Workflow to generate an **MIPD** report for the “GUIDE-IBD” study using the R-Shiny application. The individual patient dataset is uploaded as CSV file. A NONMEM® dataset is generated which is used to perform the **MAP** estimation in the modeling software NONMEM®. The NONMEM® output files can be imported in the application and specific simulation settings can be set (e.g., current dosing regimen, simulated dose and interval). The model-based dosing recommendations can be previewed and downloaded as **MIPD** report. **MAP**, maximum *a posteriori* probability; **MIPD**, model-informed precision dosing.

Over the period of February 4, 2021, and January 18, 2024 a total of 102 patients were randomized; of these, 41 patients suffering from **CD** and 46 from **UC** completed the study [212]. Interim results showed that most patients did indeed not achieve the target  $C_{min}$  of  $\geq 5$  µg/mL in the maintenance phase when applying the standard weight-based dosing regimen and required **MIPD**-based dosing adaptations [209, 210]. Moreover, a higher proportion of patients in the **MMC** arm achieved disease control at week 52 compared to the **BC** arm [212].

### 5.2.3 Automated model selection and model averaging approach

Besides using a “single-model approach” for **MIPD** (i.e., using a single **popPK** model for dose simulations), two new “multi-model approaches” using an automated model selection algorithm or automated model averaging were introduced very recently by Uster et al. and have been successfully applied for vancomycin [55, 213]. These algorithms aim to select either the best-fit model or a combination of models – informed by each model’s fit to the individual **PK** data – for the use

in Bayesian forecasting [55, 213]. In these settings, model averaging suggested a better predictive performance compared to using the best popPK model obtained from previous external evaluations [213, 214].

### 5.3 OUTLOOK FOR CLINICAL IMPLEMENTATION OF MIPD

TDM has found its place in clinical routine for specific drugs (e.g., vancomycin, gentamycin, digoxin, phenytoin) to keep the target exposure metrics within the desired therapeutic range [215]. Based on measured drug concentrations, physicians decide which drug doses and intervals to choose in order to improve individual outcomes [56]. While TDM offers advantages such as a simple implementation in the clinical setting, simple interpretation of laboratory results and simple adaptations of the dose strength or the interval [58], TDM also bears decisive limitations. In case of complex drug PK, complex relationships between specific patient characteristics and drug exposure or changing covariates over time requiring frequent dose adjustments, the interpretation of TDM results is not straightforward [58, 216]. Additionally, taking a single or a small number of blood samples can be limited to a predefined time window, may pose a suboptimal surrogate parameter for drug exposure, and may not be adequately interpreted without the use of a pharmacometric model [58]. Moreover, protocols for implementation of TDM are often not well established and clinicians often consider TDM only in cases when concerns about loss of response or immunogenicity arise [216]. Here, applying pharmacometric models in MIPD as outlined and shown above offers a powerful tool to overcome these issues.

While modeling and simulation is usually handled by pharmacometricians, dashboard precision dosing tools and clinical decision support systems (CDSS) based on popPK, PBPK and PK/PD models could serve as a user-friendly framework in the future to guide therapeutic decision making for clinicians and thus, enable MIPD “at the bedside” [24, 122, 217]. Such dashboards allow a user-friendly integration of patient-specific factors with measured concentrations to guide regimen selection toward attaining the desired therapeutic target [216]. The patient-specific input parameters include patient demographics (e.g., body weight) as well as routine laboratory results (e.g., serum albumin concentrations, immunogenicity) and are integrated with the applied drug doses, dosing scheme and measured drug concentrations to estimate patient’s individual PK parameters [122]. Subsequent individualized dosing recommendations are provided, aiming for physician-specified target exposure [122]. Several dashboards have been developed in the academic setting (e.g., TDMx [<http://www.tdmx.eu/>] and NextDose [<https://www.nextdose.org/>] based on empirical models or dosing decision support systems for drugs like simvastatin [217] or imatinib based on PBPK models), but implementation in clinical care is lacking [33]. An exemplary representation of a decision support system which leverages developed PBPK models is depicted in Figure 5.3.

In addition, commercial software exists for clinical support such as iDose® [<https://www.baysient.net/idose-product/>]. However, even a well-designed CDSS will unfold its full potential only if it is integrated in the clinical workflow (e.g., an e-prescribing system or electronic health record (EHR)) and will not

replace clinical judgement that integrates all relevant patient- and therapy-related factors – for example as implemented in the "GUIDE-IBD" study [33, 209–211]. Frymoyer et al. successfully showed that the implementation of CDSS integrated into EHR for vancomycin therapy in clinical care is feasible and provides a powerful framework improving drug therapy [33]. However, the implementation of such tools still faces multiple challenges – particularly regulatory requirements for software tools being used as medical devices – which need to be overcome in the future [24, 218].

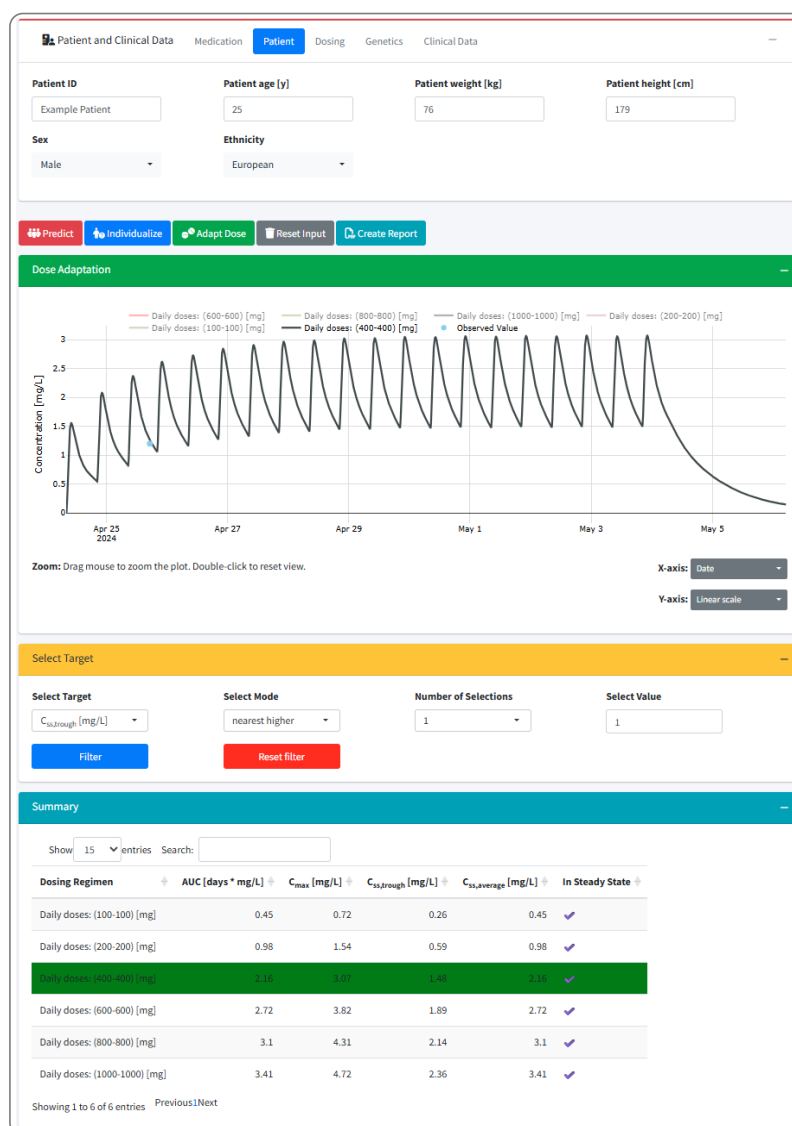


Figure 5.3: Screenshot of a decision support system based on PBPK models which were developed as part of the INSPIRATION European Union project. The screenshot depicts exemplary PBPK-based dosing simulations and corresponding dosing recommendations. For this purpose, a minimum target imatinib C<sub>min</sub> of 1000 ng/mL was selected to identify the optimal imatinib dosing regimen for the virtual patient [62, 187].

## CONCLUSIONS

---

Since **MIPD** was first introduced, efforts have been undertaken to advance drug therapy of compounds by identifying optimal doses for individual patients – particularly in therapeutic areas such as anti-infectives, oncology, immunosuppressants and anti-inflammatory drugs, where the labeled drug dose often results in suboptimal drug exposure [55]. However, these and many other therapeutic areas may benefit from continuous efforts to implement a more personalized dosing approach. Thus, this thesis delved into the novel field of **MIPD** with the aim of advancing precision dosing approaches of dasatinib, imatinib, (*E*)-clomiphene and infliximab, gaining a deeper understanding of the **PK** of these drugs by applying mechanistic and empirical pharmacometric modeling approaches, and consequently improving drug therapy outcomes.

Whole-body **PBPK** models have been thoroughly developed for the **TKIs** dasatinib and imatinib as well as for the **SERM** (*E*)-clomiphene. Enzyme-, transporter-mediated and pH-dependent **DDIs**, **DGIs** and **DDGIs** across different **CYP2D6 AS** groups were investigated, and new dosing strategies for various **CYP3A4 DDI** scenarios provided. Furthermore, with this work, powerful frameworks to individually tailor doses to the patient's need have been made available for future studies and clinical care. In addition, an external model performance evaluation for infliximab was conducted to select a pharmacometric model for application in the clinical trial “GUIDE-IBD”, supporting physicians in the selection of individually optimized dosing regimens for each patient.

For this thesis, several pharmacometric models were developed and applied to support personalized dosing strategies for patients in clinical settings. In addition, this work may contribute to the paradigm shift from a “one-size-fits-all” to a more personalized dosing approach. However, although the application of **MIPD** presents a step in the right direction, delivering the right drug via the right route and the right dose for the right patient at the right time remains an ever-present daily challenge for clinicians, calling for continuous efforts in the field of precision dosing and precision medicine.





## BIBLIOGRAPHY

---

1. Brand, A.; Allen, L.; Altman, M.; Hlava, M.; Scott, J. Beyond authorship: attribution, contribution, collaboration, and credit. *Learned Publishing* **2015**, *28*, 151–155, DOI: [10.1087/20150211](https://doi.org/10.1087/20150211).
2. Les Laboratoires Servier. Servier medical art (SMART). <https://smart.servier.com/> (accessed 10/19/2024).
3. Polasek, T. M.; Shakib, S.; Rostami-Hodjegan, A. Precision dosing in clinical medicine: present and future. *Expert review of clinical pharmacology* **2018**, *11*, 743–746, DOI: [10.1080/17512433.2018.1501271](https://doi.org/10.1080/17512433.2018.1501271).
4. Roda, G.; Jharap, B.; Neeraj, N.; Colombel, J.-F. Loss of response to anti-TNFs: definition, epidemiology, and management. *Clinical and translational gastroenterology* **2016**, *7*, e135, DOI: [10.1038/ctg.2015.63](https://doi.org/10.1038/ctg.2015.63).
5. Wong, U.; Cross, R. K. Primary and secondary nonresponse to infliximab: mechanisms and countermeasures. *Expert opinion on drug metabolism & toxicology* **2017**, *13*, 1039–1046, DOI: [10.1080/17425255.2017.1377180](https://doi.org/10.1080/17425255.2017.1377180).
6. Tyson, R. J.; Park, C. C.; Powell, J. R.; Patterson, J. H.; Weiner, D.; Watkins, P. B.; Gonzalez, D. Precision dosing priority criteria: drug, disease, and patient population variables. *Frontiers in pharmacology* **2020**, *11*, 420, DOI: [10.3389/fphar.2020.00420](https://doi.org/10.3389/fphar.2020.00420).
7. European Medicines Agency. Guideline on good pharmacovigilance practices (GVP) annex I - definitions (rev 5). 2024, [https://www.ema.europa.eu/en/documents/scientific-guideline/guideline-good-pharmacovigilance-practices-annex-i-definitions-rev-5\\_en.pdf](https://www.ema.europa.eu/en/documents/scientific-guideline/guideline-good-pharmacovigilance-practices-annex-i-definitions-rev-5_en.pdf) (accessed 03/29/2025).
8. Lazarou, J.; Pomeranz, B. H.; Corey, P. N. Incidence of adverse drug reactions in hospitalized patients: a meta-analysis of prospective studies. *JAMA* **1998**, *279*, 1200–5, DOI: [10.1001/jama.279.15.1200](https://doi.org/10.1001/jama.279.15.1200).
9. Giacomini, K. M.; Krauss, R. M.; Roden, D. M.; Eichelbaum, M.; Hayden, M. R.; Nakamura, Y. When good drugs go bad. *Nature* **2007**, *446*, 975–7, DOI: [10.1038/446975a](https://doi.org/10.1038/446975a).
10. Al Hamid, A.; Ghaleb, M.; Aljadhey, H.; Aslanpour, Z. A systematic review of hospitalization resulting from medicine-related problems in adult patients. *British journal of clinical pharmacology* **2014**, *78*, 202–17, DOI: [10.1111/bcp.12293](https://doi.org/10.1111/bcp.12293).
11. Osanlou, R.; Walker, L.; Hughes, D. A.; Burnside, G.; Pirmohamed, M. Adverse drug reactions, multimorbidity and polypharmacy: a prospective analysis of 1 month of medical admissions. *BMJ open* **2022**, *12*, e055551, DOI: [10.1136/bmjopen-2021-055551](https://doi.org/10.1136/bmjopen-2021-055551).

12. Bouvy, J. C.; De Bruin, M. L.; Koopmanschap, M. A. Epidemiology of adverse drug reactions in Europe: a review of recent observational studies. *Drug safety* **2015**, *38*, 437–53, DOI: [10.1007/s40264-015-0281-0](https://doi.org/10.1007/s40264-015-0281-0).
13. Abu, S. F.; Shafie, A. A.; Chandriah, H. Cost estimations of managing adverse drug reactions in hospitalized patients: a systematic review of study methods and their influences. *Pharmacoepidemiology* **2023**, *2*, 120–139, DOI: [10.3390/pharma2020012](https://doi.org/10.3390/pharma2020012).
14. Sultana, J.; Cutroneo, P.; Trifirò, G. Clinical and economic burden of adverse drug reactions. *Journal of pharmacology & pharmacotherapeutics* **2013**, *4*, S73–7, DOI: [10.4103/0976-500X.120957](https://doi.org/10.4103/0976-500X.120957).
15. Beijer, H. J. M.; de Blaey, C. J. Hospitalisations caused by adverse drug reactions (ADR): a meta-analysis of observational studies. *Pharmacy world & science : PWS* **2002**, *24*, 46–54, DOI: [10.1023/a:1015570104121](https://doi.org/10.1023/a:1015570104121).
16. Elliott, L. S.; Henderson, J. C.; Neradilek, M. B.; Moyer, N. A.; Ashcraft, K. C.; Thirumaran, R. K. Clinical impact of pharmacogenetic profiling with a clinical decision support tool in polypharmacy home health patients: a prospective pilot randomized controlled trial. *PloS one* **2017**, *12*, e0170905, DOI: [10.1371/journal.pone.0170905](https://doi.org/10.1371/journal.pone.0170905).
17. Nair, N. P.; Chalmers, L.; Peterson, G. M.; Bereznicki, B. J.; Castelino, R. L.; Bereznicki, L. R. Hospitalization in older patients due to adverse drug reactions – the need for a prediction tool. *Clinical Interventions in Aging* **2016**, *11*, 497–505, DOI: [10.2147/CIA.S99097](https://doi.org/10.2147/CIA.S99097).
18. Hakkarainen, K. M.; Hedna, K.; Petzold, M.; Hägg, S. Percentage of patients with preventable adverse drug reactions and preventability of adverse drug reactions – a meta-analysis. *PloS one* **2012**, *7*, e33236, DOI: [10.1371/journal.pone.0033236](https://doi.org/10.1371/journal.pone.0033236).
19. Malki, M. A.; Pearson, E. R. Drug-drug-gene interactions and adverse drug reactions. *The pharmacogenomics journal* **2020**, *20*, 355–366, DOI: [10.1038/s41397-019-0122-0](https://doi.org/10.1038/s41397-019-0122-0).
20. Jiang, H.; Lin, Y.; Ren, W.; Fang, Z.; Liu, Y.; Tan, X.; Lv, X.; Zhang, N. Adverse drug reactions and correlations with drug-drug interactions: a retrospective study of reports from 2011 to 2020. *Frontiers in pharmacology* **2022**, *13*, 923939, DOI: [10.3389/fphar.2022.923939](https://doi.org/10.3389/fphar.2022.923939).
21. Mani, S.; Lalani, S. R.; Pammi, M. Genomics and multiomics in the age of precision medicine. *Pediatric Research* **2025**, *1–12*, DOI: [10.1038/s41390-025-04021-0](https://doi.org/10.1038/s41390-025-04021-0).
22. Marques, L.; Costa, B.; Pereira, M.; Silva, A.; Santos, J.; Saldanha, L.; Silva, I.; Magalhães, P.; Schmidt, S.; Vale, N. Advancing precision medicine: a review of innovative in silico approaches for drug development, clinical pharmacology and personalized healthcare. *Pharmaceutics* **2024**, *16*, 332, DOI: [10.3390/pharmaceutics16030332](https://doi.org/10.3390/pharmaceutics16030332).
23. U.S. Food & Drug Administration. Precision medicine. 2018, <https://www.fda.gov/medical-devices/in-vitro-diagnostics/precision-medicine> (accessed 08/24/2023).

24. Darwich, A. S.; Polasek, T. M.; Aronson, J. K.; Ogungbenro, K.; Wright, D. F. B.; Achour, B.; Reny, J.-L.; Daali, Y.; Eiermann, B.; Cook, J.; Lesko, L.; McLachlan, A. J.; Rostami-Hodjegan, A. Model-informed precision dosing: background, requirements, validation, implementation, and forward trajectory of individualizing drug therapy. *Annual review of pharmacology and toxicology* **2021**, *61*, 225–245, DOI: [10.1146/annurev-pharmtox-033020-113257](https://doi.org/10.1146/annurev-pharmtox-033020-113257).
25. Jameson, J. L.; Longo, D. L. Precision medicine – personalized, problematic, and promising. *The New England journal of medicine* **2015**, *372*, 2229–34, DOI: [10.1056/NEJMs1503104](https://doi.org/10.1056/NEJMs1503104).
26. Satam, H.; Joshi, K.; Mangrolia, U.; Waghoo, S.; Zaidi, G.; Rawool, S.; Thakare, R. P.; Banday, S.; Mishra, A. K.; Das, G.; Malonia, S. K. Next-generation sequencing technology: current trends and advancements. *Biology* **2023**, *12*, 997, DOI: [10.3390/biology12070997](https://doi.org/10.3390/biology12070997).
27. Braun, T. P.; Eide, C. A.; Druker, B. J. Response and resistance to BCR-ABL1-targeted therapies. *Cancer cell* **2020**, *37*, 530–542, DOI: [10.1016/j.ccell.2020.03.006](https://doi.org/10.1016/j.ccell.2020.03.006).
28. Gonzalez, D.; Rao, G. G.; Bailey, S. C.; Brouwer, K. L. R.; Cao, Y.; Crona, D. J.; Kashuba, A. D. M.; Lee, C. R.; Morbitzer, K.; Patterson, J. H.; Wiltshire, T.; Easter, J.; Savage, S. W.; Powell, J. R. Precision dosing: public health need, proposed framework, and anticipated impact. *Clinical and translational science* **2017**, *10*, 443–454, DOI: [10.1111/cts.12490](https://doi.org/10.1111/cts.12490).
29. Grissinger, M. The five rights: a destination without a map. **2010**, *35*, 542, <https://pmc.ncbi.nlm.nih.gov/articles/PMC2957754/>.
30. Van der Lee, M.; Allard, W. G.; Vossen, R. H. A. M.; Baak-Pablo, R. F.; Menafrá, R.; Deiman, B. A. L. M.; Deenen, M. J.; Neven, P.; Johansson, I.; Gastaldello, S.; Ingelman-Sundberg, M.; Guchelaar, H.-J.; Swen, J. J.; Anvar, S. Y. Toward predicting CYP2D6-mediated variable drug response from CYP2D6 gene sequencing data. *Science translational medicine* **2021**, *13*, DOI: [10.1126/scitranslmed.abf3637](https://doi.org/10.1126/scitranslmed.abf3637).
31. Polasek, T. M.; Kirkpatrick, C. M. J.; Rostami-Hodjegan, A. Precision dosing to avoid adverse drug reactions. *Therapeutic advances in drug safety* **2019**, *10*, 2042098619894147, DOI: [10.1177/2042098619894147](https://doi.org/10.1177/2042098619894147).
32. Zhang, C.; Lei, J.; Liu, Y.; Wang, Y.; Huang, L.; Feng, Y. Therapeutic drug monitoring and pharmacogenetic testing in Northern China. *Frontiers in pharmacology* **2021**, *12*, 754380, DOI: [10.3389/fphar.2021.754380](https://doi.org/10.3389/fphar.2021.754380).
33. Frymoyer, A.; Schwenk, H. T.; Zorn, Y.; Bio, L.; Moss, J. D.; Chasmawala, B.; Faulkenberry, J.; Goswami, S.; Keizer, R. J.; Ghaskari, S. Model-informed precision dosing of vancomycin in hospitalized children: implementation and adoption at an academic children's hospital. *Frontiers in pharmacology* **2020**, *11*, 551, DOI: [10.3389/fphar.2020.00551](https://doi.org/10.3389/fphar.2020.00551).

34. Strik, A. S.; Löwenberg, M.; Mould, D. R.; Berends, S. E.; Ponsioen, C. I.; van den Brande, J. M. H.; Jansen, J. M.; Hoekman, D. R.; Brandse, J. F.; Duijvestein, M.; Gecse, K. B.; de Vries, A.; Mathôt, R. A.; D'Haens, G. R. Efficacy of dashboard driven dosing of infliximab in inflammatory bowel disease patients; a randomized controlled trial. *Scandinavian journal of gastroenterology* **2021**, *56*, 145–154, DOI: [10.1080/00365521.2020.1856405](https://doi.org/10.1080/00365521.2020.1856405).
35. Shi, L.; Zhang, Y.; Duan, L.; Huang, L.; Li, J.; Lu, J.; Zhuang, Z.; Yuan, Y.; Feng, Z.; Sun, J.; Liu, X.; Zhou, Q.; Xue, H.; Xu, J.; Tang, L. Dose optimisation of linezolid in critically ill patients based on a population pharmacokinetic model: a two-centre prospective interventional study. *International journal of antimicrobial agents* **2023**, *62*, 106881, DOI: [10.1016/j.ijantimicag.2023.106881](https://doi.org/10.1016/j.ijantimicag.2023.106881).
36. Auwerx, C.; Sadler, M. C.; Reymond, A.; Kutalik, Z. From pharmacogenetics to pharmaco-omics: milestones and future directions. *HGG advances* **2022**, *3*, 100100, DOI: [10.1016/j.xhgg.2022.100100](https://doi.org/10.1016/j.xhgg.2022.100100).
37. Pirmohamed, M. Pharmacogenetics and pharmacogenomics. *British journal of clinical pharmacology* **2001**, *52*, 345–7, DOI: [10.1046/j.0306-5251.2001.01498.x](https://doi.org/10.1046/j.0306-5251.2001.01498.x).
38. Pirmohamed, M. Pharmacogenomics: current status and future perspectives. *Nature reviews. Genetics* **2023**, *24*, 350–362, DOI: [10.1038/s41576-022-00572-8](https://doi.org/10.1038/s41576-022-00572-8).
39. Matthaei, J.; Brockmöller, J.; Tzvetkov, M. V.; Sehart, D.; Sachse-Seeboth, C.; Hjelmberg, J. B.; Möller, S.; Halekoh, U.; Hofmann, U.; Schwab, M.; Kerb, R. Heritability of metoprolol and torsemide pharmacokinetics. *Clinical pharmacology and therapeutics* **2015**, *98*, 611–21, DOI: [10.1002/cpt.258](https://doi.org/10.1002/cpt.258).
40. Roden, D. M.; Wilke, R. A.; Kroemer, H. K.; Stein, C. M. Pharmacogenomics: the genetics of variable drug responses. *Circulation* **2011**, *123*, 1661–70, DOI: [10.1161/CIRCULATIONAHA.109.914820](https://doi.org/10.1161/CIRCULATIONAHA.109.914820).
41. Kane, M. CYP2D6 overview: allele and phenotype frequencies. *Medical Genetics Summaries* **2021**, 1–34, <https://www.ncbi.nlm.nih.gov/books/NBK574601/>.
42. Taylor, C.; Crosby, I.; Yip, V.; Maguire, P.; Pirmohamed, M.; Turner, R. M. A review of the important role of CYP2D6 in pharmacogenomics. *Genes* **2020**, *11*, 1295, DOI: [10.3390/genes11111295](https://doi.org/10.3390/genes11111295).
43. Gaedigk, A. Complexities of CYP2D6 gene analysis and interpretation. *International review of psychiatry (Abingdon, England)* **2013**, *25*, 534–53, DOI: [10.3109/09540261.2013.825581](https://doi.org/10.3109/09540261.2013.825581).
44. Gaedigk, A.; Ingelman-Sundberg, M.; Miller, N. A.; Leeder, J. S.; Whirl-Carrillo, M.; Klein, T. E.; the PharmVar Steering Committee. The Pharmacogene Variation (PharmVar) Consortium: incorporation of the human cytochrome P450 (CYP) allele nomenclature database. *Clinical pharmacology and therapeutics* **2018**, *103*, 399–401, DOI: [10.1002/cpt.910](https://doi.org/10.1002/cpt.910).
45. PharmGKB. Gene-specific information tables for CYP2D6. <https://www.pharmgkb.org/page/cyp2d6RefMaterials> (accessed 10/22/2024).

46. Whirl-Carrillo, M.; McDonagh, E. M.; Hebert, J. M.; Gong, L.; Sangkuhl, K.; Thorn, C. F.; Altman, R. B.; Klein, T. E. Pharmacogenomics knowledge for personalized medicine. *Clinical pharmacology and therapeutics* **2012**, 92, 414–7, DOI: [10.1038/clpt.2012.96](https://doi.org/10.1038/clpt.2012.96).
47. Whirl-Carrillo, M.; Huddart, R.; Gong, L.; Sangkuhl, K.; Thorn, C. F.; Whalley, R.; Klein, T. E. An evidence-based framework for evaluating pharmacogenomics knowledge for personalized medicine. *Clinical pharmacology and therapeutics* **2021**, 110, 563–572, DOI: [10.1002/cpt.2350](https://doi.org/10.1002/cpt.2350).
48. Gaedigk, A.; Dinh, J. C.; Jeong, H.; Prasad, B.; Leeder, J. S. Ten years' experience with the CYP2D6 activity score: a perspective on future investigations to improve clinical predictions for precision therapeutics. *Journal of personalized medicine* **2018**, 8, 15, DOI: [10.3390/jpm8020015](https://doi.org/10.3390/jpm8020015).
49. Gaedigk, A.; Sangkuhl, K.; Whirl-Carrillo, M.; Klein, T.; Leeder, J. S. Prediction of CYP2D6 phenotype from genotype across world populations. *Genetics in medicine : official journal of the American College of Medical Genetics* **2017**, 19, 69–76, DOI: [10.1038/gim.2016.80](https://doi.org/10.1038/gim.2016.80).
50. Swen, J. J.; Wilting, I.; de Goede, A. L.; Grandia, L.; Mulder, H.; Touw, D. J.; de Boer, A.; Conemans, J. M. H.; Egberts, T. C. G.; Klungel, O. H.; Koopmans, R.; van der Weide, J.; Wilffert, B.; Guchelaar, H.-J.; Deneer, V. H. M. Pharmacogenetics: from bench to byte. *Clinical pharmacology and therapeutics* **2008**, 83, 781–7, DOI: [10.1038/sj.clpt.6100507](https://doi.org/10.1038/sj.clpt.6100507).
51. Yoon, D. Y.; Lee, S.; Ban, M. S.; Jang, I.-J.; Lee, S. Pharmacogenomic information from CPIC and DPWG guidelines and its application on drug labels. *Translational and clinical pharmacology* **2020**, 28, 189–198, DOI: [10.12793/tcp.2020.28.e18](https://doi.org/10.12793/tcp.2020.28.e18).
52. Holford, N. H.; Sheiner, L. B. Kinetics of pharmacologic response. *Pharmacology & therapeutics* **1982**, 16, 143–66, DOI: [10.1016/0163-7258\(82\)90051-1](https://doi.org/10.1016/0163-7258(82)90051-1).
53. Gross, A. S. Best practice in therapeutic drug monitoring. *British journal of clinical pharmacology* **1998**, 46, 95–9, DOI: [10.1046/j.1365-2125.1998.00770.x](https://doi.org/10.1046/j.1365-2125.1998.00770.x).
54. Touw, D. J.; Neef, C.; Thomson, A. H.; Vinks, A. A.; Cost-Effectiveness of Therapeutic Drug Monitoring Committee of the International Association for Therapeutic Drug Monitoring and Clinical Toxicology. Cost-effectiveness of therapeutic drug monitoring: a systematic review. *Therapeutic drug monitoring* **2005**, 27, 10–7, DOI: [10.1097/00007691-200502000-00004](https://doi.org/10.1097/00007691-200502000-00004).
55. Minichmayr, I. K.; Dreesen, E.; Centanni, M.; Wang, Z.; Hoffert, Y.; Friberg, L. E.; Wicha, S. G. Model-informed precision dosing: state of the art and future perspectives. *Advanced drug delivery reviews* **2024**, 215, 115421, DOI: [10.1016/j.addr.2024.115421](https://doi.org/10.1016/j.addr.2024.115421).
56. Kang, J. S.; Lee, M. H. Overview of therapeutic drug monitoring. *The Korean journal of internal medicine* **2009**, 24, 1–10, DOI: [10.3904/kjim.2009.24.1.1](https://doi.org/10.3904/kjim.2009.24.1.1).
57. Mould, D. R.; D'Haens, G.; Upton, R. N. Clinical decision support tools: the evolution of a revolution. *Clinical pharmacology and therapeutics* **2016**, 99, 405–18, DOI: [10.1002/cpt.334](https://doi.org/10.1002/cpt.334).



58. Wicha, S. G.; Märtsen, A.; Nielsen, E. I.; Koch, B. C. P.; Friberg, L. E.; Alffenaar, J.; Minichmayr, I. K.; International Society of Anti-Infective Pharmacology (ISAP), the PK/PD study group of the European Society of Clinical Microbiology, Infectious Diseases (EPASG). From therapeutic drug monitoring to model-informed precision dosing for antibiotics. *Clinical pharmacology and therapeutics* **2021**, *109*, 928–941, DOI: [10.1002/cpt.2202](https://doi.org/10.1002/cpt.2202).
59. Fox, P.; Balleine, R. L.; Lee, C.; Gao, B.; Balakrishnar, B.; Menzies, A. M.; Yeap, S. H.; Ali, S. S.; Gebiski, V.; Provan, P.; Coulter, S.; Liddle, C.; Hui, R.; Kefford, R.; Lynch, J.; Wong, M.; Wilcken, N.; Gurney, H. Dose escalation of tamoxifen in patients with low endoxifen level: evidence for therapeutic drug monitoring – the TADE study. *Clinical cancer research : an official journal of the American Association for Cancer Research* **2016**, *22*, 3164–71, DOI: [10.1158/1078-0432.CCR-15-1470](https://doi.org/10.1158/1078-0432.CCR-15-1470).
60. Lankheet, N. A. G.; Desai, I. M. E.; Mulder, S. F.; Burger, D. M.; Kweekel, D. M.; van Herpen, C. M. L.; van der Graaf, W. T. A.; van Erp, N. P. Optimizing the dose in cancer patients treated with imatinib, sunitinib and pazopanib. *British journal of clinical pharmacology* **2017**, *83*, 2195–2204, DOI: [10.1111/bcp.13327](https://doi.org/10.1111/bcp.13327).
61. Johnson-Ansah, H.; Maneglier, B.; Huguet, F.; Legros, L.; Escoffre-Barbe, M.; Gardembas, M.; Cony-Makhoul, P.; Coiteux, V.; Sutton, L.; Abarah, W.; Pouaty, C.; Pignon, J.-M.; Choufi, B.; Visanica, S.; Deau, B.; Morisset, L.; Cayssials, E.; Molimard, M.; Bouchet, S.; Mahon, F.-X.; Nicolini, F.; Aegerter, P.; Cayuela, J.-M.; Delord, M.; Bruzzoni-Giovanelli, H.; Rousselot, P.; the Groupe Français pour la LMC (Fi-LMC). Imatinib optimized therapy improves major molecular response rates in patients with chronic myeloid leukemia. *Pharmaceutics* **2022**, *14*, 1676, DOI: [10.3390/pharmaceutics14081676](https://doi.org/10.3390/pharmaceutics14081676).
62. Clarke, W. A.; Chatelut, E.; Fotoohi, A. K.; Larson, R. A.; Martin, J. H.; Mathijssen, R. H. J.; Salamone, S. J. Therapeutic drug monitoring in oncology: International Association of Therapeutic Drug Monitoring and Clinical Toxicology consensus guidelines for imatinib therapy. *European journal of cancer (Oxford, England : 1990)* **2021**, *157*, 428–440, DOI: [10.1016/j.ejca.2021.08.033](https://doi.org/10.1016/j.ejca.2021.08.033).
63. Feuerstein, J. D.; Nguyen, G. C.; Kupfer, S. S.; Falck-Ytter, Y.; Singh, S.; American Gastroenterological Association Institute Clinical Guidelines Committee. American Gastroenterological Association Institute guideline on therapeutic drug monitoring in inflammatory bowel disease. *Gastroenterology* **2017**, *153*, 827–834, DOI: [10.1053/j.gastro.2017.07.032](https://doi.org/10.1053/j.gastro.2017.07.032).
64. Fang, Z.; Zhang, H.; Guo, J.; Guo, J. Overview of therapeutic drug monitoring and clinical practice. *Talanta* **2024**, *266*, 124996, DOI: [10.1016/j.talanta.2023.124996](https://doi.org/10.1016/j.talanta.2023.124996).
65. Van der Kleij, M. B. A.; Guchelaar, N. A. D.; Mathijssen, R. H. J.; Versluis, J.; Huitema, A. D. R.; Koolen, S. L. W.; Steeghs, N. Therapeutic drug monitoring of kinase inhibitors in oncology. *Clinical pharmacokinetics* **2023**, *62*, 1333–1364, DOI: [10.1007/s40262-023-01293-9](https://doi.org/10.1007/s40262-023-01293-9).



66. Williams, P. J.; Ette, E. I. Pharmacometrics: impacting drug development and pharmacotherapy. **2006**, 1–21, DOI: [10.1002/9780470087978.ch1](https://doi.org/10.1002/9780470087978.ch1).
67. Barrett, J. S.; Fossler, M. J.; Cadieu, K. D.; Gastonguay, M. R. Pharmacometrics: a multidisciplinary field to facilitate critical thinking in drug development and translational research settings. *Journal of clinical pharmacology* **2008**, 48, 632–49, DOI: [10.1177/0091270008315318](https://doi.org/10.1177/0091270008315318).
68. Del Valle-Moreno, P.; Suarez-Casillas, P.; Mejías-Trueba, M.; Ciudad-Gutiérrez, P.; Guisado-Gil, A. B.; Gil-Navarro, M. V.; Herrera-Hidalgo, L. Model-informed precision dosing software tools for dosage regimen individualization: a scoping review. *Pharmaceutics* **2023**, 15, 1859, DOI: [10.3390/pharmaceutics15071859](https://doi.org/10.3390/pharmaceutics15071859).
69. Darwich, A. S.; Ogungbenr, K.; Hatley, O. J.; Rostami-Hodjegan, A. Role of pharmacokinetic modeling and simulation in precision dosing of anticancer drugs. *Translational Cancer Research* **2017**, 6, S1512–S1529, DOI: [10.21037/tcr.2017.09.14](https://doi.org/10.21037/tcr.2017.09.14).
70. Madabushi, R.; Seo, P.; Zhao, L.; Tegenge, M.; Zhu, H. Review: role of model-informed drug development approaches in the lifecycle of drug development and regulatory decision-making. *Pharmaceutical research* **2022**, 39, 1669–1680, DOI: [10.1007/s11095-022-03288-w](https://doi.org/10.1007/s11095-022-03288-w).
71. Hu, K.; Fu, M.; Huang, X.; He, S.; Jiao, Z.; Wang, D. Editorial: Model-informed drug development and precision dosing in clinical pharmacology practice. *Frontiers in pharmacology* **2023**, 14, 1224980, DOI: [10.3389/fphar.2023.1224980](https://doi.org/10.3389/fphar.2023.1224980).
72. Marsousi, N.; Desmeules, J. A.; Rudaz, S.; Daali, Y. Usefulness of PBPK modeling in incorporation of clinical conditions in personalized medicine. *Journal of pharmaceutical sciences* **2017**, 106, 2380–2391, DOI: [10.1016/j.xphs.2017.04.035](https://doi.org/10.1016/j.xphs.2017.04.035).
73. Kuepfer, L.; Niederalt, C.; Wendl, T.; Schlender, J.; Willmann, S.; Lippert, J.; Block, M.; Eissing, T.; Teutonico, D. Applied concepts in PBPK modeling: how to build a PBPK/PD model. *CPT: pharmacometrics & systems pharmacology* **2016**, 5, 516–531, DOI: [10.1002/psp4.12134](https://doi.org/10.1002/psp4.12134).
74. PK-Sim® documentation, <https://docs.open-systems-pharmacology.org/working-with-pk-sim/pk-sim-documentation> (accessed 08/01/2023).
75. Jones, H.; Rowland-Yeo, K. Basic concepts in physiologically based pharmacokinetic modeling in drug discovery and development. *CPT: pharmacometrics & systems pharmacology* **2013**, 2, e63, DOI: [10.1038/psp.2013.41](https://doi.org/10.1038/psp.2013.41).
76. Thelen, K.; Coboeken, K.; Willmann, S.; Dressman, J. B.; Lippert, J. Evolution of a detailed physiological model to simulate the gastrointestinal transit and absorption process in humans, part II: extension to describe performance of solid dosage forms. *Journal of pharmaceutical sciences* **2012**, 101, 1267–80, DOI: [10.1002/jps.22825](https://doi.org/10.1002/jps.22825).

77. Sjögren, E.; Tarning, J.; Barnes, K. I.; Jonsson, E. N. A physiologically-based pharmacokinetic framework for prediction of drug exposure in malnourished children. *Pharmaceutics* **2021**, *13*, 1–23, DOI: [10.3390/pharmaceutics13020204](https://doi.org/10.3390/pharmaceutics13020204).
78. Mould, D. R.; Upton, R. N. Basic concepts in population modeling, simulation, and model-based drug development-part 2: introduction to pharmacokinetic modeling methods. *CPT: pharmacometrics & systems pharmacology* **2013**, *2*, e38, DOI: [10.1038/psp.2013.14](https://doi.org/10.1038/psp.2013.14).
79. Sun, Z.; Zhao, N.; Zhao, X.; Wang, Z.; Liu, Z.; Cui, Y. Application of physiologically based pharmacokinetic modeling of novel drugs approved by the U.S. Food and Drug Administration. *European journal of pharmaceutical sciences : official journal of the European Federation for Pharmaceutical Sciences* **2024**, *200*, 106838, DOI: [10.1016/j.ejps.2024.106838](https://doi.org/10.1016/j.ejps.2024.106838).
80. Sager, J. E.; Yu, J.; Ragueneau-Majlessi, I.; Isoherranen, N. Physiologically based pharmacokinetic (PBPK) modeling and simulation approaches: a systematic review of published models, applications, and model verification. *Drug metabolism and disposition: the biological fate of chemicals* **2015**, *43*, 1823–37, DOI: [10.1124/dmd.115.065920](https://doi.org/10.1124/dmd.115.065920).
81. Lesko, L. J.; Schmidt, S. Individualization of drug therapy: history, present state, and opportunities for the future. *Clinical pharmacology and therapeutics* **2012**, *92*, 458–66, DOI: [10.1038/clpt.2012.113](https://doi.org/10.1038/clpt.2012.113).
82. U.S. Food & Drug Administration. Clinical drug interaction studies — cytochrome P450 enzyme- and transporter-mediated drug interactions guidance for industry, 2020, <https://www.regulations.gov/document/FDA-2017-D-5961-0023> (accessed 08/17/2023).
83. Fendt, R.; Hofmann, U.; Schneider, A. R. P.; Schaeffeler, E.; Burghaus, R.; Yilmaz, A.; Blank, L. M.; Kerb, R.; Lippert, J.; Schlender, J.; Schwab, M.; Kuepfer, L. Data-driven personalization of a physiologically based pharmacokinetic model for caffeine: a systematic assessment. *CPT: pharmacometrics & systems pharmacology* **2021**, *10*, 782–793, DOI: [10.1002/psp4.12646](https://doi.org/10.1002/psp4.12646).
84. Polasek, T. M.; Tucker, G. T.; Sorich, M. J.; Wiese, M. D.; Mohan, T.; Rostami-Hodjegan, A.; Korprasertthaworn, P.; Perera, V.; Rowland, A. Prediction of olanzapine exposure in individual patients using physiologically based pharmacokinetic modelling and simulation. *British journal of clinical pharmacology* **2018**, *84*, 462–476, DOI: [10.1111/bcp.13480](https://doi.org/10.1111/bcp.13480).
85. Polasek, T. M.; Rostami-Hodjegan, A. Virtual twins: understanding the data required for model-informed precision dosing. *Clinical pharmacology and therapeutics* **2020**, *107*, 742–745, DOI: [10.1002/cpt.1778](https://doi.org/10.1002/cpt.1778).
86. Vermeire, S.; Dreesen, E.; Papamichael, K.; Dubinsky, M. C. How, when, and for whom should we perform therapeutic drug monitoring? *Clinical gastroenterology and hepatology : the official clinical practice journal of the American Gastroenterological Association* **2020**, *18*, 1291–1299, DOI: [10.1016/j.cgh.2019.09.041](https://doi.org/10.1016/j.cgh.2019.09.041).

87. Faelens, R.; Wang, Z.; Bouillon, T.; Declerck, P.; Ferrante, M.; Vermeire, S.; Dreesen, E. Model-informed precision dosing during infliximab induction therapy reduces variability in exposure and endoscopic improvement between patients with ulcerative colitis. *Pharmaceutics* **2021**, *13*, 1623, DOI: [10.3390/pharmaceutics13101623](https://doi.org/10.3390/pharmaceutics13101623).
88. Roskoski, R. Properties of FDA-approved small molecule protein kinase inhibitors: a 2023 update. *Pharmacological research* **2023**, *187*, 106552, DOI: [10.1016/j.phrs.2022.106552](https://doi.org/10.1016/j.phrs.2022.106552).
89. Novartis Pharmaceuticals Corporation. Gleevec® prescribing information, 2008, [https://www.accessdata.fda.gov/drugsatfda\\_docs/label/2008/021588s024lbl.pdf](https://www.accessdata.fda.gov/drugsatfda_docs/label/2008/021588s024lbl.pdf) (accessed 03/24/2024).
90. Daley, G. Q.; Van Etten, R. A.; Baltimore, D. Induction of chronic myelogenous leukemia in mice by the P210bcr/abl gene of the Philadelphia chromosome. *Science (New York, N.Y.)* **1990**, *247*, 824–30, DOI: [10.1126/science.2406902](https://doi.org/10.1126/science.2406902).
91. Osman, A. E. G.; Deininger, M. W. Chronic myeloid leukemia: modern therapies, current challenges and future directions. *Blood reviews* **2021**, *49*, 100825, DOI: [10.1016/j.blre.2021.100825](https://doi.org/10.1016/j.blre.2021.100825).
92. Rossari, F.; Minutolo, F.; Orciuolo, E. Past, present, and future of Bcr-Abl inhibitors: from chemical development to clinical efficacy. *Journal of hematology & oncology* **2018**, *11*, 84, DOI: [10.1186/s13045-018-0624-2](https://doi.org/10.1186/s13045-018-0624-2).
93. Filppula, A. M.; Neuvonen, M.; Laitila, J.; Neuvonen, P. J.; Backman, J. T. Autoinhibition of CYP3A4 leads to important role of CYP2C8 in imatinib metabolism: variability in CYP2C8 activity may alter plasma concentrations and response. *Drug Metabolism and Disposition* **2013**, *41*, 50–59, DOI: [10.1124/dmd.112.048017](https://doi.org/10.1124/dmd.112.048017).
94. Hamada, A.; Miyano, H.; Watanabe, H.; Saito, H. Interaction of imatinib mesilate with human P-glycoprotein. *The Journal of pharmacology and experimental therapeutics* **2003**, *307*, 824–8, DOI: [10.1124/jpet.103.055574](https://doi.org/10.1124/jpet.103.055574).
95. Burger, H.; van Tol, H.; Boersma, A. W. M.; Brok, M.; Wiemer, E. A. C.; Stoter, G.; Nooter, K. Imatinib mesylate (STI571) is a substrate for the breast cancer resistance protein (BCRP)/ABCG2 drug pump. *Blood* **2004**, *104*, 2940–2, DOI: [10.1182/blood-2004-04-1398](https://doi.org/10.1182/blood-2004-04-1398).
96. Filppula, A. M.; Tornio, A.; Niemi, M.; Neuvonen, P. J.; Backman, J. T. Gemfibrozil impairs imatinib absorption and inhibits the CYP2C8-mediated formation of its main metabolite. *Clinical pharmacology and therapeutics* **2013**, *94*, 383–93, DOI: [10.1038/clpt.2013.92](https://doi.org/10.1038/clpt.2013.92).
97. Dutreix, C.; Peng, B.; Mehring, G.; Hayes, M.; Capdeville, R.; Pokorný, R.; Seiberling, M. Pharmacokinetic interaction between ketoconazole and imatinib mesylate (Gleevec) in healthy subjects. *Cancer chemotherapy and pharmacology* **2004**, *54*, 290–4, DOI: [10.1007/s00280-004-0832-z](https://doi.org/10.1007/s00280-004-0832-z).

98. Bolton, A. E.; Peng, B.; Hubert, M.; Krebs-Brown, A.; Capdeville, R.; Keller, U.; Seiberling, M. Effect of rifampicin on the pharmacokinetics of imatinib mesylate (Gleevec, STI571) in healthy subjects. *Cancer chemotherapy and pharmacology* **2004**, *53*, 102–6, DOI: [10.1007/s00280-003-0722-9](https://doi.org/10.1007/s00280-003-0722-9).
99. Gorre, M. E.; Mohammed, M.; Ellwood, K.; Hsu, N.; Paquette, R.; Rao, P. N.; Sawyers, C. L. Clinical resistance to STI-571 cancer therapy caused by BCR-ABL gene mutation or amplification. *Science (New York, N.Y.)* **2001**, *293*, 876–80, DOI: [10.1126/science.1062538](https://doi.org/10.1126/science.1062538).
100. Donato, N. J.; Wu, J. Y.; Stapley, J.; Gallick, G.; Lin, H.; Arlinghaus, R.; Talpaz, M. BCR-ABL independence and LYN kinase overexpression in chronic myelogenous leukemia cells selected for resistance to STI571. *Blood* **2003**, *101*, 690–8, DOI: [10.1182/blood.V101.2.690](https://doi.org/10.1182/blood.V101.2.690).
101. Balabanov, S.; Braig, M.; Brümmendorf, T. H. Current aspects in resistance against tyrosine kinase inhibitors in chronic myelogenous leukemia. *Drug discovery today. Technologies* **2014**, *11*, 89–99, DOI: [10.1016/j.ddtec.2014.03.003](https://doi.org/10.1016/j.ddtec.2014.03.003).
102. Bristol-Myers Squibb Company. Sprycel® prescribing information. 2010, [https://www.accessdata.fda.gov/drugsatfda\\_docs/label/2017/021986s0201bl.pdf](https://www.accessdata.fda.gov/drugsatfda_docs/label/2017/021986s0201bl.pdf) (accessed 03/01/2023).
103. O'Hare, T.; Walters, D. K.; Stoffregen, E. P.; Jia, T.; Manley, P. W.; Mestan, J.; Cowan-Jacob, S. W.; Lee, F. Y.; Heinrich, M. C.; Deininger, M. W. N.; Druker, B. J. In vitro activity of Bcr-Abl inhibitors AMN107 and BMS-354825 against clinically relevant imatinib-resistant Abl kinase domain mutants. *Cancer research* **2005**, *65*, 4500–5, DOI: [10.1158/0008-5472.CAN-05-0259](https://doi.org/10.1158/0008-5472.CAN-05-0259).
104. Shah, N. P.; Tran, C.; Lee, F. Y.; Chen, P.; Norris, D.; Sawyers, C. L. Overriding imatinib resistance with a novel ABL kinase inhibitor. *Science (New York, N.Y.)* **2004**, *305*, 399–401, DOI: [10.1126/science.1099480](https://doi.org/10.1126/science.1099480).
105. European Medicines Agency (EMA). Sprycel®: EPAR - product information, annex I - summary of product characteristics, 2024, [https://www.ema.europa.eu/en/documents/product-information/sprycel-epar-product-information\\_en.pdf](https://www.ema.europa.eu/en/documents/product-information/sprycel-epar-product-information_en.pdf) (accessed 03/29/2025).
106. Johnson, F. M.; Agrawal, S.; Burris, H.; Rosen, L.; Dhillon, N.; Hong, D.; Blackwood-Chirchir, A.; Luo, F. R.; Sy, O.; Kaul, S.; Chiappori, A. A. Phase 1 pharmacokinetic and drug-interaction study of dasatinib in patients with advanced solid tumors. *Cancer* **2010**, *116*, 1582–91, DOI: [10.1002/cncr.24927](https://doi.org/10.1002/cncr.24927).
107. Center for Drug Evaluation and Research. Clinical Pharmacology and Biopharmaceutics review(s): NDA - dasatinib, 2005, [https://www.accessdata.fda.gov/drugsatfda\\_docs/nda/2006/021986s000\\_Sprycel\\_ClinPharmR.pdf](https://www.accessdata.fda.gov/drugsatfda_docs/nda/2006/021986s000_Sprycel_ClinPharmR.pdf) (accessed 10/27/2024).
108. Eley, T.; Luo, F. R.; Agrawal, S.; Sanil, A.; Manning, J.; Li, T.; Blackwood-Chirchir, A.; Bertz, R. Phase I study of the effect of gastric acid pH modulators on the bioavailability of oral dasatinib in healthy subjects. *Journal of clinical pharmacology* **2009**, *49*, 700–9, DOI: [10.1177/0091270009333854](https://doi.org/10.1177/0091270009333854).

109. Yago, M. R.; Frymoyer, A.; Benet, L. Z.; Smelick, G. S.; Frassetto, L. A.; Ding, X.; Dean, B.; Salphati, L.; Budha, N.; Jin, J. Y.; Dresser, M. J.; Ware, J. A. The use of betaine HCl to enhance dasatinib absorption in healthy volunteers with rabeprazole-induced hypochlorhydria. *The AAPS journal* **2014**, *16*, 1358–65, DOI: [10.1208/s12248-014-9673-9](https://doi.org/10.1208/s12248-014-9673-9).
110. Sanofi-aventis U.S. LLC. Clomid® (clomiphene citrate tablets USP), 2012, [https://www.accessdata.fda.gov/drugsatfda\\_docs/label/2012/016131s026lbl.pdf](https://www.accessdata.fda.gov/drugsatfda_docs/label/2012/016131s026lbl.pdf) (accessed 10/27/2024).
111. U.S. Food & Drug Administration. Drugs@FDA: FDA-approved drugs: Clomid®, <https://www.accessdata.fda.gov/scripts/cder/daf/index.cfm?event=overview.process&ApplNo=016131> (accessed 09/14/2024).
112. Mürdter, T. E.; Kerb, R.; Turpeinen, M.; Schroth, W.; Ganchev, B.; Böhmer, G. M.; Igel, S.; Schaeffeler, E.; Zanger, U.; Brauch, H.; Schwab, M. Genetic polymorphism of cytochrome P450 2D6 determines oestrogen receptor activity of the major infertility drug clomiphene via its active metabolites. *Human molecular genetics* **2012**, *21*, 1145–54, DOI: [10.1093/hmg/ddr543](https://doi.org/10.1093/hmg/ddr543).
113. Kröner, P. Hydroxylierte Metaboliten des Clomifens : in vitro und in vivo Untersuchungen zur Bildung, Aktivität und Konjugation, Ph.D. Thesis, Eberhard-Karls-Universität Tübingen, 2018, pp 1–204.
114. Homburg, R. Clomiphene citrate—end of an era? A mini-review. *Human reproduction (Oxford, England)* **2005**, *20*, 2043–51, DOI: [10.1093/humrep/dei042](https://doi.org/10.1093/humrep/dei042).
115. Ganchev, B. Charakterisierung der metabolischen Bioaktivierung des Clomifens unter besonderer Berücksichtigung genetischer Polymorphismen des CYP450 2D6, Ph.D. Thesis, Eberhard Karls Universität Tübingen, 2014, pp 1–136.
116. Ji, M.; Kim, K.-R.; Lee, W.; Choe, W.; Chun, S.; Min, W.-K. Genetic polymorphism of CYP2D6 and clomiphene concentrations in infertile patients with ovulatory dysfunction treated with clomiphene citrate. *Journal of Korean medical science* **2016**, *31*, 310–4, DOI: [10.3346/jkms.2016.31.2.310](https://doi.org/10.3346/jkms.2016.31.2.310).
117. Ratiopharm GmbH. Clomifen-ratiopharm® 50mg tablets prescribing information. 2020, [https://www.ratiopharm.de/assets/products/de/pkg\\_insert/Clomifen-ratiopharm%C2%AE%2050%20mg%20Tabletten.pdf?pzn=3884844](https://www.ratiopharm.de/assets/products/de/pkg_insert/Clomifen-ratiopharm%C2%AE%2050%20mg%20Tabletten.pdf?pzn=3884844) (accessed 11/09/2024).
118. European Medicines Agency. Remicade® (infliximab): EPAR - summary for the public, EMA/76495/2012, 2018, [https://www.ema.europa.eu/en/documents/overview/remicade-epar-summary-public\\_en.pdf](https://www.ema.europa.eu/en/documents/overview/remicade-epar-summary-public_en.pdf) (accessed 12/22/2023).
119. European Medicines Agency. Remicade®: EPAR - product information, annex I - summary of product characteristics, EMEA/H/C/000240, 2025, [https://www.ema.europa.eu/en/documents/product-information/remicade-epar-product-information\\_en.pdf](https://www.ema.europa.eu/en/documents/product-information/remicade-epar-product-information_en.pdf) (accessed 03/29/2025).



120. Souza, R. F.; Caetano, M. A. F.; Magalhães, H. I. R.; Castelucci, P. Study of tumor necrosis factor receptor in the inflammatory bowel disease. *World journal of gastroenterology* **2023**, *29*, 2733–2746, DOI: [10.3748/wjg.v29.i18.2733](https://doi.org/10.3748/wjg.v29.i18.2733).
121. Janssen Biotech Inc. Remicade® prescribing information. 2025, <https://www.janssenlabels.com/package-insert/product-monograph/prescribing-information/REMICADE-pi.pdf> (accessed 03/30/2025).
122. Nguyen, A. L.; Gibson, P. R.; Upton, R. N.; Mould, D. R.; Sparrow, M. P. Application of a precision-dosing model to a real-world cohort of patients on infliximab maintenance therapy: drug usage and cost analysis. *Journal of clinical pharmacology* **2024**, *64*, 399–409, DOI: [10.1002/jcph.2384](https://doi.org/10.1002/jcph.2384).
123. Wolbink, G. J.; Voskuyl, A. E.; Lems, W. F.; de Groot, E.; Nurmohamed, M. T.; Tak, P. P.; Dijkmans, B. A. C.; Aarden, L. Relationship between serum trough infliximab levels, pretreatment C reactive protein levels, and clinical response to infliximab treatment in patients with rheumatoid arthritis. *Annals of the rheumatic diseases* **2005**, *64*, 704–7, DOI: [10.1136/ard.2004.030452](https://doi.org/10.1136/ard.2004.030452).
124. Adedokun, O. J.; Sandborn, W. J.; Feagan, B. G.; Rutgeerts, P.; Xu, Z.; Marano, C. W.; Johanns, J.; Zhou, H.; Davis, H. M.; Cornillie, F.; Reinisch, W. Association between serum concentration of infliximab and efficacy in adult patients with ulcerative colitis. *Gastroenterology* **2014**, *147*, 1296–1307.e5, DOI: [10.1053/j.gastro.2014.08.035](https://doi.org/10.1053/j.gastro.2014.08.035).
125. De Vries, M. K.; Wolbink, G. J.; Stapel, S. O.; de Vrieze, H.; van Denderen, J. C.; Dijkmans, B. A. C.; Aarden, L. A.; van der Horst-Bruinsma, I. E. Decreased clinical response to infliximab in ankylosing spondylitis is correlated with anti-infliximab formation. *Annals of the rheumatic diseases* **2007**, *66*, 1252–4, DOI: [10.1136/ard.2007.072397](https://doi.org/10.1136/ard.2007.072397).
126. Dannepond, C.; Maruani, A.; Machet, L.; Ternant, D.; Pintaud, G.; Samimi, M. Serum infliximab concentrations in psoriatic patients treated with infliximab: a systematic review. *Acta dermato-venereologica* **2015**, *95*, 401–6, DOI: [10.2340/00015555-1980](https://doi.org/10.2340/00015555-1980).
127. Fasanmade, A. A.; Adedokun, O. J.; Ford, J.; Hernandez, D.; Johanns, J.; Hu, C.; Davis, H. M.; Zhou, H. Population pharmacokinetic analysis of infliximab in patients with ulcerative colitis. *European journal of clinical pharmacology* **2009**, *65*, 1211–28, DOI: [10.1007/s00228-009-0718-4](https://doi.org/10.1007/s00228-009-0718-4).
128. Fasanmade, A. A.; Adedokun, O. J.; Blank, M.; Zhou, H.; Davis, H. M. Pharmacokinetic properties of infliximab in children and adults with Crohn's disease: a retrospective analysis of data from 2 phase III clinical trials. *Clinical therapeutics* **2011**, *33*, 946–64, DOI: [10.1016/j.clinthera.2011.06.002](https://doi.org/10.1016/j.clinthera.2011.06.002).
129. Brandse, J. F.; Mould, D.; Smeekes, O.; Ashruf, Y.; Kuin, S.; Strik, A.; van den Brink, G. R.; D'Haens, G. R. A real-life population pharmacokinetic study reveals factors associated with clearance and immunogenicity of infliximab in inflammatory bowel disease. *Inflammatory bowel diseases* **2017**, *23*, 650–660, DOI: [10.1097/MIB.0000000000001043](https://doi.org/10.1097/MIB.0000000000001043).

130. Edlund, H.; Steenholdt, C.; Ainsworth, M. A.; Goebgen, E.; Brynskov, J.; Thomsen, O. Ø.; Huisinga, W.; Kloft, C. Magnitude of increased infliximab clearance imposed by anti-infliximab antibodies in Crohn's disease is determined by their concentration. *The AAPS journal* **2017**, *19*, 223–233, DOI: [10.1208/s12248-016-9989-8](https://doi.org/10.1208/s12248-016-9989-8).
131. Kevans, D.; Murthy, S.; Mould, D. R.; Silverberg, M. S. Accelerated clearance of infliximab is associated with treatment failure in patients with corticosteroid-refractory acute ulcerative colitis. *Journal of Crohn's and Colitis* **2018**, *12*, 662–669, DOI: [10.1093/ecco-jcc/jjy028](https://doi.org/10.1093/ecco-jcc/jjy028).
132. Petitcollin, A.; Leuret, O.; Tron, C.; Lemaitre, F.; Verdier, M.-C.; Paintaud, G.; Bouguen, G.; Willot, S.; Bellissant, E.; Ternant, D. Modeling immunization to infliximab in children with Crohn's disease using population pharmacokinetics: a pilot study. *Inflammatory bowel diseases* **2018**, *24*, 1745–1754, DOI: [10.1093/ibd/izy129](https://doi.org/10.1093/ibd/izy129).
133. Dreesen, E.; Faelens, R.; Van Assche, G.; Ferrante, M.; Vermeire, S.; Gils, A.; Bouillon, T. Optimising infliximab induction dosing for patients with ulcerative colitis. *British journal of clinical pharmacology* **2019**, *85*, 782–795, DOI: [10.1111/bcp.13859](https://doi.org/10.1111/bcp.13859).
134. Matsuoka, K.; Hamada, S.; Shimizu, M.; Nanki, K.; Mizuno, S.; Kiyohara, H.; Arai, M.; Sugimoto, S.; Iwao, Y.; Ogata, H.; Hisamatsu, T.; Nagauma, M.; Kanai, T.; Mochizuki, M.; Hashiguchi, M. Factors contributing to the systemic clearance of infliximab with long-term administration in Japanese patients with Crohn's disease: analysis using population pharmacokinetics. *International journal of clinical pharmacology and therapeutics* **2020**, *58*, 89–102, DOI: [10.5414/CP203569](https://doi.org/10.5414/CP203569).
135. Petitcollin, A.; Brochard, C.; Siproudhis, L.; Tron, C.; Verdier, M.; Lemaitre, F.; Lucidarme, C.; Bouguen, G.; Bellissant, É. Pharmacokinetic parameters of infliximab influence the rate of relapse after de-escalation in adults with inflammatory bowel diseases. *Clinical pharmacology and therapeutics* **2019**, *106*, 605–615, DOI: [10.1002/cpt.1429](https://doi.org/10.1002/cpt.1429).
136. Bauman, L. E.; Xiong, Y.; Mizuno, T.; Minar, P.; Fukuda, T.; Dong, M.; Rosen, M. J.; Vinks, A. A. Improved population pharmacokinetic model for predicting optimized infliximab exposure in pediatric inflammatory bowel disease. *Inflammatory bowel diseases* **2020**, *26*, 429–439, DOI: [10.1093/ibd/izz143](https://doi.org/10.1093/ibd/izz143).
137. Dreesen, E.; Berends, S.; Laharie, D.; D'Haens, G.; Vermeire, S.; Gils, A.; Mathôt, R. Modelling of the relationship between infliximab exposure, faecal calprotectin and endoscopic remission in patients with Crohn's disease. *British journal of clinical pharmacology* **2021**, *87*, 106–118, DOI: [10.1111/bcp.14364](https://doi.org/10.1111/bcp.14364).
138. Grišić, A.; Dorn-Rasmussen, M.; Ungar, B.; Brynskov, J.; Ilvemark, J. F. K. F.; Bolstad, N.; Warren, D. J.; Ainsworth, M. A.; Huisinga, W.; Ben-Horin, S.; Kloft, C.; Steenholdt, C. Infliximab clearance decreases in the second and third trimesters of pregnancy in inflammatory bowel disease.



- United European gastroenterology journal* **2021**, 9, 91–101, DOI: [10.1177/2050640620964619](https://doi.org/10.1177/2050640620964619).
139. Buurman, D. J.; Maurer, J. M.; Keizer, R. J.; Kosterink, J. G. W.; Dijkstra, G. Population pharmacokinetics of infliximab in patients with inflammatory bowel disease: potential implications for dosing in clinical practice. *Alimentary pharmacology & therapeutics* **2015**, 42, 529–39, DOI: [10.1111/apt.13299](https://doi.org/10.1111/apt.13299).
  140. Kantasiripitak, W.; Verstockt, B.; Alsoud, D.; Lobatón, T.; Thomas, D.; Gils, A.; Vermeire, S.; Ferrante, M.; Dreesen, E. The effect of aging on infliximab exposure and response in patients with inflammatory bowel diseases. *British journal of clinical pharmacology* **2021**, 87, 3776–3789, DOI: [10.1111/bcp.14785](https://doi.org/10.1111/bcp.14785).
  141. Ternant, D.; Aubourg, A.; Magdelaine-Beuzelin, C.; Degenne, D.; Watier, H.; Picon, L.; Paintaud, G. Infliximab pharmacokinetics in inflammatory bowel disease patients. *Therapeutic drug monitoring* **2008**, 30, 523–9, DOI: [10.1097/FTD.0b013e318180e300](https://doi.org/10.1097/FTD.0b013e318180e300).
  142. Xu, Z.; Mould, D. R.; Hu, C.; Ford, J.; Keen, M.; Davis, H. M.; Zhou, H. Population pharmacokinetic analysis of infliximab in pediatrics using integrated data from six clinical trials - Abstract 139760. *Clin Pharmacol Drug Dev.* **2012**, 1, 203.
  143. Dotan, I.; Ron, Y.; Yanai, H.; Becker, S.; Fishman, S.; Yahav, L.; Ben Yehoyada, M.; Mould, D. R. Patient factors that increase infliximab clearance and shorten half-life in inflammatory bowel disease: a population pharmacokinetic study. *Inflammatory bowel diseases* **2014**, 20, 2247–59, DOI: [10.1097/MIB.0000000000000212](https://doi.org/10.1097/MIB.0000000000000212).
  144. Aubourg, A.; Picon, L.; Lecomte, T.; Bejan-Angoulvant, T.; Paintaud, G.; Ternant, D. A robust estimation of infliximab pharmacokinetic parameters in Crohn's disease. *European journal of clinical pharmacology* **2015**, 71, 1541–2, DOI: [10.1007/s00228-015-1942-8](https://doi.org/10.1007/s00228-015-1942-8).
  145. Ternant, D.; Berkane, Z.; Picon, L.; Gouilleux-Gruart, V.; Colombel, J.-F.; Allez, M.; Louis, E.; Paintaud, G. Assessment of the influence of inflammation and FCGR3A genotype on infliximab pharmacokinetics and time to relapse in patients with Crohn's disease. *Clinical pharmacokinetics* **2015**, 54, 551–62, DOI: [10.1007/s40262-014-0225-3](https://doi.org/10.1007/s40262-014-0225-3).
  146. Brandse, J. F.; Mathôt, R. A.; van der Kleij, D.; Rispens, T.; Ashruf, Y.; Jansen, J. M.; Rietdijk, S.; Löwenberg, M.; Ponsioen, C. Y.; Singh, S.; van den Brink, G. R.; D'Haens, G. R. Pharmacokinetic features and presence of antidrug antibodies associate with response to infliximab induction therapy in patients with moderate to severe ulcerative colitis. *Clinical gastroenterology and hepatology : the official clinical practice journal of the American Gastroenterological Association* **2016**, 14, 251–8.e1–2, DOI: [10.1016/j.cgh.2015.10.029](https://doi.org/10.1016/j.cgh.2015.10.029).
  147. Passot, C.; Mulleman, D.; Bejan-Angoulvant, T.; Aubourg, A.; Willot, S.; Lecomte, T.; Picon, L.; Goupille, P.; Paintaud, G.; Ternant, D. The underlying inflammatory chronic disease influences infliximab pharmacokinetics. *mAbs* **2016**, 8, 1407–1416, DOI: [10.1080/19420862.2016.1216741](https://doi.org/10.1080/19420862.2016.1216741).

148. Levesque, B. G.; Greenberg, G. R.; Zou, G.; Sandborn, W. J.; Singh, S.; Hauenstein, S.; Ohrmund, L.; Wong, C. J.; Stitt, L. W.; Shackelton, L. M.; King, D.; Lockton, S.; Ducharme, J.; Feagan, B. G. A prospective cohort study to determine the relationship between serum infliximab concentration and efficacy in patients with luminal Crohn's disease. *Alimentary pharmacology & therapeutics* **2014**, *39*, 1126–35, DOI: [10.1111/apt.12733](https://doi.org/10.1111/apt.12733).
149. Papamichael, K.; Rakowsky, S.; Rivera, C.; Cheifetz, A. S.; Osterman, M. T. Infliximab trough concentrations during maintenance therapy are associated with endoscopic and histologic healing in ulcerative colitis. *Alimentary pharmacology & therapeutics* **2018**, *47*, 478–484, DOI: [10.1111/apt.14458](https://doi.org/10.1111/apt.14458).
150. Kang, B.; Choi, S. Y.; Choi, Y. O.; Lee, S.-Y.; Baek, S.-Y.; Sohn, I.; Choe, B.-H.; Lee, H. J.; Choe, Y. H. Infliximab trough levels are associated with mucosal healing during maintenance treatment with infliximab in paediatric Crohn's disease. *Journal of Crohn's & colitis* **2019**, *13*, 189–197, DOI: [10.1093/ecco-jcc/jjy155](https://doi.org/10.1093/ecco-jcc/jjy155).
151. Wilson, A.; Choi, B.; Sey, M.; Ponich, T.; Beaton, M.; Kim, R. B. High infliximab trough concentrations are associated with sustained histologic remission in inflammatory bowel disease: a prospective cohort study. *BMC gastroenterology* **2021**, *21*, 77, DOI: [10.1186/s12876-021-01650-7](https://doi.org/10.1186/s12876-021-01650-7).
152. Bortlik, M.; Duricova, D.; Malickova, K.; Machkova, N.; Bouzkova, E.; Hrdlicka, L.; Komarek, A.; Lukas, M. Infliximab trough levels may predict sustained response to infliximab in patients with Crohn's disease. *Journal of Crohn's & colitis* **2013**, *7*, 736–43, DOI: [10.1016/j.crohns.2012.10.019](https://doi.org/10.1016/j.crohns.2012.10.019).
153. Yarur, A. J.; Kanagala, V.; Stein, D. J.; Czul, F.; Quintero, M. A.; Agrawal, D.; Patel, A.; Best, K.; Fox, C.; Idstein, K.; Abreu, M. T. Higher infliximab trough levels are associated with perianal fistula healing in patients with Crohn's disease. *Alimentary pharmacology & therapeutics* **2017**, *45*, 933–940, DOI: [10.1111/apt.13970](https://doi.org/10.1111/apt.13970).
154. Valentin, J. Basic anatomical and physiological data for use in radiological protection: reference values: ICRP publication 89: approved by the Commission in September 2001. *Annals of the ICRP* **2002**, *32*, 5–265, DOI: [10.1016/S0146-6453\(03\)00002-2](https://doi.org/10.1016/S0146-6453(03)00002-2).
155. National Center for Health Statistics Hyattsville MD 20782. Third National Health and Nutrition Examination Survey (NHANES III), 1997, <https://www.cdc.gov/nchs/nhanes/> (accessed 12/28/2023).
156. Open Systems Pharmacology Suite Community. PK-Sim® ontogeny database documentation, Version 7.3. 2018, <https://github.com/Open-Systems-Pharmacology/OSPSuite.Documentation/blob/master/PK-SimOntogenyDatabaseVersion7.3.pdf> (accessed 12/28/2023).
157. Schlender, J. A report including the description of the physiology base of the Japanese population implemented in PK-Sim®. 2015, [https://github.com/Open-Systems-Pharmacology/OSPSuite.Documentation/blob/master/Japanese\\_Population/Report.md](https://github.com/Open-Systems-Pharmacology/OSPSuite.Documentation/blob/master/Japanese_Population/Report.md) (accessed 08/04/2024).

158. Willmann, S.; Höhn, K.; Edginton, A.; Sevestre, M.; Solodenko, J.; Weiss, W.; Lippert, J.; Schmitt, W. Development of a physiology-based whole-body population model for assessing the influence of individual variability on the pharmacokinetics of drugs. *Journal of pharmacokinetics and pharmacodynamics* **2007**, *34*, 401–31, DOI: [10.1007/s10928-007-9053-5](https://doi.org/10.1007/s10928-007-9053-5).
159. Zhang, X.; Trame, M. N.; Lesko, L. J.; Schmidt, S. Sobol sensitivity analysis: a tool to guide the development and evaluation of systems pharmacology models. *CPT: pharmacometrics & systems pharmacology* **2015**, *4*, 69–79, DOI: [10.1002/psp4.6](https://doi.org/10.1002/psp4.6).
160. Kovar, C.; Kovar, L.; Rüdesheim, S.; Selzer, D.; Ganchev, B.; Kröner, P.; Igel, S.; Kerb, R.; Schaeffeler, E.; Mürdter, T. E.; Schwab, M.; Lehr, T. Prediction of drug-drug-gene interaction scenarios of (E)-clomiphene and its metabolites using physiologically based pharmacokinetic modeling. *Pharmaceutics* **2022**, *14*, DOI: [10.3390/pharmaceutics14122604](https://doi.org/10.3390/pharmaceutics14122604).
161. Guest, E. J.; Aarons, L.; Houston, J. B.; Rostami-Hodjegan, A.; Galetin, A. Critique of the two-fold measure of prediction success for ratios: application for the assessment of drug-drug interactions. *Drug metabolism and disposition: the biological fate of chemicals* **2011**, *39*, 170–3, DOI: [10.1124/dmd.110.036103](https://doi.org/10.1124/dmd.110.036103).
162. Wojtyniak, J.-G.; Britz, H.; Selzer, D.; Schwab, M.; Lehr, T. Data digitizing: accurate and precise data extraction for quantitative systems pharmacology and physiologically-based pharmacokinetic modeling. *CPT: pharmacometrics & systems pharmacology* **2020**, *9*, 322–331, DOI: [10.1002/psp4.12511](https://doi.org/10.1002/psp4.12511).
163. R Core Team. R: a language and environment for statistical computing. R foundation for statistical computing, Vienna, Austria. Vienna, 2021.
164. Zhao, W.; Kaguelidou, F.; Biran, V.; Zhang, D.; Allegaert, K.; Capparelli, E. V.; Holford, N.; Kimura, T.; Lo, Y.-l.; Peris, J.-e.; Thomson, A.; van den Anker, J. N.; Fakhoury, M.; Jacqz-Aigrain, E. External evaluation of population pharmacokinetic models of vancomycin in neonates: the transferability of published models to different clinical settings. *British journal of clinical pharmacology* **2013**, *75*, 1068–80, DOI: [10.1111/j.1365-2125.2012.04406.x](https://doi.org/10.1111/j.1365-2125.2012.04406.x).
165. Konecki, C.; Feliu, C.; Cazaubon, Y.; Giusti, D.; Tonye-Libyh, M.; Brix, H.; Cadiot, G.; Biron, A.; Djerada, Z. External evaluation of population pharmacokinetic models and bayes-based dosing of infliximab. *Pharmaceutics* **2021**, *13*, 0–20, DOI: [10.3390/pharmaceutics13081191](https://doi.org/10.3390/pharmaceutics13081191).
166. Brendel, K.; Dartois, C.; Comets, E.; Lemenuel-Diot, A.; Laveille, C.; Tranchand, B.; Girard, P.; Laffont, C. M.; Mentré, F. Are population pharmacokinetic and/or pharmacodynamic models adequately evaluated? A survey of the literature from 2002 to 2004. *Clinical pharmacokinetics* **2007**, *46*, 221–34, DOI: [10.2165/00003088-200746030-00003](https://doi.org/10.2165/00003088-200746030-00003).
167. Keizer, R. J.; Ter Heine, R.; Frymoyer, A.; Lesko, L. J.; Mangat, R.; Goswami, S. Model-informed precision dosing at the bedside: scientific challenges and opportunities. *CPT: pharmacometrics & systems pharmacology* **2018**, *7*, 785–787, DOI: [10.1002/psp4.12353](https://doi.org/10.1002/psp4.12353).

168. Owen, J. S.; Fiedler-Kelly, J., *Introduction to population pharmacokinetic/pharmacodynamic analysis with nonlinear mixed effects models*; John Wiley & Sons, Inc., Hoboken, New Jersey: 2014, pp 1–301.
169. Bergstrand, M.; Karlsson, M. O. Handling data below the limit of quantification in mixed effect models. *The AAPS journal* **2009**, *11*, 371–80, DOI: [10.1208/s12248-009-9112-5](https://doi.org/10.1208/s12248-009-9112-5).
170. Beal, S. L. Ways to fit a PK model with some data below the quantification limit. *Journal of pharmacokinetics and pharmacodynamics* **2001**, *28*, 481–504, DOI: [10.1023/a:1012299115260](https://doi.org/10.1023/a:1012299115260).
171. Le Louedec, F.; Puisset, F.; Thomas, F.; Chatelut, É.; White-Koning, M. Easy and reliable maximum a posteriori Bayesian estimation of pharmacokinetic parameters with the open-source R package mapbayr. *CPT: pharmacometrics & systems pharmacology* **2021**, *10*, 1208–1220, DOI: [10.1002/psp4.12689](https://doi.org/10.1002/psp4.12689).
172. Morley, S. K.; Brito, T. V.; Welling, D. T. Measures of model performance based on the log accuracy ratio. *Space Weather* **2018**, *16*, 69–88, DOI: [10.1002/2017SW001669](https://doi.org/10.1002/2017SW001669).
173. Kovar, C.; Loer, H. L. H.; Rüdesheim, S.; Fuhr, L. M.; Marok, F. Z.; Selzer, D.; Schwab, M.; Lehr, T. A physiologically-based pharmacokinetic precision dosing approach to manage dasatinib drug-drug interactions. *CPT: pharmacometrics & systems pharmacology* **2024**, *13*, 1144–1159, DOI: [10.1002/psp4.13146](https://doi.org/10.1002/psp4.13146).
174. Loer, H. L. H.; Kovar, C.; Rüdesheim, S.; Marok, F. Z.; Fuhr, L. M.; Selzer, D.; Schwab, M.; Lehr, T. Physiologically based pharmacokinetic modeling of imatinib and N-desmethyl imatinib for drug-drug interaction predictions. *CPT: pharmacometrics & systems pharmacology* **2024**, *13*, 926–940, DOI: [10.1002/psp4.13127](https://doi.org/10.1002/psp4.13127).
175. Schräpel, C.; Kovar, L.; Selzer, D.; Hofmann, U.; Tran, F.; Reinisch, W.; Schwab, M.; Lehr, T. External model performance evaluation of twelve infliximab population pharmacokinetic models in patients with inflammatory bowel disease. *Pharmaceutics* **2021**, *13*, 1368, DOI: [10.3390/pharmaceutics13091368](https://doi.org/10.3390/pharmaceutics13091368).
176. Rousselot, P.; Mollica, L.; Guilhot, J.; Guerci, A.; Nicolini, F. E.; Etienne, G.; Legros, L.; Charbonnier, A.; Coiteux, V.; Dartigeas, C.; Escoffre-Barbe, M.; Roy, L.; Cony-Makhoul, P.; Dubruille, V.; Gardembas, M.; Huguet, F.; Réa, D.; Cayssials, E.; Guilhot, F.; Bergeron, A.; Molimard, M.; Mahon, F.-X.; Cayuela, J.-M.; Busque, L.; Bouchet, S. Dasatinib dose optimisation based on therapeutic drug monitoring reduces pleural effusion rates in chronic myeloid leukaemia patients. *British journal of haematology* **2021**, *194*, 393–402, DOI: [10.1111/bjh.17654](https://doi.org/10.1111/bjh.17654).
177. Goutelle, S.; Guidi, M.; Gotta, V.; Csajka, C.; Buclin, T.; Widmer, N. From personalized to precision medicine in oncology: a model-based dosing approach to optimize achievement of imatinib target exposure. *Pharmaceutics* **2023**, *15*, 1081, DOI: [10.3390/pharmaceutics15041081](https://doi.org/10.3390/pharmaceutics15041081).

178. Dalle Fratte, C.; Gagno, S.; Roncato, R.; Polesel, J.; Zanchetta, M.; Buzzo, M.; Posocco, B.; De Mattia, E.; Borsatti, R.; Puglisi, F.; Foltran, L.; Guardascione, M.; Buonadonna, A.; Cecchin, E.; Toffoli, G. CYP2D6 and CYP2C8 pharmacogenetics and pharmacological interactions to predict imatinib plasmatic exposure in GIST patients. *British journal of clinical pharmacology* **2023**, *89*, 1089–1098, DOI: [10.1111/bcp.15551](https://doi.org/10.1111/bcp.15551).
179. He, S.; Bian, J.; Shao, Q.; Zhang, Y.; Hao, X.; Luo, X.; Feng, Y.; Huang, L. Therapeutic drug monitoring and individualized medicine of dasatinib: focus on clinical pharmacokinetics and pharmacodynamics. *Frontiers in pharmacology* **2021**, *12*, 797881, DOI: [10.3389/fphar.2021.797881](https://doi.org/10.3389/fphar.2021.797881).
180. Dai, G.; Pfister, M.; Blackwood-Chirchir, A.; Roy, A. Importance of characterizing determinants of variability in exposure: application to dasatinib in subjects with chronic myeloid leukemia. *Journal of clinical pharmacology* **2008**, *48*, 1254–69, DOI: [10.1177/0091270008320604](https://doi.org/10.1177/0091270008320604).
181. Brave, M.; Goodman, V.; Kaminskas, E.; Farrell, A.; Timmer, W.; Pope, S.; Harapanhalli, R.; Saber, H.; Morse, D.; Bullock, J.; Men, A.; Noory, C.; Ramchandani, R.; Kenna, L.; Booth, B.; Gobburu, J.; Jiang, X.; Sridhara, R.; Justice, R.; Pazdur, R. Sprycel for chronic myeloid leukemia and Philadelphia chromosome-positive acute lymphoblastic leukemia resistant to or intolerant of imatinib mesylate. *Clinical cancer research : an official journal of the American Association for Cancer Research* **2008**, *14*, 352–9, DOI: [10.1158/1078-0432.CCR-07-4175](https://doi.org/10.1158/1078-0432.CCR-07-4175).
182. Wang, X.; Roy, A.; Hochhaus, A.; Kantarjian, H. M.; Chen, T.-T.; Shah, N. P. Differential effects of dosing regimen on the safety and efficacy of dasatinib: retrospective exposure-response analysis of a Phase III study. *Clinical pharmacology : advances and applications* **2013**, *5*, 85–97, DOI: [10.2147/CPAA.S42796](https://doi.org/10.2147/CPAA.S42796).
183. Picard, S.; Titier, K.; Etienne, G.; Teilhet, E.; Ducint, D.; Bernard, M.-A.; Lassalle, R.; Marit, G.; Reiffers, J.; Begaud, B.; Moore, N.; Molimard, M.; Mahon, F.-X. Trough imatinib plasma levels are associated with both cytogenetic and molecular responses to standard-dose imatinib in chronic myeloid leukemia. *Blood* **2007**, *109*, 3496–9, DOI: [10.1182/blood-2006-07-036012](https://doi.org/10.1182/blood-2006-07-036012).
184. Guilhot, F.; Hughes, T. P.; Cortes, J.; Druker, B. J.; Baccarani, M.; Gathmann, I.; Hayes, M.; Granvil, C.; Wang, Y. Plasma exposure of imatinib and its correlation with clinical response in the tyrosine kinase inhibitor optimization and selectivity trial. *Haematologica* **2012**, *97*, 731–8, DOI: [10.3324/haematol.2011.045666](https://doi.org/10.3324/haematol.2011.045666).
185. Larson, R. A.; Druker, B. J.; Guilhot, F.; O'Brien, S. G.; Riviere, G. J.; Krahnke, T.; Gathmann, I.; Wang, Y.; IRIS (International Randomized Interferon vs STI571) Study Group. Imatinib pharmacokinetics and its correlation with response and safety in chronic-phase chronic myeloid leukemia: a subanalysis of the IRIS study. *Blood* **2008**, *111*, 4022–8, DOI: [10.1182/blood-2007-10-116475](https://doi.org/10.1182/blood-2007-10-116475).



186. Takahashi, N.; Wakita, H.; Miura, M.; Scott, S. A.; Nishii, K.; Masuko, M.; Sakai, M.; Maeda, Y.; Ishige, K.; Kashimura, M.; Fujikawa, K.; Fukazawa, M.; Katayama, T.; Monma, F.; Narita, M.; Urase, F.; Furukawa, T.; Miyazaki, Y.; Katayama, N.; Sawada, K. Correlation between imatinib pharmacokinetics and clinical response in Japanese patients with chronic-phase chronic myeloid leukemia. *Clinical pharmacology and therapeutics* **2010**, *88*, 809–13, DOI: [10.1038/clpt.2010.186](https://doi.org/10.1038/clpt.2010.186).
187. Orleni, M.; Gagno, S.; Cecchin, E.; Montico, M.; Buonadonna, A.; Fumagalli, A.; Guardascione, M.; Puglisi, F.; Toffoli, G.; Posocco, B.; Cecchin, E. Imatinib and norimatinib therapeutic monitoring using dried blood spots: analytical and clinical validation, and performance comparison of volumetric collection devices. *Journal of chromatography. B, Analytical technologies in the biomedical and life sciences* **2025**, *1255*, 124526, DOI: [10.1016/j.jchromb.2025.124526](https://doi.org/10.1016/j.jchromb.2025.124526).
188. Yu, H.; Steeghs, N.; Nijenhuis, C. M.; Schellens, J. H. M.; Beijnen, J. H.; Huitema, A. D. R. Practical guidelines for therapeutic drug monitoring of anticancer tyrosine kinase inhibitors: focus on the pharmacokinetic targets. *Clinical pharmacokinetics* **2014**, *53*, 305–25, DOI: [10.1007/s40262-014-0137-2](https://doi.org/10.1007/s40262-014-0137-2).
189. Dalle Fratte, C.; Polesel, J.; Gagno, S.; Posocco, B.; De Mattia, E.; Roncato, R.; Orleni, M.; Puglisi, F.; Guardascione, M.; Buonadonna, A.; Toffoli, G.; Cecchin, E. Impact of ABCG2 and ABCB1 polymorphisms on imatinib plasmatic exposure: an original work and meta-analysis. *International journal of molecular sciences* **2023**, *24*, 3303, DOI: [10.3390/ijms24043303](https://doi.org/10.3390/ijms24043303).
190. Rostami-Hodjegan, A.; Lennard, M. S.; Tucker, G. T.; Ledger, W. L. Monitoring plasma concentrations to individualize treatment with clomiphene citrate. *Fertility and sterility* **2004**, *81*, 1187–93, DOI: [10.1016/j.fertnstert.2003.07.044](https://doi.org/10.1016/j.fertnstert.2003.07.044).
191. Huyghe, L.; Robin, C.; Dumont, A.; Decanter, C.; Kyheng, M.; Dewailly, D.; Catteau-Jonard, S.; Robin, G. How to choose the optimal starting dose of clomiphene citrate (50 or 100 mg per day) for a first cycle of ovulation induction in anovulatory PCOS women? *Journal of clinical medicine* **2023**, *12*, 4943, DOI: [10.3390/jcm12154943](https://doi.org/10.3390/jcm12154943).
192. Kousta, E.; White, D. M.; Franks, S. Modern use of clomiphene citrate in induction of ovulation. *Human reproduction update* **1997**, *3*, 359–65, DOI: [10.1093/humupd/3.4.359](https://doi.org/10.1093/humupd/3.4.359).
193. Imani, B.; Eijkemans, M. J.; te Velde, E. R.; Habbema, J. D.; Fauser, B. C. Predictors of patients remaining anovulatory during clomiphene citrate induction of ovulation in normogonadotropic oligoamenorrheic infertility. *The Journal of clinical endocrinology and metabolism* **1998**, *83*, 2361–5, DOI: [10.1210/jcem.83.7.4919](https://doi.org/10.1210/jcem.83.7.4919).
194. Ellakwa, H. E.; Sanad, Z. F.; Hamza, H. A.; Emara, M. A.; Elsayed, M. A. Predictors of patient responses to ovulation induction with clomiphene citrate in patients with polycystic ovary syndrome experiencing infertili-

- ity. *International journal of gynaecology and obstetrics: the official organ of the International Federation of Gynaecology and Obstetrics* **2016**, 133, 59–63, DOI: [10.1016/j.ijgo.2015.09.008](https://doi.org/10.1016/j.ijgo.2015.09.008).
195. Mahran, A.; Abdelmeged, A.; El-Adawy, A. R.; Eissa, M. K.; Shaw, R. W.; Amer, S. A. The predictive value of circulating anti-Müllerian hormone in women with polycystic ovarian syndrome receiving clomiphene citrate: a prospective observational study. *The Journal of clinical endocrinology and metabolism* **2013**, 98, 4170–5, DOI: [10.1210/jc.2013-2193](https://doi.org/10.1210/jc.2013-2193).
  196. Amer, S. A.; Mahran, A.; Abdelmaged, A.; El-Adawy, A. R.; Eissa, M. K.; Shaw, R. W. The influence of circulating anti-Müllerian hormone on ovarian responsiveness to ovulation induction with gonadotrophins in women with polycystic ovarian syndrome: a pilot study. *Reproductive biology and endocrinology : RB&E* **2013**, 11, 115, DOI: [10.1186/1477-7827-11-115](https://doi.org/10.1186/1477-7827-11-115).
  197. Kim, M.-J.; Byeon, J.-Y.; Kim, Y.-H.; Kim, S.-H.; Lee, C.-M.; Jung, E. H.; Chae, W. K.; Lee, Y. J.; Jang, C.-G.; Lee, S.-Y.; Choi, C.-I. Effect of the CYP2D6\*10 allele on the pharmacokinetics of clomiphene and its active metabolites. *Archives of pharmacal research* **2018**, 41, 347–353, DOI: [10.1007/s12272-018-1005-7](https://doi.org/10.1007/s12272-018-1005-7).
  198. Ganchev, B.; Heinklele, G.; Kerb, R.; Schwab, M.; Mürdter, T. E. Quantification of clomiphene metabolite isomers in human plasma by rapid-resolution liquid chromatography-electrospray ionization-tandem mass spectrometry. *Analytical and bioanalytical chemistry* **2011**, 400, 3429–41, DOI: [10.1007/s00216-011-5045-9](https://doi.org/10.1007/s00216-011-5045-9).
  199. Kröner, P.; Heinklele, G.; Kerb, R.; Igel, S.; Schwab, M.; Mürdter, T. E. Stereoselective quantification of phase 1 and 2 metabolites of clomiphene in human plasma and urine. *Talanta* **2021**, 221, 121658, DOI: [10.1016/j.talanta.2020.121658](https://doi.org/10.1016/j.talanta.2020.121658).
  200. Teutonico, D.; Marchionni, D.; Marc, L.; Nguyen, L. Estimation of population parameter values and variability coupling non-linear mixed-effects modeling (based on SAEM algorithm) with a whole-body PBPK model, 2024, <https://www.page-meeting.org/default.asp?abstract=11055> (accessed 12/29/2024).
  201. Ford, A. C.; Sandborn, W. J.; Khan, K. J.; Hanauer, S. B.; Talley, N. J.; Moayyedi, P. Efficacy of biological therapies in inflammatory bowel disease: systematic review and meta-analysis. *The American journal of gastroenterology* **2011**, 106, 644–59, DOI: [10.1038/ajg.2011.73](https://doi.org/10.1038/ajg.2011.73).
  202. Vande Casteele, N.; Herfarth, H.; Katz, J.; Falck-Ytter, Y.; Singh, S. American Gastroenterological Association Institute technical review on the role of therapeutic drug monitoring in the management of inflammatory bowel diseases. *Gastroenterology* **2017**, 153, 835–857.e6, DOI: [10.1053/j.gastro.2017.07.031](https://doi.org/10.1053/j.gastro.2017.07.031).



203. Cheifetz, A. S.; Abreu, M. T.; Afif, W.; Cross, R. K.; Dubinsky, M. C.; Loftus, E. V.; Osterman, M. T.; Saroufim, A.; Siegel, C. A.; Yarur, A. J.; Melmed, G. Y.; Papamichael, K. A comprehensive literature review and expert consensus statement on therapeutic drug monitoring of biologics in inflammatory bowel disease. *The American journal of gastroenterology* **2021**, *116*, 2014–2025, DOI: [10.14309/ajg.0000000000001396](https://doi.org/10.14309/ajg.0000000000001396).
204. Papamichael, K.; Afif, W.; Drobne, D.; Dubinsky, M. C.; Ferrante, M.; Irving, P. M.; Kamperidis, N.; Kobayashi, T.; Kotze, P. G.; Lambert, J.; Noor, N. M.; Roblin, X.; Roda, G.; Vande Casteele, N.; Yarur, A. J.; Arebi, N.; Danese, S.; Paul, S.; Sandborn, W. J.; Vermeire, S.; Cheifetz, A. S.; Peyrin-Biroulet; the International Consortium for Therapeutic Drug Monitoring. Therapeutic drug monitoring of biologics in inflammatory bowel disease: unmet needs and future perspectives. *The lancet. Gastroenterology & hepatology* **2022**, *7*, 171–185, DOI: [10.1016/S2468-1253\(21\)00223-5](https://doi.org/10.1016/S2468-1253(21)00223-5).
205. Clarkston, K.; Tsai, Y.; Jackson, K.; Rosen, M. J.; Denson, L. A.; Minar, P. Development of infliximab target concentrations during induction in pediatric Crohn disease patients. *Journal of pediatric gastroenterology and nutrition* **2019**, *69*, 68–74, DOI: [10.1097/MPG.0000000000002304](https://doi.org/10.1097/MPG.0000000000002304).
206. Papamichael, K.; Cheifetz, A. S. Letter: infliximab concentrations during induction therapy – one size does not fit all. *Alimentary pharmacology & therapeutics* **2018**, *47*, 1334–1335, DOI: [10.1111/apt.14616](https://doi.org/10.1111/apt.14616).
207. Santacana Juncosa, E.; Rodríguez-Alonso, L.; Padullés Zamora, A.; Guardiola, J.; Rodríguez-Moranta, F.; Serra Nilsson, K.; Bas Minguet, J.; Morandeira Rego, F.; Colom Codina, H.; Padullés Zamora, N. Bayes-based dosing of infliximab in inflammatory bowel diseases: short-term efficacy. *British journal of clinical pharmacology* **2021**, *87*, 494–505, DOI: [10.1111/bcp.14410](https://doi.org/10.1111/bcp.14410).
208. Wojciechowski, J.; Upton, R. N.; Mould, D. R.; Wiese, M. D.; Foster, D. J. R. Infliximab maintenance dosing in inflammatory bowel disease: an example for in silico assessment of adaptive dosing strategies. *The AAPS journal* **2017**, *19*, 1136–1147, DOI: [10.1208/s12248-017-0082-8](https://doi.org/10.1208/s12248-017-0082-8).
209. Schräpel, C.; Hofmann, U.; Tran, F.; Schreiber, S.; Schwab, M.; Lehr, T. DPhG Annual Meeting 2022: Model-informed precision dosing (MIPD) in infliximab induction therapy to achieve target trough concentrations during the maintenance phase. **2022**.
210. Kovar, C.; Hofmann, U.; Selzer, D.; Tran, F.; Schreiber, S.; Schwab, M.; Lehr, T. eMed Meeting on Systems Medicine 2022: Early optimization of infliximab treatment using a model-informed precision dosing approach: the GUIDE-IBD study. **2022**.
211. Bundesministerium für Forschung, Technologie und Raumfahrt. GUIDE-IBD – Molekulare Therapiesteuerung bei chronisch-entzündlichen Darmerkrankungen, <https://www.gesundheitsforschung-bmbf.de/de/guide-ibd-molekulare-therapiesteuerung-bei-chronisch-entzundlichen-darmerkrankungen-9289.php> (accessed 06/09/2025).

212. Tran, F.; Aden, K.; Bernardes, J. P.; Jäckel, C.; Kovar, C.; Rüdesheim, S.; Florea, M.; Stallbaum, F.; Schrinner, F.; Nikolaus, S.; Mätzler, W.; Franke, A.; Szymczak, S.; Hofmann, U.; Lehr, T.; Schwab, M.; Dempfle, A.; Huber, S.; Wiestler, M.; Seidler, U.; Rosenstiel, P.; Schreiber, S. 987e: Biomarker-informed therapy guidance improved clinical outcomes of anti-TNF treatment in patients with inflammatory bowel disease in a multi-center, randomized, open-label, prospective clinical trial (GUIDE-IBD). *Gastroenterology* **2025**, *169*, S–2085, DOI: [10.1016/S0016-5085\(25\)05725-7](https://doi.org/10.1016/S0016-5085(25)05725-7).
213. Uster, D. W.; Stocker, S. L.; Carland, J. E.; Brett, J.; Marriott, D. J. E.; Day, R. O.; Wicha, S. G. A model averaging/selection approach improves the predictive performance of model-informed precision dosing: vancomycin as a case study. *Clinical pharmacology and therapeutics* **2021**, *109*, 175–183, DOI: [10.1002/cpt.2065](https://doi.org/10.1002/cpt.2065).
214. Kantasiripitak, W.; Outtier, A.; Wicha, S. G.; Kensert, A.; Wang, Z.; Sabino, J.; Vermeire, S.; Thomas, D.; Ferrante, M.; Dreesen, E. Multi-model averaging improves the performance of model-guided infliximab dosing in patients with inflammatory bowel diseases. *CPT: pharmacometrics & systems pharmacology* **2022**, *11*, 1045–1059, DOI: [10.1002/psp4.12813](https://doi.org/10.1002/psp4.12813).
215. Voulgaridou, G.; Paraskeva, T.; Ragia, G.; Atzemian, N.; Portokallidou, K.; Kolios, G.; Arvanitidis, K.; Manolopoulos, V. G. Therapeutic drug monitoring (TDM) implementation in public hospitals in Greece in 2003 and 2021: a comparative analysis of TDM evolution over the years. *Pharmaceutics* **2023**, *15*, 2181, DOI: [10.3390/pharmaceutics15092181](https://doi.org/10.3390/pharmaceutics15092181).
216. Mould, D. R.; Upton, R. N.; Wojciechowski, J.; Phan, B. L.; Tse, S.; Dubinsky, M. C. Dashboards for therapeutic monoclonal antibodies: learning and confirming. *The AAPS journal* **2018**, *20*, 76, DOI: [10.1208/s12248-018-0237-2](https://doi.org/10.1208/s12248-018-0237-2).
217. Wojtyniak, J.-G.; Selzer, D.; Schwab, M.; Lehr, T. Physiologically based precision dosing approach for drug-drug-gene interactions: a simvastatin network analysis. *Clinical pharmacology and therapeutics* **2021**, *109*, 201–211, DOI: [10.1002/cpt.2111](https://doi.org/10.1002/cpt.2111).
218. Dibbets, A. C.; Koldewei, C.; Osinga, E. P.; Scheepers, H. C. J.; de Wildt, S. N. Barriers and facilitators for bringing model-informed precision dosing to the patient's bedside: a systematic review. *Clinical pharmacology and therapeutics* **2025**, *117*, 633–645, DOI: [10.1002/cpt.3510](https://doi.org/10.1002/cpt.3510).

## SUPPLEMENTARY DOCUMENTS

---

### A.1 SUPPLEMENTARY DOCUMENT TO PUBLICATION I – PHYSIOLOGICALLY BASED PHARMACOKINETIC MODELING OF DASATINIB

**CPT: Pharmacometrics & Systems Pharmacology****Supplementary Material: A Physiologically-Based Pharmacokinetic Precision Dosing Approach to Manage Dasatinib Drug–Drug Interactions**

Christina Kovar<sup>1,2</sup>, Helena Leonie Hanae Loer<sup>1</sup>, Simeon Rüdesheim<sup>1,2</sup>, Laura Maria Fuhr<sup>1</sup>, Fatima Zahra Marok<sup>1</sup>, Dominik Selzer<sup>1</sup>, Matthias Schwab<sup>2,3,4</sup> and Thorsten Lehr<sup>1</sup>

<sup>1</sup>Clinical Pharmacy, Saarland University, Saarbrücken, Germany

<sup>2</sup>Dr. Margarete Fischer-Bosch Institute of Clinical Pharmacology, Stuttgart, Germany

<sup>3</sup>Departments of Clinical Pharmacology, and Pharmacy and Biochemistry, University of Tübingen, Tübingen, Germany

<sup>4</sup>Cluster of Excellence iFIT (EXC2180), Image-Guided and Functionally Instructed Tumor Therapies, University of Tübingen, Tübingen, Germany

**Funding**

Matthias Schwab was supported by the Robert Bosch Stiftung (Stuttgart, Germany), a grant from the German Federal Ministry of Education and Research (BMBF, 031L0188D, “GUIDE-IBD”) and the DFG im Rahmen der Exzellenzstrategie des Bundes und der Länder-EXC 2180-390900677. Thorsten Lehr was supported by the German Federal Ministry of Education and Research (BMBF, Horizon 2020 INSPIRATION grant 643271), under the frame of ERACoSysMed and the European Union Horizon 2021 SafePolyMed (grant 101057639).

**Conflict of Interest**

The authors declared no competing interests for this work.

**Corresponding Author**

Prof. Dr. Thorsten Lehr  
Clinical Pharmacy, Saarland University  
Campus C5 3, 66123 Saarbrücken, Germany  
ORCID: 0000-0002-8372-1465  
Phone: +49 681 302 70255  
Email: [thorsten.lehr@mx.uni-saarland.de](mailto:thorsten.lehr@mx.uni-saarland.de)

## Contents

<b>S1 PBPK Model Building</b>	<b>3</b>
S1.1 Assignment to Training and Test Dataset . . . . .	3
S1.2 Virtual Individuals . . . . .	3
S1.3 Virtual Populations . . . . .	3
S1.4 Clinical Studies . . . . .	4
S1.5 System-dependent Parameters . . . . .	6
S1.6 Drug-dependent Parameter Table . . . . .	8
<b>S2 PBPK Model Evaluation</b>	<b>9</b>
S2.1 Healthy Volunteers . . . . .	9
S2.1.1 Plasma Profiles (Linear Scale) . . . . .	9
S2.1.2 Plasma Profiles (Semilogarithmic Scale) . . . . .	11
S2.2 Cancer Patients . . . . .	13
S2.2.1 Plasma Profiles (Linear Scale) . . . . .	13
S2.2.2 Plasma Profiles (Semilogarithmic Scale) . . . . .	18
S2.2.3 Goodness-of-fit Plots . . . . .	23
S2.2.4 Residual Plot . . . . .	24
S2.3 Quantitative PBPK Model Evaluation . . . . .	25
S2.3.1 Geometric Mean Fold Error (GMFE) . . . . .	25
S2.3.2 Mean Relative Deviation (MRD) . . . . .	27
S2.4 Local Sensitivity Analysis . . . . .	29
S2.4.1 Mathematical Implementation . . . . .	29
S2.4.2 Results of the Sensitivity Analysis . . . . .	30
<b>S3 PBPK Drug–Drug Interaction (DDI) Modeling</b>	<b>31</b>
S3.1 Clinical DDI Studies . . . . .	31
S3.2 DDI Model Evaluation . . . . .	33
S3.2.1 Plasma Profiles of Enzyme-mediated DDIs (Semilogarithmic Scale) . . . . .	33
S3.2.2 Plasma Profiles of pH-Dependent DDIs (Semilogarithmic Scale) . . . . .	34
S3.2.3 Geometric Mean Fold Error (GMFE) . . . . .	35
<b>S4 PBPK Drug–Food Interaction (DFI) Modeling</b>	<b>36</b>
S4.1 DFI Model Building . . . . .	36
S4.1.1 Clinical DFI Studies . . . . .	36
S4.2 DFI Model Evaluation . . . . .	37
S4.2.1 Plasma Profiles And Goodness-of-Fit Plot of DFIs . . . . .	37
S4.2.2 Geometric Mean Fold Error (GMFE) . . . . .	39
<b>S5 Model Application &amp; Others</b>	<b>40</b>
S5.1 Exposure Simulations for Model-Informed Precision Dosing . . . . .	40
S5.1.1 Plasma Profiles of Simulated Single DDI Scenarios . . . . .	43
S5.1.2 Plasma Profiles of Simulated Multiple DDI Scenarios . . . . .	49
S5.2 CYP3A4 Autoinhibition . . . . .	50
S5.3 Pharmacokinetic Parameters: Absolute Bioavailability, Fraction Absorbed, Fraction Metabolized, Fraction Escaping Gut Wall and Hepatic Elimination . . . . .	50
<b>References</b>	<b>51</b>

## S1 PBPK Model Building

### S1.1 Assignment to Training and Test Dataset

Plasma profiles from the literature were divided into a training and a test dataset for model building (5 profiles) and evaluation (58 profiles), respectively. The plasma profiles were allocated to the training and test datasets using a non-randomized strategy to ensure comprehensive and varied data for model building. This data assortment encapsulated a wide spectrum of dosing ranges and an array of dosing regimens. In the process, we strived to maximize the number of plasma profiles for model evaluation. We specifically selected datasets with dense sampling intervals spanning a prolonged investigation period for the training dataset. An overview of all clinical studies is presented in [Table S1](#), [Table S7](#) and [Table S9](#).

### S1.2 Virtual Individuals

Virtual “mean individuals” were created for each study based on mean or mode of age, sex, body weight, height, body mass index and ethnicity from the corresponding study reports. If demographic information was not provided for a study, either a 30-year-old white American male with a body weight of 80 kg and height of 1.78 m for healthy volunteers or a 64-year-old white American male with body weight of 82 kg and height of 1.75 m for cancer patients were used according to the third National Health and Nutrition Examination Survey (NHANES) database [1].

For each compartment expressing cytochrome P450 3A4 (CYP3A4), we applied uniform parameter values for the Michaelis-Menten kinetics—specifically, the Michaelis constant ( $K_m$ ) and the catalytic constant ( $k_{cat}$ )—to model CYP3A4-mediated metabolism. In general, enzyme and transporter expressions in different tissues were implemented according to the PK-Sim<sup>®</sup> expression database.

As CML is more prevalent in men, with an average diagnosis age of 64 years, a virtual 64-year-old European male individual was used for the dosing simulations [2]. Default values for body weight (64 kg) and height (1.70 m) were derived from the International Commission on Radiological Protection (ICRP) database [3].

### S1.3 Virtual Populations

Virtual populations of 100 individuals were generated based on the respective study population demographics. Depending on the ethnicity and demographic characteristics, virtual individuals were varied by the implemented algorithm in PK-Sim<sup>®</sup> within the limits of the NHANES database for white Americans, the ICRP database for Europeans and the integrated database for Japanese population [4]. The corresponding algorithms for the generation of virtual populations have been reported by Willmann and coworkers [5].

For the studies CA180016 [6] and CA180032 [6] as well as the studies by Christopher et al. 2008 (a) [7], Vaidhyathan et al. 2019 [8] and Vargas et al. 2016 [9] an age range of 20 to 50 years for healthy volunteers was assumed, while for the studies CA180005 and CA180009 as well as the studies by Christopher et al. 2008 (b) [7] and Luo et al. 2008 [10] an age range of 20 to 80 years for cancer patients was used since information about the study populations were not available. System-dependent parameters including reference concentrations and enzyme expression variabilities are listed in [Table S2](#).

## S1.4 Clinical Studies

Table S1: Overview of clinical study data from the literature used for model development.

Clinical study	Dose [mg]	Route	N	Females [%]	Age [years]	Weight [kg]	BMI [kg/m <sup>2</sup> ]	Gastric pH	Fasted/Fed	Health Status	Dataset
Bioequivalence study [13]	140	po, tab, sd	122	-	- (18–48)	-	24.1 (-) <sup>a</sup>	2.0 <sup>b</sup>	fasted	healthy	training
Christopher 2008 (a) [7]	100	po, sol, sd	8	0	-	-	-	2.0 <sup>b</sup>	- <sup>c</sup>	healthy	test
Furlong 2012 [14]	100	po, tab, sd	20	-	-	-	-	2.0 <sup>b</sup>	fasted	healthy	training
Study CA180016 [6]	100	po, tab, sd	18	-	-	-	-	2.0 <sup>b</sup>	- <sup>c</sup>	healthy	test
Vaidhyathan 2018 (a) [8]	70	po, tab, sd	64	-	-	-	-	2.0 <sup>b</sup>	fasted	healthy	training
Vaidhyathan 2018 (b) [8]	100	po, PFOS, sd	-	-	-	-	-	2.0 <sup>b</sup>	fasted	healthy	test
Vaidhyathan 2018 (c) [8]	100	po, dispersed tab, sd	-	-	-	-	-	2.0 <sup>b</sup>	fasted	healthy	test
Vaidhyathan 2018 (d) [8]	100	po, tab, sd	-	-	-	-	-	2.0 <sup>b</sup>	fasted	healthy	test
Vargas 2016 [9]	100	po, tab, sd	-	-	28 (-) <sup>a</sup>	65 (-) <sup>a</sup>	22.7 (-) <sup>a</sup>	2.0 <sup>b</sup>	fasted	healthy	test
Araujo 2012 [15]	100	po, tab, qd, md	46	0	65 (48–83) <sup>d,e</sup>	-	-	2.0 <sup>b</sup>	- <sup>c</sup>	cancer	test
Christopher 2008 (b) [7]	180	po, tab, sd	3	-	-	-	-	2.0 <sup>b</sup>	- <sup>c</sup>	cancer	test
Demetri 2009 (a) [16]	35	po, tab, bid, md (B5D)	4	39.4 <sup>g</sup>	56 (32–81) <sup>d,g</sup>	-	-	2.0 <sup>b</sup>	fasted	cancer	test
Demetri 2009 (b) [16]	50	po, tab, bid, md (B5D)	3	39.4 <sup>g</sup>	56 (32–81) <sup>d,g</sup>	-	-	2.0 <sup>b</sup>	fasted	cancer	test
Demetri 2009 (c) [16]	70	po, tab, bid, md (B5D)	4	39.4 <sup>g</sup>	56 (32–81) <sup>d,g</sup>	-	-	2.0 <sup>b</sup>	fasted	cancer	test
Demetri 2009 (d) [16]	70	po, tab, bid, md (B7D)	3	47.1 <sup>g</sup>	59 (31–82) <sup>d,g,e</sup>	-	-	2.0 <sup>b</sup>	fasted	cancer	test
Demetri 2009 (e) [16]	90	po, tab, bid, md (B5D)	5	39.4 <sup>g</sup>	56 (32–81) <sup>d,g</sup>	-	-	2.0 <sup>b</sup>	fasted	cancer	test
Demetri 2009 (f) [16]	90	po, tab, bid, md (B7D)	5	47.1 <sup>g</sup>	59 (31–82) <sup>d,g,e</sup>	-	-	2.0 <sup>b</sup>	fasted	cancer	test
Demetri 2009 (g) [16]	100	po, tab, bid, md (B7D)	7	47.1 <sup>g</sup>	59 (31–82) <sup>d,g,e</sup>	-	-	2.0 <sup>b</sup>	fasted	cancer	test
Demetri 2009 (h) [16]	120	po, tab, bid, md (B5D)	7	39.4 <sup>g</sup>	56 (32–81) <sup>d,g</sup>	-	-	2.0 <sup>b</sup>	fasted	cancer	test
Demetri 2009 (i) [16]	120	po, tab, bid, md (B7D)	1	47.1 <sup>g</sup>	59 (31–82) <sup>d,g,e</sup>	-	-	2.0 <sup>b</sup>	fasted	cancer	test
Demetri 2009 (j) [16]	160	po, tab, bid, md (B5D)	1	39.4 <sup>g</sup>	56 (32–81) <sup>d,g</sup>	-	-	2.0 <sup>b</sup>	fasted	cancer	test
Luo 2008 [10]	90	po, tab, bid, md	-	-	-	-	-	2.0 <sup>b</sup>	- <sup>c</sup>	cancer	test
Study CA180002 (a) [6]	15	po, tab, qd, md (Q5D)	3	-	56 (15–79) <sup>d,f</sup>	-	-	2.0 <sup>b</sup>	fasted	cancer	test
Study CA180002 (b) [6]	25	po, tab, bid, md (B5D)	3	-	56 (15–79) <sup>d,f</sup>	-	-	2.0 <sup>b</sup>	fasted	cancer	test
Study CA180002 (c) [6]	30	po, tab, qd, md (Q5D)	3	-	56 (15–79) <sup>d,f</sup>	-	-	2.0 <sup>b</sup>	fasted	cancer	test
Study CA180002 (d) [6]	35	po, tab, bid, md (B5D)	8	-	56 (15–79) <sup>d,f</sup>	-	-	2.0 <sup>b</sup>	fasted	cancer	test
Study CA180002 (e) [6]	50	po, tab, bid, md (B5D)	3–5	-	56 (15–79) <sup>d,f</sup>	-	-	2.0 <sup>b</sup>	fasted	cancer	test
Study CA180002 (f) [6]	50	po, tab, bid, md (B7D)	6–8	-	56 (15–79) <sup>d,f</sup>	-	-	2.0 <sup>b</sup>	fasted	cancer	test
Study CA180002 (g) [6]	50	po, tab, qd, md (Q5D)	3	-	56 (15–79) <sup>d,f</sup>	-	-	2.0 <sup>b</sup>	fasted	cancer	test

-: unknown, **B5D**: five consecutive days bid dosing followed by two nontreatment days, **B7D**: continuous bid dosing, **bid**: twice a day, **BMI**: body mass index, **md**: multiple dose, **N**: number of participants, **PFOS**: powder for oral suspension, **po**: peroral, **Q5D**: five consecutive days once daily dosing followed by two nontreatment days, **qd**: once a day, **sd**: single dose, **sol**: solution, **tab**: tablet

<sup>a</sup> Mean (range)

<sup>b</sup> Default value in PK-Sim<sup>®</sup> for fasted state [11]

<sup>c</sup> A light-fat breakfast or fasted state was assumed

<sup>d</sup> Median (range)

<sup>e</sup> Maximum age of the NHANES database is 81 years [1]

<sup>f</sup> Values refer to the whole study population

<sup>g</sup> Values refer to the whole study population (stratified by regimen)

<sup>h</sup> Assumed (based on the reported age range of 12–17 [12])



Table S1: Overview of clinical study data from the literature used for model development (continued).

Clinical study	Dose [mg]	Route	N	Females [%]	Age [years]	Weight [kg]	BMI [kg/m <sup>2</sup> ]	Gastric pH	Fasted/Fed	Health Status	Dataset
Study CA180002 (h) [6]	70	po, tab, bid, md (B5D)	6–9	-	56 (15–79) <sup>d,f</sup>	-	-	2.0 <sup>b</sup>	fasted	cancer	test
Study CA180002 (i) [6]	70	po, tab, bid, md (B7D)	11–14	-	56 (15–79) <sup>d,f</sup>	-	-	2.0 <sup>b</sup>	fasted	cancer	test
Study CA180002 (j) [6]	75	po, tab, qd, md (Q5D)	3	-	56 (15–79) <sup>d,f</sup>	-	-	2.0 <sup>b</sup>	fasted	cancer	test
Study CA180002 (k) [6]	90	po, tab, bid, md (B7D)	11	-	56 (15–79) <sup>d,f</sup>	-	-	2.0 <sup>b</sup>	fasted	cancer	test
Study CA180002 (l) [6]	105	po, tab, qd, md (Q5D)	3	-	56 (15–79) <sup>d,f</sup>	-	-	2.0 <sup>b</sup>	fasted	cancer	test
Study CA180002 (m) [6]	120	po, tab, bid, md (B7D)	7	-	56 (15–79) <sup>d,f</sup>	-	-	2.0 <sup>b</sup>	fasted	cancer	test
Study CA180002 (n) [6]	140	po, tab, qd, md (Q5D)	3	-	56 (15–79) <sup>d,f</sup>	-	-	2.0 <sup>b</sup>	fasted	cancer	test
Study CA180002 (o) [6]	180	po, tab, qd, md (Q5D)	3	-	56 (15–79) <sup>d,f</sup>	-	-	2.0 <sup>b</sup>	fasted	cancer	test
Study CA180005 (a) [6]	70	po, tab, bid, md (B5D)	-	-	-	-	-	2.0 <sup>b</sup>	- <sup>c</sup>	cancer	test
Study CA180005 (b) [6]	70	po, tab, bid, md (B7D)	-	-	-	-	-	2.0 <sup>b</sup>	- <sup>c</sup>	cancer	test
Takahashi 2011 (a) [17]	100	po, tab, qd, md	9	77.8	58 (33–65) <sup>d</sup>	-	-	2.0 <sup>b</sup>	fed <sup>c</sup>	cancer	test
Takahashi 2011 (b) [17]	150	po, tab, qd, md	3	33.3	55 (39–63) <sup>d</sup>	-	-	2.0 <sup>b</sup>	fed <sup>c</sup>	cancer	test
Takahashi 2011 (c) [17]	200	po, tab, qd, md	4	75.0	47.5 (33–53) <sup>d</sup>	-	-	2.0 <sup>b</sup>	fed <sup>c</sup>	cancer	test
Zwaan 2013 (a) [12]	100	po, tab, qd, sd	9	-	15 <sup>h</sup> (12–17)	-	-	2.0 <sup>b</sup>	- <sup>c</sup>	cancer	test
Zwaan 2013 (b) [12]	140	po, tab, qd, sd	8	-	15 <sup>h</sup> (12–17)	-	-	2.0 <sup>b</sup>	- <sup>c</sup>	cancer	test
Zwaan 2013 (c) [12]	170	po, tab, qd, sd	9	-	15 <sup>h</sup> (12–17)	-	-	2.0 <sup>b</sup>	- <sup>c</sup>	cancer	test
Zwaan 2013 (d) [12]	200	po, tab, qd, sd	2	-	15 <sup>h</sup> (12–17)	-	-	2.0 <sup>b</sup>	- <sup>c</sup>	cancer	test

-: unknown, **B5D**: five consecutive days bid dosing followed by two nontreatment days, **B7D**: continuous bid dosing, **bid**: twice a day, **BMI**: body mass index, **md**: multiple dose,

**N**: number of participants, **PFOS**: powder for oral suspension, **po**: peroral, **Q5D**: five consecutive days once daily dosing followed by two nontreatment days, **qd**: once a day,

**sd**: single dose, **sol**: solution, **tab**: tablet

<sup>a</sup> Mean (range)

<sup>b</sup> Default value in PK-Sim<sup>®</sup> for fasted state [11]

<sup>c</sup> A light-fat breakfast or fasted state was assumed

<sup>d</sup> Median (range)

<sup>e</sup> Maximum age of the NHANES database is 81 years [1]

<sup>f</sup> Values refer to the whole study population

<sup>g</sup> Values refer to the whole study population (stratified by regimen)

<sup>h</sup> Assumed (based on the reported age range of 12–17 [12])

## S1.5 System-dependent Parameters

Table S2: System-dependent parameters and expression of relevant enzymes, transporters and processes.

Enzyme/Transporter/Processes	Mean ref. conc. [ $\mu\text{mol/L}$ ] <sup>a</sup>	GeoSD of the ref. conc. <sup>b</sup>	Relative expression in different organs <sup>c</sup>	Half-life liver [hours]	Half-life intestine [hours]
AADAC	1.00 <sup>d</sup> [18]	1.40 <sup>e</sup>	RT-PCR [26]	36	23
CYP1A2	1.80 [27]	1.63 (liver) [28]	RT-PCR [29]	39	23
CYP2A6	2.72 [27]	1.40 <sup>e</sup>	RT-PCR [29]	26	23
CYP2B6	1.56 [27]	1.40 <sup>e</sup>	RT-PCR [29]	32	23
CYP2C19	0.76 [27]	1.79 (liver) [28]	RT-PCR [29]	26	23
CYP2C8	2.56 [27]	2.05 (liver) [28]	RT-PCR [29]	23	23
CYP2D6	0.40 [27]	2.49 [28]	RT-PCR [29]	51	23
CYP3A4	4.32 [27]	1.18/1.46 (liver/duodenum) [28]	RT-PCR [29]	36 [30]	23 [31]
CYP3A5	0.04 [18]	1.40 <sup>e</sup>	RT-PCR [29]	36	23
EPHX1	1.00 <sup>d</sup> [18]	1.40 <sup>e</sup>	RT-PCR [26]	36	23
FMO3	1.00 <sup>d</sup>	1.00 [18]	RT-PCR [26]	-	23
PON3	1.00 <sup>d</sup>	1.40 <sup>e</sup>	Array [29]	36	23
UGT1A1	1.00 <sup>d</sup>	1.40 <sup>e</sup>	RT-PCR [26]	36	23
UGT1A3	1.00 <sup>d</sup>	1.40 <sup>e</sup>	RT-PCR [26]	36	23
UGT1A4	2.32 <sup>f</sup>	1.07 [28]	RT-PCR [26]	36	23
UGT2B7 <sup>g</sup>	2.78 <sup>f</sup> [32]	1.60 (liver) [28]	EST [33]	36	23
Unspecific liver lactonization	1.00 <sup>d</sup>	1.40 <sup>e</sup>	Liver only	36	23
Unspecific plasma hydrolysis	1.00 <sup>d</sup>	1.40 <sup>e</sup>	Plasma only	36	23
BCRP	1.00 <sup>d</sup>	1.35 [34]	RT-PCR <sup>h</sup> [35]	36	23
MRP2	1.00 <sup>d</sup>	1.49 [36]	Array [37]	36	23
OATP1B1	0.07 <sup>i,j</sup> [23]	1.54 [23]	RT-PCR [35]	36	-
OATP1B3	1.00 <sup>d</sup> [18]	1.54 [23]	Array [37]	36	23
P-gp	1.41 <sup>optimized</sup>	1.60 [23]	RT-PCR <sup>k</sup> [35]	36	23
Unspecific liver influx	1.00 <sup>d</sup>	1.40 <sup>e</sup>	Liver only	36	23
Unspecific hepatic clearance	-	-	-	-	-
Chemical hydrolysis	1.00	-	Ubiquitous	36	23

**AADAC**: arylacetamide deacetylase, **BCRP**: breast cancer resistance protein, **CYP**: cytochrome P450, **EST**: expressed sequence tag, **EPHX1**: epoxide hydroxylase 1, **FMO**: flavin-containing monooxygenase, **GeoSD**: geometric standard deviation, **MRP2**: multidrug resistance-associated protein 2, **OATP**: organic anion transporting polypeptide, **P-gp**: P-glycoprotein, **PON3**: paraoxonase 3, **ref. conc.**: reference concentration, **RT-PCR**: reverse transcription polymerase chain reaction, **UGT**: UDP-glucuronosyltransferase

<sup>a</sup>  $\mu\text{mol}$  protein/L in the tissue of highest expression

<sup>b</sup> Geometric standard deviation of the reference concentration

<sup>c</sup> In the different organs (PK-Sim<sup>®</sup> expression database profile)

<sup>d</sup> If no information was available, the mean ref. conc. was set to 1.0  $\mu\text{mol/L}$  and the catalytic rate constant ( $k_{\text{cat}}$ ) was optimized according to [18]

<sup>e</sup> If no information was available a moderate variability of 35% CV was assumed (= 1.40 GSD)

<sup>f</sup> Calculated from protein per mg microsomal protein  $\times$  40.0 mg microsomal protein per g liver [19]

<sup>g</sup> UGT2B7 enzyme for metabolism of fluconazole and simvastatin was implemented according to the respective publication [20, 21]

<sup>h</sup> With relative expression in blood cells set to 0.3046 [22]

<sup>i</sup> Calculated from transporter per mg membrane protein  $\times$  37.0 mg membrane protein per g liver [23]

<sup>j</sup> Differences in the implementation of the OATP1B1 ref. conc. in the rifampicin [24], simvastatin [21] and erythromycin [25] PBPK model were compensated by using the concentration of 0.07  $\mu\text{mol/L}$  [23] and optimizing the  $k_{\text{cat}}$

<sup>k</sup> With relative expression in intestinal mucosa increased by factor 3.57 [24]

**Table S3:** Relative enzymes and transporters expression in organs and tissues implemented in the dasatinib PBPK model [%]

	CYP2C8	CYP3A4	OATP1B1	OATP1B3
Data source	RT-PCR [29]	RT-PCR [29]	RT-PCR [35]	Array [37]
Blood cells	0	0	0	0
Plasma	0	0	-	-
Bone	0	0	0	3
Brain	0	0	0	3
Fat	0	0	0	0
Gonads	1	0	1	4
Heart	0	0	0	6
Kidney	0	1	0	2
Liver periportal	100	100	100	100
Liver pericentral	100	100	100	100
Lung	0	0	0	2
Muscle	0	0	0	2
Pancreas	0	0	0	1
Skin	0	0	0	1
Spleen	0	0	0	1
Duodenum mucosa	0	7	0	2
Upper jejunum mucosa	0	7	0	2
Lower jejunum mucosa	0	7	0	2
Upper ileum mucosa	0	7	0	2
Lower ileum mucosa	0	7	0	2
Cecum mucosa	0	0	0	0
Colon ascendens mucosa	0	0	0	1
Colon transversum mucosa	0	0	0	1
Colon descendens mucosa	0	0	0	1
Colon sigmoid mucosa	0	0	0	1
Rectum mucosa	0	0	0	0
Stomach non-mucosal tissue	0	0	0	1
Small intestine non-mucosal tissue	0	7	0	2
Large intestine non-mucosal tissue	0	0	0	1
Stomach lumen	0	0	-	-
Duodenum lumen	0	0	-	-
Upper jejunum lumen	0	0	-	-
Lower jejunum lumen	0	0	-	-
Upper ileum lumen	0	0	-	-
Lower ileum lumen	0	0	-	-
Cecum lumen	0	0	-	-
Colon ascendens lumen	0	0	-	-
Colon transversum lumen	0	0	-	-
Colon descendens lumen	0	0	-	-
Colon sigmoid lumen	0	0	-	-
Rectum lumen	0	0	-	-

**Array:** microarray expression profile, **CYP:** cytochrome P450, **OATP:** organic anion transporting polypeptide

## S1.6 Drug-dependent Parameter Table

Table S4: Drug-dependent parameters for dasatinib.

Parameter	Value [95% CI]	Unit	Source	Literature	Reference	Description
MW	488.01	g/mol	Literature	488.01	[39]	Molecular weight
pK <sub>a</sub> (base)	3.10, 6.80	-	Literature	3.10, 6.80	[40]	Acid dissociation constant
pK <sub>a</sub> (acid)	10.80	-	Literature	10.80	[40]	Acid dissociation constant
Solubility (pH 4.0)	0.04	mg/ml	Literature	0.04	[41]	Solubility
logP	3.59 [3.47, 3.71]	-	Optimized	2.71–4.01	[39, 40]	Lipophilicity
f <sub>u</sub>	4.00	%	Literature	4.00	[42]	Fraction unbound
CYP3A4 K <sub>m</sub> → M20 <sup>a</sup>	6.00	μmol/l	Literature	6.00	[43]	Michaelis-Menten constant
CYP3A4 k <sub>cat</sub> → M20 <sup>a</sup>	58.38 [46.19, 70.57]	1/min	Optimized	-	-	Catalytic rate constant
CYP3A4 K <sub>i</sub>	9.00	μmol/l	Literature	9.00	[44]	Inhibition Constant
CYP3A4 K <sub>inact</sub>	0.02	1/min	Literature	0.02	[44]	Maximum rate of inactivation
CYP2C8 K <sub>i</sub>	3.60	μmol/l	Literature	3.60	[44]	Dissociation Constant
OATP1B1 K <sub>i</sub>	2.33	μmol/l	Literature	2.33	[45]	Dissociation Constant
OATP1B3 K <sub>i</sub>	2.75	μmol/l	Literature	2.75	[45]	Dissociation Constant
Unspecific hepatic clearance	5.62 [3.17, 8.07]	1/min	Optimized	-	-	Elimination from plasma (first-order process in the liver)
GET (fasted)	15.00	min	Literature	15.00	[46]	Gastric emptying time
GET (fed)	103.44	min	Optimized	45–120	[47]	Gastric emptying time
GET (with Rabeprazole)	60.13	min	Optimized	-	-	Gastric emptying time
GET (with Maalox <sup>®</sup> )	31.27	min	Optimized	-	-	Gastric emptying time
GFR fraction	1.00	-	Assumed	-	-	Fraction of filtered drug in the urine
EHC continuous fraction	1.00	-	Assumed	-	-	Fraction of bile continually released
Partition coefficients	Diverse <sup>b</sup>	-	Calculated	Schmitt	[48]	Cell to plasma partition coefficients
Cellular permeability	Diverse <sup>b</sup>	cm/min	Calculated	P K-Sim Standard	[46]	Permeability into the cellular space
Intestinal permeability	1.22·10 <sup>-6</sup>	cm/s	Optimized	-	-	Transcellular intestinal permeability
Density	[6.42·10 <sup>-7</sup> , 1.80·10 <sup>-6</sup> ]	g/cm <sup>3</sup>	Literature	1.41	[49]	Density
Aqueous diffusion coefficient	1.41	cm <sup>2</sup> /min	Calculated	2.67·10 <sup>-4</sup>	-	Aqueous diffusion coefficient
Particle dissolution radius (Bin1)	2.67·10 <sup>-4</sup>	μm	Calculated	11.46 <sup>c</sup>	[8]	Mean Particle Radius
Particle dissolution radius (Bin2)	11.46	μm	Calculated	38.07 <sup>c</sup>	[8]	Mean Particle Radius
Particle dissolution radius (Bin3)	38.07	μm	Calculated	67.86 <sup>c</sup>	[8]	Mean Particle Radius

CI: confidence interval, CYP: cytochrome P450, EHC: enterohepatic circulation, GFR: glomerular filtration rate, OATP: organic anion transporting polypeptide

<sup>a</sup> Metabolite was not included in the PBPK model<sup>b</sup> Values differ across the organs<sup>c</sup> Calculated according to [38]

## S2 PBPK Model Evaluation

### S2.1 Healthy Volunteers

#### S2.1.1 Plasma Profiles (Linear Scale)

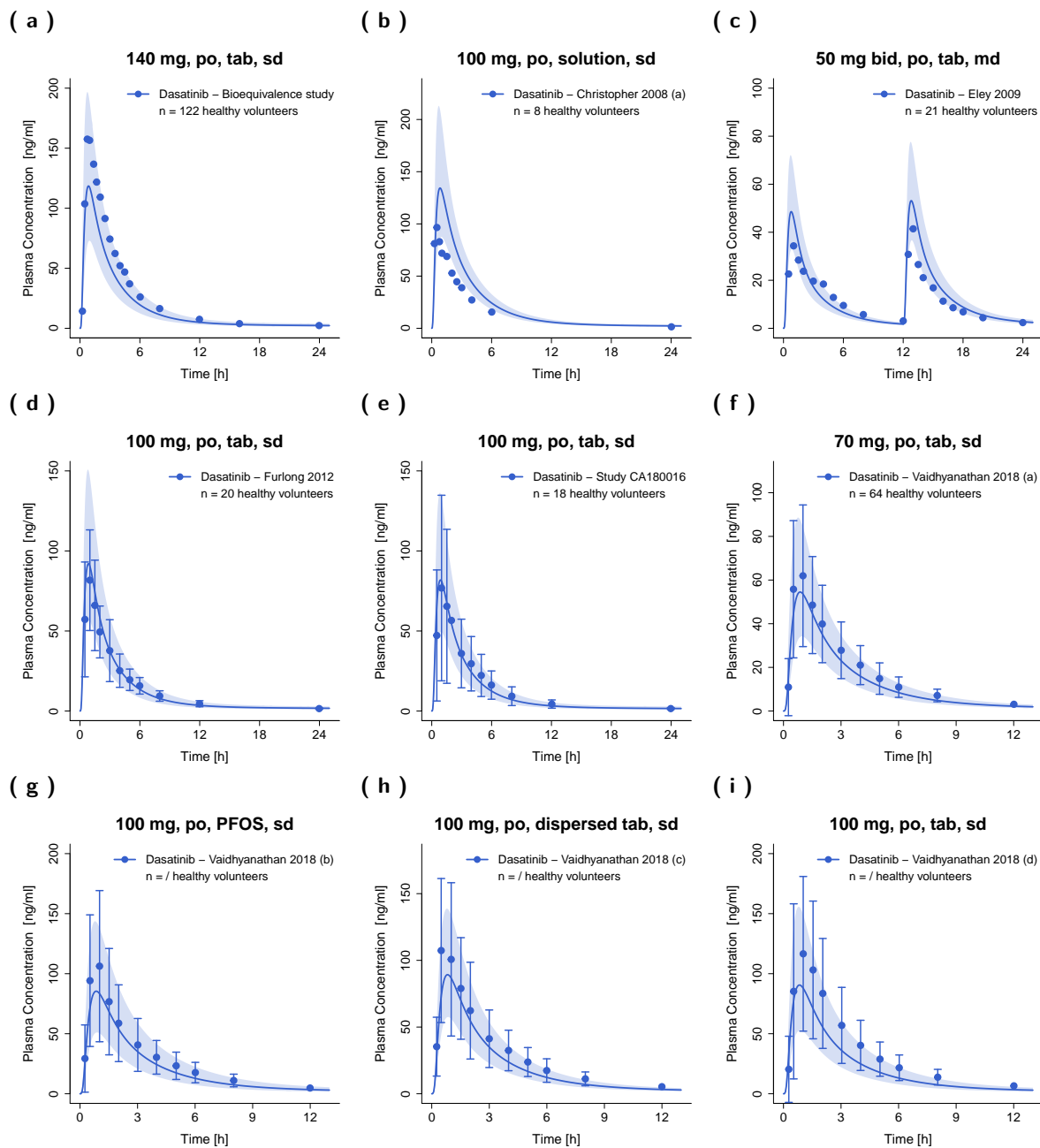


**Figure S1: Predicted and observed dasatinib plasma concentration–time profiles in healthy volunteers on a linear scale.**

Solid lines show predicted geometric mean concentration–time profiles with ribbons illustrating the corresponding geometric standard deviation of the population simulations (n=100). Points demonstrate the mean observed data with the corresponding standard deviation of dasatinib (if depicted in the respective publication). /: no information available, **bid**: twice a day, **md**: multiple dose, **n**: number of participants, **PFOS**: powder for oral suspension, **po**: peroral, **qd**: once a day, **sd**: single dose, **tab**: tablet.

(j)

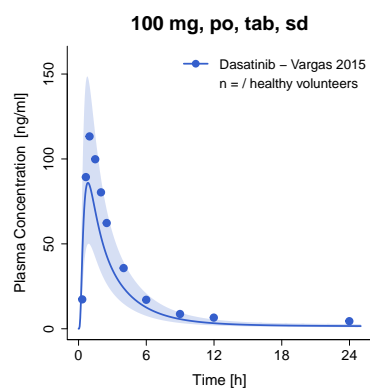


**Figure S1: (continued) Predicted and observed dasatinib plasma concentration–time profiles in healthy volunteers on a linear scale.** Solid lines show predicted geometric mean concentration–time profiles with ribbons illustrating the corresponding geometric standard deviation of the population simulations ( $n=100$ ). Points demonstrate the mean observed data with the corresponding standard deviation of dasatinib (if depicted in the respective publication). /: no information available, **bid**: twice a day, **md**: multiple dose, **n**: number of participants, **PFOS**: powder for oral suspension, **po**: peroral, **qd**: once a day, **sd**: single dose, **tab**: tablet.

## S2.1.2 Plasma Profiles (Semilogarithmic Scale)

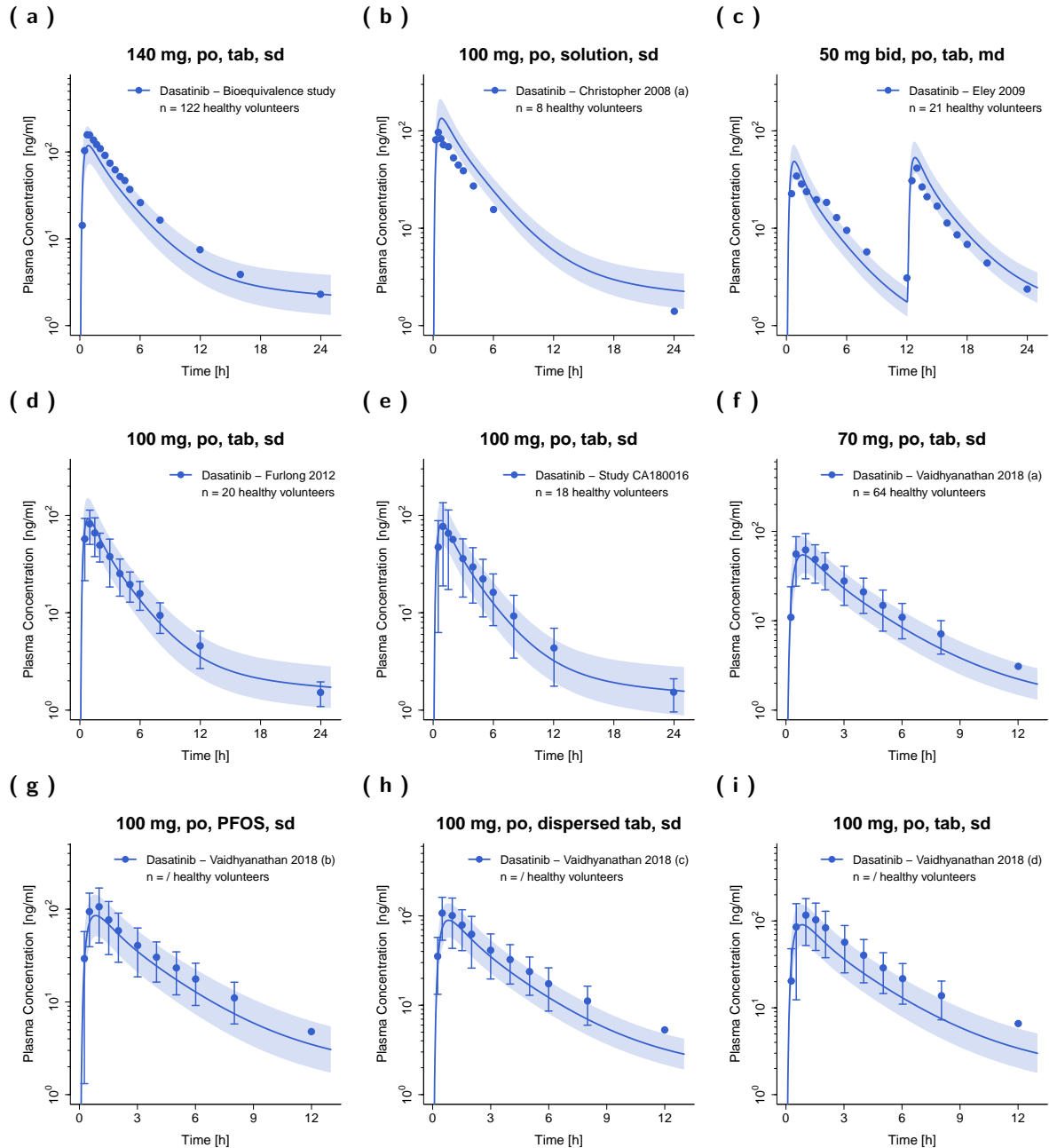


**Figure S2: Predicted and observed dasatinib plasma concentration–time profiles in healthy volunteers on a semilogarithmic scale.** Solid lines show predicted geometric mean concentration–time profiles with ribbons illustrating the corresponding geometric standard deviation of the population simulations (n=100). Points demonstrate the mean observed data with the corresponding standard deviation of dasatinib (if depicted in the respective publication). /: no information available, **bid**: twice a day, **md**: multiple dose, **n**: number of participants, **PFOS**: powder for oral suspension, **po**: peroral, **qd**: once a day, **sd**: single dose, **tab**: tablet.



(j)

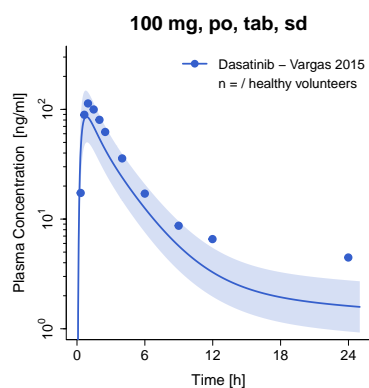


**Figure S2: (continued) Predicted and observed dasatinib plasma concentration–time profiles in healthy volunteers on a semilogarithmic scale.** Solid lines show predicted geometric mean concentration–time profiles with ribbons illustrating the corresponding geometric standard deviation of the population simulations (n=100). Points demonstrate the mean observed data with the corresponding standard deviation of dasatinib (if depicted in the respective publication). /: no information available, **bid**: twice a day, **md**: multiple dose, **n**: number of participants, **PFOS**: powder for oral suspension, **po**: peroral, **qd**: once a day, **sd**: single dose, **tab**: tablet.

## S2.2 Cancer Patients

### S2.2.1 Plasma Profiles (Linear Scale)

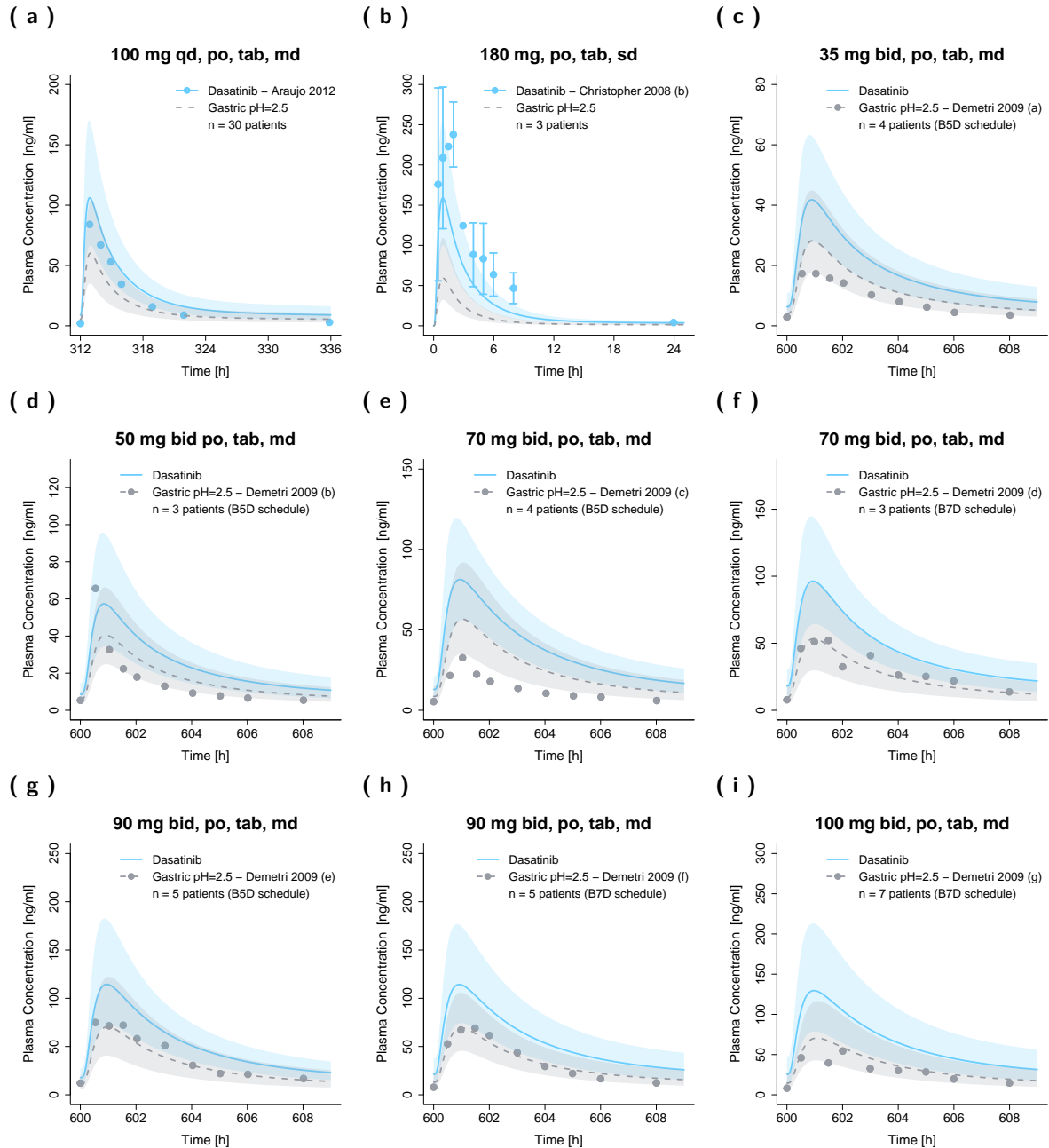


**Figure S3: Predicted and observed dasatinib plasma concentration–time profiles in cancer patients on a linear scale.** Solid and dashed lines show predicted geometric mean concentration–time profiles with gastric pH of 2.0 and 2.5, respectively, with ribbons illustrating the corresponding geometric standard deviation of the population simulations (n=100). Points demonstrate the mean observed data with the corresponding standard deviation of dasatinib (if depicted in the respective publication). /: no information available, **B5D**: five consecutive days bid dosing followed by two nontreatment days, **B7D**: seven consecutive days bid dosing, **bid**: twice a day, **md**: multiple dose, **n**: number of participants, **po**: peroral, **Q5D**: five consecutive days once daily dosing followed by two nontreatment days, **qd**: once a day, **sd**: single dose, **tab**: tablet.

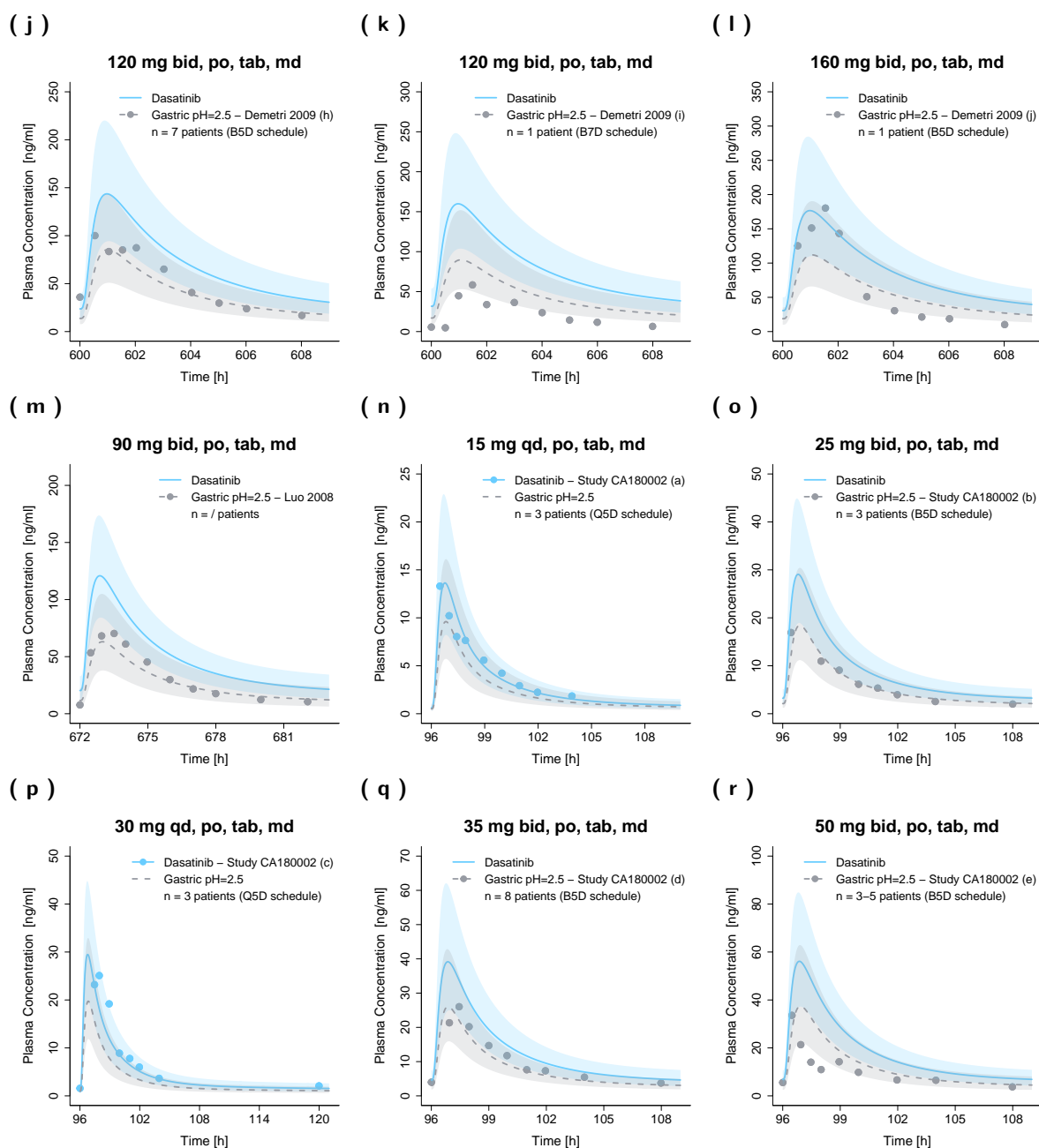


**Figure S3: (continued) Predicted and observed dasatinib plasma concentration–time profiles in cancer patients on a linear scale.** Solid and dashed lines show predicted geometric mean concentration–time profiles with gastric pH of 2.0 and 2.5, respectively, with ribbons illustrating the corresponding geometric standard deviation of the population simulations ( $n=100$ ). Points demonstrate the mean observed data with the corresponding standard deviation of dasatinib (if depicted in the respective publication). /: no information available, **B5D**: five consecutive days bid dosing followed by two nontreatment days, **B7D**: seven consecutive days bid dosing, **bid**: twice a day, **md**: multiple dose, **n**: number of participants, **po**: peroral, **Q5D**: five consecutive days once daily dosing followed by two nontreatment days, **qd**: once a day, **sd**: single dose, **tab**: tablet.

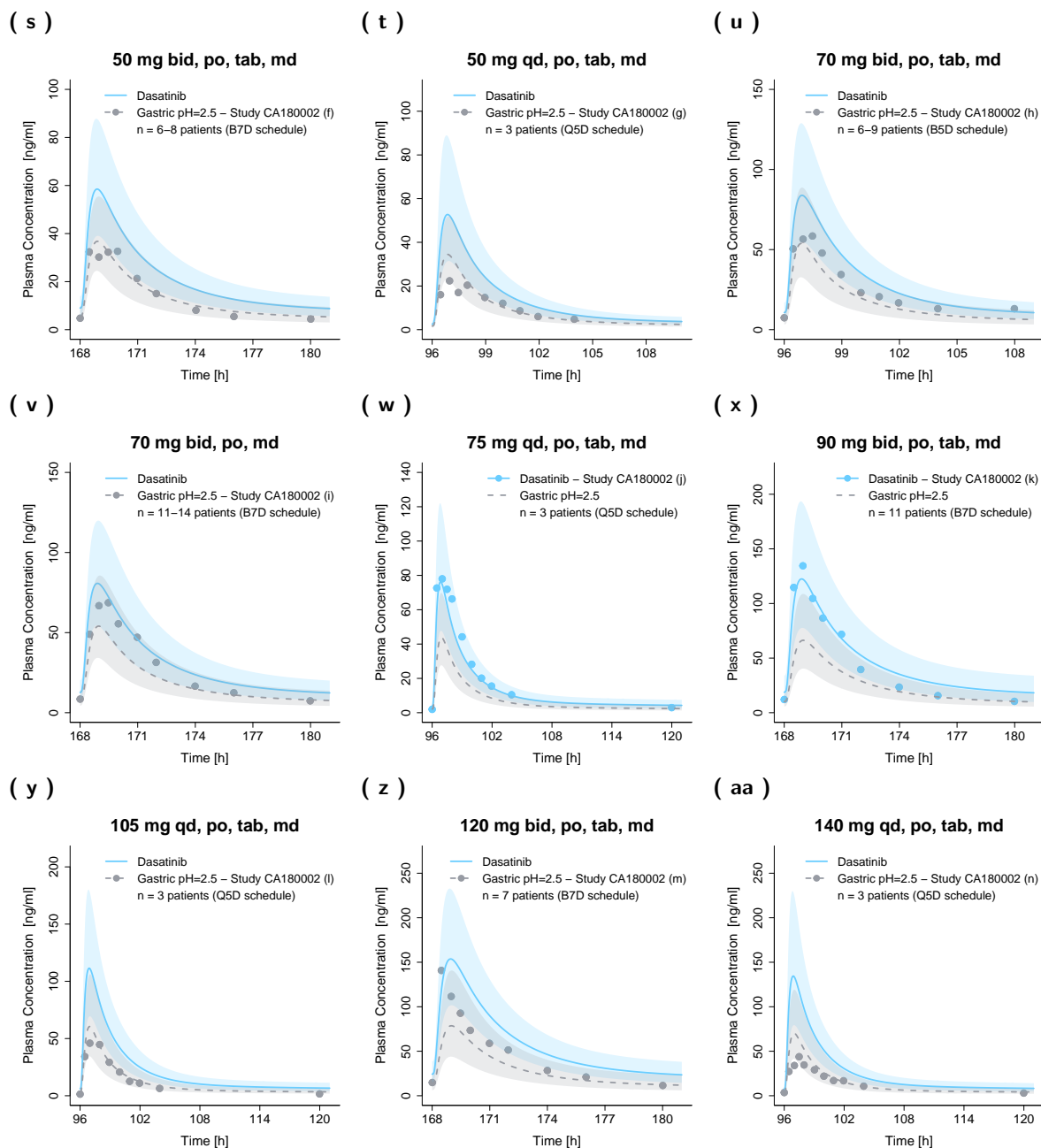


**Figure S3: (continued) Predicted and observed dasatinib plasma concentration–time profiles in cancer patients on a linear scale.** Solid and dashed lines show predicted geometric mean concentration–time profiles with gastric pH of 2.0 and 2.5, respectively, with ribbons illustrating the corresponding geometric standard deviation of the population simulations (n=100). Points demonstrate the mean observed data with the corresponding standard deviation of dasatinib (if depicted in the respective publication). /: no information available, **B5D**: five consecutive days bid dosing followed by two nontreatment days, **B7D**: seven consecutive days bid dosing, **bid**: twice a day, **md**: multiple dose, **n**: number of participants, **po**: peroral, **Q5D**: five consecutive days once daily dosing followed by two nontreatment days, **qd**: once a day, **sd**: single dose, **tab**: tablet.

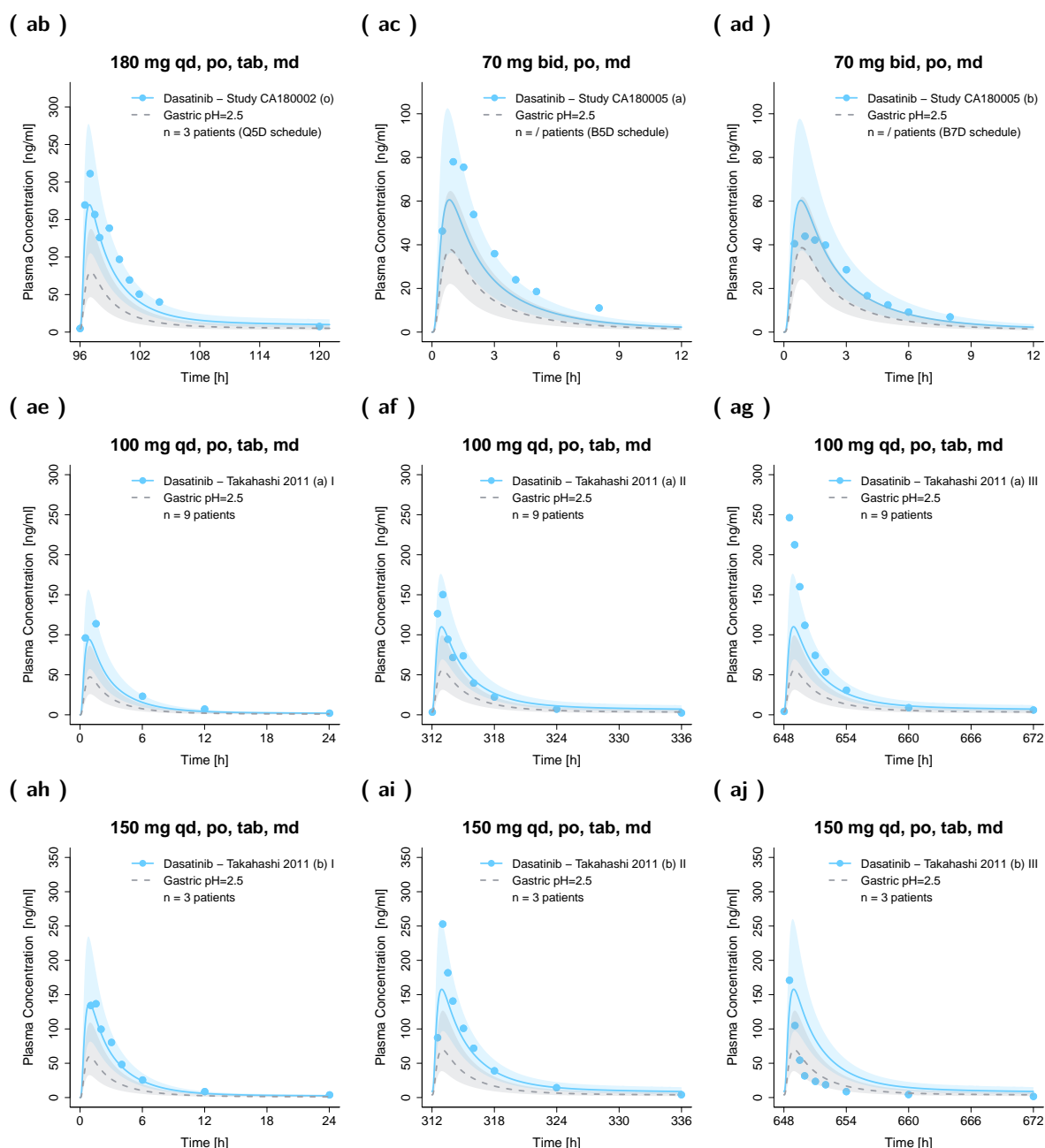


**Figure S3: (continued) Predicted and observed dasatinib plasma concentration–time profiles in cancer patients on a linear scale.** Solid and dashed lines show predicted geometric mean concentration–time profiles with gastric pH of 2.0 and 2.5, respectively, with ribbons illustrating the corresponding geometric standard deviation of the population simulations (n=100). Points demonstrate the mean observed data with the corresponding standard deviation of dasatinib (if depicted in the respective publication). /: no information available, **B5D**: five consecutive days bid dosing followed by two nontreatment days, **B7D**: seven consecutive days bid dosing, **bid**: twice a day, **md**: multiple dose, **n**: number of participants, **po**: peroral, **Q5D**: five consecutive days once daily dosing followed by two nontreatment days, **qd**: once a day, **sd**: single dose, **tab**: tablet.

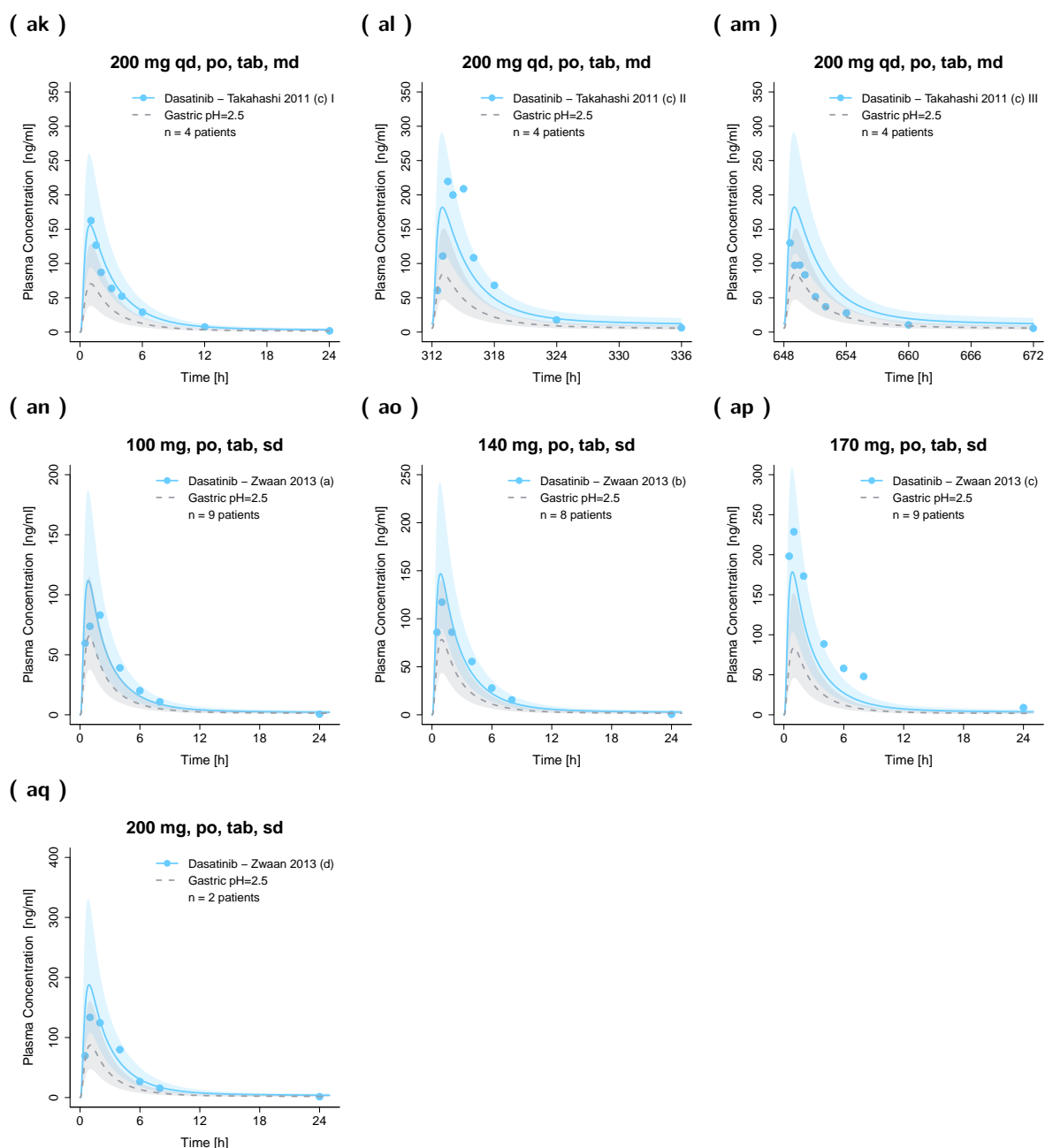


**Figure S3: (continued) Predicted and observed dasatinib plasma concentration–time profiles in cancer patients on a linear scale.** Solid and dashed lines show predicted geometric mean concentration–time profiles with gastric pH of 2.0 and 2.5, respectively, with ribbons illustrating the corresponding geometric standard deviation of the population simulations ( $n=100$ ). Points demonstrate the mean observed data with the corresponding standard deviation of dasatinib (if depicted in the respective publication). /: no information available, **B5D**: five consecutive days bid dosing followed by two nontreatment days, **B7D**: seven consecutive days bid dosing, **bid**: twice a day, **md**: multiple dose, **n**: number of participants, **po**: peroral, **Q5D**: five consecutive days once daily dosing followed by two nontreatment days, **qd**: once a day, **sd**: single dose, **tab**: tablet.

## S2.2.2 Plasma Profiles (Semilogarithmic Scale)

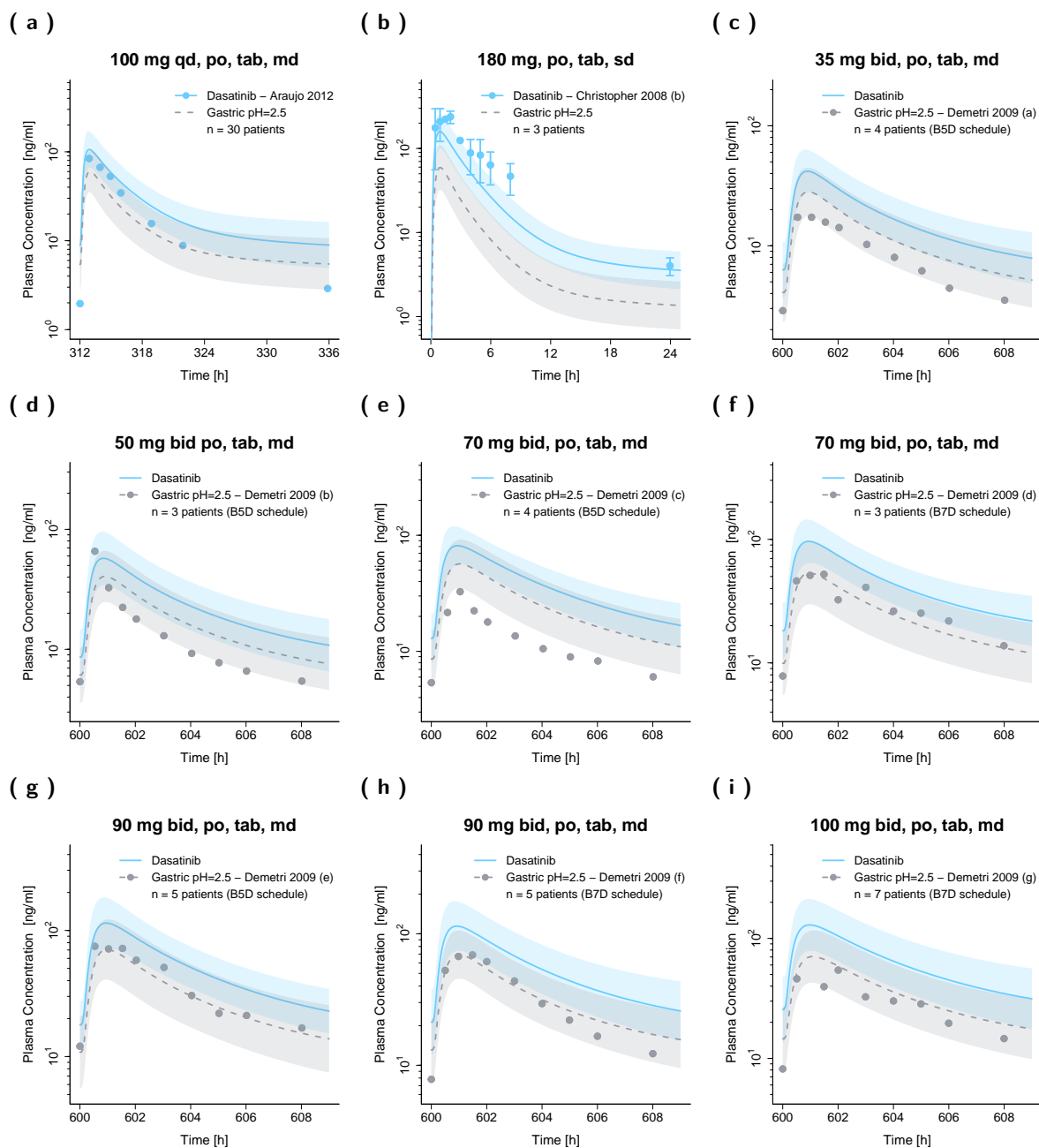


**Figure S4: Predicted and observed dasatinib plasma concentration–time profiles in cancer patients on a semilogarithmic scale.** Solid and dashed lines show predicted geometric mean concentration–time profiles with gastric pH of 2.0 and 2.5, respectively, with ribbons illustrating the corresponding geometric standard deviation of the population simulations ( $n=100$ ). Points demonstrate the mean observed data with the corresponding standard deviation of dasatinib (if depicted in the respective publication). /: no information available, **B5D**: five consecutive days bid dosing followed by two nontreatment days, **B7D**: seven consecutive days bid dosing, **bid**: twice a day, **md**: multiple dose, **n**: number of participants, **po**: peroral, **Q5D**: five consecutive days once daily dosing followed by two nontreatment days, **qd**: once a day, **sd**: single dose, **tab**: tablet.



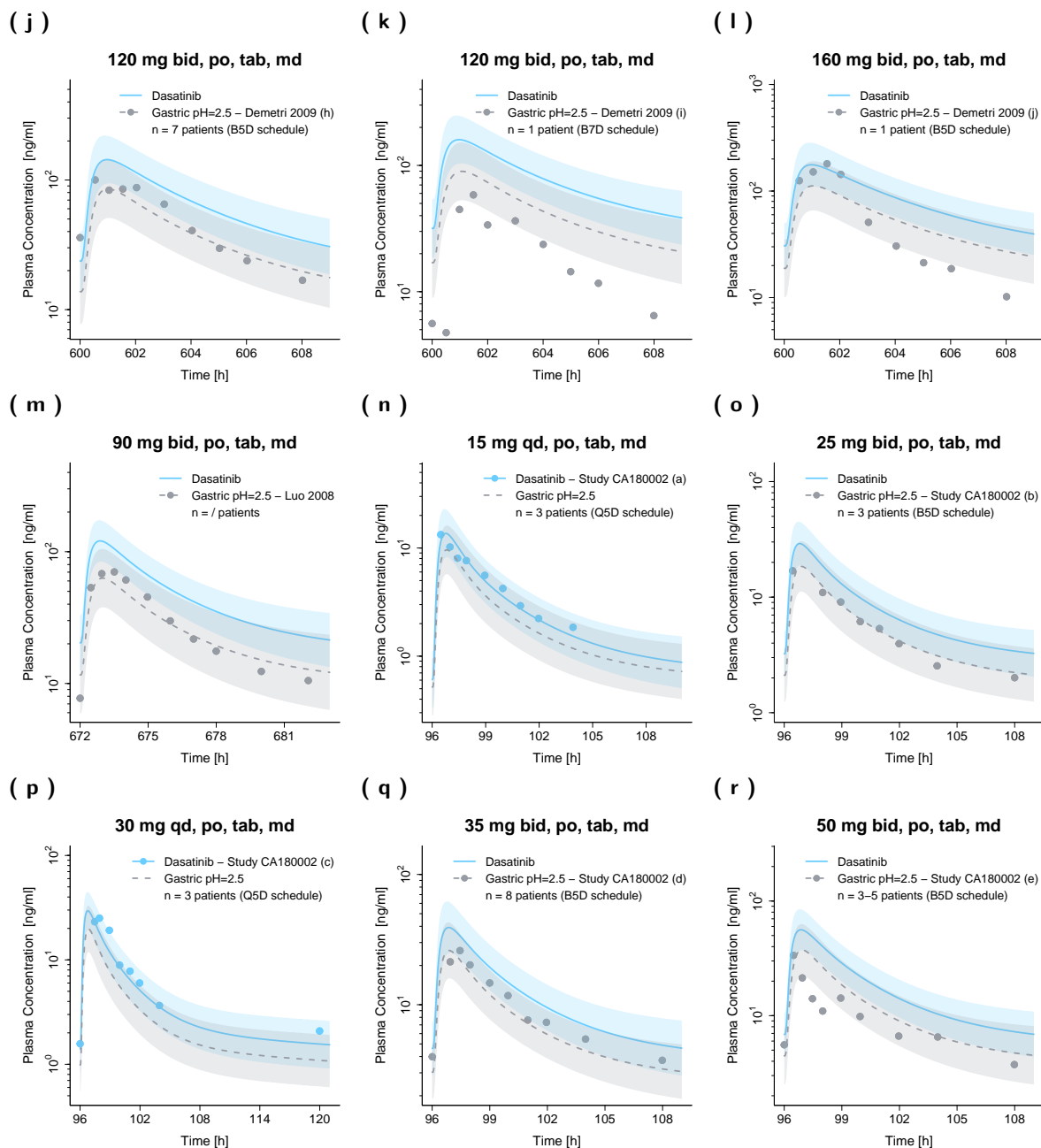


**Figure S4: (continued) Predicted and observed dasatinib plasma concentration–time profiles in cancer patients on a semilogarithmic scale.** Solid and dashed lines show predicted geometric mean concentration–time profiles with gastric pH of 2.0 and 2.5, respectively, with ribbons illustrating the corresponding geometric standard deviation of the population simulations ( $n=100$ ). Points demonstrate the mean observed data with the corresponding standard deviation of dasatinib (if depicted in the respective publication). /: no information available, **B5D**: five consecutive days bid dosing followed by two nontreatment days, **B7D**: seven consecutive days bid dosing, **bid**: twice a day, **md**: multiple dose, **n**: number of participants, **po**: peroral, **Q5D**: five consecutive days once daily dosing followed by two nontreatment days, **qd**: once a day, **sd**: single dose, **tab**: tablet.

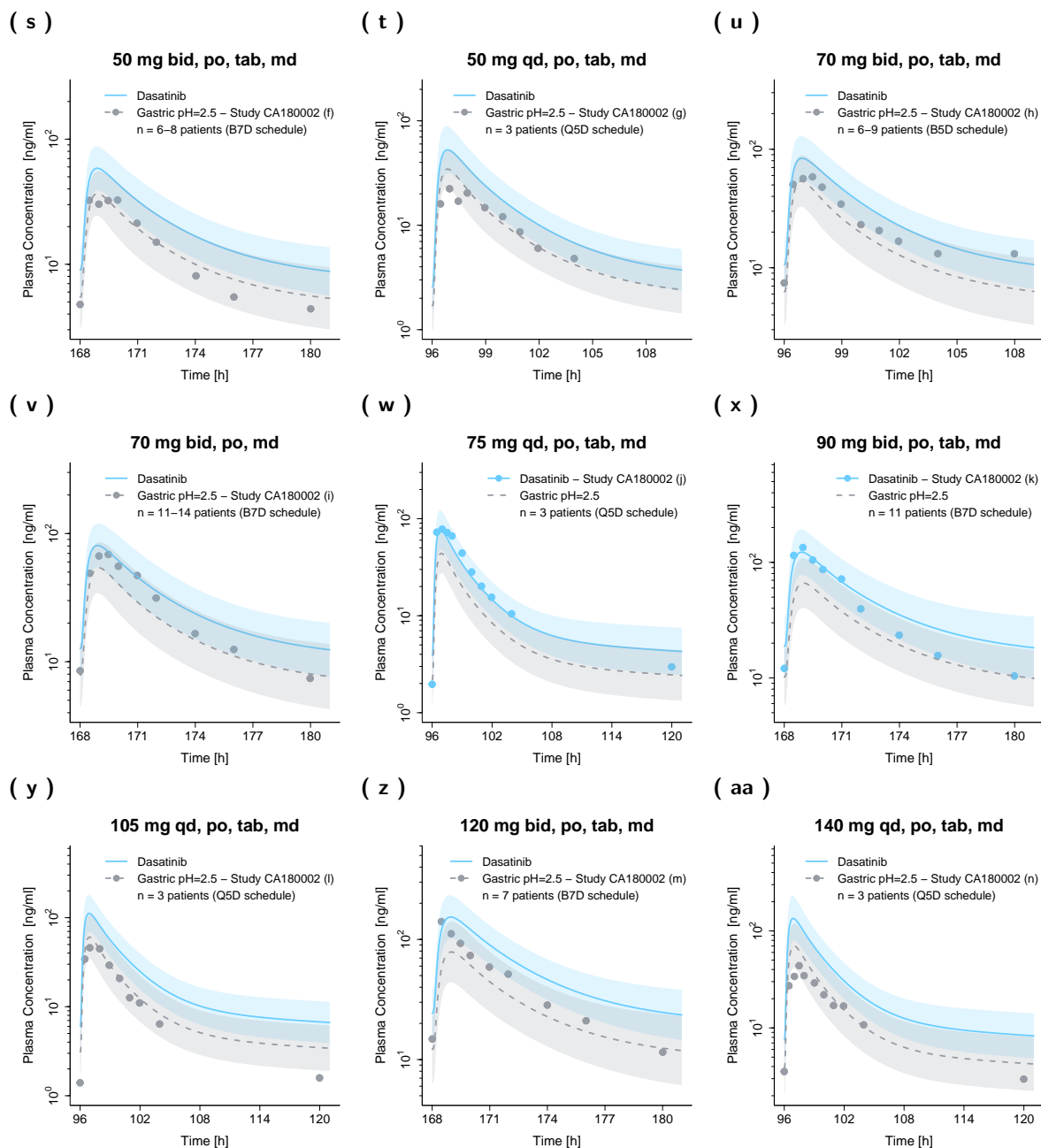


**Figure S4: (continued) Predicted and observed dasatinib plasma concentration–time profiles in cancer patients on a semilogarithmic scale.** Solid and dashed lines show predicted geometric mean concentration–time profiles with gastric pH of 2.0 and 2.5, respectively, with ribbons illustrating the corresponding geometric standard deviation of the population simulations ( $n=100$ ). Points demonstrate the mean observed data with the corresponding standard deviation of dasatinib (if depicted in the respective publication). /: no information available, **B5D**: five consecutive days bid dosing followed by two nontreatment days, **B7D**: seven consecutive days bid dosing, **bid**: twice a day, **md**: multiple dose, **n**: number of participants, **po**: peroral, **Q5D**: five consecutive days once daily dosing followed by two nontreatment days, **qd**: once a day, **sd**: single dose, **tab**: tablet.

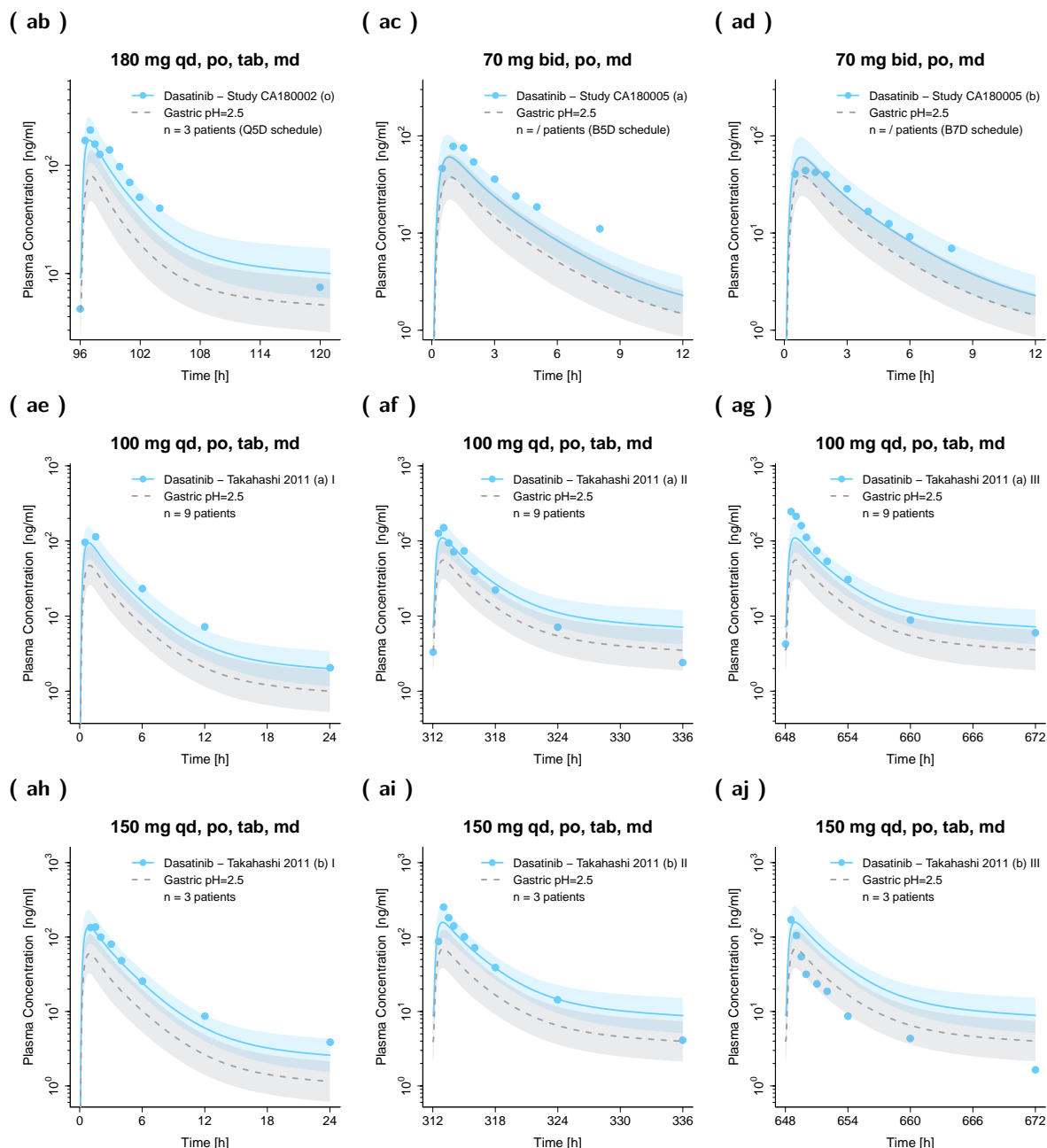


**Figure S4: (continued) Predicted and observed dasatinib plasma concentration–time profiles in cancer patients on a semilogarithmic scale.** Solid and dashed lines show predicted geometric mean concentration–time profiles with gastric pH of 2.0 and 2.5, respectively, with ribbons illustrating the corresponding geometric standard deviation of the population simulations ( $n=100$ ). Points demonstrate the mean observed data with the corresponding standard deviation of dasatinib (if depicted in the respective publication). /: no information available, **B5D**: five consecutive days bid dosing followed by two nontreatment days, **B7D**: seven consecutive days bid dosing, **bid**: twice a day, **md**: multiple dose, **n**: number of participants, **po**: peroral, **Q5D**: five consecutive days once daily dosing followed by two nontreatment days, **qd**: once a day, **sd**: single dose, **tab**: tablet.

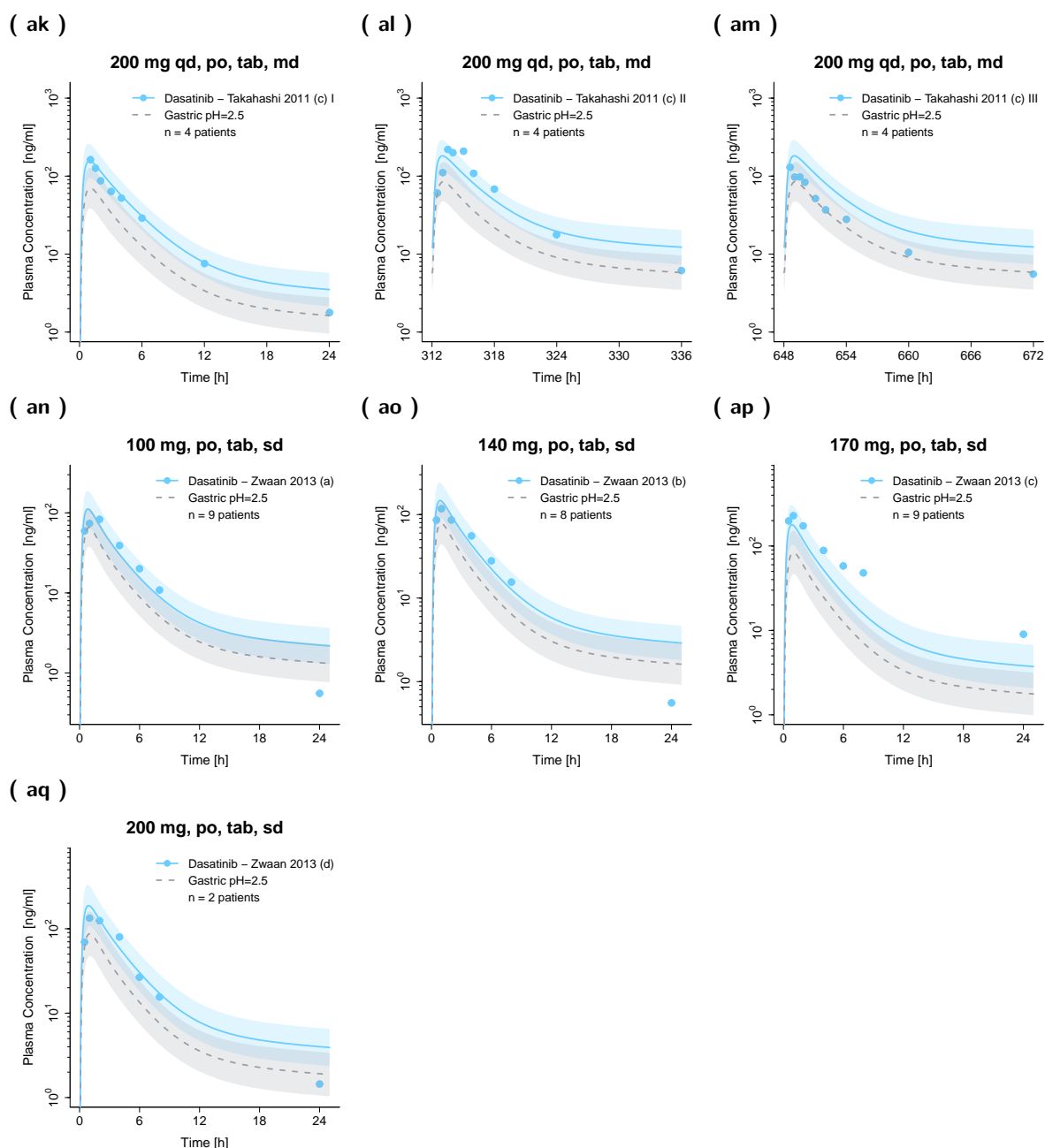


**Figure S4: (continued) Predicted and observed dasatinib plasma concentration–time profiles in cancer patients on a semilogarithmic scale.** Solid and dashed lines show predicted geometric mean concentration–time profiles with gastric pH of 2.0 and 2.5, respectively, with ribbons illustrating the corresponding geometric standard deviation of the population simulations ( $n=100$ ). Points demonstrate the mean observed data with the corresponding standard deviation of dasatinib (if depicted in the respective publication). /: no information available, **B5D**: five consecutive days bid dosing followed by two nontreatment days, **B7D**: seven consecutive days bid dosing, **bid**: twice a day, **md**: multiple dose, **n**: number of participants, **po**: peroral, **Q5D**: five consecutive days once daily dosing followed by two nontreatment days, **qd**: once a day, **sd**: single dose, **tab**: tablet.

## S2.2.3 Goodness-of-fit Plots

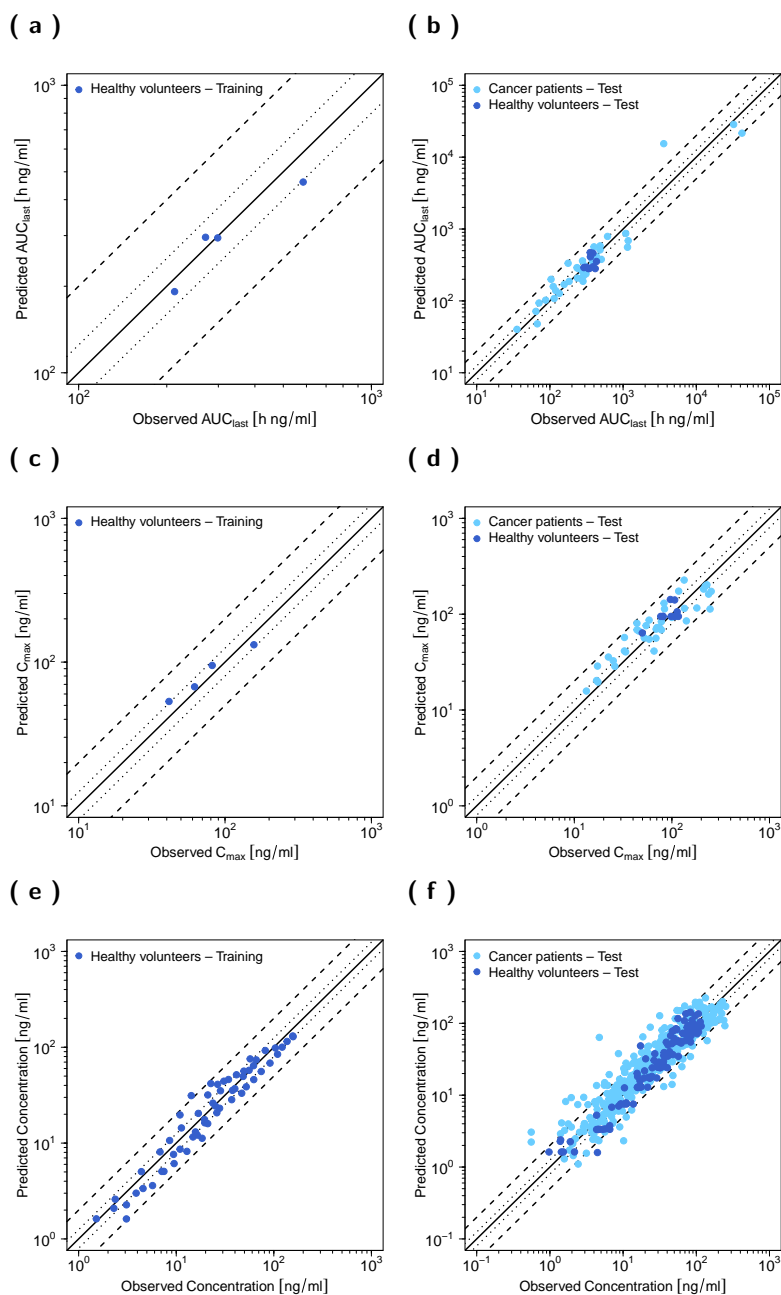


**Figure S5: Goodness-of-fit plots of predicted versus observed  $AUC_{last}$  (a–b),  $C_{max}$  (c–d) and plasma concentrations (e–f) of the training (first column) and test dataset (second column).** Solid lines mark the lines of identity, dotted lines indicate 1.25-fold and dashed lines two-fold deviation.  $AUC_{last}$ : areas under the plasma concentration–time curves from the first to the last time point of measurement,  $C_{max}$ : maximum plasma concentration.

## S2.2.4 Residual Plot

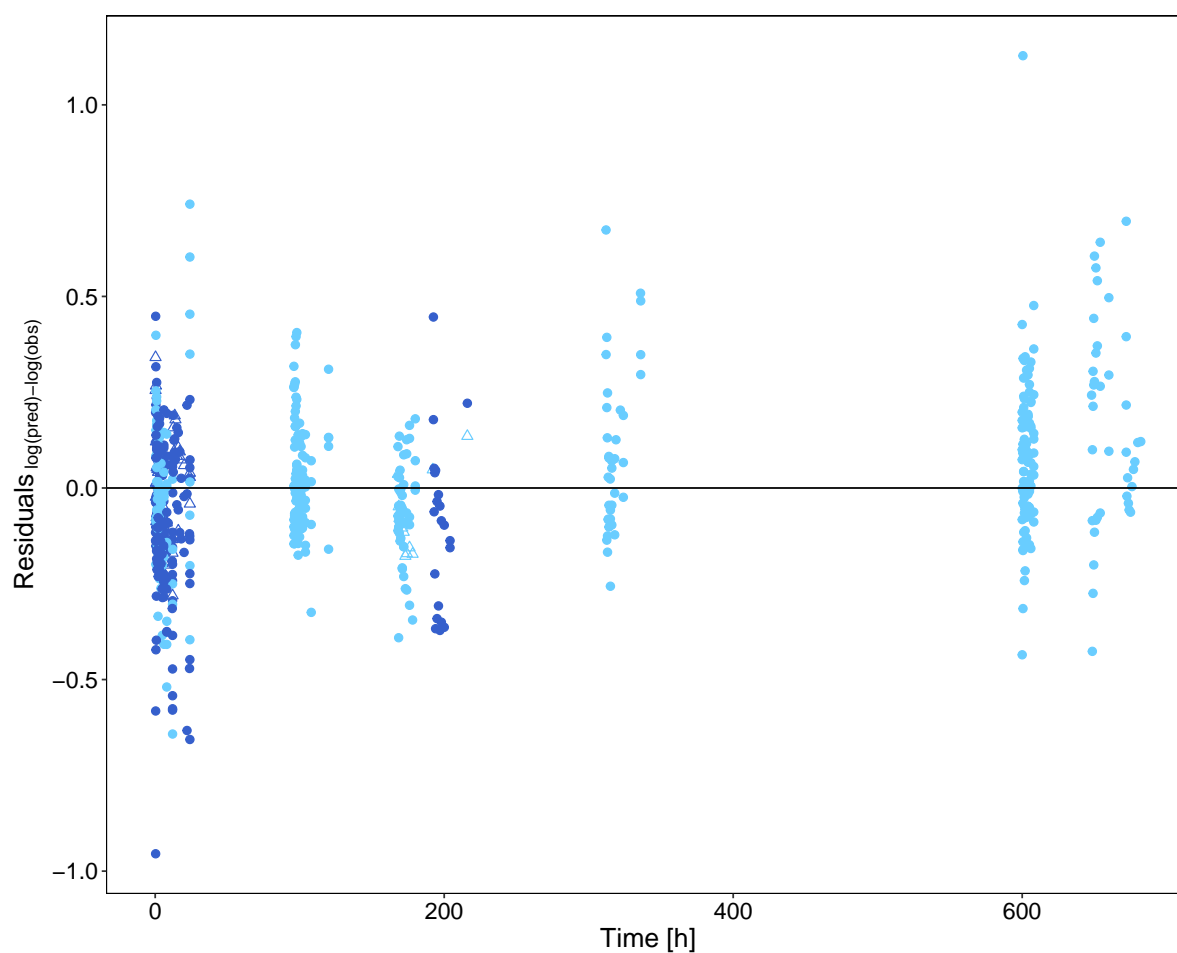


**Figure S6: Residuals versus time.** Blue and light blue symbols represent residuals from healthy volunteers and cancer patients, respectively. Triangles indicate residuals from the training dataset, while points indicate residuals from the test dataset. **Obs**: observed concentration, **pred**: predicted concentration.

## S2.3 Quantitative PBPK Model Evaluation

### S2.3.1 Geometric Mean Fold Error (GMFE)

**Table S5:** Geometric Mean Fold Error (GMFE) of  $C_{\max}$  and  $AUC_{\text{last}}$  Predictions.

Administration	Compound	$C_{\max}$			$AUC_{\text{last}}$			Reference
		Pred $\left[\frac{\text{ng}}{\text{ml}}\right]$	Obs $\left[\frac{\text{ng}}{\text{ml}}\right]$	Pred/Obs	Pred $\left[\frac{\text{ng}\cdot\text{h}}{\text{ml}}\right]$	Obs $\left[\frac{\text{ng}\cdot\text{h}}{\text{ml}}\right]$	Pred/Obs	
140 mg, po, tab, sd	Dasatinib	132.01	157.54	0.84	460.68	584.68	0.79	Bioequivalence study [13]
100 mg, po, sol, sd	Dasatinib	142.39	96.56	1.47	470.88	355.02	1.33	Christopher 2008 (a) [7]
50 mg, po, tab, bid, md	Dasatinib	53.24	41.43	1.29	295.99	271.31	1.09	Eley 2009 (control) [50]
100 mg, po, tab, sd	Dasatinib	94.78	81.72	1.16	294.52	298.60	0.99	Furlong 2012 [14]
100 mg, po, tab, sd	Dasatinib	140.72	106.81	1.32	461.41	387.37	1.19	Yago 2014 (control) [51]
100 mg, po, tab, sd	Dasatinib	94.78	81.31	1.17	292.05	323.65	0.90	Study CA180009 (fasted state (a)) [6]
100 mg, po, tab, sd	Dasatinib	63.76	49.78	1.28	410.28	357.61	1.15	Study CA180009 (with high-fat meal (b)) [6]
100 mg, po, tab, sd	Dasatinib	94.78	98.08	0.97	298.20	387.83	0.77	Study CA180009 (with light-fat meal (c)) [6]
100 mg, po, tab, sd	Dasatinib	94.78	76.82	1.23	293.25	301.65	0.97	Study CA180016 [6]
100 mg, po, tab, sd	Dasatinib	94.84	80.93	1.17	290.68	291.31	1.00	Study CA180032 (control) [6]
70 mg, po, tab, sd	Dasatinib	67.32	61.96	1.09	191.56	212.69	0.90	Vaidhyanathan 2018 (a) [8]
100 mg, po, PFOS, sd	Dasatinib	94.78	106.27	0.89	282.00	334.05	0.84	Vaidhyanathan 2018 (b) [8]
100 mg, po, dispersed tab, sd	Dasatinib	94.78	107.35	0.88	281.99	345.96	0.82	Vaidhyanathan 2018 (c) [8]
100 mg, po, tab, sd	Dasatinib	94.78	116.56	0.81	281.44	416.37	0.68	Vaidhyanathan 2018 (d) [8]
100 mg, po, tab, sd	Dasatinib	106.04	113.27	0.94	354.01	432.84	0.82	Vargas 2016 [9]
100 mg, po, tab, qd, md	Dasatinib	113.57	84.00	1.35	565.38	400.19	1.41	Araujo 2012 [15]
180 mg, po, tab, sd	Dasatinib	161.85	237.86	0.68	557.79	1149.40	0.49	Christopher 2008 (b) [7]
35 mg, po, tab, bid, md (B5D)	Dasatinib	28.74	17.28	1.66	93.48	71.05	1.32	Demetri 2009 (a) [16]
50 mg, po, tab, bid, md (B5D)	Dasatinib	41.23	65.65	0.63	139.03	120.09	1.16	Demetri 2009 (b) [16]
70 mg, po, tab, bid, md (B5D)	Dasatinib	57.16	32.64	1.75	199.85	103.69	1.93	Demetri 2009 (c) [16]
70 mg, po, tab, bid, md (B7D)	Dasatinib	56.47	52.12	1.08	207.76	238.01	0.87	Demetri 2009 (d) [16]
90 mg, po, tab, bid, md (B5D)	Dasatinib	72.10	74.88	0.96	258.15	307.42	0.84	Demetri 2009 (e) [16]
90 mg, po, tab, bid, md (B7D)	Dasatinib	69.87	69.03	1.01	263.07	273.55	0.96	Demetri 2009 (f) [16]
100 mg, po, tab, bid, md (B7D)	Dasatinib	75.90	54.40	1.40	284.12	240.30	1.18	Demetri 2009 (g) [16]
120 mg, po, tab, bid, md (B5D)	Dasatinib	92.46	100.07	0.92	339.75	396.39	0.86	Demetri 2009 (h) [16]
120 mg, po, tab, bid, md (B7D)	Dasatinib	86.73	58.42	1.48	334.03	177.28	1.88	Demetri 2009 (i) [16]
160 mg, po, tab, bid, md (B5D)	Dasatinib	116.02	180.29	0.64	413.91	433.80	0.95	Demetri 2009 (j) [16]
20 mg, po, tab, sd	Dasatinib	19.57	17.48	1.12	47.93	67.26	0.71	Johnson 2010 (control) [52]
90 mg, po, tab, bid, md	Dasatinib	72.47	70.28	1.03	306.38	301.74	1.02	Luo 2008 [10]

(continued)



**Table S5:** Geometric Mean Fold Error (GMFE) of  $C_{\max}$  and  $AUC_{\text{last}}$  Predictions (*continued*).

Administration	Compound	$C_{\max}$			$AUC_{\text{last}}$			Reference
		Pred [ $\frac{\mu\text{g}}{\text{ml}}$ ]	Obs [ $\frac{\mu\text{g}}{\text{ml}}$ ]	Pred/Obs	Pred [ $\frac{\mu\text{g}\cdot\text{h}}{\text{ml}}$ ]	Obs [ $\frac{\mu\text{g}\cdot\text{h}}{\text{ml}}$ ]	Pred/Obs	
15 mg, po, tab, qd, md (Q5D)	Dasatinib	15.77	13.30	1.19	40.22	35.50	1.13	Study CA180002 (a) [6]
25 mg, po, tab, bid, md (B5D)	Dasatinib	20.31	16.92	1.20	71.56	64.47	1.11	Study CA180002 (b) [6]
30 mg, po, tab, qd, md (Q5D)	Dasatinib	32.63	25.09	1.30	127.07	134.72	0.94	Study CA180002 (c) [6]
35 mg, po, tab, bid, md (B5D)	Dasatinib	28.55	26.02	1.10	107.80	114.35	0.94	Study CA180002 (d) [6]
50 mg, po, tab, bid, md (B5D)	Dasatinib	40.40	33.59	1.20	158.70	111.15	1.43	Study CA180002 (e) [6]
50 mg, po, tab, bid, md (B7D)	Dasatinib	41.34	32.63	1.27	169.28	156.54	1.08	Study CA180002 (f) [6]
50 mg, po, tab, qd, md (Q5D)	Dasatinib	35.72	22.36	1.60	102.44	87.51	1.17	Study CA180002 (g) [6]
70 mg, po, tab, bid, md (B5D)	Dasatinib	54.84	58.47	0.94	223.45	287.82	0.78	Study CA180002 (h) [6]
70 mg, po, tab, bid, md (B7D)	Dasatinib	56.15	68.66	0.82	237.56	311.15	0.76	Study CA180002 (i) [6]
75 mg, po, tab, qd, md (Q5D)	Dasatinib	83.54	78.00	1.07	363.20	380.49	0.95	Study CA180002 (j) [6]
90 mg, po, tab, bid, md (B7D)	Dasatinib	115.01	134.50	0.86	512.27	484.38	1.06	Study CA180002 (k) [6]
105 mg, po, tab, qd, md (Q5D)	Dasatinib	66.62	45.93	1.45	290.29	234.29	1.24	Study CA180002 (l) [6]
120 mg, po, tab, bid, md (B7D)	Dasatinib	85.07	140.79	0.60	378.38	503.90	0.75	Study CA180002 (m) [6]
140 mg, po, tab, qd, md (Q5D)	Dasatinib	80.35	43.84	1.83	360.80	278.94	1.29	Study CA180002 (n) [6]
180 mg, po, tab, qd, md (Q5D)	Dasatinib	182.78	211.15	0.87	868.30	1086.35	0.80	Study CA180002 (o) [6]
70 mg, po, tab, bid, md (B5D)	Dasatinib	68.62	78.02	0.88	187.28	283.48	0.66	Study CA180005 (a) [6]
70 mg, po, tab, bid, md (B7D)	Dasatinib	68.62	43.92	1.56	186.53	182.88	1.02	Study CA180005 (b) [6]
100 mg, po, tab, qd, md	Dasatinib	113.21	246.31	0.46	15399.80	3590.79	4.29	Takahashi 2011 (a) [17]
150 mg, po, tab, qd, md	Dasatinib	173.08	252.88	0.68	21560.86	42110.33	0.51	Takahashi 2011 (b) [17]
200 mg, po, tab, qd, md	Dasatinib	196.19	219.58	0.89	28503.51	32382.36	0.88	Takahashi 2011 (c) [17]
100 mg, po, tab, qd, sd	Dasatinib	130.21	83.05	1.57	419.24	370.40	1.13	Zwaan 2013 (a) [12]
140 mg, po, tab, qd, sd	Dasatinib	173.94	117.30	1.48	583.41	485.17	1.20	Zwaan 2013 (b) [12]
170 mg, po, tab, qd, sd	Dasatinib	202.39	228.72	0.88	688.11	1174.63	0.59	Zwaan 2013 (c) [12]
200 mg, po, tab, qd, sd	Dasatinib	226.89	133.54	1.70	789.00	613.16	1.29	Zwaan 2013 (d) [12]

GMFE: 1.29 (1.01–2.18)      GMFE: 1.27 (1.00–4.29)  
 GMFE ≤ 2: 52/53      GMFE ≤ 2: 51/53

**AUC<sub>last</sub>**: area under the plasma concentration–time curve from the first to the last time point of measurement, **B5D**: five consecutive days bid dosing followed by two nontreatment days, **B7D**: continuous bid dosing, **bid**: twice a day, **C<sub>max</sub>**: maximum plasma concentration, **DFI**, drug–food interaction, **md**: multiple dose, **Obs**: observed, **PFOS**: powder for oral suspension, **po**: peroral, **Pred**: predicted, **Q5D**: five consecutive days once daily dosing followed by two nontreatment days, **qd**: once a day, **sd**: single dose, **sol**: solution, **tab**: tablet

## S2.3.2 Mean Relative Deviation (MRD)

**Table S6:** Mean relative deviation (MRD) values of dasatinib plasma concentration predictions.

Administration	Compound	Health Status	MRD	Reference
140 mg, po, tab, sd	Dasatinib	Healthy	1.36	Bioequivalence study [13]
100 mg, po, sol, sd	Dasatinib	Healthy	1.54	Christopher 2008 (a) [7]
50 mg, po, tab, bid, md	Dasatinib	Healthy	1.43	Eley 2009 (control) [50]
100 mg, po, tab, sd	Dasatinib	Healthy	1.18	Furlong 2012 [14]
100 mg, po, tab, sd	Dasatinib	Healthy	1.37	Yago 2014 (control) [51]
100 mg, po, tab, sd	Dasatinib	Healthy	1.29	Study CA180009 (at fasted state (a)) [6]
100 mg, po, tab, sd	Dasatinib	Healthy	1.34	Study CA180009 (with high-fat meal (b)) [6]
100 mg, po, tab, sd	Dasatinib	Healthy	1.15	Study CA180009 (with light-fat meal (c)) [6]
100 mg, po, tab, sd	Dasatinib	Healthy	1.25	Study CA180016 [6]
100 mg, po, tab, sd	Dasatinib	Healthy	1.28	Study CA180032 (control) [6]
70 mg, po, tab, sd	Dasatinib	Healthy	1.31	Vaidhyanathan 2018 (a) [8]
100 mg, po, PFOS, sd	Dasatinib	Healthy	1.26	Vaidhyanathan 2018 (b) [8]
100 mg, po, dispersed tab, sd	Dasatinib	Healthy	1.32	Vaidhyanathan 2018 (c) [8]
100 mg, po, tab, sd	Dasatinib	Healthy	1.60	Vaidhyanathan 2018 (d) [8]
100 mg, po, tab, sd	Dasatinib	Healthy	1.63	Vargas 2016 [9]
100 mg, po, tab, qd, md	Dasatinib	Cancer	2.07	Araujo 2012 [15]
180 mg, po, tab, sd	Dasatinib	Cancer	2.01	Christopher 2008 (b) [7]
35 mg, po, tab, bid, md (B5D)	Dasatinib	Cancer	1.35	Demetri 2009 (a) [16]
50 mg, po, tab, bid, md (B5D)	Dasatinib	Cancer	1.49	Demetri 2009 (b) [16]
70 mg, po, tab, bid, md (B5D)	Dasatinib	Cancer	1.91	Demetri 2009 (c) [16]
70 mg, po, tab, bid, md (B7D)	Dasatinib	Cancer	1.26	Demetri 2009 (d) [16]
90 mg, po, tab, bid, md (B5D)	Dasatinib	Cancer	1.21	Demetri 2009 (e) [16]
90 mg, po, tab, bid, md (B7D))	Dasatinib	Cancer	1.19	Demetri 2009 (f) [16]
100 mg, po, tab, bid, md (B7D)	Dasatinib	Cancer	1.30	Demetri 2009 (g) [16]
120 mg, po, tab, bid, md (B5D)	Dasatinib	Cancer	1.44	Demetri 2009 (h) [16]
120 mg, po, tab, bid, md (B7D)	Dasatinib	Cancer	2.89	Demetri 2009 (i) [16]
160 mg, po, tab, bid, md (B5D)	Dasatinib	Cancer	1.66	Demetri 2009 (j) [16]
20 mg, po, tab, sd	Dasatinib	Cancer	1.64	Johnson 2010 (control) [52]
90 mg, po, tab, bid, md	Dasatinib	Cancer	1.24	Luo 2008 [10]
15 mg, po, tab, qd, md (Q5D)	Dasatinib	Cancer	1.21	Study CA180002 (a) [6]
25 mg, po, tab, bid, md (B5D)	Dasatinib	Cancer	1.13	Study CA180002 (b) [6]
30 mg, po, tab, qd, md (Q5D)	Dasatinib	Cancer	1.24	Study CA180002 (c) [6]
35 mg, po, tab, bid, md (B5D)	Dasatinib	Cancer	1.22	Study CA180002 (d) [6]
50 mg, po, tab, bid, md (B5D)	Dasatinib	Cancer	1.67	Study CA180002 (e) [6]
50 mg, po, tab, bid, md (B7D)	Dasatinib	Cancer	1.19	Study CA180002 (f) [6]
50 mg, po, tab, qd, md (Q5D)	Dasatinib	Cancer	1.33	Study CA180002 (g) [6]
70 mg, po, tab, bid, md (B5D)	Dasatinib	Cancer	1.37	Study CA180002 (h) [6]
70 mg, po, tab, bid, md (B7D)	Dasatinib	Cancer	1.30	Study CA180002 (i) [6]
75 mg, po, tab, qd, md (Q5D)	Dasatinib	Cancer	1.25	Study CA180002 (j) [6]
90 mg, po, tab, bid, md (B7D)	Dasatinib	Cancer	1.28	Study CA180002 (k) [6]
105 mg, po, tab, qd, md (Q5D)	Dasatinib	Cancer	1.47	Study CA180002 (l) [6]
120 mg, po, tab, bid, md (B7D)	Dasatinib	Cancer	1.42	Study CA180002 (m) [6]
140 mg, po, tab, qd, md (Q5D)	Dasatinib	Cancer	1.53	Study CA180002 (n) [6]
180 mg, po, tab, qd, md (Q5D)	Dasatinib	Cancer	1.34	Study CA180002 (o) [6]
70 mg, po, tab, bid, md (B5D)	Dasatinib	Cancer	1.89	Study CA180005 (a) [6]
70 mg, po, tab, bid, md (B7D)	Dasatinib	Cancer	1.36	Study CA180005 (b) [6]
100 mg, po, tab, qd, md	Dasatinib	Cancer	1.58	Takahashi 2011 (a) [17]
150 mg, po, tab, qd, md	Dasatinib	Cancer	2.08	Takahashi 2011 (b) [17]
200 mg, po, tab, qd, md	Dasatinib	Cancer	1.72	Takahashi 2011 (c) [17]

(continued)

**Table S6:** Mean relative deviation (MRD) values of dasatinib plasma concentration predictions (*continued*).

Study	Compound	Health Status	MRD	Reference
100 mg, po, tab, qd, sd	Dasatinib	Cancer	1.84	Zwaan 2013 (a) [12]
140 mg, po, tab, qd, sd	Dasatinib	Cancer	2.00	Zwaan 2013 (b) [12]
170 mg, po, tab, qd, sd	Dasatinib	Cancer	1.78	Zwaan 2013 (c) [12]
200 mg, po, tab, qd, sd	Dasatinib	Cancer	1.81	Zwaan 2013 (d) [12]
<b>Overall MRD: 1.54 (1.13–2.89)</b>				
<b>49/53 MRD <math>\leq 2</math></b>				

**B5D:** five consecutive days bid dosing followed by two nontreatment days, **B7D:** continuous bid dosing, **bid:** twice a day, **DFI:** drug–food interaction, **md:** multiple dose, **PFOS:** powder for oral suspension, **po:** peroral, **Q5D:** five consecutive days once daily dosing followed by two nontreatment days, **qd:** once a day, **sd:** single dose, **sol:** solution, **tab:** tablet

## S2.4 Local Sensitivity Analysis

### S2.4.1 Mathematical Implementation

A sensitivity analysis was conducted by calculating the impact of single parameter changes (local sensitivity analysis) on the predicted  $AUC_{inf}$ . Here, the relative change of  $AUC_{inf}$  at steady-state after peroral administration of 100 mg dasatinib daily to the relative variation of model input parameters was calculated according to [Equation S1](#). Parameters were included in the sensitivity analysis, if they were optimized (I), assumed to affect  $AUC_{inf}$  (II) or might have a strong impact due to their use in the calculation of permeabilities or partition coefficients (III). A relative perturbation of 1000% (variation range 10.0, maximum number of 9 steps) was utilized. Parameters were considered sensitive if their sensitivity value was equal or greater than  $|0.5|$ . For instance, a sensitivity of  $+0.5$  implies that a 100% increase of the examined parameter value leads to a 50% increase of the simulated  $AUC_{inf}$ .

$$S = \frac{\Delta AUC_{inf}}{\Delta p} \cdot \frac{p}{AUC_{inf}} \quad (S1)$$

$S$  = sensitivity of the  $AUC_{inf}$  to the examined model parameter,  $\Delta AUC_{inf}$  = change of the  $AUC_{inf}$ ,  $AUC_{inf}$  = simulated  $AUC_{inf}$  with the original parameter value,  $p$  = original model parameter value,  $\Delta p$  = variation of the model parameter value

## S2.4.2 Results of the Sensitivity Analysis

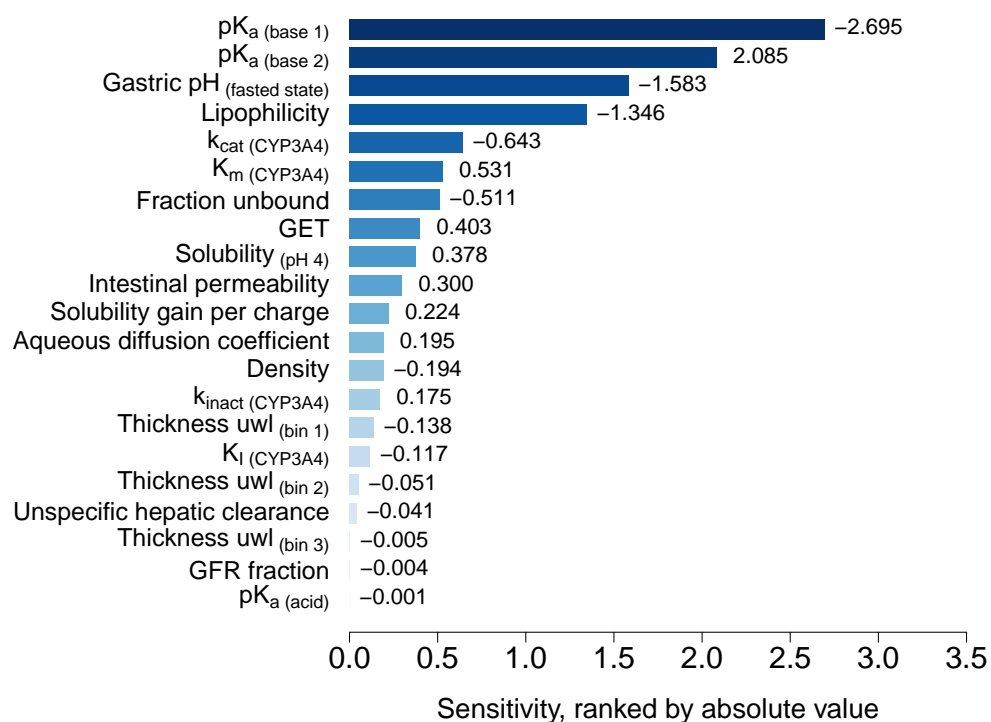


**Figure S7: Sensitivity analysis of the dasatinib PBPK model.** CYP: cytochrome P450, GET: gastric emptying time, GFR: glomerular filtration rate,  $k_{cat}$ : catalytic rate constant,  $K_I$ : inhibition constant,  $k_{inact}$ : maximum rate of inactivation,  $K_m$ : Michaelis-Menten constant,  $pK_a$ : acid dissociation constant, uwl: unstirred water layer.

S3 PBPK Drug–Drug Interaction (DDI) Modeling  
S3.1 Clinical DDI Studies

Table S7: Overview of clinical study data from the literature used for DDI model development.

Clinical study	Dosing of Perpetrator Drug	Dosing of Victim Drug	Gastric pH	N	Females [%]	Age [years]	BMI [kg/m <sup>2</sup> ]	Health Status	Dataset
(a) Enzyme-mediated DDIs									
<i>Ketoconazole</i>									
Johnson 2010 (control) [52]	200 mg, tab, bid, md (D3–D8)	20 mg, tab, qd, md (D1–D8)	2.0 <sup>a</sup>	18	43	57.5 (23–80) <sup>b</sup>	-	-	cancer test
Johnson 2010 (DDI) [52]		20 mg, tab, qd, md (D1–D8)	2.0 <sup>a</sup>	18	43	57.5 (23–80) <sup>b</sup>	-	-	cancer training
<i>Rifampicin</i>									
Study CA180032 (control) [6]	600 mg, tab, qd, md (D2–D9) <sup>d</sup>	100 mg, tab, sd (D1) <sup>c</sup>	2.0 <sup>a</sup>	20	-	-	-	-	healthy test
Study CA180032 (DDI) [6]		100 mg, tab, sd (D8) <sup>c</sup>	2.0 <sup>a</sup>	20	-	-	-	-	healthy test
<i>Dasatinib</i>									
Study CA180022 (control) [6]	100 mg, tab, sd (D8)	80 mg, tab, sd (D1)	2.0 <sup>a</sup>	48	58	40 (18–50) <sup>e</sup>	25.8 (20.9–31.7) <sup>e</sup>	healthy	test
Study CA180022 (DDI) [6]		80 mg, tab, sd (D8)	2.0 <sup>a</sup>	48	58	40 (18–50) <sup>e</sup>	25.8 (20.9–31.7) <sup>e</sup>	healthy	test
(b) pH-dependent DDIs									
<i>Rabeprazole</i>									
Yago 2014 (control) [51]	20 mg, tab, bid, md (D1–D4) <sup>f</sup> 20 mg, tab, bid, md (D1–D4) <sup>f</sup> + 1500 mg BHCl	100 mg, tab, sd	0.6 (0.5–1.8) <sup>b</sup>	10	10	38 (23–59) <sup>e</sup>	- (21.6–29.1)	healthy	test
Yago 2014 (DDI (a)) [51]		100 mg, tab, sd (D4)	4.1 (2.8–5.2) <sup>e</sup>	10	10	38 (23–59) <sup>e</sup>	- (21.6–29.1)	healthy	test
Yago 2014 (DDI (b)) [51]		100 mg, tab, sd (D4) <sup>g</sup>	0.7 (0.5–3.6) <sup>e</sup>	10	10	38 (23–59) <sup>e</sup>	- (21.6–29.1)	healthy	test

-: unknown, **bid**: twice a day, **BHCI**: betaine hydrochloride, **BMI**: body mass index, **D**: day, **DDI**: drug–drug interaction, **md**: multiple dose, **N**: number of participants, **qd**: once a day, **sd**: single dose, **tab**: tablet

<sup>a</sup> Default value in PK-Sim® for fasted state [11]

<sup>b</sup> Median (range)

<sup>c</sup> Administration of 100 mg dasatinib at 9:00 AM

<sup>d</sup> Administration of 600 mg rifampicin at 9:00 PM

<sup>e</sup> Mean (range)

<sup>f</sup> Single dose rabeprazole at D4

<sup>g</sup> Dasatinib administration following five minutes after BHCI administration

<sup>h</sup> Dasatinib was administered two hours before and ten hours after famotidine intake, respectively

<sup>i</sup> Dasatinib was administered two hours after and concomitantly with Maalox®, respectively

Table S7: Overview of clinical study data from the literature used for DDI model development (continued).

Clinical study	Dosing of Perpetrator Drug	Dosing of Victim Drug	Gastric pH	N	Females [%]	Age [years]	BMI [kg/m <sup>2</sup> ]	Health Status	Dataset
<i>Famotidine</i>									
Eley 2009 (control) [50]									
Eley 2009 (DDI (a)) [50]	40 mg, tab, bid, md	Dasatinib 50 mg, tab, bid, md	2.0 <sup>a</sup>	22	0	29 (19–47) <sup>e</sup>	25.1 (18.8–29.6) <sup>e</sup>	healthy	training
		50 mg, tab, bid, md <sup>b</sup>	2.8 [53]	22	0	29 (19–47) <sup>e</sup>	25.1 (18.8–29.6) <sup>e</sup>	healthy	test
<i>Maalox®</i>									
Eley 2009 (control) [50]									
Eley 2009 (DDI (b)) [50]	30 ml, liquid, bid, md	Dasatinib 50 mg, tab, bid, md	2.0 <sup>a</sup>	22	0	29 (19–47) <sup>e</sup>	25.1 (18.8–29.6) <sup>e</sup>	healthy	training
		50 mg, tab, bid, md <sup>i</sup>	3.0 [54]	22	0	29 (19–47) <sup>e</sup>	25.1 (18.8–29.6) <sup>e</sup>	healthy	test

-: unknown, **bid**: twice a day, **BHCl**: betaine hydrochloride, **BMI**: body mass index, **D**: day, **DDI**: drug–drug interaction, **md**: multiple dose, **N**: number of participants, **qd**: once a day, **sd**: single dose, **tab**: tablet

<sup>a</sup> Default value in PK-Sim<sup>®</sup> for fasted state [11]  
<sup>b</sup> Median (range)  
<sup>c</sup> Administration of 100 mg dasatinib at 9:00 AM  
<sup>d</sup> Administration of 600 mg rifampicin at 9:00 PM  
<sup>e</sup> Mean (range)  
<sup>f</sup> Single dose rabeprazole at D4  
<sup>g</sup> Dasatinib administration following five minutes after BHCl administration  
<sup>h</sup> Dasatinib was administered two hours before and ten hours after famotidine intake, respectively  
<sup>i</sup> Dasatinib was administered two hours after and concomitantly with Maalox<sup>®</sup>, respectively



## S3.2 DDI Model Evaluation

### S3.2.1 Plasma Profiles of Enzyme-mediated DDIs (Semilogarithmic Scale)

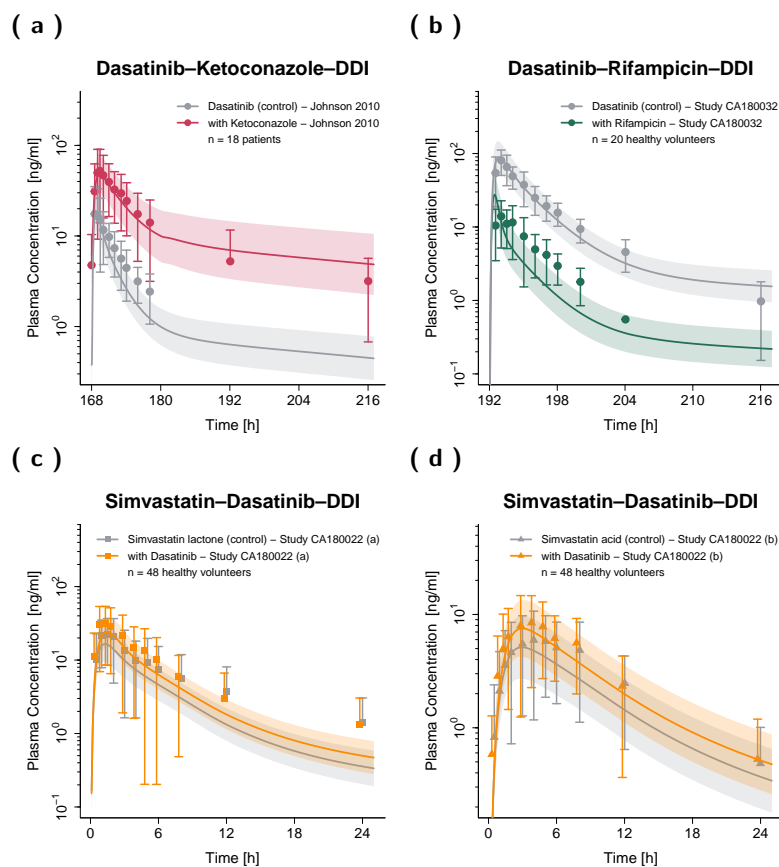


**Figure S8:** Predicted and observed plasma concentration–time profiles for enzyme-mediated DDIs with dasatinib acting as victim (a–b) and perpetrator drug (c–d) on a semilogarithmic scale. The solid lines show predicted geometric mean concentration–time profiles with and without intake of the perpetrator drug and ribbons show the corresponding geometric standard deviation of the population simulations ( $n=100$ ). Points depict mean observed data and corresponding standard deviation of dasatinib, while squares and triangles depict the observed data and corresponding standard deviation of simvastatin lactone and simvastatin acid, respectively. /: no information available, DDIs: drug–drug interactions,  $n$ : number of participants.

## S3.2.2 Plasma Profiles of pH-Dependent DDIs (Semilogarithmic Scale)

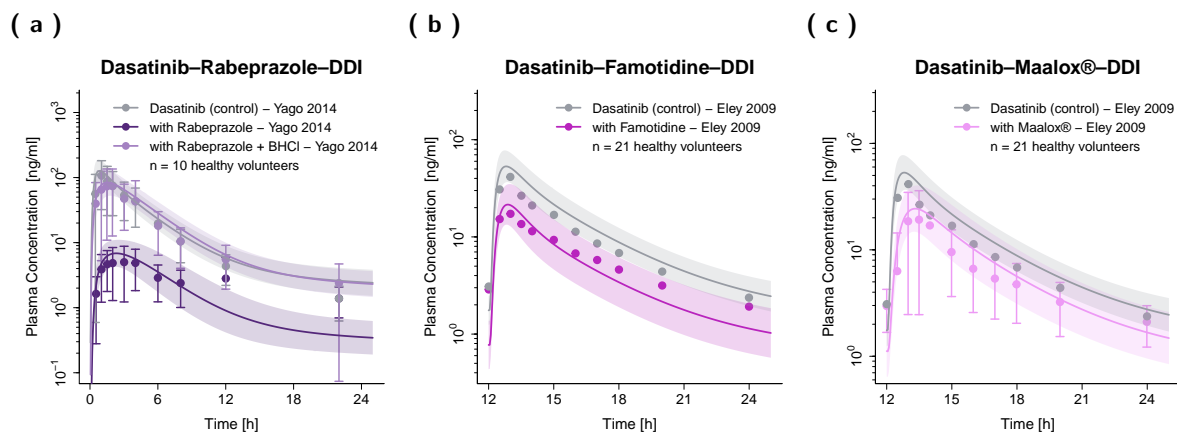


**Figure S9: Predicted and observed plasma concentration–time profiles for the pH-dependent DDIs on a semilogarithmic scale.** The solid lines show predicted geometric mean concentration–time profiles with and without the intake of perpetrator drug and ribbons show the corresponding geometric standard deviation of the population simulations (n=100). Points depict mean observed data and corresponding standard deviation of dasatinib (if depicted in the respective publication). **BHCl**: betaine hydrochloride, **DDIs**: drug–drug interactions, **n**: number of participants.

S3.2.3 Geometric Mean Fold Error (GMFE)

Table S8: Geometric Mean Fold Error (GMFE) of C<sub>max</sub> and AUC<sub>last</sub> DDI ratios.

Administration	Compound	C <sub>max</sub> DDI Ratio			AUC <sub>last</sub> DDI Ratio			Reference
		Pred [1]	Obs [1]	Pred/Obs	Pred [1]	Obs [1]	Pred/Obs	
Dasatinib–Ketoconazole–DDI	Dasatinib	2.17	2.99	0.73	9.14	7.65	1.19	Johnson 2010 [52]
Dasatinib–Rifampicin–DDI	Dasatinib	0.31	0.17	1.79	0.11	0.17	0.64	Study CA180032 [6]
Simvastatin–Dasatinib–DDI	Simvastatin lactone	1.48	1.38	1.07	1.47	1.23	1.20	Study CA180022 [6]
Simvastatin–Dasatinib–DDI	Simvastatin acid	1.52	1.43	1.06	1.45	1.19	1.22	Study CA180022 [6]
Dasatinib–Famotidine–DDI	Dasatinib	0.44	0.42	1.05	0.24	0.27	0.88	Eley 2009 [50]
Dasatinib–Maalox <sup>®</sup> –DDI	Dasatinib	0.45	0.46	0.97	0.31	0.28	1.09	Eley 2009 [50]
Dasatinib–Rabeprazole–DDI	Dasatinib	0.05	0.05	1.16	0.10	0.15	0.68	Yago 2014 [51]
Dasatinib–Rabeprazole–BHCI–DDI	Dasatinib	0.66	0.69	0.95	1.02	0.92	1.10	Yago 2014 [51]
		GMFE: 1.18 (1.03–1.79)			GMFE: 1.24 (1.09–1.57)			
		GMFE ≤ 2: 08/08			GMFE ≤ 2: 08/08			
		Guest limits: 08/08			Guest limits: 08/08			

AUC<sub>last</sub>: area under the plasma concentration–time curve from the first to the last time point of measurement, BHCl: betaine hydrochloride,  
C<sub>max</sub>: maximum plasma concentration, DDI: drug–drug interaction, Obs: observed, Pred: predicted

## S4 PBPK Drug–Food Interaction (DFI) Modeling

### S4.1 DFI Model Building

Studies have shown that the intake of both light and high-fat meals only marginally influences the pharmacokinetics (PK) of dasatinib. During light-fat meal ingestion, the maximum concentration ( $C_{\max}$ ) and area under the concentration–time curve (AUC) increased by 22% and 21%, respectively. The time to peak concentration ( $T_{\max}$ ) remained unaffected. In contrast, high-fat meal consumption led to a 24% decrease in  $C_{\max}$  and a 14% increase in AUC, along with a one-hour delay in  $T_{\max}$ , when compared to a fasted state [6]. The plasma concentration–time profiles of the DFI study investigating dasatinib exposure in the fasted state, after light-fat and high-fat breakfast were included in the model development (Table S9). The observed dasatinib data during ingestion of a light-fat meal (which only slightly impacted the PK of dasatinib) could be well predicted using the dasatinib model parameters of the fasted state, while the delay in  $T_{\max}$  after a high-fat meal intake could be covered by prolonging the gastric emptying time from 15.0 minutes (default setting in PK-Sim® for the fasted state) to 103.4 minutes.

#### S4.1.1 Clinical DFI Studies

**Table S9:** Overview of clinical study data from the literature used for DFI model development.

Clinical study	Dosing of dasatinib		Meal	N	Females [%]	Age [years]	BMI [kg/m <sup>2</sup> ]	Health Status	Dataset
Study CA180009 (control)) [6]	100 mg, tab, qd, sd		Fasted state	48	-	-	-	healthy	test
Study CA180009 (DFI (a)) [6]	100 mg, tab, qd, sd	Light breakfast (319 kcal)		48	-	-	-	healthy	test
Study CA180009 (DFI (b)) [6]	100 mg, tab, qd, sd	High-fat breakfast (985 kcal)		48	-	-	-	healthy	test

**BMI:** body mass index, **D:** day, **DFI:** drug–food interaction, **N:** number of subjects, **qd:** once a day, **sd:** single dose, **tab:** tablet

## S4.2 DFI Model Evaluation

### S4.2.1 Plasma Profiles And Goodness-of-Fit Plot of DFIs

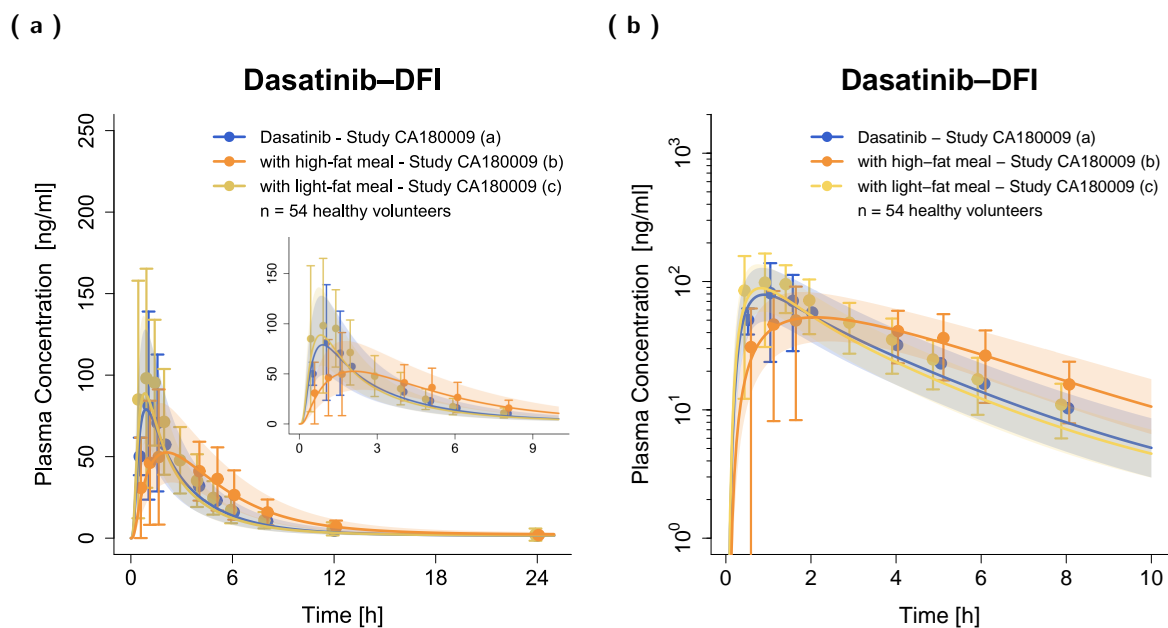


**Figure S10: Predicted and observed plasma concentration–time profiles for the DFIs.** Blue, yellow and orange lines show predicted geometric mean concentration–time profiles at fasted state, after light-fat and after high-fat breakfast, respectively. Ribbons show the corresponding geometric standard deviation of the population simulations ( $n=100$ ). Points depict mean observed data and corresponding standard deviation of dasatinib. **DFI:** drug–food interaction, **n:** number of participants.

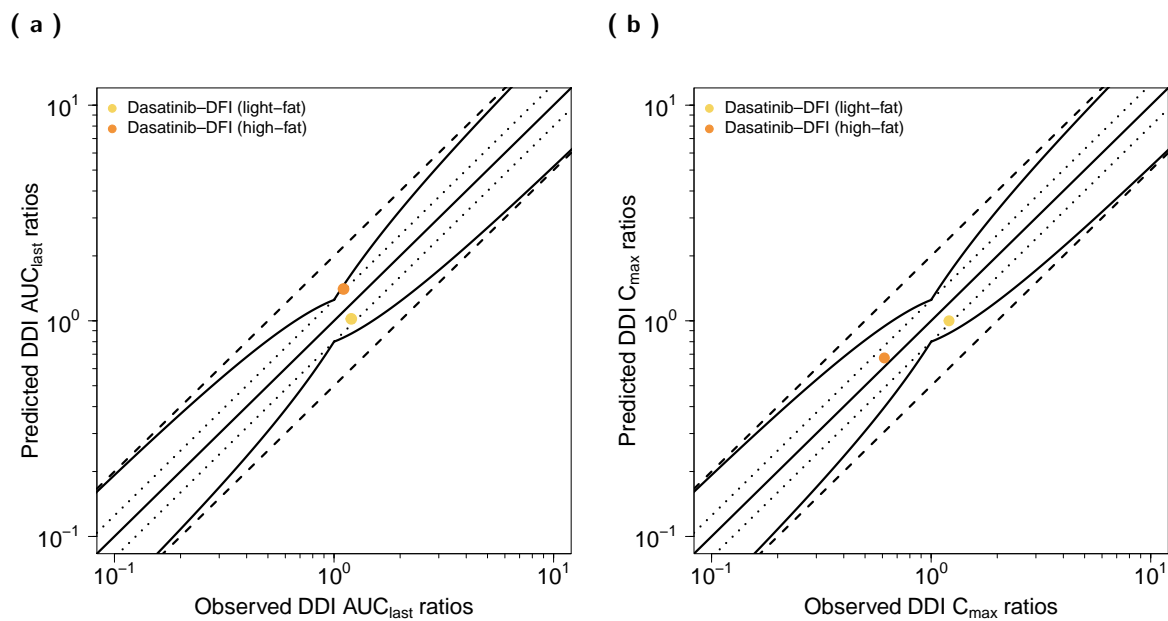


**Figure S11: Predicted versus observed DFI  $AUC_{last}$  ratios (a) and DFI  $C_{max}$  ratios (b) of dasatinib.** The straight solid lines mark the lines of identity, the curved lines show the limits of the predictive measure proposed by Guest et al. with 1.25-fold variability [55]. Dotted lines indicate 1.25-fold and dashed lines two-fold deviation.  $AUC_{last}$ : area under the plasma concentration–time curve from the first to the last time point of measurement,  $C_{max}$ : maximum plasma concentration, **DFI**: drug–food interaction.

S4.2.2 Geometric Mean Fold Error (GMFE)

Table S10: Geometric Mean Fold Error (GMFE) of C<sub>max</sub> and AUC<sub>last</sub> DFI ratios.

Administration	Compound	C <sub>max</sub> DFI Ratio			AUC <sub>last</sub> DFI Ratio			Reference
		Pred [1]	Obs [1]	Pred/Obs	Pred [1]	Obs [1]	Pred/Obs	
100 mg, po, tab, sd	Dasatinib	0.67	0.61	1.10	1.40	1.10	1.27	Study CA180009 (b) [6]
100 mg, po, tab, sd	Dasatinib	1.00	1.21	0.83	1.02	1.20	0.85	Study CA180009 (c) [6]
<b>GMFE: 1.15 (1.21–1.10)</b>								
<b>GMFE ≤ 2: 02/02</b>								
<b>Guest limits: 02/02</b>								
<b>GMFE: 1.22 (1.17–1.27)</b>								
<b>GMFE ≤ 2: 02/02</b>								
<b>Guest limits: 02/02</b>								

AUC<sub>last</sub>: area under the plasma concentration–time curve from the first to the last time point of measurement,  
C<sub>max</sub>: maximum plasma concentration, DFI, drug–food interaction, Obs: observed, Pred: predicted



## S5 Model Application & Others

### S5.1 Exposure Simulations for Model-Informed Precision Dosing

The developed PBPK model of dasatinib was coupled with previously published PBPK models of carbamazepine [56] (version 11), clarithromycin [24] (version 11), efavirenz [56, 57] (version 11), erythromycin [25] (version 11), fluconazole [20] (version 11), fluvoxamine [58] (version 11), grapefruit juice [59] (version 11), itraconazole [24] (version 11), ketoconazole [60] (version 11), rifampicin [24] (version 11), simvastatin [21] (version 9) and voriconazole [61] (version 11). The drug-dependent parameters of the compounds were adapted from the respective publications. Modifications of drug-dependent parameters are shown in Table S11.

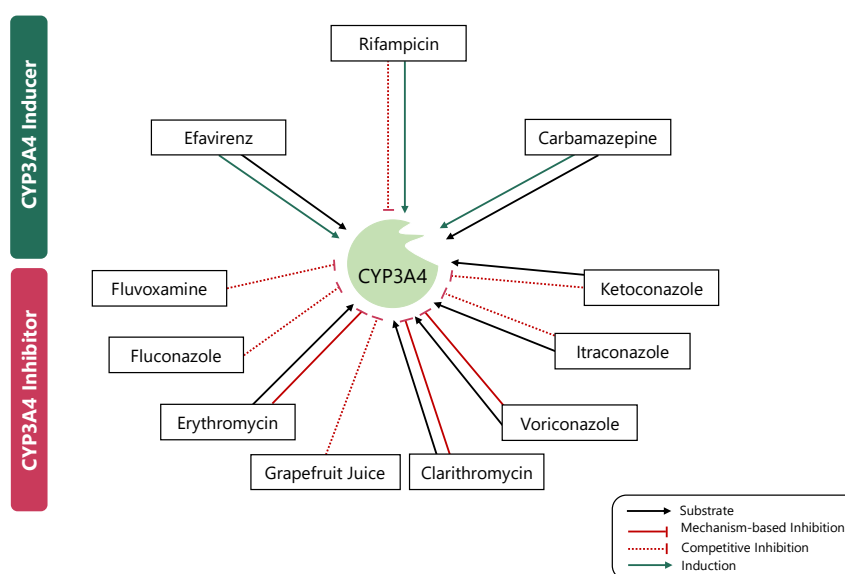


**Figure S12: Overview of investigated DDI scenarios.** The developed dasatinib PBPK model was coupled with previously published PBPK perpetrator models of clarithromycin, erythromycin, fluconazole, fluvoxamine, grapefruit juice, itraconazole, ketoconazole and voriconazole as CYP3A4 inhibitors as well as of carbamazepine, efavirenz and rifampicin as CYP3A4 inducers. **DDI**: drug–drug interaction, **PBPK**: physiologically based pharmacokinetic.

**Table S11:** Modified drug-dependent parameters of the PBPK models from the literature.

PBPK model	Modified parameter	Published parameter	Reason for Modification
Efavirenz [56, 57]	modified according to [56]	see [57]	-
Erythromycin [25]	OATP1B1 $k_{cat}$ = 19.29 1/min	OATP1B1 $k_{cat}$ = 1.35 1/min	Different OATP1B1 ref. conc.
Rifampicin [24]	OATP1B1 $k_{cat}$ = 74.43 1/min	OATP1B1 $k_{cat}$ = 5.21 1/min	Different OATP1B1 ref. conc.
Simvastatin [21]	OATP1B1 $k_{cat}$ = 146.41 1/min	OATP1B1 $k_{cat}$ = 10.25 1/min	Different OATP1B1 ref. conc.

$k_{cat}$ : catalytic rate constant, **OATP**: organic anion transporting polypeptide, **ref. conc.**: reference concentration

**Table S12:** Overview of model-based dose adaptations for dasatinib within various DDI scenarios based on the exposure matching principle.

Perpetrator	Dosing of Perpetrator	Dosing of Dasatinib	AUC <sub>ss</sub> Ratio <sup>1</sup>	AUC <sub>ss</sub> Ratio <sup>2</sup> (adapted)	Adapted Dasatinib Dose
<b>Strong CYP3A4 Inhibitors</b>					
Clarithromycin	250 mg, bid	100 mg, qd	1.85	0.99	50 mg, qd
	250 mg, bid	140 mg, qd	1.76	0.96	70 mg, qd
Clarithromycin	500 mg, bid	100 mg, qd	3.37	1.11	30 mg, qd
	500 mg, bid	140 mg, qd	3.21	1.05	40 mg, qd
Itraconazole (fed state)	200 mg, bid	100 mg, qd	4.59	1.03	20 mg, qd
	200 mg, bid	140 mg, qd	4.36	1.09	30 mg, qd
Ketoconazole	200 mg, bid	100 mg, qd	3.75	0.84	20 mg, qd
	200 mg, bid	140 mg, qd	3.59	0.88	30 mg, qd
Voriconazole	400 mg, qd (D1) + 200 mg, bid	100 mg, qd	3.01	0.98	30 mg, qd
	400 mg, qd (D1) + 200 mg, bid	140 mg, qd	2.87	0.93	40 mg, qd
<b>Moderate CYP3A4 Inhibitors</b>					
Erythromycin	500 mg, tid	100 mg, qd	2.12	0.93	40 mg, qd
	500 mg, tid	140 mg, qd	1.84	0.97	60 mg, qd
Erythromycin	500 mg, qid	100 mg, qd	2.31	1.01	40 mg, qd
	500 mg, qid	140 mg, qd	2.19	1.05	60 mg, qd
Fluconazole	200 mg, qd	100 mg, qd	2.11	1.09	50 mg, qd
	200 mg, qd	140 mg, qd	2.04	0.93	60 mg, qd
Fluconazole	400 mg, qd	100 mg, qd	2.70	0.87	30 mg, qd
	400 mg, qd	140 mg, qd	2.59	1.01	50 mg, qd
Fluvoxamine (+0 h)	100 mg, qd	100 mg, qd	1.15	1.04	90 mg, qd
	100 mg, qd	140 mg, qd	1.12	0.98	120 mg, qd

-: Dose adaptations could not be provided, **AUC<sub>ss</sub>**: steady state area under the concentration–time curve, **bid**: twice a day, **D**: day, **IR**: immediate release, **qd**: once daily, **qid**: four times a day, **sd**: single dose, **tab**: tablet, **tid**: three times a day

<sup>1</sup> AUC<sub>ss</sub> Ratio was calculated dividing AUC<sub>ss</sub> of the DDI setting (with 100 or 140 mg dasatinib) by the corresponding AUC<sub>ss</sub> of the control scenario.

<sup>2</sup> AUC<sub>ss</sub> Ratio (adapted) was calculated dividing AUC<sub>ss</sub> of the DDI setting using the model-based adapted dose of dasatinib by the corresponding AUC<sub>ss</sub> of the control scenario.

<sup>3</sup> Rifampicin is also a weak CYP3A4 inhibitor; administrations were simulated to be concomitantly with dasatinib administrations.

**Table S12:** Overview of model-based dose adaptations for dasatinib within various DDI scenarios based on the exposure matching principle.

Perpetrator	Dosing of Perpetrator	Dosing of Dasatinib	AUC <sub>ss</sub> Ratio	AUC <sub>ss</sub> Ratio (adapted)	Adapted Dasatinib Dose
Fluoxamine (+12 h)	100 mg, qd	100 mg, qd	1.02	1.02	100 mg, qd
	100 mg, qd	140 mg, qd	1.02	1.02	140 mg, qd
Grapefruit Juice	250 ml, qd	100 mg, qd	1.40	1.02	70 mg, qd
	250 ml, qd	140 mg, qd	1.33	1.00	100 mg, qd
Grapefruit Juice	250 ml, sd	100 mg, qd	1.13	1.02	90 mg, qd
	250 ml, sd	140 mg, qd	1.10	1.03	130 mg, qd
<b>Strong CYP3A4 Inducers</b>					
Carbamazepine (IR tab, fed state)	400 mg, tid	100 mg, qd	0.30	1.01	250 mg, qd
	400 mg, tid	140 mg, qd	0.35	0.99	340 mg, qd
Rifampicin <sup>3</sup>	600 mg, qd	100 mg, qd	0.50	1.01	230 mg, qd
	600 mg, qd	140 mg, qd	0.48	1.00	360 mg, qd
<b>Moderate CYP3A4 Inducers</b>					
Efavirenz (+ 0 h)	600 mg, qd	100 mg, qd	0.34	0.99	240 mg, qd
	600 mg, qd	140 mg, qd	0.37	1.00	340 mg, qd
Efavirenz (+12 h)	600 mg, qd	100 mg, qd	0.23	1.00	310 mg, qd
	600 mg, qd	140 mg, qd	-	-	-

-: Dose adaptations could not be provided, **AUC<sub>ss</sub>**: steady state area under the concentration-time curve, **bid**: twice a day, **D**: day, **IR**: immediate release, **qd**: once daily, **qid**: four times a day, **sd**: single dose, **tab**: tablet, **tid**: three times a day

<sup>1</sup> AUC<sub>ss</sub> Ratio was calculated dividing AUC<sub>ss</sub> of the DDI setting (with 100 or 140 mg dasatinib) by the corresponding AUC<sub>ss</sub> of the control scenario.

<sup>2</sup> AUC<sub>ss</sub> Ratio (adapted) was calculated dividing AUC<sub>ss</sub> of the DDI setting using the model-based adapted dose of dasatinib by the corresponding AUC<sub>ss</sub> of the control scenario.

<sup>3</sup> Rifampicin is also a weak CYP3A4 inhibitor; administrations were simulated to be concomitantly with dasatinib administrations.

## S5.1.1 Plasma Profiles of Simulated Single DDI Scenarios

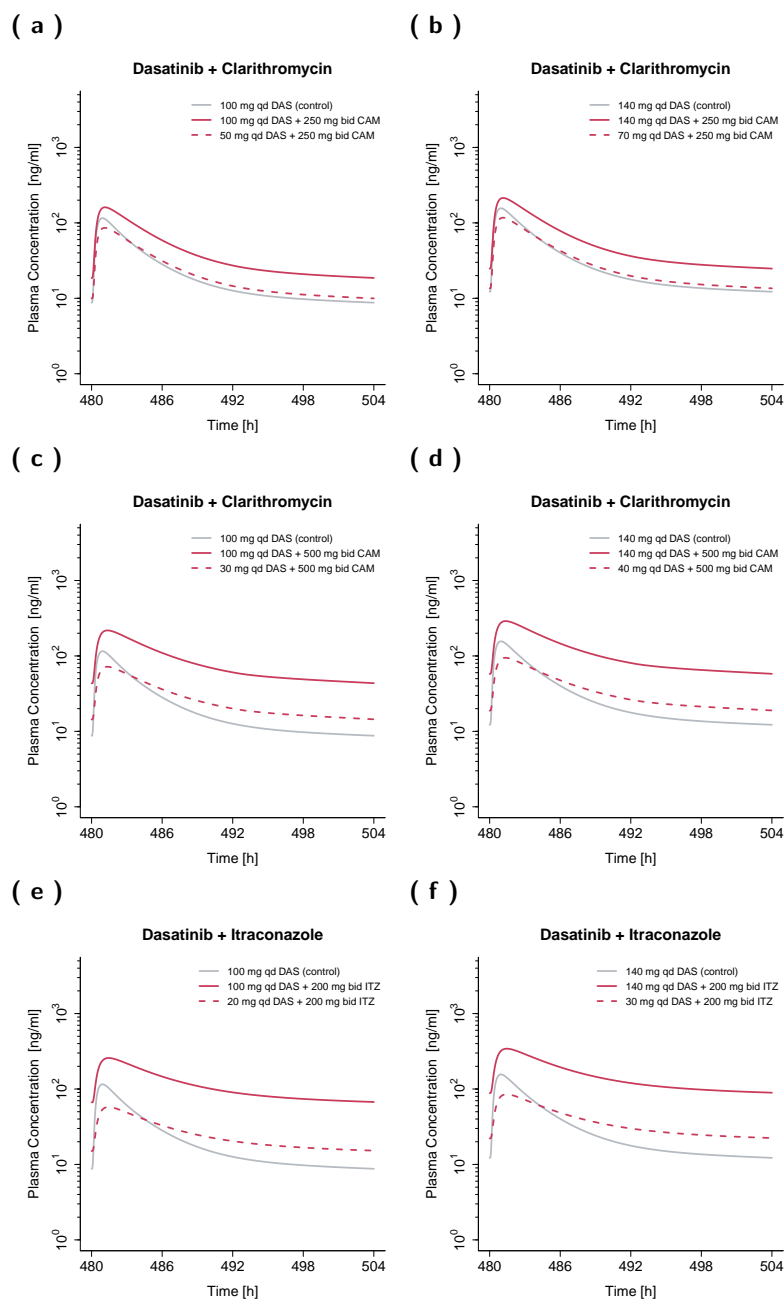


**Figure S13: Model-based dose adaptations for dasatinib within various single DDI scenarios including moderate and strong CYP3A4 inhibitors and inducers.** The first and second column represent the simulation results after administration of 100 mg and 140 mg dasatinib daily, respectively. Colored and grey solid lines show simulated mean concentration–time profiles with and without intake of a perpetrator drug, respectively. Dashed lines represent the simulated mean concentration–time profiles in presence of a perpetrator drug, using an adapted dose of dasatinib. **Bid**: twice a day, **CAM**: clarithromycin, **CBZ**: carbamazepine, **D**: day, **DAS**: dasatinib, **DDI**: drug–drug interaction, **EFV**: efavirenz, **ERY**: erythromycin, **FLV**: fluvoxamine, **FLZ**: fluconazole, **GFJ**: grapefruit juice, **ITZ**: itraconazole, **KCZ**: ketoconazole, **qd**: once a day, **qid**: four times a day, **RIF**: rifampicin, **sd**: single dose, **tid**: three times a day, **VRC**: voriconazole.

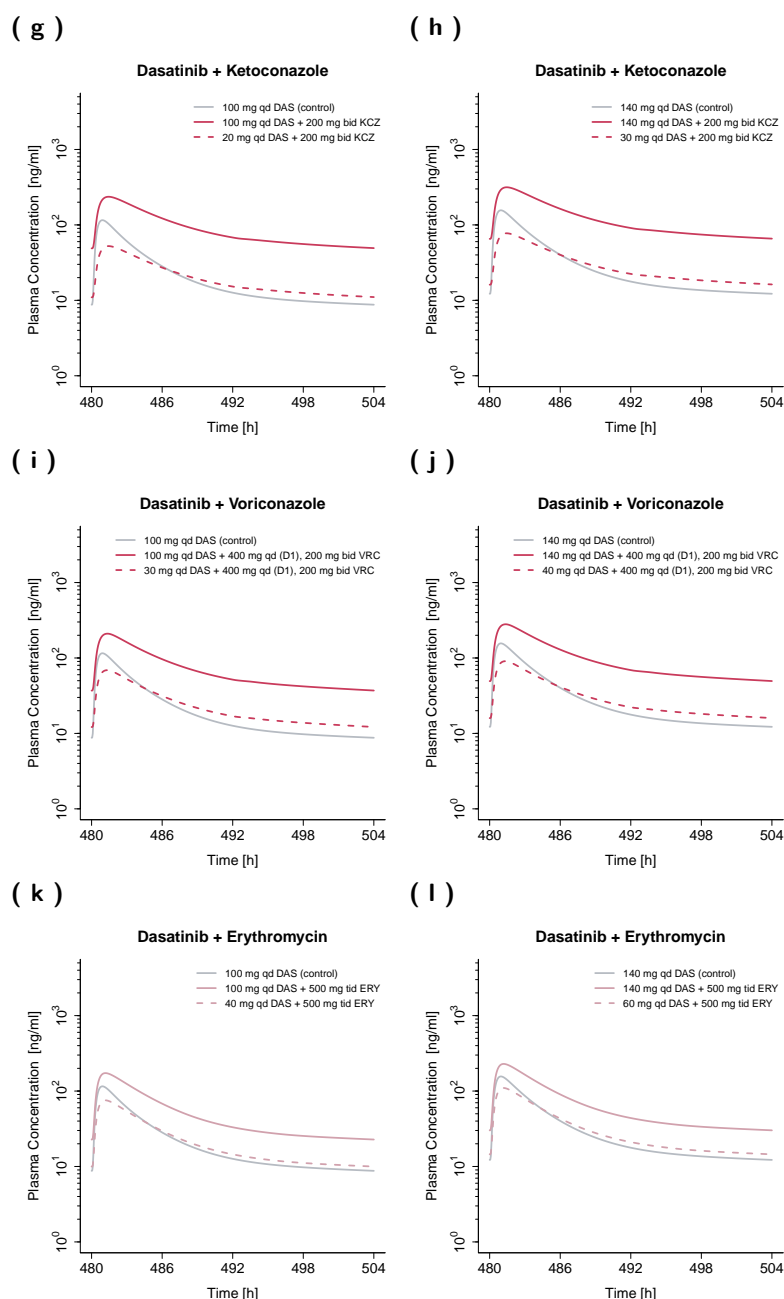


**Figure S13: (continued) Model-based dose adaptations for dasatinib within various single DDI scenarios including moderate and strong CYP3A4 inhibitors and inducers.** The first and second column represent the simulation results after administration of 100 mg and 140 mg dasatinib daily, respectively. Colored and grey solid lines show simulated mean concentration–time profiles with and without intake of a perpetrator drug, respectively. Dashed lines represent the simulated mean concentration–time profiles in presence of a perpetrator drug, using an adapted dose of dasatinib. **Bid:** twice a day, **CAM:** clarithromycin, **CBZ:** carbamazepine, **D:** day, **DAS:** dasatinib, **DDI:** drug–drug interaction, **EFV:** efavirenz, **ERY:** erythromycin, **FLV:** fluvoxamine, **FLZ:** fluconazole, **GFJ:** grapefruit juice, **ITZ:** itraconazole, **KCZ:** ketoconazole, **qd:** once a day, **qid:** four times a day, **RIF:** rifampicin, **sd:** single dose, **tid:** three times a day, **VRC:** voriconazole.

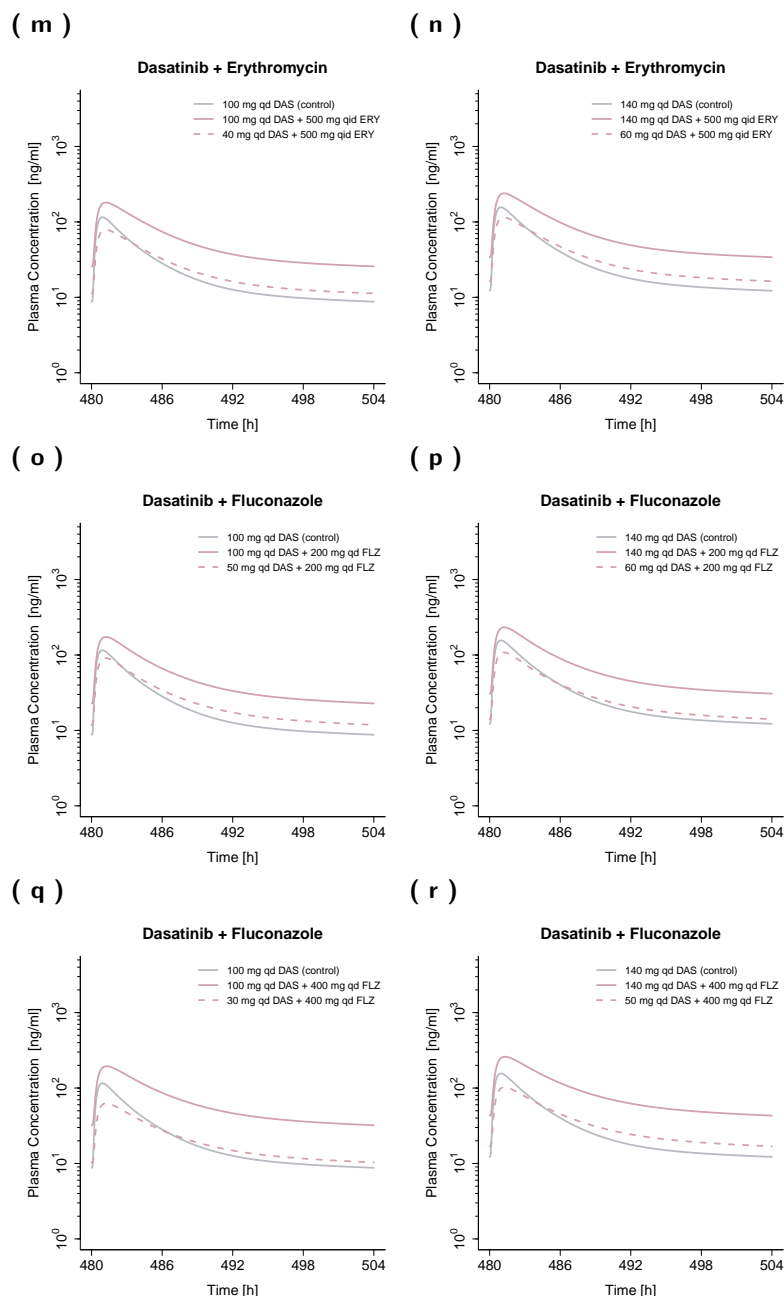


**Figure S13: (continued) Model-based dose adaptations for dasatinib within various single DDI scenarios including moderate and strong CYP3A4 inhibitors and inducers.** The first and second column represent the simulation results after administration of 100 mg and 140 mg dasatinib daily, respectively. Colored and grey solid lines show simulated mean concentration–time profiles with and without intake of a perpetrator drug, respectively. Dashed lines represent the simulated mean concentration–time profiles in presence of a perpetrator drug, using an adapted dose of dasatinib. **Bid:** twice a day, **CAM:** clarithromycin, **CBZ:** carbamazepine, **D:** day, **DAS:** dasatinib, **DDI:** drug–drug interaction, **EFV:** efavirenz, **ERY:** erythromycin, **FLV:** fluvoxamine, **FLZ:** fluconazole, **GFJ:** grapefruit juice, **ITZ:** itraconazole, **KCZ:** ketoconazole, **qd:** once a day, **qid:** four times a day, **RIF:** rifampicin, **sd:** single dose, **tid:** three times a day, **VRC:** voriconazole.

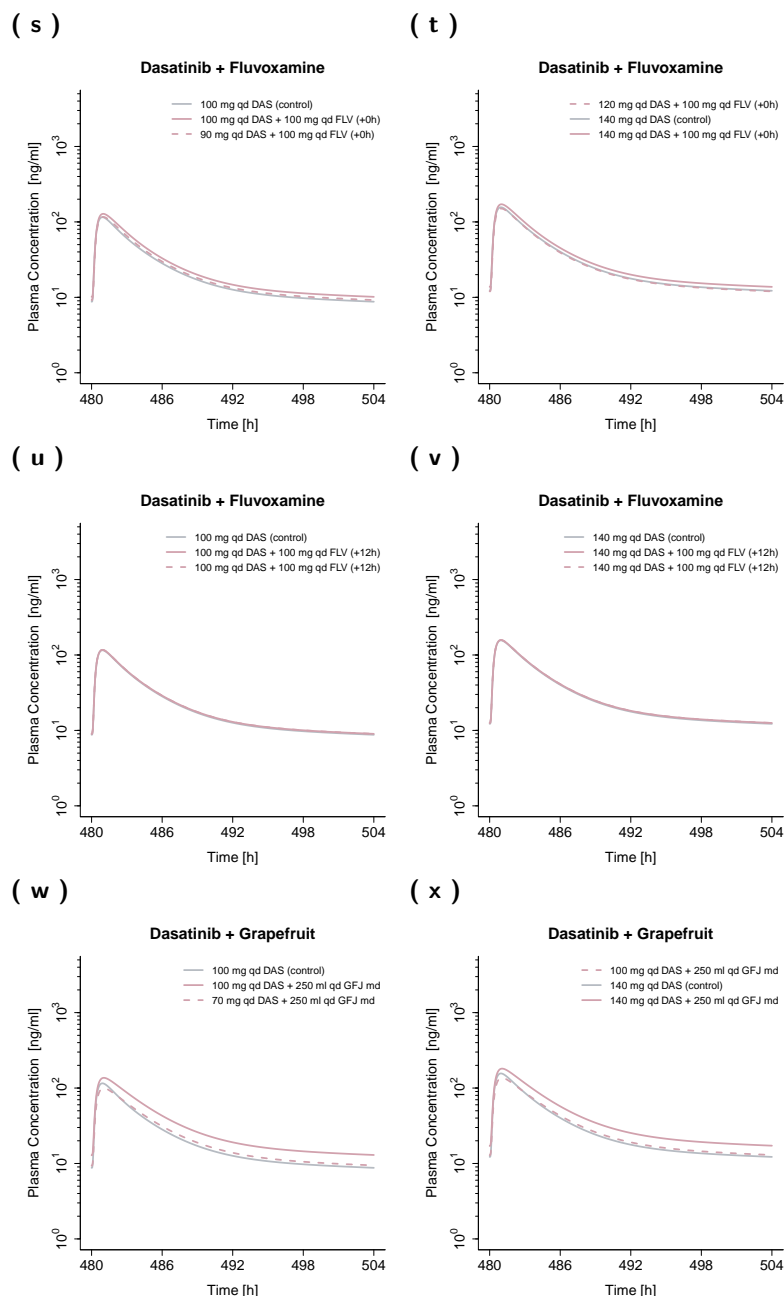


**Figure S13: (continued) Model-based dose adaptations for dasatinib within various single DDI scenarios including moderate and strong CYP3A4 inhibitors and inducers.** The first and second column represent the simulation results after administration of 100 mg and 140 mg dasatinib daily, respectively. Colored and grey solid lines show simulated mean concentration–time profiles with and without intake of a perpetrator drug, respectively. Dashed lines represent the simulated mean concentration–time profiles in presence of a perpetrator drug, using an adapted dose of dasatinib. **Bid:** twice a day, **CAM:** clarithromycin, **CBZ:** carbamazepine, **D:** day, **DAS:** dasatinib, **DDI:** drug–drug interaction, **EFV:** efavirenz, **ERY:** erythromycin, **FLV:** fluvoxamine, **FLZ:** fluconazole, **GFJ:** grapefruit juice, **ITZ:** itraconazole, **KCZ:** ketoconazole, **qd:** once a day, **qid:** four times a day, **RIF:** rifampicin, **sd:** single dose, **tid:** three times a day, **VRC:** voriconazole.



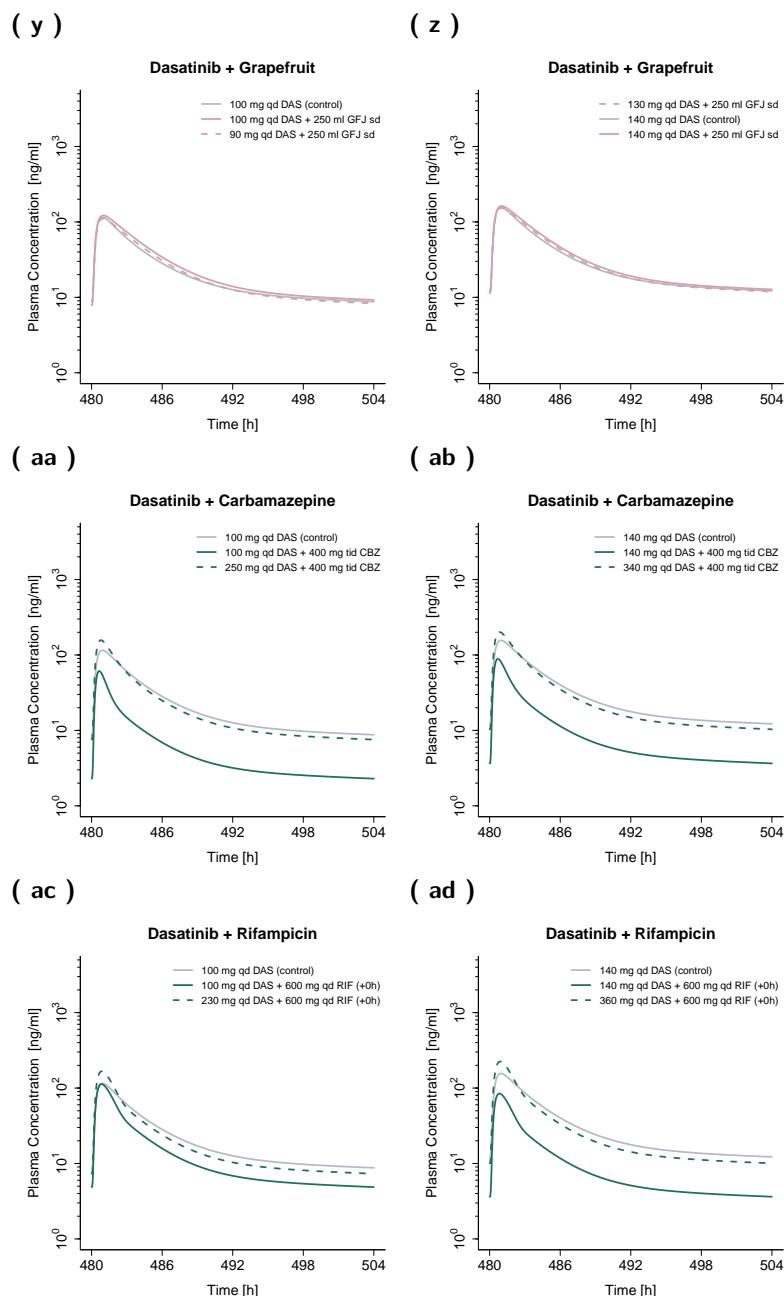


**Figure S13: (continued) Model-based dose adaptations for dasatinib within various single DDI scenarios including moderate and strong CYP3A4 inhibitors and inducers.** The first and second column represent the simulation results after administration of 100 mg and 140 mg dasatinib daily, respectively. Colored and grey solid lines show simulated mean concentration–time profiles with and without intake of a perpetrator drug, respectively. Dashed lines represent the simulated mean concentration–time profiles in presence of a perpetrator drug, using an adapted dose of dasatinib. **Bid:** twice a day, **CAM:** clarithromycin, **CBZ:** carbamazepine, **D:** day, **DAS:** dasatinib, **DDI:** drug–drug interaction, **EFV:** efavirenz, **ERY:** erythromycin, **FLV:** fluvoxamine, **FLZ:** fluconazole, **GFJ:** grapefruit juice, **ITZ:** itraconazole, **KCZ:** ketoconazole, **qd:** once a day, **qid:** four times a day, **RIF:** rifampicin, **sd:** single dose, **tid:** three times a day, **VRC:** voriconazole.

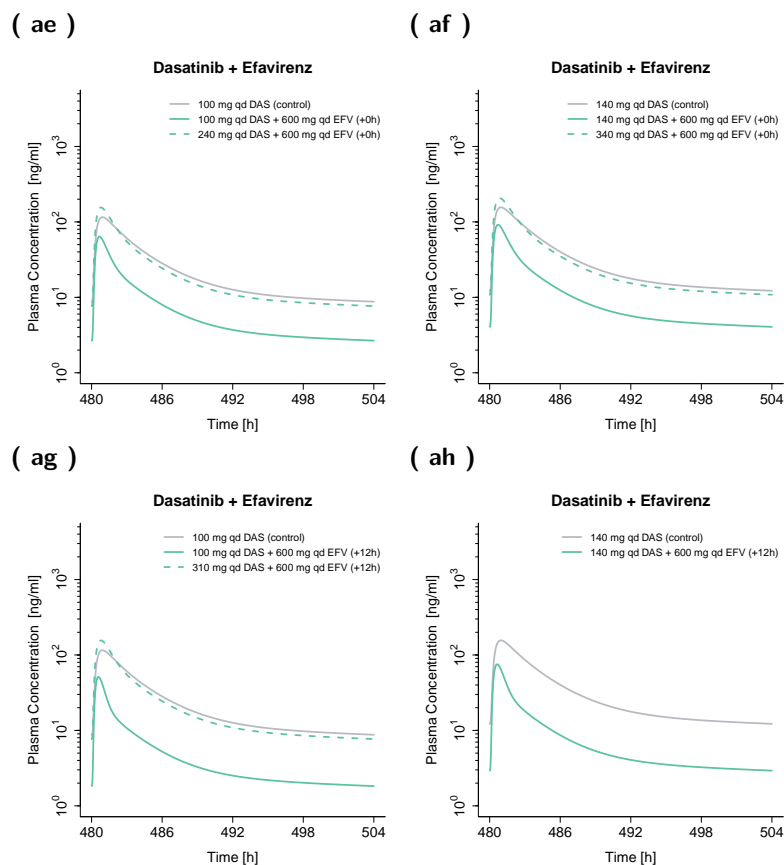


**Figure S13: (continued) Model-based dose adaptations for dasatinib within various single DDI scenarios including moderate and strong CYP3A4 inhibitors and inducers.** The first and second column represent the simulation results after administration of 100 mg and 140 mg dasatinib daily, respectively. Colored and grey solid lines show simulated mean concentration–time profiles with and without intake of a perpetrator drug, respectively. Dashed lines represent the simulated mean concentration–time profiles in presence of a perpetrator drug, using an adapted dose of dasatinib. **Bid:** twice a day, **CAM:** clarithromycin, **CBZ:** carbamazepine, **D:** day, **DAS:** dasatinib, **DDI:** drug–drug interaction, **EFV:** efavirenz, **ERY:** erythromycin, **FLV:** fluvoxamine, **FLZ:** fluconazole, **GFJ:** grapefruit juice, **ITZ:** itraconazole, **KCZ:** ketoconazole, **qd:** once a day, **qid:** four times a day, **RIF:** rifampicin, **sd:** single dose, **tid:** three times a day, **VRC:** voriconazole.

## S5.1.2 Plasma Profiles of Simulated Multiple DDI Scenarios

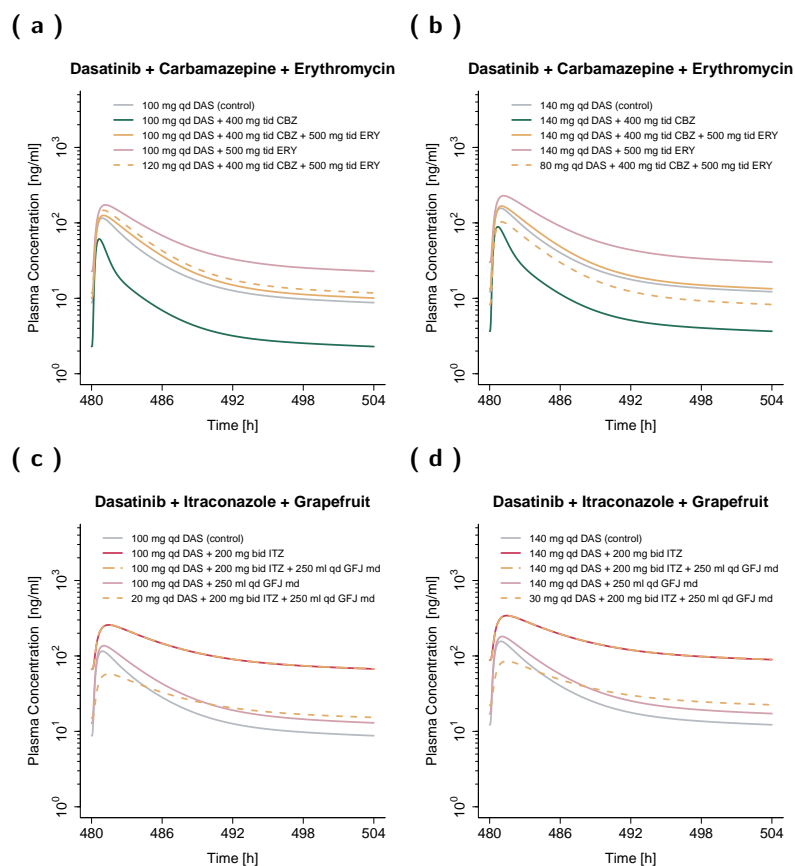


**Figure S14: Model-based dose adaptations for dasatinib within multiple DDIs.** The first and second column represent the simulation results after administration of 100 mg and 140 mg dasatinib daily, respectively. Colored and grey solid lines show simulated mean concentration–time profiles with and without intake of perpetrator drug(s), respectively. Dashed lines represent the simulated mean concentration–time profiles in presence of perpetrator drug(s), using an adapted dose of dasatinib. **Bid**: twice a day, **CBZ**: carbamazepine, **DAS**: dasatinib, **DDI**: drug–drug interaction, **ERY**: erythromycin, **GFJ**: grapefruit juice, **ITZ**: itraconazole, **qd**: once a day, **tid**: three times a day.

## S5.2 CYP3A4 Autoinhibition

Dasatinib exhibits time-dependent inhibition of CYP3A4 according to *in vitro* studies [44, 62] affecting the exposure of CYP3A4 substrates (e.g., simvastatin) [6], but also its own metabolism. CYP3A4 time-dependent inhibition by dasatinib results in a slight supra-proportional increase in exposure of 16% comparing area under the concentration–time curve (AUC) from zero to infinity after single dose administration and AUC steady state ( $AUC_{ss}$ ) (see Table S13). Moreover, the time-dependent inhibition showed no or only minor effects on the performed prospective DDI simulations with dasatinib as victim drug (e.g., no impact on  $AUC_{ss}$  during itraconazole DDI and 7% higher  $AUC_{ss}$  during fluvoxamine DDI).

**Table S13:** Impact of CYP3A4 autoinhibition on dasatinib exposure.

Dasatinib Dosing Regimen	$AUC_{inf}$	$AUC_{ss}$	$AUC_{ss}/AUC_{inf}$
20 mg, sd	0.19	-	1.07
20 mg, qd	-	0.20	1.07
100 mg, sd	1.06	-	1.16
100 mg, qd	-	1.24	1.16
140 mg, sd	1.51	-	1.15
140 mg, qd	-	1.73	1.15
360 mg, sd	3.09	-	1.11
360 mg, qd	-	3.42	1.11
420 mg, sd	3.26	-	1.10
420 mg, qd	-	3.58	1.10

$AUC_{inf}$ : area under the concentration–time curve from zero to infinity,

$AUC_{ss}$ : steady state area under the concentration–time curve,

CYP: cytochrome P450, qd: once a day, sd: single dose

## S5.3 Pharmacokinetic Parameters: Absolute Bioavailability, Fraction Absorbed, Fraction Metabolized, Fraction Escaping Gut Wall and Hepatic Elimination

**Table S14:** Overview of simulated  $F_a$ ,  $F_g$ ,  $F_h$ ,  $F_m$  and BA.

Dasatinib Dosing Regimen	$F_a$ (%)	$F_g$ (%)	$F_h$ (%)	$F_m$ (%)	BA (%)
20 mg, sd	80	47	64	94	24
100 mg, sd	69	64	63	93	28
140 mg, sd	65	68	63	92	28
360 mg, sd	45	79	62	91	22
420 mg, sd	41	79	62	90	20

BA: absolute bioavailability, CYP: cytochrome P450,  $F_a$ : fraction absorbed,

$F_g$ : fraction escaping gut wall elimination,  $F_h$ : fraction escaping hepatic elimination

$F_m$ : fraction metabolized via CYP3A4, sd: single dose

## References

- [1] National Center for Health Statistics (1997) Third National Health and Nutrition Examination Survey (NHANES III). Tech. rep., Hyattsville, MD 20782
- [2] American Cancer Society (2022) Cancer Facts and Figures. <https://www.cancer.org/cancer/chronic-myeloid-leukemia/about/statistics.html>, available online (accessed: 2023-02-01)
- [3] Valentin J (2002) Basic anatomical and physiological data for use in radiological protection: reference values. A report of age- and gender-related differences in the anatomical and physiological characteristics of reference individuals. ICRP Publication 89. *Annals of the ICRP* 32(3-4):5–265
- [4] Schlender J (2015) A report including the description of the physiology base of the Japanese population implemented in PK-Sim<sup>®</sup>. [https://github.com/Open-Systems-Pharmacology/OSPSuite.Documentation/blob/master/Japanese\\_Population/Report.md](https://github.com/Open-Systems-Pharmacology/OSPSuite.Documentation/blob/master/Japanese_Population/Report.md), available online (accessed: 2022-08-04)
- [5] Willmann S, Höhn K, Edginton A, Sevestre M, Solodenko J, Weiss W, Lippert J, Schmitt W (2007) Development of a physiology-based whole-body population model for assessing the influence of individual variability on the pharmacokinetics of drugs. *Journal of pharmacokinetics and pharmacodynamics* 34(3):401–31
- [6] Center for Drug Evaluation (2005) Clinical Pharmacology and Biopharmaceutics Review(s): NDA Review - Dasatinib. [https://www.accessdata.fda.gov/drugsatfda\\_docs/nda/2006/021986s000\\_Sprycel\\_ClinPharmR.pdf](https://www.accessdata.fda.gov/drugsatfda_docs/nda/2006/021986s000_Sprycel_ClinPharmR.pdf), available online (accessed: 2022-08-04)
- [7] Christopher LJ, Cui D, Wu C, Luo R, Manning JA, Bonacorsi SJ, Lago M, Allentoff A, Lee FYF, McCann B, Galbraith S, Reitberg DP, He K, Barros A, Blackwood-Chirchir A, Humphreys WG, Iyer RA (2008) Metabolism and disposition of dasatinib after oral administration to humans. *Drug metabolism and disposition: the biological fate of chemicals* 36(7):1357–64
- [8] Vaidhyanathan S, Wang X, Crison J, Varia S, Gao JZH, Saxena A, Good D (2019) Bioequivalence Comparison of Pediatric Dasatinib Formulations and Elucidation of Absorption Mechanisms Through Integrated PBPK Modeling. *Journal of pharmaceutical sciences* 108(1):741–749
- [9] Vargas M, Villarraga E (2016) Bioequivalence Study of Two Dasatinib 100 mg Formulations in Healthy Colombians. *Journal of Bioequivalence & Bioavailability* 09(01):302–305
- [10] Luo FR, Barrett YC, Yang Z, Camuso A, McGlinchey K, Wen ML, Smykla R, Fager K, Wild R, Palme H, Galbraith S, Blackwood-Chirchir A, Lee FY (2008) Identification and validation of phospho-SRC, a novel and potential pharmacodynamic biomarker for dasatinib (SPRYCEL), a multi-targeted kinase inhibitor. *Cancer chemotherapy and pharmacology* 62(6):1065–74
- [11] Willmann S, Schmitt W, Keldenich J, Lippert J, Dressman JB (2004) A physiological model for the estimation of the fraction dose absorbed in humans. *Journal of medicinal chemistry* 47(16):4022–31
- [12] Zwaan CM, Rizzari C, Mechinaud F, Lancaster DL, Lehrnbecher T, van der Velden VHJ, Beverloo BB, den Boer ML, Pieters R, Reinhardt D, Dworzak M, Rosenberg J, Manos G, Agrawal S, Strauss L, Baruchel A, Kearns PR (2013) Dasatinib in children and adolescents with relapsed or refractory leukemia: results of the CA180-018 phase I dose-escalation study of the Innovative Therapies for Children with Cancer Consortium. *Journal of clinical oncology : official journal of the American Society of Clinical Oncology* 31(19):2460–8

- [13] Synthon Hispania SL (2019) Public Assessment Report (Decentralised Procedure): Dasatinib Synthon Hispania 20 mg ; 50 mg ; 70 mg ; 80 mg ; 100 mg ; 140 mg Filmtabletten. [https://file.wuxuwang.com/hma/DE\\_H\\_5896\\_003\\_PAR.pdf](https://file.wuxuwang.com/hma/DE_H_5896_003_PAR.pdf), available online (accessed: 2022-05-05)
- [14] Furlong MT, Agrawal S, Hawthorne D, Lago M, Unger S, Krueger L, Stouffer B (2012) A validated LC-MS/MS assay for the simultaneous determination of the anti-leukemic agent dasatinib and two pharmacologically active metabolites in human plasma: application to a clinical pharmacokinetic study. *Journal of pharmaceutical and biomedical analysis* 58(1):130–5
- [15] Araujo JC, Mathew P, Armstrong AJ, Braud EL, Posadas E, Lonberg M, Gallick GE, Trudel GC, Paliwal P, Agrawal S, Logothetis CJ (2012) Dasatinib combined with docetaxel for castration-resistant prostate cancer: results from a phase 1-2 study. *Cancer* 118(1):63–71
- [16] Demetri GD, Lo Russo P, MacPherson IRJ, Wang D, Morgan JA, Brunton VG, Paliwal P, Agrawal S, Voi M, Evans TRJ (2009) Phase I dose-escalation and pharmacokinetic study of dasatinib in patients with advanced solid tumors. *Clinical cancer research : an official journal of the American Association for Cancer Research* 15(19):6232–40
- [17] Takahashi S, Miyazaki M, Okamoto I, Ito Y, Ueda K, Seriu T, Nakagawa K, Hatake K (2011) Phase I study of dasatinib (BMS-354825) in Japanese patients with solid tumors. *Cancer science* 102(11):2058–64
- [18] Meyer M, Schneekener S, Ludewig B, Kuepfer L, Lippert J (2012) Using expression data for quantification of active processes in physiologically based pharmacokinetic modeling. *Drug metabolism and disposition: the biological fate of chemicals* 40(5):892–901
- [19] Scotcher D, Billington S, Brown J, Jones CR, Brown CDA, Rostami-Hodjegan A, Galetin A (2017) Microsomal and Cytosolic Scaling Factors in Dog and Human Kidney Cortex and Application for In Vitro-In Vivo Extrapolation of Renal Metabolic Clearance. *Drug metabolism and disposition: the biological fate of chemicals* 45(5):556–568
- [20] Eriksson J, Solodenko J (2021) Building and evaluation of a PBPK model for Fluconazole in healthy adults. <https://github.com/Open-Systems-Pharmacology/OSP-PBPK-Model-Library/tree/master/Fluconazole>, available online (accessed: 2023-08-17)
- [21] Wojtyniak JG, Selzer D, Schwab M, Lehr T (2021) Physiologically Based Precision Dosing Approach for Drug-Drug-Gene Interactions: A Simvastatin Network Analysis. *Clinical pharmacology and therapeutics* 109(1):201–211
- [22] Shi P, Liao M, Chuang BC, Griffin R, Shi J, Hyer M, Fallon JK, Smith PC, Li C, Xia CQ (2018) Efflux transporter breast cancer resistance protein dominantly expresses on the membrane of red blood cells, hinders partitioning of its substrates into the cells, and alters drug-drug interaction profiles. *Xenobiotica; the fate of foreign compounds in biological systems* 48(11):1173–1183
- [23] Prasad B, Evers R, Gupta A, Hop CECA, Salphati L, Shukla S, Ambudkar SV, Unadkat JD (2014) Interindividual variability in hepatic organic anion-transporting polypeptides and P-glycoprotein (ABCB1) protein expression: quantification by liquid chromatography tandem mass spectroscopy and influence of genotype, age, and sex. *Drug metabolism and disposition: the biological fate of chemicals* 42(1):78–88
- [24] Hanke N, Frechen S, Moj D, Britz H, Eissing T, Wendl T, Lehr T (2018) PBPK Models for CYP3A4 and P-gp DDI Prediction: A Modeling Network of Rifampicin, Itraconazole, Clarithromycin, Midazolam, Alfentanil, and Digoxin. *CPT: pharmacometrics & systems pharmacology* 7(10):647–659

- [25] Dallmann A, Solodenko J, Wendl T, Frechen S (2022) Building and Evaluation of a PBPK Model for Erythromycin in Healthy Adults. [https://github.com/Open-Systems-Pharmacology/OSP-PBPK-Model-Library/blob/master/Erythromycin/Erythromycin\\_evaluation\\_report.pdf](https://github.com/Open-Systems-Pharmacology/OSP-PBPK-Model-Library/blob/master/Erythromycin/Erythromycin_evaluation_report.pdf), available online (accessed: 2022-10-18)
- [26] Nishimura M, Naito S (2006) Tissue-specific mRNA expression profiles of human phase I metabolizing enzymes except for cytochrome P450 and phase II metabolizing enzymes. *Drug metabolism and pharmacokinetics* 21(5):357–74
- [27] Rodrigues AD (1999) Integrated cytochrome P450 reaction phenotyping: attempting to bridge the gap between cDNA-expressed cytochromes P450 and native human liver microsomes. *Biochemical pharmacology* 57(5):465–80
- [28] Open Systems Pharmacology Suite Community (2018) PK-Sim® Ontogeny Database Documentation, Version 7.3. <https://github.com/Open-Systems-Pharmacology/OSPSuite.Documentation/blob/master/PK-SimOntogenyDatabaseVersion7.3.pdf>, available online (accessed: 2020-03-25)
- [29] Nishimura M, Yaguti H, Yoshitsugu H, Naito S, Satoh T (2003) Tissue distribution of mRNA expression of human cytochrome P450 isoforms assessed by high-sensitivity real-time reverse transcription PCR. *Yakugaku zasshi : Journal of the Pharmaceutical Society of Japan* 123(5):369–75
- [30] Rowland Yeo K, Walsky RL, Jamei M, Rostami-Hodjegan A, Tucker GT (2011) Prediction of time-dependent CYP3A4 drug-drug interactions by physiologically based pharmacokinetic modelling: impact of inactivation parameters and enzyme turnover. *European journal of pharmaceutical sciences : official journal of the European Federation for Pharmaceutical Sciences* 43(3):160–73
- [31] Greenblatt DJ, von Moltke LL, Harmatz JS, Chen G, Weemhoff JL, Jen C, Kelley CJ, LeDuc BW, Zinny MA (2003) Time course of recovery of cytochrome p450 3A function after single doses of grapefruit juice. *Clinical pharmacology and therapeutics* 74(2):121–9
- [32] Margaillan G, Rouleau M, Klein K, Fallon JK, Caron P, Villeneuve L, Smith PC, Zanger UM, Guillemette C (2015) Multiplexed Targeted Quantitative Proteomics Predicts Hepatic Glucuronidation Potential. *Drug metabolism and disposition: the biological fate of chemicals* 43(9):1331–5
- [33] National Center for Biotechnology Information (NCBI) (2010) Expressed Sequence Tags (EST) from UniGene.
- [34] Prasad B, Lai Y, Lin Y, Unadkat JD (2013) Interindividual variability in the hepatic expression of the human breast cancer resistance protein (BCRP/ABCG2): effect of age, sex, and genotype. *Journal of pharmaceutical sciences* 102(3):787–93
- [35] Nishimura M, Naito S (2005) Tissue-specific mRNA expression profiles of human ATP-binding cassette and solute carrier transporter superfamilies. *Drug metabolism and pharmacokinetics* 20(6):452–77
- [36] Deo AK, Prasad B, Balogh L, Lai Y, Unadkat JD (2012) Interindividual variability in hepatic expression of the multidrug resistance-associated protein 2 (MRP2/ABCC2): quantification by liquid chromatography/tandem mass spectrometry. *Drug metabolism and disposition: the biological fate of chemicals* 40(5):852–5



- [37] Kolesnikov N, Hastings E, Keays M, Melnichuk O, Tang YA, Williams E, Dylag M, Kurbatova N, Brandizi M, Burdett T, Megy K, Pilicheva E, Rustici G, Tikhonov A, Parkinson H, Petryszak R, Sarkans U, Brazma A (2015) ArrayExpress update—simplifying data submissions. *Nucleic acids research* 43(Database issue):D1113–6
- [38] Andre Dallmann (2021) IVIC with the particle dissolution module implemented in OSP. <https://github.com/AndreDlm/IVIVC-with-particle-dissolution-module-in-OSP>, available online (accessed: 2023-01-05)
- [39] Developed by ChemAxon (2009) Chemicalize was used for prediction of dasatinib properties. <https://chemicalize.com/>, available online (accessed: 2022-05-03)
- [40] Hořínková J, Šíma M, Slanař O (2019) Pharmacokinetics of Dasatinib. *Prague medical report* 120(2-3):52–63
- [41] Tsume Y, Takeuchi S, Matsui K, Amidon GE, Amidon GL (2015) In vitro dissolution methodology, mini-Gastrointestinal Simulator (mGIS), predicts better in vivo dissolution of a weak base drug, dasatinib. *European journal of pharmaceutical sciences : official journal of the European Federation for Pharmaceutical Sciences* 76:203–12
- [42] Watanabe R, Esaki T, Kawashima H, Natsume-Kitatani Y, Nagao C, Ohashi R, Mizuguchi K (2018) Predicting Fraction Unbound in Human Plasma from Chemical Structure: Improved Accuracy in the Low Value Ranges. *Molecular pharmaceutics* 15(11):5302–5311
- [43] Wang L, Christopher LJ, Cui D, Li W, Iyer R, Humphreys WG, Zhang D (2008) Identification of the human enzymes involved in the oxidative metabolism of dasatinib: an effective approach for determining metabolite formation kinetics. *Drug metabolism and disposition: the biological fate of chemicals* 36(9):1828–39
- [44] Chang M, Bathena S, Christopher LJ, Shen H, Roy A (2022) Prediction of drug-drug interaction potential mediated by transporters between dasatinib and metformin, pravastatin, and rosuvastatin using physiologically based pharmacokinetic modeling. *Cancer chemotherapy and pharmacology* 89(3):383–392
- [45] Pahwa S, Alam K, Crowe A, Farasyn T, Neuhoﬀ S, Hatley O, Ding K, Yue W (2017) Pre-treatment With Rifampicin and Tyrosine Kinase Inhibitor Dasatinib Potentiates the Inhibitory Effects Toward OATP1B1- and OATP1B3-Mediated Transport. *Journal of pharmaceutical sciences* 106(8):2123–2135
- [46] Open Systems Pharmacology Suite Community (2021) Open Systems Pharmacology Suite Manual. <https://raw.githubusercontent.com/Open-Systems-Pharmacology/OSPSuite.Documentation/master/OpenSystemsPharmacologySuite.pdf>, available online (accessed: 2023-05-04)
- [47] Fisher RS, Rock E, Malmud LS (1987) Effects of meal composition on gallbladder and gastric emptying in man. *Digestive diseases and sciences* 32(12):1337–44
- [48] Schmitt W (2008) General approach for the calculation of tissue to plasma partition coefficients. *Toxicology in vitro : an international journal published in association with BIBRA* 22(2):457–67
- [49] ChemicalBook (2006) ChemicalBook was used for collection of chemical information of dasatinib. <https://www.chemicalbook.com/>, available online (accessed: 2023-01-05)

- [50] Eley T, Luo FR, Agrawal S, Sanil A, Manning J, Li T, Blackwood-Chirchir A, Bertz R (2009) Phase I study of the effect of gastric acid pH modulators on the bioavailability of oral dasatinib in healthy subjects. *Journal of clinical pharmacology* 49(6):700–9
- [51] Yago MR, Frymoyer A, Benet LZ, Smelick GS, Frassetto LA, Ding X, Dean B, Salphati L, Budha N, Jin JY, Dresser MJ, Ware JA (2014) The use of betaine HCl to enhance dasatinib absorption in healthy volunteers with rabeprazole-induced hypochlorhydria. *The AAPS journal* 16(6):1358–65
- [52] Johnson FM, Agrawal S, Burris H, Rosen L, Dhillon N, Hong D, Blackwood-Chirchir A, Luo FR, Sy O, Kaul S, Chiappori AA (2010) Phase 1 pharmacokinetic and drug-interaction study of dasatinib in patients with advanced solid tumors. *Cancer* 116(6):1582–91
- [53] Okada M, Yao T, Sakurai T, Arita M, Okabe N, Iida M, Okada Y, Koga T (1992) A comparative study of once-a-day morning and once-a-day bedtime administration of 40 mg famotidine in treating gastric ulcers. *The American journal of gastroenterology* 87(8):1009–13
- [54] Dennis L Decktor, Malcolm Robinson SG (1995) Comparative Effects of Liquid Antacids on Esophageal and Gastric pH in Patients with Heartburn. *American journal of therapeutics* 2(7):481–486
- [55] Guest EJ, Aarons L, Houston JB, Rostami-Hodjegan A, Galetin A (2011) Critique of the two-fold measure of prediction success for ratios: application for the assessment of drug-drug interactions. *Drug metabolism and disposition: the biological fate of chemicals* 39(2):170–3
- [56] Fuhr LM, Marok FZ, Hanke N, Selzer D, Lehr T (2021) Pharmacokinetics of the CYP3A4 and CYP2B6 Inducer Carbamazepine and Its Drug-Drug Interaction Potential: A Physiologically Based Pharmacokinetic Modeling Approach. *Pharmaceutics* 13(2):1–21
- [57] Wendl T, Frechen S, Solodenko J, Dallmann A (2021) Building and Evaluation of a PBPK Model for Efavirenz in Healthy Adults. [https://github.com/Open-Systems-Pharmacology/OSP-PBPK-Model-Library/blob/master/Efavirenz/efavirenz\\_evaluation\\_report.pdf](https://github.com/Open-Systems-Pharmacology/OSP-PBPK-Model-Library/blob/master/Efavirenz/efavirenz_evaluation_report.pdf), available online (accessed: 2022-10-18)
- [58] Britz H, Hanke N, Volz AK, Spigset O, Schwab M, Eissing T, Wendl T, Frechen S, Lehr T (2019) Physiologically-Based Pharmacokinetic Models for CYP1A2 Drug–Drug Interaction Prediction: A Modeling Network of Fluvoxamine, Theophylline, Caffeine, Rifampicin, and Midazolam. *CPT: Pharmacometrics and Systems Pharmacology* 8(5):296–307
- [59] Fuhr LM, Marok FZ, Fuhr U, Selzer D, Lehr T (2023) Physiologically based pharmacokinetic modeling of bergamottin and 6,7-dihydroxybergamottin to describe CYP3A4 mediated grapefruit-drug interactions. *Clinical pharmacology and therapeutics* (031):0–2
- [60] Marok FZ, Wojtyniak JG, Fuhr LM, Selzer D, Schwab M, Weiss J, Haefeli WE, Lehr T (2023) A Physiologically Based Pharmacokinetic Model of Ketoconazole and Its Metabolites as Drug–Drug Interaction Perpetrators. *Pharmaceutics* 15(2)
- [61] Li X, Frechen S, Moj D, Lehr T, Taubert M, Hsin CH, Mikus G, Neuvonen PJ, Olkkola KT, Saari TI, Fuhr U (2020) A Physiologically Based Pharmacokinetic Model of Voriconazole Integrating Time-Dependent Inhibition of CYP3A4, Genetic Polymorphisms of CYP2C19 and Predictions of Drug-Drug Interactions. *Clinical pharmacokinetics* 59(6):781–808
- [62] Li X, He Y, Ruiz CH, Koenig M, Cameron MD, Vojtkovsky T (2009) Characterization of dasatinib and its structural analogs as CYP3A4 mechanism-based inactivators and the proposed bioactivation pathways. *Drug metabolism and disposition: the biological fate of chemicals* 37(6):1242–50

A.2 SUPPLEMENTARY DOCUMENT TO PUBLICATION II – PHYSIOLOGICALLY  
BASED PHARMACOKINETIC MODELING OF IMATINIB

CPT: PHARMACOMETRICS &amp; SYSTEMS PHARMACOLOGY

# Physiologically Based Pharmacokinetic Modeling of Imatinib and N-Desmethyl Imatinib for Drug-Drug Interaction Predictions

Supplement S1 - Model Information and Evaluation

Helena Leonie Hanae Loer<sup>1</sup>, Christina Kovar<sup>1,2</sup>, Simeon Rüdesheim<sup>1,2</sup>, Fatima Zahra Marok<sup>1</sup>, Laura Maria Fuhr<sup>1</sup>, Dominik Selzer<sup>1</sup>, Matthias Schwab<sup>2,3,4</sup>, Thorsten Lehr<sup>1</sup>

<sup>1</sup>Clinical Pharmacy, Saarland University, 66123 Saarbrücken, Germany

<sup>2</sup>Dr. Margarete Fischer-Bosch-Institute of Clinical Pharmacology, 70376 Stuttgart, Germany

<sup>3</sup>Departments of Clinical Pharmacology, and Pharmacy and Biochemistry, University of Tübingen, 72076 Tübingen, Germany

<sup>4</sup>Cluster of Excellence iFIT (EXC2180), Image-Guided and Functionally Instructed Tumor Therapies, University of Tübingen, 69120 Tübingen, Germany

**Funding:**

Matthias Schwab was supported by the Robert Bosch Stiftung (Stuttgart, Germany), a grant from the German Federal Ministry of Education and Research (BMBF, 031L0188D, “GUIDE-IBD”) and the DFG im Rahmen der Exzellenzstrategie des Bundes und der Länder-EXC 2180-390900677.

Thorsten Lehr was supported by the German Federal Ministry of Education and Research (BMBF, Horizon 2020 INSPIRATION grant 643271), under the frame of ERACoSysMed and the European Union Horizon 2021 SafePolyMed (grant 101057639).

**Conflict of Interest:**

The authors declared no competing interests for this work.

**Corresponding Author:**

Thorsten Lehr, PhD  
Clinical Pharmacy  
Saarland University  
Campus C4 3  
66123 Saarbrücken  
Germany

# Contents

<b>S1 Physiologically Based Pharmacokinetic Model Building</b>	<b>3</b>
S1.1 System-Dependent Parameters . . . . .	3
S1.2 Equations . . . . .	6
S1.2.1 Weibull Function . . . . .	6
S1.2.2 Michaelis-Menten Kinetics . . . . .	6
S1.3 Clinical Study Data . . . . .	7
S1.4 Drug-Dependent Parameters . . . . .	9
<b>S2 Physiologically Based Pharmacokinetic Model Evaluation</b>	<b>11</b>
S2.1 Plasma Concentration-Time Profiles (Semilogarithmic) . . . . .	11
S2.2 Plasma Concentration-Time Profiles (Linear) . . . . .	16
S2.3 Urinary Excretion Profiles . . . . .	20
S2.4 Goodness-of-Fit Plots . . . . .	21
S2.5 MRD of Plasma Concentration Predictions . . . . .	22
S2.6 Predicted and Observed $AUC_{last}$ and $C_{max}$ Values . . . . .	24
S2.7 Local Sensitivity Analysis . . . . .	26
S2.7.1 Methods . . . . .	26
S2.7.2 Results . . . . .	26
<b>S3 Drug-Drug Interaction Modeling</b>	<b>28</b>
S3.1 Clinical Study Data . . . . .	28
S3.2 Drug-Dependent Parameters of DDI Partners . . . . .	29
S3.2.1 Rifampicin . . . . .	29
S3.2.2 Ketoconazole . . . . .	30
S3.2.3 Gemfibrozil . . . . .	32
S3.2.4 Simvastatin . . . . .	33
S3.2.5 Metoprolol . . . . .	34
S3.3 Plasma Concentration-Time Profiles (Semilogarithmic) . . . . .	36
S3.4 Plasma Concentration-Time Profiles (Linear) . . . . .	37
S3.5 DDI $AUC_{last}$ and DDI $C_{max}$ Ratio Goodness-of-Fit Plots . . . . .	38
S3.6 Predicted and Observed DDI $AUC_{last}$ and DDI $C_{max}$ Ratios . . . . .	39
S3.7 Comparison of CYP3A Perpetrator Effects – SD vs. MD Imatinib Administration . . . . .	40
<b>Bibliography</b>	<b>42</b>

# S1 Physiologically Based Pharmacokinetic Model Building

## S1.1 System-Dependent Parameters

**Table S1:** System-dependent parameters

Enzyme/ Transporter	Reference concentration		Localization/ Direction	Half-life liver [h]	Half-life intestine [h]
	Mean <sup>a</sup> [μmol/L]	GeoSD <sup>b</sup>			
AADAC	1.00 <sup>c</sup>	1.40 <sup>d</sup>	intracellular	36	23
CYP2C8	2.56 [1]	2.05 [2]	intracellular	23	23
CYP2D6	0.40 [1]	2.49 [2]	intracellular	51	23
CYP3A4	4.32 [1]	1.18 (liver) [2] 1.45 (duodenum) [2]	intracellular	36	23
FMO3	1.00 <sup>c</sup>	1.40 <sup>d</sup>	intracellular	36	23
PON3	1.00 <sup>c</sup>	1.40 <sup>d</sup>	intracellular	36	23
UGT1A1	1.00 <sup>c</sup>	1.40 <sup>d</sup>	intracellular	36	23
UGT1A3	1.00 <sup>c</sup>	1.40 <sup>d</sup>	intracellular	36	23
UGT1A4	2.32 <sup>e</sup> [3]	1.07 [2]	intracellular	36	23
UGT2B7	2.78 [4]	1.60 [2]	intracellular	36	23
Chemical hydrolysis <sup>f</sup>	1.00 <sup>c</sup>	-	-	36	23
Liver lactonization <sup>g</sup>	1.00 <sup>c</sup>	1.40 <sup>d</sup>	-	36	23
Plasma hydrolysis <sup>f</sup>	1.00 <sup>c</sup>	1.40 <sup>d</sup>	-	36	23
BCRP	1.00 <sup>c</sup>	1.35 [5]	efflux	36	23
MRP2	1.00 <sup>c</sup>	1.49 [6]	efflux	36	23
OATP1B1	0.07 <sup>h</sup> [7]	1.54 [7]	influx	36	23
OATP1B3	1.00 <sup>c</sup>	1.54 [7]	influx	36	23
P-gp	1.41 [8]	1.60 [7]	efflux	36	23
Liver influx <sup>i</sup>	1.00 <sup>c</sup>	1.40 <sup>d</sup>	influx	36	23

AADAC: arylacetamide deacetylase, BCRP: breast cancer resistance protein, CYP: cytochrome P450, FMO: flavin-containing monooxygenase, MRP: multidrug resistance-associated protein, OATP: organic-anion-transporting polypeptide, P-gp: P-glycoprotein, PON: paraoxonase, UGT: uridine 5'-diphosphoglucuronosyltransferase.

<sup>a</sup>: μmol protein/L in the tissue of highest expression

<sup>b</sup>: geometric standard deviation of the reference concentration

<sup>c</sup>: if no information was available, the mean reference concentration was set to 1.00 μmol/L and the catalytic rate constant was optimized according to [9]

<sup>d</sup>: if no information was available, a moderate variability of 35% coefficient of variation was assumed

<sup>e</sup>: calculated from protein per mg microsomal protein x 40.0 mg microsomal protein per g liver [10]

<sup>f</sup>: simvastatin

<sup>g</sup>: simvastatin hydroxy acid

<sup>h</sup>: calculated from transporter per mg membrane protein x 37.0 mg membrane protein per g liver [7]

<sup>i</sup>: gemfibrozil

**Table S2:** Relative expression of implemented enzymes and transporters in organs and tissues [%]

Data source	AADAC	CYP2C8	CYP2D6	CYP3A4	FMO3	PON3	UGT1A1	UGT1A3	UGT1A4	UGT2B7
	RT-PCR [12]	RT-PCR [13]	RT-PCR [13]	RT-PCR [13]	RT-PCR [12]	Array [14]	RT-PCR [12]	RT-PCR [12]	RT-PCR [12]	EST [15]
Blood cells	0	0	0	0	0	0	0	0	0	0
Plasma	0	0	0	0	0	0	0	0	0	0
Bone	0	0	0	0	1	8	0	0	0	0
Brain	0	0	1	0	0	6	0	0	0	8
Fat	0	0	0	0	0	0	0	0	0	0
Gonads	0	1	77	0	0	15	0	0	0	13
Heart	0	0	0	0	0	5	0	0	0	0
Kidney	0	0	2	1	0	12	8	8	0	100
Liver periportal	100	100	100	100	100	100	100	100	100	23
Liver pericentral	100	100	100	100	100	18	100	100	100	23
Lung	3	0	2	0	2	0	0	0	0	0
Muscle	0	0	0	0	1	4	0	0	0	0
Pancreas	15	0	0	0	0	7	0	0	0	0
Skin	0	0	0	0	0	13	0	0	0	3
Spleen	0	0	0	0	0	6	0	0	0	0
Duodenum mucosa	25	0	9	7	0	9	32	32	0	4
Upper jejunum mucosa	25	0	9	7	0	9	32	32	0	4
Lower jejunum mucosa	25	0	9	7	0	9	32	32	0	4
Upper ileum mucosa	25	0	9	7	0	9	32	32	0	4
Lower ileum mucosa	25	0	9	7	0	9	32	32	0	4
Cecum mucosa	0	0	0	0	0	0	0	0	0	0
Colon ascendens mucosa	0	0	0	0	0	6	3	3	0	0
Colon transversum mucosa	0	0	0	0	0	6	3	3	0	0
Colon descendens mucosa	0	0	0	0	0	6	3	3	0	0
Colon sigmoid mucosa	0	0	0	0	0	6	3	3	0	0
Rectum mucosa	0	0	0	0	0	0	0	0	0	0
Stomach non-muc. tissue	8	0	0	0	1	9	2	2	0	13
Small intestine non-muc. tissue	25	0	9	7	0	9	32	32	0	4
Large intestine non-muc. tissue	0	0	0	0	0	6	3	3	0	0
Stomach lumen	0	0	0	0	0	0	0	0	0	0
Duodenum lumen	0	0	0	0	0	0	0	0	0	0
Upper jejunum lumen	0	0	0	0	0	0	0	0	0	0
Lower jejunum lumen	0	0	0	0	0	0	0	0	0	0
Upper ileum lumen	0	0	0	0	0	0	0	0	0	0
Lower ileum lumen	0	0	0	0	0	0	0	0	0	0
Cecum lumen	0	0	0	0	0	0	0	0	0	0
Colon ascendens lumen	0	0	0	0	0	0	0	0	0	0
Colon transversum lumen	0	0	0	0	0	0	0	0	0	0
Colon descendens lumen	0	0	0	0	0	0	0	0	0	0
Colon sigmoid lumen	0	0	0	0	0	0	0	0	0	0
Rectum lumen	0	0	0	0	0	0	0	0	0	0

<sup>a</sup>: with the relative expression in blood cells set to 0.3046 [11], <sup>b</sup>: with the relative expression in intestinal mucosa increased by factor 3.57, <sup>c</sup>: gemfibrozil, AADAC: arylacetamide deacetylase, Array: microarray expression profile, BCRP: breast cancer resistance protein, CYP: cytochrome P450, EST: expressed sequence tags, FMO: flavin-containing monooxygenase, MRP: multidrug resistance-associated protein, muc.: mucosal, OATP: organic-anion-transporting polypeptide, P-gp: P-glycoprotein, PON: paraoxonase, RT-PCR: reverse transcription polymerase chain reaction, UGT: uridine 5'-diphospho-glucuronosyltransferase.



**Table S2:** Relative expression of implemented enzymes and transporters in organs and tissues [%] (*continued*)

Data source	Chemical hydrolysis	Liver lactonization	Plasma hydrolysis	BCRP	MRP2	OATP1B1	OATP1B3	P-gp	Liver influx <sup>c</sup>
	-	-	-	RT-PCR <sup>a</sup> [16]	Array [14]	RT-PCR [16]	Array [14]	RT-PCR <sup>b</sup> [16]	-
Blood cells	0	0	0	30	0	0	0	0	0
Plasma	0	0	100	-	-	-	-	-	-
Bone	66	0	0	21	7	0	3	2	0
Brain	73	0	0	46	6	0	3	8	0
Fat	73	0	0	0	0	0	0	0	0
Gonads	66	0	0	27	9	1	4	2	0
Heart	73	0	0	11	5	0	6	4	0
Kidney	82	0	0	9	59	0	2	71	0
Liver periportal	83	100	0	28	100	100	100	19	100
Liver pericentral	83	100	0	28	100	100	100	19	100
Lung	36	0	0	22	6	0	2	7	0
Muscle	52	0	0	3	31	0	2	1	0
Pancreas	96	0	0	1	56	0	1	1	0
Skin	66	0	0	0	3	0	0	0	0
Spleen	66	0	0	6	7	0	1	7	0
Duodenum mucosa	88	0	0	100	50	0	2	100	0
Upper jejunum mucosa	88	0	0	100	50	0	2	100	0
Lower jejunum mucosa	88	0	0	100	50	0	2	100	0
Upper ileum mucosa	88	0	0	100	50	0	2	100	0
Lower ileum mucosa	88	0	0	100	50	0	2	100	0
Cecum mucosa	88	0	0	0	0	0	0	0	0
Colon ascendens mucosa	88	0	0	16	12	0	1	40	0
Colon transversum mucosa	88	0	0	16	12	0	1	40	0
Colon descendens mucosa	88	0	0	16	12	0	1	40	0
Colon sigmoid mucosa	88	0	0	16	12	0	1	40	0
Rectum mucosa	88	0	0	0	0	0	0	0	0
Stomach non-muc. tissue	96	0	0	4	5	0	1	3	0
Small intestine non-muc. tissue	96	0	0	100	50	0	2	28	0
Large intestine non-muc. tissue	83	0	0	16	12	0	1	11	0
Stomach lumen	0	0	0	-	-	-	-	-	-
Duodenum lumen	10	0	0	-	-	-	-	-	-
Upper jejunum lumen	10	0	0	-	-	-	-	-	-
Lower jejunum lumen	60	0	0	-	-	-	-	-	-
Upper ileum lumen	100	0	0	-	-	-	-	-	-
Lower ileum lumen	81	0	0	-	-	-	-	-	-
Cecum lumen	10	0	0	-	-	-	-	-	-
Colon ascendens lumen	10	0	0	-	-	-	-	-	-
Colon transversum lumen	10	0	0	-	-	-	-	-	-
Colon descendens lumen	35	0	0	-	-	-	-	-	-
Colon sigmoid lumen	35	0	0	-	-	-	-	-	-
Rectum lumen	35	0	0	-	-	-	-	-	-

<sup>a</sup>: with the relative expression in blood cells set to 0.3046 [11], <sup>b</sup>: with the relative expression in intestinal mucosa increased by factor 3.57, <sup>c</sup>: genfibrozil, AADAC: arylacetamide deacetylase, Array: microarray expression profile, BCRP: breast cancer resistance protein, CYP: cytochrome P450, EST: expressed sequence tags, FMO: flavin-containing monooxygenase, MRP: multidrug resistance-associated protein, muc.: mucosal, OATP: organic-anion-transporting polypeptide, P-gp: P-glycoprotein, PON: paraoxonase, RT-PCR: reverse transcription polymerase chain reaction, UGT: uridine 5'-diphospho-glucuronosyltransferase.

## S1.2 Equations

### S1.2.1 Weibull Function

$$f_d(t) = 1 - \exp\left(\frac{-(t - t_{lag})^b}{a}\right) \quad (S1)$$

where  $f_d(t)$  = fraction of administered dose dissolved at time  $t$ ,  $t_{lag}$  = lag time between drug intake and start of the dissolution process,  $b$  = shape parameter,  $a$  = scale parameter.

### S1.2.2 Michaelis-Menten Kinetics

$$v = \frac{v_{max} \cdot [S]}{K_M + [S]} = \frac{k_{cat} \cdot [E] \cdot [S]}{K_M + [S]} \quad (S2)$$

where  $v$  = reaction velocity,  $v_{max}$  = maximum reaction velocity,  $[S]$  = free substrate concentration,  $K_M$  = Michaelis-Menten constant,  $k_{cat}$  = catalytic rate constant, and  $[E]$  = enzyme concentration.

## S1.3 Clinical Study Data

Table S3: Clinical studies of imatinib used for PBPK model development

Imatinib dosing regimen		n	Females [%]	Ethnicity <sup>a</sup>	Age [years]	Weight [kg]	Height [cm]	Compound(s) measured	Dataset	Reference
Route	Dose [mg]									
iv (inf, 1 h, SD)	100	17 (healthy)	18	White American	(40–58)	73.3±7 (62–88)	-	Ima	training	Peng 2004 [17]
po (-, QD)	25	3 (CML patients)	34	White American	53.11±12.99	80.05±17.72	-	Ima	test	Peng 2004 [18]
po (-, SD)	50	3 (CML patients)	34	White American	53.11±12.99	80.05±17.72	-	Ima	test	Peng 2004 [18]
po (-, QD)	50	3 (CML patients)	34	White American	53.11±12.99	80.05±17.72	-	Ima	test	Peng 2004 [18]
po (-, QD)	85	3 (CML patients)	34	White American	53.11±12.99	80.05±17.72	-	Ima	test	Peng 2004 [18]
po (tab, SD)	100	1 (healthy)	67	European	(25–34)	-	-	Ima	test	Zidan 2018 [19]
po (tab, SD)	100	1 (healthy)	67	European	(25–34)	-	-	Ima	test	Zidan 2018 [19]
po (tab, SD)	100	1 (healthy)	67	European	(25–34)	-	-	Ima	test	Zidan 2018 [19]
po (tab, SD)	100	37 (healthy)	-	European	32.4±9.84	75.0±7.63	177.4±7.12	Ima, NDMI	test	Ostrowicz 2014 [20]
po (tab, SD)	200	10 (healthy)	20	European	24±3	72±13	-	Ima, NDMI	training	Filppula 2013 [21]
po (tab, SD)	200	23 (healthy)	0	Asian	29±7	69.5±8.1	175.8±6	Ima	training	Jung 2014 [22]
po (cap, SD)	200	14 (healthy)	7	European	(35–59)	(64–103)	-	Ima, NDMI	test	Dutreix 2004 [23]
po (cap, SD)	200	4 (healthy)	0	European	-	(61.8–85.7)	-	Ima, NDMI	test	Gschwind 2005 [24]
po (tab, SD)	200	1 (healthy)	-	European	-	-	-	Ima, NDMI	test	Golabchifar 2011 [25]
po (-, SD)	200	27 (healthy)	-	Asian	-	-	-	Ima	test	Yang 2013 [26]
po (-, QD)	350	5 (CML patients)	34	White American	53.11±12.99	80.05±17.72	-	Ima	test	Peng 2004 [18]
po (-, SD)	400	12 (healthy)	50	White American	28.3±11.9 (21–57)	72.2±16.6 (50.9–101)	-	Ima, NDMI	training	Frye 2004 [27]
po (tab, SD)	400	33 (healthy)	18	White American	38.3±11.83 (19–60)	75.52±10.77 (57.6–101.7)	176.6±8.24 (161–194)	Ima, NDMI	training	Nikolova 2004 [28]
po (cap, SD)	400	17 (healthy)	18	White American	(40–58)	73.3±7 (62–88)	-	Ima	test	Peng 2004 [17]
po (cap, SD)	400	33 (healthy)	18	White American	38.3±11.83 (19–60)	75.52±10.77 (57.6–101.7)	176.6±8.24 (161–194)	Ima, NDMI	test	Nikolova 2004 [28]
po (tab, SD)	400	33 (healthy)	18	White American	38.3±11.83 (19–60)	75.52±10.77 (57.6–101.7)	176.6±8.24 (161–194)	Ima, NDMI	test	Nikolova 2004 [28]
po (-, SD)	400	26 (healthy)	31	European	24±3	72±12	175±8	Ima	test	Pena 2020 [29]

-: not given, <sup>a</sup>: implemented, BID: twice daily, cap: capsule, CML: chronic myeloid leukemia, GIST: gastrointestinal stromal tumor, Ima: imatinib, inf: infusion, iv: intravenous, n: number of participants, NDMI: N-desmethyl imatinib, po: oral, QD: once daily, SD: single dose, tab: tablet; values for age, weight, and height are shown as mean ± standard deviation (range).

Table S3: Clinical studies of imatinib used for PBPK model development (*continued*)

Imatinib dosing regimen		n	Females [%]	Ethnicity <sup>a</sup>	Age [years]	Weight [kg]	Height [cm]	Compound(s) measured	Dataset	Reference
Route	Dose [mg]									
po (tab, SD)	400	30 (healthy)	0	Mexican American	27.8±6.5	71.2±9.8	171±9	Ima	test	Parrillo-Campiglia 2009 [30]
po (-, SD)	400	10 (healthy)	30	White American	43.7±6.4	80.5±6.0	-	Ima	test	Smith 2004 [31]
po (-, SD)	400	11 (healthy)	-	White American	-	-	-	Ima, NDMI	test	Tawbi 2014 [32]
po (cap, SD)	400	24 (healthy)	0	Asian	36.5±1.70	62.8±1.66 (60.0–66.5)	168 (163–173)	Ima, NDMI	test	Zhang 2014 [33]
po (-, SD)	400	12 (healthy)	50	White American	(20–51)	-	-	Ima, NDMI	test	Sparano 2009 [34]
po (cap, SD)	400	12 (CML patients)	46	European	43±10	69.2±8.2	174±12	Ima, NDMI	test	Mohajeri 2015 [35]
po (tab, SD)	400	12 (CML patients)	46	European	(19–63)	(40.6–89.9)	(158–190)	Ima, NDMI	test	Mohajeri 2015 [35]
po (tab, SD)	400	12 (CML patients)	46	European	43±10	69.2±8.2	174±12	Ima, NDMI	test	Mohajeri 2015 [35]
po (tab, SD)	400	12 (CML patients)	46	European	(19–63)	(40.6–89.9)	(158–190)	Ima, NDMI	test	Mohajeri 2015 [35]
po (tab, SD)	400	21 (healthy)	0	European	(19–63)	(40.6–89.9)	(158–190)	Ima, NDMI	test	Mohajeri 2015 [35]
po (cap, SD)	400	14 (healthy)	7	European	39±11	78.7±9.4	175.4±7.4	Ima	test	Jawhari 2011 [36]
po (tab, SD)	400	37 (healthy)	-	European	49.8±8.2	74.4±8.1	172±6	Ima	test	Bolton 2004 [37]
po (-, SD)	400	12 (healthy)	50	White American	(40–64)	(61.5–90.0)	(165–186)	Ima, NDMI	test	Ostrowicz 2014 [20]
po (-, SD)	400	4 (CML patients)	34	White American	53.11±12.99	80.05±17.72	-	Ima, NDMI	test	Egorin 2009 [38]
po (tab, QD)	400	40 (CML patients)	20	Asian	40.95	58.21±8.41	163±8.07	Ima	test	Peng 2004 [18]
po (-, QD)	400	12 (GIST patients)	20	White American	(20–67)	(41–79)	(148–182)	Ima, NDMI	test	Arora 2016 [39]
po (-, QD)	400	5 (CML patients)	34	White American	53.11±12.99	80.05±17.72	-	Ima	test	Eechoute 2011 [40]
po (-, BID)	400	4 (CML patients)	34	White American	53.11±12.99	80.05±17.72	-	Ima	test	Peng 2004 [18]
po (-, BID)	500	6 (CML patients)	34	White American	53.11±12.99	80.05±17.72	-	Ima	test	Peng 2004 [18]
po (-, QD)	600	9 (CML patients)	34	White American	53.11±12.99	80.05±17.72	-	Ima	test	Peng 2004 [18]
po (-, SD)	750	6 (CML patients)	34	White American	53.11±12.99	80.05±17.72	-	Ima	test	Peng 2004 [18]

-: not given, <sup>a</sup>: implemented, BID: twice daily, cap: capsule, CML: chronic myeloid leukemia, GIST: gastrointestinal stromal tumor, Ima: imatinib, iv: intravenous, n: number of participants, NDMI: N-desmethyl imatinib, po: oral, QD: once daily, SD: single dose, tab: tablet; values for age, weight, and height are shown as mean ± standard deviation (range).

## S1.4 Drug-Dependent Parameters

Table S4: Drug-dependent parameters of the final imatinib PBPK model

Parameter	Unit	Value	Source	Literature	Reference	Description
<b>Imatinib</b>						
Molecular weight	g/mol	493.62	Lit.	493.62	[42]	Molecular weight
pK <sub>a1</sub> , acid		12.69	Lit.	12.69	[42]	Acid dissociation constant
pK <sub>a2</sub> , base		7.84	Lit.	7.84	[42]	Acid dissociation constant
pK <sub>a3</sub> , base		4.27	Lit.	4.27	[42]	Acid dissociation constant
Solubility (pH)	mg/mL	0.04 (7.4)	Lit.	0.04 (7.4)	[42]	Solubility
Lipophilicity	log units	3.25	Opt.	2.89–4.53	[42–44]	Lipophilicity
f <sub>u</sub>	%	3.0 (AGP)	Lit.	3.0–5.1	[31, 45, 46]	Fraction unbound
CYP2C8 K <sub>M</sub> → NDMI	μmol/L	3.85	Lit.	3.85 <sup>a</sup>	[47]	Michaelis-Menten constant
CYP2C8 k <sub>cat</sub> → NDMI	1/min	2.20	Opt.	4.07	[47]	Catalytic rate constant
CYP3A4 K <sub>M</sub> → NDMI	μmol/L	12.96	Lit.	12.96 <sup>a</sup>	[47]	Michaelis-Menten constant
CYP3A4 k <sub>cat</sub> → NDMI	1/min	2.59	Opt.	13.30	[47]	Catalytic rate constant
CYP3A4 CL → sink	1/min	0.42	Opt.	0.06	[47]	Clearance
P-gp K <sub>M</sub>	μmol/L	4.09	Opt.	-	-	Michaelis-Menten constant
P-gp k <sub>cat</sub>	1/min	2.98	Opt.	-	-	Transport rate constant
GFR fraction		1 <sup>b</sup>	Asm.	-	-	Filtered drug in the urine
EHC continuous fraction		1	Asm.	-	-	Bile fraction continuously released
Intestinal permeability	cm/min	3.52 · 10 <sup>-5</sup>	Opt.	1.08±0.18 · 10 <sup>-4</sup>	[48]	Transcellular intestinal permeability
Cellular permeability	cm/min	3.52 · 10 <sup>-3</sup>	Calc.	PK-Sim Standard	[49]	Permeability into the cellular space
Partition coefficients			Calc.	Schmitt	[50]	Organ-plasma partition coefficients
Dissolution time (Weibull)	min	4.36	Lit.	4.36 <sup>c</sup>	[19]	Dissolution time (50%)
Dissolution shape (Weibull)		0.44	Lit.	0.44 <sup>c</sup>	[19]	Dissolution shape
CYP2C8 K <sub>i</sub>	μmol/L	7.56	Lit.	7.56 <sup>a</sup>	[51]	Diss. const. inhibitor-enzyme complex (CI)
CYP2D6 K <sub>i</sub>	μmol/L	6.75	Lit.	6.75 <sup>a</sup>	[51]	Diss. const. inhibitor-enzyme complex (CI)
CYP3A4 K <sub>i</sub>	μmol/L	11.40	Lit.	11.40 <sup>a</sup>	[51]	Conc. for half-maximal inactivation (MBI)
CYP3A4 k <sub>inact</sub>	1/min	0.07	Lit.	0.07	[51]	Maximum inactivation rate constant (MBI)
BCRP K <sub>i</sub>	μmol/L	0.47	Lit.	0.47	[52]	Diss. const. inhibitor-transporter complex (CI)
P-gp K <sub>i</sub>	μmol/L	8.00	Lit.	1.21–18.3	[44, 52, 53]	Diss. const. inhibitor-transporter complex (CI)

-: not available, <sup>a</sup>: *in vitro* values corrected for binding in the assay (f<sub>u,mic</sub>), <sup>b</sup>: a GFR fraction of 1 corresponds to passive glomerular filtration of a compound, <sup>c</sup>: obtained from literature dissolution profile according to [41], AGP: α1-acid glycoprotein, asm.: assumed, BCRP: breast cancer resistance protein, calc.: calculated, CI: competitive inhibition, conc.: concentration, CYP: cytochrome P450, diss. const.: dissociation constant, EHC: enterohepatic circulation, GFR: glomerular filtration rate, lit.: literature, MBI: mechanism-based inactivation, opt.: optimized, P-gp: P-glycoprotein.

Table S4: Drug-dependent parameters of the final imatinib PBPK model (*continued*)

Parameter	Unit	Value	Source	Literature	Reference	Description
<b>N-Desmethy1 Imatinib</b>						
Molecular weight	g/mol	479.59	Lit.	479.59	[54]	Molecular weight
pKa <sub>1</sub> , acid		12.69	Lit.	12.69	[54]	Acid dissociation constant
pKa <sub>2</sub> , base		9.23	Lit.	9.23	[54]	Acid dissociation constant
pKa <sub>3</sub> , base		4.45	Lit.	4.45	[54]	Acid dissociation constant
Solubility (pH)	mg/mL	0.37 (7.4)	Lit.	0.37 (7.4)	[54]	Solubility
Lipophilicity	log units	3.07	Opt.	4.00	[54]	Lipophilicity
f <sub>a</sub>	%	3.6 (AGP)	Lit.	3.6–5	[45, 46]	Fraction unbound
CYP2C8 CL → sink	1/min	0.01	Opt.	1.91 · 10 <sup>-3</sup>	[47]	Clearance
CYP3A4 CL → sink	1/min	2.43 · 10 <sup>-5</sup>	Opt.	7.21 · 10 <sup>-3</sup>	[47]	Clearance
CL <sub>hep</sub> → sink	1/min	7.22	Opt.	-	-	Unspecific hepatic clearance
GFR fraction		1 <sup>b</sup>	Asm.	-	-	Filtered drug in the urine
EHC continuous fraction		1	Asm.	-	-	Bile fraction continuously released
Intestinal permeability	cm/min	1.64 · 10 <sup>-5</sup>	Calc.	-	-	Transcellular intestinal permeability
Cellular permeability	cm/min	2.81 · 10 <sup>-3</sup>	Calc.	PK-Sim Standard	[49]	Permeability into the cellular space
Partition coefficients				PK-Sim Standard	[49]	Organ-plasma partition coefficients
CYP2C8 K <sub>i</sub>	μmol/L	11.52	Lit.	11.52 <sup>a</sup>	[51]	Diss. const. inhibitor-enzyme complex (CI)
CYP2D6 K <sub>i</sub>	μmol/L	12.15	Lit.	12.15 <sup>a</sup>	[51]	Diss. const. inhibitor-enzyme complex (CI)
CYP3A4 K <sub>i</sub>	μmol/L	16.29	Lit.	16.29 <sup>a</sup>	[51]	Diss. const. inhibitor-enzyme complex (CI)

-: not available, <sup>a</sup>: *in vitro* values corrected for binding in the assay (f<sub>u,mic</sub>), <sup>b</sup>: a GFR fraction of 1 corresponds to passive glomerular filtration of a compound, <sup>c</sup>: obtained from literature dissolution profile according to [41], AGP: α1-acid glycoprotein, asm.: assumed, BCRP: breast cancer resistance protein, calc.: calculated, CI: competitive inhibition, conc.: concentration, CYP: cytochrome P450, diss. const.: dissociation constant, EHC: enterohepatic circulation, GFR: glomerular filtration rate, lit.: literature, MBI: mechanism-based inactivation, opt.: optimized, P-gp: P-glycoprotein.

## S2 Physiologically Based Pharmacokinetic Model Evaluation

### S2.1 Plasma Concentration-Time Profiles (Semilogarithmic)

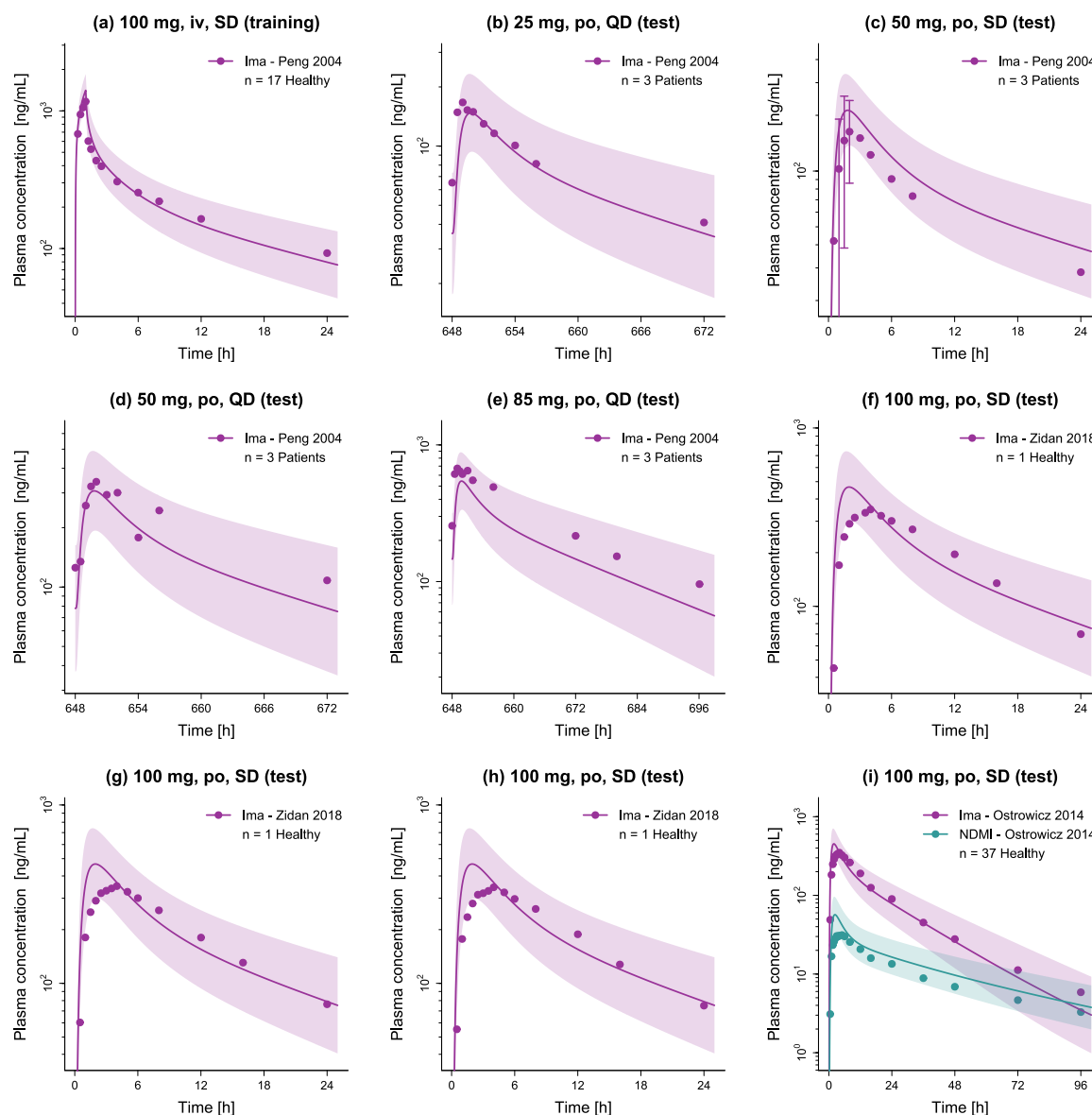


**Figure S1:** Semilogarithmic plots of predicted and observed plasma concentration-time profiles of imatinib and N-desmethyl imatinib. Solid lines and ribbons represent population predictions (n = 1000; geometric mean and geometric standard deviation), while corresponding observed data are shown as dots (± standard deviation, if available) [17–20]. Healthy: healthy subjects, Ima: imatinib, iv: intravenous, n: number of study participants, NDMI: N-desmethyl imatinib, Patients: cancer patients, po: oral, QD: once daily, SD: single dose.



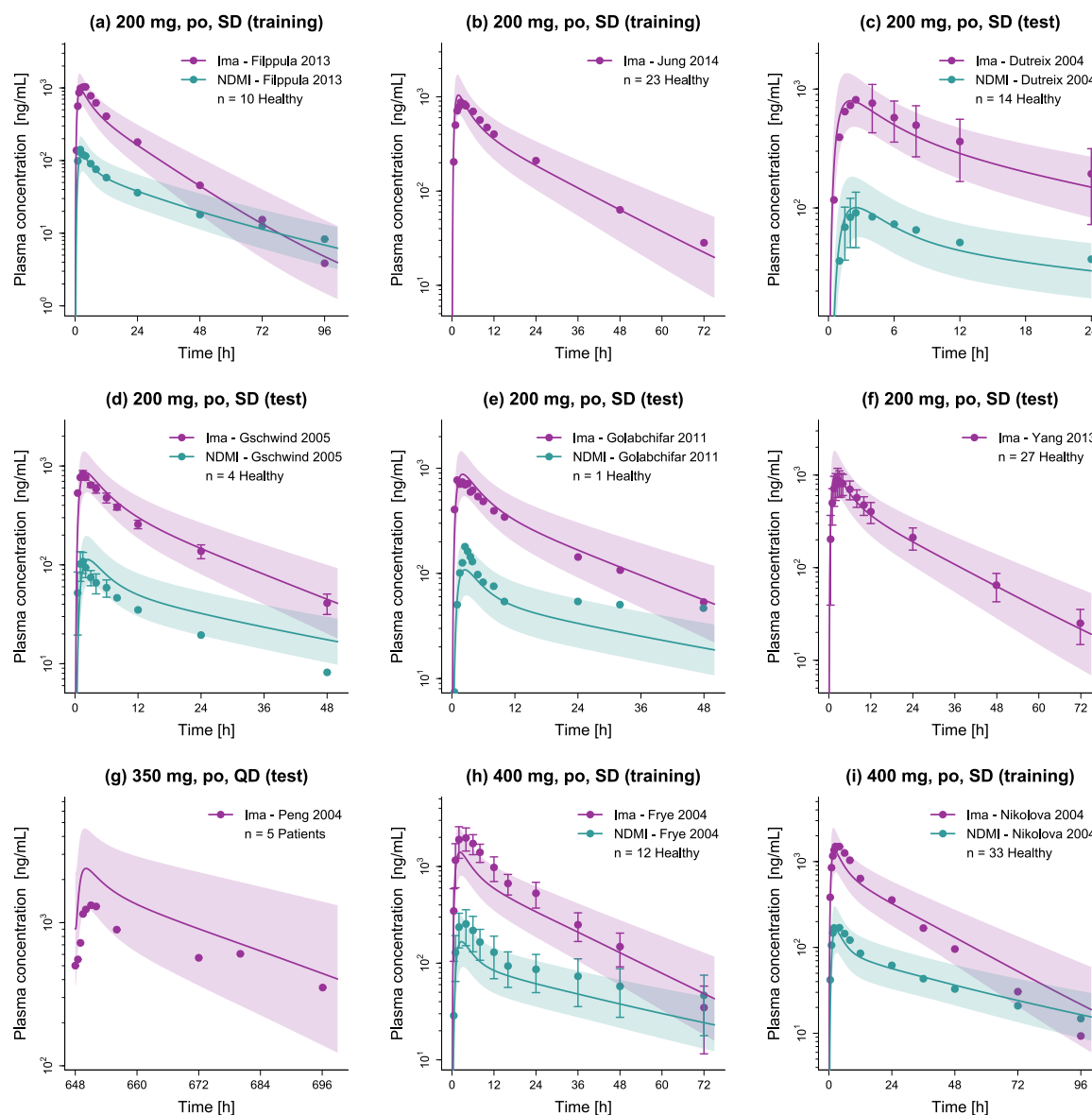


**Figure S2:** Semilogarithmic plots of predicted and observed plasma concentration-time profiles of imatinib and N-desmethyl imatinib. Solid lines and ribbons represent population predictions ( $n = 1000$ ; geometric mean and geometric standard deviation), while corresponding observed data are shown as dots ( $\pm$  standard deviation, if available) [18, 21–28]. Healthy, healthy subjects, Ima: imatinib,  $n$ : number of study participants, NDMI: N-desmethyl imatinib, Patients: cancer patients, po: oral, QD: once daily, SD: single dose.

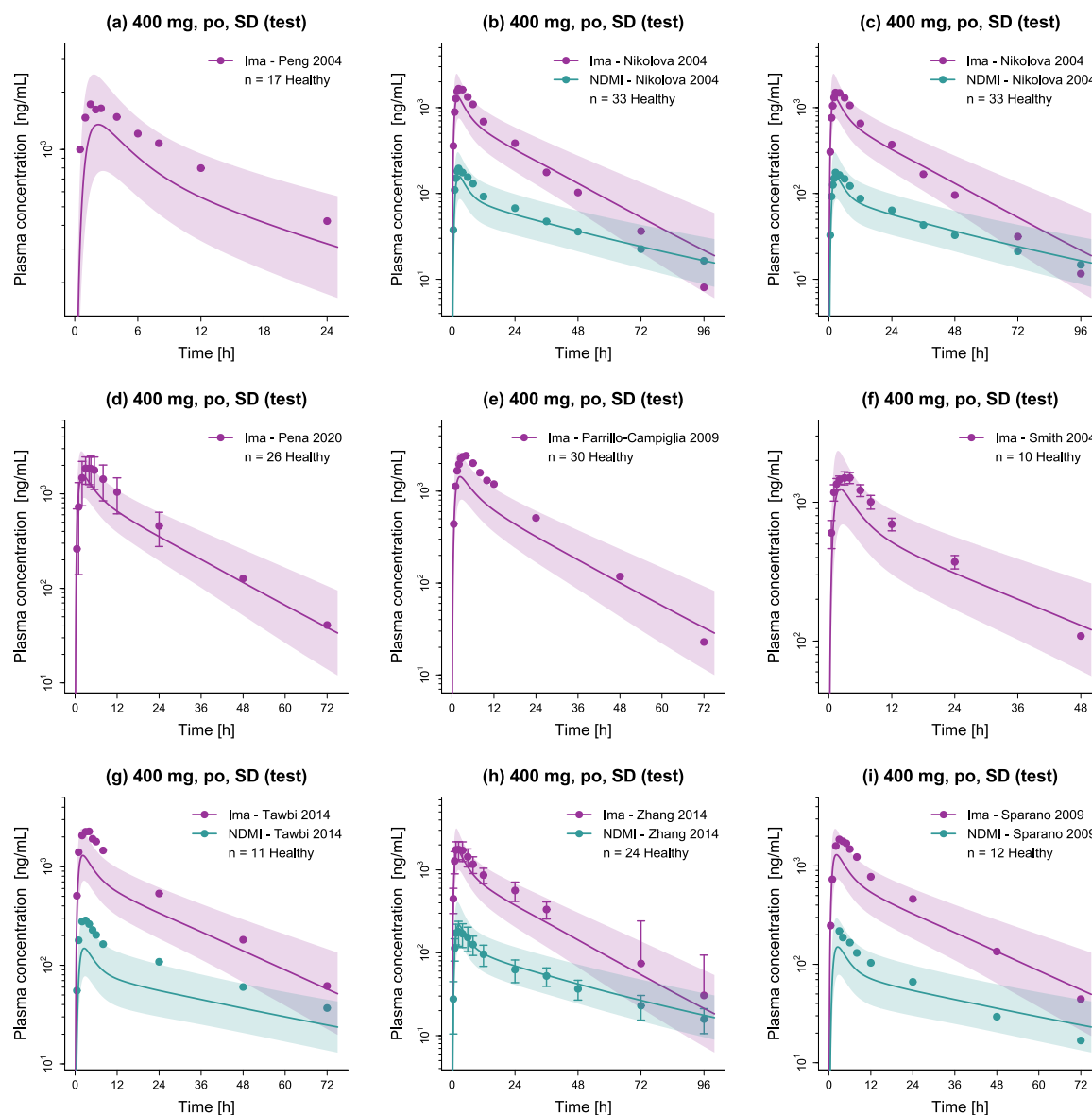


**Figure S3:** Semilogarithmic plots of predicted and observed plasma concentration-time profiles of imatinib and N-desmethyl imatinib. Solid lines and ribbons represent population predictions (n = 1000; geometric mean and geometric standard deviation), while corresponding observed data are shown as dots (± standard deviation, if available) [17, 28–34]. Healthy: healthy subjects, Ima: imatinib, n: number of study participants, NDMI: N-desmethyl imatinib, po: oral, SD: single dose.

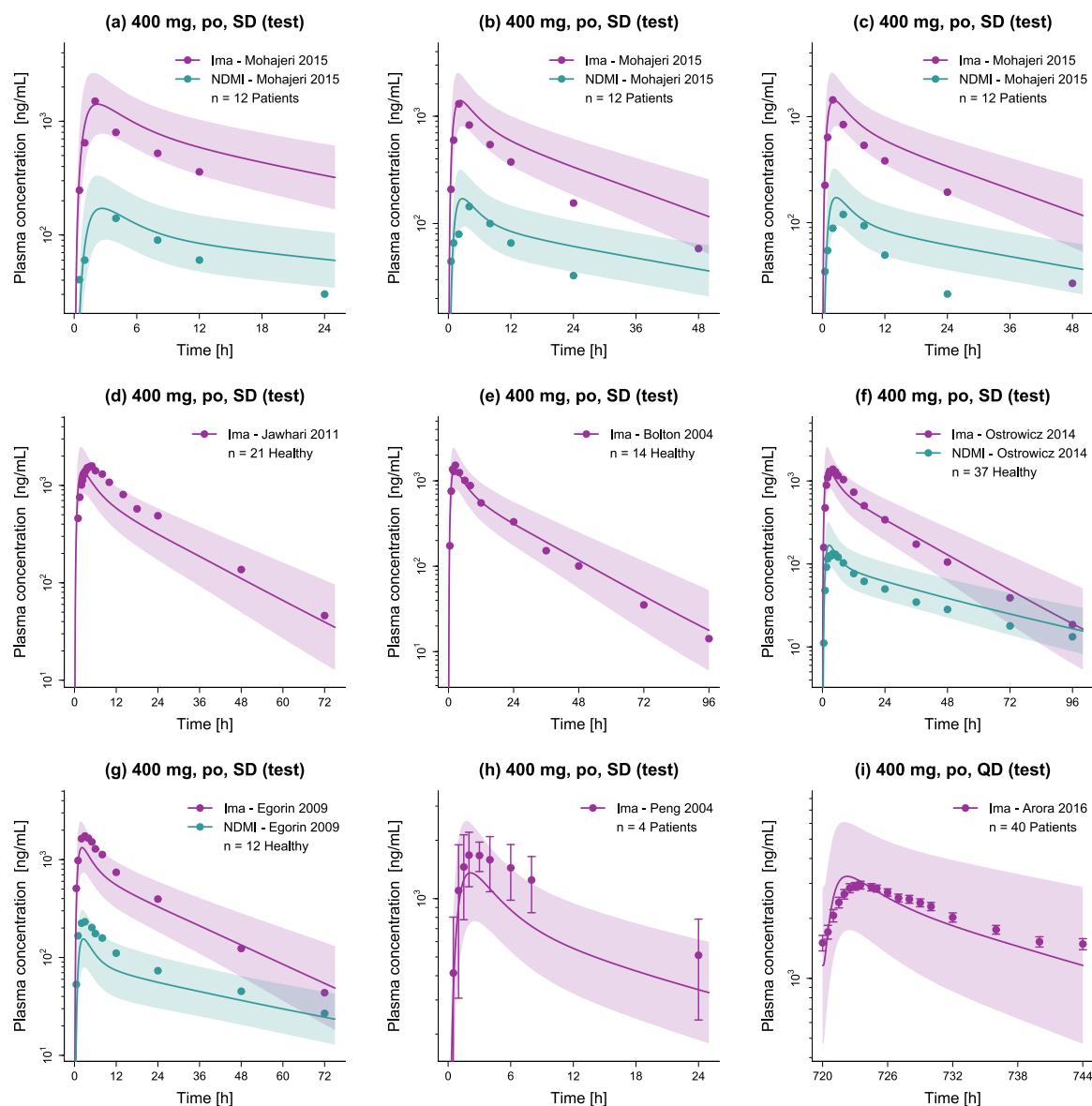


**Figure S4:** Semilogarithmic plots of predicted and observed plasma concentration-time profiles of imatinib and N-desmethyl imatinib. Solid lines and ribbons represent population predictions ( $n = 1000$ ; geometric mean and geometric standard deviation), while corresponding observed data are shown as dots ( $\pm$  standard deviation, if available) [18, 20, 35–39]. Healthy: healthy subjects, Ima: imatinib, n: number of study participants, NDMI: N-desmethyl imatinib, Patients: cancer patients, po: oral, QD: once daily, SD: single dose.

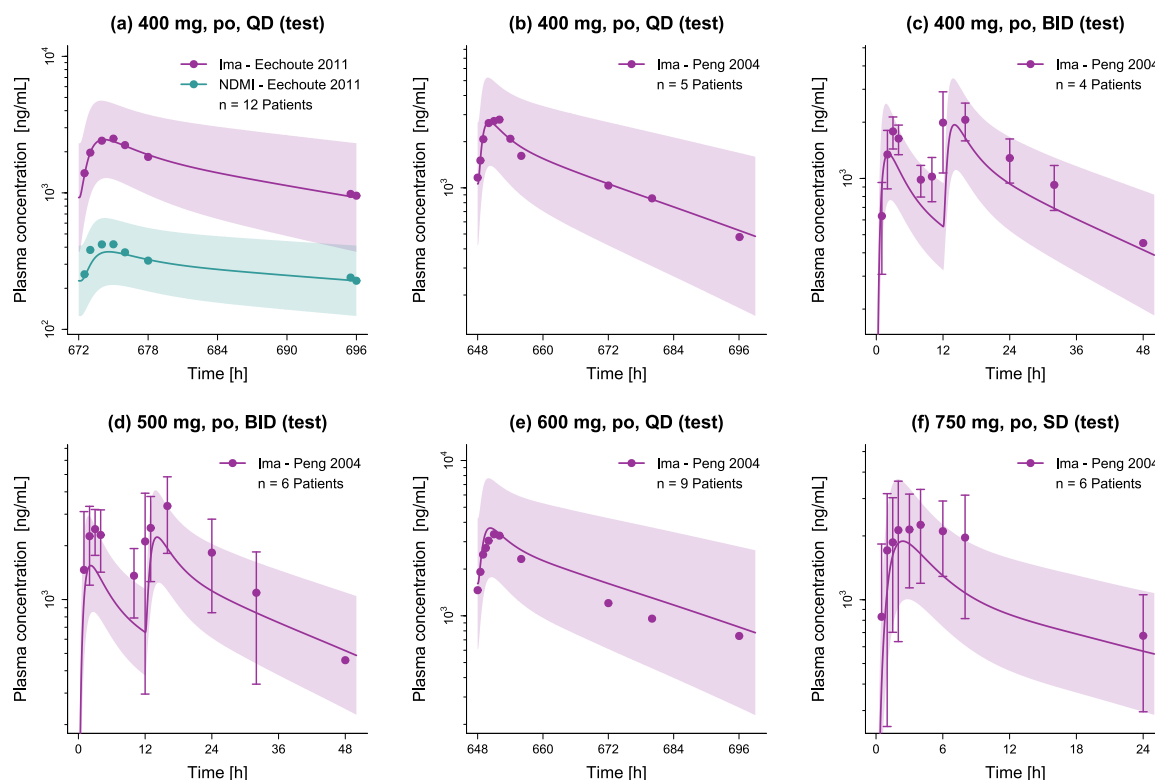


**Figure S5:** Semilogarithmic plots of predicted and observed plasma concentration-time profiles of imatinib and N-desmethyl imatinib. Solid lines and ribbons represent population predictions ( $n = 1000$ ; geometric mean and geometric standard deviation), while corresponding observed data are shown as dots ( $\pm$  standard deviation, if available) [18, 40]. BID: twice daily, Ima: imatinib, n: number of study participants, NDMI: N-desmethyl imatinib, Patients: cancer patients, po: oral, QD: once daily, SD: single dose.

## S2.2 Plasma Concentration-Time Profiles (Linear)

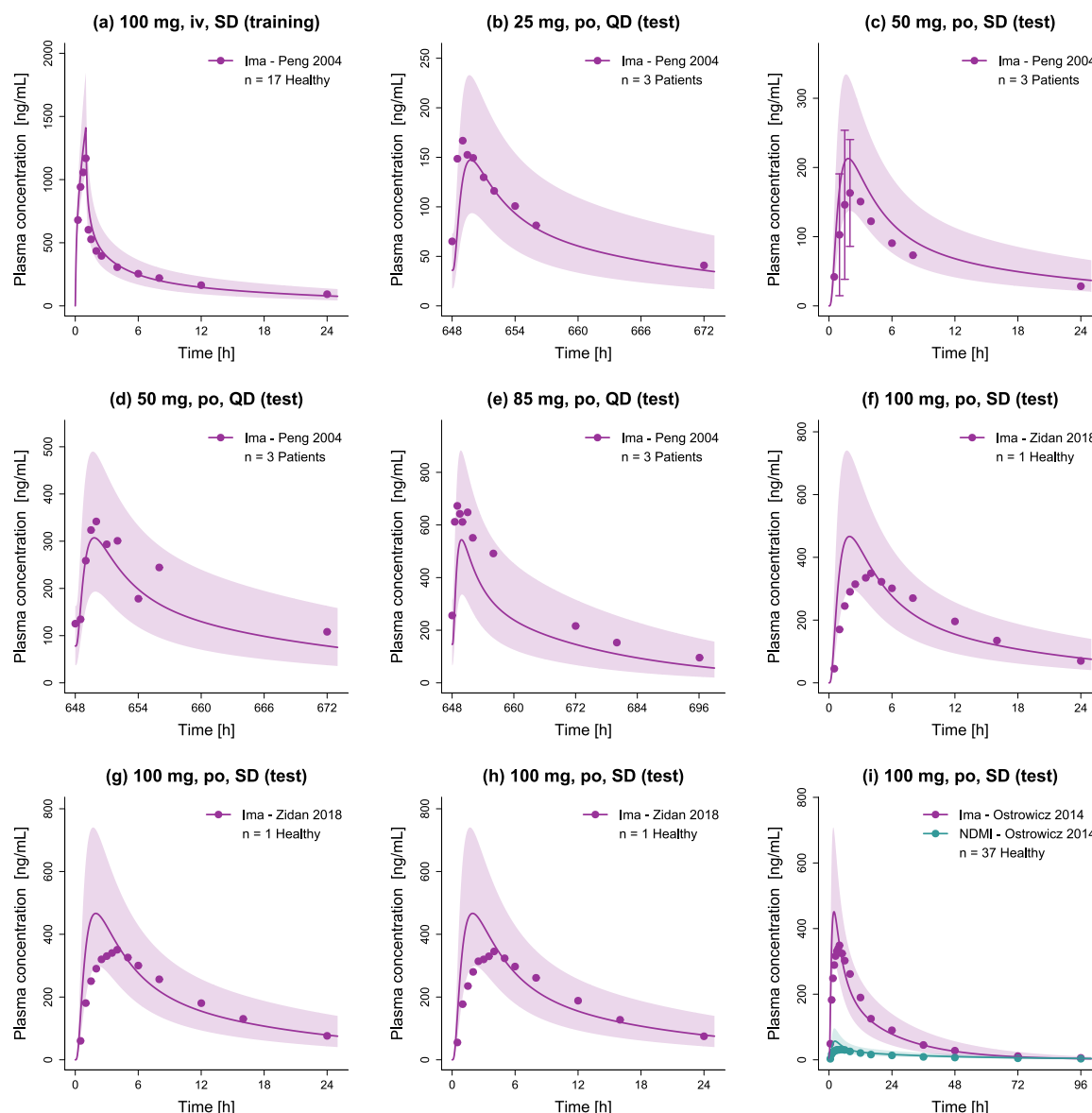


**Figure S6:** Linear plots of predicted and observed plasma concentration-time profiles of imatinib and N-desmethyl imatinib. Solid lines and ribbons represent population predictions ( $n = 1000$ ; geometric mean and geometric standard deviation), while corresponding observed data are shown as dots ( $\pm$  standard deviation, if available) [17–20]. Healthy: healthy subjects, Ima: imatinib, iv: intravenous, n: number of study participants, NDMI: N-desmethyl imatinib, Patients: cancer patients, po: oral, QD: once daily, SD: single dose.

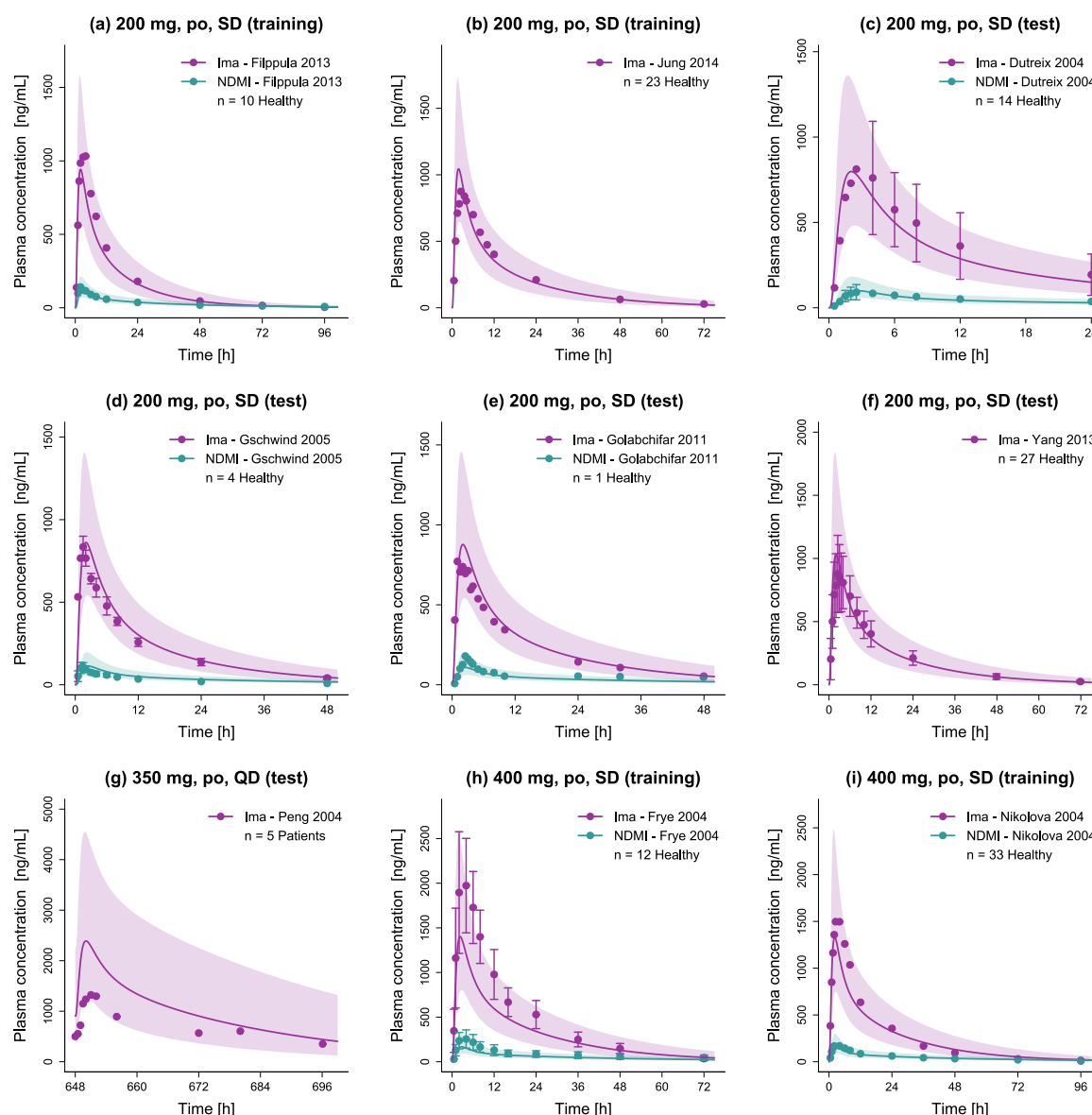


**Figure S7:** Linear plots of predicted and observed plasma concentration-time profiles of imatinib and N-desmethyl imatinib. Solid lines and ribbons represent population predictions ( $n = 1000$ ; geometric mean and geometric standard deviation), while corresponding observed data are shown as dots ( $\pm$  standard deviation, if available) [18, 21–28]. Healthy: healthy subjects, Ima: imatinib, n: number of study participants, NDMI: N-desmethyl imatinib, Patients: cancer patients, po: oral, QD: once daily, SD: single dose.

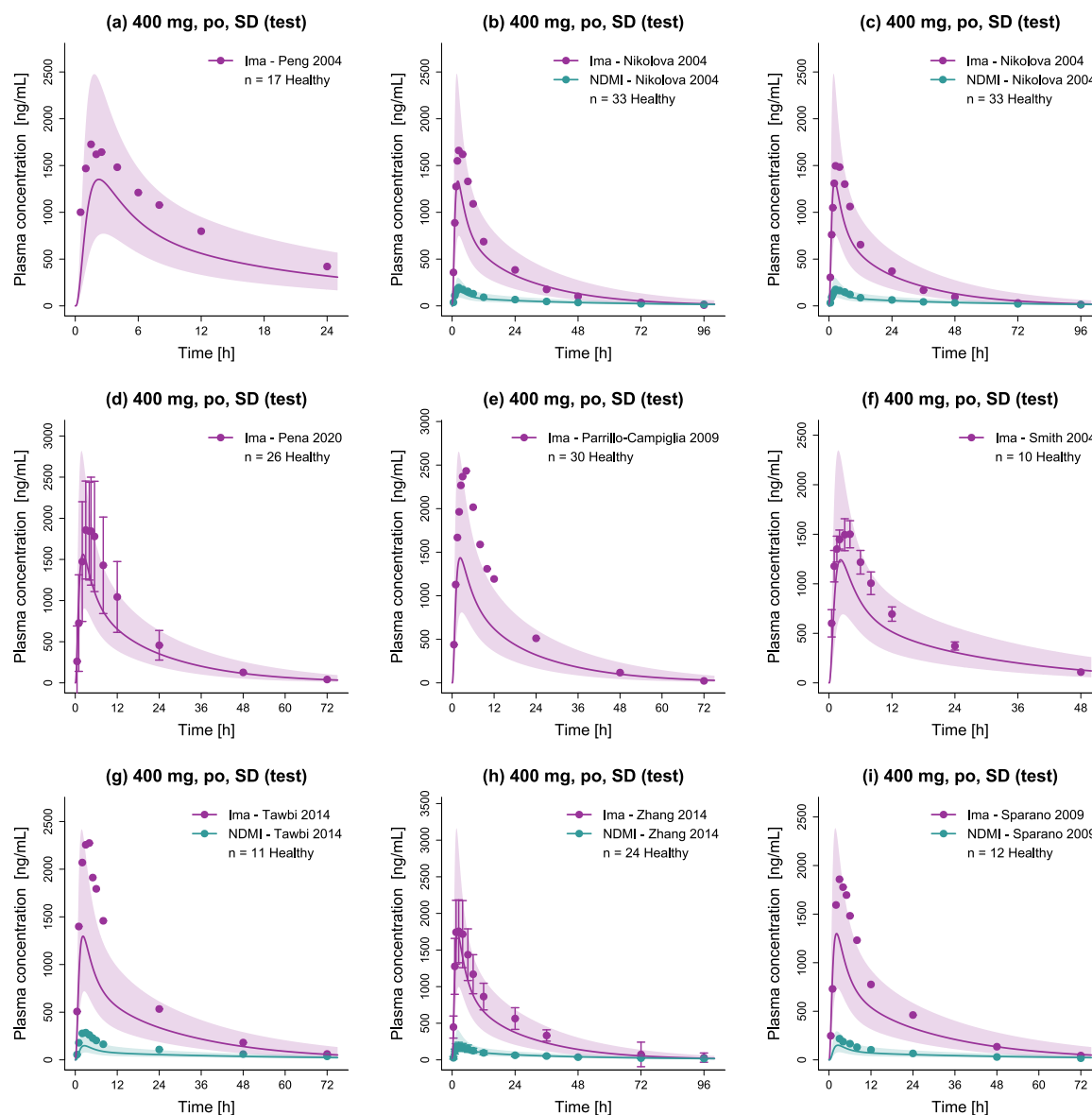


**Figure S8:** Linear plots of predicted and observed plasma concentration-time profiles of imatinib and N-desmethyl imatinib. Solid lines and ribbons represent population predictions ( $n = 1000$ ; geometric mean and geometric standard deviation), while corresponding observed data are shown as dots ( $\pm$  standard deviation, if available) [17, 28–34]. Healthy: healthy subjects, Ima: imatinib, n: number of study participants, NDMI: N-desmethyl imatinib, po: oral, SD: single dose.



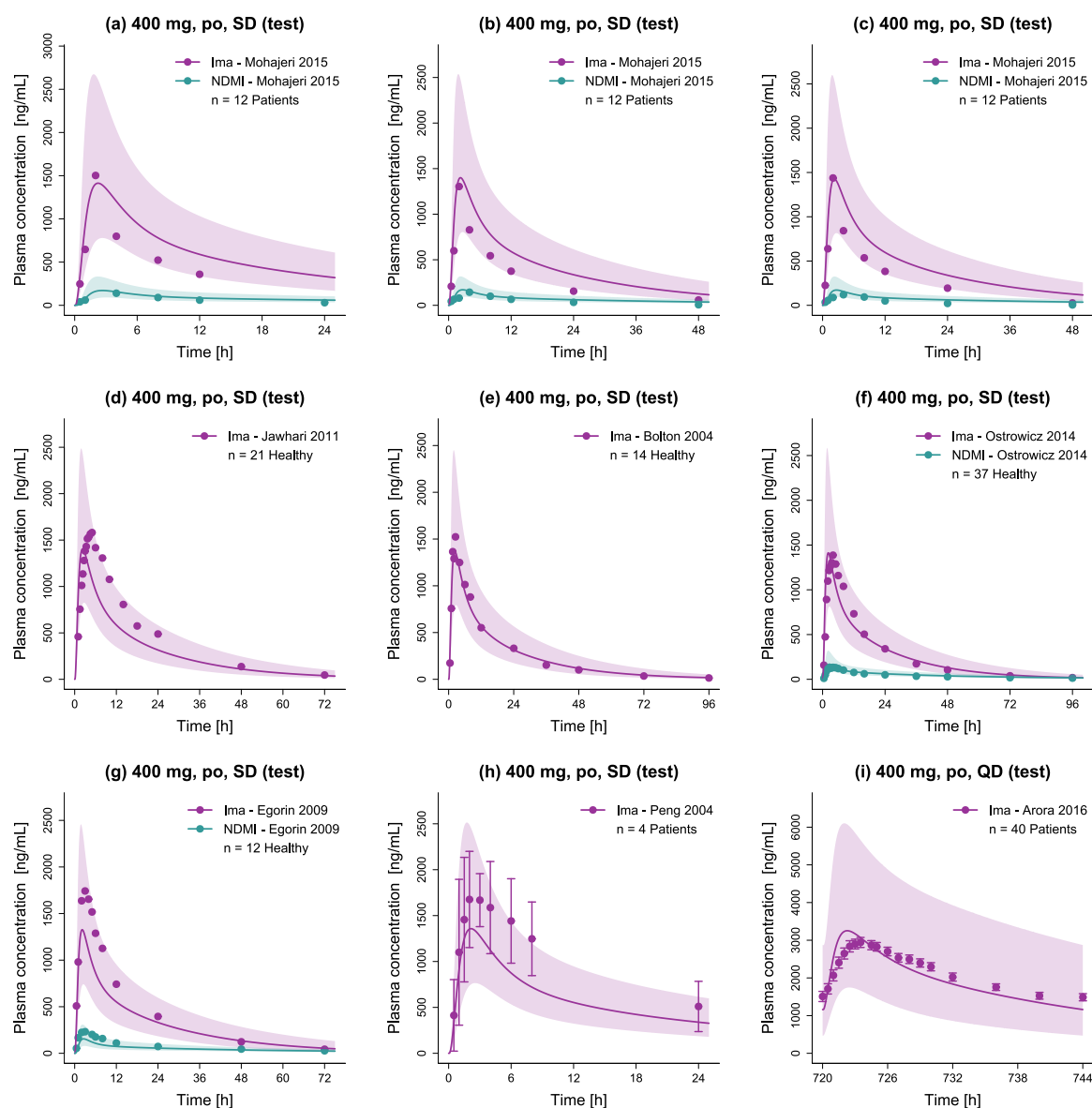


**Figure S9:** Linear plots of predicted and observed plasma concentration-time profiles of imatinib and N-desmethyl imatinib. Solid lines and ribbons represent population predictions ( $n = 1000$ ; geometric mean and geometric standard deviation), while corresponding observed data are shown as dots ( $\pm$  standard deviation, if available) [18, 20, 35–39]. Healthy: healthy subjects, Ima: imatinib, n: number of study participants, NDMI: N-desmethyl imatinib, Patients: cancer patients, po: oral, QD: once daily, SD: single dose.

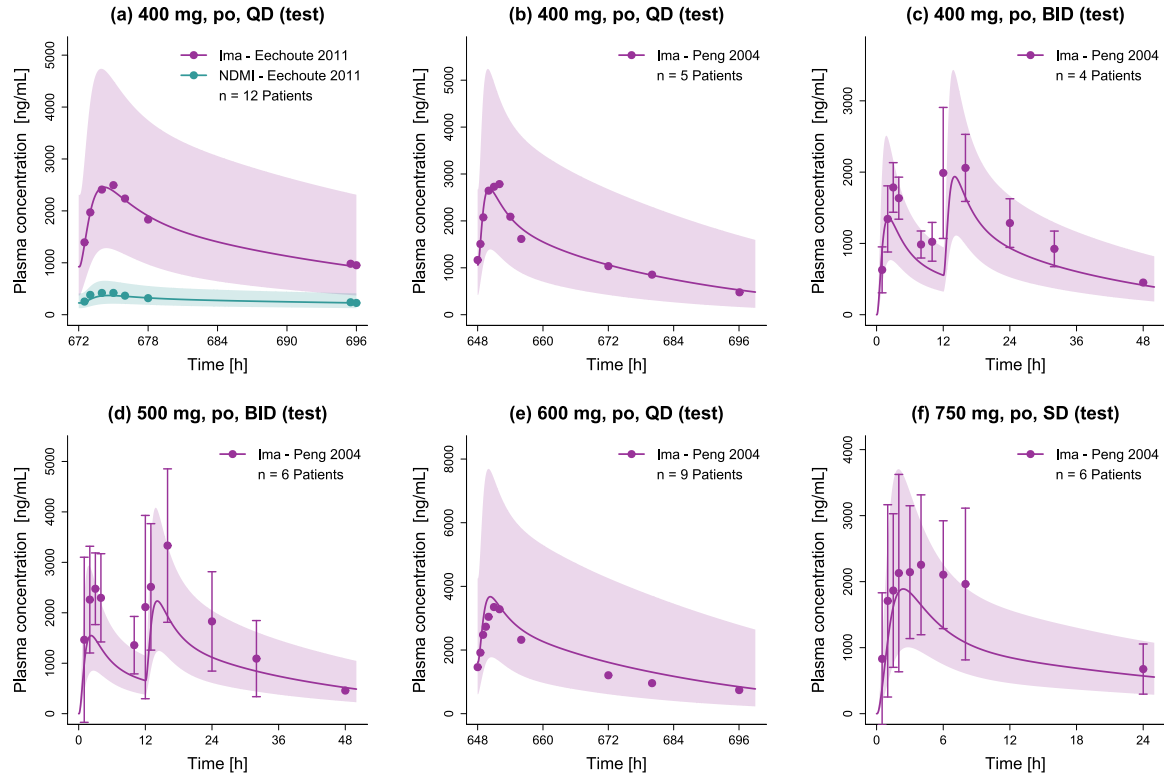


**Figure S10:** Linear plots of predicted and observed plasma concentration-time profiles of imatinib and N-desmethyl imatinib. Solid lines and ribbons represent population predictions ( $n = 1000$ ; geometric mean and geometric standard deviation), while corresponding observed data are shown as dots ( $\pm$  standard deviation, if available) [18, 40]. BID: twice daily, Ima: imatinib, n: number of study participants, NDMI: N-desmethyl imatinib, Patients: cancer patients, po: oral, QD: once daily, SD: single dose.

### S2.3 Urinary Excretion Profiles

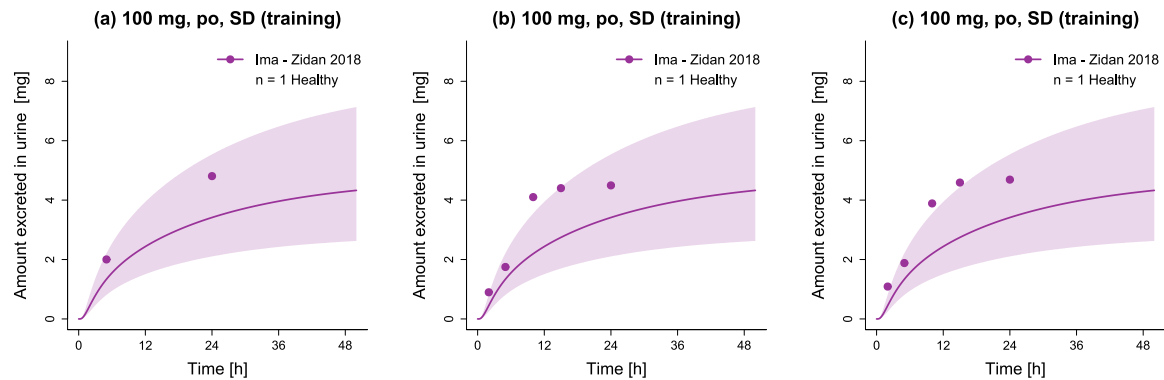


**Figure S11:** Cumulative amount excreted in urine of imatinib. Solid lines and ribbons represent population predictions ( $n = 1000$ ; geometric mean and geometric standard deviation), while corresponding observed data are shown as dots [19]. Healthy: healthy subjects, Ima: imatinib, n: number of study participants, po: oral, SD: single dose.

## S2.4 Goodness-of-Fit Plots

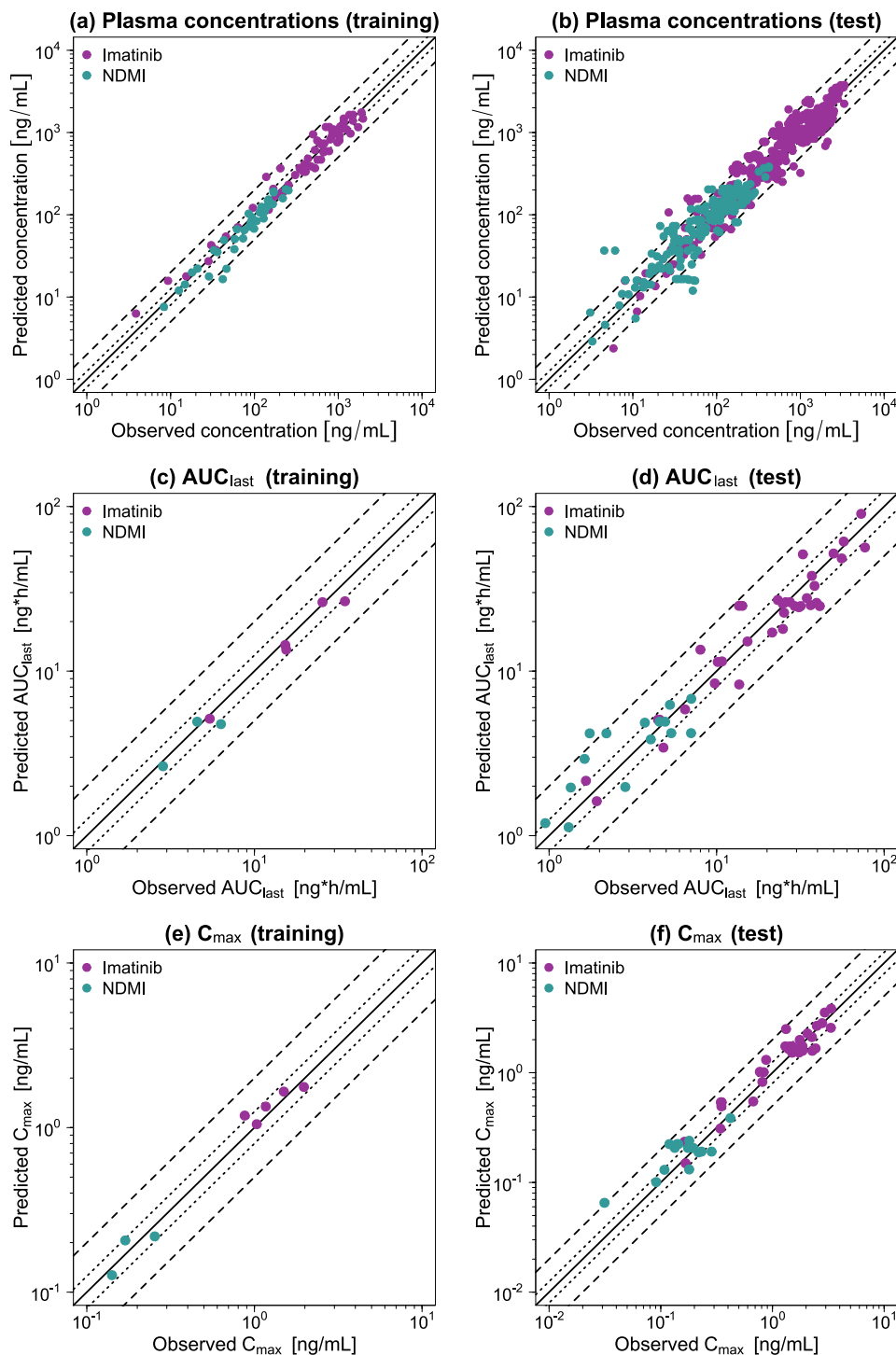


**Figure S12:** Goodness-of-fit plots of the final imatinib model. Stratified by training (left column) and test dataset (right column), predicted plasma concentration measurements (a–b) as well as  $AUC_{last}$  (c–d) and  $C_{max}$  (e–f) values are plotted against corresponding observed data. The solid line represents the line of identity, while dotted lines indicate 1.25-fold and dashed lines twofold deviation from the respective observed value.  $AUC_{last}$ : area under the curve determined between first and last plasma concentration measurements,  $C_{max}$ : maximum plasma concentration, NDMI: N-desmethyl imatinib.

## S2.5 MRD of Plasma Concentration Predictions

**Table S5:** MRD values of plasma concentration predictions

Compound	Imatinib dosing regimen		n	Dataset	MRD	Reference
	Route	Dose [mg]				
Ima	iv (inf, 1 h, SD)	100	17 (healthy)	training	1.13	Peng 2004 [17]
Ima	po (-, QD)	25	3 (CML patients)	test	1.43	Peng 2004 [18]
Ima	po (-, SD)	50	3 (CML patients)	test	1.49	Peng 2004 [18]
Ima	po (-, QD)	50	3 (CML patients)	test	1.32	Peng 2004 [18]
Ima	po (-, QD)	85	3 (CML patients)	test	1.63	Peng 2004 [18]
Ima	po (tab, SD)	100	1 (healthy)	test	1.71	Zidan 2018 [19]
Ima	po (tab, SD)	100	1 (healthy)	test	1.59	Zidan 2018 [19]
Ima	po (tab, SD)	100	1 (healthy)	test	1.64	Zidan 2018 [19]
Ima	po (tab, SD)	100	37 (healthy)	test	1.61	Ostrowicz 2014 [20]
Ima	po (tab, SD)	200	10 (healthy)	training	1.36	Filppula 2013 [21]
Ima	po (tab, SD)	200	23 (healthy)	training	1.37	Jung 2014 [22]
Ima	po (cap, SD)	200	14 (healthy)	test	1.13	Dutreix 2004 [23]
Ima	po (cap, SD)	200	4 (healthy)	test	1.33	Gschwind 2005 [24]
Ima	po (tab, SD)	200	1 (healthy)	test	1.29	Golabchifar 2011 [25]
Ima	po (-, SD)	200	27 (healthy)	test	1.43	Yang 2013 [26]
Ima	po (-, QD)	350	5 (CML patients)	test	1.87	Peng 2004 [18]
Ima	po (-, SD)	400	12 (healthy)	training	1.28	Frye 2004 [27]
Ima	po (tab, SD)	400	33 (healthy)	training	1.25	Nikolova 2004 [28]
Ima	po (cap, SD)	400	17 (healthy)	test	1.52	Peng 2004 [17]
Ima	po (cap, SD)	400	33 (healthy)	test	1.25	Nikolova 2004 [28]
Ima	po (tab, SD)	400	33 (healthy)	test	1.23	Nikolova 2004 [28]
Ima	po (-, SD)	400	26 (healthy)	test	1.31	Pena 2020 [29]
Ima	po (tab, SD)	400	30 (healthy)	test	1.42	Parrillo-Campiglia [30]
Ima	po (-, SD)	400	10 (healthy)	test	1.28	Smith 2004 [31]
Ima	po (-, SD)	400	11 (healthy)	test	1.54	Tawbi 2014 [32]
Ima	po (cap, SD)	400	24 (healthy)	test	1.14	Zhang 2014 [33]
Ima	po (-, SD)	400	12 (healthy)	test	1.32	Sparano 2009 [34]
Ima	po (cap, SD)	400	12 (CML patients)	test	1.72	Mohajeri 2015 [35]
Ima	po (tab, SD)	400	12 (CML patients)	test	1.84	Mohajeri 2015 [35]
Ima	po (tab, SD)	400	12 (CML patients)	test	2.02	Mohajeri 2015 [35]
Ima	po (tab, SD)	400	21 (healthy)	test	1.40	Jawhari 2011 [36]
Ima	po (cap, SD)	400	14 (healthy)	test	1.31	Bolton 2004 [37]
Ima	po (tab, SD)	400	37 (healthy)	test	1.38	Ostrowicz 2014 [20]
Ima	po (-, SD)	400	12 (healthy)	test	1.23	Egorin 2009 [38]
Ima	po (-, SD)	400	4 (CML patients)	test	1.25	Peng 2004 [18]
Ima	po (tab, QD)	400	40 (CML patients)	test	1.15	Arora 2016 [39]
Ima	po (-, QD)	400	12 (GIST patients)	test	1.07	Eechoute 2011 [40]
Ima	po (-, QD)	400	5 (CML patients)	test	1.09	Peng 2004 [18]
Ima	po (-, BID)	400	4 (CML patients)	test	1.46	Peng 2004 [18]
Ima	po (-, BID)	500	6 (CML patients)	test	1.56	Peng 2004 [18]
Ima	po (-, QD)	600	9 (CML patients)	test	1.24	Peng 2004 [18]
Ima	po (-, SD)	750	6 (CML patients)	test	1.45	Peng 2004 [18]

-: not given, BID: twice daily, cap: capsule, CML: chronic myeloid leukemia, GIST: gastrointestinal stromal tumor, Ima: imatinib, inf: infusion, iv: intravenous, MRD: mean relative deviation, n: number of participants, NDMI: N-desmethyl imatinib, po: oral, QD: once daily, SD: single dose, tab: tablet.

**Table S5:** MRD values of plasma concentration predictions (*continued*)

Compound	Imatinib dosing regimen		n	Dataset	MRD	Reference
	Route	Dose [mg]				
NDMI	po (tab, SD)	100	37 (healthy)	test	1.71	Ostrowicz 2014 [20]
NDMI	po (tab, SD)	200	10 (healthy)	training	1.17	Filppula 2013 [21]
NDMI	po (cap, SD)	200	14 (healthy)	test	1.29	Dutreix 2004 [23]
NDMI	po (cap, SD)	200	4 (healthy)	test	1.85	Gschwind 2005 [24]
NDMI	po (tab, SD)	200	1 (healthy)	test	1.48	Golabchifar 2011 [25]
NDMI	po (-, SD)	400	12 (healthy)	training	1.42	Frye 2004 [27]
NDMI	po (tab, SD)	400	33 (healthy)	training	1.42	Nikolova 2004 [28]
NDMI	po (cap, SD)	400	33 (healthy)	test	1.27	Nikolova 2004 [28]
NDMI	po (tab, SD)	400	33 (healthy)	test	1.25	Nikolova 2004 [28]
NDMI	po (-, SD)	400	11 (healthy)	test	1.84	Tawbi 2014 [32]
NDMI	po (cap, SD)	400	24 (healthy)	test	1.21	Zhang 2014 [33]
NDMI	po (-, SD)	400	12 (healthy)	test	1.21	Sparano 2009 [34]
NDMI	po (cap, SD)	400	12 (CML patients)	test	1.92	Mohajeri 2015 [35]
NDMI	po (tab, SD)	400	12 (CML patients)	test	2.44	Mohajeri 2015 [35]
NDMI	po (tab, SD)	400	12 (CML patients)	test	2.81	Mohajeri 2015 [35]
NDMI	po (tab, SD)	400	37 (healthy)	test	1.44	Ostrowicz 2014 [20]
NDMI	po (-, SD)	400	12 (healthy)	test	1.61	Egorin 2009 [38]
NDMI	po (-, QD)	400	12 (GIST patients)	test	1.13	Eechoute 2011 [40]
Training dataset mean MRD (range)				1.29 (1.13–1.42)		
Test dataset mean MRD (range)				1.48 (1.07–2.81)		
Imatinib mean MRD (range)				1.41 (1.07–2.02)		
NDMI mean MRD (range)				1.58 (1.13–2.81)		
Overall mean MRD (range)				1.46 (1.07–2.81)		
MRD $\leq 2$				57/60		

-: not given, BID: twice daily, cap: capsule, CML: chronic myeloid leukemia, GIST: gastrointestinal stromal tumor, Ima: imatinib, inf: infusion, iv: intravenous, MRD: mean relative deviation, n: number of participants, NDMI: N-desmethyl imatinib, po: oral, QD: once daily, SD: single dose, tab: tablet.

## S2.6 Predicted and Observed $AUC_{last}$ and $C_{max}$ Values

Table S6: Predicted versus observed  $AUC_{last}$  and  $C_{max}$  values

Comp.	Imatinib dosing regimen		n	Dataset	$AUC_{last}$		$C_{max}$		Reference
	Route	Dose [mg]			Pred [ $\frac{ng \cdot h}{mL}$ ]	Obs [ $\frac{ng \cdot h}{mL}$ ]	Pred [ $\frac{ng}{mL}$ ]	Obs [ $\frac{ng}{mL}$ ]	
Ima	iv (inf, 1 h, SD)	100	17 (healthy)	training	5135.03	5413.67	1341.86	1168.54	Peng 2004 [17]
Ima	po (-, QD)	25	3 (CML patients)	test	1620.46	1925.88	149.64	166.80	Peng 2004 [18]
Ima	po (-, SD)	50	3 (CML patients)	test	2156.03	1659.50	234.92	163.17	Peng 2004 [18]
Ima	po (-, QD)	50	3 (CML patients)	test	3427.70	4812.66	309.81	341.81	Peng 2004 [18]
Ima	po (-, QD)	85	3 (CML patients)	test	8292.80	13640.36	546.95	672.65	Peng 2004 [18]
Ima	po (tab, SD)	100	1 (healthy)	test	5065.99	4567.07	537.48	349.13	Zidan 2018 [19]
Ima	po (tab, SD)	100	1 (healthy)	test	5066.65	4492.26	537.48	350.70	Zidan 2018 [19]
Ima	po (tab, SD)	100	1 (healthy)	test	5066.65	4472.12	537.48	345.41	Zidan 2018 [19]
Ima	po (tab, SD)	100	37 (healthy)	test	5850.56	6480.78	493.80	348.87	Ostrowicz 2014 [20]
Ima	po (tab, SD)	200	10 (healthy)	training	13491.87	15477.34	1048.55	1032.35	Filippula 2013 [21]
Ima	po (tab, SD)	200	23 (healthy)	training	14406.34	15278.67	1182.78	874.95	Jung 2014 [22]
Ima	po (cap, SD)	200	14 (healthy)	test	8422.16	9750.92	824.82	812.31	Dutreix 2004 [23]
Ima	po (cap, SD)	200	4 (healthy)	test	11361.68	10162.66	1011.29	834.99	Gschwind 2005 [24]
Ima	po (tab, SD)	200	1 (healthy)	test	11457.06	10770.52	1019.34	771.20	Golabchifar 2011 [25]
Ima	po (-, SD)	200	27 (healthy)	test	15141.20	15286.99	1310.48	877.81	Yang 2013 [26]
Ima	po (-, QD)	350	5 (CML patients)	test	51224.25	32731.62	2499.24	1322.70	Peng 2004 [18]
Ima	po (-, SD)	400	12 (healthy)	training	26558.01	34680.72	1765.16	1972.90	Frye 2004 [27]
Ima	po (tab, SD)	400	33 (healthy)	training	26233.38	25471.37	1654.84	1497.23	Nikolova 2004 [28]
Ima	po (cap, SD)	400	17 (healthy)	test	17158.16	21458.79	1525.15	1726.61	Peng 2004 [17]
Ima	po (cap, SD)	400	33 (healthy)	test	26231.76	27407.94	1654.84	1660.68	Nikolova 2004 [28]
Ima	po (tab, SD)	400	33 (healthy)	test	26231.72	25845.92	1654.84	1496.76	Nikolova 2004 [28]
Ima	po (-, SD)	400	26 (healthy)	test	27754.49	34577.78	1744.23	1857.26	Pena 2020 [29]
Ima	po (tab, SD)	400	30 (healthy)	test	25977.11	39524.46	1665.92	2432.85	Parrillo-Campiglia [30]
Ima	po (-, SD)	400	10 (healthy)	test	24833.59	41273.28	1583.45	2274.30	Smith 2004 [31]
Ima	po (cap, SD)	400	11 (healthy)	test	32955.63	38422.97	1991.31	1755.60	Tawbi 2014 [32]
Ima	po (-, SD)	400	24 (healthy)	test	24834.21	31739.96	1583.46	1858.33	Zhang 2014 [33]
Ima	po (cap, SD)	400	12 (healthy)	test	13494.94	8003.87	1739.85	1502.51	Sparano 2009 [34]
Ima	po (tab, SD)	400	12 (CML patients)	test	24921.36	13603.14	1740.06	1303.70	Mohajeri 2015 [35]
Ima	po (tab, SD)	400	12 (CML patients)	test	24917.20	14231.96	1739.83	1437.86	Mohajeri 2015 [35]
Ima	po (tab, SD)	400	21 (healthy)	test	24426.74	30992.29	1558.62	1580.92	Mohajeri 2015 [36]
Ima	po (cap, SD)	400	14 (healthy)	test	27039.91	23183.57	1602.67	1523.50	Bolton 2004 [37]
Ima	po (tab, SD)	400	37 (healthy)	test	25659.89	24839.39	1652.22	1386.64	Ostrowicz 2014 [20]
Ima	po (-, SD)	400	12 (healthy)	test	24830.21	29259.96	1583.31	1742.20	Egorin 2009 [38]
Ima	po (-, SD)	400	4 (CML patients)	test	18042.33	24873.97	1590.22	1675.79	Peng 2004 [18]

-: not given,  $AUC_{last}$ : area under the plasma concentration-time curve determined between first and last concentration measurements, BID: twice daily, cap: capsule,  $C_{max}$ : maximum plasma concentration, CML: chronic myeloid leukemia, comp.: compound, GST: gastrointestinal stromal tumor, GMFE: geometric mean fold error, Ima: imatinib, inf: infusion, iv: intravenous, NDMI: N-desmethyl imatinib, n: number of participants, obs: observed, po: oral, pred: predicted, QD: once daily, SD: single dose, tab: tablet.

Table S6: Predicted versus observed  $AUC_{last}$  and  $C_{max}$  values (continued)

Comp.	Imatinib dosing regimen		n	Dataset	$AUC_{last}$		$C_{max}$		Reference
	Route	Dose [mg]			Pred [ $\frac{ng}{mL}$ ]	Obs [ $\frac{ng}{mL}$ ]	Pred [ $\frac{ng}{mL}$ ]	Obs [ $\frac{ng}{mL}$ ]	
Ima	po (tab, QD)	400	40 (CML patients)	test	51824.07	49892.23	3536.39	2941.33	Arora 2016 [39]
Ima	po (-, QD)	400	12 (GIST patients)	test	37924.07	37036.92	2673.46	2495.52	Echoute 2011 [40]
Ima	po (-, QD)	400	5 (CML patients)	test	61263.32	57407.51	2829.41	2784.60	Peng 2004 [18]
Ima	po (-, BID)	400	4 (CML patients)	test	48390.10	55826.05	2279.51	2059.17	Peng 2004 [18]
Ima	po (-, BID)	500	6 (CML patients)	test	56400.59	76859.29	2566.09	3332.50	Peng 2004 [18]
Ima	po (-, QD)	600	9 (CML patients)	test	90308.34	729947.50	3832.97	3350.20	Peng 2004 [18]
Ima	po (-, SD)	750	6 (CML patients)	test	25158.86	36417.12	2111.84	2255.24	Peng 2004 [18]
NDMI	po (tab, SD)	100	37 (healthy)	test	1191.65	948.99	65.20	31.30	Ostrowicz 2014 [20]
NDMI	po (tab, SD)	200	10 (healthy)	training	2642.06	2848.15	126.85	141.26	Filippula 2013 [21]
NDMI	po (cap, SD)	200	14 (healthy)	test	1125.55	1308.30	100.75	90.94	Duttreix 2004 [23]
NDMI	po (cap, SD)	200	4 (healthy)	test	1961.24	1347.14	130.29	107.86	Gschwind 2005 [24]
NDMI	po (tab, SD)	200	1 (healthy)	test	1975.89	2850.58	131.29	179.59	Golabchifar 2011 [25]
NDMI	po (-, SD)	400	12 (healthy)	training	4762.88	6313.61	218.23	254.29	Frye 2004 [27]
NDMI	po (tab, SD)	400	33 (healthy)	training	4925.99	4555.57	206.22	169.55	Nikolova 2004 [28]
NDMI	po (cap, SD)	400	33 (healthy)	test	4925.99	4927.30	206.22	195.45	Nikolova 2004 [28]
NDMI	po (tab, SD)	400	33 (healthy)	test	495.99	4565.31	206.22	175.30	Nikolova 2004 [28]
NDMI	po (-, SD)	400	11 (healthy)	test	4198.97	7038.25	191.02	285.15	Tawbi 2014 [32]
NDMI	po (cap, SD)	400	24 (healthy)	test	6239.45	5264.18	239.88	179.60	Zhang 2014 [33]
NDMI	po (-, SD)	400	12 (healthy)	test	3845.99	4044.45	187.88	218.01	Sparano 2009 [34]
NDMI	po (cap, SD)	400	12 (CML patients)	test	2927.40	1628.46	180	140.04	Mohajeri 2015 [35]
NDMI	po (tab, SD)	400	12 (CML patients)	test	4186.14	2199.09	223.49	143.83	Mohajeri 2015 [35]
NDMI	po (tab, SD)	400	12 (CML patients)	test	4185.71	1747.22	223.48	119.49	Mohajeri 2015 [35]
NDMI	po (tab, SD)	400	37 (healthy)	test	4859.00	3728.96	206.58	133.46	Ostrowicz 2014 [20]
NDMI	po (-, SD)	400	12 (healthy)	test	4198.54	5361.34	191.01	231.64	Egorin 2009 [38]
NDMI	po (-, QD)	400	12 (GIST patients)	test	6789.87	7060.68	386.00	420.01	Echoute 2011 [40]
Training dataset mean GMFE (range)					1.14 (1.03-1.33)		1.18 (1.11-1.35)		
Test dataset mean GMFE (range)					1.31 (1.00-2.40)		1.27 (1.00-2.08)		
Imatinib mean GMFE (range)					1.25 (1.01-1.83)		1.22 (1.00-1.89)		
NDMI mean GMFE (range)					1.36 (1.00-2.40)		1.35 (1.06-2.08)		
Overall mean GMFE (range)					1.28 (1.00-2.40)		1.26 (1.00-2.08)		
GMFE $\leq 2$					59/60		59/60		

-: not given,  $AUC_{last}$ : area under the plasma concentration-time curve determined between first and last concentration measurements, BID: twice daily, cap: capsule,  $C_{max}$ : maximum plasma concentration, CML: chronic myeloid leukemia, comp.: compound, GIST: gastrointestinal stromal tumor, GMFE: geometric mean fold error, Ima: imatinib, inf: infusion, iv: intravenous, NDMI: N-desmethyl imatinib, n: number of participants, obs: observed, po: oral, pred: predicted, QD: once daily, SD: single dose, tab: tablet.

## S2.7 Local Sensitivity Analysis

### S2.7.1 Methods

Local sensitivity analyses were performed for imatinib and N-desmethyl imatinib, by calculating the sensitivity to single parameter changes according to Equation S3. A relative perturbation of 10% was applied (variation range 0.1, maximum number of 2 steps) and parameters included were either optimized or assumed to affect  $AUC_{last}$ .

$$S = \frac{\Delta AUC_{last}}{\Delta p} \cdot \frac{p}{AUC_{last}} \quad (S3)$$

where  $S$  = sensitivity,  $\Delta AUC_{last}$  = change of  $AUC_{last}$ ,  $\Delta p$  = change of the analyzed parameter value,  $p$  = original parameter value, and  $AUC_{last}$  = simulated  $AUC_{last}$  with the original parameter value.

The threshold for sensitivity was set at  $|0.5|$ , which corresponds to a 50% change in simulated  $AUC_{last}$  given a 100% change in the parameter value examined.

### S2.7.2 Results

**Table S7:** Parameters evaluated during the local sensitivity analyses

Compound	Parameter	Source	Compound	Parameter	Source
Ima	pKa <sub>1</sub> , acid	Lit.	Ima	CYP3A4 K <sub>i</sub> MBI	Lit.
Ima	pKa <sub>2</sub> , base	Lit.	Ima	CYP3A4 K <sub>I</sub> MBI	Lit.
Ima	pKa <sub>3</sub> , base	Lit.	Ima	CYP3A4 k <sub>inact</sub> MBI	Lit.
Ima	Solubility	Lit.	Ima	P-gp K <sub>i</sub> CI	Lit.
Ima	Lipophilicity	Opt.	NDMI	pKa <sub>1</sub> , acid	Lit.
Ima	Fraction unbound	Lit.	NDMI	pKa <sub>2</sub> , base	Lit.
Ima	CYP2C8 K <sub>M</sub>	Lit.	NDMI	pKa <sub>3</sub> , base	Lit.
Ima	CYP2C8 k <sub>cat</sub>	Opt.	NDMI	Solubility	Lit.
Ima	CYP3A4 K <sub>M</sub>	Lit.	NDMI	Lipophilicity	Opt.
Ima	CYP3A4 k <sub>cat</sub>	Opt.	NDMI	Fraction unbound	Lit.
Ima	CYP3A4 CL	Opt.	NDMI	CYP2C8 CL	Opt.
Ima	P-gp K <sub>M</sub>	Opt.	NDMI	CYP3A4 CL	Opt.
Ima	P-gp k <sub>cat</sub>	Opt.	NDMI	Hepatic CL	Opt.
Ima	GFR fraction	Asm.	NDMI	GFR fraction	Asm.
Ima	Intestinal permeability	Opt.	NDMI	CYP2C8 K <sub>i</sub> CI	Lit.
Ima	CYP2C8 K <sub>i</sub> CI	Lit.	NDMI	CYP3A4 K <sub>i</sub> CI	Lit.

Asm.: assumed, CI: competitive inhibition, CYP: cytochrome P450, GFR: glomerular filtration rate, Ima: imatinib, k<sub>cat</sub>: catalytic/transport rate constant, K<sub>i</sub>: dissociation constant inhibitor-enzyme/transporter complex, K<sub>I</sub>: concentration for half-maximal inactivation, k<sub>inact</sub>: maximum inactivation rate constant, K<sub>M</sub>: Michaelis-Menten constant, lit.: literature, MBI: mechanism-based inactivation, NDMI: N-desmethyl imatinib, opt.: optimized, pKa: acid dissociation constant, P-gp: P-glycoprotein.



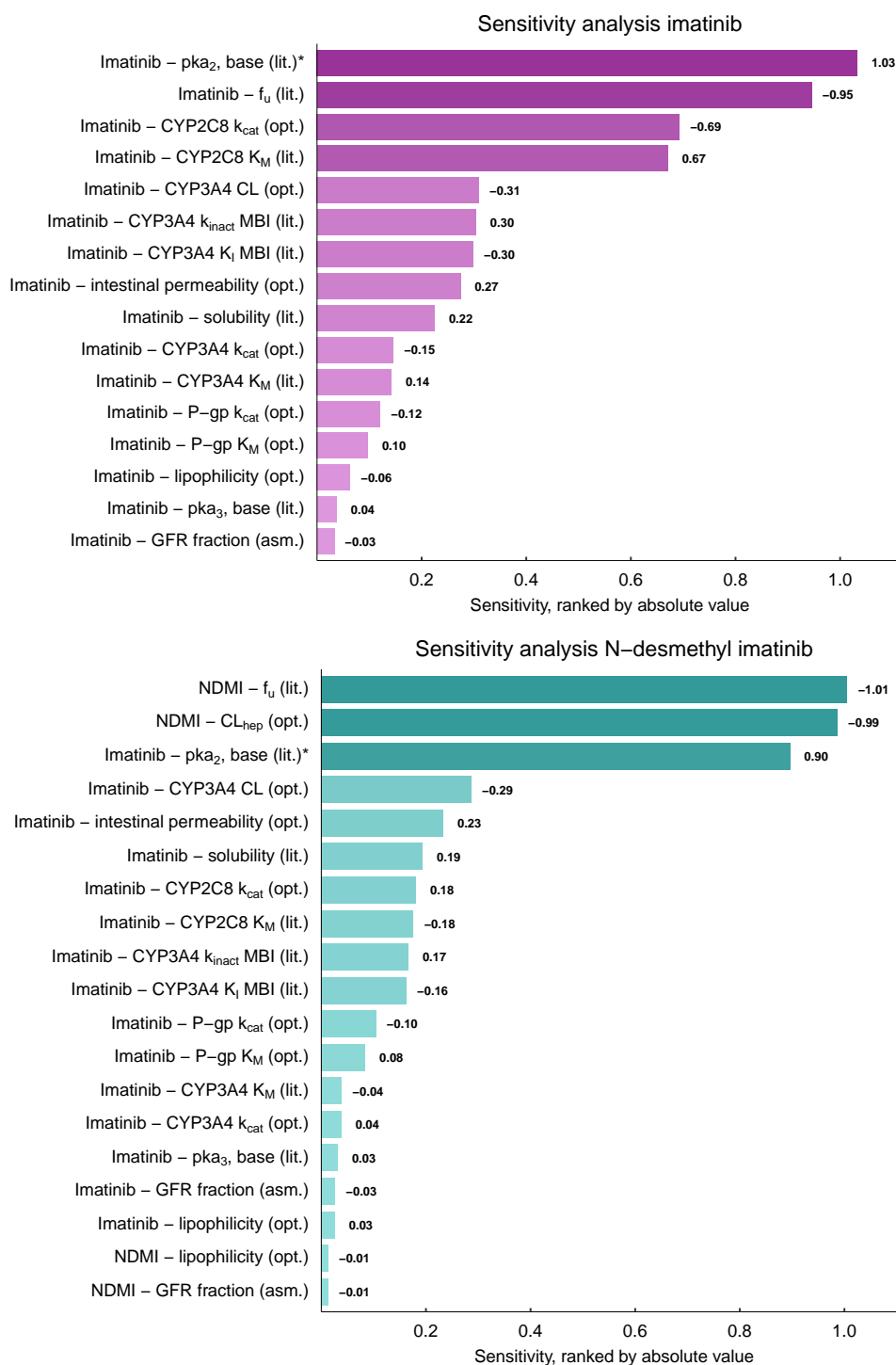


**Figure S13:** Imatinib model sensitivity analysis (400 mg, once daily [18]). Presented are parameters with a calculated sensitivity different from 0.00. Asm.: assumed, CI: competitive inhibition, CYP: cytochrome P450,  $f_u$ : fraction unbound, GFR: glomerular filtration rate,  $k_{cat}$ : catalytic/transport rate constant,  $K_i$ : dissociation constant inhibitor-enzyme/transporter complex,  $K_I$ : concentration for half-maximal inactivation,  $k_{inact}$ : maximum inactivation rate constant,  $K_M$ : Michaelis-Menten constant, lit.: literature, MBI: mechanism-based inactivation, NDMI: N-desmethyl imatinib, opt.: optimized, pKa: acid dissociation constant, P-gp: P-glycoprotein. \*: Due to the proximity of the model parameter (7.84) to the physiological pH of 7.4, an increase of 10% causes only a small change in imatinib and NDMI AUC values, while a reduction of 10% is associated with a large decrease in exposure.

## S3 Drug-Drug Interaction Modeling

### S3.1 Clinical Study Data

Table S8: Imatinib DDI model study table

Victim application [mg]	Perpetrator application [mg]	n	Females [%]	Ethnicity <sup>a</sup>	Age [years]	Weight [kg]	Height [cm]	Compound(s) measured	Reference
<b>Imatinib</b> d8: 400 po (cap, SD)	<b>Rifampicin</b> d1–11: 600 po (, QD)	14 (healthy)	7	European	49.8±8.2 (40–64)	74.4±8.1 (61.5–90.0)	172±6 (165–186)	Ima	Bolton 2004 [37]
<b>Imatinib</b> d1: 200 po (cap, SD)	<b>Ketoconazole</b> d1: 400 po (, SD)	14 (healthy)	7	European	(35–59)	(64–103)	-	Ima, NDMI	Dutrex 2004 [23]
<b>Imatinib</b> d3: 200 po (tab, SD)	<b>Gemfibrozil</b> d1–6: 600 po (tab, BID)	10 (healthy)	20	European	24±3	72±13	-	Ima, NDMI	Filippula 2013 [21]
<b>Simvastatin</b> d7: 40 po (tab, SD)	<b>Imatinib</b> d1–7: 400 po (cap, QD)	20 (CML patients)	50	European	50.5±13.4	(53–111)	(158–192)	Simva, Simva-Acid	O’Brien 2003 [55]
<b>Metoprolol</b> d7: 100 po (tab, SD)	<b>Imatinib</b> d1–9: 400 po (cap, BID)	13 (CML patients) CYP2D6 NMs	-	Asian	40.6±13.2	73.7±12.6	-	Meto, OH-Meto	Wang 2008 [56]
<b>Metoprolol</b> d7: 100 po (tab, SD)	<b>Imatinib</b> d1–9: 400 po (cap, BID)	6 (CML patients) CYP2D6 IMs	-	Asian	39.8±6.1	72.3±8.0	-	Meto, OH-Meto	Wang 2008 [56]

-: not given, <sup>a</sup>: implemented, BID: twice daily, cap: capsule, CYP: cytochrome P450, d: day, DDI: drug-drug interaction, IM: intermediate metabolizer, Ima: imatinib, Meto: metoprolol, n: number of participants, NDMI: N-desmethyl imatinib, NM: normal metabolizer, OH-Meto: hydroxymetoprolol, po: oral, QD: once daily, SD: single dose, Simva: simvastatin, Simva-Acid: simvastatin hydroxy acid, tab: tablet; values for age, weight, and height are presented as mean ± standard deviation (range).

## S3.2 Drug-Dependent Parameters of DDI Partners

### S3.2.1 Rifampicin

**Table S9:** Drug-dependent parameters of the rifampicin PBPK model [8]

Parameter	Unit	Value	Description
<b>Rifampicin</b>			
Molecular weight	g/mol	822.94	Molecular weight
pKa <sub>1</sub> , base		7.90	Acid dissociation constant
pKa <sub>2</sub> , acid		1.70	Acid dissociation constant
Solubility (pH)	mg/L	2800.00 (7.5)	Solubility
Lipophilicity		2.50	Lipophilicity
f <sub>u</sub>	%	17.00	Fraction unbound
AADAC K <sub>M</sub> → sink	μmol/L	195.10	Michaelis-Menten constant
AADAC k <sub>cat</sub> → sink	1/min	9.87	Catalytic rate constant
OATP1B1 K <sub>M</sub>	μmol/L	1.50	Michaelis-Menten constant
OATP1B1 k <sub>cat</sub>	1/min	74.43 <sup>a</sup>	Transport rate constant
P-gp K <sub>M</sub>	μmol/L	55.00	Michaelis-Menten constant
P-gp k <sub>cat</sub>	1/min	0.61	Transport rate constant
GFR fraction		1 <sup>b</sup>	Filtered drug in the urine
EHC continuous fraction		1	Bile fraction continuously released
Intestinal permeability	cm/min	1.24 · 10 <sup>-5</sup>	Transcellular intestinal permeability
Cellular permeability	cm/min	PK-Sim Standard, 2.93 · 10 <sup>-5</sup>	Permeability into the cellular space
Partition coefficients		Rodgers + Rowland	Organ-plasma partition coefficients
Formulation		Solution	Formulation used in predictions
Induction EC <sub>50</sub>	μmol/L	0.34	Conc. for half-maximal induction
AADAC E <sub>max</sub>		0.99	Maximum induction effect
CYP2C8 E <sub>max</sub>		3.20	Maximum induction effect
CYP2C8 K <sub>i</sub>	μmol/L	30.20	Diss. const. inhibitor-enzyme complex
CYP3A4 E <sub>max</sub>		9.00	Maximum induction effect
CYP3A4 K <sub>i</sub>	μmol/L	18.50	Diss. const. inhibitor-enzyme complex
OATP1B1 E <sub>max</sub>		0.38	Maximum induction effect
OATP1B1 K <sub>i</sub>	μmol/L	0.48	Diss. const. inhibitor-transporter complex
P-gp E <sub>max</sub>		2.50	Maximum induction effect
P-gp K <sub>i</sub>	μmol/L	169.00	Diss. const. inhibitor-transporter complex

<sup>a</sup>: adjusted due to different reference concentrations in the original model and imatinib model, <sup>b</sup>: a GFR fraction of 1 corresponds to passive glomerular filtration of a compound, AADAC: arylacetamide deacetylase, conc.: concentration, CYP: cytochrome P450, diss. const.: dissociation constant, EHC: enterohepatic circulation, GFR: glomerular filtration rate, OATP: organic-anion-transporting polypeptide, P-gp: P-glycoprotein.

## S3.2.2 Ketoconazole

Table S10: Drug-dependent parameters of the ketoconazole PBPK model [58]

Parameter	Unit	Value	Description
<b>Ketoconazole</b>			
Molecular weight	g/mol	531.43	Molecular weight
pKa <sub>1</sub> , base		6.51	Acid dissociation constant
pKa <sub>2</sub> , base		2.94	Acid dissociation constant
Solubility (pH)	mg/L	4.34 (7.40)	Solubility
Lipophilicity	log units	2.52	Lipophilicity
f <sub>u</sub>	%	1	Fraction unbound
AADAC K <sub>M</sub> → ND-Keto	μmol/L	1.88	Michaelis-Menten constant
AADAC k <sub>cat</sub> → ND-Keto	1/min	0.87	Catalytic rate constant
CYP3A4 K <sub>M</sub> → sink	μmol/L	8.46 · 10 <sup>-3</sup>	Michaelis-Menten constant
CYP3A4 k <sub>cat</sub> → sink	1/min	0.10	Catalytic rate constant
UGT1A4 K <sub>M</sub> → sink	μmol/L	7.00	Michaelis-Menten constant
UGT1A4 k <sub>cat</sub> → sink	1/min	0.31	Catalytic rate constant
P-gp K <sub>M</sub>	μmol/L	0.04	Michaelis-Menten constant
P-gp k <sub>cat</sub>	1/min	0.33	Transport rate constant
GFR fraction		1 <sup>a</sup>	Filtered drug in the urine
EHC continuous fraction		1	Bile fraction continuously released
Intestinal permeability	cm/min	9.95 · 10 <sup>-6</sup> (fed)	Transcellular intestinal permeability
GET	min	45 (fed)	Gastric emptying time
Cellular permeability	cm/min	PK-Sim Standard 7.18 · 10 <sup>-4</sup>	Permeability into the cellular space
Partition coefficients		Berezhkovskiy	Organ-plasma partition coefficients
Particle radius Bin1	nm	11.75	Particle dissolution radius
Particle radius Bin2	nm	111.06	Particle dissolution radius
Particle radius Bin3	nm	205.46	Particle dissolution radius
Density	g/cm <sup>3</sup>	1.40	Density
Aqueous diffusion coefficient	dm <sup>2</sup> /min	3.75 · 10 <sup>-7</sup>	Aqueous diffusion coefficient
CYP2C8 K <sub>i</sub>	μmol/L	2.50 <sup>b</sup>	Diss. const. inhibitor-enzyme complex
CYP3A4 K <sub>i</sub>	μmol/L	8.46 · 10 <sup>-3</sup>	Diss. const. inhibitor-enzyme complex
P-gp K <sub>i</sub>	μmol/L	0.04	Diss. const. inhibitor-transporter complex
<b>N-Deacetyl-Ketoconazole</b>			
Molecular weight	g/mol	489.40	Molecular weight
pKa <sub>1</sub> , base		8.90	Acid dissociation constant
pKa <sub>2</sub> , base		6.42	Acid dissociation constant
pKa <sub>3</sub> , base		0.20	Acid dissociation constant
Solubility (pH)	mg/mL	1.24 (6.50)	Solubility
Lipophilicity	log units	3.75	Lipophilicity
f <sub>u</sub>	%	1	Fraction unbound
FMO3 K <sub>M</sub> → OH-Keto	μmol/L	1.17	Michaelis-Menten constant
FMO3 k <sub>cat</sub> → OH-Keto	1/min	378.65	Catalytic rate constant
GFR fraction		1 <sup>a</sup>	Filtered drug in the urine
EHC continuous fraction		1	Bile fraction continuously released
Intestinal permeability	cm/min	1.08 · 10 <sup>-4</sup>	Transcellular intestinal permeability
Cellular permeability	cm/min	Charge dependent Schmitt, 0.02	Permeability into the cellular space
Partition coefficients		Rodgers + Rowland	Organ-plasma partition coefficients
CYP2C8 K <sub>i</sub>	μmol/L	2.50 <sup>b</sup>	Diss. const. inhibitor-enzyme complex
CYP3A4 K <sub>i</sub>	μmol/L	0.02	Diss. const. inhibitor-enzyme complex
P-gp K <sub>i</sub>	μmol/L	0.12	Diss. const. inhibitor-transporter complex

<sup>a</sup>: a GFR fraction of 1 corresponds to passive glomerular filtration of a compound, <sup>b</sup>: added to the model [57], AADAC: arylacetamide deacetylase, CYP: cytochrome P450, diss. const.: dissociation constant, EHC: enterohepatic circulation, FMO: flavin-containing monooxygenase, Gemfi-Glu: gemfibrozil-glucuronide, GFR: glomerular filtration rate, MBI: mechanism-based inactivation, MRP: multidrug resistance-associated protein, ND-Keto: N-deacetyl-ketoconazole, OATP: organic-anion-transporting polypeptide, OH-Keto: N-deacetyl-N-hydroxy-ketoconazole, P-gp: P-glycoprotein, UGT: uridine 5'-diphospho-glucuronosyltransferase.

**Table S10:** Drug-dependent parameters of the ketoconazole PBPK model [58] (*continued*)

Parameter	Unit	Value	Description
<b>N-Deacetyl-N-Hydroxy-Ketoconazole</b>			
Molecular weight	g/mol	505.40	Molecular weight
pKa <sub>1</sub> , base		6.42	Acid dissociation constant
pKa <sub>2</sub> , base		3.42	Acid dissociation constant
Solubility (pH)	mg/mL	$4.40 \cdot 10^{-3}$ (6.50)	Solubility
Lipophilicity	log units	4.20	Lipophilicity
f <sub>u</sub>	%	1	Fraction unbound
FMO3 CL → sink	Lμmol/min	0.09	Clearance
GFR fraction		1 <sup>a</sup>	Filtered drug in the urine
EHC continuous fraction		1	Bile fraction continuously released
Intestinal permeability	cm/min	$2.60 \cdot 10^{-4}$	Transcellular intestinal permeability
Cellular permeability	cm/min	Charge dependent Schmitt, 0	Permeability into the cellular space
Partition coefficients		Berezhkovskiy	Organ-plasma partition coefficients
CYP2C8 K <sub>i</sub>	μmol/L	2.50 <sup>b</sup>	Diss. const. inhibitor-enzyme complex
CYP3A4 K <sub>i</sub>	μmol/L	0.02	Diss. const. inhibitor-enzyme complex
P-gp K <sub>i</sub>	μmol/L	0.12	Diss. const. inhibitor-transporter complex

<sup>a</sup>: a GFR fraction of 1 corresponds to passive glomerular filtration of a compound, <sup>b</sup>: added to the model [57], AADAC: arylacetamide deacetylase, CYP: cytochrome P450, diss. const.: dissociation constant, EHC: enterohepatic circulation, FMO: flavin-containing monooxygenase, Gemfi-Glu: gemfibrozil-glucuronide, GFR: glomerular filtration rate, MBI: mechanism-based inactivation, MRP: multidrug resistance-associated protein, ND-Keto: N-deacetyl-ketoconazole, OATP: organic-anion-transporting polypeptide, OH-Keto: N-deacetyl-N-hydroxy-ketoconazole, P-gp: P-glycoprotein, UGT: uridine 5'-diphospho-glucuronosyltransferase.

## S3.2.3 Gemfibrozil

Table S11: Drug-dependent parameters of the gemfibrozil PBPK model [59]

Parameter	Unit	Value	Description
<b>Gemfibrozil</b>			
Molecular weight	g/mol	250.33	Molecular weight
pKa, acid		4.70	Acid dissociation constant
Solubility (pH)	mg/mL	0.17 (5.90)	Solubility
Lipophilicity	log units	2.80	Lipophilicity
$f_u$	%	0.65	Fraction unbound
UGT2B7 $K_M \rightarrow$ Gemfi-Glu	$\mu\text{mol/L}$	2.20	Michaelis-Menten constant
UGT2B7 $k_{\text{cat}} \rightarrow$ Gemfi-Glu	1/min	18.67 <sup>a</sup>	Catalytic rate constant
Liver influx $K_M$	$\mu\text{mol/L}$	2.39	Michaelis-Menten constant
Liver influx $k_{\text{cat}}$	1/min	39.26 <sup>b</sup>	Transport rate constant
GFR fraction		1 <sup>c</sup>	Filtered drug in the urine
EHC continuous fraction		1	Bile fraction continuously released
Intestinal permeability	cm/min	$6.62 \cdot 10^{-3}$	Transcellular intestinal permeability
Cellular permeability	cm/min	Charge dependent Schmitt 0.07	Permeability into the cellular space
Partition coefficients		Berezhkovskiy	Organ-plasma partition coefficients
Dissolution time (Weibull)	min	24.45	Dissolution time (50%)
Dissolution shape (Weibull)		1.56	Dissolution shape
CYP2C8 $K_i$	$\mu\text{mol/L}$	30.40	Diss. const. inhibitor-enzyme complex
OATP1B1 $K_i$	$\mu\text{mol/L}$	25.20	Diss. const. inhibitor-transporter complex
<b>Gemfibrozil-Glucuronide</b>			
Molecular weight	g/mol	426.46	Molecular weight
pKa, acid		2.68	Acid dissociation constant
Solubility (pH)	mg/L	789.00 (7.00)	Solubility
Lipophilicity	log units	1.41	Lipophilicity
$f_u$	%	12	Fraction unbound
MRP2 $K_M$	$\mu\text{mol/L}$	21.49	Michaelis-Menten constant
MRP2 $k_{\text{cat}}$	1/min	7.13	Transport rate constant
OATP1B1 $K_M$	$\mu\text{mol/L}$	0.43	Michaelis-Menten constant
OATP1B1 $k_{\text{cat}}$	1/min	147.00 <sup>b</sup>	Transport rate constant
GFR fraction		1 <sup>c</sup>	Filtered drug in the urine
EHC continuous fraction		1	Bile fraction continuously released
Intestinal permeability	cm/min	$5.98 \cdot 10^{-7}$	Transcellular intestinal permeability
Cellular permeability	cm/min	PK-Sim Standard, $1.22 \cdot 10^{-4}$	Permeability into the cellular space
Partition coefficients		PK-Sim Standard	Organ-plasma partition coefficients
CYP2C8 $K_i$	$\mu\text{mol/L}$	20.00	Conc. for half-maximal inactivation
CYP2C8 $k_{\text{inact}}$	1/min	0.21	Maximum inactivation rate constant
OATP1B1 $K_i$	$\mu\text{mol/L}$	22.60	Diss. const. inhibitor-transporter complex

<sup>a</sup>: adjusted due to different reference concentrations in the original model and imatinib model, <sup>b</sup>: adapted when migrating the model from PK-Sim® version 9 to 10, <sup>c</sup>: a GFR fraction of 1 corresponds to passive glomerular filtration of a compound, conc.: concentration, CYP: cytochrome P450, diss. const.: dissociation constant, EHC: enterohepatic circulation, Gemfi-Glu: gemfibrozil-glucuronide, GFR: glomerular filtration rate, MRP: multidrug resistance-associated protein, OATP: organic-anion-transporting polypeptide, UGT: uridine 5'-diphospho-glucuronosyltransferase.

## S3.2.4 Simvastatin

Table S12: Drug-dependent parameters of the simvastatin PBPK model (PK-Sim® V9) [60]

Parameter	Unit	Value	Description
<b>Simvastatin</b>			
Molecular weight	g/mol	418.57	Molecular weight
Solubility (pH)	mg/L	16.40 (5.00)	Solubility
Lipophilicity	log units	4.68	Lipophilicity
$f_u$	%	1.34	Fraction unbound
CYP3A4 $K_M \rightarrow$ sink	$\mu\text{mol/L}$	21.00	Michaelis-Menten constant
CYP3A4 $k_{\text{cat}} \rightarrow$ sink	1/min	5194.04	Catalytic rate constant
PON3 $K_M \rightarrow$ Simva-Acid	$\mu\text{mol/L}$	840.00	Michaelis-Menten constant
PON3 $k_{\text{cat}} \rightarrow$ Simva-Acid	1/min	4952.08	Catalytic rate constant
Chemical hydrolysis CL $\rightarrow$ Simva-Acid	L/ $\mu\text{mol/min}$	$9.80 \cdot 10^{-4}$	Clearance
Plasma hydrolysis CL $\rightarrow$ Simva-Acid	L/ $\mu\text{mol/min}$	0.06	Clearance
BCRP $K_M$	$\mu\text{mol/L}$	5.00	Michaelis-Menten constant
BCRP $k_{\text{cat}}$	1/min	7.50	Transport rate constant
GFR fraction		1 <sup>a</sup>	Filtered drug in the urine
EHC continuous fraction		1	Bile fraction continuously released
Intestinal permeability	cm/min	$1.08 \cdot 10^{-3}$	Transcellular intestinal permeability
Cellular permeability	cm/min	PK-Sim Standard	Permeability into the cellular space
		0.26	
Partition coefficients		Berezhkovskiy	Organ-plasma partition coefficients
Dissolution time (Weibull)	min	86.38	Dissolution time (50%)
Dissolution shape (Weibull)		1.30	Dissolution shape
CYP2C8 $K_i$	$\mu\text{mol/L}$	1.10	Diss. const. inhibitor-enzyme complex
CYP3A4 $K_i$	$\mu\text{mol/L}$	0.16	Diss. const. inhibitor-enzyme complex
OATP1B1 $K_i$	$\mu\text{mol/L}$	5.00	Diss. const. inhibitor-transporter complex
P-gp $K_i$	$\mu\text{mol/L}$	4.60	Diss. const. inhibitor-transporter complex
<b>Simvastatin Hydroxy Acid</b>			
Molecular weight	g/mol	436.60	Molecular weight
pKa, acid		4.20	Acid dissociation constant
Solubility (pH)	mg/L	13.09 (6.84)	Solubility
Lipophilicity	log units	1.45	Lipophilicity
$f_u$	%	5.68	Fraction unbound
CYP2C8 $K_M \rightarrow$ sink	$\mu\text{mol/L}$	36.00	Michaelis-Menten constant
CYP2C8 $k_{\text{cat}} \rightarrow$ sink	1/min	52.30	Catalytic rate constant
CYP3A4 $K_M \rightarrow$ sink	$\mu\text{mol/L}$	26.00	Michaelis-Menten constant
CYP3A4 $k_{\text{cat}} \rightarrow$ sink	1/min	31.00	Catalytic rate constant
UGT1A1 $K_M \rightarrow$ sink	$\mu\text{mol/L}$	349.00	Michaelis-Menten constant
UGT1A1 $k_{\text{cat}} \rightarrow$ sink	1/min	6.50	Catalytic rate constant
UGT1A3 $K_M \rightarrow$ sink	$\mu\text{mol/L}$	349.00	Michaelis-Menten constant
UGT1A3 $k_{\text{cat}} \rightarrow$ sink	1/min	6.50	Catalytic rate constant
Liver lactonization CL $\rightarrow$ sink	L/ $\mu\text{mol/min}$	$2.43 \cdot 10^{-3}$	Clearance
OATP1B1 $K_M$	$\mu\text{mol/L}$	2.00	Michaelis-Menten constant
OATP1B1 $k_{\text{cat}}$	1/min	146.43 <sup>b</sup>	Transport rate constant
OATP1B3 $K_M$	$\mu\text{mol/L}$	2.00	Michaelis-Menten constant
OATP1B3 $k_{\text{cat}}$	1/min	2.15	Transport rate constant
P-gp $K_M$	$\mu\text{mol/L}$	10.00	Michaelis-Menten constant
P-gp $k_{\text{cat}}$	1/min	50.00	Transport rate constant
GFR fraction		1 <sup>a</sup>	Filtered drug in the urine
EHC continuous fraction		1	Bile fraction continuously released
Intestinal permeability	cm/min	$5.92 \cdot 10^{-7}$	Transcellular intestinal permeability
Cellular permeability	cm/min	Schmitt, $1.17 \cdot 10^{-4}$	Permeability into the cellular space
Partition coefficients		Charge dependent Schmitt normalized to PK-Sim	Organ-plasma partition coefficients
CYP2C8 $K_i$	$\mu\text{mol/L}$	41.10	Diss. const. inhibitor-enzyme complex
CYP3A4 $K_i$	$\mu\text{mol/L}$	69.60	Diss. const. inhibitor-enzyme complex
BCRP $K_i$	$\mu\text{mol/L}$	18.00	Diss. const. inhibitor-transporter complex
OATP1B1 $K_i$	$\mu\text{mol/L}$	3.60	Diss. const. inhibitor-transporter complex

<sup>a</sup>: a GFR fraction of 1 corresponds to passive glomerular filtration of a compound, <sup>b</sup>: adjusted due to different reference concentrations in the original model and imatinib model, BCRP: breast cancer resistance protein, CYP: cytochrome P450, diss. const.: dissociation constant, EHC: enterohepatic circulation, GFR: glomerular filtration rate, MRP: multidrug resistance-associated protein, OATP: organic-anion-transporting polypeptide, P-gp: P-glycoprotein, PON: paraoxonase, Simva-Acid: simvastatin hydroxy acid, UGT: uridine 5'-diphospho-glucuronosyltransferase.

## S3.2.5 Metoprolol

**Table S13:** Drug-dependent parameters of the metoprolol PBPK model [61]

Parameter	Unit	Value	Description
<b>R-Metoprolol</b>			
Molecular weight	g/mol	267.36	Molecular weight
pKa, base		9.70	Acid dissociation constant
Solubility (pH)	mg/mL	1000.00 (7.40)	Solubility
Lipophilicity	log units	1.77	Lipophilicity
$f_u$	%	88	Fraction unbound
CYP2D6 $K_M \rightarrow$ OH-Meto	$\mu\text{mol/L}$	10.08	Michaelis-Menten constant
CYP2D6 $k_{\text{cat}}$ NM $\rightarrow$ OH-Meto	1/min	5.73	Catalytic rate constant
CYP2D6 $k_{\text{cat}}$ IM $\rightarrow$ OH-Meto	1/min	1.65	Catalytic rate constant
CYP2D6 $K_M \rightarrow$ sink	$\mu\text{mol/L}$	8.82	Michaelis-Menten constant
CYP2D6 $k_{\text{cat}}$ NM $\rightarrow$ sink	1/min	9.40	Catalytic rate constant
CYP2D6 $k_{\text{cat}}$ IM $\rightarrow$ sink	1/min	2.70	Catalytic rate constant
CYP3A4 CL $\rightarrow$ sink	1/min	0.02 <sup>a</sup>	Clearance
GFR fraction		1 <sup>b</sup>	Filtered drug in the urine
EHC continuous fraction		1	Bile fraction continuously released
Intestinal permeability	cm/min	$4.14 \cdot 10^{-5}$	Transcellular intestinal permeability
Cellular permeability	cm/min	PK-Sim Standard $4.64 \cdot 10^{-3}$	Permeability into the cellular space
Partition coefficients		Rodgers + Rowland	Organ-plasma partition coefficients
Dissolution time (Weibull)	min	12.31	Dissolution time (50%)
Dissolution shape (Weibull)		0.72	Dissolution shape
<b>S-Metoprolol</b>			
Molecular weight	g/mol	267.36	Molecular weight
pKa, base		9.70	Acid dissociation constant
Solubility (pH)	mg/mL	1000.00 (7.40)	Solubility
Lipophilicity	log units	1.77	Lipophilicity
$f_u$	%	88	Fraction unbound
CYP2D6 $K_M \rightarrow$ OH-Meto	$\mu\text{mol/L}$	10.75	Michaelis-Menten constant
CYP2D6 $k_{\text{cat}}$ NM $\rightarrow$ OH-Meto	1/min	6.30	Catalytic rate constant
CYP2D6 $k_{\text{cat}}$ IM $\rightarrow$ OH-Meto	1/min	1.82	Catalytic rate constant
CYP2D6 $K_M \rightarrow$ sink	$\mu\text{mol/L}$	12.43	Michaelis-Menten constant
CYP2D6 $k_{\text{cat}}$ NM $\rightarrow$ sink	1/min	7.89	Catalytic rate constant
CYP2D6 $k_{\text{cat}}$ IM $\rightarrow$ sink	1/min	2.27	Catalytic rate constant
CYP3A4 CL $\rightarrow$ sink	1/min	0.02 <sup>a</sup>	Clearance
GFR fraction		1 <sup>b</sup>	Filtered drug in the urine
EHC continuous fraction		1	Bile fraction continuously released
Intestinal permeability	cm/min	$4.14 \cdot 10^{-5}$	Transcellular intestinal permeability
Cellular permeability	cm/min	PK-Sim Standard $4.64 \cdot 10^{-3}$	Permeability into the cellular space
Partition coefficients		Rodgers + Rowland	Organ-plasma partition coefficients
Dissolution time (Weibull)	min	12.31	Dissolution time (50%)
Dissolution shape (Weibull)		0.72	Dissolution shape

<sup>a</sup>: included in the model instead of a non-specific hepatic clearance process, <sup>b</sup>: a GFR fraction of 1 corresponds to passive glomerular filtration of a compound, CYP: cytochrome P450, EHC: enterohepatic circulation, GFR: glomerular filtration rate, IM: intermediate metabolizer, NM: normal metabolizer, OH-Meto: hydroxymetoprolol.



**Table S13:** Drug-dependent parameters of the metoprolol PBPK model [61] (*continued*)

Parameter	Unit	Value	Description
<b>Hydroxymetoprolol</b>			
Molecular weight	g/mol	283.36	Molecular weight
pKa <sub>1</sub> , base		9.67	Acid dissociation constant
pKa <sub>2</sub> , acid		13.55	Acid dissociation constant
Solubility (pH)	mg/L	1430.00 (7.00)	Solubility
Lipophilicity	log units	0.87	Lipophilicity
f <sub>u</sub>	%	63	Fraction unbound
Hepatic CL → sink	l/min	0.34	Clearance
GFR fraction		1 <sup>b</sup>	Filtered drug in the urine
EHC continuous fraction		1	Bile fraction continuously released
Intestinal permeability	cm/min	$1.08 \cdot 10^{-6}$	Transcellular intestinal permeability
Cellular permeability	cm/min	PK-Sim Standard $4.08 \cdot 10^{-4}$	Permeability into the cellular space
Partition coefficients		Rodgers + Rowland	Organ-plasma partition coefficients

<sup>a</sup>: included in the model instead of a non-specific hepatic clearance process, <sup>b</sup>: a GFR fraction of 1 corresponds to passive glomerular filtration of a compound, CYP: cytochrome P450, EHC: enterohepatic circulation, GFR: glomerular filtration rate, IM: intermediate metabolizer, NM: normal metabolizer, OH-Meto: hydroxymetoprolol.

### S3.3 Plasma Concentration-Time Profiles (Semilogarithmic)

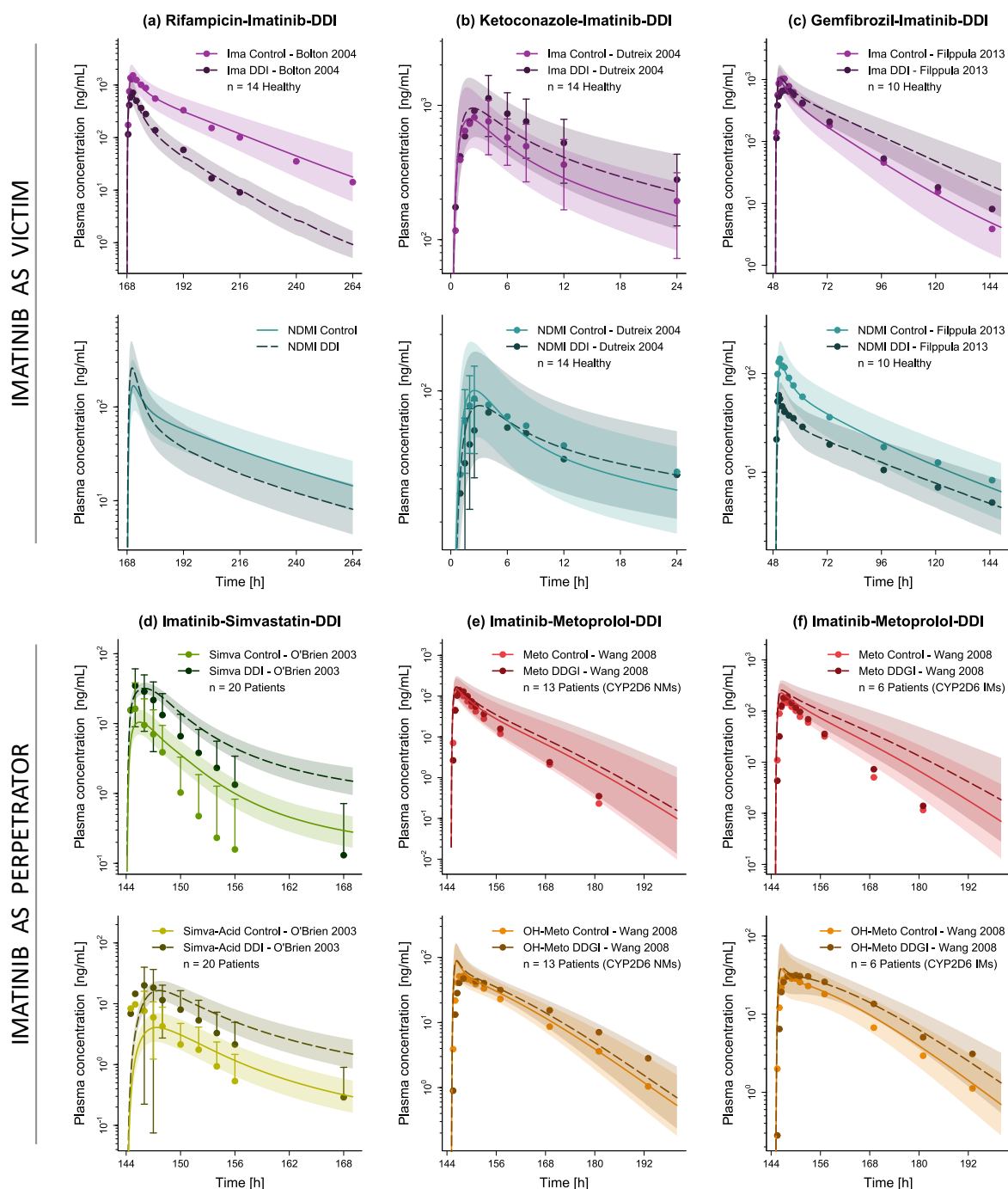


**Figure S14:** Evaluation of the modeled drug-drug interaction network. Presented are predicted plasma concentration-time profiles (semilogarithmic) of each victim drug (imatinib (a–c), simvastatin (d), metoprolol (e–f)) without (Control) and with (DDI) intake of the respective perpetrator drug (rifampicin (a), ketoconazole (b), gemfibrozil (c), imatinib (d–f)), alongside corresponding observed data [21, 23, 37, 55, 56]. Solid (Control) and dashed (DDI) lines and ribbons represent model population predictions ( $n = 1000$ ; geometric mean and geometric standard deviation), while corresponding observed data are shown as dots ( $\pm$  standard deviation, if available). CYP: cytochrome P450, DDI: drug-drug interaction, Healthy: healthy subjects, IM: intermediate metabolizer, Ima: imatinib, Meto: metoprolol, n: number of study participants, NDMI: N-desmethyl imatinib, NM: normal metabolizer, OH-Meto: hydroxymetoprolol, Patients: cancer patients, Simva: simvastatin, Simva-Acid: simvastatin hydroxy acid.

## S3.4 Plasma Concentration-Time Profiles (Linear)

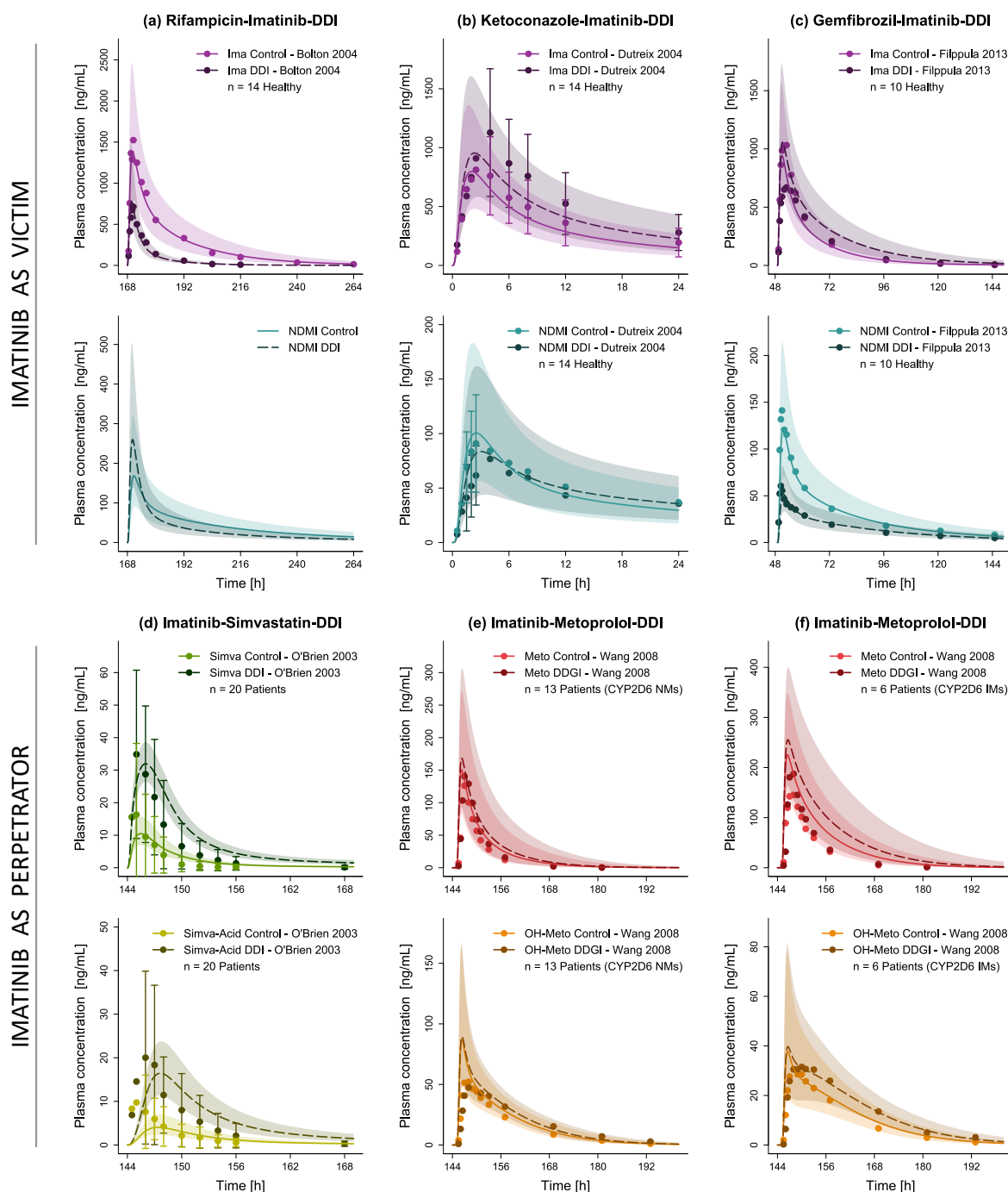


**Figure S15:** Evaluation of the modeled drug-drug interaction network. Presented are predicted plasma concentration-time profiles (linear) of each victim drug (imatinib (a–c), simvastatin (d), metoprolol (e–f)) without (Control) and with (DDI) intake of the respective perpetrator drug (rifampicin (a), ketoconazole (b), gemfibrozil (c), imatinib (d–f)), alongside corresponding observed data [21, 23, 37, 55, 56]. Solid (Control) and dashed (DDI) lines and ribbons represent model population predictions ( $n = 1000$ ; geometric mean and geometric standard deviation), while corresponding observed data are shown as dots ( $\pm$  standard deviation, if available). CYP: cytochrome P450, DDI: drug-drug interaction, Healthy: healthy subjects, IM: intermediate metabolizer, Ima: imatinib, Meto: metoprolol, n: number of study participants, NDMI: N-desmethyl imatinib, NM: normal metabolizer, Patients: cancer patients, OH-Meto: hydroxymetoprolol, Simva: simvastatin, Simva-Acid: simvastatin hydroxy acid.

### S3.5 DDI $AUC_{last}$ and DDI $C_{max}$ Ratio Goodness-of-Fit Plots

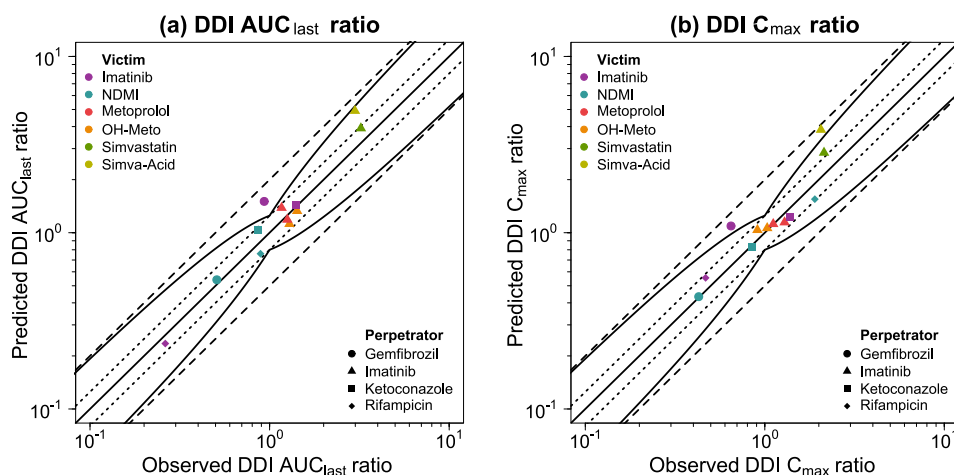


**Figure S16:** Evaluation of the modeled drug-drug interaction network. Predicted versus observed DDI  $AUC_{last}$  (a) and DDI  $C_{max}$  (b) ratios are shown with the solid line representing the line of identity, dotted lines indicating 1.25-fold and dashed lines twofold deviation from the respective observed value. Curved lines mark the prediction success limits proposed by Guest et al. [62] including 20% variability.  $AUC_{last}$ : area under the curve determined between first and last plasma concentration measurements,  $C_{max}$ : maximum plasma concentration, DDI: drug-drug interaction, NDMI: N-desmethyl imatinib, OH-Meto: hydroxymetoprolol, Simva-Acid: simvastatin hydroxy acid.

S3.6 Predicted and Observed DDI  $AUC_{last}$  and DDI  $C_{max}$  RatiosTable S14: Predicted versus observed DDI  $AUC_{last}$  and DDI  $C_{max}$  ratios

Victim application [mg]	Perpetrator application [mg]	n	Compound	DDI AUC <sub>last</sub> ratio		DDI C <sub>max</sub> ratio		Reference		
				Pred	Obs	Pred/Obs	Pred		Obs	Pred/Obs
<b>Imatinib</b> d8: 400 po (cap, SD)	<b>Rifampicin</b> d1–11: 600 po (–, QD)	14 (healthy)	Ima NDMI	0.24	0.26	0.90	0.55	0.47	1.18 0.82	Bolton 2004 [37]
				0.76	0.89	0.85	1.55	1.90		
<b>Imatinib</b> d1: 200 po (cap, SD)	<b>Ketoconazole</b> d1: 400 po (–, SD)	14 (healthy)	Ima NDMI	1.44	1.40	1.02	1.24	1.39	0.89 0.99	Duttreix 2004 [23]
				1.04	0.86	1.21	0.83	0.84		
<b>Imatinib</b> d3: 200 po (tab, SD)	<b>Gemfibrozil</b> d1–6: 600 po (tab, BID)	10 (healthy)	Ima NDMI	1.51	0.93	1.61	1.09	0.65	1.68 1.01	Filppula 2013 [21]
				0.54	0.51	1.06	0.43	0.43		
<b>Simvastatin</b> d7: 40 po (tab, SD)	<b>Imatinib</b> d1–7: 400 po (cap, QD)	20 (CML patients)	Simva Simva-Acid	3.91	3.22	1.21	2.84	2.14	1.33 1.87	O'Brien 2003 [55]
				4.91	2.99	1.65	3.84	2.05		
<b>Metoprolol</b> d7: 100 po (tab, SD)	<b>Imatinib</b> d1–9: 400 po (cap, BID)	13 (CML patients) CYP2D6 NMs	Meto OH-Meto	1.19	1.26	0.94	1.12	1.11	1.01 1.14	Wang 2008 [56]
				1.12	1.29	0.87	1.04	0.91		
<b>Metoprolol</b> d7: 100 po (tab, SD)	<b>Imatinib</b> d1–9: 400 po (cap, BID)	6 (CML patients) CYP2D6 IMs	Meto OH-Meto	1.38	1.17	1.19	1.15	1.29	0.89 1.03	Wang 2008 [56]
				1.33	1.42	0.93	1.06	1.03		
Overall mean GMFE (range) GMFE ≤ 2				1.21 (1.02–1.65) 12/12		1.23 (1.01–1.87) 12/12				

-: not given,  $AUC_{last}$ : area under the plasma concentration-time curve determined between first and last concentration measurements, BID: twice daily, cap: capsule,  $C_{max}$ : maximum plasma concentration, CYP: cytochrome P450, d: day, DDI: drug-drug interaction, GMFE: geometric mean fold error, IM: intermediate metabolizer, Ima: imatinib, Meto: metoprolol, n: number of participants, NDMI: N-desmethyl imatinib, NM: normal metabolizer, OH-Meto: hydroxy-metoprolol, po: oral, QD: once daily, SD: single dose, Simva: simvastatin, Simva-Acid: simvastatin hydroxy acid, tab: tablet.

### S3.7 Comparison of CYP3A Perpetrator Effects – SD vs. MD Imatinib Administration

In DDI studies involving CYP3A perpetrators, ketoconazole was observed to increase imatinib exposure by 40% after SD-administration, while ritonavir showed almost no effect on the steady-state AUC of imatinib [23, 63].

A detailed description and evaluation of the modeled ketoconazole-imatinib-DDI [23] can be found in Sections S3.1–S3.6.

The ritonavir-imatinib-DDI study by van Erp et al. [63] was not included in the developed DDI network due to limited reproducibility. Eleven patients were enrolled, six of whom were women, with an average age of 62 years. The influence of ritonavir on imatinib exposure at steady-state was investigated. Participants received imatinib doses equivalent to 100% on study days 1 and 5 and 50% on days 2, 3, and 4 of the doses given prior to participation in the study, which ranged from 400 to 800 mg once daily. Ritonavir was co-administered (600 mg once daily) on days 2, 3, and 4.

Since the AUC and  $C_{\max}$  values for imatinib and NDMI were reported as dose-normalized means for all patients and additionally the number of patients receiving each dose was not specified, the DDI study could not be accurately recreated in our model without bias. Here, we assumed a daily dose of 400 mg (100%) imatinib to simulate the ritonavir-imatinib-DDI and assessed the performance of our model in predicting the steady-state AUC of imatinib. The effect was compared to the impact of ketoconazole on imatinib SD-administration. For this, the imatinib model was coupled with a recently published ritonavir model [64]. Drug-dependent parameters of ritonavir are presented in Table S16. Figure S17 presents the goodness-of-fit plots of the ketoconazole-imatinib and ritonavir-imatinib DDI ratios, with respective values listed in Table S15.

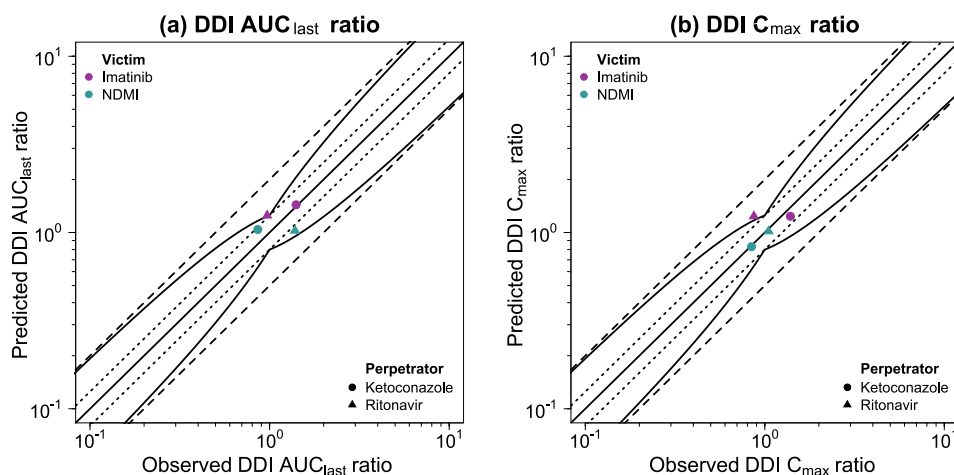


**Figure S17:** Predicted versus observed DDI  $AUC_{\text{last}}$  (a) and DDI  $C_{\max}$  (b) ratios are shown with the solid line representing the line of identity, dotted lines indicating 1.25-fold and dashed lines twofold deviation from the respective observed value. Curved lines mark the prediction success limits proposed by Guest et al. [62] including 20% variability.  $AUC_{\text{last}}$ : area under the curve determined between first and last plasma concentration measurements,  $C_{\max}$ : maximum plasma concentration, DDI: drug-drug interaction, NDMI: N-desmethyl imatinib.

**Table S15:** Predicted versus observed DDI  $AUC_{last}$  and DDI  $C_{max}$  ratios

Perpetrator	Compound	DDI $AUC_{last}$ ratio			DDI $C_{max}$ ratio			Reference
		Pred	Obs	Pred/Obs	Pred	Obs	Pred/Obs	
<b>KET</b>	Ima	1.44	1.40	1.02	1.24	1.39	0.89	Dutreix 2004 [23]
	NDMI	1.04	0.86	1.21	0.83	0.84	0.99	
<b>RIT</b>	Ima	1.25	0.97	1.29	1.24	0.87	1.42	van Erp 2007 [63]
	NDMI	1.02	1.39	0.74	1.02	1.05	0.97	
Overall mean GMFE (range)		1.22 (1.02–1.35)			1.15 (1.01–1.42)			
GMFE $\leq 2$		4/4			4/4			

$AUC_{last}$ : area under the plasma concentration-time curve determined between first and last concentration measurements,  $C_{max}$ : maximum plasma concentration, DDI: drug-drug interaction, GMFE: geometric mean fold error, Ima: imatinib, KET: ketoconazole, NDMI: N-desmethyl imatinib, RIT: ritonavir.

**Table S16:** Drug-dependent parameters of the ritonavir PBPK model [64]

Parameter	Unit	Value	Description
<b>Ritonavir</b>			
Molecular weight	g/mol	721.00	Molecular weight
pKa <sub>1</sub> , base		1.90	Acid dissociation constant
pKa <sub>2</sub> , base		2.60	Acid dissociation constant
Solubility (pH)	µg/mL	60.00 (7.0)	Solubility
Lipophilicity		3.90	Lipophilicity
f <sub>u</sub>	%	2.00	Fraction unbound
CYP2D6 K <sub>M</sub> → sink	µmol/L	1.00	Michaelis-Menten constant
CYP2D6 k <sub>cat</sub> → sink	1/min	3.00	Catalytic rate constant
CYP3A4 K <sub>M</sub> → sink	µmol/L	0.07	Michaelis-Menten constant
CYP3A4 k <sub>cat</sub> → sink	1/min	1.10	Catalytic rate constant
P-gp K <sub>M</sub>	µmol/L	0.13	Michaelis-Menten constant
P-gp k <sub>cat</sub>	1/min	0.70	Transport rate constant
GFR fraction		1 <sup>a</sup>	Filtered drug in the urine
EHC continuous fraction		1	Bile fraction continuously released
Intestinal permeability	cm/min	6.50 · 10 <sup>-5</sup>	Transcellular intestinal permeability
Cellular permeability	cm/min	PK-Sim Standard, 1.63 · 10 <sup>-3</sup>	Permeability into the cellular space
Partition coefficients		Rodgers + Rowland	Organ-plasma partition coefficients
Particle radius	µm	10.00	Particle dissolution radius
Induction EC <sub>50</sub>	µmol/L	0.17	Conc. for half-maximal induction
CYP3A4 E <sub>max</sub>		7.47	Maximum induction effect
CYP2D6 K <sub>i</sub>	µmol/L	0.04	Diss. const. inhibitor-enzyme complex
CYP3A4 K <sub>i</sub>	µmol/L	0.25	Diss. const. inhibitor-enzyme complex
CYP3A4 K <sub>I</sub>	µmol/L	0.20	Conc. for half-maximal inactivation
CYP3A4 k <sub>inact</sub>	1/min	0.40	Maximum inactivation rate constant
P-gp K <sub>i</sub>	µmol/L	4.2 <sup>b</sup>	Diss. const. inhibitor-transporter complex

<sup>a</sup>: a GFR fraction of 1 corresponds to passive glomerular filtration of a compound, <sup>b</sup>: added to the model [65], conc.: concentration, CYP: cytochrome P450, diss. const.: dissociation constant, EHC: enterohepatic circulation, GFR: glomerular filtration rate, P-gp: P-glycoprotein.

## Bibliography

- [1] AD Rodrigues. Integrated cytochrome P450 reaction phenotyping. Attempting to bridge the gap between cDNA-expressed cytochromes P450 and native human liver microsomes. *Biochemical Pharmacology*, 57(5): 465–480, 1999. doi: 10.1016/s0006-2952(98)00268-8.
- [2] Open Systems Pharmacology Suite Community PK-Sim®Ontogeny Database Documentation, Available online (accessed on 30 April 2022). URL <https://github.com/Open-Systems-Pharmacology/OSPSuite.Documentation/blob/master/PK-SimOntogenyDatabaseVersion7.3.pdf>.
- [3] B Achour, A Dantonio, M Niosi, JJ Novak, JK Fallon, J Barber, PC Smith, A Rostami-Hodjegan, and TC Goosen. Quantitative characterization of major hepatic UDP-glucuronosyltransferase enzymes in human liver microsomes: Comparison of two proteomic methods and correlation with catalytic activity. *Drug metabolism and disposition: the biological fate of chemicals*, 45(10):1102–1112, 2017. doi: 10.1124/dmd.117.076703.
- [4] G Margaillan, M Rouleau, JK Fallon, P Caron, L Villeneuve, V Turcotte, PC Smith, MS Joy, and C Guillemette. Quantitative profiling of Human renal UDP-glucuronosyltransferases and glucuronidation activity: A comparison of normal and tumoral kidney tissues. *Drug Metabolism and Disposition*, 43(4):611–619, 2015. doi: 10.1124/dmd.114.062877.
- [5] B Prasad, Y Lai, Y Lin, and JD Unadkat. Interindividual variability in the hepatic expression of the human breast cancer resistance protein (BCRP/ABCG2): effect of age, sex, and genotype. *Journal of pharmaceutical sciences*, 102(3):787–793, 2013. doi: 10.1002/jps.23436.
- [6] AK Deo, B Prasad, L Balogh, Y Lai, and JD Unadkat. Interindividual variability in hepatic expression of the multidrug resistance-associated protein 2 (MRP2/ABCC2): quantification by liquid chromatography/tandem mass spectrometry. *Drug Metabolism and Disposition*, 40(5):852–855, 2012. doi: 10.1124/dmd.111.043810.
- [7] B Prasad, R Evers, A Gupta, CECA Hop, L Salphati, S Shukla, S Ambudkar, and JD Unadkat. Interindividual variability in hepatic OATPs and P-glycoprotein (ABCB1) protein expression: Quantification by LC-MS/MS and influence of genotype, age and sex. *Drug metabolism and disposition: the biological fate of chemicals*, 42(1):78–88, 2014. doi: 10.1124/dmd.113.053819.
- [8] N Hanke, S Frechen, D Moj, H Britz, T Eissing, T Wendl, and T Lehr. PBPK models for CYP3A4 and P-gp DDI prediction: A modeling network of rifampicin, itraconazole, clarithromycin, midazolam, alfentanil, and digoxin. *CPT: Pharmacometrics and Systems Pharmacology*, 7(10):647–659, 2018. doi: 10.1002/psp4.12343.
- [9] M Meyer, S Schneckener, B Ludewig, L Kuepfer, and J Lippert. Using expression data for quantification of active processes in physiologically based pharmacokinetic modeling. *Drug metabolism and disposition: the biological fate of chemicals*, 40(5):892–901, 2012. doi: 10.1124/dmd.111.043174.
- [10] D Scotcher, S Billington, J Brown, CR Jones, CDA Brown, A Rostami-Hodjegan, and A Galetin. Microsomal and cytosolic scaling factors in dog and human kidney cortex and application for in vitro-in vivo extrapolation of renal metabolic clearance. *Drug Metabolism and Disposition*, 45(5):556–568, 2017. doi: 10.1124/dmd.117.075242.
- [11] P Shi, M Liao, C Chuang, R Griffin, J Shi, M Hyer, JK Fallon, PC Smith, C Li, and CQ Xia. Efflux transporter breast cancer resistance protein dominantly expresses on the membrane of red blood cells, hinders partitioning of its substrates into the cells, and alters drug–drug interaction profiles. *Xenobiotica*, 48(11):1173–1183, 2018. doi: 10.1080/00498254.2017.1397812.
- [12] M Nishimura and S Naito. Tissue-specific mRNA expression profiles of human phase I metabolizing enzymes except for cytochrome P450 and phase II metabolizing enzymes. *Drug metabolism and pharmacokinetics*, 21(5):357–374, 2006. doi: 10.2133/dmpk.21.357.
- [13] M Nishimura, H Yaguti, H Yoshitsugu, and S Naito. Tissue distribution of mRNA expression of human cytochrome P450 isoforms assessed by high-sensitivity real-time reverse transcription PCR. *Journal of the Pharmaceutical Society of Japan*, 123(5):369–375, 2003. doi: 10.1248/yakushi.123.369.



- [14] N Kolesnikov, E Hastings, M Keays, O Melnichuk, YA Tang, E Williams, M Dylag, N Kurbatova, M Brandizi, T Burdett, K Megy, E Pilicheva, G Rustici, A Tikhonov, H Parkinson, R Petryszak, U Sarkans, and A Brazma. ArrayExpress update-simplifying data submissions. *Nucleic Acids Research*, 43(D1):D1113–D1116, 2015. doi: 10.1093/nar/gku1057.
- [15] National Center for Biotechnology Information (NCBI) (2010) Expressed Sequence Tags (EST) from UniGene.
- [16] M Nishimura and S Naito. Tissue-specific mRNA expression profiles of human ATP-binding cassette and solute carrier transporter superfamilies. *Drug metabolism and pharmacokinetics*, 20(6):452–477, 2005. doi: 10.2133/dmpk.20.452.
- [17] B Peng, C Dutreix, G Mehring, MJ Hayes, M Ben-Am, M Seiberling, R Pokorny, R Cupdeville, and P Lloyd. Absolute bioavailability of imatinib (Glivec®) orally versus intravenous infusion. *Journal of Clinical Pharmacology*, 44(2):158–162, 2004. doi: 10.1177/0091270003262101.
- [18] B Peng, M Hayes, D Resta, A Racine-Poon, BJ Druker, M Talpaz, CL Sawyers, M Rosamilia, J Ford, P Lloyd, and R Capdeville. Pharmacokinetics and pharmacodynamics of imatinib in a phase I trial with chronic myeloid leukemia patients. *Journal of Clinical Oncology*, 22(5):935–942, 2004. doi: 10.1200/JCO.2004.03.050.
- [19] DW Zidan, WS Hassan, MS Elmasry, and AA Shalaby. A novel spectrofluorimetric method for determination of imatinib in pure, pharmaceutical preparation, human plasma, and human urine. *Luminescence*, 33(1):232–242, 2018. doi: 10.1002/bio.3406.
- [20] A Ostrowicz, P Mikołajczak, M Wierzbicka, and P Boguradzki. Bioequivalence study of 400 and 100 mg imatinib film-coated tablets in healthy volunteers. *Acta Poloniae Pharmaceutica - Drug Research*, 71(5): 843–854, 2014.
- [21] AM Filppula, A Tornio, M Niemi, PJ Neuvonen, and JT Backman. Gemfibrozil impairs imatinib absorption and inhibits the CYP2C8-mediated formation of its main metabolite. *Clinical Pharmacology and Therapeutics*, 94(3):383–393, 2013. doi: 10.1038/clpt.2013.92.
- [22] JA Jung, N Kim, JS Yang, TE Kim, JR Kim, GS Song, H Kim, JW Ko, and W Huh. Bioequivalence study of two imatinib formulations after single-dose administration in healthy Korean male volunteers. *Drug Research*, 64(12):651–655, 2014. doi: 10.1055/s-0034-1367059.
- [23] C Dutreix, B Peng, G Mehring, M Hayes, R Capdeville, R Pokorny, and M Seiberling. Pharmacokinetic interaction between ketoconazole and imatinib mesylate (Glivec) in healthy subjects. *Cancer Chemotherapy and Pharmacology*, 54(4):290–294, 2004. doi: 10.1007/s00280-004-0832-z.
- [24] HP Gschwind, U Pfaar, F Waldmeier, M Zollinger, C Sayer, P Zbinden, M Hayes, R Pokorny, M Seiberling, M Ben-Am, B Peng, and G Gross. Metabolism and disposition of imatinib mesylate in healthy volunteers. *Drug Metabolism and Disposition*, 33(10):1503–1512, 2005. doi: 10.1124/dmd.105.004283.
- [25] AA Golabchifar, MR Rouini, B Shafaghi, S Rezaee, A Foroumadi, and MR Khoshayand. Optimization of the simultaneous determination of imatinib and its major metabolite, CGP74588, in human plasma by a rapid HPLC method using D-optimal experimental design. *Talanta*, 85(5):2320–2329, 2011. doi: 10.1016/j.talanta.2011.07.093.
- [26] JS Yang, EG Cho, W Huh, JW Ko, JA Jung, and SY Lee. Rapid determination of imatinib in human plasma by liquid chromatography-tandem mass spectrometry: Application to a pharmacokinetic study. *Bulletin of the Korean Chemical Society*, 34(8):2425–2430, 2013. doi: 10.5012/bkcs.2013.34.8.2425.
- [27] RF Frye, SM Fitzgerald, TF Lagattuta, MW Hruska, and MJ Egorin. Effect of St John’s wort on imatinib mesylate pharmacokinetics. *Clinical Pharmacology and Therapeutics*, 76(4):323–329, 2004. doi: 10.1016/j.clpt.2004.06.007.
- [28] Z Nikolova, B Peng, M Hubert, M Seiberling, U Keller, YY Ho, H Schran, and R Capdeville. Bioequivalence, safety, and tolerability of imatinib tablets compared with capsules. *Cancer Chemotherapy and Pharmacology*, 53(5):433–438, 2004. doi: 10.1007/s00280-003-0756-z.
- [29] MA Pena, J Muriel, M Saiz-Rodríguez, AM Borobia, F Abad-Santos, J Frías, and AM Peiró. Effect of cytochrome P450 and ABCB1 polymorphisms on imatinib pharmacokinetics after single-dose administration to healthy subjects. *Clinical Drug Investigation*, 40(7):617–628, 2020. doi: 10.1007/s40261-020-00921-7.

- [30] S Parrillo-Campiglia, MC Ercoli, O Umpierrez, P Rodríguez, S Márquez, C Guarneri, FT Estevez-Parrillo, M Laurenz, and FE Estevez-Carrizo. Bioequivalence of two film-coated tablets of imatinib mesylate 400 mg: A randomized, open-label, single-dose, fasting, two-period, two-sequence crossover comparison in healthy male South American volunteers. *Clinical Therapeutics*, 31(10):2224–2232, 2009. doi: 10.1016/j.clinthera.2009.10.009.
- [31] P Smith, JM Bullock, BM Booker, CE Haas, CS Berenson, and WJ Jusko. The influence of St. John’s wort on the pharmacokinetics and protein binding of imatinib mesylate. *Pharmacotherapy*, 24(11):1508–1514, 2004. doi: 10.1592/phco.24.16.1508.50958.
- [32] H Tawbi, SM Christner, Y Lin, M Johnson, ET Mowrey, C Cherrin, E Chu, JJ Lee, S Puhalla, R Stoller, LR Appleman, BM Miller, and JH Beumer. Calcium carbonate does not affect imatinib pharmacokinetics in healthy volunteers. *Cancer Chemotherapy and Pharmacology*, 73(1):207–211, 2014. doi: 10.1007/s00280-013-2337-0.
- [33] Y Zhang, S Qiang, Z Yu, W Zhang, Z Xu, L Yang, A Wen, and T Hang. LC-MS-MS determination of imatinib and N-desmethyl imatinib in human plasma. *Journal of Chromatographic Science*, 52(4):344–350, 2014. doi: 10.1093/chromsci/bmt037.
- [34] BA Sparano, MJ Egorin, RA Parise, J Walters, KA Komazec, RL Redner, and JH Beumer. Effect of antacid on imatinib absorption. *Cancer Chemotherapy and Pharmacology*, 63(3):525–528, 2009. doi: 10.1007/s00280-008-0778-7.
- [35] E Mohajeri, B Kalantari-Khandani, A Pardakhty, M Safavi, and M Ansari. Comparative pharmacokinetic evaluation and bioequivalence study of three different formulations of imatinib mesylate in CML patients. *International Journal of Hematology-Oncology and Stem Cell Research*, 9(4):165–172, 2015.
- [36] D Jawhari, M Alswisi, and M Ghannam. Bioavailability of a new generic formulation of imatinib mesylate 400mg tablets versus glivec in healthy male adult volunteers. *Journal of Bioequivalence and Bioavailability*, 3(7):161–164, 2011. doi: 10.4172/jbb.1000077.
- [37] AE Bolton, B Peng, M Hubert, A Krebs-Brown, R Capdeville, U Keller, and M Seiberling. Effect of rifampicin on the pharmacokinetics of imatinib mesylate (Gleevec, STI571) in healthy subjects. *Cancer Chemotherapy and Pharmacology*, 53(2):102–106, 2004. doi: 10.1007/s00280-003-0722-9.
- [38] MJ Egorin, DD Shah, SM Christner, MA Yerk, KA Komazec, LR Appleman, RL Redner, BM Miller, and JH Beumer. Effect of a proton pump inhibitor on the pharmacokinetics of imatinib. *British Journal of Clinical Pharmacology*, 68(3):370–374, 2009. doi: 10.1111/j.1365-2125.2009.03466.x.
- [39] R Arora, M Sharma, T Monif, and S Iyer. A multi-centric bioequivalence trial in Ph+ chronic myeloid leukemia patients to assess bioequivalence and safety evaluation of generic imatinib mesylate 400 mg tablets. *Cancer Research and Treatment*, 48(3):1120–1129, 2016. doi: 10.4143/crt.2015.436.
- [40] K Eechoute, RM Franke, WJ Loos, LA Scherckenbach, I Boere, J Verweij, H Gurney, RB Kim, RG Tirona, RHJ Mathijssen, and A Sparreboom. Environmental and genetic factors affecting transport of imatinib by OATP1A2. *Clinical Pharmacology and Therapeutics*, 89(6):816–820, 2011. doi: 10.1038/clpt.2011.42.
- [41] F Langenbucher. Linearization of dissolution rate by the Weibull distribution. *J Pharm Pharmac*, 24(12):979–981, 1972. doi: 10.1111/j.2042-7158.1972.tb08930.x.
- [42] ChemAxon Imatinib, Available online (accessed on 9 September 2022). URL <https://chemicalize.com/app/calculation>.
- [43] T Minematsu and KM Giacomini. Interactions of tyrosine kinase inhibitors with organic cation transporters and multidrug and toxic compound extrusion proteins. *Molecular Cancer Therapeutics*, 10(3):531–539, 2011. doi: 10.1158/1535-7163.MCT-10-0731.
- [44] T Hegedus, L Orfi, A Seprodi, A Váradi, B Sarkadi, and G Kéri. Interaction of tyrosine kinase inhibitors with the human multidrug transporter proteins, MDR1 and MRP1. *Biochimica et Biophysica Acta - Molecular Basis of Disease*, 1587(2-3):318–325, 2002. doi: 10.1016/S0925-4439(02)00095-9.
- [45] Fachinformation Glivec(R) Filmtabletten, Available online (accessed on 9 September 2022). URL <https://klinischeforschung.novartis.de/dokumente/fachinformationen-glivec-filmtabletten/>.

- [46] C Arellano, P Gandia, T Lafont, R Jongejan, and E Chatelut. Determination of unbound fraction of imatinib and N-desmethyl imatinib, validation of an UPLC-MS/MS assay and ultrafiltration method. *Journal of Chromatography B: Analytical Technologies in the Biomedical and Life Sciences*, 907:94–100, 2012. doi: 10.1016/j.jchromb.2012.09.007.
- [47] AM Filppula, M Neuvonen, J Laitila, PJ Neuvonen, and JT Backman. Autoinhibition of CYP3A4 leads to important role of CYP2C8 in imatinib metabolism: Variability in CYP2C8 activity may alter plasma concentrations and response. *Drug Metabolism and Disposition*, 41(1):50–59, 2013. doi: 10.1124/dmd.112.048017.
- [48] E Kralj, S Žakelj, J Trontelj, R Roškar, P Černelč, and A Kristl. Absorption and elimination of imatinib through the rat intestine in vitro. *International Journal of Pharmaceutics*, 460(1-2):144–149, 2014. doi: 10.1016/j.ijpharm.2013.10.054.
- [49] Open Systems Pharmacology Suite Community. Open Systems Pharmacology Suite Manual, Version 7.4 2018, Available online (accessed on 28 September 2021). URL <https://docs.open-systems-pharmacology.org/working-with-pk-sim/pk-sim-documentation>.
- [50] W Schmitt. General approach for the calculation of tissue to plasma partition coefficients. *Toxicology in Vitro*, 22(2):457–467, 2008. doi: 10.1016/j.tiv.2007.09.010.
- [51] AM Filppula, J Laitila, PJ Neuvonen, and Janne T Backman. Potent mechanism-based inhibition of CYP3A4 by imatinib explains its liability to interact with CYP3A4 substrates. *British Journal of Pharmacology*, 165(8):2787–2798, 2012. doi: 10.1111/j.1476-5381.2011.01732.x.
- [52] R D’Cunha, S Bae, DJ Murry, and G An. TKI combination therapy: strategy to enhance dasatinib uptake by inhibiting Pgp- and BCRP-mediated efflux. *Biopharmaceutics and drug disposition*, 37(7):397–408, 2016. doi: 10.1002/bdd.2022.
- [53] A Hamada, H Miyano, H Watanabe, and H Saito. Interaction of imatinib mesilate with human P-glycoprotein. *Journal of Pharmacology and Experimental Therapeutics*, 307(2):824–828, 2003. doi: 10.1124/jpet.103.055574.
- [54] ChemAxon N-Desmethyl Imatinib, Available online (accessed on 9 September 2022). URL <https://chemicalize.com/app/calculation>.
- [55] SG O’Brien, P Meinhardt, E Bond, J Beck, B Peng, C Dutreix, G Mehring, S Milosavljev, C Huber, R Capdeville, and T Fischer. Effects of imatinib mesylate (ST1571, Glivec) on the pharmacokinetics of simvastatin, a cytochrome P450 3A4 substrate, in patients with chronic myeloid leukaemia. *British Journal of Cancer*, 89(10):1855–1859, 2003. doi: 10.1038/sj.bjc.6601152.
- [56] Y Wang, L Zhou, C Dutreix, E Leroy, Q Yin, V Sethuraman, GJ Riviere, OQP Yin, H Schran, and ZX Shen. Effects of imatinib (Glivec) on the pharmacokinetics of metoprolol, a CYP2D6 substrate, in Chinese patients with chronic myelogenous leukaemia. *British Journal of Clinical Pharmacology*, 65(6): 885–892, 2008. doi: 10.1111/j.1365-2125.2008.03150.x.
- [57] Chin Eng Ong, Sally Coulter, Donald J. Birkett, C. Ramana Bhasker, and John O. Miners. The xenobiotic inhibitor profile of cytochrome P4502C8. *British Journal of Clinical Pharmacology*, 50(6):573–580, 2000. doi: 10.1046/j.1365-2125.2000.00316.x.
- [58] FZ Marok, JG Wojtyniak, LM Fuhr, D Selzer, M Schwab, J Weiss, WE Haefeli, and Thorsten Lehr. A physiologically based pharmacokinetic model of ketoconazole and its metabolites as drug–drug interaction perpetrators. *Pharmaceutics*, 12(2):679, 2023. doi: 10.3390/pharmaceutics13030331.
- [59] D Türk, N Hanke, S Wolf, S Frechen, T Eissing, T Wendl, M Schwab, and T Lehr. Physiologically based pharmacokinetic models for prediction of complex CYP2C8 and OATP1B1 (SLCO1B1) drug–drug–gene interactions: a modeling network of gemfibrozil, repaglinide, pioglitazone, rifampicin, clarithromycin and itraconazole. *Clinical Pharmacokinetics*, 58(12):1595–1607, 2019. doi: 10.1007/s40262-019-00777-x.
- [60] JG Wojtyniak, D Selzer, M Schwab, and T Lehr. Physiologically based precision dosing approach for drug–drug–gene interactions: A simvastatin network analysis. *Clinical Pharmacology and Therapeutics*, 109(1):201–211, 2021. doi: 10.1002/cpt.2111.

- [61] S Rüdesheim, JG Wojtyniak, D Selzer, N Hanke, F Mahfoud, M Schwab, and T Lehr. Physiologically based pharmacokinetic modeling of metoprolol enantiomers and  $\alpha$ -hydroxymetoprolol to describe CYP2D6 drug-gene interactions. *Pharmaceutics*, 12(12):1200, 2020. doi: 10.3390/pharmaceutics12121200.
- [62] EJ Guest, L Aarons, JB Houston, A Rostami-Hodjegan, and A Galetin. Critique of the two-fold measure of prediction success for ratios: Application for the assessment of drug-drug interactions. *Drug Metabolism and Disposition*, 39(2):170–173, 2011. doi: 10.1124/dmd.110.036103.
- [63] NP Van Erp, H Gelderblom, MO Karlsson, J Li, M Zhao, J Ouwerkerk, JW Nortier, HJ Guchelaar, SD Baker, and A Sparreboom. Influence of CYP3A4 inhibition on the steady-state pharmacokinetics of imatinib. *Clinical Cancer Research*, 13(24):7394–7400, 2007. ISSN 10780432. doi: 10.1158/1078-0432.CCR-07-0346.
- [64] L Zheng, W Zhang, KT Olkkola, A Dallmann, L Ni, Y Zhao, L Wang, Q Zhang, and W Hu. Physiologically based pharmacokinetic modeling of ritonavir-oxycodone drug interactions and its implication for dosing strategy. *European Journal of Pharmaceutical Sciences*, 194:106697, 2024. ISSN 18790720. doi: 10.1016/j.ejps.2024.106697.
- [65] Á Telbisz, C Ambrus, O Móznér, E Szabó, G Várady, É Bakos, B Sarkadi, and C Özvegy-Laczka. Interactions of potential anti-COVID-19 compounds with multispecific ABC and OATP drug transporters. *Pharmaceutics*, 13(1):81, 2021. ISSN 19994923. doi: 10.3390/pharmaceutics13010081.

A.3 SUPPLEMENTARY DOCUMENT TO PUBLICATION III – PHYSIOLOGICALLY  
BASED PHARMACOKINETIC MODELING OF (E)-CLOMIPHENE AND ITS  
MAIN METABOLITES

## Pharmaceutics

# Supplementary Materials: Prediction of Drug-Drug-Gene Interaction Scenarios of (*E*)-Clomiphene and its Metabolites Using Physiologically Based Pharmacokinetic Modeling

Christina Kovar <sup>1,2</sup>, Lukas Kovar <sup>1</sup>, Simeon Rüdesheim <sup>1,2</sup>, Dominik Selzer <sup>1</sup>, Boian Ganchev <sup>2</sup>, Patrick Kröner <sup>2</sup>, Svitlana Igel <sup>2</sup>, Reinhold Kerb <sup>2</sup>, Elke Schaeffeler <sup>2</sup>, Thomas E. Mürdter <sup>2</sup>, Matthias Schwab <sup>2,3</sup> and Thorsten Lehr <sup>1,\*</sup>

<sup>1</sup> Clinical Pharmacy, Saarland University, 66123 Saarbrücken, Germany

<sup>2</sup> Dr. Margarete Fischer-Bosch Institute of Clinical Pharmacology, University of Tübingen, 70376 Stuttgart, Germany

<sup>3</sup> Departments of Clinical Pharmacology, Pharmacy and Biochemistry, University of Tübingen, 72076 Tübingen, Germany

\* Correspondence: thorsten.lehr@mx.uni-saarland.de; Tel.: +49-681-302-70255

## Contents

<b>S1 PBPK Model Building</b>	<b>3</b>
S1.1 Clinical Studies . . . . .	3
S1.2 System-dependent Parameters and Virtual Populations . . . . .	5
S1.3 Supplementary Information on ( <i>E</i> )-clomiphene PBPK Model Building . . . . .	7
S1.4 Drug-dependent Parameter Tables . . . . .	8
S1.5 Calculation of Fractions Metabolized . . . . .	11
S1.6 Formulations . . . . .	12
S1.7 Handling Data Below the Lower Limit of Quantification (LLOQ) . . . . .	12
<b>S2 Drug-Gene-Interaction (DGI) Modeling</b>	<b>13</b>
S2.1 CYP2D6 <i>in vitro</i> Scaling Factors . . . . .	13
<b>S3 Drug-Drug-(Gene)-Interaction (DD(G)I) Modeling</b>	<b>13</b>
S3.1 Clarithromycin and Paroxetine . . . . .	13
<b>S4 PBPK Model Evaluation</b>	<b>14</b>
S4.1 Evaluation of the DGI Model . . . . .	14
S4.1.1 Plasma Profiles (Linear Scale) . . . . .	14
S4.1.2 Plasma Profiles (Semilogarithmic Scale) . . . . .	17
S4.1.3 Goodness-of-Fit Plots . . . . .	20
S4.1.4 Renal Excretion Profiles (Linear Scale) . . . . .	22
S4.1.5 Plasma Profiles from Literature (Linear Scale) . . . . .	25
S4.1.6 Plasma Profiles from Literature (Semilogarithmic Scale) . . . . .	26
S4.1.7 Goodness-of-Fit Plots (from Literature) . . . . .	27
S4.2 Evaluation of the DD(G)I Model . . . . .	28
S4.2.1 Plasma Profiles (Linear Scale) . . . . .	28
S4.2.2 Plasma Profiles (Semilogarithmic Scale) . . . . .	31
S4.2.3 Goodness-of-Fit Plots . . . . .	34
S4.2.4 Renal Excretion Profiles (Linear Scale) . . . . .	36
S4.3 Quantitative PBPK Model Evaluation . . . . .	39
S4.3.1 Mean Relative Deviation (MRD) . . . . .	39
S4.3.2 Geometric Mean Fold Error (GMFE) . . . . .	41
S4.4 Local Sensitivity Analysis . . . . .	48
S4.4.1 Mathematical Implementation . . . . .	48
S4.4.2 Results of the Sensitivity Analysis . . . . .	49
<b>S5 Molecular</b>	<b>50</b>
<b>References</b>	<b>51</b>

## S1. PBPK Model Building

### S1.1. Clinical Studies

Plasma and renal excretion profiles of (*E*)-clomiphene ((*E*)-Clom) and its metabolites from a pharmacokinetic panel study with 20 healthy female volunteers, that were assigned to six different cytochrome P450 (CYP) 2D6 activity scores (AS), were available for model building and evaluation (see Table 1 in the main manuscript for demographic information). The pharmacokinetic panel study was complemented with digitized data from published clinical studies (study search criteria were (a) studies with intravenous or oral (*E*)-Clom administration and (b) reported pharmacokinetic data of (*E*)-Clom and/or its metabolites (*E*)-4-hydroxyclophene ((*E*)-4-OH-Clom), (*E*)-N-desethylclomiphene ((*E*)-DE-Clom) and (*E*)-4-hydroxy-N-desethylclomiphene ((*E*)-4-OH-DE-Clom). Data originating from two single dose and two multiple dose studies with oral (*E*)-Clom administration could be integrated. To the best of our knowledge, plasma profiles of (*E*)-Clom and its metabolites after intravenous administration were not publicly available. Information on the identified and integrated published clinical studies are listed in Table S2. As CYP2D6 AS and phenotype of corresponding study participants were not reported, CYP2D6 catalytic rate constants ( $k_{\text{cat}}$ ) values in the PBPK model were estimated (see Table S1).

**Table S1.** Optimized CYP2D6  $k_{\text{cat}}$  values for each study.

CYP2D6 $k_{\text{cat}}$ values	Mikkelsen et al. 1986 [1]	Study Ratioph. 1991 [2]	Wiehle et al. 2013 (a) [3]	Wiehle et al. 2013 (b)[3]	Wiehle et al. 2013 (c) [3]	Miller et al. 2018 [4]
( <i>E</i> )-Clom $\rightarrow$ ( <i>E</i> )-4-OH-Clom	213.0	283.1	87.7	124.1	43.3	18.1
( <i>E</i> )-Clom $\rightarrow$ undef.	90.6	120.5	37.3	52.8	18.4	7.7
( <i>E</i> )-Clom $\rightarrow$ ( <i>E</i> )-DE-Clom	84.4	112.1	34.8	49.1	17.1	7.2

CYP: cytochrome P450, (***E***)-4-OH-Clom: (*E*)-4-hydroxyclophene, (***E***)-Clom: (*E*)-clomiphene, (***E***)-DE-Clom: (*E*)-N-desethylclomiphene,  $k_{\text{cat}}$ : catalytic rate constant, **Ratioph.**: Ratiopharm<sup>®</sup> GmbH, **undef.**: undefined metabolite

Of note, in the pharmacokinetic panel study, two study participants with the *CYP2D6* genotypes <sup>\*</sup>9/<sup>\*</sup>10 and <sup>\*</sup>9/<sup>\*</sup>41 had been classified as AS=0.75. Here, a high interindividual variability in the plasma profiles could be observed. The study participant genotyped as <sup>\*</sup>9/<sup>\*</sup>41 showed unexpectedly high (*E*)-Clom plasma concentrations for an AS=0.75 individual with (*E*)-Clom levels comparable with those of poor metabolizers (PM). Since the allele haplotype <sup>\*</sup>41 has shown a high dispersion in CYP2D6 enzyme activity, the respective individual was excluded from the dataset [5].



Table S2. Overview of clinical study data from literature used for model evaluation.

Clinical study	Route	Dose [mg] <sup>a</sup>	E/Z ratio	n	Females [%]	Age [years] <sup>b</sup>	Weight [kg] <sup>b</sup>	BMI [kg/m <sup>2</sup> ] <sup>b</sup>	Metabolites measured	CYP2D6 genotyped
Mikkelsen et al. 1986 [1]	po, tab, s.d.	50	- <sup>c</sup>	23	100	32	62.4	-	no	no
Study Ratioph. 1991 [2]	po, tab, s.d.	50	62/38	18	-	-	-	-	no	no
Wiehle et al. 2013 (a) [3]	po, caps, m.d.	6.25	100/0	16	0	53.3±10.2	-	34.7±7.2	no	no
Wiehle et al. 2013 (b) [3]	po, caps, m.d.	12.5	100/0	14	0	53.3±10.2	-	34.7±7.2	no	no
Wiehle et al. 2013 (c) [3]	po, caps, m.d.	25	100/0	16	0	53.3±10.2	-	34.7±7.2	no	no
Miller et al. 2018 [4]	po, tab, m.d.	50	62/38	12	0	31.5±3.6	77.9±8.2	24.4±2.4	no	no

**BMI:** body mass index, **caps:** capsule, **CYP:** cytochrome P450, **E/Z:** (E)-/(Z)-cloniphenene, **m.d.:** multiple dose, **n:** number of subjects, **po:** per oral,

**Ratioph.:** Ratiopharm® GmbH, **s.d.:** single dose, **tab:** tablet

<sup>a</sup> (E)-/(Z)-cloniphenene citrate

<sup>b</sup> mean (±SD) if applicable

<sup>c</sup> E/Z-ratio of 62/38 was assumed

## S1.2. System-dependent Parameters and Virtual Populations

Virtual individuals were created in PK-Sim<sup>®</sup>, using the published information on the respective study population, including mode of ethnicity and gender as well as mean values of age, weight and height. For the study population in the study from Ratiopharm<sup>®</sup> GmbH [2], demographic information were not provided. Here, the default values of a 30-year-old male European individual with body weight of 73 kg and height of 176 cm according to the International Commission on Radiological Protection (ICRP) reference values were used [6]. Distribution and abundance of enzymes in the different tissues was implemented according to the PK-Sim<sup>®</sup> expression database [7]. For the generation of virtual populations, 1000 individuals were created according to the respective study population demographics. Demographic characteristics of virtual individuals were varied within the ICRP [6] and the third National Health and Nutrition Examination Survey (NHANES) [8] limits by an implemented algorithm in PK-Sim<sup>®</sup>. The corresponding algorithms for the generation of virtual populations have been reported by Willmann and coworkers [9]. For the study by Mikkelsen et al. [1] and the study from Ratiopharm<sup>®</sup> GmbH [2] an age range of 20 to 50 years was assumed.

Variabilities for CYP2B6 and CYP3A4 enzyme abundances in the virtual populations were integrated and variability in CYP2D6 abundance was allowed for study populations that were not genotyped and thus not stratified by CYP2D6 AS. For the pharmacokinetic panel study, CYP2D6  $k_{cat}$  values differ across CYP2D6 AS groups, already accounting for varying CYP2D6 abundance and/or activity. Thus, CYP2D6 expression variability was set to 0 for the respective population simulations.

System-dependent parameters including reference concentrations and enzyme expression variabilities are listed in [Table S3](#).

Table S3. System-dependent parameters and expression of relevant enzymes.

Enzyme / Processes	Mean reference concentration [μmol/L] <sup>a</sup>	GeoSD of the reference concentration	Relative expression in different organs <sup>b</sup>	Half-life liver [hours]	Half-life intestine [hours]
<b>Enzymes</b>					
CYP2B6	1.56 [10]	1.40 <sup>c</sup>	RT-PCR [11]	32	23
CYP2D6	0.40 [10]	0 <sup>d</sup>	RT-PCR [11]	51	23
CYP3A4	4.32 [10]	1.18 (liver)[7] 1.45 (duodenum)[7]	RT-PCR [11]	36 [12]	23 [13]
<b>Processes</b>					
Unspec. hep. CL of (E)-4-OH-Clom	-	1.40 <sup>c</sup>			
Unspec. hep. CL of (E)-4-OH-DE-Clom	-	1.40 <sup>c</sup>			

**CYP**: cytochrome P450, **(E)-4-OH-Clom**: (E)-4-hydroxyclophiphen, **(E)-4-OH-DE-Clom**: (E)-4-hydroxy-N-desethylclomiphene, **GeoSD**: geometric standard deviation, **RT-PCR**: reverse transcription polymerase chain reaction, **unspec. hep. CL**: unspecific hepatic clearance

<sup>a</sup> [μmol protein/L] in the tissue of the highest expression

<sup>b</sup> PK-Sim<sup>®</sup> expression database profile

<sup>c</sup> geometric standard deviation with coefficient of variation (CV) of 35 % assumed

<sup>d</sup> as described in Section 1.2

### S1.3. Supplementary Information on (*E*)-clomiphen PBPK Model Building

The parent-metabolite PBPK model of (*E*)-Clom was developed using a middle-out approach, combining information on drug- and system-specific parameters from literature with a parameter estimation step based on clinical trial data [14]. *In vitro*, *in silico* and clinical *in vivo* data were combined to inform model input parameters [14]. Information about absorption, distribution, metabolism and excretion (ADME) processes were used to incorporate relevant enzymes.

Metabolism via CYP enzymes was implemented as Michaelis-Menten kinetic processes. To account for nonspecific binding in *in vitro* assays, apparent Michaelis-Menten constant ( $K_m$ ) values informed from literature were adjusted by the free fraction of drug compound as suggested by Obach and Austin et al. [15, 16].  $K_m$  and  $v_{max}$  values were available only for composite metabolic pathway reactions, while parameters for each specific CYP enzyme involved in the respective pathway were not reported. When multiple CYP enzymes were incorporated in one metabolic pathway (see Figure 2 in the main manuscript), identical  $K_m$  values were allocated to each CYP enzyme and the corresponding  $k_{cat}$  estimated with a fixed ratio based on *in vitro* results on the metabolic enzyme activities [17, 18].

In the PBPK model, three metabolic pathways were implemented for the parent compound (*E*)-Clom: metabolism to (*E*)-DE-Clom, metabolism to (*E*)-4-OH-Clom and metabolism to (*Z*)-3-hydroxyclophiphen (implemented as an undefined metabolite). The latter enzymatic pathway, mediated via CYP2D6, was estimated with a 1.8-fold higher intrinsic clearance compared to the formation of (*E*)-4-OH-Clom in the PBPK model according to literature [19]. Further, the formation of (*E*)-DE-Clom is primarily catalyzed by CYP3A4 and to some extent by CYP2D6 [17, 18]. This was integrated by accounting for the 80:20 metabolic ratio of CYP3A4 to CYP2D6 reported by Mazzarino and coworkers [20]. (*E*)-DE-Clom itself is also metabolized via CYP3A4 and CYP2D6 to (*E*)-N,N-didesethylclomiphen (implemented as an undefined metabolite) [17, 18]. As previously described, the ratio of the corresponding measured *in vitro* metabolic enzyme activities was used during the parameter estimation step for optimization of  $k_{cat}$  values ( $k_{cat, CYP3A4} = 0.13 * k_{cat, CYP2D6}$ ) [17, 18].

## S1.4. Drug-dependent Parameter Tables

Table S4. Drug-dependent parameters for (*E*)-clomiphene.

Parameter	Value	Unit	Source	Literature	Reference	Description
MW	405.96	g/mol	Literature	405.96	[22]	Molecular weight
pK <sub>a</sub> (base)	9.31	-	Literature	9.31	[23]	Acid dissociation constant
Solubility (pH 6.8)	0.0138	mg/ml	Literature	0.0138	[24]	Solubility
logP	5.67	-	Optimized	5.18, 6.08, 6.48, 6.65	[23, 25–27]	Lipophilicity
f <sub>u</sub>	0.08	%	Optimized	1.42 <sup>a</sup>	[21]	Fraction unbound
CYP2D6 K <sub>m</sub> → ( <i>E</i> )-4-OH-Clom	0.13	μmol/l	Literature	0.13 <sup>b</sup>	[19]	Michaelis-Menten constant
CYP2D6 k <sub>cat</sub> → ( <i>E</i> )-4-OH-Clom	306.4 <sup>c</sup>	1/min	Optimized	-	-	Catalytic rate constant
CYP2D6 K <sub>m</sub> → undef.	0.03	μmol/l	Literature	0.03 <sup>b</sup>	[19]	Michaelis-Menten constant
CYP2D6 k <sub>cat</sub> → undef.	130.4 <sup>c</sup>	1/min	Optimized	-	-	Catalytic rate constant
CYP2B6 K <sub>m</sub> → ( <i>E</i> )-4-OH-Clom	0.60	μmol/l	Literature	0.60 <sup>b</sup>	[17, 18]	Michaelis-Menten constant
CYP2B6 k <sub>cat</sub> → ( <i>E</i> )-4-OH-Clom	7.5	1/min	Optimized	-	-	Catalytic rate constant
CYP2D6 K <sub>m</sub> → ( <i>E</i> )-DE-Clom	0.78	μmol/l	Literature	0.78 <sup>b</sup>	[17, 18]	Michaelis-Menten constant
CYP2D6 k <sub>cat</sub> → ( <i>E</i> )-DE-Clom	121.4 <sup>c</sup>	1/min	Optimized	-	-	Catalytic rate constant
CYP3A4 K <sub>m</sub> → ( <i>E</i> )-DE-Clom	0.78	μmol/l	Literature	0.78 <sup>b</sup>	[17, 18]	Michaelis-Menten constant
CYP3A4 k <sub>cat</sub> → ( <i>E</i> )-DE-Clom	45.0	1/min	Optimized	-	-	Catalytic rate constant
GFR fraction	0.92	-	Optimized	-	-	Fraction of filtered drug in the urine
EHC continuous fraction	1.00	-	Assumed	-	-	Fraction of bile continually released
Partition coefficients	Diverse <sup>d</sup>	-	Calculated	Schmitt	[28]	Cell to plasma partition coefficients
Cellular permeability	Diverse <sup>d</sup>	cm/min	Calculated	Ch. dep. Schmitt	[29]	Permeability into the cellular space
Intestinal permeability	0.08	cm/min	Optimized	-	-	Transcellular intestinal permeability
Tablet Weibull time	6.80	min	Assumed	-	<sup>e</sup>	Dissolution time (50 % dissolved)
Tablet Weibull shape	0.47	-	Assumed	-	<sup>e</sup>	Dissolution profile shape

**Ch. dep. Schmitt:** Charge dependent Schmitt calculation method, **CYP:** cytochrome P450, **(*E*)-4-OH-Clom:** (*E*)-4-hydroxyclophene, **(*E*)-DE-Clom:** (*E*)-N-desethylclomiphene, **EHC:** enterohepatic circulation, **GFR:** glomerular filtration rate, **IM:** intermediate metabolizers, **IVSF:** *in vitro* scaling factor, **NM:** normal metabolizers, **UM:** ultrarapid metabolizers, **undef.:** undefined metabolite

<sup>a</sup> f<sub>u</sub> was estimated with the classification model by Watanabe et al. [21]

<sup>b</sup> K<sub>m</sub> values from literature were adapted with the calculated f<sub>u,inc</sub>=0.024, considering nonspecific binding in *in vitro* assays according to [15, 16]

<sup>c</sup> Only CYP2D6 k<sub>cat</sub> values of NM are shown while IM- and UM-k<sub>cat</sub> values were extrapolated according to Equation 1 in the main manuscript (IVSFs represented in Table S8)

<sup>d</sup> values differ across the organs

<sup>e</sup> see Section 1.6

**Table S5.** Drug-dependent parameters for (*E*)-N-desethylclomiphene.

Parameter	Value	Unit	Source	Literature	Reference	Description
MW	377.91	g/mol	Literature	377.91	[30]	Molecular weight
pK <sub>a</sub> (base)	8.14	-	Optimized	9.59	[30]	Acid dissociation constant
Solubility (pH 6.5)	0.46	mg/ml	Literature	0.46	[30]	Solubility
logP	4.17	-	Optimized	5.74, 6.4	[30, 31]	Lipophilicity
f <sub>u</sub>	0.86	%	Optimized	1.37 <sup>a</sup>	[21]	Fraction unbound
CYP2D6 K <sub>m</sub> → ( <i>E</i> )-4-OH-DE-Clom	0.49	μmol/l	Literature	0.49 <sup>b</sup>	[17, 18]	Michaelis-Menten constant
CYP2D6 k <sub>cat</sub> → ( <i>E</i> )-4-OH-DE-Clom	64.5 <sup>c</sup>	1/min	Optimized	-	-	Catalytic rate constant
CYP2D6 K <sub>m</sub> → undef.	0.97	μmol/l	Literature	0.97 <sup>b</sup>	[17, 18]	Michaelis-Menten constant
CYP2D6 k <sub>cat</sub> → undef.	5.8 <sup>c</sup>	1/min	Optimized	-	-	Catalytic rate constant
CYP3A4 K <sub>m</sub> → undef.	0.97	μmol/l	Literature	0.97 <sup>b</sup>	[17, 18]	Michaelis-Menten constant
CYP3A4 k <sub>cat</sub> → undef.	0.8	1/min	Optimized	-	-	Catalytic rate constant
GFR fraction	0.10	-	Optimized	-	-	Fraction of filtered drug in the urine
EHC continuous fraction	1.00	-	Assumed	-	-	Fraction of bile continually released
Partition coefficients	Diverse <sup>d</sup>	-	Calculated	R&R	[32, 33]	Cell to plasma partition coefficients
Cellular permeability	Diverse <sup>d</sup>	cm/min	Calculated	Ch. dep. Schmitt	[29]	Permeability into the cellular space

**Ch. dep. Schmitt:** Charge dependent Schmitt calculation method, **CYP:** cytochrome P450,

**(*E*)-4-OH-DE-Clom:** (*E*)-4-hydroxy-N-desethylclomiphene, **EHC:** enterohepatic circulation, **GFR:** glomerular filtration rate,

**IM:** intermediate metabolizers, **IVSF:** *in vitro* scaling factor, **NM:** normal metabolizers, **R&R:** Rodgers and Rowland calculation method,

**UM:** ultrarapid metabolizers, **undef.:** undefined metabolite

<sup>a</sup> f<sub>u</sub> was estimated with the classification model by Watanabe et al. [21]

<sup>b</sup> K<sub>m</sub> values from literature were adapted with the calculated f<sub>u,inc</sub>=0.059, considering nonspecific binding in *in vitro* assays according to [15, 16]

<sup>c</sup> Only CYP2D6 k<sub>cat</sub> values of NM are shown while IM- and UM-k<sub>cat</sub> values were extrapolated according to Equation 1 in the main manuscript (IVSFs represented in Table S8)

<sup>d</sup> values differ across the organs

**Table S6.** Drug-dependent parameters for (*E*)-4-hydroxyclophene.

Parameter	Value	Unit	Source	Literature	Reference	Description
MW	421.97	g/mol	Literature	421.97	[34]	Molecular weight
pK <sub>a</sub> (acid)	8.64	-	Literature	8.64	[34]	Acid dissociation constant
pK <sub>a</sub> (base)	7.90	-	Optimized	9.41	[34]	Acid dissociation constant
Solubility (pH 6.5)	0.06	mg/ml	Literature	0.06	[34]	Solubility
logP	5.50	-	Optimized	5.31, 5.64	[25, 34]	Lipophilicity
f <sub>u</sub>	0.45	%	Optimized	0.6, 1.33 <sup>a</sup>	[21, 35]	Fraction unbound
CYP2D6 K <sub>m</sub> → undef.	3.60	μmol/l	Literature	3.60 <sup>b</sup>	[19]	Michaelis-Menten constant
CYP2D6 k <sub>cat</sub> → undef.	855.2 <sup>c</sup>	1/min	Optimized	-	-	Catalytic rate constant
CYP3A4 K <sub>m</sub> → ( <i>E</i> )-4-OH-DE-Clom	3.40	μmol/l	Literature	3.40 <sup>b</sup>	[17, 18]	Michaelis-Menten constant
CYP3A4 k <sub>cat</sub> → ( <i>E</i> )-4-OH-DE-Clom	19.5	1/min	Optimized	-	-	Catalytic rate constant
Unspec. hep. CL → undef.	23.78	1/min	Optimized	-	-	Elimination from plasma (first-order process in the liver)
GFR fraction	0.24	-	Optimized	-	-	Fraction of filtered drug in the urine
EHC continuous fraction	1.00	-	Assumed	-	-	Fraction of bile continually released
Partition coefficients	Diverse <sup>d</sup>	-	Calculated	Berez.	[36]	Cell to plasma partition coefficients
Cellular permeability	2.23	cm/min	Calculated	PK-Sim	[37]	Permeability into the cellular space

**Berez.:** Berezhkovskiy calculation method, **CYP:** cytochrome P450, **(*E*)-4-OH-DE-Clom:** (*E*)-4-hydroxy-N-desethylclomiphene,

**EHC:** enterohepatic circulation, **GFR:** glomerular filtration rate, **IM:** intermediate metabolizers, **IVSF:** *in vitro* scaling factor,

**NM:** normal metabolizers, **PK-Sim:** PK-Sim standard calculation method, **UM:** ultrarapid metabolizers, **undef.:** undefined metabolite,

**unspec. hep. CL:** unspecific hepatic clearance

<sup>a</sup> f<sub>u</sub> was estimated with the classification model by Watanabe et al. [21]

<sup>b</sup> K<sub>m</sub> values from literature were adapted with the calculated f<sub>u,inc</sub>=0.099, considering nonspecific binding in *in vitro* assays according to [15, 16]

<sup>c</sup> Only CYP2D6 k<sub>cat</sub> values of NM are shown while IM- and UM-k<sub>cat</sub> values were extrapolated according to Equation 1 in the main manuscript (IVSFs represented in Table S8)

<sup>d</sup> values differ across the organs

**Table S7.** Drug-dependent parameters for (*E*)-4-hydroxy-N-desethyl-clomiphene.

Parameter	Value	Unit	Source	Literature	Reference	Description
MW	393.91	g/mol	Literature	393.91	[38]	Molecular weight
pK <sub>a</sub> (acid)	8.69	-	Literature	8.69	[38]	Acid dissociation constant
pK <sub>a</sub> (base)	9.65	-	Literature	9.65	[38]	Acid dissociation constant
Solubility (pH 6.5)	0.17	mg/ml	Literature	0.17	[38]	Solubility
logP	3.71	-	Optimized	4.47	[38]	Lipophilicity
f <sub>u</sub>	1.32	%	Calculated	1.32 <sup>a</sup>	[21]	Fraction unbound
CYP2D6 K <sub>m</sub> → undef.	8.86	μmol/l	Assumed	8.86 <sup>b,c</sup>	-	Michaelis-Menten constant
CYP2D6 k <sub>cat</sub> → undef.	211.7 <sup>d</sup>	1/min	Optimized	-	-	Catalytic rate constant
Unsp. hep. CL → undef.	8.50	1/min	Optimized	-	-	Elimination from plasma (first-order process in the liver)
GFR fraction	0.13	-	Optimized	-	-	Fraction of filtered drug in the urine
EHC continuous fraction	1.00	-	Assumed	-	-	Fraction of bile continually released
Partition coefficients	Diverse <sup>e</sup>	-	Calculated	Schmitt	[28]	Cell to plasma partition coefficients
Cellular permeability	Diverse <sup>e</sup>	cm/min	Calculated	Ch. dep. Schmitt	[29]	Permeability into the cellular space

**Ch. dep. Schmitt:** Charge dependent Schmitt calculation method, **CYP:** cytochrome P450, **(E)-4-OH-Clom:** (*E*)-4-hydroxyclophene, **(E)-4-OH-DE-Clom:** (*E*)-4-hydroxy-N-desethylclomiphene, **EHC:** enterohepatic circulation, **GFR:** glomerular filtration rate,

**IM:** intermediate metabolizers, **IVSF:** *in vitro* scaling factor, **NM:** normal metabolizers, **UM:** ultrarapid metabolizers,

**undef.:** undefined metabolite, **unsp. hep. CL:** unspecific hepatic clearance

<sup>a</sup> f<sub>u</sub> was estimated with the classification model by Watanabe et al. [21]

<sup>b</sup> K<sub>m</sub> values from literature were adapted with the calculated f<sub>u,inc</sub>=0.243, considering nonspecific binding in *in vitro* assays according to [15, 16]

<sup>c</sup> K<sub>m</sub> value for CYP2D6-mediated hydroxylation of (*E*)-4-OH-DE-Clom was assumed to be equal to K<sub>m</sub> value of the CYP2D6-mediated hydroxylation of (*E*)-4-OH-Clom

<sup>d</sup> Only CYP2D6 k<sub>cat</sub> values of NM are shown while IM- and UM-k<sub>cat</sub> values were extrapolated according to Equation 1 in the main manuscript (IVSFs represented in Table S8)

<sup>e</sup> values differ across the organs

## S1.5. Calculation of Fractions Metabolized

The fraction metabolized (f<sub>m</sub>) of (*E*)-Clom via CYP2D6 was calculated according to Equation S1, using the observed relative AUC<sub>last</sub> increase between the PM population and the control group (normal metabolizers (NM)) [39]. Calculation yielded a CYP2D6 f<sub>m</sub> of ~90%. In addition, data from the CYP2D6 NM population in the clarithromycin DDI scenario (CYP3A4 inhibition) was used to estimate f<sub>m</sub> of (*E*)-Clom via CYP3A4 to inform model development regarding CYP3A4-dependent (*E*)-Clom degradation. For this, the observed relative AUC<sub>last</sub> increase in the NM population between the DDI scenario with CYP3A4 inhibition and the control scenario without inhibition was used, yielding a CYP3A4 f<sub>m</sub> of about 13%. Of note, a complete CYP3A4 inhibition through clarithromycin was assumed, given the strong and mechanism-based inhibition through clarithromycin, which was administered twice a day for four days before the victim drug, (*E*)-Clom, was administered.

$$\frac{1}{1 - f_m} = \frac{AUC_{last, effect, AS=i}}{AUC_{last, control}} \quad (S1)$$

In case of CYP2D6 f<sub>m</sub> calculation, AUC<sub>last, effect</sub> represents the AUC<sub>last</sub> of (*E*)-Clom for the PM population, while AUC<sub>last, control</sub> represents the AUC<sub>last</sub> of (*E*)-Clom for the NM population. For



calculation of the CYP3A4  $f_m$ ,  $AUC_{last, effect}$  represents the  $AUC_{last}$  of (*E*)-Clom for the NM population in the DDI scenario with clarithromycin, while  $AUC_{last, control}$  represents the  $AUC_{last}$  of (*E*)-Clom for the NM population without concomitant clarithromycin administration.

### S1.6. Formulations

Dissolution profiles for clomiphene citrate tablets and (*E*)-Clom citrate capsules were not publicly available. However, according to the U.S. pharmacopoeia, the dissolution rate within the first 30 minutes of clomiphene citrate tablets is required to be at least 75% [40]. This information was used to inform the dissolution shape and time (50% dissolved) parameters of a Weibull function, which was employed as the formulation in PK-Sim<sup>®</sup> (mathematical implementation see Equation S2 and Equation S3). The respective parameter values are represented in Table S4.

$$m = 1 - \exp\left(\frac{-(t - T_{lag})^\beta}{\alpha}\right) \quad (S2)$$

$$\text{with } \alpha = (T_d)^\beta \quad (S3)$$

Here,  $m$  represents the fraction of dissolved drug at time  $t$ ,  $T_{lag}$  is the lag time before onset of dissolution,  $\alpha$  is the scaling parameter,  $\beta$  the shape parameter and  $T_d$  the time needed to dissolve 63% of the formulation [37].

### S1.7. Handling Data Below the Lower Limit of Quantification (LLOQ)

In the pharmacokinetic panel study used for model building and evaluation, 9% of measured concentrations fell below the lower limit of quantification (LLOQ). For handling lower limit of quantification (LLOQ) data, a combination of the M5 and M6 method [41] was used. Below limit of quantification (BLQ) individual plasma concentrations were substituted by LLOQ/2. Subsequently, mean concentrations were calculated for each CYP2D6 activity score (AS) and only the first BLQ data was used for model building and evaluation, while subsequent concentrations were excluded. During the initial period of metabolite formation, BLQ data also appeared in the ascending branch of the plasma profiles. In this case, the last BLQ concentration was included in the data, while BLQ concentrations before this time point were discarded.

## S2. Drug-Gene-Interaction (DGI) Modeling

### S2.1. CYP2D6 *in vitro* Scaling Factors

The estimated CYP2D6  $k_{cat}$  values for the NM population were extrapolated to the intermediate metabolizers (IM) (AS=0.5, AS=0.75 and AS=1) and ultrarapid metabolizers (UM) populations according to Equation 1 in the main manuscript, using *in vitro* scaling factors (IVSFs). Determination of IVSFs were based on AS-specific *in vitro* metabolite formation rates relative to the corresponding formation rate in NM as a reference. The respective IVSFs for each CYP2D6-dependent pathway are depicted in Table S8. Measured *in vitro* data for (*E*)-4-OH-Clom and (*E*)-4-OH-DE-Clom AS-specific formation rates were available, while mean values were assumed for the remaining CYP2D6-dependent metabolic pathways [17].

**Table S8.** Employed *in vitro* scaling factors (IVSFs) for individual CYP2D6 activity scores.

CYP2D6-mediated metabolic pathways	AS=0	AS=0.5	AS=0.75	AS=1	AS=2	AS=3
( <i>E</i> )-Clom → ( <i>E</i> )-4-OH-Clom	0	0.19	0.27	0.57	1	1.52
( <i>E</i> )-Clom → ( <i>E</i> )-DE-Clom	0	0.17	0.23	0.51	1	1.41
( <i>E</i> )-Clom → undef.	0	0.17	0.23	0.51	1	1.41
( <i>E</i> )-4-OH-Clom → undef.	0	0.17	0.23	0.51	1	1.41
( <i>E</i> )-4-OH-DE-Clom → undef.	0	0.17	0.23	0.51	1	1.41
( <i>E</i> )-DE-Clom → ( <i>E</i> )-4-OH-DE-Clom	0	0.16	0.19	0.44	1	1.30
( <i>E</i> )-DE-Clom → undef.	0	0.17	0.23	0.51	1	1.41

AS: CYP2D6 activity score, CYP: cytochrome P450, (***E***)-4-OH-Clom: (*E*)-4-hydroxyclophiphen, (***E***)-4-OH-DE-Clom: (*E*)-4-hydroxy-N-desethylclomiphene, (***E***)-Clom: (*E*)-clomiphene, (***E***)-DE-Clom: (*E*)-N-desethylclomiphene, undef.: undefined metabolite

## S3. Drug-Drug-(Gene)-Interaction (DD(G)I) Modeling

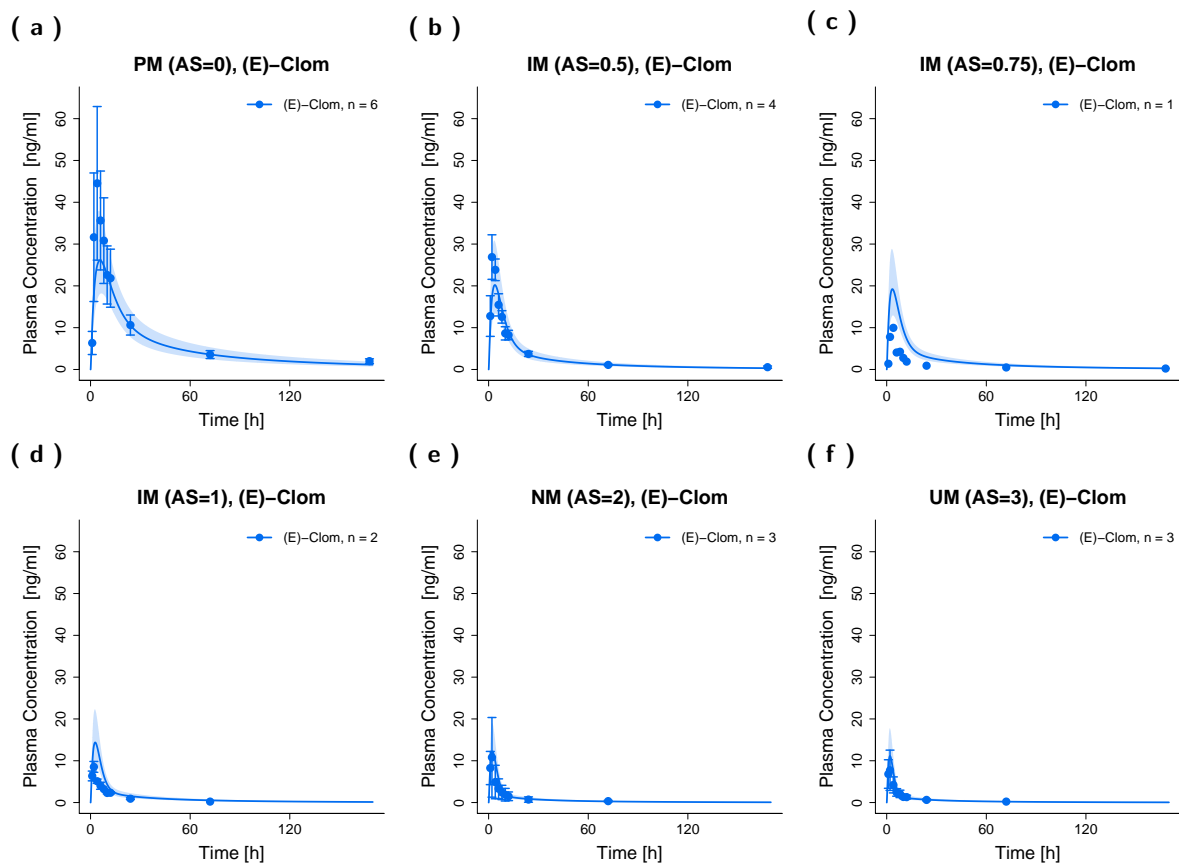
### S3.1. Clarithromycin and Paroxetine

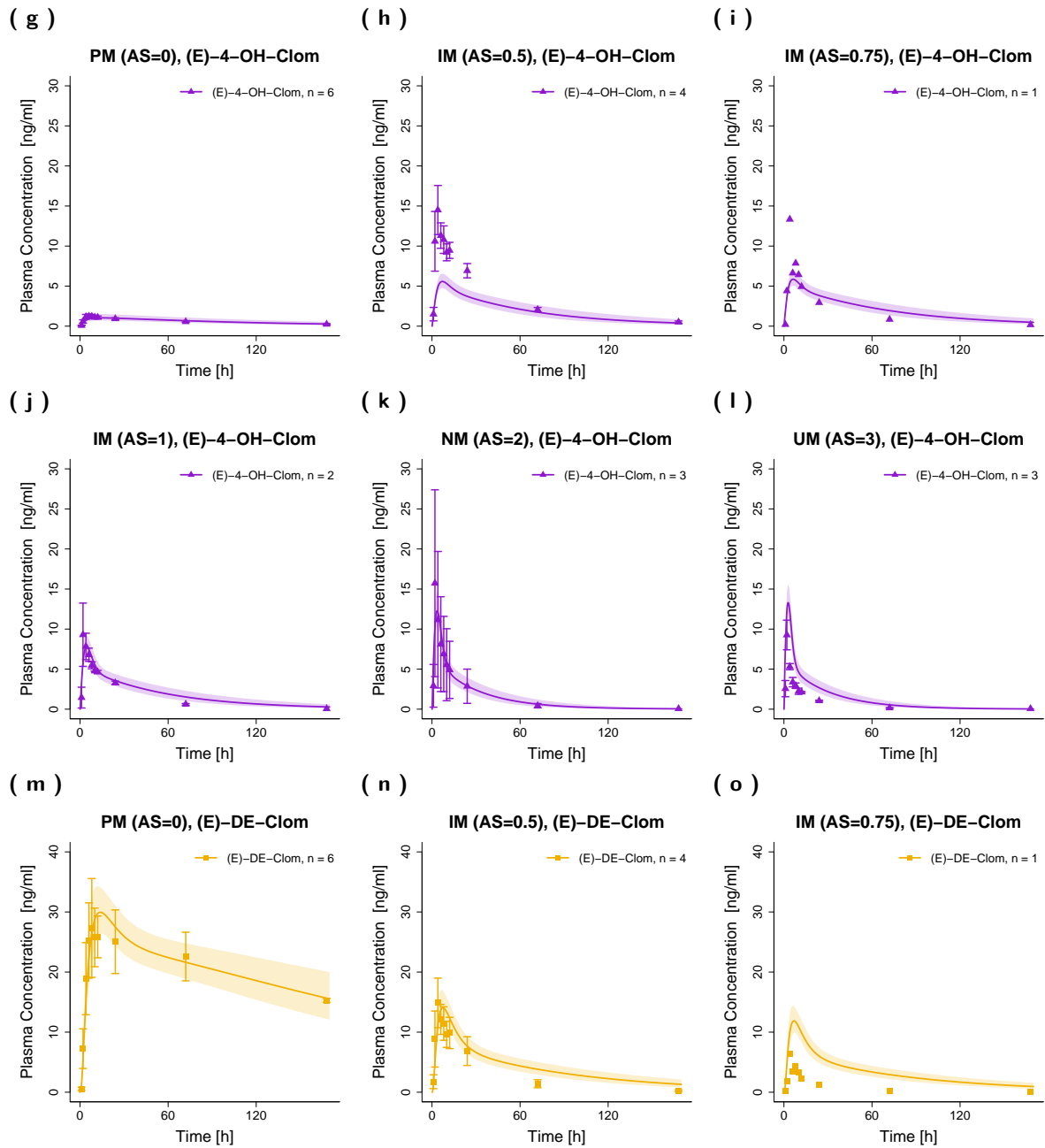
Clarithromycin acts as a mechanism-based inhibitor of CYP3A4, while paroxetine inhibits CYP2D6 and to a minor extent CYP3A4 [42]. Inhibition mechanisms of CYP3A4 and CYP2D6 were implemented according to the PK-Sim<sup>®</sup> manual [37]. Two previously published PBPK models of clarithromycin [43] and paroxetine [44] were applied and coupled with the developed parent-metabolite PBPK model of (*E*)-Clom to assess the model prediction performance in the DD(G)I setting. Interaction parameters were used as published in the respective perpetrator PBPK models.

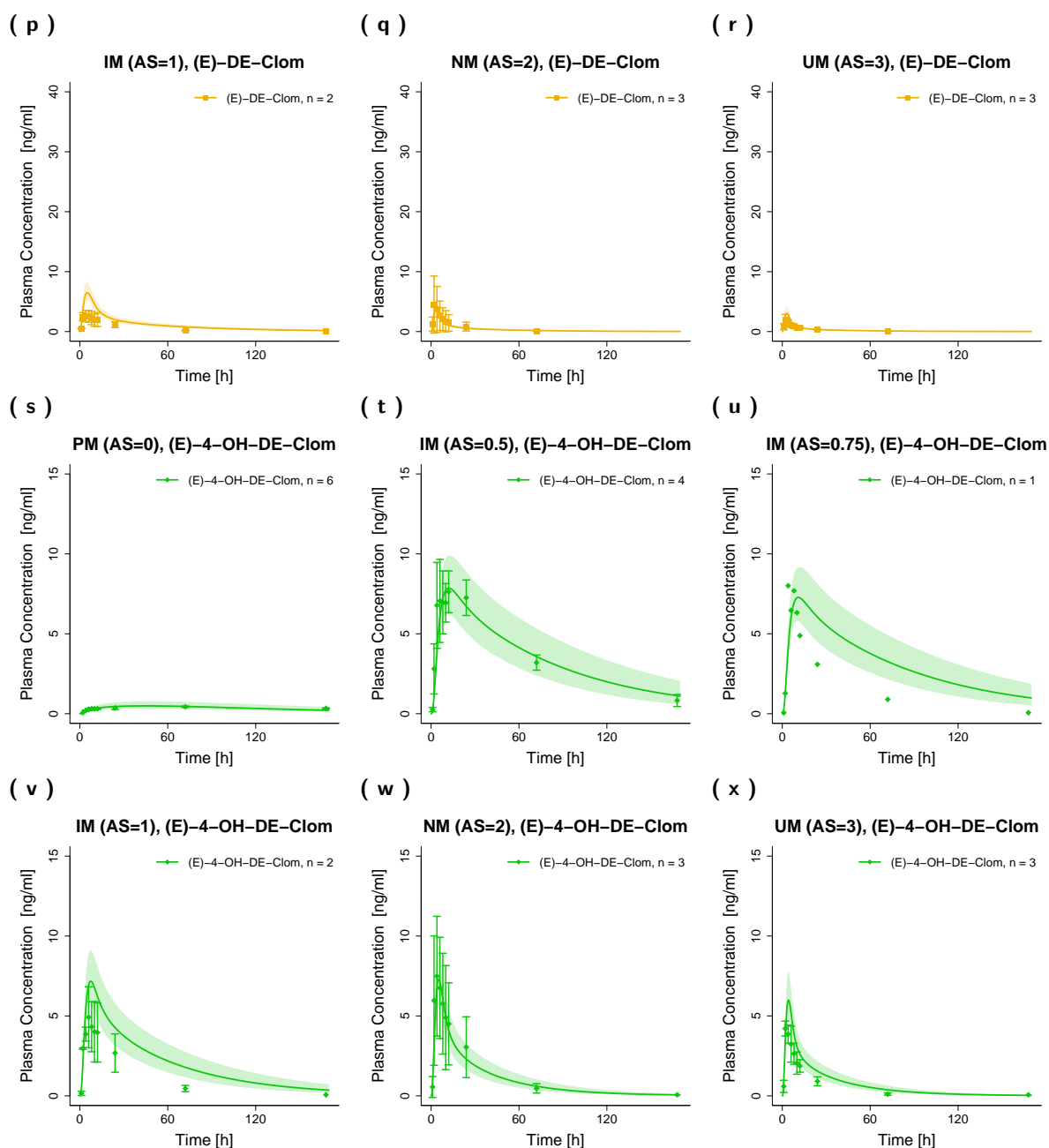
## S4. PBPK Model Evaluation

### S4.1. Evaluation of the DGI Model

#### S4.1.1. Plasma Profiles (Linear Scale)

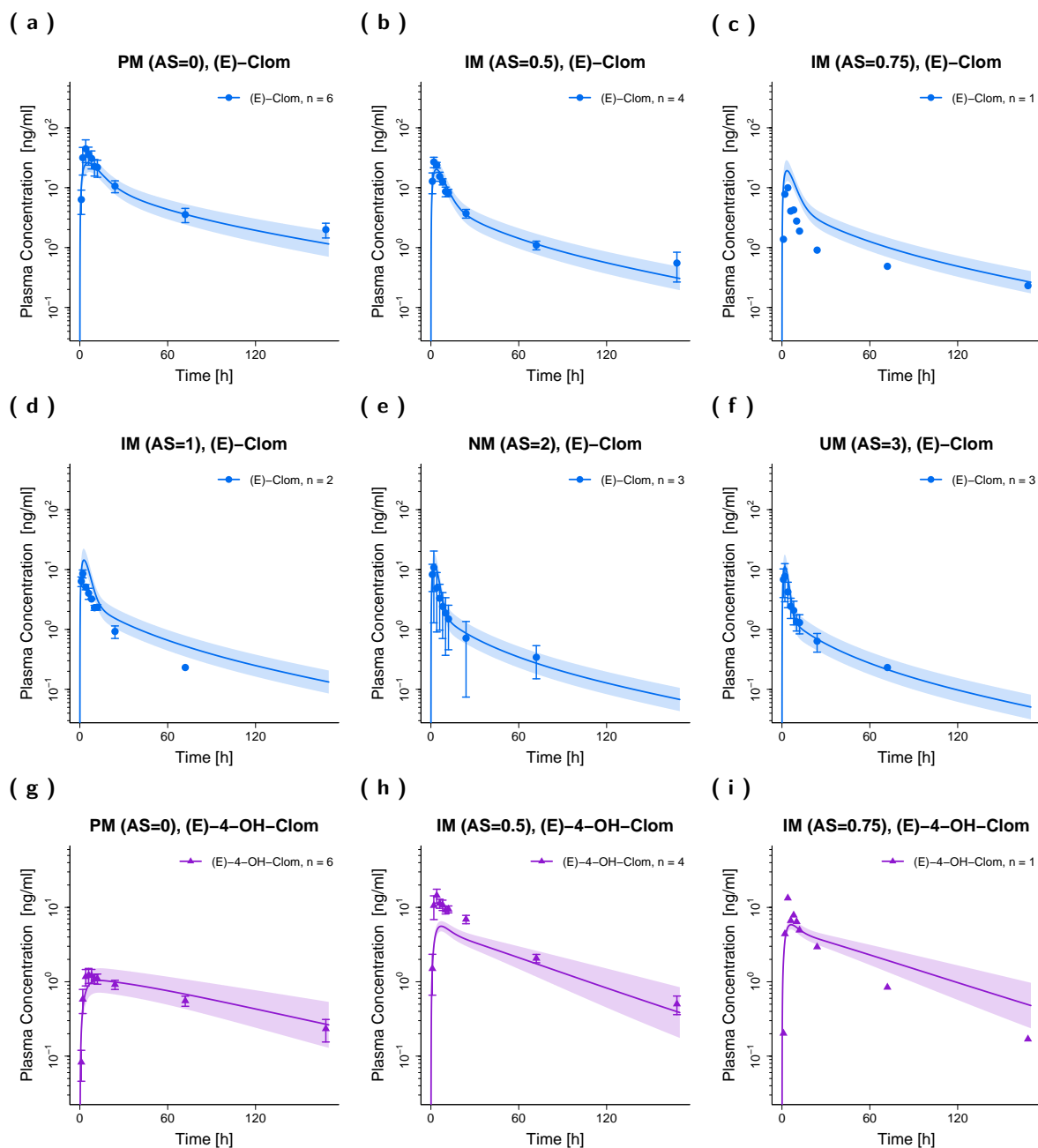


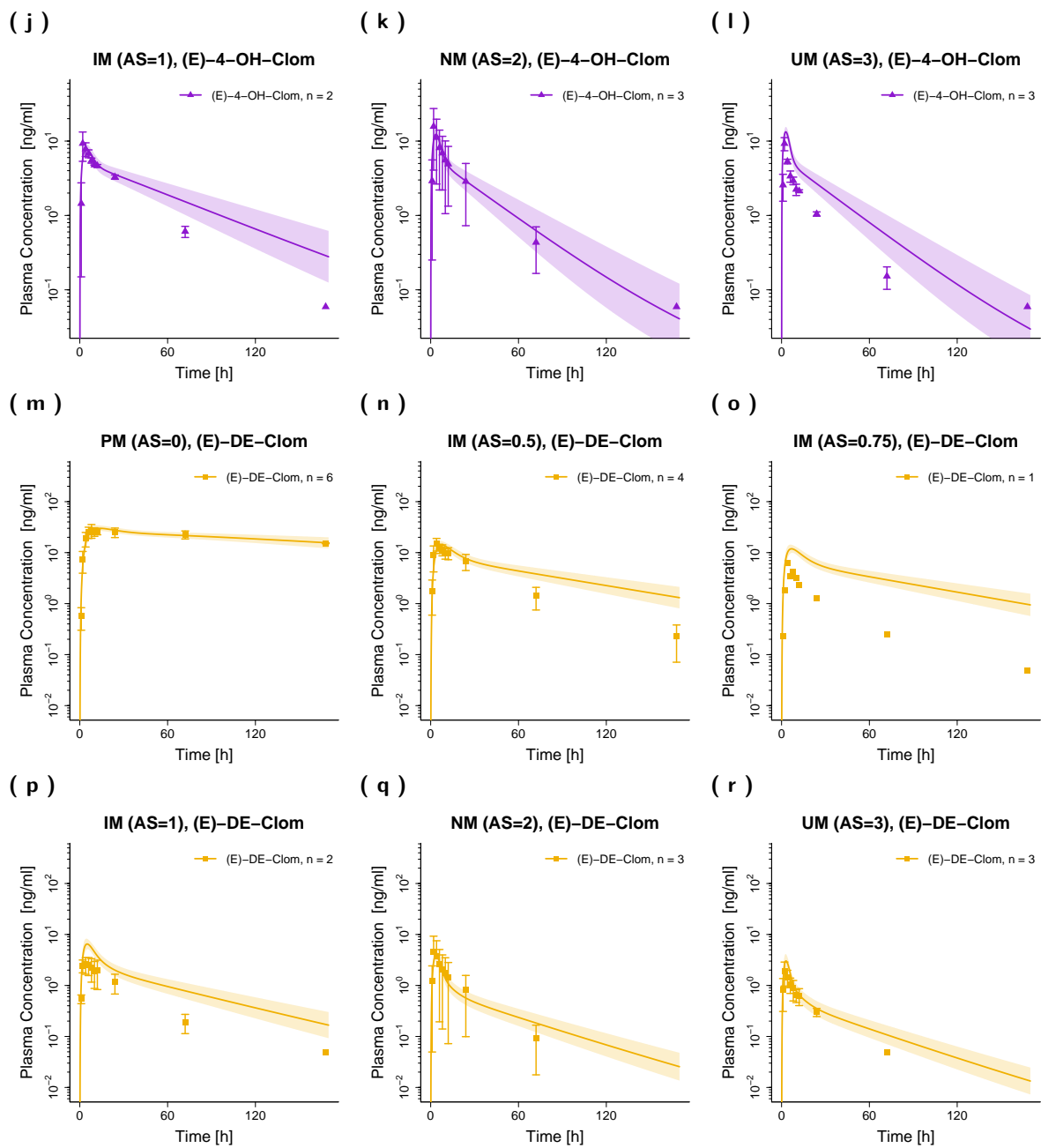


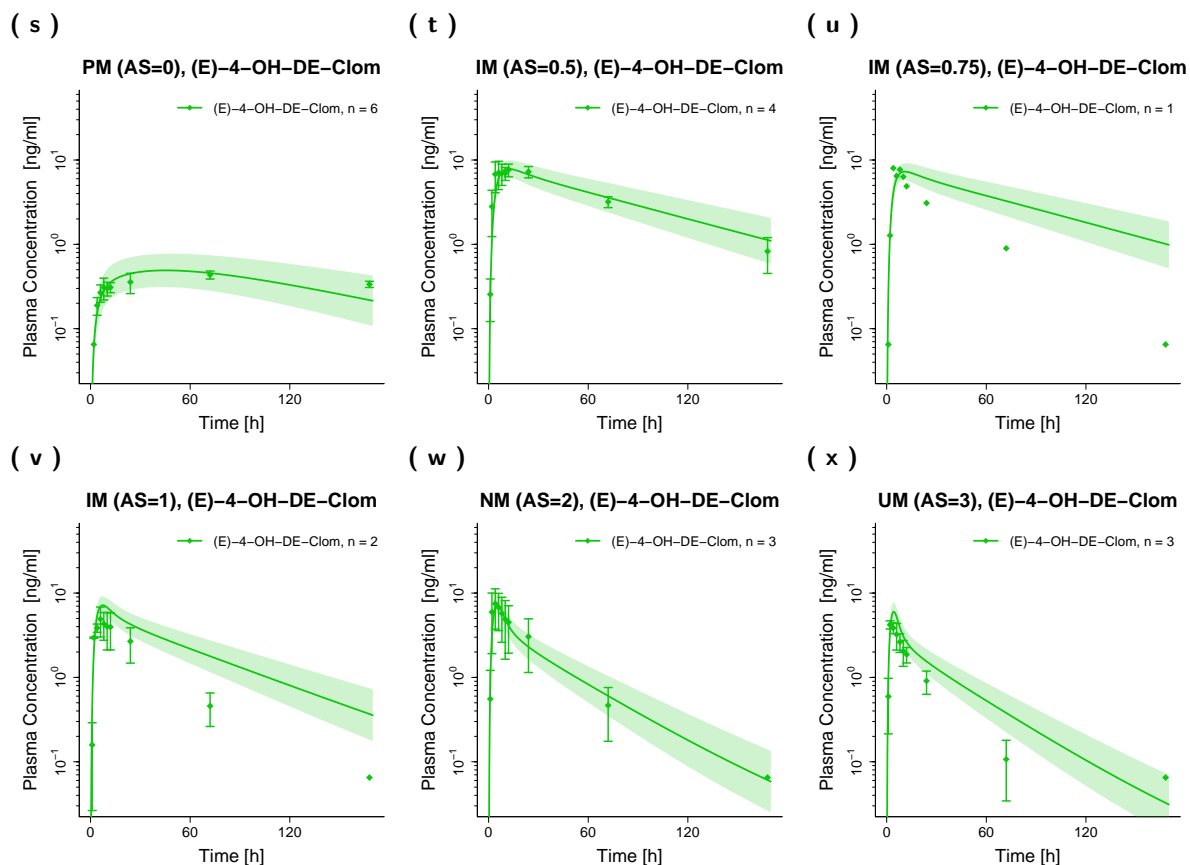


**Figure S1. Predicted and observed plasma concentration-time profiles (linear scale) of (E)-Clom (a-f), (E)-4-OH-Clom (g-l), (E)-DE-Clom (m-r) and (E)-4-OH-DE-Clom (s-x) for DGI scenarios.** Solid lines depict predicted geometric mean concentration-time profiles in PM, IM, NM and UM. The respective semitransparent areas show the geometric standard deviation of the population simulations (n=1000). Mean observed data are shown as symbols with the corresponding standard deviation. **AS**, CYP2D6 activity score; **DGI**, drug-gene inter-action; **(E)-4-OH-Clom**, (E)-4-hydroxyclophene; **(E)-4-OH-DE-Clom**, (E)-4-hydroxy-N-desethylclomiphene; **(E)-Clom**, (E)-clomiphene; **(E)-DE-Clom**, (E)-N-desethylclomiphene; **IM**, intermediate metabolizers; **n**, number of subjects; **NM**, normal metabolizers; **PM**, poor metabolizers; **UM**, ultrarapid metabolizers.

## S4.1.2. Plasma Profiles (Semilogarithmic Scale)



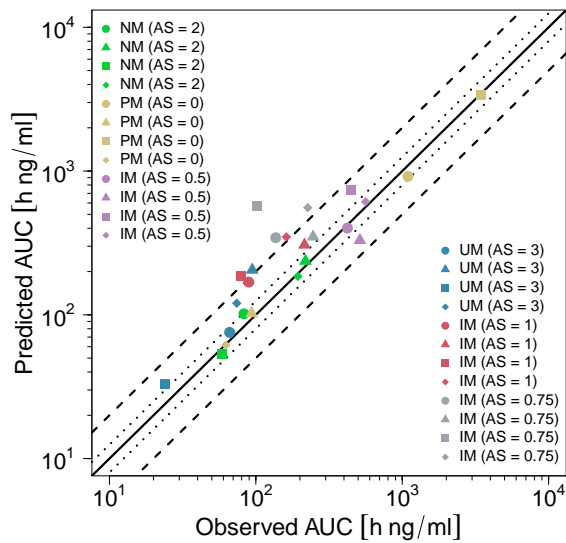
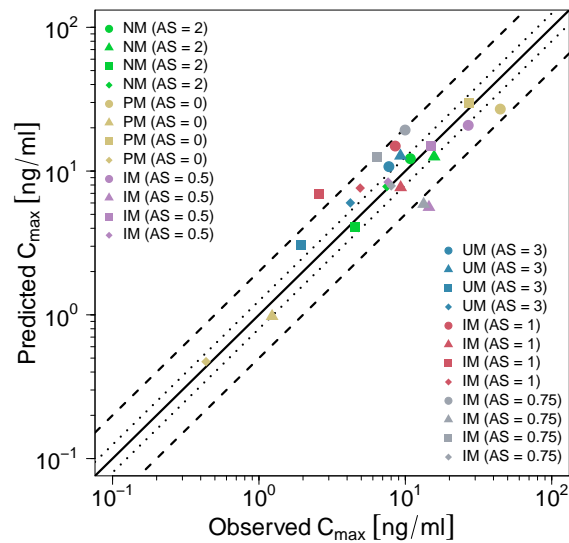




**Figure S2. Predicted and observed plasma concentration-time profiles (semilogarithmic scale) of (*E*)-Clom (a–f), (*E*)-4-OH-Clom (g–l), (*E*)-DE-Clom (m–r) and (*E*)-4-OH-DE-Clom (s–x) for DGI scenarios.** Solid lines depict predicted geometric mean concentration-time profiles in the PM, IM, NM and UM populations. The respective semitransparent areas show the geometric standard deviation of the population simulations ( $n=1000$ ). Mean observed data are shown as symbols with the corresponding standard deviation. **AS**, CYP2D6 activity score; **DGI**, drug-gene interaction; (*E*)-4-OH-Clom, (*E*)-4-hydroxyclophene; (*E*)-4-OH-DE-Clom, (*E*)-4-hydroxy-*N*-desethylclomiphene; (*E*)-Clom, (*E*)-clomiphene; (*E*)-DE-Clom, (*E*)-*N*-desethylclomiphene; IM, intermediate metabolizers; n, number of subjects; NM, normal metabolizers; PM, poor metabolizers; UM, ultrarapid metabolizers.



## S4.1.3. Goodness-of-Fit Plots

(a)  $AUC_{last}$ (b)  $C_{max}$ 

(c) Plasma concentrations

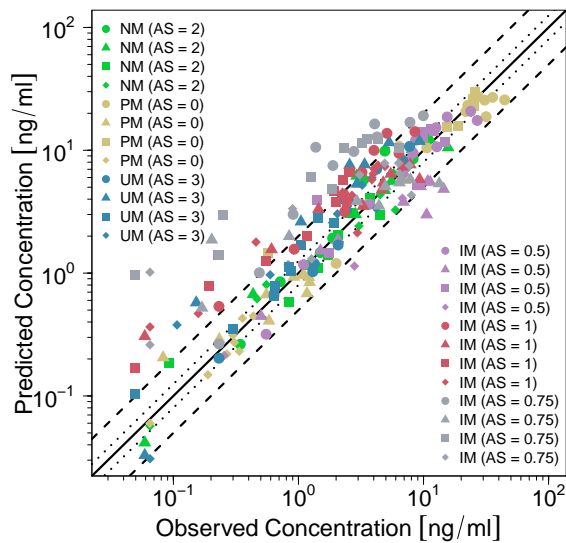
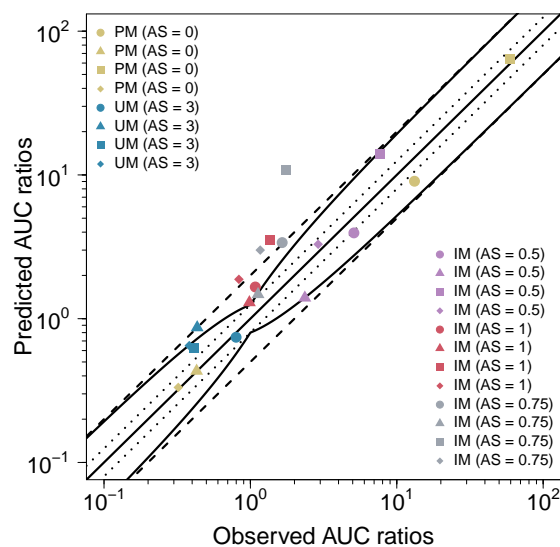
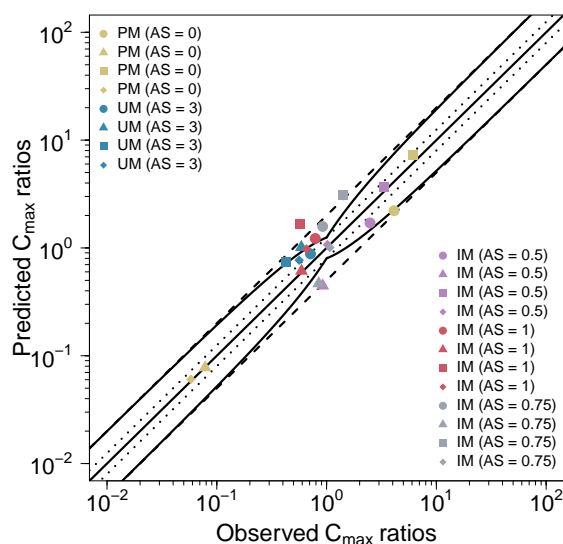
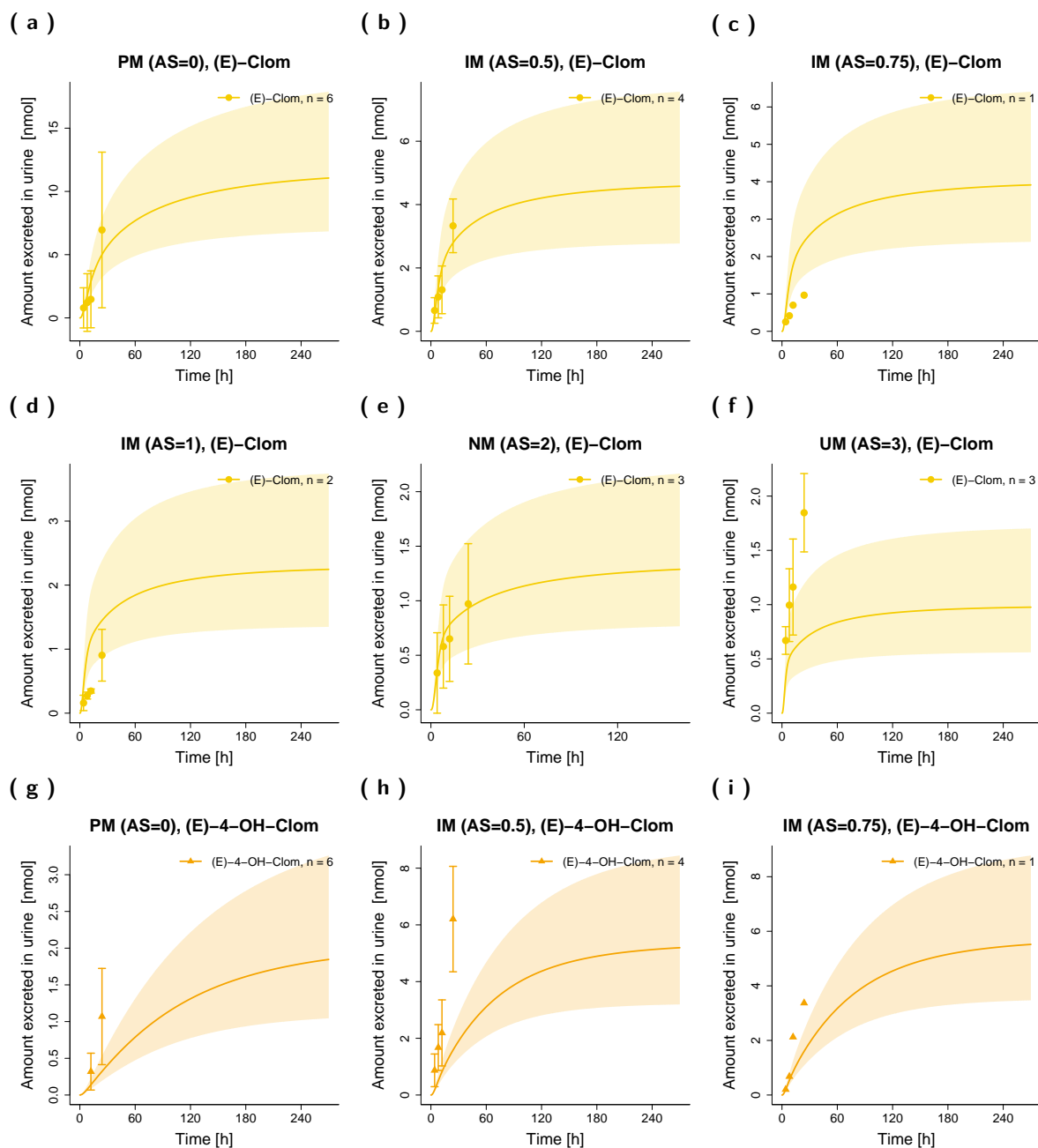


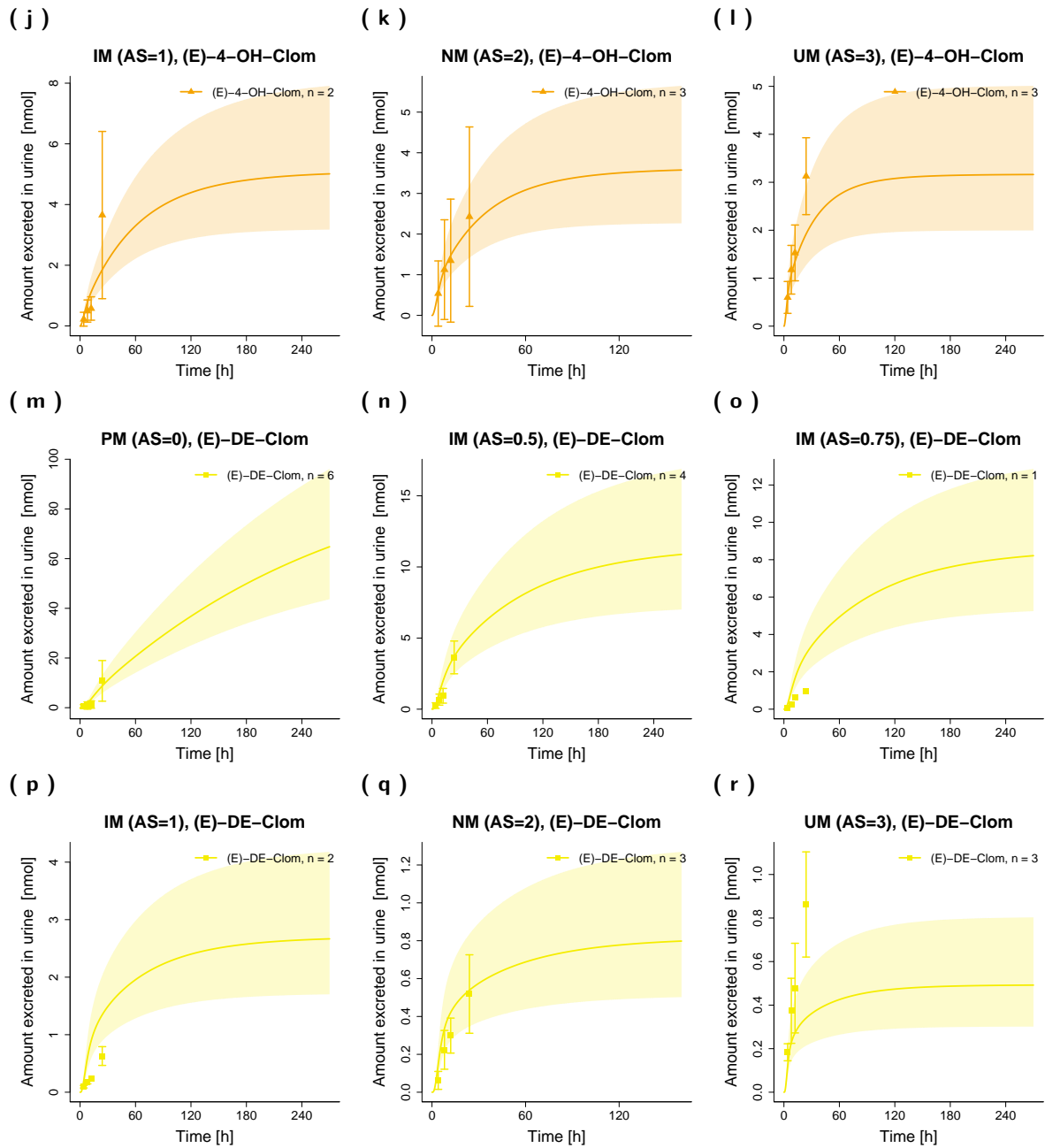
Figure S3. Predicted versus observed  $AUC_{last}$  (a),  $C_{max}$  (b) and plasma concentrations (c) of (E)-Clom (circles), (E)-4-OH-Clom (triangles), (E)-DE-Clom (squares) and (E)-4-OH-DE-Clom (diamonds) in PM, IM, NM and UM (DGI scenarios). The black solid lines mark the lines of identity. Black dotted lines indicate 1.25-fold, black dashed lines indicate 2-fold deviation. AS, CYP2D6 activity score; DGI, drug-gene interaction; (E)-4-OH-Clom, (E)-4-hydroxyclophene; (E)-4-OH-DE-Clom, (E)-4-hydroxy-N-desethylclomiphene; (E)-Clom, (E)-clomiphene; (E)-DE-Clom, (E)-N-desethylclomiphene; IM, intermediate metabolizers; NM, normal metabolizers; PM, poor metabolizers; UM, ultrarapid metabolizers.

(a)  $AUC_{last}$ (b)  $C_{max}$ 

**Figure S4.** Predicted versus observed DGI  $AUC_{last}$  (a) and  $C_{max}$  (b) ratios of (*E*)-Clom (circles), (*E*)-4-OH-Clom (tri-angles), (*E*)-DE-Clom (squares) and (*E*)-4-OH-DE-Clom (diamonds) in PM, IM and UM. The straight black lines mark the lines of identity, the curved solid black lines show the limits of the predictive measure proposed by Guest et al. with 1.25-fold variability [46]. Black dotted lines indicate 1.25-fold, black dashed lines indicate 2-fold deviation. AS, CYP2D6 activity score; (*E*)-4-OH-Clom, (*E*)-4-hydroxyclophene; (*E*)-4-OH-DE-Clom, (*E*)-4-hydroxy-N-desethylclomiphene; (*E*)-Clom, (*E*)-clomiphene; (*E*)-DE-Clom, (*E*)-N-desethylclomiphene; IM, intermediate metabolizers; PM, poor metabolizers; UM, ultrarapid metabolizers.

## S4.1.4. Renal Excretion Profiles (Linear Scale)





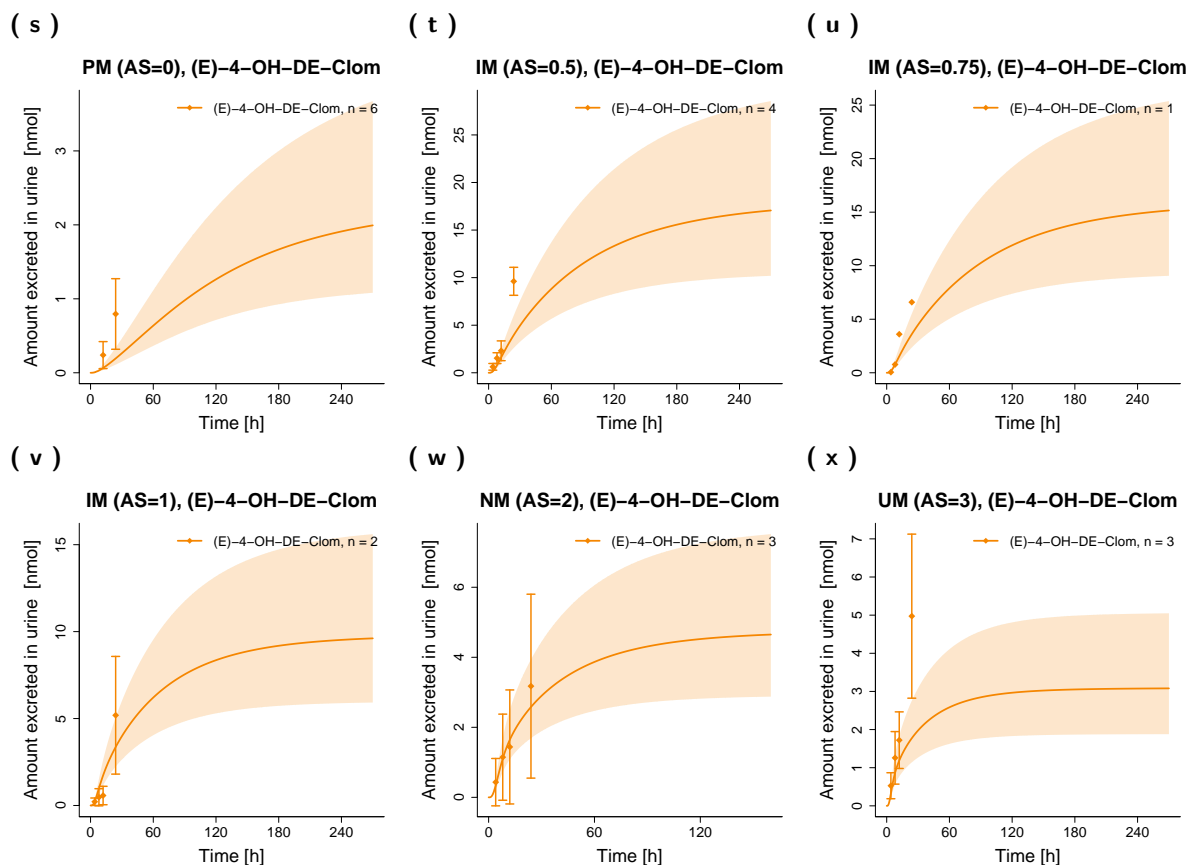
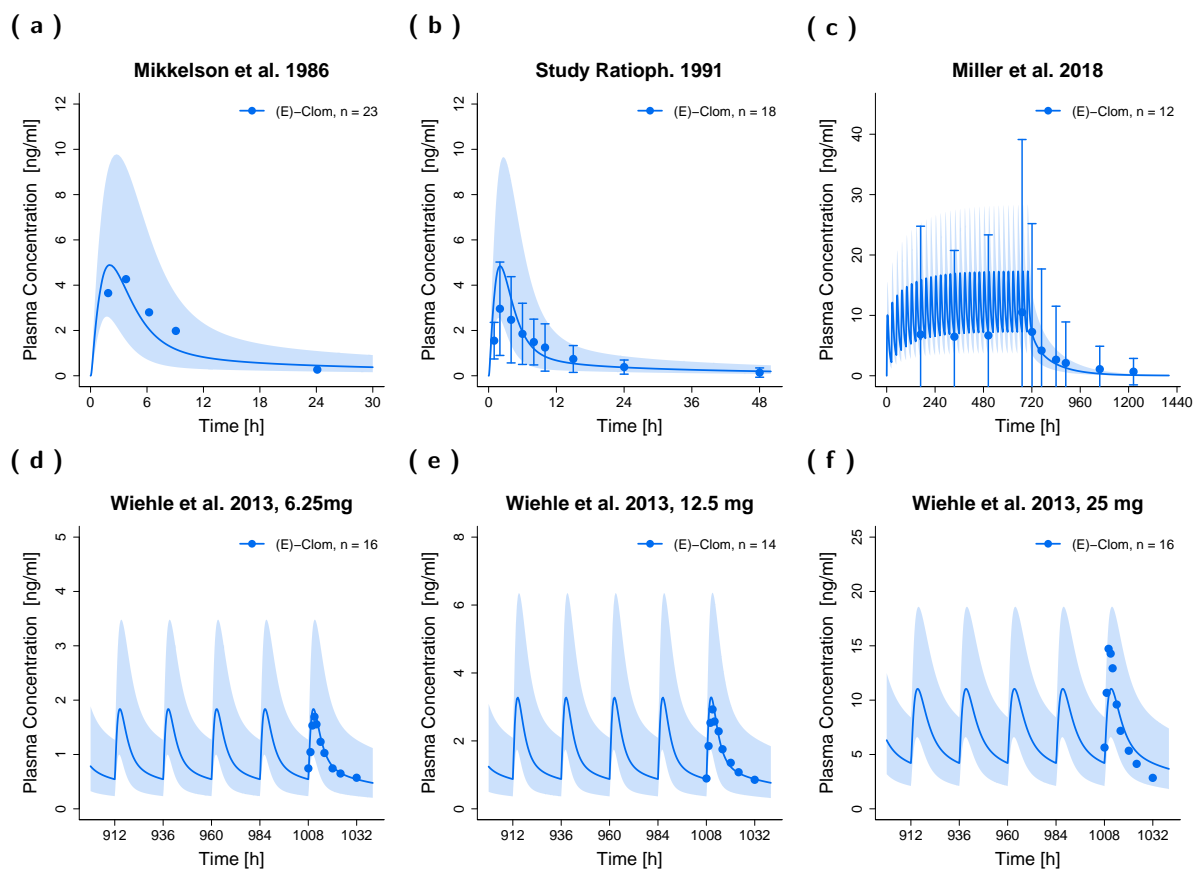
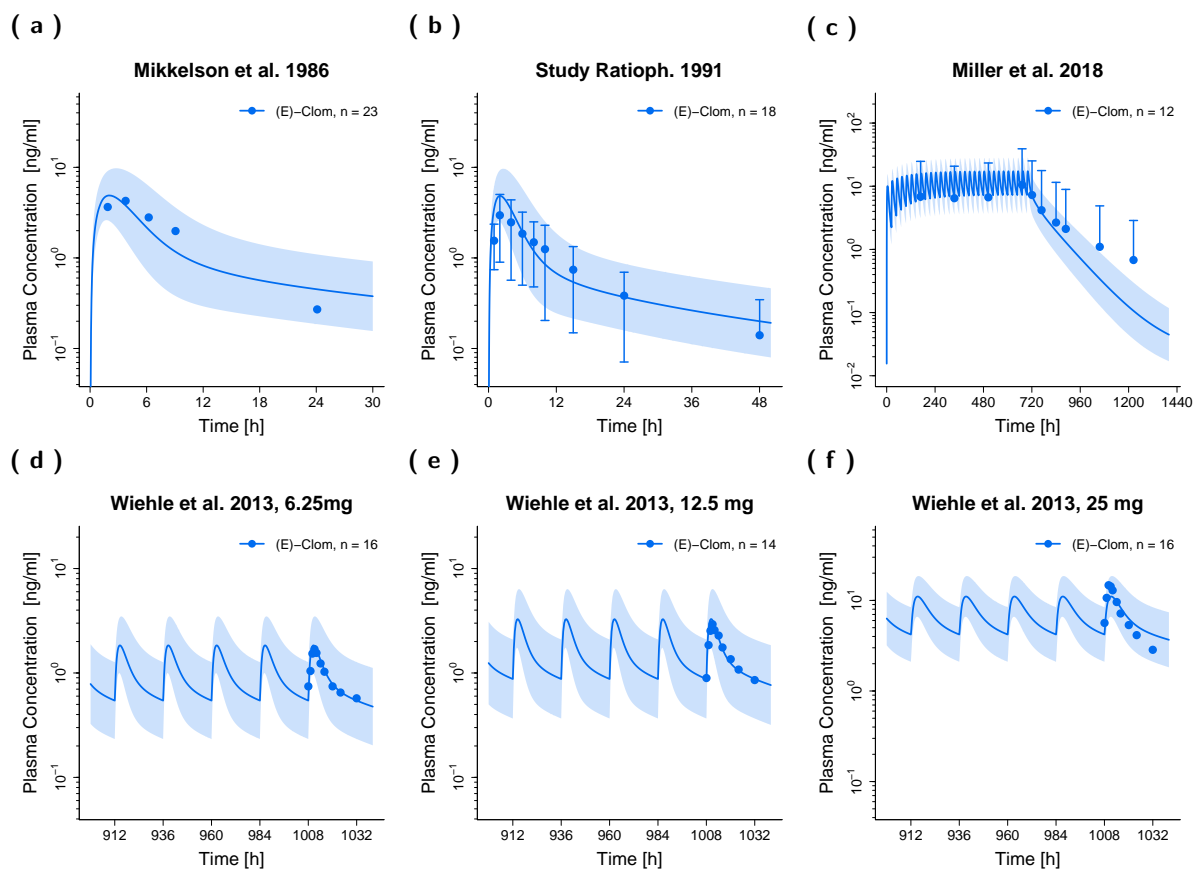


**Figure S5.** Predicted and observed renal excretion profiles (linear scale) of (E)-Clom (a–f), (E)-4-OH-Clom (g–i), (E)-DE-Clom (m–r) and (E)-4-OH-DE-Clom (s–x) for DGI scenarios. Solid lines depict predicted geometric mean profiles in PM, IM, NM and UM. The respective semitransparent areas show the geometric standard deviation of the population simulations ( $n=1000$ ). Mean observed data are shown as symbols with the corresponding standard deviation. **AS**, CYP2D6 activity score; **DGI**, drug-gene interaction; **(E)-4-OH-Clom**, (E)-4-hydroxyclophene; **(E)-4-OH-DE-Clom**, (E)-4-hydroxy-N-desethylclomiphene; **(E)-Clom**, (E)-clomiphene; **(E)-DE-Clom**, (E)-N-desethylclomiphene; **IM**, intermediate metabolizers; **n**, number of subjects; **NM**, normal metabolizers; **PM**, poor metabolizers; **UM**, ultrarapid metabolizers.

## S4.1.5. Plasma Profiles from Literature (Linear Scale)

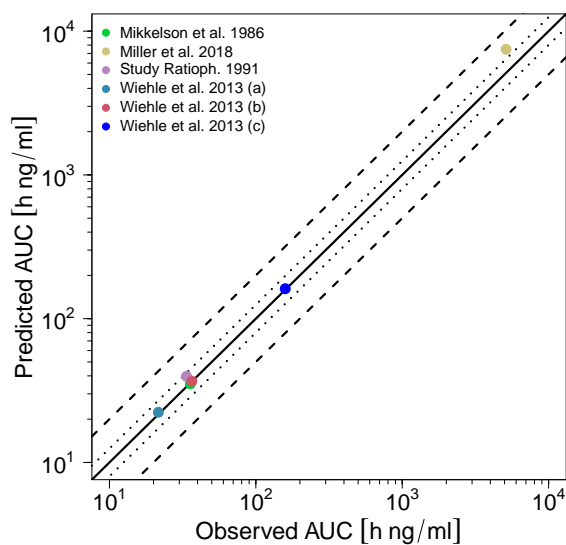
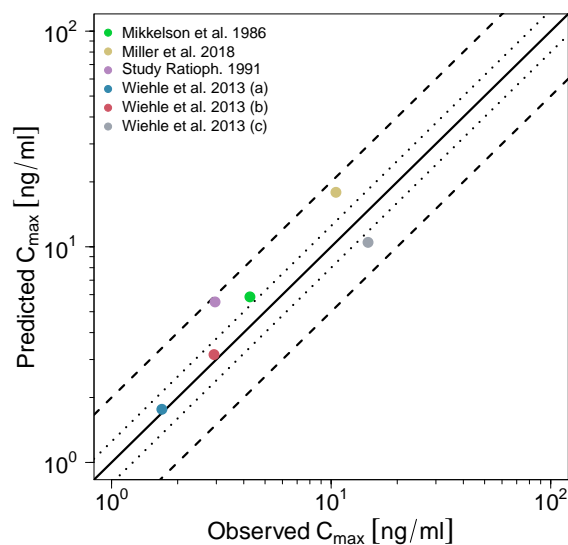


## S4.1.6. Plasma Profiles from Literature (Semilogarithmic Scale)



**Figure S7. Predicted and observed plasma concentration-time profiles (semilogarithmic scale) of digitized studies from literature after single (a,b) and multiple (c-f) dosing.** Solid lines depict predicted geometric mean concentration-time profiles of (E)-Clom. The respective semitransparent areas show the geometric standard deviation of the population simulations (n=1000). Mean observed data are shown as symbols with the corresponding standard deviation. (E)-Clom, (E)-clomiphene; n, number of subjects; Ratioph., Ratiopharm® GmbH.

## S4.1.7. Goodness-of-Fit Plots (from Literature)

(a)  $AUC_{last}$ (b)  $C_{max}$ 

(c) Plasma concentrations

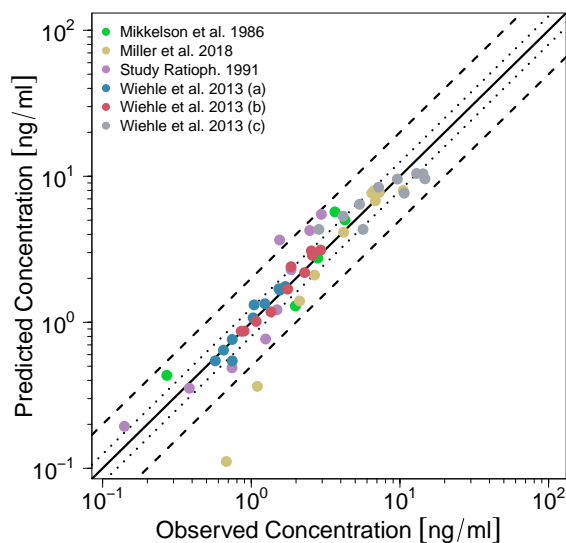
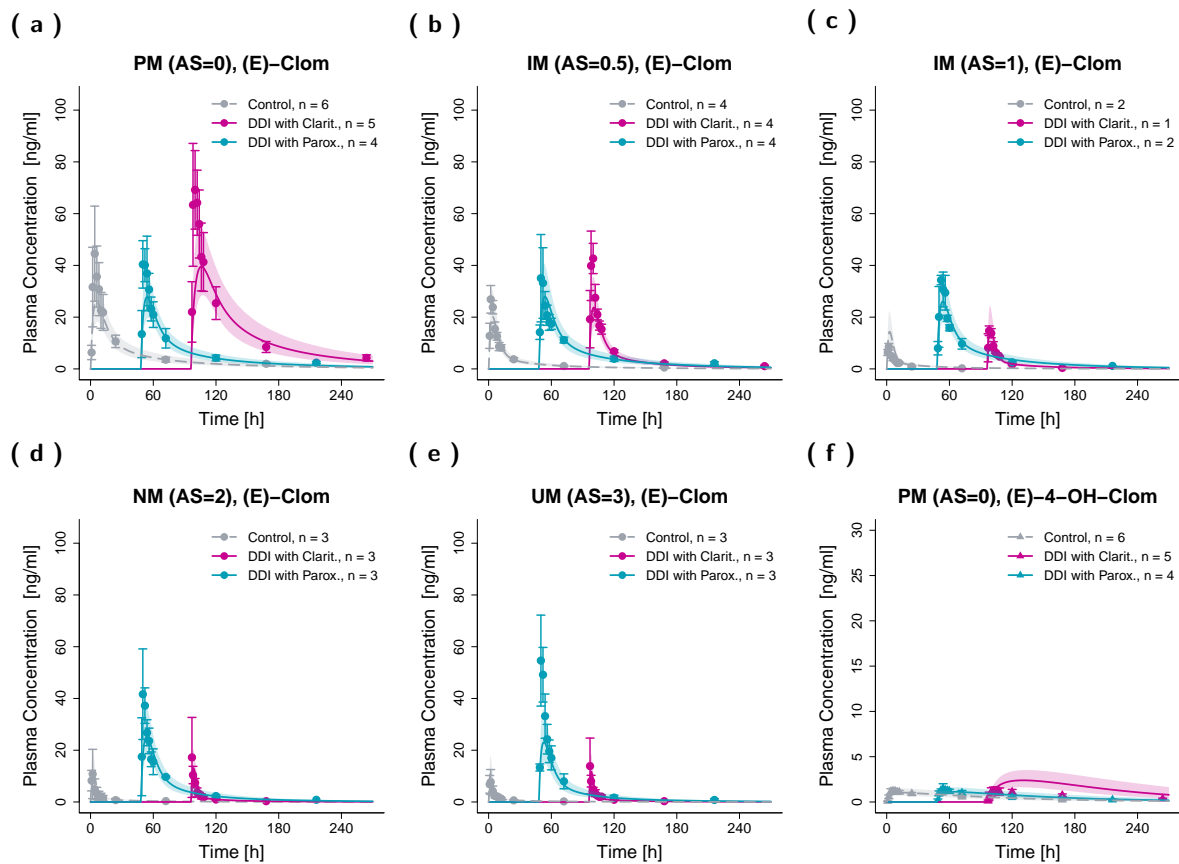


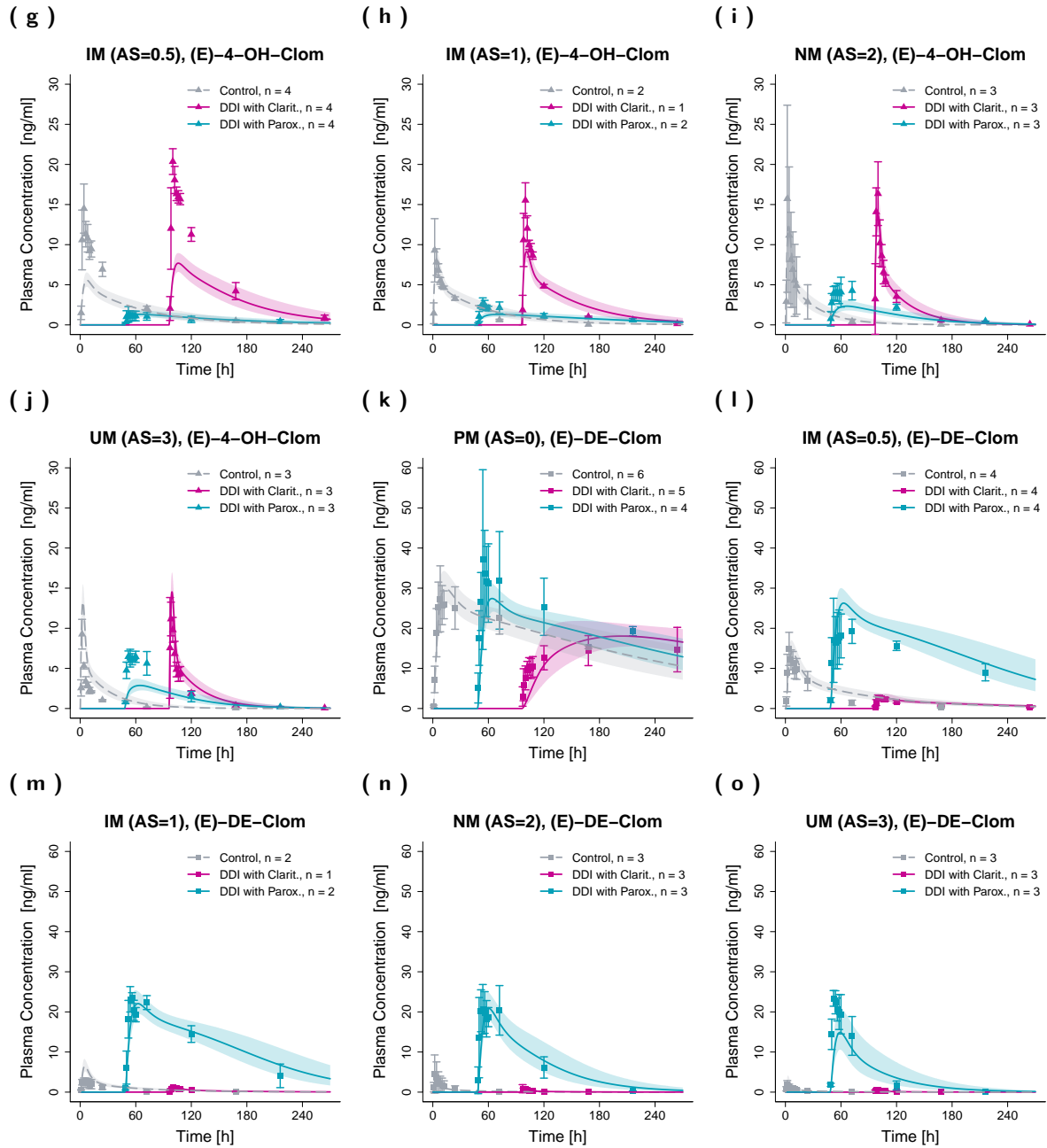
Figure S8. Predicted versus observed (a)  $AUC_{last}$ , (b)  $C_{max}$  and (c) plasma concentrations of (*E*)-Clom. The black solid lines mark the lines of identity. Black dotted lines indicate 1.25-fold, black dashed lines indicate 2-fold deviation. **Ratioph.**, Ratiopharm® GmbH.



## S4.2. Evaluation of the DD(G)I Model

## S4.2.1. Plasma Profiles (Linear Scale)





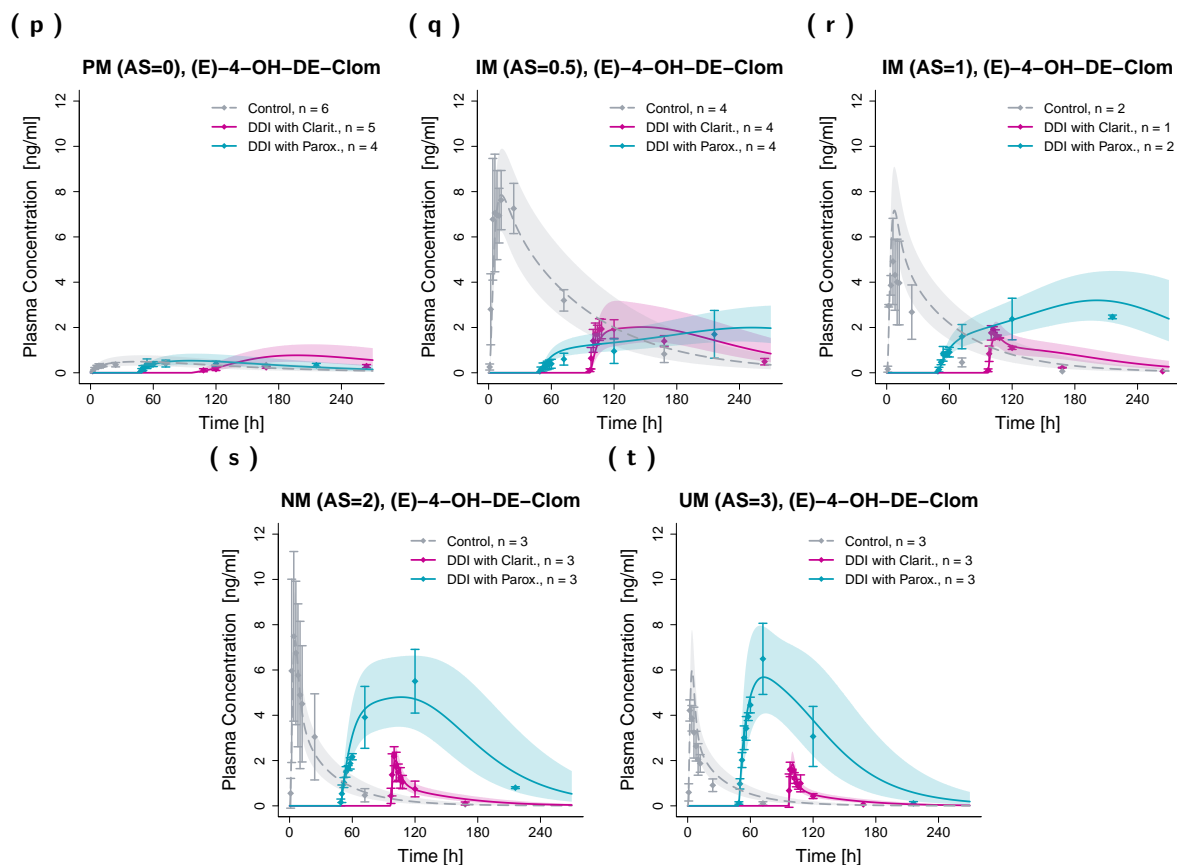
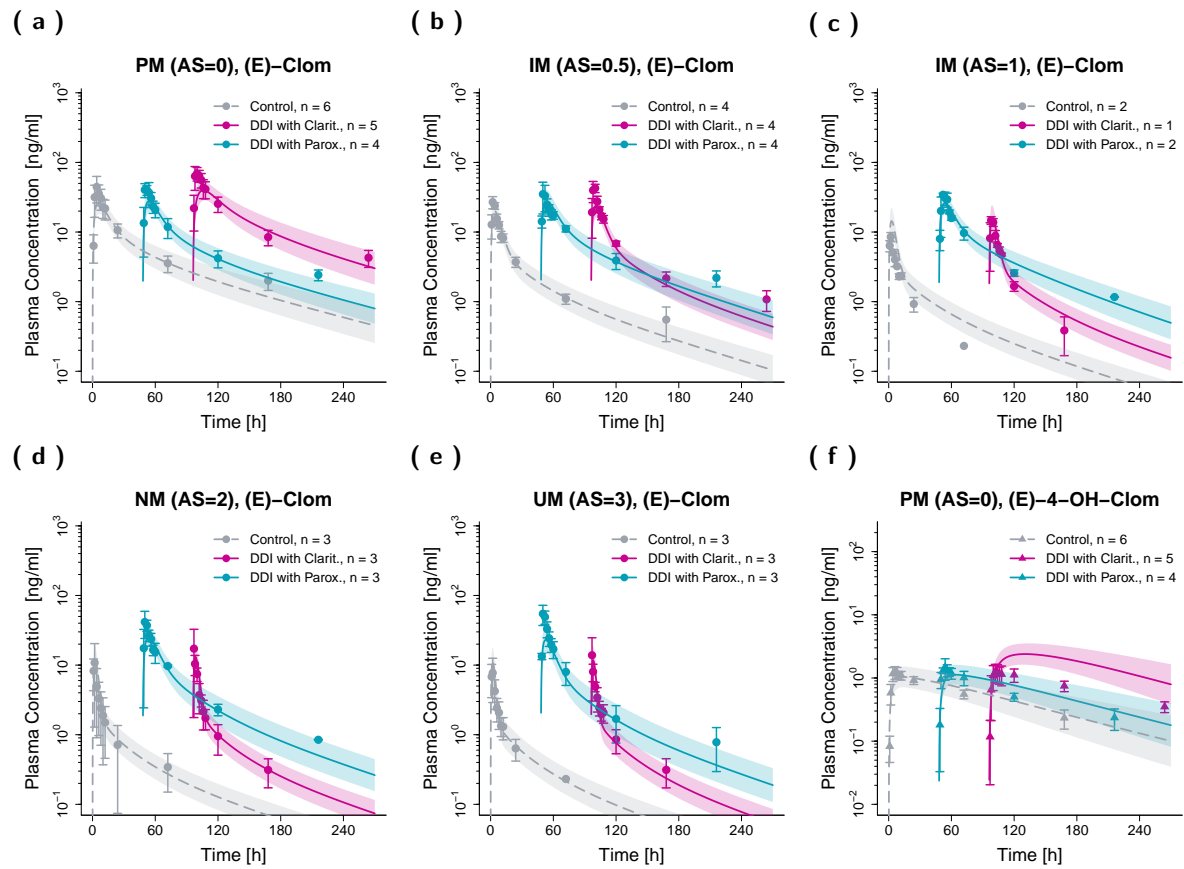
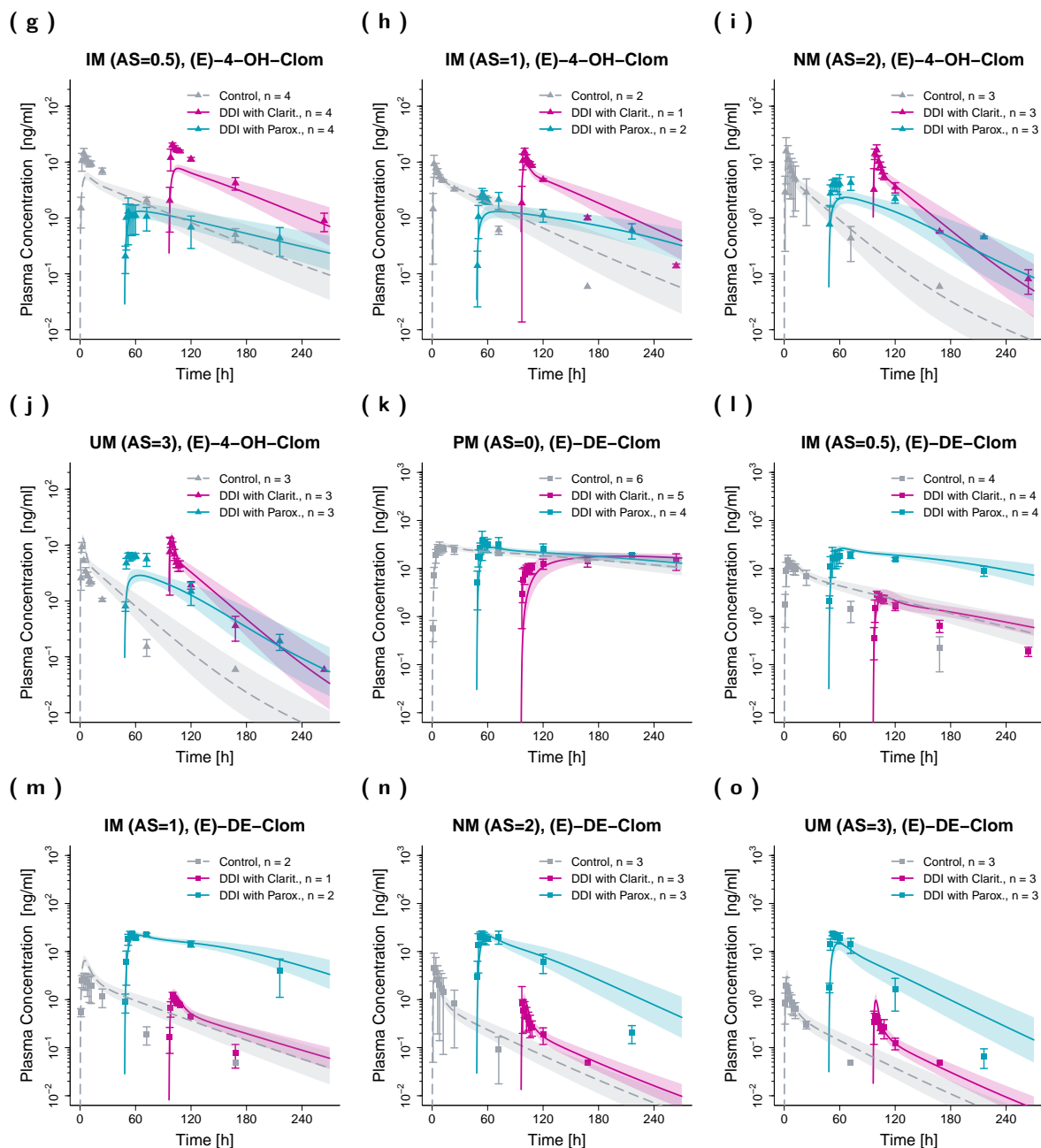


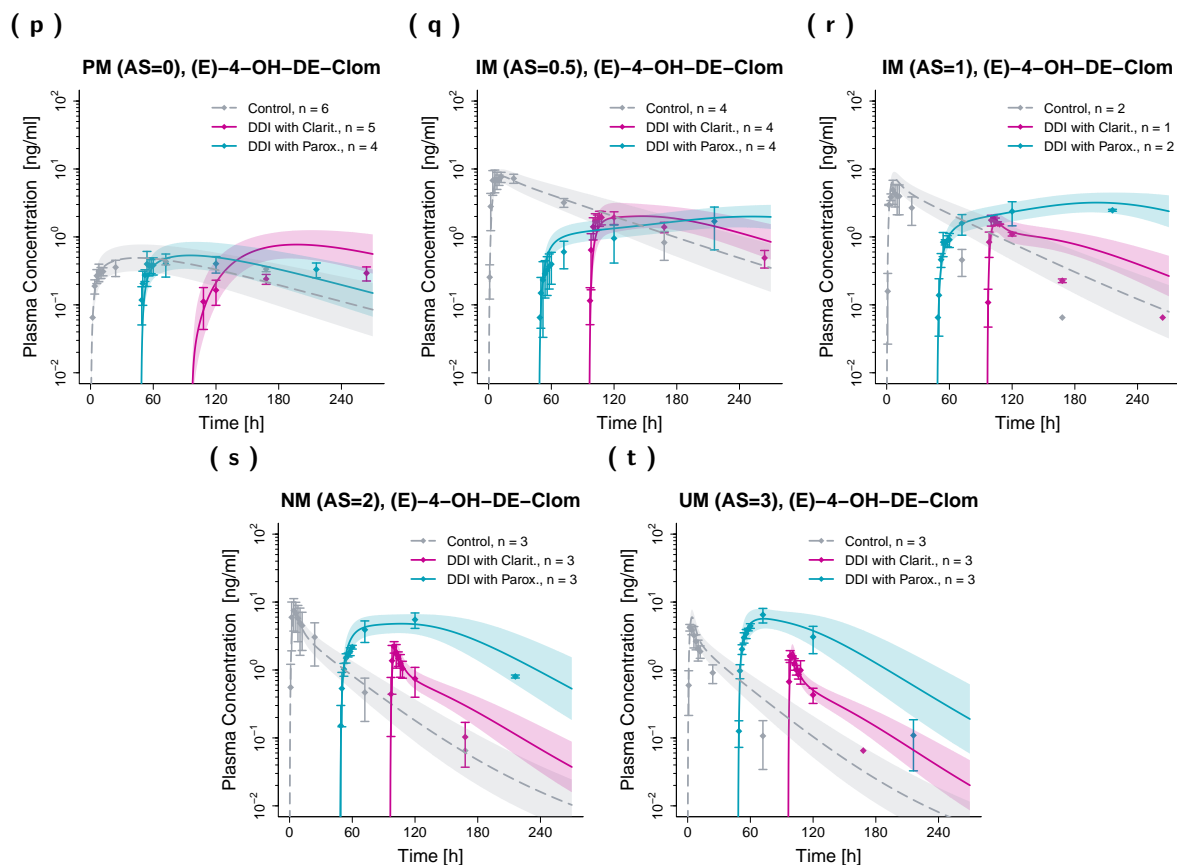
Figure S9. Predicted and observed plasma concentration-time profiles (linear scale) of (E)-Clom (a-e),

(E)-4-OH-Clom (f-j), (E)-DE-Clom (k-o) and (E)-4-OH-DE-Clom (p-t) for DD(G)I scenarios in PM, IM, NM and UM. Grey dashed lines depict the predicted geometric mean concentration-time profiles without clarithromycin and paroxetine (control), turquoise lines represent the predicted geometric mean profiles in presence of paroxetine and pink lines the predicted geometric mean profiles in presence of clarithromycin (DD(G)I). The respective semitransparent areas show the geometric standard deviation of the population simulations (n=1000). Mean observed data are shown as symbols with the corresponding standard deviation. For a better visibility, DD(G)I scenarios were plotted with a time offset with  $t=0$  at the first dose of the perpetrator drug. **AS**, CYP2D6 activity score; **Clarit.**, clarithromycin; **DD(G)I**, drug-drug and drug-drug-gene interactions; **(E)-4-OH-Clom**, (E)-4-hydroxyclophene; **(E)-4-OH-DE-Clom**, (E)-4-hydroxy-N-desethylclomiphene; **(E)-Clom**, (E)-clomiphene; **(E)-DE-Clom**, (E)-N-desethylclomiphene; **IM**, intermediate metabolizers; **n**, number of subjects; **NM**, normal metabolizers; **Parox.**, paroxetine; **PM**, poor metabolizers; **UM**, ultrarapid metabolizers.

## S4.2.2. Plasma Profiles (Semilogarithmic Scale)

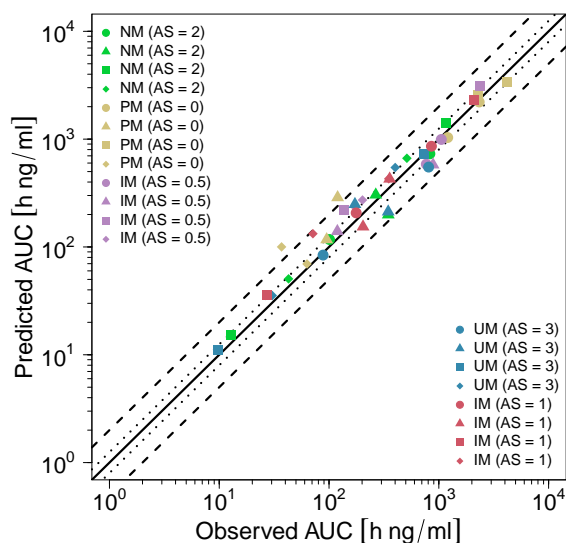
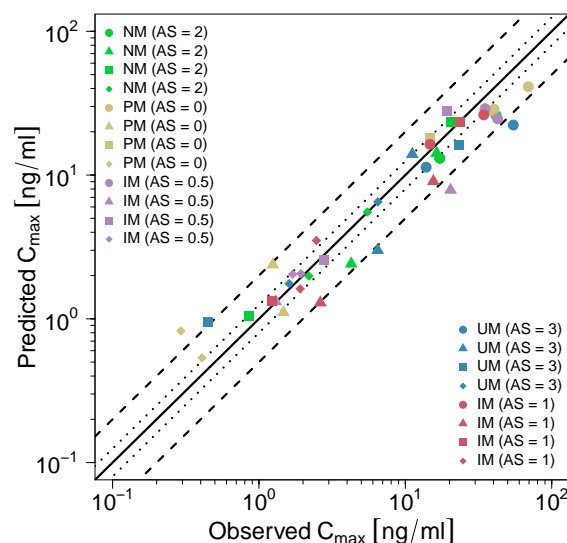




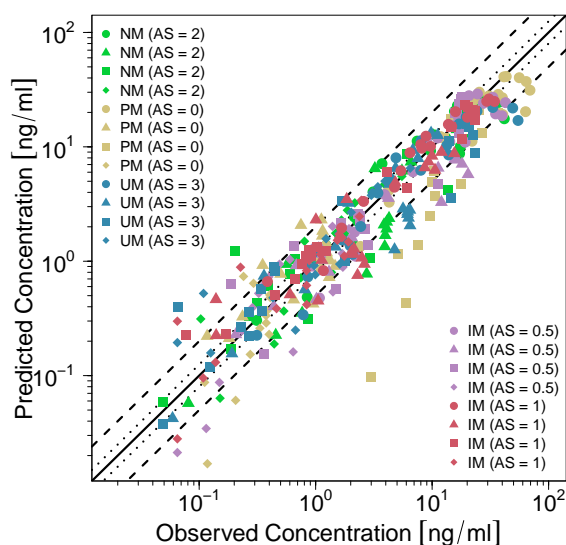


**Figure S10. Predicted and observed plasma concentration-time profiles (semilogarithmic scale) of (E)-Clom (a-e), (E)-4-OH-Clom (f-j), (E)-DE-Clom (k-o) and (E)-4-OH-DE-Clom (p-t) for DD(G)I scenarios in PM, IM, NM and UM.** Grey dashed lines depict the predicted geometric mean concentration-time profiles without clarithromycin and paroxetine (control), turquoise lines represent the predicted geometric mean profiles in presence of paroxetine and pink lines the predicted geometric mean profiles in presence of clarithromycin. The respective semitransparent areas show the geometric standard deviation of the population simulations ( $n=1000$ ). Mean observed data are shown as symbols with the corresponding standard deviation. For a better visibility, DD(G)I scenarios were plotted with a time offset with  $t=0$  at the first dose of the perpetrator drug. **AS**, CYP2D6 activity score; **Clarit.**, clarithromycin; **DD(G)I**, drug-drug and drug-drug-gene interactions; **(E)-4-OH-Clom**, (E)-4-hydroxyclophene; **(E)-4-OH-DE-Clom**, (E)-4-hydroxy-N-desethylclomiphene; **(E)-Clom**, (E)-clomiphene; **(E)-DE-Clom**, (E)-N-desethylclomiphene; **IM**, intermediate metabolizers; **n**, number of subjects; **NM**, normal metabolizers; **Parox.**, paroxetine; **PM**, poor metabolizers; **UM**, ultrarapid metabolizers.

## S4.2.3. Goodness-of-Fit Plots

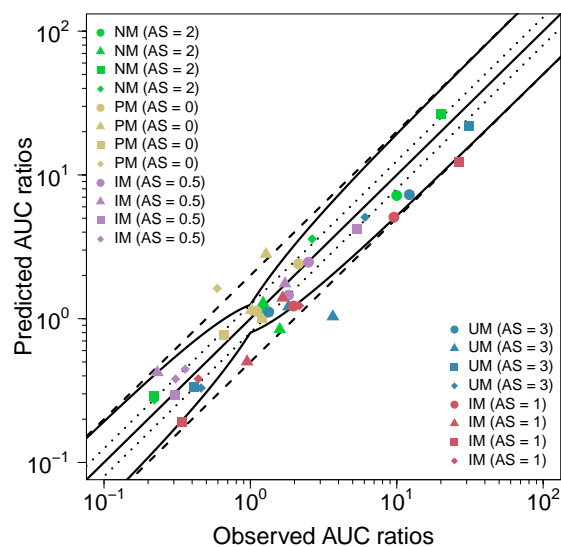
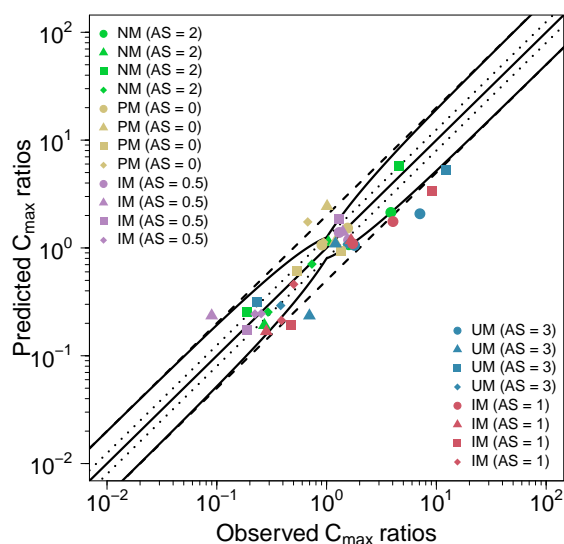
(a)  $AUC_{last}$ (b)  $C_{max}$ 

(c) Plasma concentrations



**Figure S11.** Predicted versus observed  $AUC_{last}$  (a),  $C_{max}$  (b) and plasma concentrations (c) of (*E*)-Clom (circles), (*E*)-4-OH-Clom (triangles), (*E*)-DE-Clom (squares) and (*E*)-4-OH-DE-Clom (diamonds) for DD(G)I scenarios with clarithromycin and paroxetine, respectively in PM, IM, NM and UM. The black solid lines mark the lines of identity. Black dotted lines indicate 1.25-fold, black dashed lines indicate 2-fold deviation. AS, CYP2D6 activity score; DD(G)I, drug-drug and drug-drug-gene interactions; (*E*)-4-OH-Clom, (*E*)-4-hydroxyclophene; (*E*)-4-OH-DE-Clom, (*E*)-4-hydroxy-N-desethylclomiphene; (*E*)-Clom, (*E*)-clomiphene; (*E*)-DE-Clom, (*E*)-N-desethylclomiphene; IM, intermediate metabolizers; NM, normal metabolizers; PM, poor metabolizers; UM, ultrarapid metabolizers.

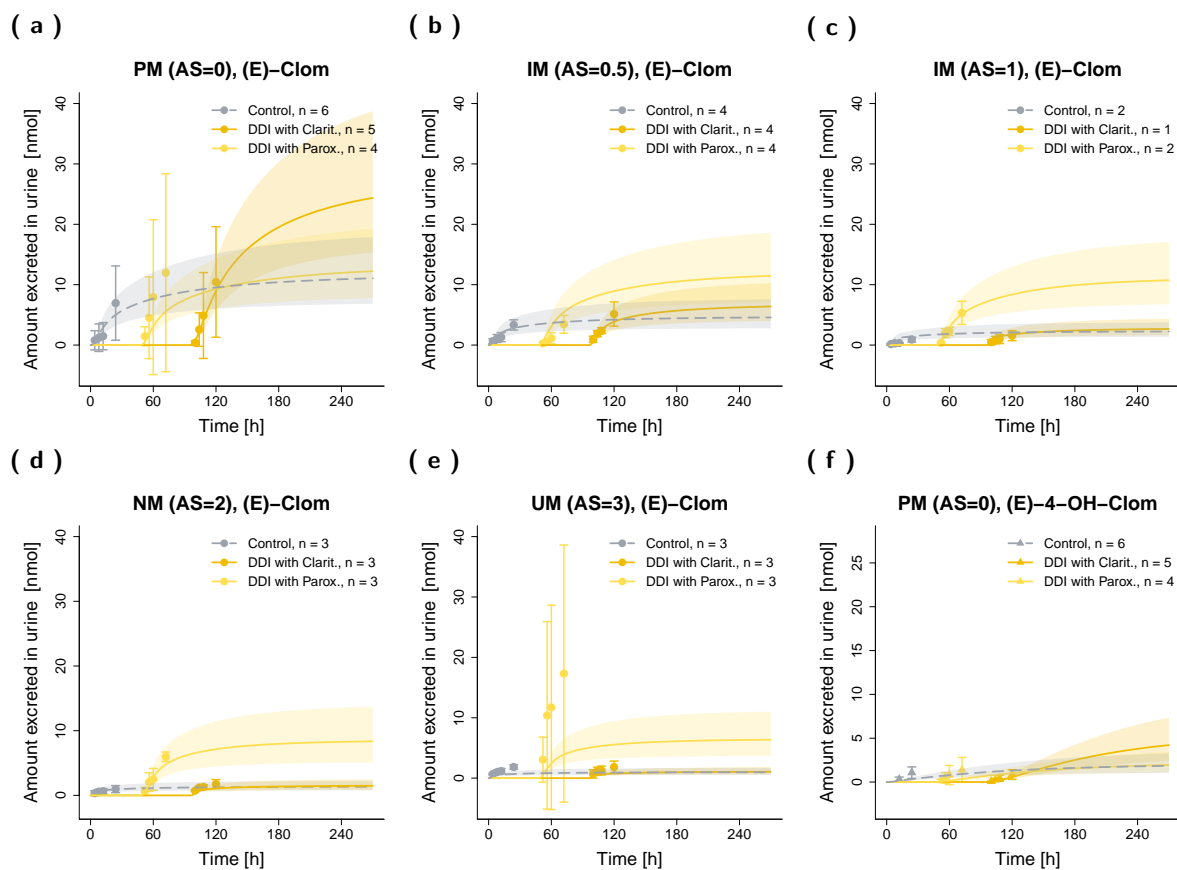
## (a) AUC

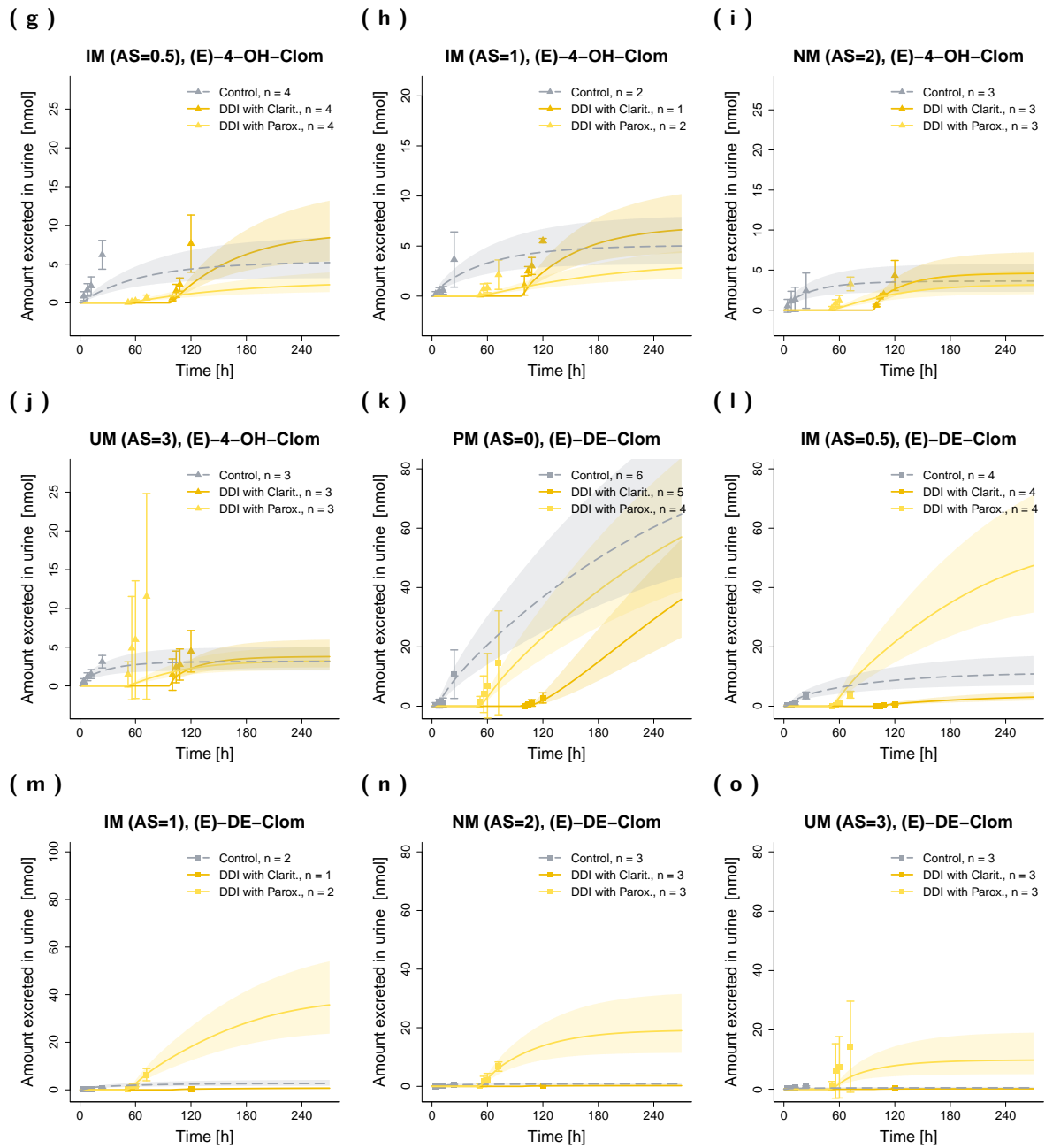
(b)  $C_{\max}$ 

**Figure S12.** Predicted versus observed DD(G)I AUC<sub>last</sub> (a) and  $C_{\max}$  (b) ratios of (*E*)-Clom (circles), (*E*)-4-OH-Clom (triangles), (*E*)-DE-Clom (squares) and (*E*)-4-OH-DE-Clom (diamonds) in PM, IM, NM and UM. The straight black lines mark the lines of identity, the curved black lines show the limits of the predictive measure proposed by Guest et al. with 1.25-fold variability [46]. Black dotted lines indicate 1.25-fold, black dashed lines indicate 2-fold deviation. AS, CYP2D6 activity score; DD(G)I, drug-drug and drug-drug-gene interactions; (*E*)-4-OH-Clom, (*E*)-4-hydroxyclophiphen; (*E*)-4-OH-DE-Clom, (*E*)-4-hydroxy-N-desethylclomiphene; (*E*)-Clom, (*E*)-clomiphene; (*E*)-DE-Clom, (*E*)-N-desethylclomiphene; IM, intermediate metabolizers; NM, normal metabolizers, PM, poor metabolizers; UM, ultrarapid metabolizers.



## S4.2.4. Renal Excretion Profiles (Linear Scale)





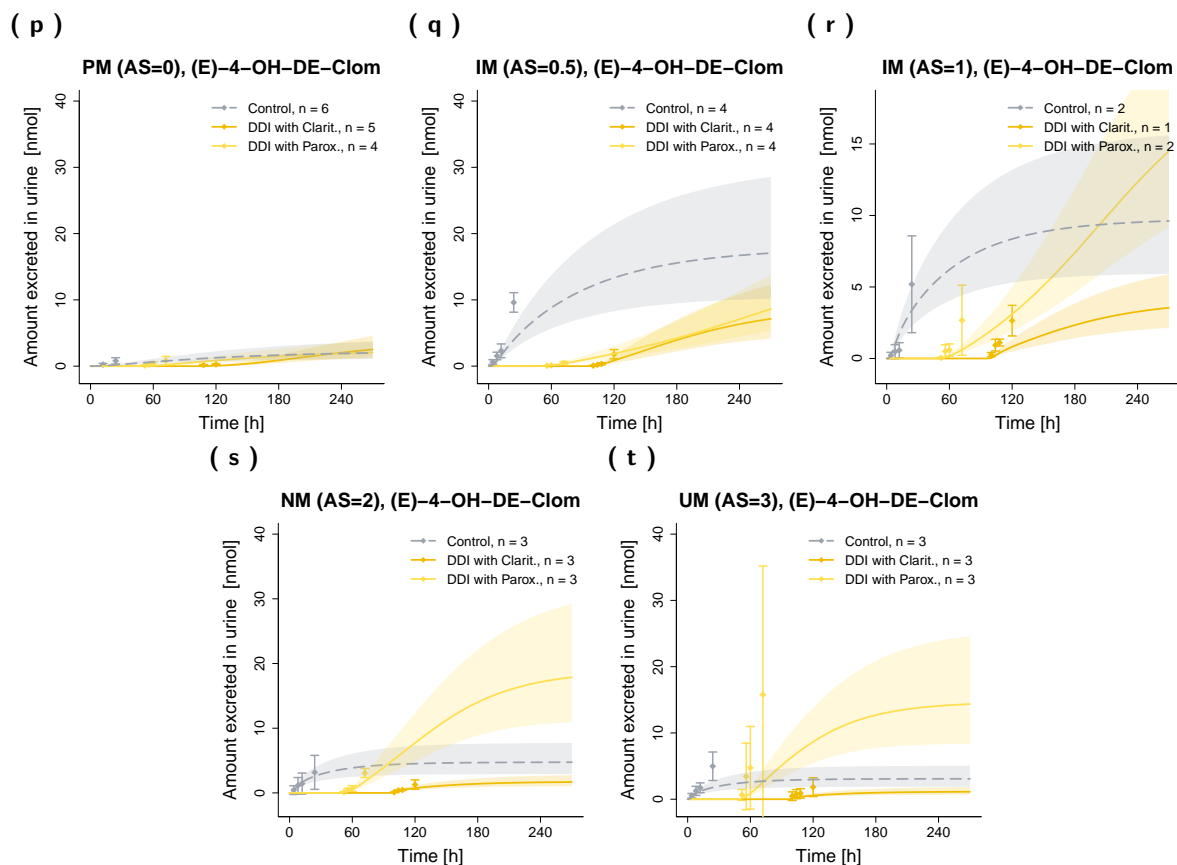


**Figure S13.** Predicted and observed renal excretion profiles (linear scale) of (E)-Clom (a–e), (E)-4-OH-Clom (f–j), (E)-DE-Clom (k–o) and (E)-4-OH-DE-Clom (p–t) for DD(G)I scenarios in PM, IM, NM and UM. Grey dashed lines depict the predicted geometric mean profiles in a absence of clarithromycin and paroxetine (control), yellow solid lines represent the predicted geometric mean profiles in presence of paroxetine and orange solid lines represent the predicted geometric mean profiles in presence of clarithromycin (DD(G)I). The respective semitransparent areas show the geometric standard deviation of the population simulations (n=1000). Mean observed data are shown as symbols with the corresponding standard deviation. For a better visibility, DD(G)I scenarios were plotted with a time offset with t=0 at the first dose of the perpetrator drug. AS, CYP2D6 activity score; Clarit., clarithromycin; DD(G)I, drug-drug and drug-drug-gene interactions; (E)-4-OH-Clom, (E)-4-hydroxyclophene; (E)-4-OH-DE-Clom, (E)-4-hydroxy-N-desethylclomiphene; (E)-Clom, (E)-clomiphene; (E)-DE-Clom, (E)-N-desethylclomiphene; IM, intermediate metabolizers; n, number of subjects; NM, normal metabolizers; Parox., paroxetine; PM, poor metabolizers; UM, ultrarapid metabolizers.

### S4.3. Quantitative PBPK Model Evaluation

#### S4.3.1. Mean Relative Deviation (MRD)

**Table S9.** Mean relative deviation (MRD) values of DGI plasma concentration predictions.

Study	Compound	MRD	Reference
PK Panel Study, PM (AS = 0)	( <i>E</i> )-4-OH-Clom	1.49	[19]
PK Panel Study, PM (AS = 0)	( <i>E</i> )-4-OH-DE-Clom	1.20	[19]
PK Panel Study, PM (AS = 0)	( <i>E</i> )-Clom	1.42	[19]
PK Panel Study, PM (AS = 0)	( <i>E</i> )-DE-Clom	1.38	[19]
PK Panel Study, IM (AS = 0.5)	( <i>E</i> )-4-OH-Clom	2.00	[19]
PK Panel Study, IM (AS = 0.5)	( <i>E</i> )-4-OH-DE-Clom	1.44	[19]
PK Panel Study, IM (AS = 0.5)	( <i>E</i> )-Clom	1.31	[19]
PK Panel Study, IM (AS = 0.5)	( <i>E</i> )-DE-Clom	2.04	[19]
PK Panel Study, IM (AS = 0.75)	( <i>E</i> )-4-OH-Clom	2.45	[19]
PK Panel Study, IM (AS = 0.75)	( <i>E</i> )-4-OH-DE-Clom	3.04	[19]
PK Panel Study, IM (AS = 0.75)	( <i>E</i> )-Clom	3.24	[19]
PK Panel Study, IM (AS = 0.75)	( <i>E</i> )-DE-Clom	5.42	[19]
PK Panel Study, IM (AS = 1)	( <i>E</i> )-4-OH-Clom	1.96	[19]
PK Panel Study, IM (AS = 1)	( <i>E</i> )-4-OH-DE-Clom	2.38	[19]
PK Panel Study, IM (AS = 1)	( <i>E</i> )-Clom	1.99	[19]
PK Panel Study, IM (AS = 1)	( <i>E</i> )-DE-Clom	2.52	[19]
PK Panel Study, NM (AS = 2)	( <i>E</i> )-4-OH-Clom	1.40	[19]
PK Panel Study, NM (AS = 2)	( <i>E</i> )-4-OH-DE-Clom	1.30	[19]
PK Panel Study, NM (AS = 2)	( <i>E</i> )-Clom	1.39	[19]
PK Panel Study, NM (AS = 2)	( <i>E</i> )-DE-Clom	1.38	[19]
PK Panel Study, UM (AS = 3)	( <i>E</i> )-4-OH-Clom	2.26	[19]
PK Panel Study, UM (AS = 3)	( <i>E</i> )-4-OH-DE-Clom	1.81	[19]
PK Panel Study, UM (AS = 3)	( <i>E</i> )-Clom	1.30	[19]
PK Panel Study, UM (AS = 3)	( <i>E</i> )-DE-Clom	1.50	[19]
Mikkelsen et al. 1986	( <i>E</i> )-Clom	1.43	[1]
Miller et al. 2018	( <i>E</i> )-Clom	2.01	[4]
Study Ratioph. 1991	( <i>E</i> )-Clom	1.61	[2]
Wiehle et al. 2013 (a)	( <i>E</i> )-Clom	1.14	[3]
Wiehle et al. 2013 (b)	( <i>E</i> )-Clom	1.13	[3]
Wiehle et al. 2013 (c)	( <i>E</i> )-Clom	1.33	[3]

**Overall MRD: 1.95 (1.13–5.42)**

**21/30 MRD  $\leq 2$**

**AS:** CYP2D6 activity score, **DGI:** drug-gene interaction, **(*E*)-4-OH-Clom:** (*E*)-4-hydroxyclophene, **(*E*)-4-OH-DE-Clom:** (*E*)-4-hydroxy-N-desethylclomiphene, **(*E*)-Clom:** (*E*)-clomiphene, **(*E*)-DE-Clom:** (*E*)-N-desethylclomiphene, **IM:** intermediate metabolizers, **NM:** normal metabolizers, **PK:** pharmacokinetic, **PM:** poor metabolizers, **UM:** ultrarapid metabolizers, **Ratioph.:** Ratiopharm® GmbH

**Table S10.** Mean relative deviation (MRD) values of DD(G)I plasma concentration predictions.

Study	Compound	Perpetrator	MRD	Reference
PK Panel Study, PM (AS = 0)	( <i>E</i> )-4-OH-Clom	Clarithromycin	1.80	[19]
PK Panel Study, PM (AS = 0)	( <i>E</i> )-4-OH-Clom	Paroxetine	1.50	[19]
PK Panel Study, PM (AS = 0)	( <i>E</i> )-4-OH-DE-Clom	Clarithromycin	2.04	[19]
PK Panel Study, PM (AS = 0)	( <i>E</i> )-4-OH-DE-Clom	Paroxetine	2.18	[19]
PK Panel Study, PM (AS = 0)	( <i>E</i> )-Clom	Clarithromycin	1.72	[19]
PK Panel Study, PM (AS = 0)	( <i>E</i> )-Clom	Paroxetine	1.41	[19]
PK Panel Study, PM (AS = 0)	( <i>E</i> )-DE-Clom	Clarithromycin	4.87	[19]
PK Panel Study, PM (AS = 0)	( <i>E</i> )-DE-Clom	Paroxetine	2.04	[19]
PK Panel Study, IM (AS = 0.5)	( <i>E</i> )-4-OH-Clom	Clarithromycin	2.18	[19]
PK Panel Study, IM (AS = 0.5)	( <i>E</i> )-4-OH-Clom	Paroxetine	1.38	[19]
PK Panel Study, IM (AS = 0.5)	( <i>E</i> )-4-OH-DE-Clom	Clarithromycin	2.11	[19]
PK Panel Study, IM (AS = 0.5)	( <i>E</i> )-4-OH-DE-Clom	Paroxetine	1.73	[19]
PK Panel Study, IM (AS = 0.5)	( <i>E</i> )-Clom	Clarithromycin	1.55	[19]
PK Panel Study, IM (AS = 0.5)	( <i>E</i> )-Clom	Paroxetine	1.43	[19]
PK Panel Study, IM (AS = 0.5)	( <i>E</i> )-DE-Clom	Clarithromycin	1.92	[19]
PK Panel Study, IM (AS = 0.5)	( <i>E</i> )-DE-Clom	Paroxetine	1.53	[19]
PK Panel Study, IM (AS = 1)	( <i>E</i> )-4-OH-Clom	Clarithromycin	1.79	[19]
PK Panel Study, IM (AS = 1)	( <i>E</i> )-4-OH-Clom	Paroxetine	2.01	[19]
PK Panel Study, IM (AS = 1)	( <i>E</i> )-4-OH-DE-Clom	Clarithromycin	2.03	[19]
PK Panel Study, IM (AS = 1)	( <i>E</i> )-4-OH-DE-Clom	Paroxetine	1.38	[19]
PK Panel Study, IM (AS = 1)	( <i>E</i> )-Clom	Clarithromycin	1.30	[19]
PK Panel Study, IM (AS = 1)	( <i>E</i> )-Clom	Paroxetine	1.25	[19]
PK Panel Study, IM (AS = 1)	( <i>E</i> )-DE-Clom	Clarithromycin	1.53	[19]
PK Panel Study, IM (AS = 1)	( <i>E</i> )-DE-Clom	Paroxetine	1.29	[19]
PK Panel Study, NM (AS = 2)	( <i>E</i> )-4-OH-Clom	Clarithromycin	1.38	[19]
PK Panel Study, NM (AS = 2)	( <i>E</i> )-4-OH-Clom	Paroxetine	2.23	[19]
PK Panel Study, NM (AS = 2)	( <i>E</i> )-4-OH-DE-Clom	Clarithromycin	1.67	[19]
PK Panel Study, NM (AS = 2)	( <i>E</i> )-4-OH-DE-Clom	Paroxetine	1.52	[19]
PK Panel Study, NM (AS = 2)	( <i>E</i> )-Clom	Clarithromycin	1.44	[19]
PK Panel Study, NM (AS = 2)	( <i>E</i> )-Clom	Paroxetine	1.51	[19]
PK Panel Study, NM (AS = 2)	( <i>E</i> )-DE-Clom	Clarithromycin	1.62	[19]
PK Panel Study, NM (AS = 2)	( <i>E</i> )-DE-Clom	Paroxetine	2.19	[19]
PK Panel Study, UM (AS = 3)	( <i>E</i> )-4-OH-Clom	Clarithromycin	1.42	[19]
PK Panel Study, UM (AS = 3)	( <i>E</i> )-4-OH-Clom	Paroxetine	2.28	[19]
PK Panel Study, UM (AS = 3)	( <i>E</i> )-4-OH-DE-Clom	Clarithromycin	1.72	[19]
PK Panel Study, UM (AS = 3)	( <i>E</i> )-4-OH-DE-Clom	Paroxetine	1.71	[19]
PK Panel Study, UM (AS = 3)	( <i>E</i> )-Clom	Clarithromycin	1.46	[19]
PK Panel Study, UM (AS = 3)	( <i>E</i> )-Clom	Paroxetine	1.74	[19]
PK Panel Study, UM (AS = 3)	( <i>E</i> )-DE-Clom	Clarithromycin	1.47	[19]
PK Panel Study, UM (AS = 3)	( <i>E</i> )-DE-Clom	Paroxetine	2.38	[19]

**Overall MRD: 1.83 (1.25–4.87)****28/40 MRD ≤ 2****AS:** CYP2D6 activity score, **DD(G)I:** drug-drug and drug-drug-gene interactions, **(*E*)-4-OH-Clom:****(*E*)-4-hydroxyclophene, (*E*)-4-OH-DE-Clom:** (*E*)-4-hydroxy-N-desethylclomiphene, **(*E*)-Clom:** (*E*)-clomiphene,**(*E*)-DE-Clom:** (*E*)-N-desethylclomiphene, **IM:** intermediate metabolizers, **NM:** normal metabolizers,**PK:** pharmacokinetic, **PM:** poor metabolizers, **UM:** ultrarapid metabolizers

## S4.3.2. Geometric Mean Fold Error (GMFE)

Table S11. Geometric Mean Fold Error (GMFE) of  $AUC_{last}$  and  $C_{max}$  DGI Predictions.

Study	Compound	$AUC_{last}$			$C_{max}$			Reference
		Pred $\left[\frac{ng}{ml}\right]$	Obs $\left[\frac{ng}{ml}\right]$	Pred/Obs	Pred $\left[\frac{ng}{ml}\right]$	Obs $\left[\frac{ng}{ml}\right]$	Pred/Obs	
PK Panel Study, PM (AS = 0)	(E)-Clom	919.01	1095.56	0.84	27.00	44.53	0.61	[19]
PK Panel Study, PM (AS = 0)	(E)-4-OH-Clom	102.28	93.66	1.09	0.98	1.23	0.79	[19]
PK Panel Study, PM (AS = 0)	(E)-DE-Clom	3389.54	3473.88	0.98	29.59	27.34	1.08	[19]
PK Panel Study, PM (AS = 0)	(E)-4-OH-DE-Clom	61.68	62.33	0.99	0.47	0.44	1.09	[19]
PK Panel Study, IM (AS = 0.5)	(E)-Clom	401.77	422.50	0.95	20.81	26.89	0.77	[19]
PK Panel Study, IM (AS = 0.5)	(E)-4-OH-Clom	330.20	513.99	0.64	5.61	14.50	0.39	[19]
PK Panel Study, IM (AS = 0.5)	(E)-DE-Clom	741.34	446.69	1.66	14.89	14.86	1.00	[19]
PK Panel Study, IM (AS = 0.5)	(E)-4-OH-DE-Clom	610.91	562.68	1.09	8.39	7.63	1.10	[19]
PK Panel Study, IM (AS = 0.75)	(E)-Clom	344.04	136.73	2.52	19.30	9.96	1.94	[19]
PK Panel Study, IM (AS = 0.75)	(E)-4-OH-Clom	349.10	246.20	1.42	5.89	13.33	0.44	[19]
PK Panel Study, IM (AS = 0.75)	(E)-DE-Clom	575.65	102.23	5.63	12.62	6.39	1.98	[19]
PK Panel Study, IM (AS = 0.75)	(E)-4-OH-DE-Clom	556.31	226.19	2.46	7.89	8.01	0.98	[19]
PK Panel Study, IM (AS = 1)	(E)-Clom	168.98	89.54	1.89	14.93	8.53	1.75	[19]
PK Panel Study, IM (AS = 1)	(E)-4-OH-Clom	306.54	214.87	1.43	7.69	9.29	0.83	[19]
PK Panel Study, IM (AS = 1)	(E)-DE-Clom	187.42	79.09	2.37	6.88	2.59	2.66	[19]
PK Panel Study, IM (AS = 1)	(E)-4-OH-DE-Clom	348.35	161.70	2.15	7.62	4.92	1.55	[19]
PK Panel Study, NM (AS = 2)	(E)-Clom	101.66	82.93	1.23	12.20	10.82	1.13	[19]
PK Panel Study, NM (AS = 2)	(E)-4-OH-Clom	236.46	218.30	1.08	12.59	15.72	0.80	[19]
PK Panel Study, NM (AS = 2)	(E)-DE-Clom	53.16	58.47	0.91	4.09	4.50	0.91	[19]
PK Panel Study, NM (AS = 2)	(E)-4-OH-DE-Clom	185.45	193.74	0.96	7.81	7.49	1.04	[19]
PK Panel Study, UM (AS = 3)	(E)-Clom	75.53	66.21	1.14	10.74	7.72	1.39	[19]
PK Panel Study, UM (AS = 3)	(E)-4-OH-Clom	205.20	94.52	2.17	12.76	9.26	1.38	[19]
PK Panel Study, UM (AS = 3)	(E)-DE-Clom	32.98	23.91	1.38	3.05	1.93	1.58	[19]
PK Panel Study, UM (AS = 3)	(E)-4-OH-DE-Clom	120.44	74.07	1.63	6.01	4.21	1.43	[19]
Mikkelsen et al. 1986	(E)-Clom	35.20	35.70	0.99	5.86	4.27	1.37	[1]
Miller et al. 2018	(E)-Clom	7484.01	5121.29	1.46	17.89	10.51	1.70	[4]
Study Ratioph. 1991	(E)-Clom	39.73	33.60	1.18	5.55	2.96	1.88	[2]
Wiehle et al. 2013 (a)	(E)-Clom	22.34	21.59	1.03	1.76	1.69	1.04	[3]
Wiehle et al. 2013 (b)	(E)-Clom	36.73	36.53	1.01	3.16	2.93	1.08	[3]
Wiehle et al. 2013 (c)	(E)-Clom	161.63	158.86	1.02	10.49	14.72	0.71	[3]
				GMFE: 1.43 (1.01–5.63)	GMFE: 1.41 (1.00–2.66)			

(continued)

Table S11. continued

Study	Compound	Pred $\left[\frac{\text{ng}\cdot\text{h}}{\text{ml}}\right]$	Obs $\left[\frac{\text{ng}\cdot\text{h}}{\text{ml}}\right]$	Pred/Obs	Pred $\left[\frac{\text{ng}}{\text{ml}}\right]$	Obs $\left[\frac{\text{ng}}{\text{ml}}\right]$	Pred/Obs	Reference
GMFE $\leq$ 2: 24/30								
GMFE $\leq$ 2: 27/30								

**AS:** CYP2D6 activity score, **DGI:** drug-gene interaction, **(E)-4-OH-Clom:** (E)-4-hydroxyclophiphen, **(E)-4-OH-DE-Clom:** (E)-4-hydroxy-N-desethylclomiphene, **(E)-Clom:** (E)-clomiphene, **(E)-DE-Clom:** (E)-N-desethylclomiphene, **IM:** intermediate metabolizers, **NM:** normal metabolizers, **Obs:** observed, **PK:** pharmacokinetic, **PM:** poor metabolizers, **Pred:** predicted, **UM:** ultrarapid metabolizers, **Ratioph.**: Ratiopharm® GmbH

Table S12. Geometric Mean Fold Error (GMFE) of DGI AUC<sub>last</sub> and C<sub>max</sub> ratios.

Study	Compound	AUC <sub>last</sub> Ratio				C <sub>max</sub> Ratio				Reference
		Pred [1]	Obs [1]	Pred/Obs		Pred [1]	Obs [1]	Pred/Obs		
PK Panel Study, PM (AS = 0)	(E)-Clom	9.04	13.21	0.68		2.21	4.12	0.54	[19]	
PK Panel Study, PM (AS = 0)	(E)-4-OH-Clom	0.43	0.43	1.01		0.08	0.08	0.99	[19]	
PK Panel Study, PM (AS = 0)	(E)-DE-Clom	63.77	59.41	1.07		7.23	6.07	1.19	[19]	
PK Panel Study, PM (AS = 0)	(E)-4-OH-DE-Clom	0.33	0.32	1.03		0.06	0.06	1.04	[19]	
PK Panel Study, IM (AS = 0.5)	(E)-Clom	3.95	5.09	0.78		1.71	2.49	0.69	[19]	
PK Panel Study, IM (AS = 0.5)	(E)-4-OH-Clom	1.40	2.35	0.59		0.45	0.92	0.48	[19]	
PK Panel Study, IM (AS = 0.5)	(E)-DE-Clom	13.95	7.64	1.83		3.64	3.30	1.10	[19]	
PK Panel Study, IM (AS = 0.5)	(E)-4-OH-DE-Clom	3.29	2.90	1.13		1.07	1.02	1.05	[19]	
PK Panel Study, IM (AS = 0.75)	(E)-Clom	3.38	1.65	2.05		1.58	0.92	1.72	[19]	
PK Panel Study, IM (AS = 0.75)	(E)-4-OH-Clom	1.48	1.13	1.31		0.47	0.85	0.55	[19]	
PK Panel Study, IM (AS = 0.75)	(E)-DE-Clom	10.83	1.75	6.19		3.08	1.42	2.17	[19]	
PK Panel Study, IM (AS = 0.75)	(E)-4-OH-DE-Clom	3.00	1.17	2.57		1.01	1.07	0.94	[19]	
PK Panel Study, IM (AS = 1)	(E)-Clom	1.66	1.08	1.54		1.22	0.79	1.55	[19]	
PK Panel Study, IM (AS = 1)	(E)-4-OH-Clom	1.30	0.98	1.32		0.61	0.59	1.03	[19]	
PK Panel Study, IM (AS = 1)	(E)-DE-Clom	3.53	1.35	2.61		1.68	0.57	2.92	[19]	
PK Panel Study, IM (AS = 1)	(E)-4-OH-DE-Clom	1.88	0.83	2.25		0.98	0.66	1.49	[19]	
PK Panel Study, UM (AS = 3)	(E)-Clom	0.74	0.80	0.93		0.88	0.71	1.23	[19]	
PK Panel Study, UM (AS = 3)	(E)-4-OH-Clom	0.87	0.43	2.00		1.01	0.59	1.72	[19]	
PK Panel Study, UM (AS = 3)	(E)-DE-Clom	0.62	0.41	1.52		0.75	0.43	1.74	[19]	
PK Panel Study, UM (AS = 3)	(E)-4-OH-DE-Clom	0.65	0.38	1.70		0.77	0.56	1.37	[19]	
AS: CYP2D6 activity score, <b>DGI</b> : drug-gene interaction, <b>(E)-4-OH-Clom</b> : (E)-4-hydroxyclophenene, <b>(E)-4-OH-DE-Clom</b> : (E)-4-hydroxy-N-desethylclomiphene, <b>(E)-Clom</b> : (E)-clomiphene, <b>(E)-DE-Clom</b> : (E)-N-desethylclomiphene, <b>IM</b> : intermediate metabolizers, <b>NM</b> : normal metabolizers, <b>Obs</b> : observed, <b>PK</b> : pharmacokinetic, <b>PM</b> : poor metabolizers, <b>Pred</b> : predicted, <b>UM</b> : ultrarapid metabolizers										
		GMFE: 1.65 (1.00–6.19)				GMFE: 1.46 (1.00–2.95)				
		GMFE ≤ 2: 14/20				GMFE ≤ 2: 17/20				
		Guest limits: 12/20				Guest limits: 10/20				



Table S13. Geometric Mean Fold Error (GMFE) of AUC<sub>last</sub> and C<sub>max</sub> DD(G) Predictions.

Study	Compound	Perpetrator	AUC <sub>last</sub>		C <sub>max</sub>		Reference
			Pred $\left[\frac{\mu\text{g}\cdot\text{h}}{\text{ml}}\right]$	Obs $\left[\frac{\mu\text{g}\cdot\text{h}}{\text{ml}}\right]$	Pred $\left[\frac{\text{ng}}{\text{ml}}\right]$	Obs $\left[\frac{\text{ng}}{\text{ml}}\right]$	
PK Panel Study, PM (AS = 0)	(E)-Clom	Clarithromycin	2211.99	2332.83	41.25	69.18	[19]
PK Panel Study, PM (AS = 0)	(E)-4-OH-Clom	Clarithromycin	287.69	119.75	2.38	1.24	[19]
PK Panel Study, PM (AS = 0)	(E)-DE-Clom	Clarithromycin	2592.38	2282.03	18.17	14.69	[19]
PK Panel Study, PM (AS = 0)	(E)-4-OH-DE-Clom	Clarithromycin	100.11	36.96	0.82	0.29	[19]
PK Panel Study, IM (AS = 0.5)	(E)-Clom	Clarithromycin	585.91	769.47	24.64	42.67	[19]
PK Panel Study, IM (AS = 0.5)	(E)-4-OH-Clom	Clarithromycin	578.95	885.93	7.88	20.35	[19]
PK Panel Study, IM (AS = 0.5)	(E)-DE-Clom	Clarithromycin	219.84	135.87	2.58	2.79	[19]
PK Panel Study, IM (AS = 0.5)	(E)-4-OH-DE-Clom	Clarithromycin	272.46	201.78	2.06	1.93	[19]
PK Panel Study, IM (AS = 1)	(E)-Clom	Clarithromycin	207.03	176.77	16.37	14.74	[19]
PK Panel Study, IM (AS = 1)	(E)-4-OH-Clom	Clarithromycin	427.82	356.60	9.05	15.53	[19]
PK Panel Study, IM (AS = 1)	(E)-DE-Clom	Clarithromycin	35.98	26.96	1.33	1.22	[19]
PK Panel Study, IM (AS = 1)	(E)-4-OH-DE-Clom	Clarithromycin	132.72	71.32	1.62	1.91	[19]
PK Panel Study, NM (AS = 2)	(E)-Clom	Clarithromycin	117.25	100.98	13.07	17.22	[19]
PK Panel Study, NM (AS = 2)	(E)-4-OH-Clom	Clarithromycin	304.50	266.53	14.21	16.36	[19]
PK Panel Study, NM (AS = 2)	(E)-DE-Clom	Clarithromycin	15.33	12.85	1.05	0.85	[19]
PK Panel Study, NM (AS = 2)	(E)-4-OH-DE-Clom	Clarithromycin	50.59	42.79	1.98	2.19	[19]
PK Panel Study, UM (AS = 3)	(E)-Clom	Clarithromycin	84.09	88.29	11.34	13.87	[19]
PK Panel Study, UM (AS = 3)	(E)-4-OH-Clom	Clarithromycin	248.86	172.19	13.96	11.16	[19]
PK Panel Study, UM (AS = 3)	(E)-DE-Clom	Clarithromycin	11.10	9.79	0.96	0.45	[19]
PK Panel Study, UM (AS = 3)	(E)-4-OH-DE-Clom	Clarithromycin	35.43	30.40	1.76	1.61	[19]
PK Panel Study, PM (AS = 0)	(E)-Clom	Paroxetine	1035.07	1204.78	28.75	40.39	[19]
PK Panel Study, PM (AS = 0)	(E)-4-OH-Clom	Paroxetine	117.15	95.18	1.11	1.47	[19]
PK Panel Study, PM (AS = 0)	(E)-DE-Clom	Paroxetine	3405.95	4195.92	27.95	37.12	[19]
PK Panel Study, PM (AS = 0)	(E)-4-OH-DE-Clom	Paroxetine	69.53	63.01	0.54	0.41	[19]
PK Panel Study, IM (AS = 0.5)	(E)-Clom	Paroxetine	993.64	1053.60	28.98	35.05	[19]
PK Panel Study, IM (AS = 0.5)	(E)-4-OH-Clom	Paroxetine	139.64	119.04	1.32	1.30	[19]
PK Panel Study, IM (AS = 0.5)	(E)-DE-Clom	Paroxetine	3094.26	2384.31	27.70	19.23	[19]
PK Panel Study, IM (AS = 0.5)	(E)-4-OH-DE-Clom	Paroxetine	232.51	173.56	2.05	1.70	[19]
PK Panel Study, IM (AS = 1)	(E)-Clom	Paroxetine	858.97	855.99	26.24	34.32	[19]
PK Panel Study, IM (AS = 1)	(E)-4-OH-Clom	Paroxetine	153.97	204.03	1.30	2.62	[19]
PK Panel Study, IM (AS = 1)	(E)-DE-Clom	Paroxetine	2288.71	2104.81	23.38	23.47	[19]
PK Panel Study, IM (AS = 1)	(E)-4-OH-DE-Clom	Paroxetine	428.74	349.83	3.51	2.47	[19]
PK Panel Study, NM (AS = 2)	(E)-Clom	Paroxetine	731.17	828.75	26.03	41.65	[19]

(continued)

Table S13. continued

Study	Compound	Perpetrator	Pred $\left[\frac{\text{ng}\cdot\text{h}}{\text{ml}}\right]$	Obs $\left[\frac{\text{ng}\cdot\text{h}}{\text{ml}}\right]$	Pred/Obs	Pred $\left[\frac{\text{ng}}{\text{ml}}\right]$	Obs $\left[\frac{\text{ng}}{\text{ml}}\right]$	Pred/Obs	Reference
PK Panel Study, NM (AS = 2)	(E)-4-OH-Clom	Paroxetine	199.16	346.58	0.57	2.41	4.27	0.57	[19]
PK Panel Study, NM (AS = 2)	(E)-DE-Clom	Paroxetine	1421.08	1170.81	1.21	23.33	20.66	1.13	[19]
PK Panel Study, NM (AS = 2)	(E)-4-OH-DE-Clom	Paroxetine	664.56	511.87	1.30	5.53	5.50	1.01	[19]
PK Panel Study, UM (AS = 3)	(E)-Clom	Paroxetine	550.74	806.88	0.68	22.29	54.63	0.41	[19]
PK Panel Study, UM (AS = 3)	(E)-4-OH-Clom	Paroxetine	212.08	345.90	0.61	3.00	6.46	0.46	[19]
PK Panel Study, UM (AS = 3)	(E)-DE-Clom	Paroxetine	722.15	739.59	0.98	16.09	23.37	0.69	[19]
PK Panel Study, UM (AS = 3)	(E)-4-OH-DE-Clom	Paroxetine	545.59	400.60	1.36	6.51	6.49	1.00	[19]

GMFE: 1.30 (1.00–2.71) GMFE: 1.40 (1.00–2.83)  
GMFE ≤ 2: 38/40 GMFE ≤ 2: 34/40

AS: CYP2D6 activity score, DD(G)I: drug-drug and drug-drug-gene interactions, (E)-4-OH-Clom: (E)-4-hydroxyclomiphene, (E)-4-OH-DE-Clom: (E)-4-hydroxy-N-desethylclomiphene, (E)-Clom: (E)-clomiphene, (E)-DE-Clom: (E)-N-desethylclomiphene, IM: intermediate metabolizers, NM: normal metabolizers, Obs: observed, PK: pharmacokinetic, PM: poor metabolizers, Pred: predicted, UM: ultrarapid metabolizers

**Table S14.** Geometric Mean Fold Error (GMFE) of DD(G)I AUC<sub>last</sub> and C<sub>max</sub> ratios.

Study	Compound	Perpetrator	AUC <sub>last</sub> Ratio				C <sub>max</sub> Ratio				Reference		
			Pred [1]		Obs [1]		Pred/Obs		Pred [1]			Obs [1]	
			Pred [1]	Obs [1]	Pred/Obs	Pred/Obs	Pred [1]	Obs [1]	Pred/Obs	Pred/Obs			
PK Panel Study, PM (AS = 0)	(E)-Clom	Clarithromycin	2.41	2.13	1.13	1.13	1.53	1.55	0.98	[19]			
PK Panel Study, PM (AS = 0)	(E)-4-OH-Clom	Clarithromycin	2.81	1.28	2.20	2.20	2.44	1.01	2.41	[19]			
PK Panel Study, PM (AS = 0)	(E)-DE-Clom	Clarithromycin	0.76	0.66	1.16	1.16	0.61	0.54	1.14	[19]			
PK Panel Study, PM (AS = 0)	(E)-4-OH-DE-Clom	Clarithromycin	1.62	0.59	2.74	2.74	1.74	0.67	2.59	[19]			
PK Panel Study, IM (AS = 0.5)	(E)-Clom	Clarithromycin	1.46	1.82	0.80	0.80	1.18	1.59	0.75	[19]			
PK Panel Study, IM (AS = 0.5)	(E)-4-OH-Clom	Clarithromycin	1.75	1.72	1.02	1.02	1.41	1.40	1.00	[19]			
PK Panel Study, IM (AS = 0.5)	(E)-DE-Clom	Clarithromycin	0.30	0.30	0.97	0.97	0.17	0.19	0.92	[19]			
PK Panel Study, IM (AS = 0.5)	(E)-4-OH-DE-Clom	Clarithromycin	0.45	0.36	1.24	1.24	0.25	0.25	0.97	[19]			
PK Panel Study, IM (AS = 1)	(E)-Clom	Clarithromycin	1.23	1.97	0.62	0.62	1.10	1.73	0.63	[19]			
PK Panel Study, IM (AS = 1)	(E)-4-OH-Clom	Clarithromycin	1.40	1.66	0.84	0.84	1.18	1.67	0.70	[19]			
PK Panel Study, IM (AS = 1)	(E)-DE-Clom	Clarithromycin	0.19	0.34	0.56	0.56	0.19	0.47	0.41	[19]			
PK Panel Study, IM (AS = 1)	(E)-4-OH-DE-Clom	Clarithromycin	0.38	0.44	0.86	0.86	0.21	0.39	0.55	[19]			
PK Panel Study, NM (AS = 2)	(E)-Clom	Clarithromycin	1.15	1.22	0.95	0.95	1.07	1.59	0.67	[19]			
PK Panel Study, NM (AS = 2)	(E)-4-OH-Clom	Clarithromycin	1.29	1.22	1.05	1.05	1.13	1.04	1.08	[19]			
PK Panel Study, NM (AS = 2)	(E)-DE-Clom	Clarithromycin	0.29	0.22	1.31	1.31	0.26	0.19	1.36	[19]			
PK Panel Study, NM (AS = 2)	(E)-4-OH-DE-Clom	Clarithromycin	0.27	0.22	1.24	1.24	0.25	0.29	0.87	[19]			
PK Panel Study, UM (AS = 3)	(E)-Clom	Clarithromycin	1.11	1.33	0.84	0.84	1.06	1.80	0.59	[19]			
PK Panel Study, UM (AS = 3)	(E)-4-OH-Clom	Clarithromycin	1.21	1.82	0.67	0.67	1.09	1.20	0.91	[19]			
PK Panel Study, UM (AS = 3)	(E)-DE-Clom	Clarithromycin	0.34	0.41	0.82	0.82	0.31	0.23	1.33	[19]			
PK Panel Study, UM (AS = 3)	(E)-4-OH-DE-Clom	Clarithromycin	0.33	0.46	0.72	0.72	0.29	0.38	0.77	[19]			
PK Panel Study, PM (AS = 0)	(E)-Clom	Paroxetine	1.13	1.10	1.02	1.02	1.07	0.91	1.17	[19]			
PK Panel Study, PM (AS = 0)	(E)-4-OH-Clom	Paroxetine	1.15	1.02	1.13	1.13	1.13	1.19	0.95	[19]			
PK Panel Study, PM (AS = 0)	(E)-DE-Clom	Paroxetine	1.00	1.21	0.83	0.83	0.94	1.36	0.70	[19]			
PK Panel Study, PM (AS = 0)	(E)-4-OH-DE-Clom	Paroxetine	1.13	1.01	1.12	1.12	1.13	0.94	1.21	[19]			
PK Panel Study, IM (AS = 0.5)	(E)-Clom	Paroxetine	2.47	2.49	0.99	0.99	1.39	1.30	1.07	[19]			
PK Panel Study, IM (AS = 0.5)	(E)-4-OH-Clom	Paroxetine	0.42	0.23	1.83	1.83	0.24	0.09	2.62	[19]			
PK Panel Study, IM (AS = 0.5)	(E)-DE-Clom	Paroxetine	4.17	5.34	0.78	0.78	1.86	1.29	1.44	[19]			
PK Panel Study, IM (AS = 0.5)	(E)-4-OH-DE-Clom	Paroxetine	0.38	0.31	1.23	1.23	0.24	0.22	1.10	[19]			
PK Panel Study, IM (AS = 1)	(E)-Clom	Paroxetine	5.08	9.56	0.53	0.53	1.76	4.02	0.44	[19]			
PK Panel Study, IM (AS = 1)	(E)-4-OH-Clom	Paroxetine	0.50	0.95	0.53	0.53	0.17	0.28	0.60	[19]			
PK Panel Study, IM (AS = 1)	(E)-DE-Clom	Paroxetine	12.21	26.61	0.46	0.46	3.40	9.07	0.37	[19]			
PK Panel Study, IM (AS = 1)	(E)-4-OH-DE-Clom	Paroxetine	1.23	2.16	0.57	0.57	0.46	0.50	0.92	[19]			
PK Panel Study, NM (AS = 2)	(E)-Clom	Paroxetine	7.19	9.99	0.72	0.72	2.13	3.85	0.55	[19]			

(continued)

Table S14. *continued*

Study	Compound	Perpetrator	Pred [1]	Obs [1]	Pred/Obs	Pred [1]	Obs [1]	Pred/Obs	Reference
PK Panel Study, NM (AS = 2)	( <i>E</i> )-4-OH-Clom	Paroxetine	0.84	1.59	0.53	0.19	0.27	0.71	[19]
PK Panel Study, NM (AS = 2)	( <i>E</i> )-DE-Clom	Paroxetine	26.73	20.02	1.34	5.70	4.59	1.24	[19]
PK Panel Study, NM (AS = 2)	( <i>E</i> )-4-OH-DE-Clom	Paroxetine	3.58	2.64	1.36	0.71	0.74	0.96	[19]
PK Panel Study, UM (AS = 3)	( <i>E</i> )-Clom	Paroxetine	7.29	12.19	0.60	2.08	7.08	0.29	[19]
PK Panel Study, UM (AS = 3)	( <i>E</i> )-4-OH-Clom	Paroxetine	1.03	3.66	0.28	0.24	0.70	0.34	[19]
PK Panel Study, UM (AS = 3)	( <i>E</i> )-DE-Clom	Paroxetine	21.90	30.93	0.71	5.27	12.14	0.43	[19]
PK Panel Study, UM (AS = 3)	( <i>E</i> )-4-OH-DE-Clom	Paroxetine	5.08	6.07	0.84	1.08	1.54	0.70	[19]
			<b>GMFE: 1.40 (1.00-3.55)</b>		<b>GMFE: 1.50 (1.00-3.40)</b>				
			<b>GMFE <math>\leq</math> 2: 36/40</b>		<b>GMFE <math>\leq</math> 2: 31/40</b>				
			<b>Guest limits: 29/40</b>		<b>Guest limits: 23/40</b>				

**AS:** CYP2D6 activity score, **DD(G)I:** drug-drug and drug-drug-gene interactions, (*E*)-4-OH-Clom: (*E*)-4-hydroxyclophiphen, (*E*)-4-OH-DE-Clom: (*E*)-4-hydroxy-N-desethylclomiphene, (*E*)-Clom: (*E*)-clomiphene, (*E*)-DE-Clom: (*E*)-N-desethylclomiphene, **IM:** intermediate metabolizers, **NM:** normal metabolizers, **Obs:** observed, **PK:** pharmacokinetic, **PM:** poor metabolizers, **Pred:** predicted, **UM:** ultrarapid metabolizers

## S4.4. Local Sensitivity Analysis

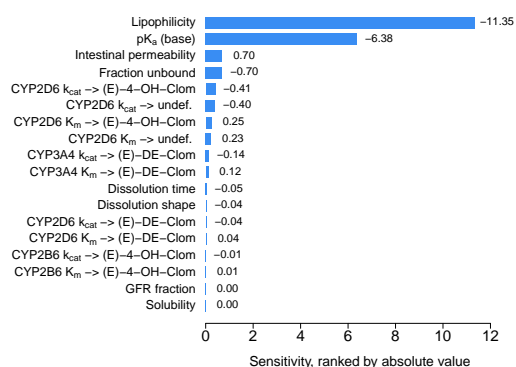
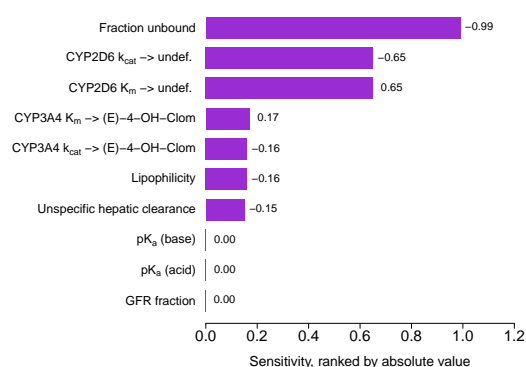
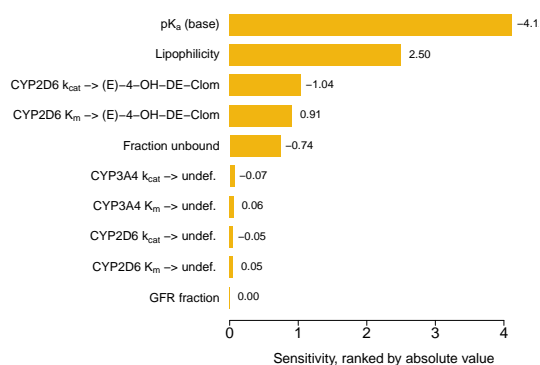
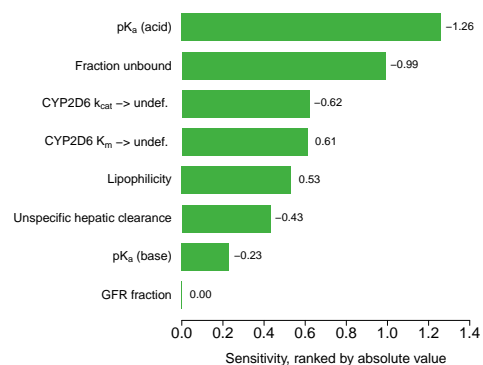
### S4.4.1. Mathematical Implementation

A sensitivity analysis of the developed model was conducted to explore the impact of single parameter changes (local sensitivity analysis) on the predicted  $AUC_{inf}$ . According to [Equation S4](#), the relative change of  $AUC_{inf}$  after oral application of a single dose of 100 mg clomiphen citrate to the relative variation of model input parameters was calculated. All optimized parameters as well as parameters that might have a strong impact because of calculation methods employed in the model (e.g., lipophilicity) were integrated in the sensitivity analysis and a relative perturbation of 10% was used.

$$S = \frac{\Delta AUC_{inf}}{\Delta p} \cdot \frac{p}{AUC_{inf}} \quad (S4)$$

$S$  is the sensitivity of the  $AUC_{inf}$  to the examined model parameter,  $\Delta AUC_{inf}$  is the change of the  $AUC_{inf}$ ,  $AUC_{inf}$  represents the simulated  $AUC_{inf}$  with the original parameter value,  $p$  is the original model parameter value and  $\Delta p$  the variation of the model parameter value. A sensitivity value of +1.0 signifies that a 10% increase of the examined parameter causes a 10% increase of the simulated  $AUC_{inf}$ .

## S4.4.2. Results of the Sensitivity Analysis

( a ) Sensitivity Analysis (*E*)-Clom( b ) Sensitivity Analysis (*E*)-4-OH-Clom( c ) Sensitivity Analysis (*E*)-Clom( d ) Sensitivity Analysis (*E*)-4-OH-Clom

**Figure S14. Sensitivity analysis of the PBPK model for (*E*)-Clom, (*E*)-4-OH-Clom, (*E*)-DE-Clom and (*E*)-4-OH-DE-Clom.** CYP, cytochrome P450; (*E*)-4-OH-Clom, (*E*)-4-hydroxyclophene; (*E*)-4-OH-DE-Clom, (*E*)-4-hydroxy-N-desethylclomiphene; (*E*)-Clom, (*E*)-clomiphene; (*E*)-DE-Clom, (*E*)-N-desethylclomiphene; GFR, glomerular filtration rate; k<sub>cat</sub>, catalytic rate constant; K<sub>m</sub>, Michaelis-Menten constant; pK<sub>a</sub>, acid dissociation constant; undef., undefined metabolite.

## S5. Molecular Structures

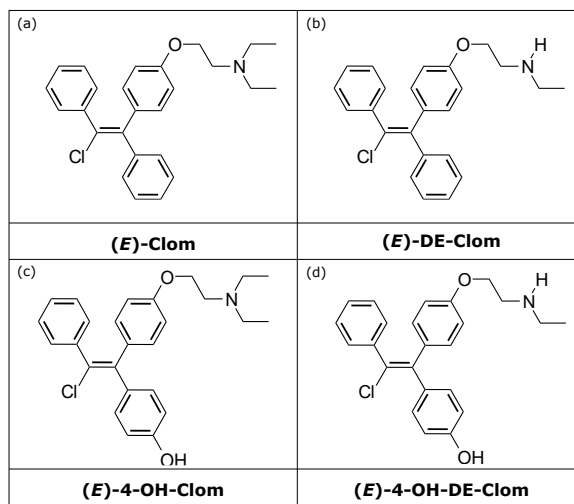


Figure S15. Molecular structures of (*E*)-Clom (a) and its metabolites (*E*)-DE-Clom (b), (*E*)-4-OH-Clom (c) and (*E*)-4-OH-DE-Clom (d). (*E*)-4-OH-Clom, (*E*)-4-hydroxyclophene; (*E*)-4-OH-DE-Clom, (*E*)-4-hydroxy-N-desethylclomiphene; (*E*)-Clom, (*E*)-clomiphene; (*E*)-DE-Clom, (*E*)-N-desethylclomiphene.

## References

- [1] Mikkelsen TJ, Kroboth PD, Cameron WJ, Dittert LW, Chungi V, Manberg PJ (1986) Single-dose pharmacokinetics of clomiphene citrate in normal volunteers\*\*Supported by a grant from Serono Laboratories, Inc., Randolph, Massachusetts. *Fertility and Sterility* 46(3):392–396
- [2] Ratiopharm® GmbH (2016) Clomifen-ratiopharm® 50 mg Tabletten (Study 1991). <https://www.ratiopharm.de/produkte/details/praeparate/paeparatedaten/detail/pzn-3884844.html>, available online (accessed: 2021-11-23)
- [3] Wiehle R, Cunningham GR, Pitteloud N, Wike J, Hsu K, Fontenot GK, Rosner M, Dwyer A, Podolski J (2013) Testosterone Restoration by Enclomiphene Citrate in Men with Secondary Hypogonadism: Pharmacodynamics and Pharmacokinetics. *BJU international* 112(8):1188–1200
- [4] Miller GD, Moore C, Nair V, Hill B, Willick SE, Rogol AD, Eichner D (2019) Hypothalamic-Pituitary-Testicular Axis Effects and Urinary Detection Following Clomiphene Administration in Males. *The Journal of clinical endocrinology and metabolism* 104(3):906–914
- [5] van der Lee M, Allard WG, Vossen RHAM, Baak-Pablo RF, Menafrá R, Deiman BALM, Deenen MJ, Neven P, Johansson I, Gastaldello S, Ingelman-Sundberg M, Guchelaar HJ, Swen JJ, Anvar SY (2021) Toward predicting CYP2D6-mediated variable drug response from CYP2D6 gene sequencing data. *Science translational medicine* 13(603)
- [6] Valentin J (2002) Basic anatomical and physiological data for use in radiological protection: reference values. A report of age- and gender-related differences in the anatomical and physiological characteristics of reference individuals. ICRP Publication 89. *Annals of the ICRP* 32(3-4):5–265
- [7] Open Systems Pharmacology Suite Community (2018) PK-Sim® Ontogeny Database Documentation, Version 7.3. <https://github.com/Open-Systems-Pharmacology/OSPSuite.Documentation/blob/master/PK-SimOntogenyDatabaseVersion7.3.pdf>, available online (accessed: 2020-03-25)
- [8] National Center for Health Statistics (1997) Third National Health and Nutrition Examination Survey (NHANES III). Tech. rep., Hyattsville, MD 20782
- [9] Willmann S, Höhn K, Edginton A, Sevestre M, Solodenko J, Weiss W, Lippert J, Schmitt W (2007) Development of a physiology-based whole-body population model for assessing the influence of individual variability on the pharmacokinetics of drugs. *Journal of pharmacokinetics and pharmacodynamics* 34(3):401–31
- [10] Rodrigues AD (1999) Integrated cytochrome P450 reaction phenotyping: attempting to bridge the gap between cDNA-expressed cytochromes P450 and native human liver microsomes. *Biochemical pharmacology* 57(5):465–80
- [11] Nishimura M, Yaguti H, Yoshitsugu H, Naito S, Satoh T (2003) Tissue distribution of mRNA expression of human cytochrome P450 isoforms assessed by high-sensitivity real-time reverse transcription PCR. *Yakugaku zasshi : Journal of the Pharmaceutical Society of Japan* 123(5):369–75
- [12] Rowland Yeo K, Walsky RL, Jamei M, Rostami-Hodjegan A, Tucker GT (2011) Prediction of time-dependent CYP3A4 drug-drug interactions by physiologically based pharmacokinetic modelling: impact of inactivation parameters and enzyme turnover. *European journal of pharmaceutical sciences : official journal of the European Federation for Pharmaceutical Sciences* 43(3):160–73



- [13] Greenblatt DJ, von Moltke LL, Harmatz JS, Chen G, Weemhoff JL, Jen C, Kelley CJ, LeDuc BW, Zinny MA (2003) Time course of recovery of cytochrome p450 3A function after single doses of grapefruit juice. *Clinical pharmacology and therapeutics* 74(2):121–9
- [14] Tsamandouras N, Rostami-Hodjegan A, Aarons L (2015) Combining the 'bottom up' and 'top down' approaches in pharmacokinetic modelling: fitting PBPK models to observed clinical data. *British journal of clinical pharmacology* 79(1):48–55
- [15] Austin RP, Barton P, Cockroft SL, Wenlock MC, Riley RJ (2002) The influence of nonspecific microsomal binding on apparent intrinsic clearance, and its prediction from physicochemical properties. *Drug metabolism and disposition: the biological fate of chemicals* 30(12):1497–503
- [16] Obach RS (1997) Nonspecific binding to microsomes: impact on scale-up of in vitro intrinsic clearance to hepatic clearance as assessed through examination of warfarin, imipramine, and propranolol. *Drug metabolism and disposition: the biological fate of chemicals* 25(12):1359–69
- [17] Mürdter TE, Kerb R, Turpeinen M, Schroth W, Ganchev B, Böhmer GM, Igel S, Schaeffeler E, Zanger U, Brauch H, Schwab M (2012) Genetic polymorphism of cytochrome P450 2D6 determines oestrogen receptor activity of the major infertility drug clomiphene via its active metabolites. *Human molecular genetics* 21(5):1145–54
- [18] Ganchev B (2014) Charakterisierung der metabolischen Bioaktivierung des Clomifens unter besonderer Berücksichtigung genetischer Polymorphismen. PhD thesis, Eberhard Karls University Tübingen
- [19] Kröner P (2018) Hydroxylierte Metaboliten des Clomifens : in vitro und in vivo Untersuchungen zur Bildung, Aktivität und Konjugation. PhD thesis, Eberhard-Karls-University Tübingen
- [20] Mazzarino M, Biava M, de la Torre X, Fiacco I, Botrè F (2013) Characterization of the biotransformation pathways of clomiphene, tamoxifen and toremifene as assessed by LC-MS/(MS) following in vitro and excretion studies. *Analytical and bioanalytical chemistry* 405(16):5467–87
- [21] Watanabe R, Esaki T, Kawashima H, Natsume-Kitatani Y, Nagao C, Ohashi R, Mizuguchi K (2018) Predicting Fraction Unbound in Human Plasma from Chemical Structure: Improved Accuracy in the Low Value Ranges. *Molecular pharmaceutics* 15(11):5302–5311
- [22] Siramshetty VB, Grishagin I, Nguyen cT, Peryea T, Skovpen Y, Stroganov O, Katzel D, Sheils T, Jadhav A, Mathé EA, Southall NT (2022) NCATS Inxight Drugs: a comprehensive and curated portal for translational research. *Nucleic acids research* 50(D1):D1307–D1316
- [23] Developed by ChemAxon (2009) (<http://www.chemaxon.com>), chemicalize was used for prediction of (E)-clomiphene properties. <https://chemicalize.com/>, available online (accessed: 2021-08-09)
- [24] Das P, Prajapati M, Maity A (2020) Study of equilibrium solubility of Clomiphene Citrate as model compound by Saturation orbital shake flask method 3(4):843–847
- [25] Smith DA, Dalvie D (2012) Why do metabolites circulate? *Xenobiotica; the fate of foreign compounds in biological systems* 42(1):107–26
- [26] Wishart DS, Knox C, Guo AC, Shrivastava S, Hassanali M, Stothard P, Chang Z, Woolsey J (2006) DrugBank: a comprehensive resource for in silico drug discovery and exploration. *Nucleic acids research* 34(Database issue):D668–72

- [27] Güngör S, Delgado-Charro MB, Masini-Etévé V, Potts RO, Guy RH (2013) Transdermal flux predictions for selected selective oestrogen receptor modulators (SERMs): comparison with experimental results. *Journal of controlled release : official journal of the Controlled Release Society* 172(3):601–6
- [28] Schmitt W (2008) General approach for the calculation of tissue to plasma partition coefficients. *Toxicology in vitro : an international journal published in association with BIBRA* 22(2):457–67
- [29] Kawai R, Lemaire M, Steimer JL, Bruelisauer A, Niederberger W, Rowland M (1994) Physiologically based pharmacokinetic study on a cyclosporin derivative, SDZ IMM 125. *Journal of pharmacokinetics and biopharmaceutics* 22(5):327–65
- [30] Developed by ChemAxon (2009) (<http://www.chemaxon.com>), chemicalize was used for prediction of (E)-N-desethylclomiphene properties. <https://chemicalize.com/>, available online (accessed: 2021-08-09)
- [31] Kim S, Chen J, Cheng T, Gindulyte A, He J, He S, Li Q, Shoemaker BA, Thiessen PA, Yu B, Zaslavsky L, Zhang J, Bolton EE (2021) PubChem in 2021: new data content and improved web interfaces. *Nucleic acids research* 49(D1):D1388–D1395
- [32] Rodgers T, Leahy D, Rowland M (2005) Physiologically based pharmacokinetic modeling 1: predicting the tissue distribution of moderate-to-strong bases. *Journal of pharmaceutical sciences* 94(6):1259–76
- [33] Rodgers T, Rowland M (2006) Physiologically based pharmacokinetic modelling 2: predicting the tissue distribution of acids, very weak bases, neutrals and zwitterions. *Journal of pharmaceutical sciences* 95(6):1238–57
- [34] Developed by ChemAxon (2009) (<http://www.chemaxon.com>), chemicalize was used for prediction of (E)-4-hydroxyclophene properties. <https://chemicalize.com/>, available online (accessed: 2021-08-09)
- [35] European Medicines Agency (2018) Assessment Report EnCyzix. [https://www.ema.europa.eu/en/documents/assessment-report/encyzix-epar-public-assessment-report\\_en.pdf](https://www.ema.europa.eu/en/documents/assessment-report/encyzix-epar-public-assessment-report_en.pdf), available online (accessed: 2021-08-12)
- [36] Berezhkovskiy LM (2004) Volume of distribution at steady state for a linear pharmacokinetic system with peripheral elimination. *Journal of pharmaceutical sciences* 93(6):1628–40
- [37] Open Systems Pharmacology Suite Community (2021) Open Systems Pharmacology Suite Manual. <https://raw.githubusercontent.com/Open-Systems-Pharmacology/OSPSuite.Documentation/master/OpenSystemsPharmacologySuite.pdf>, available online (accessed: 2022-02-19)
- [38] Developed by ChemAxon (2009) (<http://www.chemaxon.com>), chemicalize was used for prediction of (E)-4-hydroxy-N-desethylclomiphene properties. <https://chemicalize.com/>, available online (accessed: 2021-08-09)
- [39] T’jollyn H, Snoeys J, Vermeulen A, Michelet R, Cuyckens F, Mannens G, Van Peer A, Annaert P, Allegaert K, Van Bocxlaer J, Boussery K (2015) Physiologically Based Pharmacokinetic Predictions of Tramadol Exposure Throughout Pediatric Life: an Analysis of the Different Clearance Contributors with Emphasis on CYP2D6 Maturation. *The AAPS journal* 17(6):1376–87

- [40] United States Pharmacopeial Convention (2006) United States Pharmacopeia and National Formulary (USP 29-NF 24). p 553, [http://www.pharmacoepia.cn/v29240/usp29nf24s0\\_m18490.html](http://www.pharmacoepia.cn/v29240/usp29nf24s0_m18490.html), available online (accessed: 2021-08-24)
- [41] Beal SL (2001) Ways to fit a PK model with some data below the quantification limit. *Journal of pharmacokinetics and pharmacodynamics* 28(5):481–504
- [42] Obach RS, Walsky RL, Venkatakrishnan K (2007) Mechanism-based inactivation of human cytochrome p450 enzymes and the prediction of drug-drug interactions. *Drug metabolism and disposition: the biological fate of chemicals* 35(2):246–55
- [43] Hanke N, Frechen S, Moj D, Britz H, Eissing T, Wendl T, Lehr T (2018) PBPK Models for CYP3A4 and P-gp DDI Prediction: A Modeling Network of Rifampicin, Itraconazole, Clarithromycin, Midazolam, Alfentanil, and Digoxin. *CPT: pharmacometrics & systems pharmacology* 7(10):647–659
- [44] Rüdeshiem S, Selzer D, Mürdter T, Igel S, Kerb R, Schwab M, Lehr T (2022) Physiologically Based Pharmacokinetic Modeling to Describe the CYP2D6 Activity Score-Dependent Metabolism of Paroxetine, Atomoxetine and Risperidone. *Pharmaceutics* 14(8):1734
- [45] Guest EJ, Aarons L, Houston JB, Rostami-Hodjegan A, Galetin A (2011) Critique of the two-fold measure of prediction success for ratios: application for the assessment of drug-drug interactions. *Drug metabolism and disposition: the biological fate of chemicals* 39(2):170–3

A.4 SUPPLEMENTARY DOCUMENT TO PUBLICATION IV – EXTERNAL PERFORMANCE EVALUATION OF INFLIXIMAB POPULATION PHARMACOKINETIC MODELS

# Supplementary Material: External Model Performance Evaluation of Twelve Infliximab Population Pharmacokinetic Models in Patients with Inflammatory Bowel Disease

Christina Schräpel, Lukas Kovar, Dominik Selzer, Ute Hofmann, Florian Tran, Walter Reinisch, Matthias Schwab and Thorsten Lehr

## 1. Assumptions for model implementations of investigated population pharmacokinetic models

In the publication by Brandse et al. 2016, the additive residual error of 0.26 was reported without a unit [1]. The unit  $\mu\text{g/mL}$ , which was used throughout the respective publication to report IFX concentrations was assumed. In the publication by Buurman et al. 2015 [2], the equation for calculating the central volume of distribution was presented as

$$V_i = V_{pop} * 0.964 * (HBI - 6) \quad (S1)$$

with HBI being the Harvey-Bradshaw index and  $V_{pop}$  being the central volume of distribution of the typical patient. Using this equation,  $V_i$  would become negative for HBI values  $< 6$ . The respective publication reported an HBI range of the internal dataset of 3–24. With the help of information from the text (“For  $V$ , a significant and clinically relevant effect was found for the HBI at baseline, a higher value resulting in lower values of  $V$ ” [2]) and from Table 3 ( $\theta_{HBI}$  is  $-3.6$  per HBI point) in the respective publication [2], the equation was changed to:

$$V_i = V_{pop} \times (1 - 0.036 \times (HBI - 6)) \quad (S2)$$

indicating a lower central volume of distribution with higher HBI values.

In the publication by Aubourg et al. 2015, contradictory units were displayed for the clearance (CL) and inter-compartmental clearance (Q) parameters (L/h and L/day, respectively) when comparing values from text and Table 1 [3]. However, in Table 1, also CL and Q parameters from other infliximab population pharmacokinetic models were displayed. By comparing these parameters to the respective publications, it becomes clear, that the correct unit is L/h which was used for our model implementation.

For predictions with the model by Edlund et al. 2017 (III), ADA concentrations reported below the lower limit of quantification were treated as zero as suggested in the respective publication [4].

The full-text version of the publication by Xu et al. 2012 [5] could not be identified. As a result, the information for model implementation were gathered from the abstract as well as from the publication by Wojciechowski and coworkers [6], who used the model by Xu et al. 2012 to simulate individual pharmacokinetic parameters for a virtual study population and who reported the modeling information of the model by Xu et al. 2012.

For model predictions with time-varying covariates, changes in covariates over time were acknowledged (e.g. change in ADA status, HBI, weight) and used for model computations. Missing continuous covariates were imputed by median values and missing categorical covariates by the mode (most frequent value).

## 2 Predictive model performance evaluation

### 2.1. Goodness-of-fit plots

The goodness-of-fit plot showing the individual predicted versus observed serum infliximab concentrations for the population pharmacokinetic model by Petitcollin et al. 2018 [7] including the concentration which was cut-off in the main manuscript is depicted in Figure S1.

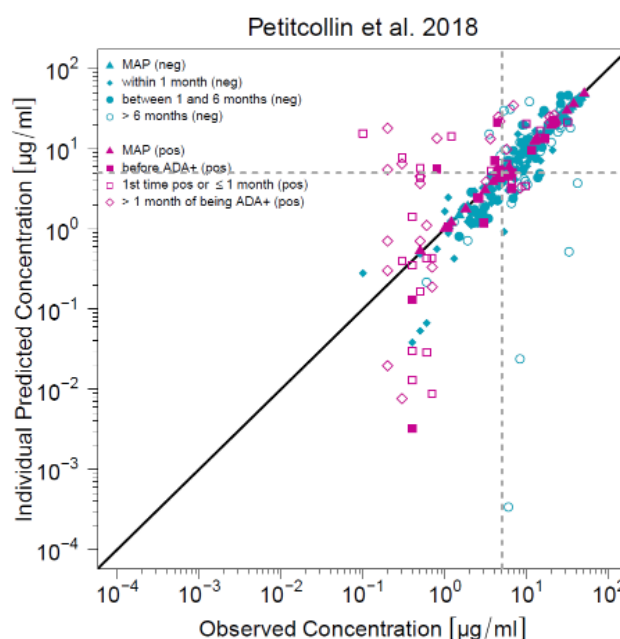


**Figure S1.** Individual predicted versus observed serum infliximab concentrations for the population pharmacokinetic model by Petitcollin et al. 2018. Concentrations of anti-drug antibody (ADA) negative patients are shown in turquoise, concentrations of ADA positive patients in pink. Concentrations used for maximum a posteriori (MAP) estimation ( $C_{MAP}$ ) are depicted as triangles, the remaining symbols depict predictions in different time intervals after  $C_{MAP}$ . The black solid line represents the line of identity, grey dashed lines mark the target trough concentration of 5 µg/mL. (neg): ADA negative patients; (pos): ADA positive patients.

## 2.2 Accuracy and bias of model predictions

The calculated median symmetric accuracy ( $\zeta$ ) and symmetric signed percentage bias (SSPB) values for all included population pharmacokinetic models are shown in Tables S1 to S4. Tables S1 and S2 list the results for model predictions with fixed covariates determined at the time of the first measured serum infliximab concentration of each patient ( $C_{MAP}$ ), while Tables S3 and S4 list the results for model predictions with time-varying covariates. Tables S1 and S3 provide the calculated  $\zeta$  and SSPB values for the ADA negative patient cohort. Tables S2 and S4 provide the  $\zeta$  and SSPB values for the ADA positive patient cohort. In addition, Figures S2 and S3 show the corresponding visual depiction of  $\zeta$  and SSPB values.

**Table S1.**  $\zeta$  and SSPB values for model predictions with fixed covariates at time of  $C_{MAP}$  for ADA negative patients.

Model	$\zeta$ (%)					SSPB (%)				
	MAP	< 1 m	1–6 m	> 6 m	all pred	MAP	< 1 m	1–6 m	> 6 m	all pred
Aubourg et al. 2015	9.2	20.8	32.1	54.7	28.0	−8.3	17.3	19.0	5.0	15.6
Brandse et al. 2016	23.7	33.7	28.9	49.3	33.2	−23.7	−27.8	−21.9	−18.0	−22.0
Buurman et al. 2015	18.8	43.8	35.0	65.2	43.5	−1.6	40.4	15.3	21.2	27.5
Edlund et al. 2017 (I)	6.2	26.5	28.0	53.8	33.1	−1.5	11.5	17.6	11.0	13.4
Edlund et al. 2017 (II)	5.1	24.6	27.3	53.5	30.5	−1.9	12.0	17.0	9.2	12.0
Edlund et al. 2017 (III)	4.5	23.2	27.2	54.5	29.1	−2.4	11.8	16.1	8.5	12.5
Fasanmade et al. 2009	16.1	24.9	23.5	50.6	27.3	−14.1	−3.5	0.4	−6.1	−2.6
Fasanmade et al. 2011 (a)	14.7	24.7	21.0	54.9	26.4	−14.4	−8.6	1.0	−2.2	−5.3
Fasanmade et al. 2011 (a/c)	13.3	23.6	21.5	53.0	25.5	−12.9	−8.5	0.3	−1.2	−5.2
Passot et al. 2016	0.3	33.1	46.4	49.3	37.7	−0.2	26.9	41.0	20.2	26.6
Petitcollin et al. 2018	2.5	30.0	34.9	69.3	39.5	−2.5	−20.1	−8.6	−37.3	−19.8
Xu et al. 2012	18.0	25.6	20.4	57.5	27.1	−16.9	1.6	−3.2	−6.5	−0.6

a: adults; a/c: adults/children; ADA: anti-drug antibody; m: month; pred: predicted; SSPB: symmetric signed percentage bias;  $\zeta$ : median symmetric accuracy. Abbreviations for time intervals refer to descriptions in the main manuscript.

**Table S2.**  $\zeta$  and SSPB values for model predictions with fixed covariates at time of  $C_{MAP}$  for ADA positive patients.

Model	$\zeta$ [%]					SSPB [%]				
	MAP	before ADA+	1 <sup>st</sup> time ADA+ or $\leq$ 1 m	> 1 m after ADA+	all pred	MAP	before ADA+	1 <sup>st</sup> time ADA+ or $\leq$ 1 m	> 1 m after ADA+	all pred
Aubourg et al. 2015	10.7	33.9	98.2	301.9	92.8	-5.2	32.8	82.6	301.9	78.7
Brandse et al. 2016	18.4	51.5	278.6	384.4	214.9	-12.8	-30.0	-66.2	180.7	8.1
Buurman et al. 2015	43.1	88.9	361.4	175.1	144.8	22.3	70.0	361.4	175.1	144.8
Edlund et al. 2017 (I)	10.6	41.3	72.1	300.4	86.4	-9.5	-7.5	30.1	300.4	51.1
Edlund et al. 2017 (II)	6.8	23.9	77.3	344.3	85.4	0.4	7.8	9.4	344.3	37.6
Edlund et al. 2017 (III)	5.2	24.9	91.2	205.5	90.8	-0.3	6.3	-9.4	205.5	25.9
Fasanmade et al. 2009	15.1	31.9	79.9	330.1	111.7	-2.9	-4.3	-2.0	330.1	48.4
Fasanmade et al. 2011 (a)	15.8	28.5	107.5	250.9	85.1	-9.9	-25.6	13.5	191.6	14.1
Fasanmade et al. 2011 (a/c)	14.1	29.9	95.4	254.1	83.6	-9.2	-13.8	5.5	200.6	15.6
Passot et al. 2016	0.3	17.1	144.5	347.7	128.0	0.1	14.5	78.4	330.1	73.0
Petitcollin et al. 2018	2.3	29.4	106.3	269.9	108.5	-2.0	-10.7	-0.5	77.6	16.4
Xu et al. 2012	16.5	38.7	80.7	303.3	77.1	-8.3	3.5	54.3	303.3	50.1

$\zeta$ : median symmetric accuracy; a: adults; a/c: adults/children; ADA: anti-drug antibody, ADA+: anti-drug antibody positive; m: month; pred: predicted; SSPB: symmetric signed percentage bias. Abbreviations for time intervals refer to descriptions in the main manuscript.

**Table S3.**  $\zeta$  and SSPB values for model predictions with time-varying covariates for ADA negative patients.

Model	$\zeta$ [%]					SSPB [%]				
	MAP	< 1 m	1 - 6 m	> 6 m	all pred	MAP	< 1 m	1 - 6 m	> 6 m	all pred
Aubourg et al. 2015	9.2	20.9	32.2	54.7	27.8	-8.3	17.3	19.1	5.7	15.6
Brandse et al. 2016	23.7	33.5	30.5	45.9	33.1	-23.7	-27.9	-26.3	-21.6	-22.6
Buurman et al. 2015	18.8	44.9	31.0	55.8	44.3	-1.6	43.4	15.2	19.3	26.7
Edlund et al. 2017 (I)	6.2	27.3	26.5	54.2	31.0	-1.5	11.5	16.0	10.5	12.9
Edlund et al. 2017 (II)	5.1	24.6	27.0	52.9	30.2	-1.9	12.0	14.4	10.3	11.9
Edlund et al. 2017 (III)	4.5	23.2	25.3	52.5	28.6	-2.4	11.8	10.9	-1.8	10.4
Fasanmade et al. 2009	16.1	25.1	24.1	47.7	26.0	-14.1	-3.6	0.6	-3.3	-2.5
Fasanmade et al. 2011 (a)	14.7	24.5	16.4	55.0	25.5	-14.4	-8.3	-2.5	-1.2	-5.1
Fasanmade et al. 2011 (a/c)	13.3	23.4	20.1	52.9	24.9	-12.9	-8.8	-1.4	0.2	-5.5
Passot et al. 2016	0.3	33.1	46.4	49.8	37.5	-0.2	27.1	41.0	16.6	26.4
Petitcollin et al. 2018	2.5	30.3	36.3	79.9	42.0	-2.5	-20.7	-16.5	-48.2	-22.0
Xu et al. 2012	18.0	25.2	16.6	57.3	26.8	-16.9	1.3	-5.4	-6.2	-3.9

$\zeta$ : median symmetric accuracy; a: adults; a/c: adults/children; ADA: anti-drug antibody; m: month; pred: predicted; SSPB: symmetric signed percentage bias. Abbreviations for time intervals refer to descriptions in the main manuscript.

**Table S4.**  $\zeta$  and SSPB values for model predictions with time-varying covariates for ADA positive patients.

Model	$\zeta$ [%]					SSPB [%]				
	MAP	before ADA+	1 <sup>st</sup> time ADA+ or $\leq$ 1 m	> 1 m after ADA+	all pred	MAP	before ADA+	1 <sup>st</sup> time ADA+ or $\leq$ 1 m	> 1 m after ADA+	all pred
Aubourg et al. 2015	10.7	33.9	98.2	305.8	92.8	-5.2	32.8	85.2	305.8	79.7
Brandse et al. 2016	18.4	52.5	288.9	231.2	156.7	-12.8	-21.0	-113.3	-141.0	-56.5
Buurman et al. 2015	43.1	88.9	156.3	137.9	130.6	22.3	70.0	128.7	103.1	103.6
Edlund et al. 2017 (I)	10.6	40.6	72.1	309.9	82.2	-9.5	-7.5	30.1	309.9	51.7
Edlund et al. 2017 (II)	6.8	23.9	114.6	156.0	86.5	0.4	7.8	9.4	142.9	22.4
Edlund et al. 2017 (III)	5.2	24.9	109.8	129.5	71.2	-0.3	6.3	-14.4	11.4	6.4
Fasanmade et al. 2009	15.1	28.9	197.0	188.7	93.9	-2.9	-3.8	-33.3	153.8	14.3
Fasanmade et al. 2011 (a)	15.8	30.0	114.2	125.6	77.0	-9.9	-15.3	-18.7	77.0	-1.1
Fasanmade et al. 2011 (a/c)	14.1	31.0	95.4	132.3	77.8	-9.2	-13.8	-11.2	79.0	-1.9
Passot et al. 2016	0.3	17.1	144.5	354.8	127.8	0.1	14.5	78.4	340.0	66.9
Petitcollin et al. 2018	2.3	75.3	214.4	399.5	183.1	-2.0	-18.6	12.3	43.1	1.8
Xu et al. 2012	16.5	38.1	98.8	161.0	86.7	-8.3	2.9	51.6	134.9	58.8

$\zeta$ : median symmetric accuracy; a: adults; a/c: adults/children; ADA: anti-drug antibody, ADA+: anti-drug antibody positive; m: month; pred: predicted; SSPB: symmetric signed percentage bias. Abbreviations for time intervals refer to descriptions in the main manuscript.



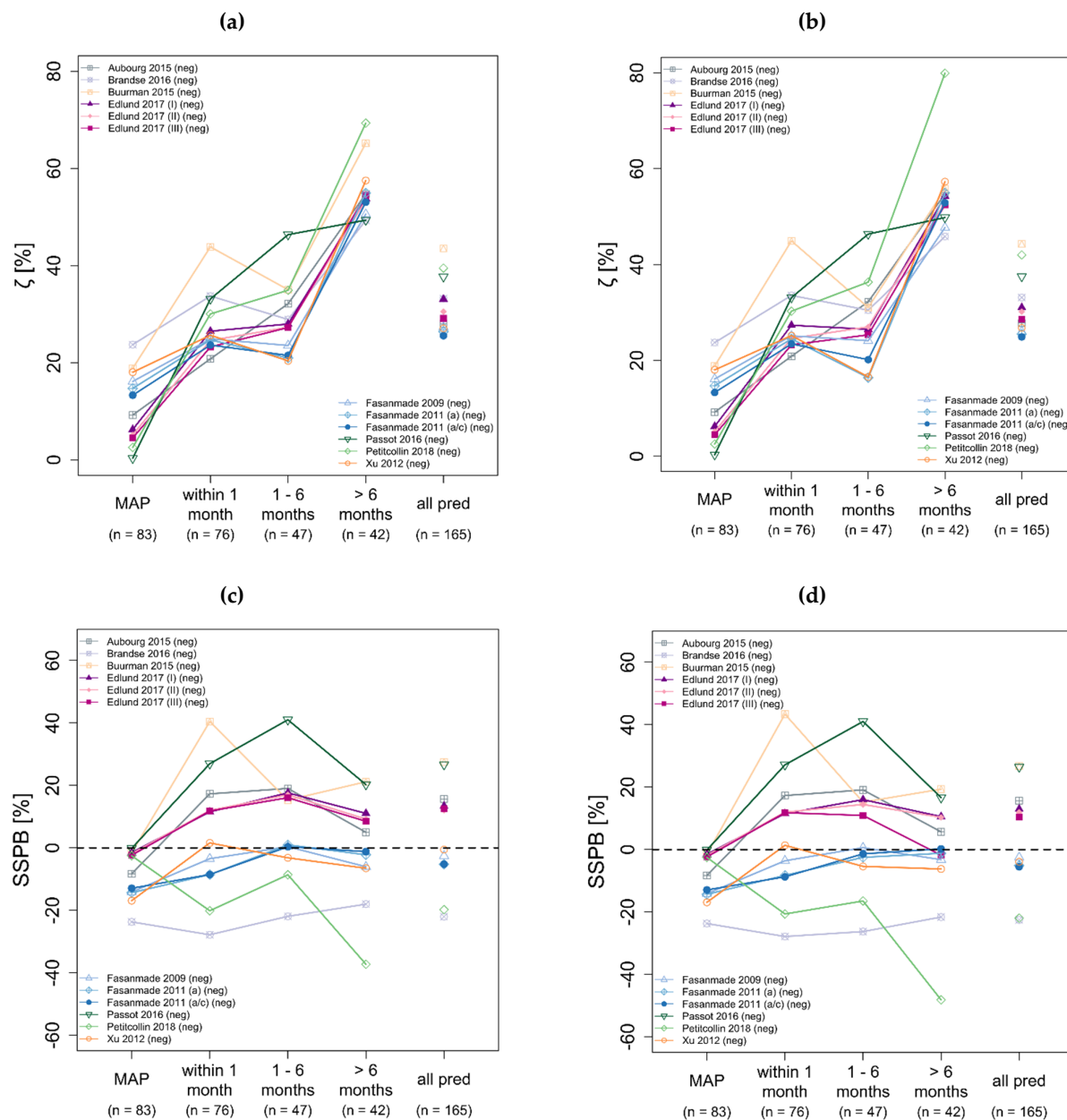


**Figure S2.** Model prediction accuracy ( $\zeta$ , **a** and **b**) and bias (SSPB, **c** and **d**) for anti-drug antibody (ADA) negative patients over time. The left panel shows  $\zeta$  and SSPB values for model predictions with fixed covariates determined at the time of the first measured serum infliximab concentration of each patient ( $C_{MAP}$ ), the right panel shows  $\zeta$  and SSPB values for model predictions with time-varying covariates. “all pred” covers all predicted concentrations excluding  $C_{MAP}$ . Numbers in parentheses refer to the number of observed concentrations in the respective time interval. (neg): ADA negative patients, pred: predictions; SSPB: symmetric signed percentage bias;  $\zeta$ : median symmetric accuracy.

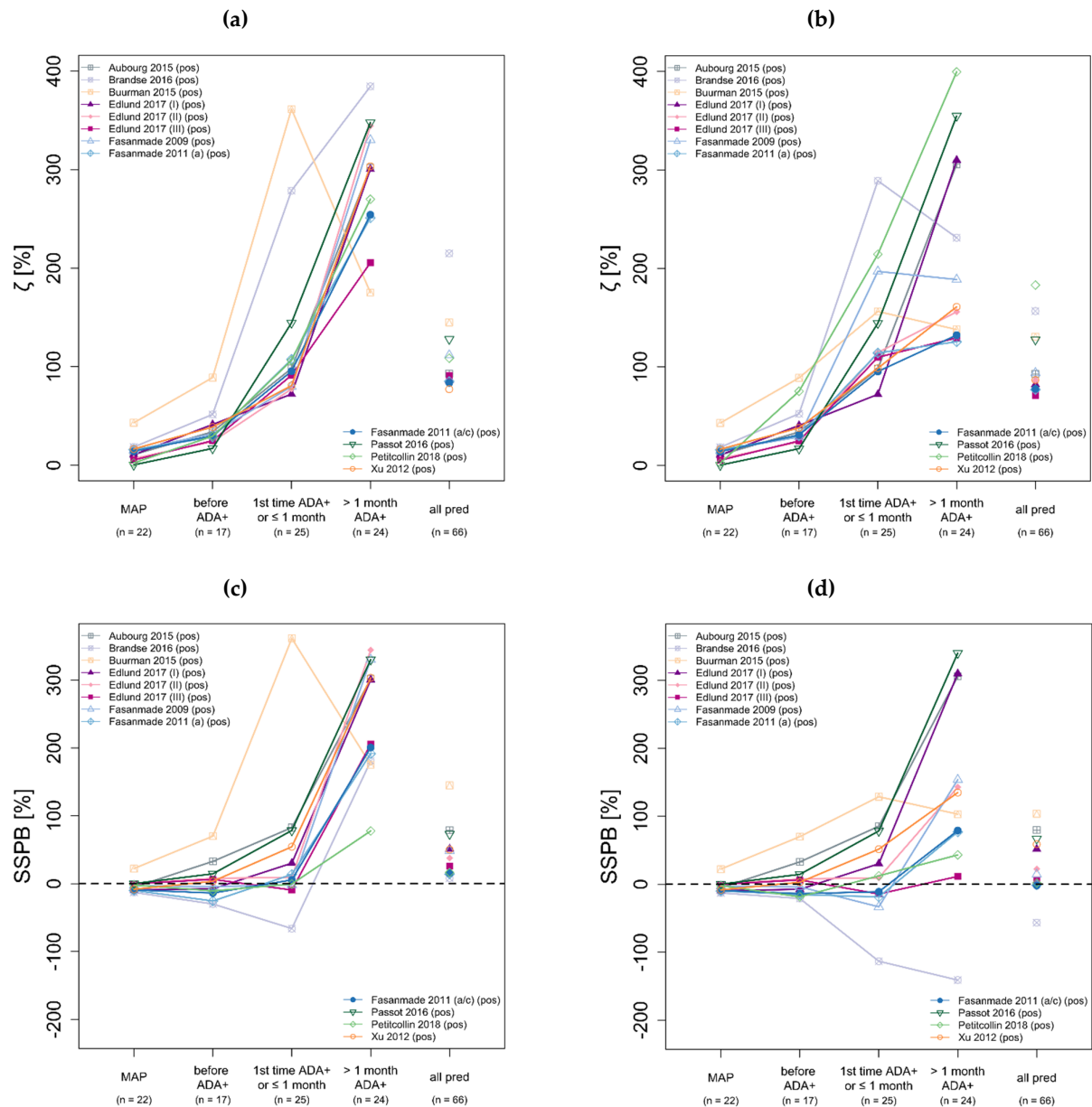


**Figure S3.** Model prediction accuracy ( $\zeta$ , **a** and **b**) and bias (SSPB, **c** and **d**) for anti-drug antibody (ADA) positive patients over time. The left panel shows  $\zeta$  and SSPB values for model predictions with fixed covariates determined at the time of the first measured serum infliximab concentration of each patient ( $C_{MAP}$ ), the right panel shows  $\zeta$  and SSPB values for model predictions with time-varying covariates. “all pred” covers all predicted concentrations excluding  $C_{MAP}$ . Numbers in parentheses refer to the number of observed concentrations in the respective time interval. (pos): ADA positive patients, pred: predictions; SSPB: symmetric signed percentage bias;  $\zeta$ : median symmetric accuracy.

### 2.3 Prediction- and variability-corrected visual predictive checks (pvcVPCs)

In this section, the pvcVPC for the population pharmacokinetic model by Petitcollin et al. 2018 is shown with automatic (full range) y-axis limits.

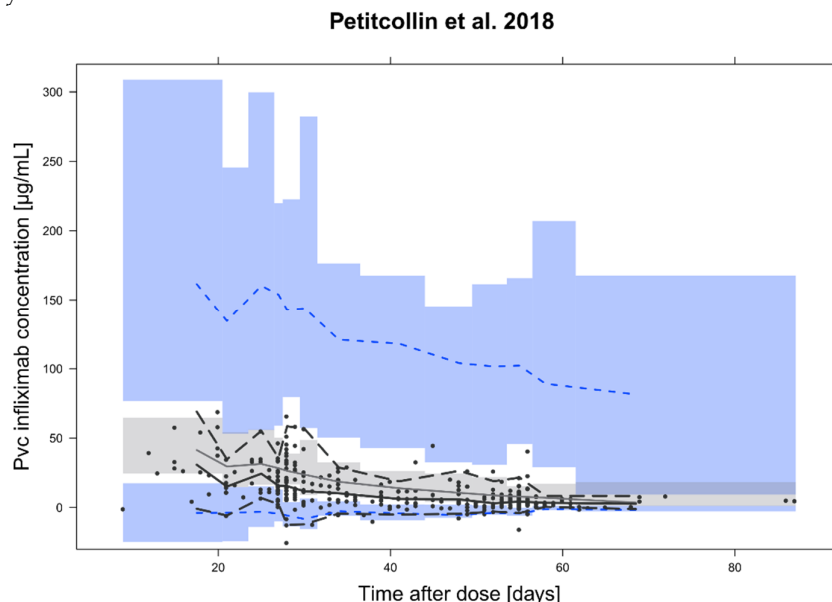


**Figure S4.** Prediction- and variability-corrected visual predictive check (pvcVPC) of serum infliximab concentrations for the population pharmacokinetic model by Petitcollin et al. 2018. Prediction- and variability-corrected observed concentrations are shown as black circles, observed median is depicted as black solid line, 5<sup>th</sup> and 95<sup>th</sup> data percentiles as black dashed lines. The model simulations (n=1000 replicates) are depicted as grey solid line (median) and blue dashed lines (5<sup>th</sup> and 95<sup>th</sup> percentiles). Colored areas represent the simulation-based 95% confidence intervals for the corresponding model-predicted median (grey areas) and 5<sup>th</sup> and 95<sup>th</sup> percentiles (blue areas). Pvc: prediction- and variability-corrected.

### References

1. Brandse, J.F.; Mathôt, R.A.; van der Kleij, D.; Rispens, T.; Ashruf, Y.; Jansen, J.M.; Rietdijk, S.; Löwenberg, M.; Ponsioen, C.Y.; Singh, S.; et al. Pharmacokinetic Features and Presence of Antidrug Antibodies Associate With Response to Infliximab Induction Therapy in Patients With Moderate to Severe Ulcerative Colitis. *Clin. Gastroenterol. Hepatol.* **2016**, *14*, 251–258.e2, doi:10.1016/j.cgh.2015.10.029.
2. Buurman, D.J.; Maurer, J.M.; Keizer, R.J.; Kosterink, J.G.W.; Dijkstra, G. Population pharmacokinetics of infliximab in patients with inflammatory bowel disease: Potential implications for dosing in clinical practice. *Aliment. Pharmacol. Ther.* **2015**, *42*, 529–539, doi:10.1111/apt.13299.
3. Aubourg, A.; Picon, L.; Lecomte, T.; Bejan-Angoulvant, T.; Paintaud, G.; Ternant, D. A robust estimation of infliximab pharmacokinetic parameters in Crohn's disease. *Eur. J. Clin. Pharmacol.* **2015**, *71*, 1541–1542, doi:10.1007/s00228-015-1942-8.
4. Edlund, H.; Steenholdt, C.; Ainsworth, M.A.; Goebgen, E.; Brynskov, J.; Thomsen, O.; Huisinga, W.; Kloft, C. Magnitude of Increased Infliximab Clearance Imposed by Anti-infliximab Antibodies in Crohn's Disease Is Determined by Their Concentration. *AAPS J.* **2017**, *19*, 223–233, doi:10.1208/s12248-016-9989-8.
5. Xu, Z.; Mould, D.; Hu, C.; Al, E. Population pharmacokinetic analysis of infliximab in pediatrics using integrated data from six clinical trials. *Clin Pharmacol Drug Dev.* **2012**, *1*, 203.
6. Wojciechowski, J.; Upton, R.N.; Mould, D.R.; Wiese, M.D.; Foster, D.J.R. Infliximab Maintenance Dosing in Inflammatory Bowel Disease: an Example for In Silico Assessment of Adaptive Dosing Strategies. *AAPS J.* **2017**, *19*, 1136–1147, doi:10.1208/s12248-017-0082-8.
7. Petitcollin, A.; Leuret, O.; Tron, C.; Lemaitre, F.; Verdier, M.C.; Paintaud, G.; Bouguen, G.; Willot, S.; Bellissant, E.; Ternant, D. Modeling Immunization to Infliximab in Children with Crohn's Disease Using Population Pharmacokinetics: A Pilot Study. *Inflamm. Bowel Dis.* **2018**, *24*, 1745–1754, doi:10.1093/ibd/izy129.

## PUBLICATION HISTORY

## B.1 RESEARCH ARTICLES

- I Kovar, C., Loer, H. L. H., Rüdesheim, S., Fuhr, L. M., Marok, F. Z., Selzer, D., Schwab, M., & Lehr, T. (2024). A physiologically-based pharmacokinetic precision dosing approach to manage dasatinib drug-drug interactions. *CPT: pharmacometrics & systems pharmacology*, 13(7), 1144–1159. DOI: [10.1002/psp4.13146](https://doi.org/10.1002/psp4.13146).
- II Loer, H. L. H., Kovar, C., Rüdesheim, S., Marok, F. Z., Fuhr, L. M., Selzer, D., Schwab, M., & Lehr, T. (2024). Physiologically based pharmacokinetic modeling of imatinib and N-desmethyl imatinib for drug-drug interaction predictions. *CPT: pharmacometrics & systems pharmacology*, 13(6), 926–940. DOI: [10.1002/psp4.13127](https://doi.org/10.1002/psp4.13127).
- III Kovar, C., Kovar, L., Rüdesheim, S., Selzer, D., Ganchev, B., Kröner, P., Igel, S., Kerb, R., Schaeffeler, E., Mürdter, T. E., Schwab, M., & Lehr, T. (2022). Prediction of drug-drug-gene interaction scenarios of (E)-clomiphene and its metabolites using physiologically based pharmacokinetic modeling. *Pharmaceutics*, 14(12), 2604. DOI: [10.3390/pharmaceutics14122604](https://doi.org/10.3390/pharmaceutics14122604).
- IV Schräpel, C., Kovar, L., Selzer, D., Hofmann, U., Tran, F., Reinisch, W., Schwab, M., & Lehr, T. (2021). External model performance evaluation of twelve infliximab population pharmacokinetic models in patients with inflammatory bowel disease. *Pharmaceutics*, 13(9), 1368. DOI: [10.3390/pharmaceutics13091368](https://doi.org/10.3390/pharmaceutics13091368).
- V Kovar, L., Schräpel, C., Selzer, D., Kohl, Y., Bals, R., Schwab, M., & Lehr, T. (2020). Physiologically-based pharmacokinetic (PBPK) modeling of buprenorphine in adults, children and preterm neonates. *Pharmaceutics*, 12(6), 578. DOI: [10.3390/pharmaceutics12060578](https://doi.org/10.3390/pharmaceutics12060578).

## B.2 CONFERENCE ABSTRACTS

- I Tran, F., Aden, K., Bernardes, J. P., Jäckel, C., Kovar, C., Rüdesheim, S., Florea, M., Stallbaum, F., Schrinner, F., Nikolaus S., Maetzler W., Franke, A., Syzmz-cak, S., Hofmann, U., Lehr, T., Schwab, M., Dempfle, A., Huber, S., Wiestler, M., Seidler, U., Rosenstiel, P., Schreiber, S. (2025). Biomarker-informed therapy guidance improved clinical outcomes of anti-TNF treatment in patients with inflammatory bowel disease in a multi-center, randomized, open-label, prospective clinical trial (GUIDE-IBD). *Gastroenterology*, 169, S–2085. DOI: [10.1016/S0016-5085\(25\)05725-7](https://doi.org/10.1016/S0016-5085(25)05725-7).
- II Kovar, C., Loer, H. L. H., Schwab, M., & Lehr, T. (2023) Physiologically based pharmacokinetic modeling of dasatinib to describe enzyme-mediated and pH-dependent drug–drug interaction scenarios. PAGE 31, Abstr 10589 [[www.page-meeting.org/?abstract=10589](http://www.page-meeting.org/?abstract=10589)].
- III Loer, H. L. H., Kovar, C., Schwab, M., & Lehr, T. (2023). Physiologically based pharmacokinetic modeling of imatinib and its main metabolite for drug–drug interaction predictions. PAGE 31, Abstr 10583 [[www.page-meeting.org/?abstract=10583](http://www.page-meeting.org/?abstract=10583)]
- IV Kovar, C., Hofmann, U., Selzer, D., Tran, F., Schreiber, S., Schwab, M., & Lehr, T. (2022). Early optimization of infliximab treatment using a model-informed precision dosing approach: the GUIDE-IBD study. e:Med Meeting 2022 on Systems Medicine.
- V Schräpel, C., Hofmann, U., Tran, F., Schreiber, S., Schwab, M., & Lehr, T. (2022) Model-informed precision dosing (MIPD) in infliximab induction therapy to achieve target trough concentrations during the maintenance phase. DPhG Annual Meeting.
- VI Schräpel, C., Kovar, L., Rüdesheim, S., Ganchev, B., Kröner, P., Igel, S., Kerb, R., Mürdter, T. E., Schwab, M., & Lehr, T. (2021). Physiologically based pharmacokinetic (PBPK) modeling of (E)-clomiphene drug-drug-gene interactions with CYP2D6 and clarithromycin. PAGE 29, Abstr 9819 [[www.page-meeting.org/?abstract=9819](http://www.page-meeting.org/?abstract=9819)].
- VII Schräpel, C., Kovar, L., Hofmann, U., Reinisch, W., Schwab, M. & Lehr, T. (2020). Predictive model performance of population pharmacokinetic (popPK) and physiologically based pharmacokinetic (PBPK) models for infliximab concentrations. e:Med Kick-off Meeting on Systems Medicine, digital.

## B.3 OTHERS

I Kovar, L., Jan-Georg, W., Schräpel, C. & Lehr, T. (2020). Pharmakometrie erklärt: Wie verändert sie die moderne Pharmazie? PZ Prisma, 26, 217–230.

